National Oceanography Centre
NATURAL ENVIRONMENT RESEARCH COUNCIL

UNIVERSITY OF Southampton

UNIVERSITY OF SOUTHAMPTON

Faculty Of Natural And Environmental Sciences

School of Ocean and Earth Science

Investigating the influence of fine-scale physical processes on the spatio-temporal distribution of marine megavertebrates off southwest UK

by

Sophia Butler-Cowdry

Thesis for the degree of Doctor of Philosophy

March 2015

UNIVERSITY OF SOUTHAMPTON

ABSTRACT

FACULTY OF NATURAL AND ENVIRONMENTAL SCIENCE

Ocean and Earth Sciences

Thesis for the degree of Doctor of Philosophy

INVESTIGATING THE INFLUENCE OF FINE-SCALE PHYSICAL PROCESSES ON THE SPATIO-TEMPORAL DISTRIBUTION OF MARINE MEGAVERTEBRATES OFF SOUTHWEST UK

Sophia Butler-Cowdry

The primary aim of this PhD research is to describe environmental controls on distribution patterns of free-ranging marine top predators in tidally-dominated coastal waters off southwest UK, at a spatial resolution of metres to hundreds of metres, and a temporal resolution of hours to months. As human impacts increase in the nearshore zone (e.g. wet renewables), the need to better understand such fine-scale controls on distribution is critical, particularly as highly mobile marine megavertebrates in southwest coastal waters are amongst some of the region's most threatened species (e.g. basking sharks *Cetorhinus maximus*, harbour porpoises *Phocoena phocoena*, and the critically-endangered Balearic shearwater *Puffinus mauretanicus*). Current policy drivers (e.g. Marine Protected Area designation and management) require the development of appropriate low-cost methodologies for land-based data collection, in order to provide robust scientific evidence on fine-scale habitat use of these threatened species.

To improve understanding of how the physical environment influences habitat use of vulnerable marine predators, a complementary and multi-disciplinary suite of techniques for data collection and analyses was developed. This methodological 'toolbox' included: a theodolite to collect highly-accurate (<50 m) positions of animals at sea; acoustic data loggers to collect continuous, subsurface echolocation data on cetacean presence; fine scale (1-m) resolution seafloor bathymetry; novel radar-derived sea surface metrics; and temporally highly-resolved (30-min) met-ocean data (e.g. weather and tides). These data were integrated into statistical predictive models to identify significant drivers of distribution; information that can be used to inform local policy at the study sites and provide new knowledge on the target species.

To test the utility of the methods, two contrasting locations of different physical habitat were selected as study sites: the tidally-swept, high-energy, bedrock-dominated Runnel Stone Reef off the southwest tip of the UK mainland; and St Ives Bay, a shallow, sediment-dominated, gently-sloping bay on the northwest Cornish coast. Both sites are known 'hotspots' for top predators, and both have an urgent requirement for species' distribution data to meet current and future management requirements.

Theodolite sightings data were collected at both study sites for a variety of small cetaceans and seabird species. All target species were influenced by small-scale topographic features at the scale of metres to tens of metres, with areas of steeper slopes and strong tidal flows (i.e. tidal-topographic fronts) forming particular hotspots. At St Ives Bay, shallow sheltered nearshore habitats were preferentially utilised. Small-scale commercial fishing activity showed significant overlap with target species' distributions, highlighting the additional importance of these sites for human predators. Significant relationships with tidal flow parameters (e.g. current direction and tidal range) provided further insights into the physical processes driving these clustered sightings.

Acoustic data collected from the Runnel Stone Reef provided valuable supporting data on porpoise and dolphin activity, including a strong diel pattern and fine-scale spatial variation in habitat use that was species-specific. The importance of accounting for variability in survey conditions (e.g. acoustic noise, and wind, cloud and sea state) across land-based and subsurface analyses was also highlighted.

The methodological toolbox developed and successfully applied in this study, comprising high-resolution visual and acoustic data, and a variety of environmental parameters, provides a relatively low-cost and effective method for determining fine-scale habitat use of mobile top predators in dynamic, topographically-complex nearshore environments, where vessel-based surveys may be impractical.

“The greatness of a nation and its moral

progress can be measured by the way

its animals are treated…”

Mahatama Gandhi c. 1890

Table of Contents

List of Tables

List of Figures

List of Appendices

DECLARATION OF AUTHORSHIP

I, Sophia Butler-Cowdry, declare that this thesis,

Investigating the influence of fine-scale physical processes on the spatio-temporal distribution of marine megavertebrates off southwest UK

and the work presented in it, are my own, and have been generated by me, as the result of my own original research.

I confirm that:

1. This work was done wholly or mainly while in candidature for a research degree at this University;
2. Where any part of this thesis has previously been submitted for a degree or any other qualification at this University or any other institution, this has been clearly stated;
3. Where I have consulted the published work of others, this is always clearly attributed;
4. Where I have quoted from the work of others, the source is always given. With the exception of such quotations, this thesis is entirely my own work;
5. I have acknowledged all main sources of help;
6. Where the thesis is based on work done by myself jointly with others, I have made clear exactly what was done by others and what I have contributed myself;
7. Parts of this work have been published in Jones et al. (2014a); see Appendix A.

Signed: .....

Date: .....

Acknowledgements

Thank you to my main supervisor, Dr Russell Wynn, for creating this project, time spent in the field (an incredible experience of which I am very grateful), and for having faith in me enough to carry it out, despite my rather unconventional background. Thanks to my co-supervisor, Dr Simon Ingram, for his feedback and continual support, particularly defining survey strategy. I am especially grateful to Simon, and Dr Mark Davidson of Plymouth University, for their support and belief in me at the beginning of my scientific career as an arts student; their motivation pushed me through my master's degree. Between them, they instilled in me the confidence to apply for a PhD in Marine Science, a path I had not even considered, let alone thought possible, thank you. Thanks to my co-supervisor, Dr Justin Dix, for helpful comments.

Clare Embling has been phenomenal in the depth and breadth of advice given throughout this project, from analysis and coding, to feedback and moral support; thank you for everything. Travis Mason provided invaluable support with environmental data processing; help that was greatly appreciated, thank you. Thanks to Tim Le Bas in the office next door for support with bathymetry datasets and general computer issues. Nick Tregenza of Chelonia, your input and advice on acoustic data processing and analysis were much valued, I am enormously grateful. Thanks to Duncan and Hannah Jones of Marine Discovery Penzance for your friendship, and to Dan Murphy for commitment in the field, beautiful photography and help with acoustic data processing; I am very grateful to all of you, and look forward to our paths crossing again.

I would like to thank Andrew Colenutt for his enormous contribution during fieldwork, help acquiring environmental data, and continued support during writing-up. To Ted Chappell, not only a huge thank you for your time, but for sharing with me your vast local knowledge. Also, to your wife, Sue, for making me so welcome in your home during fieldwork; I am so grateful to both of you for your kindness and warmth. Thanks to John Swann in the field whose wonderful company was much valued and expert knowledge an inspiration; I look forward to time spent along the beautiful Cornish coast with you again. To John Chappell, thank you for your friendly, informative visits in the field and for supplying data from your weather station. I am also grateful to Jeff Hardman for the special arrangements at his property in Sennen Cove that provided a comfortable and useful base for myself and volunteers during fieldwork.

To my PhD colleagues, Alice Jones, Rhiannon Meier, Lavinia Suberg, Matt Hodgkinson and Jessica Klar; thank you all so much for your help, advice and encouragement throughout the

journey, it has meant so much to me and I will always be grateful. Alice, your guidance on the project throughout, including data handling and GIS, was invaluable, and I thank you for your time, patience and friendship; Australia is lucky to have you. Matt, you helped me during so many 'crisis' moments, thank you for your patience, kindness, and access to the most well-stocked biscuit drawer. I thank Rhiannon, in particular, for her unwavering support and phone calls, help with statistics and analysis, and for becoming a wonderful friend; I couldn't have got through it without you, and I thank you from the bottom of my heart for everything.

Some thanks to my friends. Thomas Hinman, thank you for being a rock throughout my scientific journey, from the first moments at Plymouth, just a few years ago, when I couldn't even interpret a plot showing simple correlation, to rescuing me in the library in the middle of the night when I lost half my work before a deadline in the morning, and for time spent during surveys in your favourite part of England. Thank you for your encouragement, belief in me, and for always making me see the bigger picture; your friendship and insight mean the world to me, and I value it to my core. To CJ (Christina McClay) and Phil Beenham, thank you both for your kindness, laughter, friendship, and support in the field when I needed it most, I will always be grateful; you both contributed so much to the wonderful memories of Cornwall I now hold dear, thank you for our time together. Finally, to Heywood Beacon, who was brave enough to enter a time of my life that most would consider madness, the writing-up. Thank you for your unconditional support through some extreme emotions, and for your patience, kindness and encouragement when I was on the verge; I am enormously grateful.

Lastly, and most importantly, thank you to both my parents who have provided me with many opportunities in life with no questions asked, only that I act constructively and consciously. It has been a long time coming (understatement) but I hope I have done you proud. I believe I have now built a sufficient foundation for myself on which to do whatever I choose to make this world a little better, but I could not have achieved any of my successes without your support, generosity (beyond the call of duty) and unconditional love. My father is one of my greatest inspirations: his patience, intelligence, foresight, sheer ability to manage everything in all our lives simultaneously, and his words of wisdom; you amaze me and will continue to inspire me to be the very best I can be, always.

I hope this work can motivate others to choose the environment over their ego, and see that the world is a huge and beautiful place that requires respect, compassion and understanding. Humans are the guardians of that world, and we should live up to the duty demanded of us.

Chapter 1 Introduction to the Thesis

This thesis is the result of a four-year PhD project at the National Oceanography Centre (NOC), Southampton. PhD funding was provided by University of Southampton, with additional support from the NOC component of the UK Marine Environmental Mapping Programme (MAREMAP).

The thesis is presented in seven chapters, outlined below:

1. Introductory chapter outlining the aims, objectives and rationale of the research project. The introduction also contains an overview of the literature relevant to all the substantive science chapters (Chapters 3-6), focusing on small-scale physical processes and their influence on marine megavertebrates in the nearshore environment. Each of the science chapters contains an introduction with chapter-specific literature.
2. Methods chapter detailing field survey set-up and environmental data collection. This chapter also includes a section on data quality and descriptions of the study sites. The information presented is broadly relevant to the substantive science chapters, though each also includes chapter-specific survey methodologies and analytical techniques.
3. Influence of physical controls on the fine-scale habitat use of harbour porpoises. This chapter describes spatial and temporal patterns in theodolite (visual sightings) data collected over tidally-swept rocky reef habitat to improve understanding of the environmental controls driving their distribution.
4. Influence of physical controls on the fine-scale habitat use of harbour porpoises and dolphins. This chapter describes temporal patterns in the acoustic (subsurface echolocation) data collected at three locations around the reef survey site to contribute to knowledge on the environmental drivers of distribution. Patterns are compared between species, sites and years within the study area.
5. Influence of physical controls on the fine-scale habitat use of foraging seabird aggregations. This chapter describes spatial and temporal patterns in theodolite (visual sightings) data over the reef survey site to improve understanding of the environmental controls driving the distribution of foraging aggregations, considered a proxy for prey availability.
6. Influence of physical controls on the fine-scale habitat use of foraging seabirds and cetaceans. This chapter describes spatial and temporal patterns in theodolite (visual sightings) data collected from a shallow bay, where recent bycatch incidents highlight the

need to improve knowledge of the environmental controls driving seabird distribution to inform local fisheries' management.

7. Overall conclusions. Synthesis of key findings from Chapters 3-6, including suggestions for future work.

1.1 Project Description

Data collected for this project were used to investigate the influence of small-scale physical processes on the distribution of top marine predators at two contrasting coastal sites off Cornwall, southwest UK, at a resolution of metres to tens of metres. Although progress has been made describing the spatio-temporal drivers of distribution of highly mobile marine species, some key questions still remain, particularly at such fine scale in the nearshore environment. The project sought to explain the influence of these fine-scale processes by collecting locational data on a variety of marine megavertebrates observable from shore, with focus on: harbour porpoises *Phocoena phocoena*, listed under Annex II and IV of the EU Habitats Directive; other cetaceans, including bottlenose *Tursiops truncatus* and common *Delphinus delphis* dolphins; and various seabird species, including northern gannets *Morus bassanus*, black-legged kittiwakes *Rissa tridactyla* and the critically-endangered Balearic shearwater *Puffinus mauretanicus*.

Data were collected using a suite of complementary techniques, including: a theodolite, acoustic data loggers, high resolution (1-m scale) bathymetry, novel radar-derived tidal flow imagery, and highly resolved (30-minute) environmental data; these data were integrated into statistical models to identify significant drivers of species' distribution. Results contribute to knowledge on the fine-scale habitat use of highly mobile marine animals, and provide insight into the static and dynamic variables that support ecologically-important areas within coastal environments.

Developing appropriate low-cost methodologies for land-based data collection in order to determine patterns of habitat use for a variety of species is of critical value in the face of ever-increasing anthropogenic impacts in the nearshore zone, including marine spatial planning and renewables. Understanding fine-scale controls on distribution has implications for the location and design of protected areas, as well as local fisheries management. The efficacy of field methods and analytical techniques developed in this project (i.e. a methodological 'toolbox') may serve UK (e.g. Defra) and international (e.g. EU) requirements to identify cost-efficient

methods for the designation and/or monitoring of marine protected areas in the future, including effective and appropriate monitoring and management regimes.

1.2 Aims

The aims of the thesis fall under three main themes:

Ecology (overarching theme of the research)

i. To describe the fine-scale spatial and temporal distribution patterns of harbour porpoises, dolphins, and foraging seabird aggregations at two contrasting coastal locations off southwest UK.

Management and Policy

ii. To improve understanding of how the physical environment influences fine-scale habitat preferences of highly mobile marine species in order to better inform management regimes, including conservation and marine spatial planning.

Methodological Toolbox

iii. To develop a multi-disciplinary suite of complementary techniques that can be applied as a methodological 'toolbox' at coastal locations amenable to shore-based observations, in order to determine fine-scale habitat use of highly mobile marine species (where appropriately-resolved covariate data exist).

1.3 Research Questions

A number of research questions were generated in three key areas:

Spatial

In the nearshore zone, do certain bathymetric (fixed) habitat variables influence the spatial distribution of particular highly mobile marine animals? Do higher trophic level species aggregate in spatially-constrained areas (i.e. do they exhibit clustering behaviours)? Do disparate species exhibit similar habitat preferences within the same location? Do observed associations with identifiable features vary depending on survey method?

Temporal

In tidally-dominated environments, does tidal state, including the spring-neap cycle, influence the fine-scale distribution of marine species? Do dynamic processes result in varying spatio-temporal patterns (i.e. does core habitat vary spatially according to wind vector and/or tidal flow direction)? Are patterns site-specific? Do other factors influence distribution, such as survey variability (e.g. wind strength, wind direction, cloud cover, sea state)? To what extent are responses dependent on survey method, species, site, or year? Are there diurnal patterns in species occurrence data?

Interaction Between Tide and Topography

Are high energy, nearshore (<6 km offshore) tidal-topographic boundaries (small-scale fronts) important habitat areas for higher trophic level species? Do highly mobile marine animals aggregate along these fronts? Do disparate species exhibit similar habitat preferences within the same location? Is tidal-topographic influence site-specific, or can inferences be made on its predictability? Are there implications for species conservation and management?

1.4 Objectives

The objectives were designed to answer the research questions:

i. To collect fine-scale visual sightings data of the focal species to describe spatial and temporal distribution patterns (using a theodolite – the primary survey method).
ii. To collect acoustic data of cetacean species to describe subsurface spatial and temporal distribution patterns (using static acoustic data loggers – an alternative survey method).
iii. To incorporate high resolution multibeam bathymetry data to provide fine-scale physical habitat information.
iv. To acquire remotely-sensed (radar) data to infer surface current flow dynamics.
v. To acquire and collate a suite of measured, highly-resolved environmental variables relevant to survey effort to provide evidence of dynamic controls on observed species distribution.
vi. To construct statistical models that integrate animal response data with static and dynamic environmental variables in order to identify significant factors driving fine-scale habitat use, and predict zones of higher relative use within the study areas.

vii. To interpret results within the context of policy to better inform marine spatial planning, fisheries and conservation management.

viii. To discuss utility of the complimentary suite of techniques developed in the study (the methodological 'toolbox') and its application for identifying fine-scale habitat preferences of highly mobile marine species at other constrained coastal locations.

1.5 Rationale

Ecology

In the face of ever-increasing anthropogenic disturbance in coastal waters (Witt et al., 2012b; Waggitt & Scott, 2014), the marine environment is subject to a range of threats. Potentially damaging activities include, but are not limited to: fishing, development of marine renewables, oil, gas and aggregate extraction, shipping, recreation, and waste disposal, all of which can impact on the habitat and availability of prey to apex marine predators (e.g. basking sharks *Cetorhinus maximus*, dolphins, porpoises and seabirds), collectively referred to as 'megavertebrates'. Furthermore, marine megavertebrates in coastal environments are often amongst some of the most threatened species (e.g. porpoises and seabirds; IUCN, 2014), as they depend on specific environmental conditions at a limited number of suitable locations for the successful capture of prey (Scott et al., 2010; Witt et al., 2013). These highly mobile marine species are therefore in need of effective management measures to avoid long-term decline in population and distribution (Thompson et al., 2000; Cañadas & Hammond, 2006). However, detailed information on their fine-scale movements in relation to environmental variables, both static and dynamic, is currently inadequate (Embling et al., 2010) though urgently needed to robustly assess their realised and potential interactions with anthropogenic activities at small scales (McClellan et al., 2014). Additionally, as human impacts increase in tidally-swept environments (e.g. in the form of wet renewables, such as tidal stream turbines; Waggitt & Scott, 2014), improved understanding of the fine-scale distributions of vulnerable species in dynamic coastal waters will be fundamental to carrying out effective Environmental Impact Assessments (EIAs) to mitigate any adverse effects.

The relationship between static variables (e.g. seabed topography), complex water dynamics and biota, is a challenging area of environmental science (Kim et al., 2009; McPhee-Shaw et al., 2011; Sveegaard et al., 2012a). A decade ago, Wilson et al. (2004) reported that knowledge on the oceanographic, biological and anthropogenic factors that drive distribution patterns

remained basic. However, despite the evidence base having grown in recent years (Booth et al., 2013; Embling et al., 2013; Scott et al., 2013; Sharples et al., 2013a), there is a continued and urgent need to improve information on habitat use in relation to environmental variables (Jones et al., 2014a), particularly concerning the fine-scale drivers of distribution in coastal waters (discussed further in Section 1.6). Many previous studies of the marine environment have attempted to link environmental data with spatio-temporal distribution of various trophic level species; these include: plankton (Franks, 1992b, 1992a; Hao et al., 2003; Genin, 2004; Bertrand et al., 2008; Scott et al., 2010), demersal fish (Zheng, 2002), squid (Sanchez et al., 2008), ocean sunfish *Mola mola* (Sims & Southall, 2002; Houghton et al., 2006), seabirds (Abrams & Griffiths, 1981; Haney, 1986; Camphuysen et al., 2006; Camphuysen, 2011; Camphuysen et al., 2012; Lascelles et al., 2012; Thaxter et al., 2012), cetaceans and pinnipeds (Cañadas et al., 2002; Hamazaki, 2002; Macleod et al., 2004; Cañadas et al., 2005; MacLeod & Zuur, 2005; Kaschner et al., 2006; Redfern et al., 2006; MacLeod et al., 2007b), and sharks (Sims & Merrett, 1997; Sims et al., 2003; Sims et al., 2005).

It is clear that dynamic coastal systems require appropriate, and adaptable, conservation and monitoring methods if a sustainable, ecosystem-based approach to managing the marine environment is to be applied (Lascelles et al., 2012; Ronconi et al., 2012). However, the literature supports the fact it is first necessary to improve knowledge on how the physical environment affects habitat preferences of top predators by providing robust scientific evidence on the drivers controlling their distribution. This is particularly important as these animals are often considered 'indicator' species (Montevecchi, 1993), likely indicative of localised zones of enhanced prey availability, or 'hotspot' areas. Shifts in the distribution and/or habitat preferences of these higher trophic level species can have significant ecological implications, thus ensuring the health of other key aspects of marine ecosystems (Hooker & Gerber, 2004). Since it is generally assumed that areas of greatest usage reflect higher quality habitat (Bailey & Thompson, 2010; Pirotta et al., 2013), the value of identifying and quantifying controls on short-term (days to weeks) distribution and small-scale (tens of metres) concentrations of these highly mobile marine species is clear.

Management

Spatial management regimes and anthropogenic activites (e.g. conservation, fisheries, wind farms, telecommunications, waste disposal) are often concentrated in the coastal zone but robust scientific evidence is lacking, and key questions still remain, on how marine predators at the top of the food chain actually use this habitat. Many of these species are protected under

UK (e.g. Marine and Coastal Access Act 2009) and international conventions (e.g. Habitats Directive 92/43/EEC; Birds Directive 2009/147/EC). Threatened, rare and vulnerable bird species require specific conservation measures by Member States for their protection, such as the designation of Special Protection Areas (SPAs). Annex II marine animals, for example, which include several species of cetaceans, e.g. bottlenose dolphin and porpoise, require Special Areas of Conservation (SACs). The aim is to ensure their natural range is not reduced, nor likely to be reduced, in the near future (Article 4). Indeed, one of the main aims of the Habitats Directive is to 'maintain or restore, at favourable conservation status, natural habitats and species of wild fauna and flora of Community interest' (Article 2.2) by designating a network of ecologically-coherent protected areas across the EU, known as 'Natura 2000'.

The designation of SACs, and marine SPAs for seabirds, will contribute to this network, so acquiring sufficient scientific evidence on the fine-scale distributions of protected species is vital for Government to be able to make informed proposals to the European Commission on site selection. This can be problematic for wide-ranging species, as sites can only be proposed where there are 'clearly identifiable areas…essential for their life and reproduction' (Article 4.1) but the distribution and relative abundance of many listed species remain poorly understood (JNCC, 2009). Additionally, according to European guidance in Annex III, a protected species may only be excluded from consideration from site selection where the 'populations are too small to be naturally viable, or where the species occur only as vagrants', i.e. outside their natural range. It is clearly essential to adequately determine a population's occurrence, or persistence, over time within an area to contribute to the evidence base required for the site selection process.

In 2009, the Marine and Coastal Access Act paved the way for the establishment of Marine Conservation Zones (MCZs) to be designated in English waters by 2013, as part of a wider network of Marine Protected Areas (MPAs) around the UK and across Europe. MCZs generally aim to protect a range of 'nationally important marine wildlife, habitats, geology and geomorphology' to ensure the long-term sustainability of marine resources (JNCC, 2009), and will contribute to the European-wide Natura 2000. Although English MCZs are not specifically designated for mobile species, cetaceans and seabirds are listed as supporting features at some sites. In September 2011, regional steering groups, set up under the Marine and Coastal Access Act, recommended 127 MCZ sites to JNCC, Natural England (NE), and the MCZ Science Advisory Panel. In November 2013, Defra designated 27 of these sites in a first tranche. Defra subsequently funded additional survey work to fill the 'gaps in evidence used to support the

recommendations' (GOV.UK, 2014) with the aim of designating a second tranche in 2016, followed by a third and final tranche. Additionaly, in UK waters, 108 SACs, and 108 SPAs with marine components, have been designated, as well as two Marine Nature Reserves (MNRs). This means ~9.5% of UK waters are now listed as MPAs.

The timely designation of MPAs would have enabled the UK Government to meet its on-going European and international marine conservation commitments, which aim to achieve Good Environmental Status ('GES') across Europe's seas by 2020 under the EU Marine Strategy Framework Directive (2008/56/EEC). However, the key challenge the UK Government has faced is making informed decisions on which areas to protect and how to manage them when they do not always have the best evidence available. As a result of delaying designation of SACs for harbour porpoises in 2013, for example, the UK Government became the subject of legal infraction proceedings that were issued by the European Commission (ClientEarth, 2013). Furthermore, management regimes responsible for site designation and/or monitoring in coastal waters often lack a clear set of scientific tools to assist them in the process, which this study helps provide.

Methodological Toolbox

The development of intelligent and cost-effective survey methods to support future MPA designation for mobile species is timely. The study of nearshore phenomena and ongoing processes is clearly limited by time, finances and the physical constraints of acquiring scientifically-robust evidence in challenging, tidally-dominated environments. The dynamic nature of small-scale tidal-topographic fronts (discussed further in Section 1.6), and the fine-scale distributions of species that utilise them for foraging, cannot be easily or directly measured using conventional methods, e.g. boat-based surveys. They must be inferred from land-based visual and/or *in situ* acoustic monitoring, where relevant. When animal observations are combined with geophysical and hydrographic data on seafloor topography, water column characteristics, and met-ocean data, such as weather and tides, improved knowledge on distribution can be achieved. Furthermore, by integrating precise locations of indicator species collected in the field with advanced mapping software, layers of spatial data can be superimposed to relate characteristics of the physical environment to spatial observations. Integration of these data into statistical models, accompanied by a suite of dynamic (temporal) variables, enables any significant relationships between the response of the animals and certain aspects of their environment to be quantitatively identified. Developing a suite of complementary and multi-disciplinary techniques can be considered a

methodological 'toolbox', which can be usefully applied in constrained, topographically-complex high energy environments, which are often hotspot areas for top predators, where controls on distribution are variable, and otherwise challenging to quantify.

Overview of Primary Survey Method (land-based observations)

Shore-based methods offered the opportunity to develop the methodological toolbox and collect the data required by management in order to better understand how complex free-ranging animals use dynamic coastal systems. The suite of complementary tools was used to provide robust evidence and improve knowledge on the fine-scale drivers of distribution of the focal species.

Land-based observation studies offer a cost-effective and non-intrusive alternative to boat-based and aerial surveys (Denardo et al., 2001). When the precise height and location of a land observation point are known, a theodolite can be used during visual surveys to accurately measure the positions of highly mobile marine species in the nearshore zone (Kruse, 1991; Wursig et al., 1991; Mayo & Goodson, 1993). Theodolites have been used since the 1970s to successfully study a variety of cetaceans around the world (Wursig & Wursig, 1979; Acevedo, 1991; Kruse, 1991; Goodson & Mayo, 1995). The theodolite method provides accurate data on the distances to individual animals, or groups of animals (Sagnol et al., 2014) from the operator, although it cannot be used to explore group spatial structure (inter-animal distances) as a stand-alone method (Denardo et al., 2001). Additionally, since observations of marine animals are made from a distance, their behaviour is unaffected by the recording method (vs. boat-based surveys, for example); this means recorded positional locations are 'true' markers of target species' surface distribution. The utility of the theodolite method is highlighted in this project, as well as others (e.g. Kruse, 1991; Goodson & Mayo, 1995; Harzen, 2002), when used in conjunction with highly-resolved environmental data, such as bathymetry. Visual spatial analyses can reveal extremely fine-scale habitat associations between identifiable seafloor features and species' locations.

Site Selection

Two contrasting coastal locations of different physical habitat (detailed further in Section 2.4) were selected to meet the project's objectives, not only as an opportunity to compare application of the same suite of techniques, i.e. as test sites for the methods, but where there existed strong policy drivers to collect critical information on the fine-scale controls of habitat use for a variety of vulnerable marine species.

The primary study area, the highly-dynamic environment of the Runnel Stone Reef off the headland at Gwennap Head, is located off the southwest peninsula of the UK mainland. The reef also falls within the recommended MCZ of Land's End (Runnel Stone). The study area hosts a wide variety of migratory and resident marine megavertebrate populations, which include vulnerable species such as harbour porpoises, basking sharks, dolphins, ocean sunfish, and seabirds, which can be monitored during localised feeding events or on longer distance foraging movements and migrations between the Western Channel and the Celtic Sea. The effort-based visual observations provide valuable baseline data that have been analysed to evaluate and quantify fine-scale temporal and spatial distribution patterns of the target species (cetaceans and seabirds) in relation to an array of environmental parameters. These included local and regional scale meteorology (e.g. wind direction and wind speed), sea surface physics (e.g. sea state, current flow direction and flow velocity), tidal state and fine-scale seafloor topography.

The second study area was the expansive gently-sloping sandy bay of St Ives, off the north Cornish coast, southwest UK. It is an important mid-winter foraging area for a variety of seabirds, including auks (family Alcidae), gannets, and Balearic shearwaters, as well as host to several resident cetacean populations. It has a vibrant inshore fishing industry, but recent incidents involving incidental seabird bycatch in local fishers' gillnets invoked a byelaw-enforced time-space closure of some parts of the bay (see Appendix B: co-authored report for NE, RSPB and the Cornish Inshore Fisheries Conservation Agency). It is vital that fine-scale temporal and spatial distribution of seabird foraging events is better understood, to more usefully inform local management and mitigate future incidents that negatively impact on both seabird fatalities and the economic interests of local fishers. The effort-based visual survey data have been analysed to quantify and evaluate fine-scale temporal and spatial distribution patterns of foraging events and the relationships with a variety of environmental parameters (similar to those at Gwennap Head, as described above).

It is clear that dynamic nearshore frontal regions, such as the Runnel Stone Reef, or highly-utilised inshore areas, such as the shallow bay of St Ives, present a challenge for determining correct management practices, particularly as vulnerable marine species must co-exist alongside anthropogenic activities. Through the integration of precise theodolite mapping with site-specific high resolution bathymetry data, and a suite of temporal variables (that also includes, where relevant: acoustic data, acoustic Doppler current profiler (ADCP) flow data, and radar-derived tidal flow metrics), this novel project draws together a unique suite of fine-

scale qualitative and quantitative information to improve understanding of how fine-scale processes impact the distribution of wide-ranging species in two contrasting coastal environments, which can be used to more effectively inform management.

Site selection enabled a demonstration of the utility of the methodological toolbox for application at contrasting coastal sites with varying management issues and different focal species. Despite their physical differences (i.e. tidally-swept rocky reef off Gwennap Head vs. sheltered and shallow bay at St Ives), both sites were amenable to the same types of methods, i.e. shore-based surveys, so the same toolbox could be applied and its (adaptable) value demonstrated. However, for broader applicability, it is important that the multi-disciplinary techniques developed in this study are adequately described and tested, so the toolbox can be applied at other localised coastal environments, not only around the UK, but further afield. Using methods that are both cost-efficient and effective for monitoring the fine-scale habitat use of highly mobile marine species is particularly useful where there are strong policy drivers to do so, such as the increasing need for effective EIAs required for marine spatial planning purposes, and/or where the techniques would help answer similar scientific questions as those posed in this study.

1.6 Fine-Scale Physical Processes as Drivers of Animal Distribution

This section focuses on the fine-scale physical processes most relevant to nearshore coastal habitats in tidally-dominated environments, and their influence on the distribution of mobile marine species.

1.6.1 Bio-Physical Coupling and Fronts

Increased understanding of the ecological links with the physical environment will serve in the effective planning and management of MPAs in the future (Cañadas et al., 2005; Embling et al., 2010; Booth et al., 2013; Jones et al., 2014a). Improved understanding of the bio-physical processes linking predators to their prey helps in an ecosystem, best-practice approach to species and habitat conservation. Mechanistic links in the marine environment, such as frontal processes (described below), influence everything from primary productivity (Wolanski & Hamner, 1988; Sharples, 2007; Scott et al., 2010), trophic transfer (Hao et al., 2003; Genin, 2004; Bertrand et al., 2008), to fish (Maravelias, 1999; Embling et al., 2013) and other top predators (Booth et al., 2013; Scott et al., 2013; McClellan et al., 2014). Several studies have

focussed on the relationships between mobile species and oceanic fronts (Sims & Southall, 2002; Scales et al., 2014).

Highly-mobile marine species must forage effectively to increase prey encounter rates (Sims et al., 2006), so, relative to the heterogeneous landscape of the open ocean, frontal regions, for example, may be considered hotspots, offering improved foraging opportunities to a variety of free-ranging and highly mobile marine top predators, including seabirds, cetaceans and sharks (Decker & Hunt, 1996; Sveegaard et al., 2012a). In shelf seas, there are many types of frontal systems, which include: wind-driven upwelling fronts, tidally-generated fronts and topographically-formed fronts (described further below). They are regions of strong physico-chemical contrast, i.e. horizontal gradients of temperature (thermocline), salinity (halocline) and/or density (pycnocline), at the boundary between two separate bodies of water (Franks, 1992a), which result in stratification. Fronts can also form in shear zones that separate flows of different velocities (Farmer et al., 1995; Nash & Moum, 2001). The front is created as the pycnocline bends from the horizontal, either at the surface or below, which separates the lighter surface water from the dense deep water. Furthermore, since the width of the front refers to the horizontal extent of the density gradient, the frontal region will normally be wider than the front itself (Franks, 1992a) and may include sites of turbulent mixing (Gargett, 1988), which breaks down stratification.

Coastal winds can cause upwelling or downwelling fronts due to Ekman transport, which (in the Northern Hemisphere) moves the coastal water to the right of the wind direction. Depending on wind direction, water either rises from below to replace water moving away from the shore (coastal upwelling) or, when the water flows toward the shoreline, water stacks up along it and has nowhere to go but down (coastal downwelling). Areas of coastal upwelling tend to be characterised by high concentrations of nutrients, resulting in high biological activity and rich marine life (Trujillo & Thurman, 2008). In the absence of any circulation, many of the ocean's nutrients would be unavailable to surface feeding organisms.

Tidally-dominated environments are of particular interest since interaction between tidal flows and topography often results in spatially and temporally predictable aggregations of prey (Genin, 2004; Embling et al., 2013; Sharples et al., 2013a), which higher trophic species can exploit (Yen, 2004; Ingram et al., 2007; Embling et al., 2012; Jones et al., 2014a). Results that evidence this temporal and spatial predictability of marine species distribution will help in the face of increasingly-widespread marine spatial planning activities (Sveegaard et al., 2011b; Waggitt & Scott, 2014).

1.6.2 Tidal-Topographic Interaction

Tidal-mixing fronts at larger scales (10s to 100s km) separate tidally-mixed and seasonally-stratified shelf seas (Farmer et al., 1995), and are often sites of 'massive' dinoflagellate blooms in waters off the British Isles (Franks, 1992b). In frontal regions at smaller scales (<several km), debris and organisms accumulate in zones of convergence (Wolanski & Hamner, 1988; Franks, 1992a), where topography interacts with prevailing tidal flows causing secondary currents. These small-scale, 'tidal-topographic' fronts cause complex downstream currents (e.g. island wakes and eddies) to form in the lee of features such as headlands and reefs, with their associated topographic 'highs'. This latter spatial process occurs at relatively finer scales, compared to ocean or shelf fronts, and is the focus of this study.

Tidal-topographic fronts are likely to contribute to dynamic, small-scale physical processes operating in tidally-dominated environments at localised coastal locations where there is complex bathymetry, and may exert a first order control on the distribution of the target species, as regions of enhanced biological activity (Wolanski & Hamner, 1988; Franks, 1992b, 1992a; Farmer et al., 1995; Hao et al., 2003; Scott et al., 2010; Embling et al., 2013; Scott et al., 2013; Sharples et al., 2013a). Hunt et al. (1998) found strong tidal currents passing over a submerged reef in the Aleutians, a chain of volcanic islands in the North Pacific, caused upwelling on the upstream side of the reef, and zones of surface convergence on the downstream side. Three species of auklets (family Alcidae) partitioned foraging habitat along this gradient demonstrating that the strength of the tidal current was positively related to the number of birds present, and, when the tide reversed, so did the sides of the reef occupied by the auklet species.

Interestingly, tidal-topographic processes were recognised by the Northern Ireland Environment Agency (NIEA) in its 2012 report. NIEA officially designated two SACs within its jurisdiction (the Maiden Islands, and Skerries and Causeway) based on protecting physical habitat of European-importance, including sand banks, reefs and sea caves, as well as harbour porpoises. However, the EA also acknowledged the existence of locally-important oceanographic features within these habitats (NIEA, 2011) and expressly identified them due to their interaction with strong tidal currents (i.e. tidal-topographic interaction), which were noted to cause tide races and eddies. The NIEA recognised the specific importance of these fine-scale physical features on local biodiversity through enhanced foraging opportunities. As discussed, these processes can initiate a bottom-up cascade resulting in aggregations of prey

items and localised zones of enhanced productivity for higher trophic level species, i.e. foraging hotspots.

Summary

It is clear there are strong policy drivers to acquire robust and improved evidence linking marine species to their environment through small-scale physical interactions, which this project aims to do. Additionally, the contrasting locations of the study sites, combined with a variety of species of interest, means the methodological toolbox may be of applied interest. Both sites host a variety of protected species that urgently require increased knowledge of the factors driving their distribution, particularly at very fine-scales. Contributing to knowledge on fine-scale habitat use in coastal waters by applying a tried-and-tested methodological toolbox may be used to more appropriately inform conservation, fisheries and marine spatial planning management in the future, at other constrained locations that are amenable to land-based studies (and where appropriately-resolved environmental covariate data exist).

Chapter 2 Methods and Environment

Detailed field site descriptions are provided at the end of this chapter (Section 2.4), after the sections on survey methods, data quality and environmental data collection, which are relevant to both.

2.1 Survey Methods

2.1.1 Theodolite Setup Procedure

A land-based observation team of at least two observers with 10x binoculars and 30x telescopes searched for target species at sea (Figure 2.1). When species were detected, one observer operated the theodolite (Leica FlexLine TS02 Total Station), equipped with a 30x monocular eyepiece, to measure and record horizontal ("Hz") and vertical ("V") angles from the watch point to the waterline at the centre of the animal, or group of animals (detailed further in survey methodology sections of relevant chapters), to a precision of 0.0018° of arc.

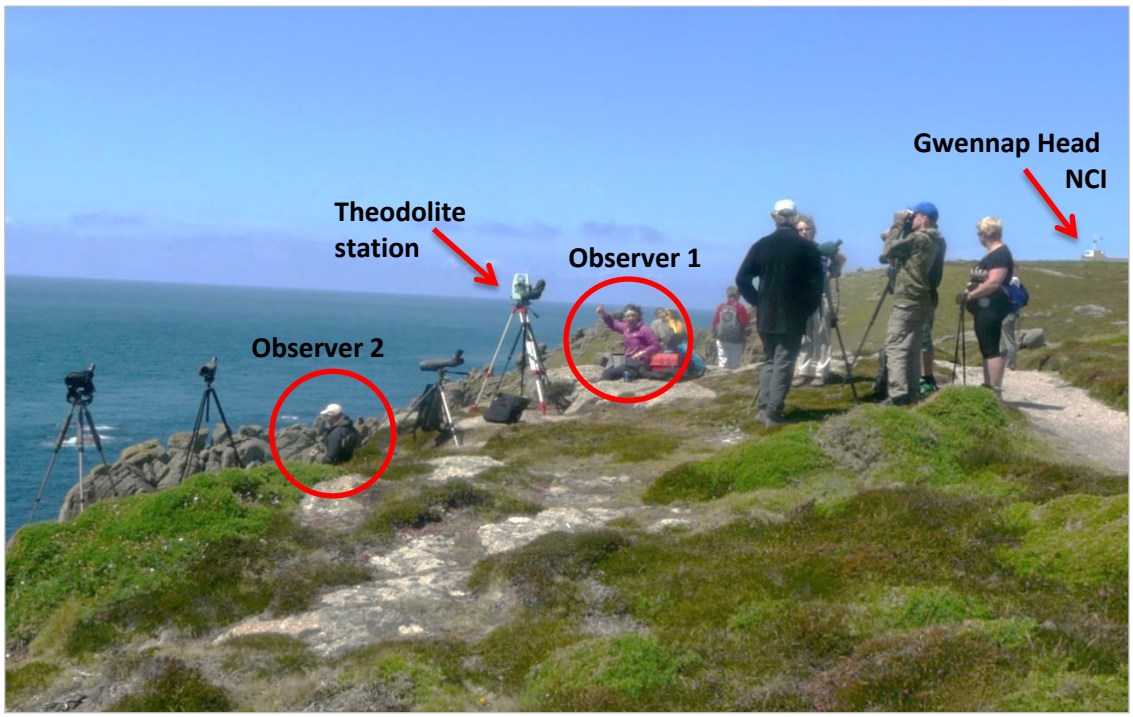

Figure 2.1. Typical survey day in the field (at Gwennap Head) with team of observers.
A minimum of two dedicated observers were each equipped with binoculars and telescope. The theodolite was set up each day over a measured point, and a geographical reference point at a sufficient distance was used to calibrate/zero the horizontal angle at regular intervals during surveys. (Photograph © A Colenutt 2012).

Using the theodolite's laser plummet, its tripod was set up each day directly over a precisely-surveyed point, measured at the beginning of the study using a Trible differential GPS. The theodolite was levelled using the tribrach's three thumbscrews, fine-tuned using its internal precision mechanism, and checked at frequent intervals throughout the day to maintain accuracy. Vertical angles were measured with respect to the zenith to serve as the y-axis of a Cartesian (x,y) coordinate system. Horizontal angles were zeroed and measured counter-clockwise along an imaginary line connecting the instrument to a pre-established geographical reference point at each study site, serving as the x-axis. These were zeroed at regular intervals throughout survey days to ensure correct calibration. At Gwennap, the NCI (National Coastwatch Institution) station's flagpole was used (shown in Figure 2.1); at St Ives, the obelisk of Knill's Monument in Carbis Bay was selected. Both reference points were precisely measured in the field using a differential GPS.

Only given the theodolite height above sea level could recorded V and Hz angles be used to accurately calculate target locations at the sea surface (in Eastings and Northings). Therefore, measurements of tidal changes in the instrument's height above sea level were also recorded (protocol outlined below), so necessary tidal height corrections could be carried out during data processing (see Section 2.1.2) and applied to each recorded, target feature observation (see also Wursig et al., 1991).

To acquire the necessary tidal data on theodolite height above sea level, the following steps were followed: 1) On the first day of survey, select a near-as-vertical-face-as-possible where the theodolite operator has a clear line of sight to the changing waterline level. (At Gwennap, a sheer rocky face in the immediate bay to the right below the watch point was selected; at St Ives, the concrete wall of the pier's steps to the right of the watch point, just beyond the car park was used). 2) Using the most vertical area of the vertical feature, establish an imaginary vertical line and hold the manufacturer's reflective prism anywhere above the waterline. 3) Fire the theodolite's electronic distance measurement (EDM) laser at the prism and record the horizontal distance in metres. 4) At frequent intervals during surveys (the more often, the more precise the tide-corrected coordinates), use the theodolite to record V angles of the rising and falling waterline, directly-below where the prism had been held, i.e. along the same imaginary vertical plane.

For this study, tidal measurements recorded every 30 minutes were deemed sufficient intervals, not only for practical purposes, but any increased accuracy using finer time intervals would be offset given the error in practical terms of recording V angle measurements of a

choppy waterline (see Section 2.2.1 for details on accuracy; also Bailey & Lusseau, 2004). It should be noted the horizontal distance to the prism can be measured at any time during the survey, not necessarily at the start, as it is only required during data processing. (However, it is important that the same vertical plane is always used to measure the waterline's V angles, below where the prism was held).

2.1.2 Theodolite Data Processing

Data from the theodolite was uploaded onto a computer using the manufacturer's software, FlexOffice, version 2.0 (Leica Geosystems). It was then downloaded from the programme and saved as a spread sheet via an ASCII format file (.frt) that had been expressly written to extract the desired information, namely, "Point ID" (the theodolite recording number), date, time, and the V and Hz angles. Each observation recorded in the field (see survey methodology sections in the relevant chapters) was noted down with its corresponding theodolite Point ID. Using a series of trigonometric formulas in Excel, by taking into account the curvature of the Earth, the varying height of the instrument due to tide (see calculations below), and the GPS locations of both the survey site and the reference point on which the Hz angle was zeroed, the angles were converted into Eastings and Northings, so each observation could be assigned a set of precise and accurate coordinates (see Section 2.2.2 on Field Calibration). These data were saved as .csv files, a format compatible for loading into ArcGIS® ("GIS") v.10 (ESRI, 2012).

To calculate the changing height of the instrument relative to sea level every 30 minutes of survey, necessary for the trigonometric functions to convert the Hz and V angles into accurate Eastings and Northings, the waterline V angle data were used, which had been collected in the field (according to the protocol described in Section 2.1.1). Resultant tide-corrected height values were applied to all observation data within the relevant 30-minute survey unit. The following calculation was used:

$$Ht = \tan(V\ waterline - 90) \times horizontal\ distance\ to\ prism$$

where, Ht is tide-corrected height of the instrument above sea level, $V\ waterline$ is the V angle recording of the waterline, measured every 30 minutes, and $horizontal\ distance\ to\ prism$ is the laser-measured horizontal distance (m) to the vertical plane above the waterline from where tidal measurements were taken.

2.1.3 Conventional Visual Monitoring

Along with theodolite monitoring, visual estimates of an animal's location (compass bearing from the watch point and a visual estimate of distance to the sighting) were sometimes noted. (Section 2.2.3 presents results from data collected of an animal's location using these different visual survey methodologies).

An effort-based monitoring programme, SeaWatch South West (SWSW; SeaWatch SW, 2014), was also based at a nearby watch point on Gwennap Head. Experienced observers collected visual sightings data over consecutive days between June and September, across years 2007-12. The survey used conventional visual monitoring techniques, as described above, and all 'effort' was standardised (Jones, 2012). Theodolite data from this project were used to calibrate locations of the SWSW's visually-estimated sightings (Jones, 2012, p. 29). Additionally, results from the double-observer trials (Section 3.2.2) carried out in this project were used to calculate a detection function for porpoises at the Runnel Stone Reef. This detection function was retrospectively applied to the SWSW porpoise dataset, and subsequently published in the co-authored Jones et al. (2014a) paper, which presents and analyses the SWSW visual sightings porpoise data in detail (Appendix A). Subsets of data from the SWSW surveys have also been re-analysed in this project to visually compare porpoise (Chapter 3) and foraging seabird (Chapter 5) habitat through time, and when collected using different methods.

2.2 Theodolite Data Quality

2.2.1 Accuracy

Accuracy of the theodolite method was estimated by introducing ±1-m error in the height calculations at various distances from the St Ives (Figure 2.2-A) and Gwennap Head (Figure 2.2-B) watch points; for example, if tidal height measurements were inaccurate (see Section 2.1.1). The '0' height error was taken as the average measured heights of the relevant observation stations (~24 m at St Ives; ~47 m at Gwennap Head).

Using trigonometry to calculate coordinates from theodolite angles means error is magnified with increasing range from the observation station, as reported in other studies (e.g. Bailey & Lusseau, 2004; Hastie et al., 2004). Error is also greater at lower altitudes. This means any error in tidal height measurements will have more effect at St Ives, where not only is the survey

extent delimited at a greater distance from the watch point, than at Gwennap Head (6 km, rather than 3 km), the watch point is also lower. (Delimiting the survey areas is discussed in the relevant chapters).

Although possible errors are larger at St Ives (given a ±1-m error in height above sea level), the accuracy was considered acceptable, as the target species were foraging seabird aggregations often highly (>200 m) dispersed, and therefore covered areas of at least a substantial part of that error, even at 6 km where it is ±260 m (Figure 2.2-A). At 0.5 km from the watch point, the error is 17 m, which increases to 60 m at 2 km. At Gwennap Head, the maximum error at the furthest extent of the survey region (at 3 km) is 60 m (Figure 2.2-B). At 0.6 km from the watch point the error is 12 m, which increases to 40 m at 2 km.

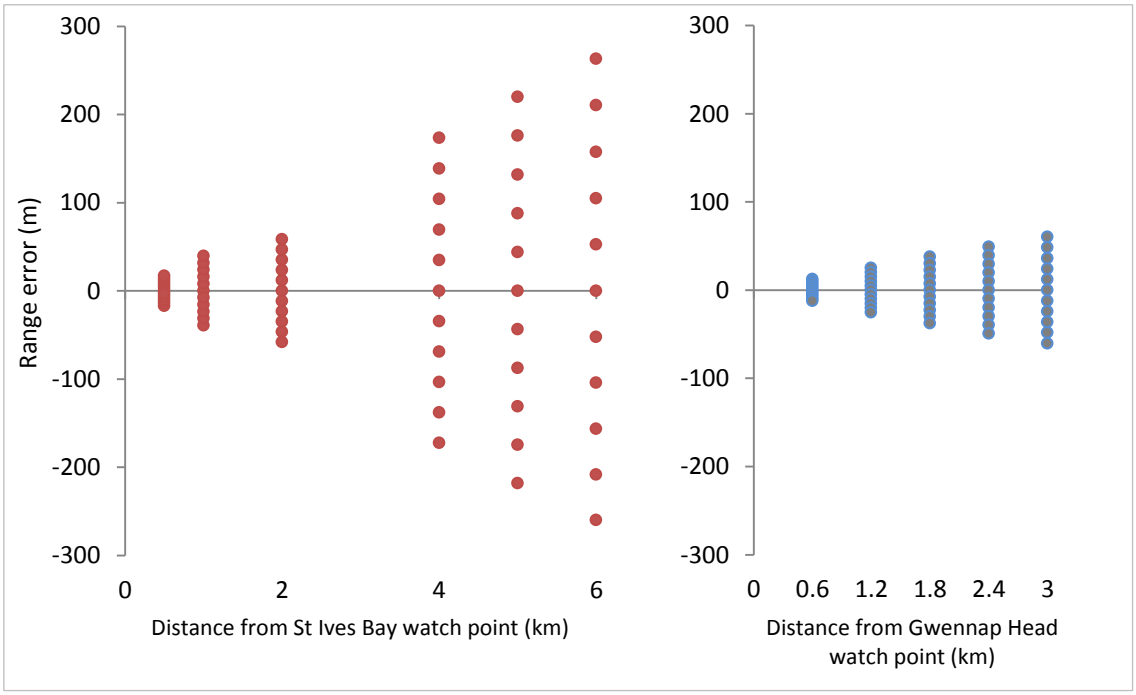

Figure 2.2. Accuracy of theodolite method with distance from observer, given ±1 m introduced error. Increasing error with range from the watch points at A): St Ives Bay, and B): Gwennap Head, given an introduced height error of ±1 m.

Additionally, statistical analyses were carried out on spatial sightings data that were gridded at 500 m at St Ives and 600 m at Gwennap Head (discussed further in the relevant chapters). This method accounted for the maximum errors when determining statistical significance of spatial drivers of distribution.

2.2.2 Field Calibration

The theodolite method was calibrated at various intervals during fieldwork using objects of known position in the survey areas (see also Sagnol et al., 2014). The shallowest topographic features (e.g. pinnacles) at Gwennap Head (Figure 2.3) and St Ives (Figure 2.4), indicated by dark orange areas in the bathymetry (see Section 2.3.1), were often exposed during certain times of low water. They were 'fixed' by the theodolite and then mapped in GIS; other permanent features, such as cardinal marks and headlands, were also mapped. (It should be noted the same observer operated the theodolite during all field sessions, and therefore responsible for all theodolite data used in this study).

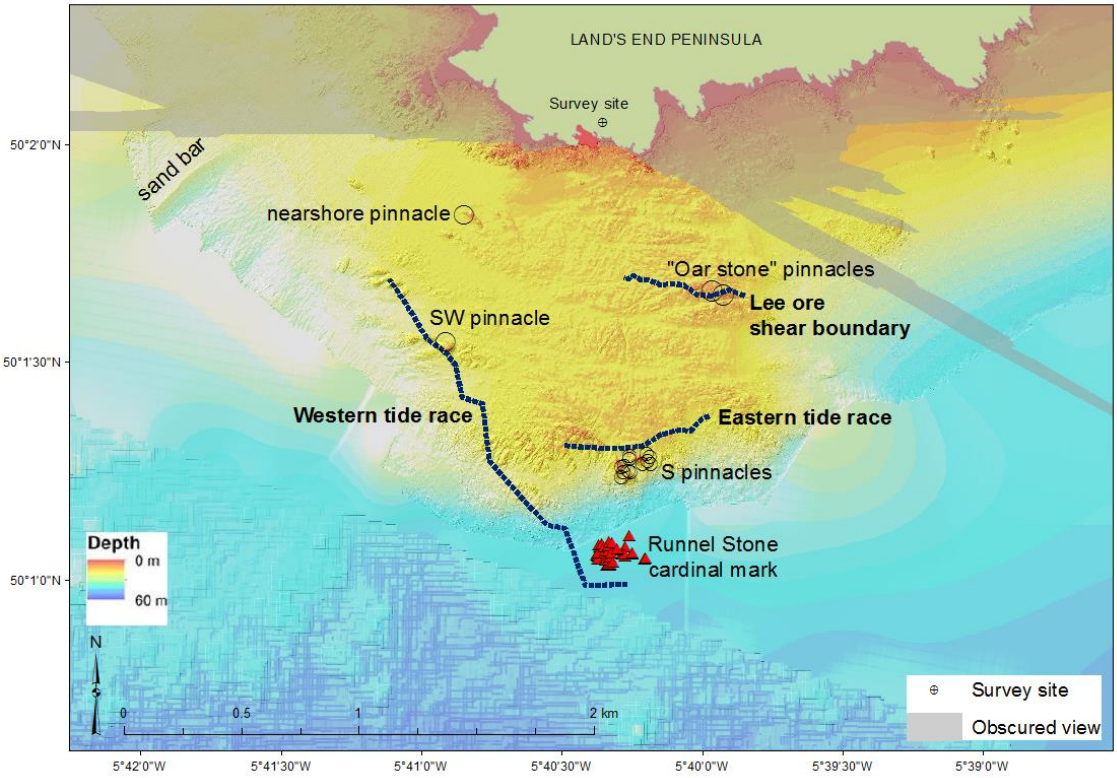

Figure 2.3. Surface expressions of underlying bathymetry visible from Gwennap Head watch point. Visible expressions of static bathymetric features at the sea surface fixed by the theodolite demonstrates a methodological accuracy of ±20 m within a km of the watch point, and ±200 m at the furthest extent of the survey area, where the Runnel Stone cardinal mark was tracked over a complete tidal cycle. High resolution (1 m) bathymetry data (courtesy of CCO/MCA © Crown copyright). Increasing depth represented by colours red to blue. Obscured areas of the sea surface due to land topography are shaded out, as precisely traced in the field using the theodolite.

At Gwennap Head, visible surface expressions of the underlying bathymetry, including turbulent 'boils' at the sea surface i.e. lee eddies (Largier, 1992; Nash & Moum, 2001), located

over confined regions of topographic highs (e.g. oar stone and SW pinnacles) were fixed (Figure 2.3). 'Tide races' were also traced in the field by the theodolite at both study sites, as evidenced by highly-visible spatially-constrained areas of turbulent water. By plotting theodolite-recorded surface expressions of static bathymetric features over the fine-scale bathymetry layers in GIS, accuracy of the theodolite method could be visually assessed.

At Gwennap Head, the pinnacles were fixed with a maximum error of ±20 m (Figure 2.3). However, near-exact locations were fixed in some areas demonstrating accuracy and reliability of the theodolite (and tidal-correction) methods used in this project. Some of the error, primarily around features that were not actually exposed (i.e. represented by surface expressions only), particularly at St Ives (Figure 2.4), was due to the fact fixes of where the water was breaking were variable, and depended on factors such as tidal flow direction and sea conditions.

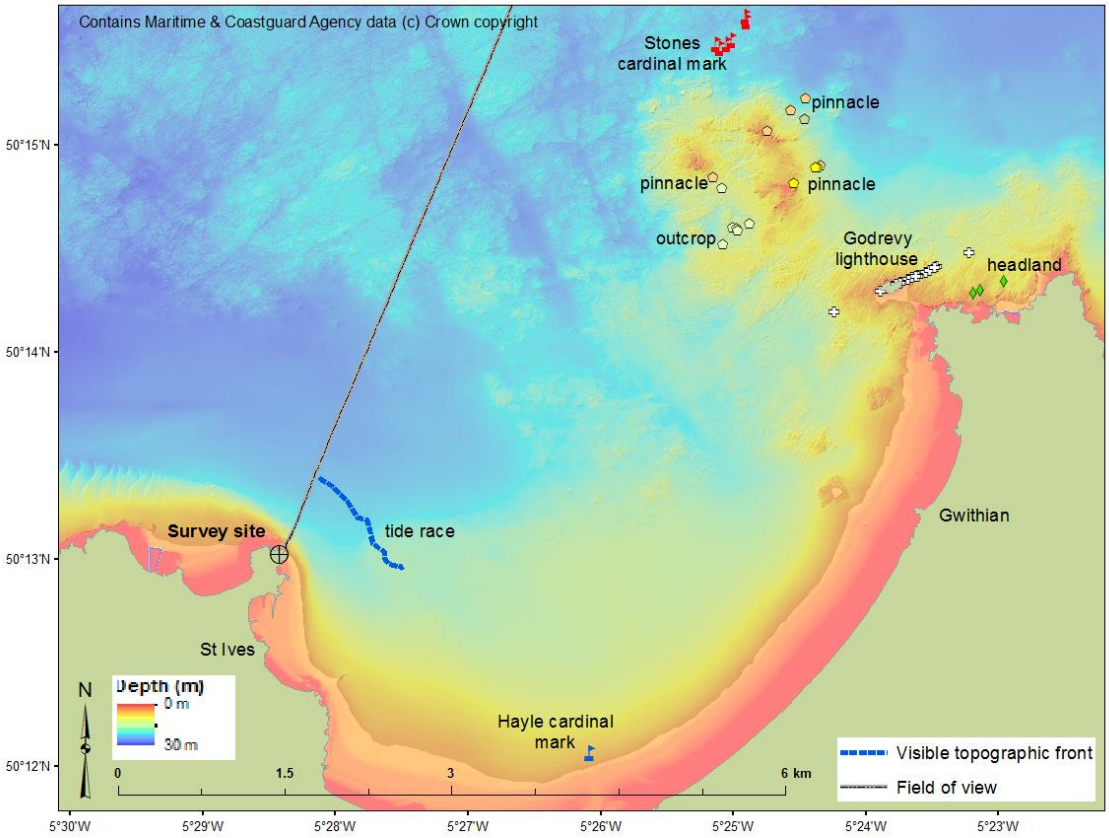

Figure 2.4. Surface expressions of underlying bathymetry visible from the St Ives Bay watch point. Visible expressions of static bathymetric features at the sea surface fixed by the theodolite demonstrates a methodological accuracy of ±30 m within 3 km of the watch point, and ±250 m at the furthest extent of the survey area, where the Stones cardinal mark was tracked over a complete tidal cycle. High resolution (1 m) bathymetry data (courtesy of CCO/MCA © Crown copyright). Increasing depth represented by colours red to blue.

The fixes of cardinal marks at both locations helped calibrate the theodolite method and also investigate their range of movement over a complete tidal cycle, as they are often used as visual cues during conventional visual monitoring surveys (e.g. SWSW), so this information was important for quality control purposes, as some visually-estimated sightings data were used in this study. Their positions varied by ±200 m, but these maximum errors occurred at the furthest extents of both survey regions, where the methodological error is greatest (see Section 2.2.1). The locational errors justify the grid cell sizes selected to account for this during relative-density analyses at the two study sites (discussed in the relevant chapters).

2.2.3 Theodolite vs. Conventional Visual Monitoring

To demonstrate the value of the theodolite method in comparison to conventional visual monitoring (see Section 2.1.3), two observers surveyed from the same location and recorded sightings of the same harbour porpoises *Phocoena phocoena*.

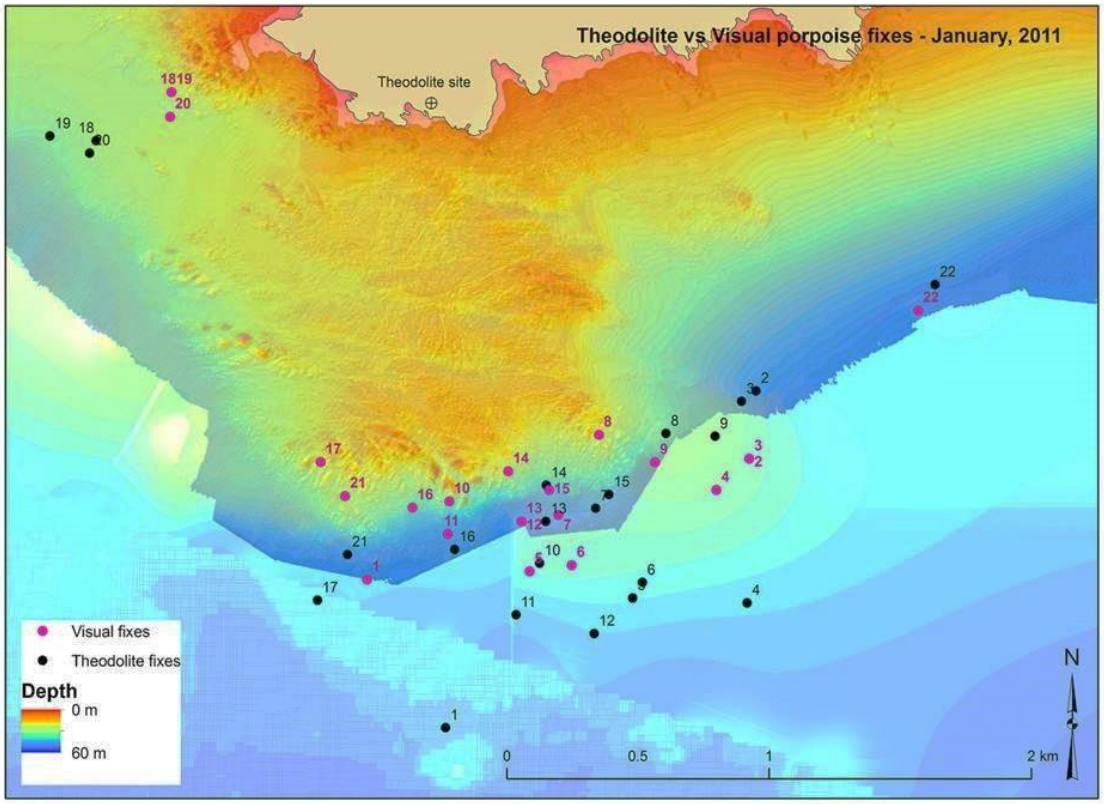

Figure 2.5. Harbour porpoise locations mapped using a theodolite vs. conventional visual monitoring. Sightings (n = 22) were recorded simultaneously by the theodolite observer and an additional observer using a compass and visually-estimated distances to the animal. High resolution (1 m) bathymetry data (courtesy of CCO/MCA © Crown copyright). Increasing depth represented by colours red to blue.

One observer fixed and recorded an animal's position on the theodolite, while the other noted its visually-estimated location. Comparative observations are plotted in Figure 2.5.

The average bearing error of the visual estimates compared to the theodolite fixes is ±12.9°, and the average error in the distance between the visual estimate of the sighting and the 'true' location (as measured by the theodolite) is an under-estimation of 316 m. On average, it appears the theodolite method is approximately five times more accurate than visually-estimated data.

2.3 Environmental Data Collection

Data were collected for the two study sites in southwest UK, the Runnel Stone Reef off Gwennap Head, and St Ives Bay (see Section 2.4 for detailed field site descriptions).

2.3.1 Bathymetry Data

The nearshore (<2 km offshore) data at Gwennap Head ('Lizard Point to Land's End') and St Ives ('Hartland Point to Land's End') were collected by the Plymouth Coastal Observatory (Figure 2.6).

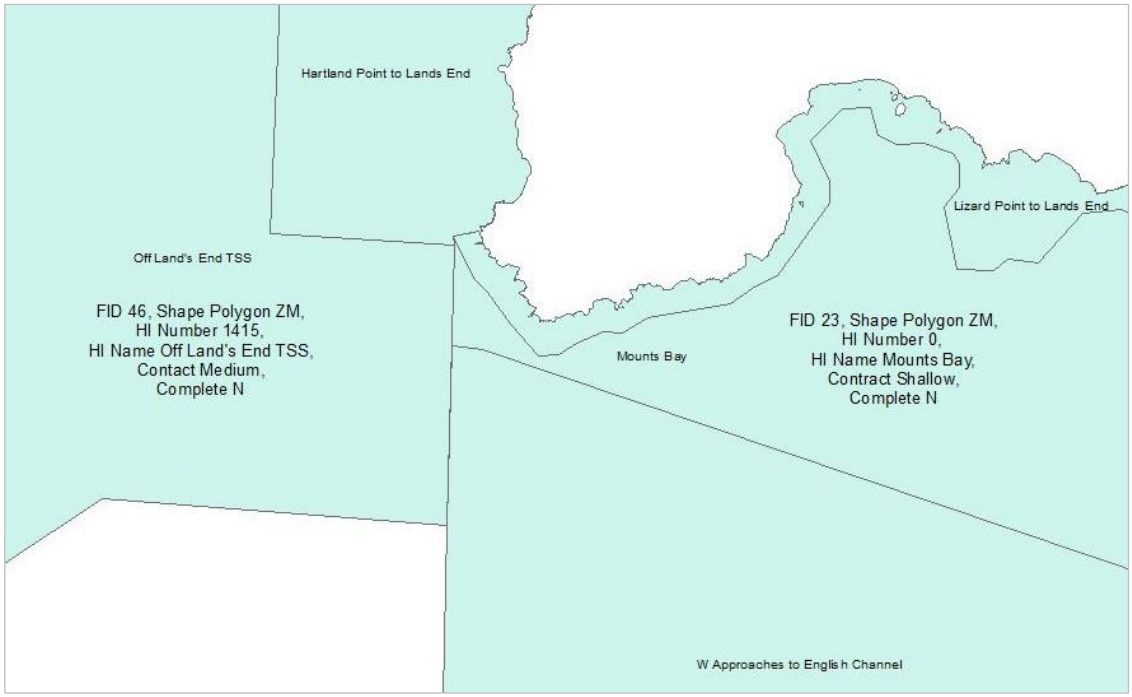

Figure 2.6. MCA/CHP bathymetry survey regions © Crown Copyright (as of 04/11/2013).

Surveys were conducted according to the International Hydrography Organisation standard (IHO Order 1a) using a single-beam echosounder coupled with a differential GPS allowing for positional accuracy of <1-m. Data were collected as part of the Southwest Strategic Regional Coastal Monitoring Programme and provided courtesy of the Channel Coastal Observatory (CCO, 2011) through their online data catalogue.

The offshore bathymetry data at Gwennap Head ('W Approaches to English Channel') were collected at 12-m resolution using a multi-beam echo-sounder, as part of the Maritime and Coastguard Agency Civil Hydrography Programme (MCA CHP © Crown copyright), and released under Open Government License. Missing areas within the survey area (not-yet-complete 'Mounts Bay') either side of the spatial join were then interpolated using the weighted average function in ArcGIS, to provide the most realistic fit between the fine-scale nearshore data and the coarser resolution, offshore data.

The MCA CHP base bathymetry layer at St Ives Bay was spatially joined in GIS to LiDAR-derived data, previously collected by the CCO to survey the site's intertidal regions. The LiDAR data were initially imported into GIS as an ERDAS IMAGINE file, as the raster's altitude values needed converting from vertical ordnance datum (relative to mean sea level) into chart datum (relative to LAT) for compatibility with the sonar-derived bathymetry data layers.

The combined bathymetry layers at both Gwennap Head and St Ives are used as the base layers for all species distribution maps in the analyses, as well as to create rasters of the bathymetry-derived static variables, benthic slope (degrees, i.e. inclination of slope) and aspect (degrees from North, i.e. compass direction), using the relevant Spatial Analyst tools in GIS (ArcToolbox > Spatial Analyst Tools > Surface > Aspect/Slope). Aspect identified the downslope direction of the maximum rate of change in value from each cell within the bathymetry raster relative to its neighbours, i.e. slope direction. Slope identified the gradient, or rate of maximum change, from each cell within the bathymetry raster.

2.3.2 Environmental Data

Data on survey conditions and other environmental variables, e.g. sea state and Beaufort (BFT) wind force, wind direction (bearing), visibility (km), cloud cover (oktas) and glare (0-5), as given in Appendix C, were collected in the field at both study sites every 30-minutes of survey effort, and recorded on standardised recording forms (Appendix D).

Wind data

Runnel Stone Reef: time series wind data were obtained courtesy of John Chappell's Instromet weather station (http://www.landsendweather.info/) lying 2 km ESE of Land's End at Trebehor. The anemometer is mast-mounted 7.6 m above ground and records hourly measurements of wind speed (mph) and wind direction (bearing), which were interpolated to match the 30-minute interval survey effort times. Wind speeds were converted to km h^{-1}.

St Ives: wind metrics from the *Seven Stones Lightship* offshore of Land's End, lying at 50.103° N and 6.100° W, were obtained courtesy of the UK Met Office. Hourly data on wind direction (bearing) and speed (knots) were interpolated to match the 30-minute interval survey effort times. Wind speeds were converted to km h^{-1}.

Wave data and sea surface temperature

Gwennap Head: relevant archives were downloaded via the CCO from the Penzance *Datawell BV Directional Waverider Buoy* (Mk III), lying 18 km east of Gwennap Head at 50.113° N, 05.504° W. Recorded 30-minute averages of significant wave height (Hs, in m) and sea surface temperature (SST, in °C) were matched to survey effort times.

Acoustic analyses at Gwennap Head: relevant archives were downloaded from the Penzance *Waverider* buoy. Recorded 30-minute measurements of Hs (m) were averaged and matched to survey effort hours.

St Ives: relevant archives were downloaded via the CCO from the Perranporth *Datawell BV Directional Waverider Buoy* (Mk III), lying 40 km east of St Ives at 50.353° N, 05.174° W. Recorded 30-minute averages of Hs (m), SST (°C) and wave direction (bearing) were matched to survey effort times.

Tidal data

Using the offshore tidal computation software, POLPRED v.2.4.1(POLPRED, 2013), predictions were made of tidal elevations and currents. The UK continental shelf model, CS20, was used to extract metrics for both sites. It is a true, 3D model that gives higher resolution in the vertical dimension (sigmas). Three sigma levels, which are specified fractions of the water column, independent of absolute depth, were selected and compared: Sigma 1 (sea bed), Sigma 16 (mid-water column depth) and Sigma 31 (surface waters). See Appendix E for graphic comparisons of the spatial predictions using the different sigma levels at Gwennap Head.

Patterns did not vary between the sigma data, so Sigma 16 (describing the mid-water layer) was selected for subsequent use in temporal analyses at both study sites, as it was considered the most relevant layer likely to influence prey distribution of the target species, opposed to the surface or bottom waters only. Additionally, two modes of prediction were used: 'single location' (generating time series information), and 'spatial' (enabling prediction over a specified area at a single point in time), used only for data exploration purposes at Gwennap Head (to compare with ADCP data and radar imagery, as described in the following sections).

A subset of the predicted tidal data for St Ives Bay were compared to accurate, measured tide tables for the area (not available for Gwennap Head), and found to be in close agreement, which justified reliable use of the predicted data.

Gwennap Head: predicted metrics used, and averaged for the burst, were tidal flow speed (m-s^{-1}), flow direction (bearing), tide height relative to LAT (m), tidal range (m), and times of high and low waters.

Acoustic analyses at Gwennap Head: predicted metrics used, and averaged for the burst, were tidal flow speed (m-s^{-1}), flow direction (bearing), tide height relative to LAT (m), tidal range (m), and times of high and low waters.

St Ives: predicted metrics used, and averaged for the burst, were tidal range (m), and times of high and low waters.

Tidal hour

For all analyses, a continuous metric, "tidal hour", was calculated for each unit of survey effort using the predicted HW times. This metric represented time in the tidal cycle (i.e. tidal state relative to the nearest HW) and ranged in values from approximately HW-6.3 to HW+6.3.

Flow Group

Gwennap Head: tidal flows in the area are not typical for a semi-diurnal coastal location in the Western Channel based on information from experienced local fishermen and the Gwennap Head NCI (schematics provided in Appendix F). Using the tidal hour metric, tidal flow groups were allocated to each unit of survey effort and provided in Table 2.1. The information was visually checked against hourly images of radar-derived current flow metrics (see Section 2.3.3), and found to be in close agreement.

Table 2.1. Local flow patterns within the Runnel Stone Reef survey area over a complete tidal cycle. Characteristics inferred from local-scale schematics provided by the Gwennap Head National Coastwatch Institute (Appendix F), originally drawn by local fishermen.

Tidal hour (relative to nearest HW, where HW = 0)	**Flow group**	**Flow description**
-6 (LW) to -5	1	Strong westward – full strength (full)
-5 to -4	2	Westward – gradually slowing (moderate)
-4 to -3	2	Westward – gradually slowing (moderate)
-3 to -2	2	Westward – gradually slowing (moderate)
-2 to -1	3	slackening – starting to turn W to E
-1 to 0	4	Eastward – slowly increasing (moderate)
0 to +1	4	Eastward – full strength (full)
+1 to +2	4	Eastward – full strength (full)
+2 to +3	3	slackening – tide quickly turns E to W
+3 to +4	1	Strong westward – full strength (full)
+4 to +5	1	Strong westward – full strength (full)
+5 to +6 (LW)	1	Strong westward – full strength (full)

Time of day

Gwennap Head: time of day (GMT) was re-calculated as a continuous metric, "DayHr", which is a ratio between sunrise and sunset, to compensate for the varying lengths of day during the survey period.

Acoustic analyses: time of day (GMT) remained unchanged, as data were collected continuously each 24-hour period over three consecutive summer months each year.

St Ives: time of day (GMT) was given as hours post-sunrise. This metric was deemed more practical than 'DayHr' within the context of fisheries' management and informing policy, as surveys only took place over two consecutive winter months.

2.3.3 Radar Installation

Remote bathymetric mapping has developed to provide methods of digitally-recorded images of the sea surface (Figure 2.7) with high spatial (7.5-m) and temporal (2-s) resolution (Bell, 2008; Hessner & Bell, 2009). Bathymetric inversion techniques based on wave property analysis (Bell & Osler, 2011) can be applied to mapped wavelengths from radar image sequences to produce inferred bathymetric maps of the scanned areas, up to 4 km (Bell, 2011).

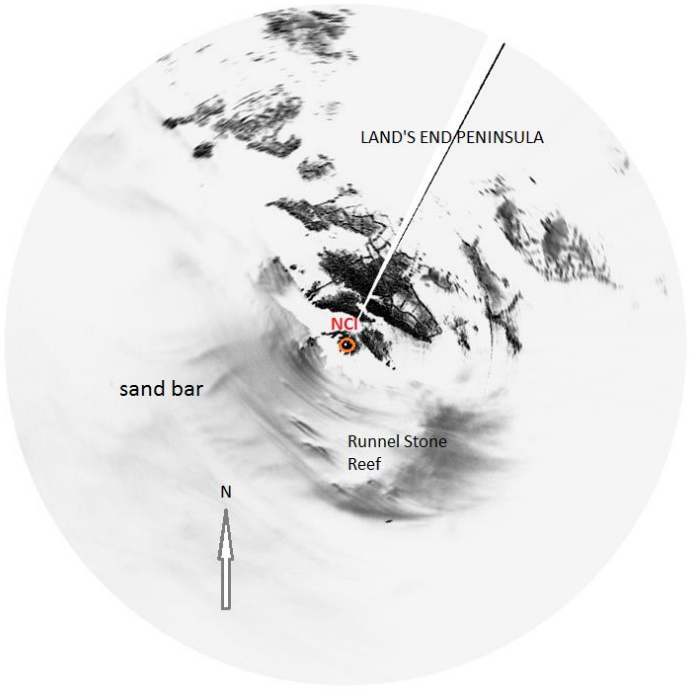

Figure 2.7. Snapshot of a radar video scan collected at the Gwennap Head watch point.
An X-band marine radar station was installed at the Gwennap Head NCI (denoted by red circle) to record 10-minute video scans each hour. Dark areas indicate field boundaries on the land; Runnel Stone Reef shown as whiter area south of the land; linear 'shadows' to the east of topographic highs indicate eastward tidal flows during this recording; sand waves clearly visible on the sea floor to the north-west of the western reef margin (Figure 2.3 shows same features visible in the measured bathymetry data). (Image courtesy of P Bell).

Other hydrodynamic data can also be extracted, including mean current direction and velocities (Hessner & Bell, 2009). In collaboration with Dr Paul Bell at the NOC Liverpool, a shore-based X-band marine radar station was installed at the Gwennap Head NCI, approximately 500 m north-west of the watch point and collected data from mid-August until mid-October, 2011. The radar station recorded 10-minute video scans each hour (Figure 2.7), and covered an area extending to 3.8 km. These hourly recordings were designed to coincide with the 10-minute intensive searches that were carried out every 30-minutes as part of the theodolite survey methodology. The radar was set up in a GPS coordinate system, so return data could be linked to geographic coordinates, which enabled acquisition of a complimentary visual dataset of tidal flow dynamics (speed and vector) across the survey region at ~160 m resolution. Only a few days of data were retrieved due to technical problems with the recording system. However, two, hourly-series of radar scans over a complete tidal cycle were retrieved, and tidal flow plots calculated by P. Bell in Matlab using his most robust, quality-controlled algorithms (as of 22/02/2015). The radar-derived images of surface flow dynamics

were recorded during periods around spring (16/09/2011) and neap (05/10/2011) tides, and provided in Appendix E.

2.3.4 ADCP Survey

ADCP data were successfully acquired at the Runnel Stone Reef study site (Figure 2.8) for the PhD research project by A. Jones (2013), that was subsequently published (Jones et al., 2014a). The survey was designed to highlight any small-scale tidal-topographic flow features that may be relevant in the context of the species sightings data. The survey was conducted aboard the University of Southampton's research vessel *R.V. Callista* on 11th July 2011 using a hull-mounted RDI Workhorse Mariner ADCP. Data were recorded via a linked computer running WinRiver software, v.2. The ADCP was set at 600 kHz to give a depth range of approximately 50 m with 1-m vertical bins, and a ping rate of 2 Hz (2 cycles per second). ADCP software recorded the latitude and longitude of the boat position from the vessel's GPS system, whilst bottom tracking was used to determine speed and direction of travel.

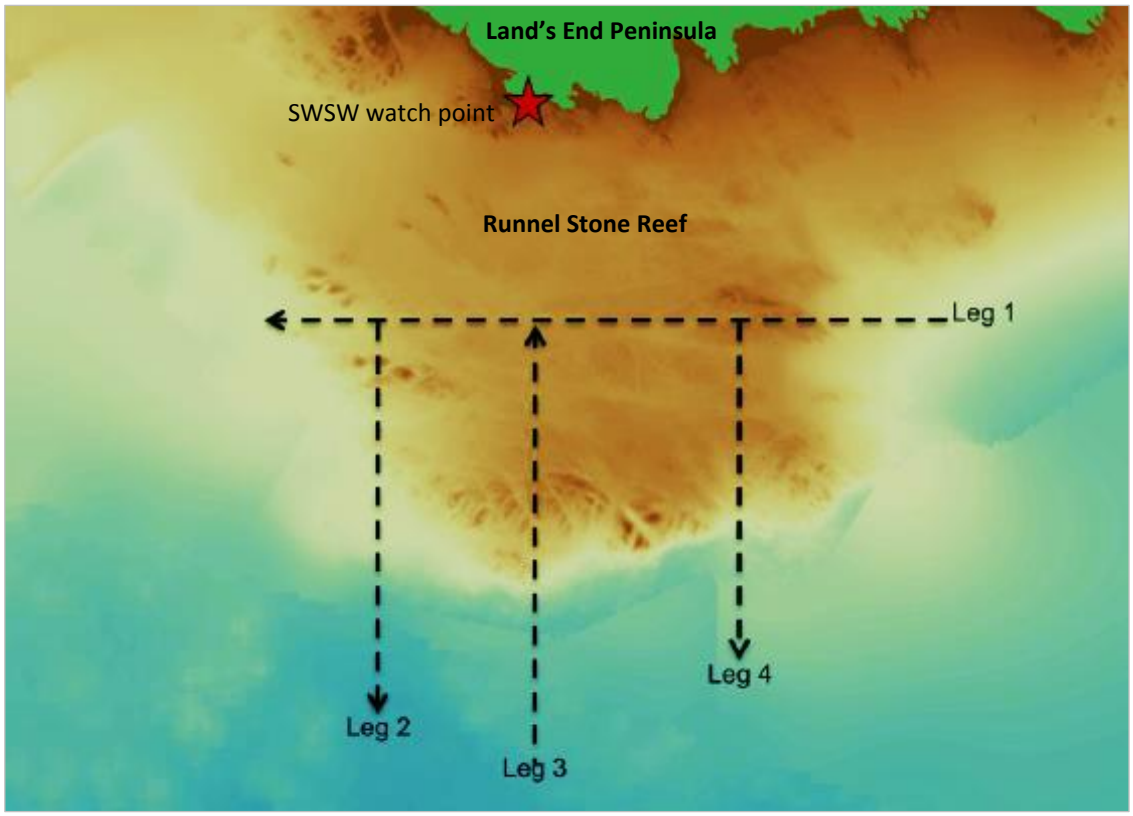

Figure 2.8. ADCP survey transect route at the Runnel Stone Reef study site.
The survey was split into discreet 'legs', labelled 1-4, and covered a complete 12.6-hour tidal cycle on 11th July, 2011. High resolution (1 m) bathymetry data (courtesy of CCO/MCA © Crown copyright). Increasing depth represented by colours dark brown to dark blue. Map adapted from Jones (2012) p. 73, showing the SeaWatch South West watch point used in their study during the ADCP survey.

The survey covered a complete 12.6-hour semi-diurnal tidal cycle, two days after a neap tide, and was split into four discreet transects, or 'legs' (Figure 2.8). The transect route was designed as a compromise between length and topographic coverage, so a minimum of nine repeats could be conducted over a complete tidal cycle (enabling current flow comparison between discreet legs), whilst maximising the possibility of identifying any zones of fine-scale topographic feature-flow interaction. The data were processed by Dr Phil Hosegood at Plymouth University, and used to more fully understand the complex interaction between small-scale topography and hydrodynamics through the water column in the survey area. It should be noted that, since interpolation between transects was not possible for this dataset, the oceanography can only be interpreted across the transect lines themselves, not between them. Detailed interpretation of the flow features and hydrodynamic environment can be found in Jones et al. (2014a); see Appendix A (pp. 38-45 of the paper).

2.4 Survey Sites

2.4.1 Runnel Stone Reef

The Runnel Stone Reef extends off the most south-westerly tip of the Land's End peninsula, Cornwall, UK (Figure 2.9). The reef is horseshoe-shaped of rocky substrate, with a plateau <20 m water depth, that extends 1.5 km to the south into deeper waters. It has steeper slopes at its eastern and southern margins, relative to its western edge, and is an area of topographic highs and lows. There are shallow pinnacles at the southern reef margin, the Runnel Stone, and other topographic features over the plateau that are exposed or, at least, expressed by areas of turbulent water at the sea surface during periods of sufficiently low water (see Section 2.2.2). Waters around the Runnel Stone Reef host an abundance of marine species that are observed on a daily basis (SeaWatch SW, 2014) and commonly include: several species of dolphin, harbour porpoises, basking sharks *Cetorhinus maximus* and seabirds (Pikesley et al., 2011; Hardy et al., 2012; Leeney et al., 2012). Waters off Land's End generally are a principal shipping route utilised by many sectors, e.g. transportation, tourist, recreational, small- and large-scale fishing, and the military.

The shore observation site was atop the rocky cliff between the headlands of Gwennap Head and Hella Point, 47 m above sea level at 50°02'08.80" N and 05°40'31.14" W (Figure 2.9). The entire survey area, defined as the area within which marine life could be observed, comprised approximately 80 km^2.

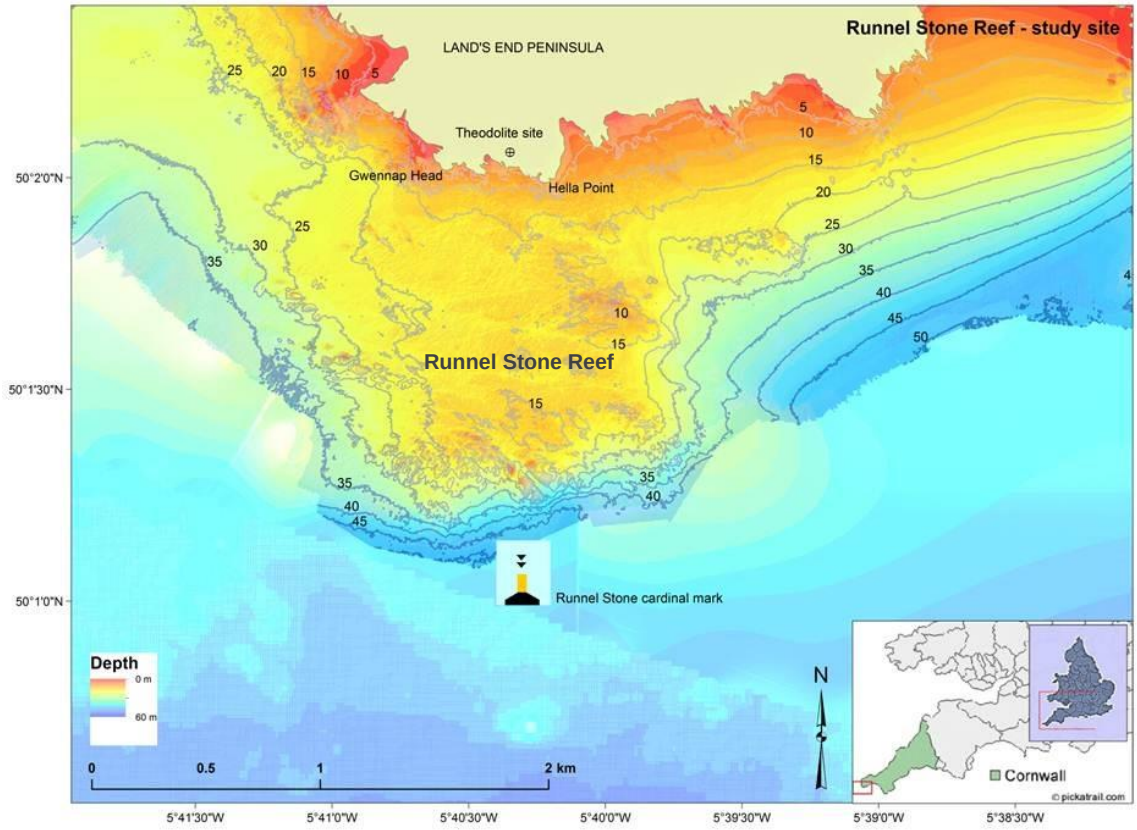

Figure 2.9. Runnel Stone Reef study site off the headland at Gwennap Head, southwest UK.
High resolution (1 m) bathymetry data (courtesy of CCO/MCA © Crown copyright) and 5 m depth contours. Increasing depth represented by colours red to purple; observation station located at survey site 'crosshairs'; Runnel Stone cardinal mark 1.6 km due south of the watch point.

The study site falls within the Land's End (Runnel Stone) recommended MCZ (Figure 2.10) and will be designated during Defra's second tranche in 2016. The protection of foraging areas of marine species is widely recognised as a key component of the MCZ process and was a supporting factor identified by the south-west's steering group, Finding Sanctuary, when recommending this area (JNCC, 2009).

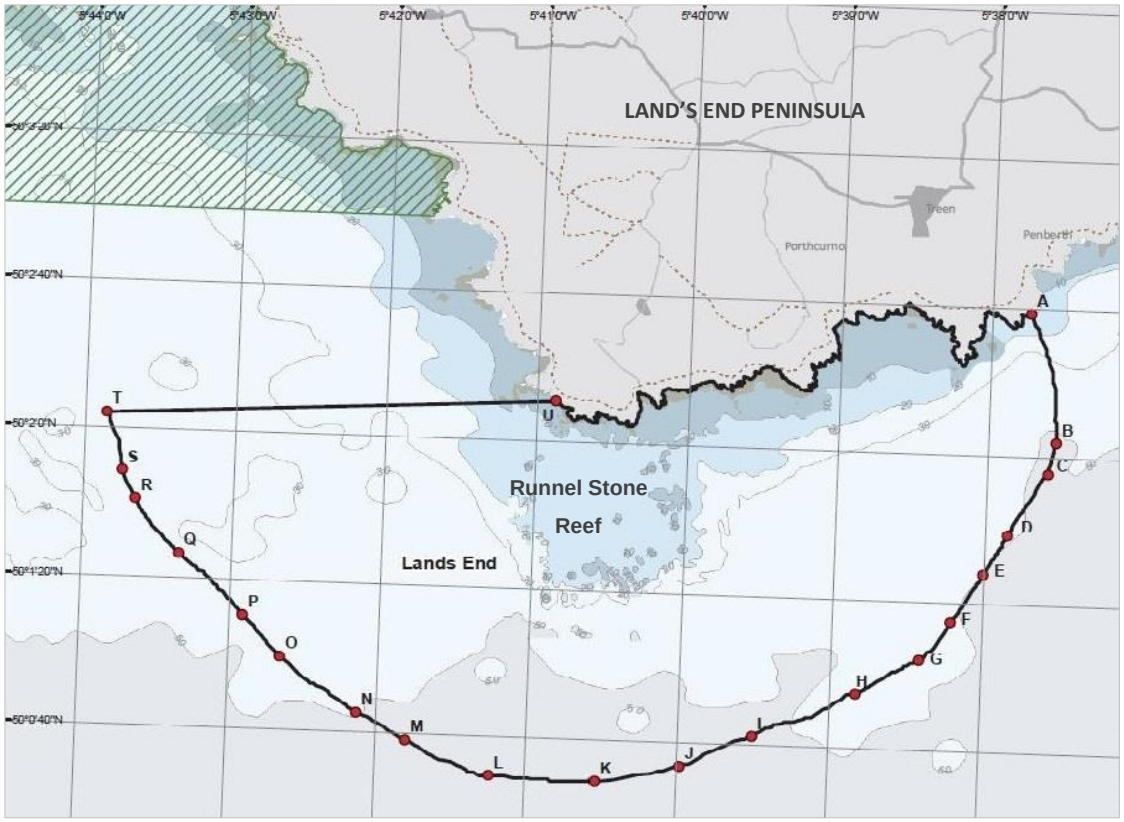

Figure 2.10. Land's End (Runnel Stone) recommended Marine Conservation Zone (rMCZ).
The Runnel Stone Reef study site falls within the rMCZ of Land's End (Runnel Stone) off the tip of southwest UK, and is depicted by the mid-blue and dark blue shading between points 'U' and 'K'. (Image © Finding Sanctuary 2011).

There was an unobstructed field of view in nearly all southerly directions up to and beyond 5 km (Figure 2.11), though visibility was dependent on weather conditions. The main point of reference within the survey area was the Runnel Stone cardinal mark, ~1.6 km from the watch point, anchored south of the Runnel Stone pinnacles at 50°1'8.22" N, 5°40'22.18" W.

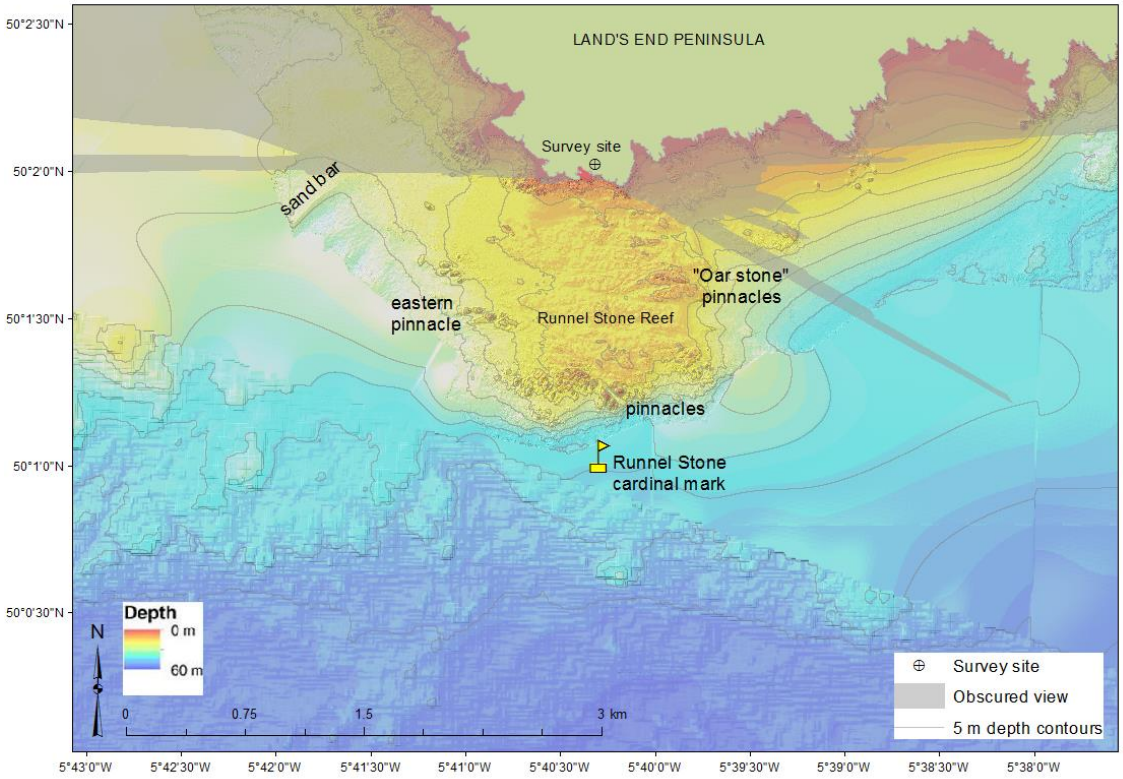

Figure 2.11. Field of View of the Runnel Stone Reef study area from the Gwennap Head watch point. Field of view from the watch point where sea watching can occur mapped onto high resolution (1 m) bathymetry data (courtesy of CCO/MCA © Crown copyright) with 5 m depth contours. Obscured areas due to land topography shaded out, as precisely traced in the field by the theodolite.

The survey area is a topographically-complex (Figure 2.9) high energy environment that includes a boundary between the shallow, fast-flowing water over the reef plateau and the deeper, slower water off the reef edge. This is further complicated by the topography and high tidal flow rates of the surrounding waters, since the peninsula lies between the Western Approaches to the English Channel and the Celtic Sea. The survey area is exposed to the full force of prevailing Atlantic winds. The tide is semi-diurnal (0.035), with two high waters (HW) per day, and a spring-neap cycle phase of 14.8-days (POLPRED, 2013). The mean neap tidal range is 2.42 m and spring tidal range is 4.72 m. In the mid-water column (Sigma 16), current speeds reach 0.21 m s^{-1} during neaps, and 1.64 m s^{-1} during springs; at the surface (Sigma 31), current speeds reach 0.14 m s^{-1} during neaps, and 1.73 m s^{-1} during springs (POLPRED, 2013).

High tidal flow and exposure to south-westerly swell, together with the topography, i.e. a protruding headland and a shallow (<20 m) rocky reef feature, means the area is subject to extreme tidal forcing. Water flows slower at the reef edge but, in the shallower water over the reef plateau, the tidal streams speed up. Counter-currents and eddies form visible surface

'boils' (Figure 2.12) downstream of topographic highs, or 'tidal intrusion fronts' (Largier, 1992). When tidal flows are sufficiently high, various tidal boundaries form at the interface of the two primary water masses, differentiated by their flow speeds, and are often evidenced by visibly turbulent water (Figure 2.13). These 'tide races' form near the reef edge during certain tidal flow directions, and are associated with areas of topographic highs (see Section 2.2.2).

Figure 2.12. Tidal intrusion fronts characterised by strong surface convergence.
Visibly turbulent water seen from the watch point where tidal flows interact with topographic features, often resulting in the accumulation of surface debris, foam, and surfactants along the plunge line (Largier, 1992).

The 'western tide race' was measured at HW+2.5, during eastward flows (see Table 2.1), i.e. water flowing into the Channel, against the western reef edge. Tide races in the eastern quadrant were measured at HW+6, during westward flows, i.e. water flowing out of the Channel against the eastern reef edge. The eastern tide races include the 'lee ore shear boundary' around the Oar Stone, which is a broad shallow pinnacle (<8 m water depth) and, the other, labelled 'eastern tide race', runs along the southern reef edge during westward flows past the shallow (<5 m) pinnacles of the Runnel Stone itself, near the cardinal mark.

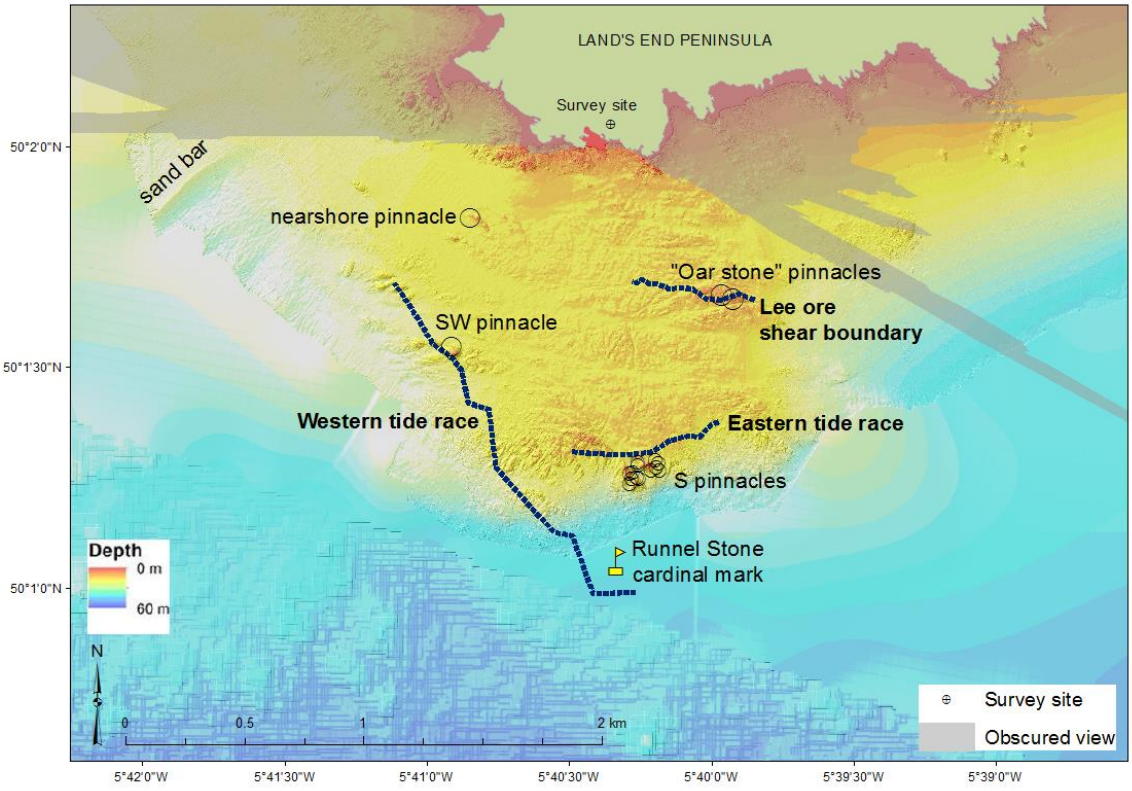

Figure 2.13. Fine-scale tidal-topographic features at the Runnel Stone Reef study site.
During periods of sufficiently high tidal flows, water masses of differing speeds interact with bathymetric features forming areas of visibly turbulent water at the sea surface, or tide 'races'. Fronts traced accurately in the field using the theodolite. Shallowest pinnacles mapped when exposed at sea surface during periods of sufficiently low water. High resolution (1 m) bathymetry data (courtesy of CCO/MCA © Crown copyright). Obscured areas due to land topography shaded out, as precisely traced in the field by the theodolite.

On a clear day, the reef edge itself is clearly demarcated by the contrast in water colour between the deeper areas beyond the reef, and the shallow areas of the reef plateau (Figure 2.14) due to marked differences in light absorption through the water column.

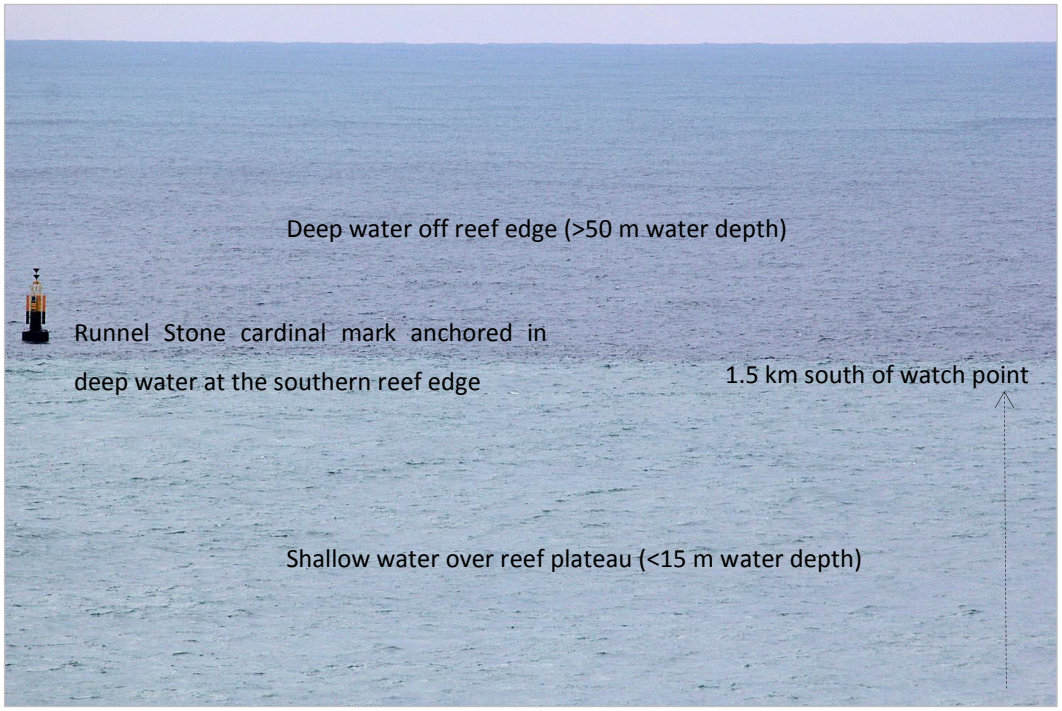

Figure 2.14. Reef edge clearly demarcated by colours of different water masses due to depth change. Waters over reef plateau appear brighter, as more daylight is reflected off the shallow, rocky substrate beneath whereas waters of relatively deeper depths appear darker, as more light is absorbed by the water column. Runnel Stone cardinal mark is anchored 1.6 km south of the watch point in approximately 50 m water depth, at the southern reef edge. (Photograph © A Colenutt 2012).

2.4.1.1 Environmental Data Results (Runnel Stone Reef)

The wind rose (Figure 2.15) calculated in WindRosePRO3, v.3.1.54 (Enviroware, 2013) shows prominent wind bearing and wind speeds encountered at the Gwennap Head watch point. Recorded wind measurements from the Land's End weather station (see Section 2.3.2) indicate ~60% of winds were north-westerlies (i.e. offshore), while ~40% blew from the south (i.e. onshore) directly at the watch point. Generally, the south-easterlies reached faster (>12 km hr^{-1}) speeds during surveys.

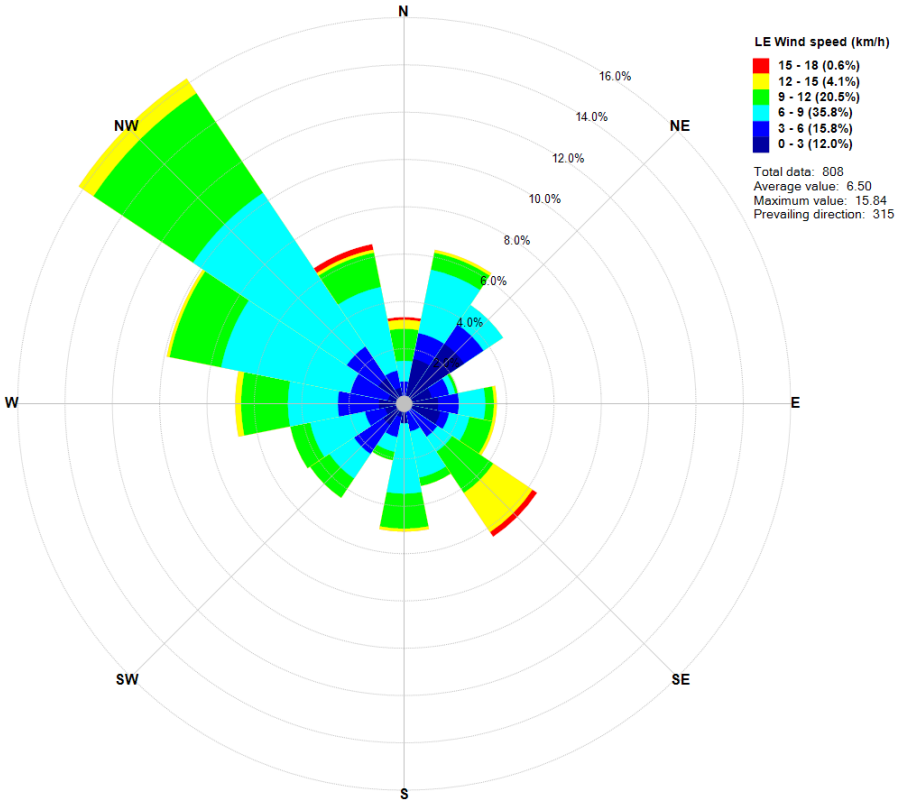

Figure 2.15. Wind rose showing speeds and bearing during surveys at Gwennap Head.
Wind rose calculated in WindRosePRO3 (Enviroware, 2013) using Land's End weather station data used in the analyses (n = 808 30-minute units of survey effort).

Tidal rose (Figure 2.16) calculated with Polpred-predicted data using Sigma 16 in WindRosePRO3 to show prominent flow speeds and direction in the survey area used in the Runnel Stone Reef analyses. Flows were predominently (~60%) north-westward (ebbing) and stronger than south-eastward flooding tides.

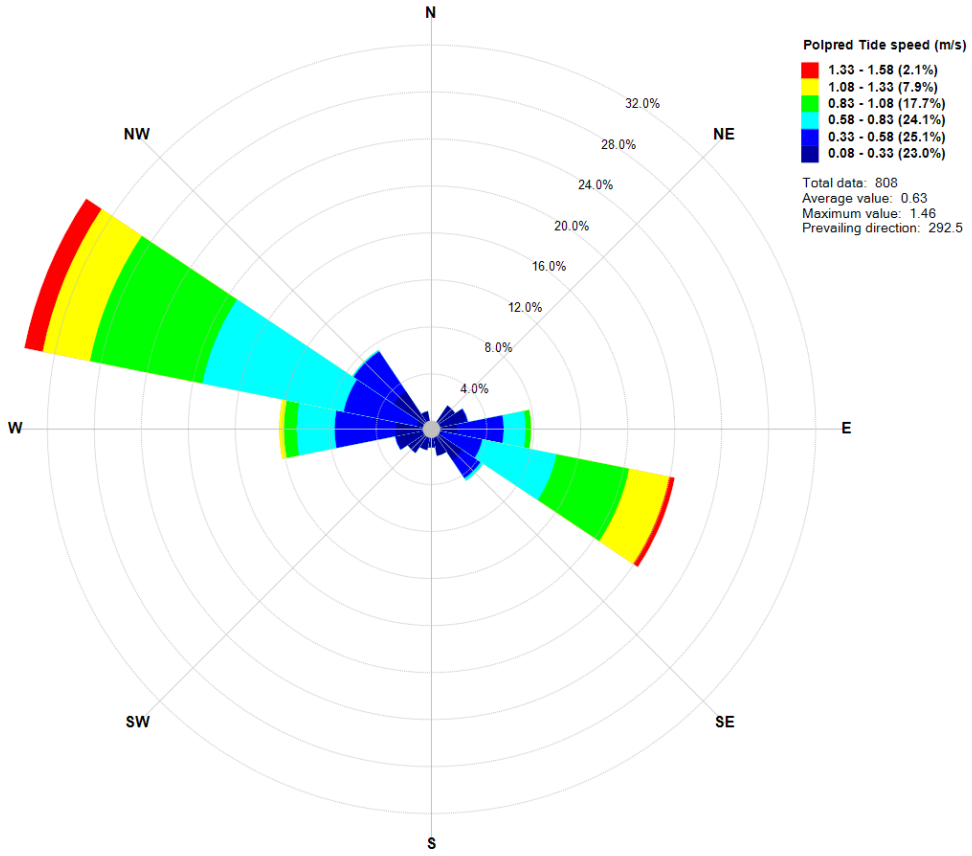

Figure 2.16. Tidal rose showing flow speeds and direction during surveys at Gwennap Head.
Wind rose calculated in WindRosePRO3 (Enviroware, 2013) using Polpred predicted tidal data used in the analyses (n = 808 30-minute units of survey effort).

Figure 2.17 shows radar-derived current vectors for a ‘typical’ hour during westward (Figure 2.17-A), eastward (Figure 2.17-B), and slack water (Figure 2.17-C) flows in the survey area out to a 3.8 km range from the watch point. The images selected are instantaneous results to be used as examples of currents for these particular tidal states, and can vary depending on a variety of factors, such as weather conditions, phase in the spring-neap cycle, and different tidal amplitudes between the semi-diurnal tides on any particular day (pers. comm. P. Bell, 2015).

Radar-derived plots and Polpred-predicted schematics for each hour of the tidal cycle are provided in Appendix E to highlight additional key tidal flow features around the Runnel Stone Reef, evidencing flow complexity in the region for each hour of the tidal cycle.

Results from the ADCP survey are shown in the co-authored paper provided in Appendix A.

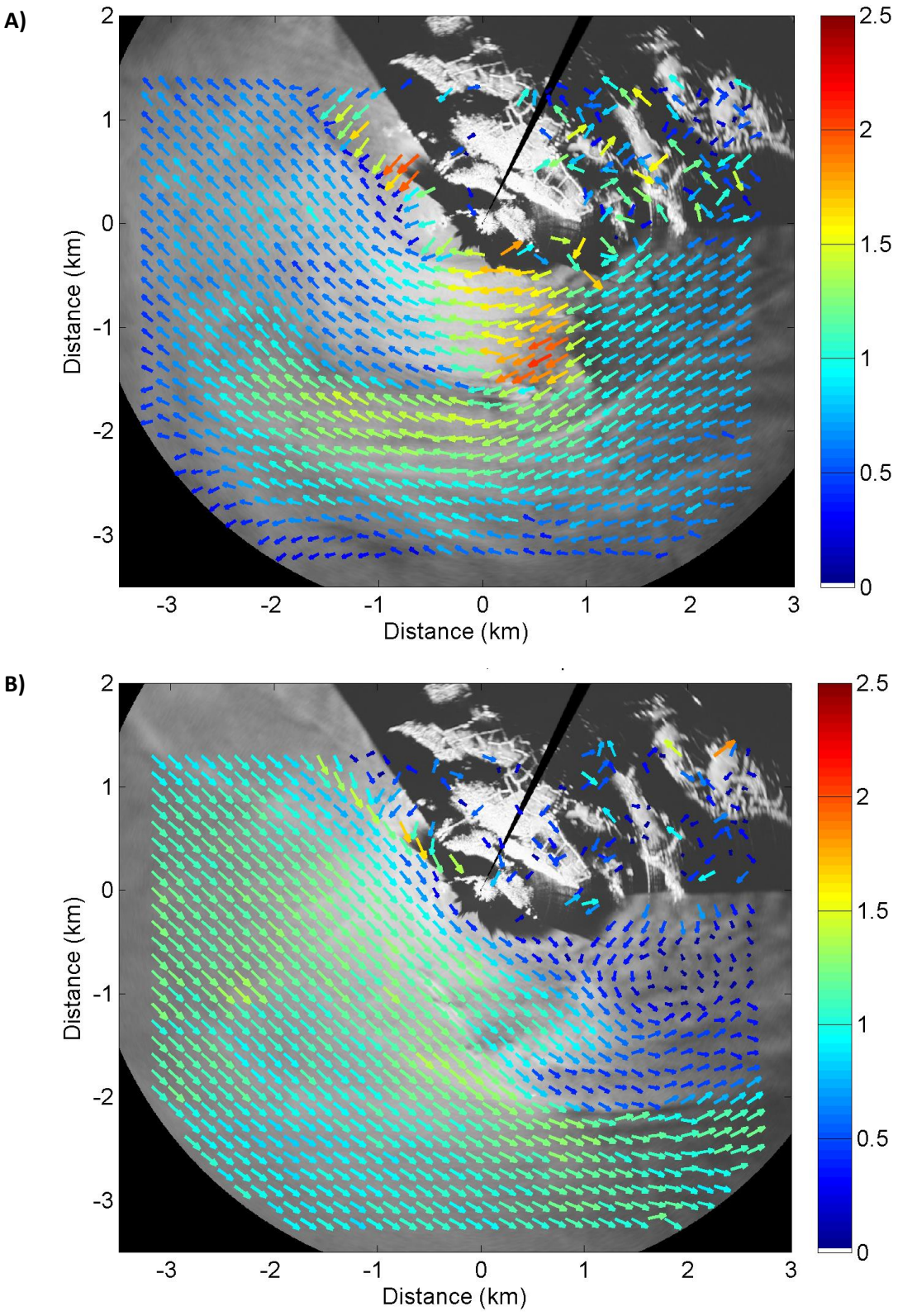
A)
B)
Distance (km)
Distance (km)
2
1
0
-1
-2
-3
2.5
2
1.5
1
0.5
0

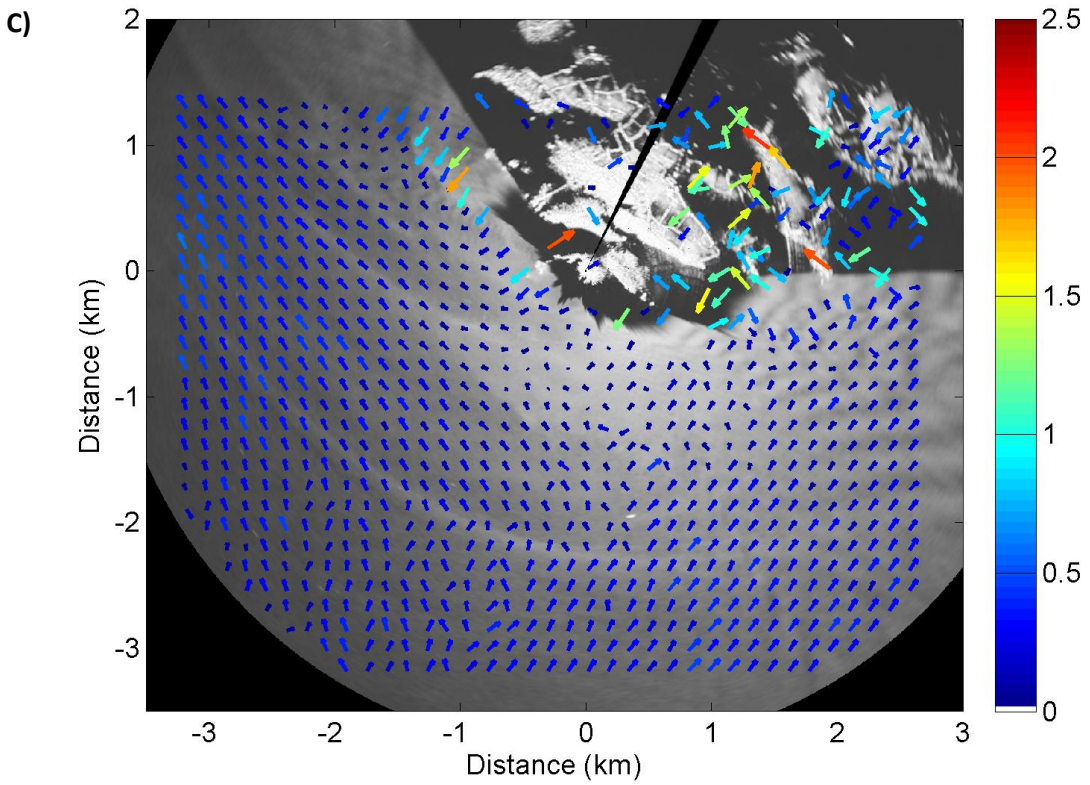

Figure 2.17. Radar-derived current vectors given tidal flow group at the Runnel Stone Reef. A): westward flow (tidal hours HW-6 to -2, and HW+3 to +6), B): eastward flow (tidal hours HW-1 to HW+2), and C) slack water (tidal hours HW-2 to -1, and HW+2 to +3). Current vectors scale logarithmically with speed; vectors coloured according to colour scale in m s^{-1} (blue = 0 m s^{-1}; red = 2.5 m s^{-1}). Black and white area in the top right corner is the headland; the image is oriented North; bright spot at ~(0.3 km, -1.5 km) is the Runnel Stone cardinal mark. Flows calculated during a spring tide on 16/09/2011. (Images courtesy of P Bell).

2.4.2 St Ives Bay

St Ives Bay is situated on the north Cornish coast, southwest UK (Figure 2.18) and is exposed primarily to northerly onshore winds. It is a crescent-shaped, shallow (<30 m) environment with a gently sloping shoreline. It is a known, locally-important winter foraging area for several species of auk (family Alcidae), including Europe's only critically-endangered seabird, the Balearic shearwater *Puffinus mauretanicus*. The bay hosts resident populations of several cetacean species, including harbour porpoise and bottlenose dolphin, which visit on a regular basis (Appendix B). Waters around St Ives are intensively used by the inshore fishing fleet, tourist and recreational sectors. The tide is semi-diurnal (0.027), with two high waters per day. There is a mean spring tidal range of 5.9 m, and neap tidal range of 3.0 m. In the mid-water column (Sigma 16) and at the surface (Sigma 31), current flows reach 0.11 m s^{-1} during spring tides, and 0.02 m s^{-1} during neaps (POLPRED, 2013).

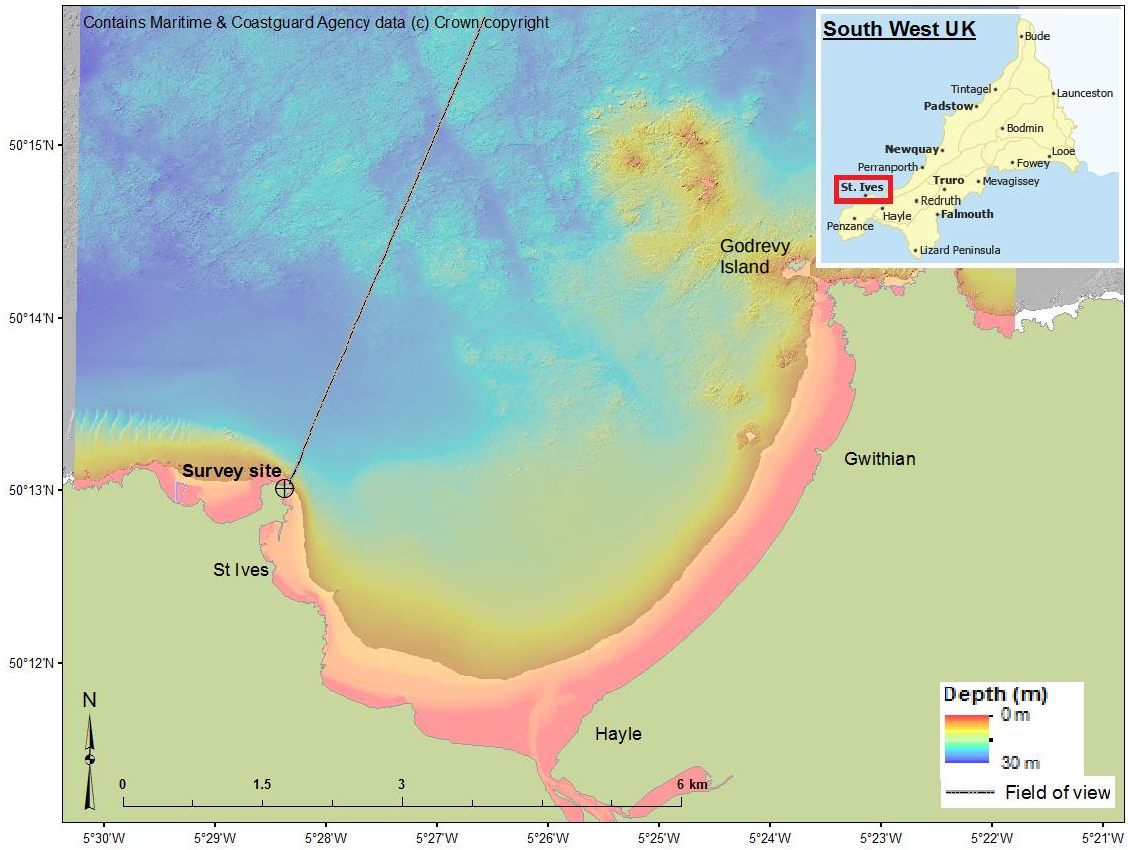

Figure 2.18. St Ives Bay study site, southwest UK.
Field of view extends 6 km from the watch point, denoted by the crosshairs, covering a 35 km^2 survey area to the east of the grey line. High resolution (1 m) bathymetry data (courtesy of CCO/MCA © Crown copyright).

The shore observation site was located 24.2 m above sea level, at 05°28'31.64" W and 50°13'3.79" N (Figure 2.18). Precise GPS coordinates of the location were obtained by the Plymouth CCO using a differential GPS. The watch point was situated on the concrete plinth immediately below the St Ives NCI station (Figure 2.19) on 'the Island' at St Ives, selected due to its ease of access, option of shelter during inclement weather, and because it provided an unobstructed view of the bay to the north-east, out to >6 km. The study area comprised approximately 35 km^2 and was defined as the area within which marine life could be observed and recorded.

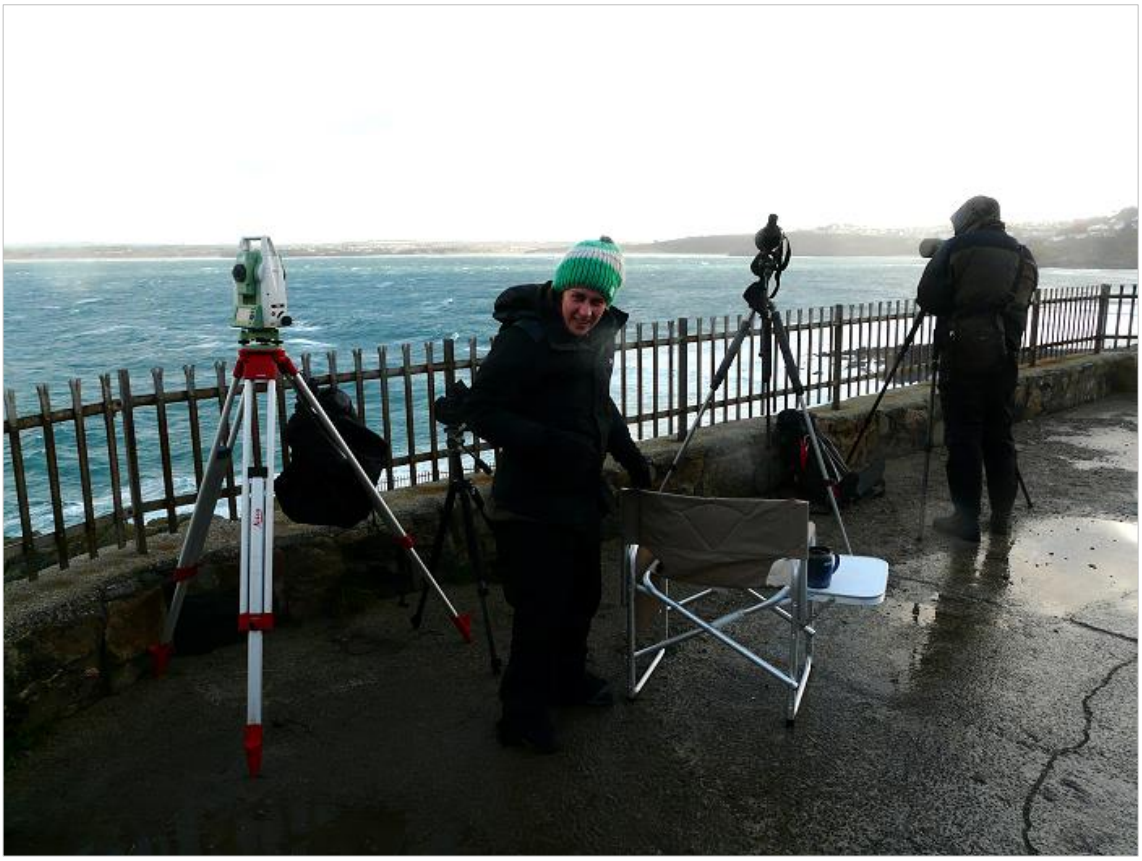

Figure 2.19. Photograph of St Ives Bay watch point showing unobstructed view out to ~6 km. (Photograph © A Colenutt 2013).

The main points of reference were the Stones cardinal mark anchored to the NNE, ~6 km from the watch point, Godrevy Lighthouse atop Godrevy Island 6 km to the northeast at 05°23'57" W and 50°14'31" N, and Gwithian Beach and the Hayle Estuary, delimiting the far east and south-eastern extents of the survey area. There are various protruding headland features, including the Island itself, St Ives Headland at Porthminster, and the headland at Godrevy (Figure 2.20).

There are several shallow pinnacles in the bay, clearly seen in the fine-scale bathymetry (denoted by areas of dark orange) to the north-west of Godrevy Island, which are exposed at certain times of low water and visible from the watch point. There is some particularly steep topography on the western edges of the bay near the watch point, where water depth ranges between 1 m and 21 m, within a constrained 500 m area. A tidal boundary (marked by dashed blue line in Figure 2.20) is often evidenced by visibly turbulent water at the sea surface during certain periods of the tidal cycle, as currents converge and are forced around the sharp corner of the cliff feature. The resultant tide race runs adjacent to the underlying steep bathymetry, at a slight offset (~500 m further offshore) in deeper water.

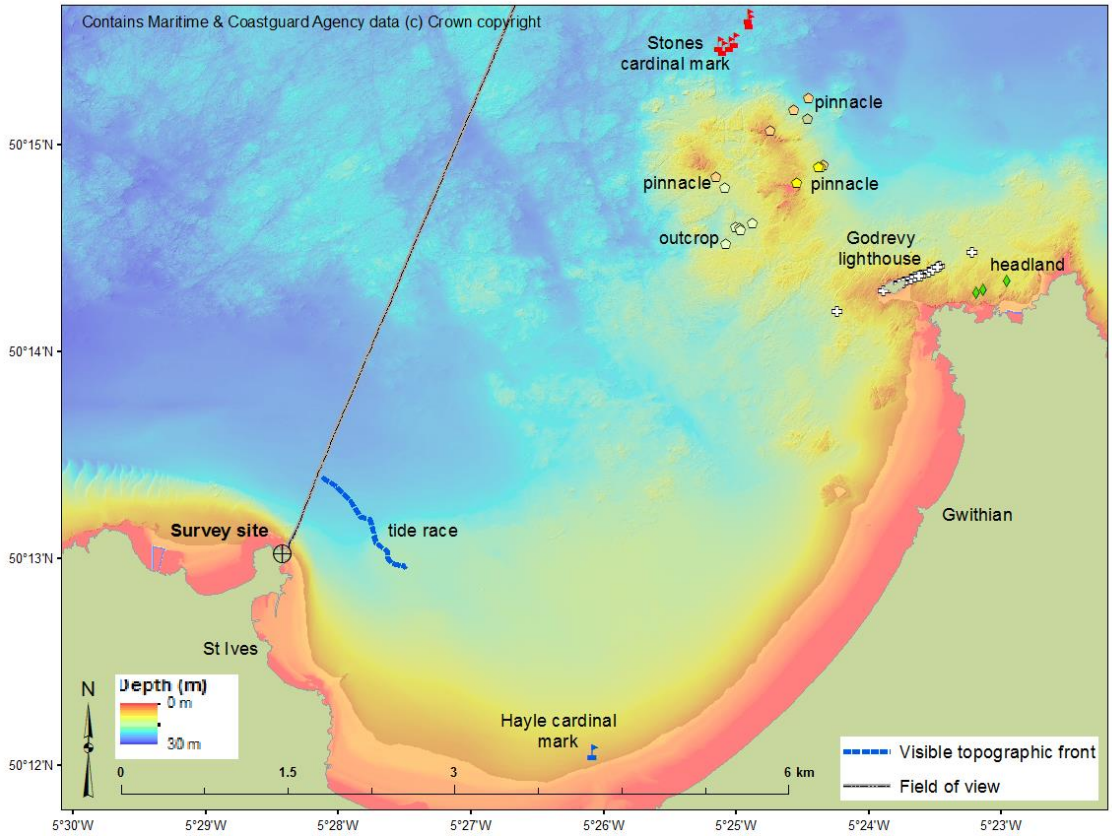

Figure 2.20. Small-scale tidal-topographic front at the St Ives Bay study site, seen at HW+3.
During periods of sufficiently high tidal flow, currents interact around the area of steep topography forming a path of visibly turbulent water at the sea surface. Front traced accurately in the field using the theodolite. High resolution (1 m) bathymetry data (courtesy of CCO/MCA © Crown copyright).

2.4.2.1 Environmental Data Results (St Ives Bay)

Wind rose calculated in WindRosePRO3 using the Seven Stones Lightship data to show prominent wind bearing and wind speeds encountered at the St Ives Bay watch point during the *first* field session in December 2012 (Figure 2.21). Winds were primarily north-westerlies or south-easterlies. The fastest wind speeds were measured during northerlies, i.e. onshore.

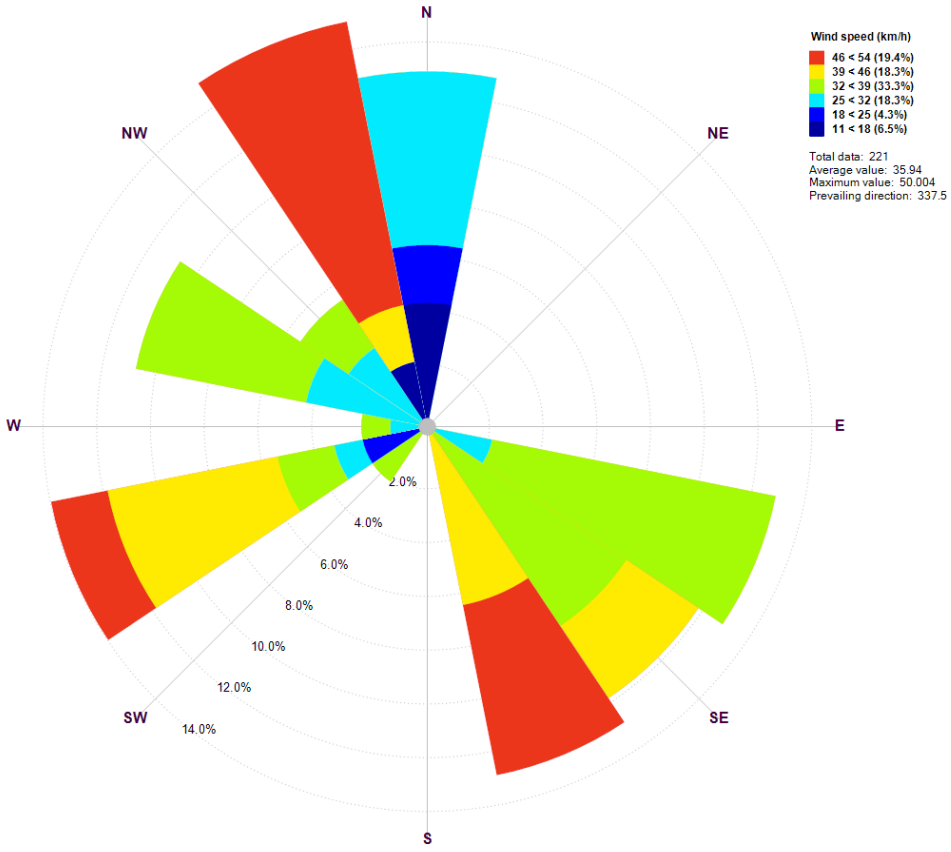

Figure 2.21. Wind rose showing speeds and bearing during surveys at St Ives Bay, December 2012. Wind rose calculated in WindRosePRO3 (Enviroware, 2013) using Seven Stones Lightship data for December 2012.

Wind rose to show wind conditions encountered during the *second* field session in January 2013 (Figure 2.22). Unlike December (Figure 2.21), the majority of winds during January were north-easterlies, with a few strong north-westerlies. Generally, wind speeds were slower in January than in December. There is an absence of southerly (offshore) winds.

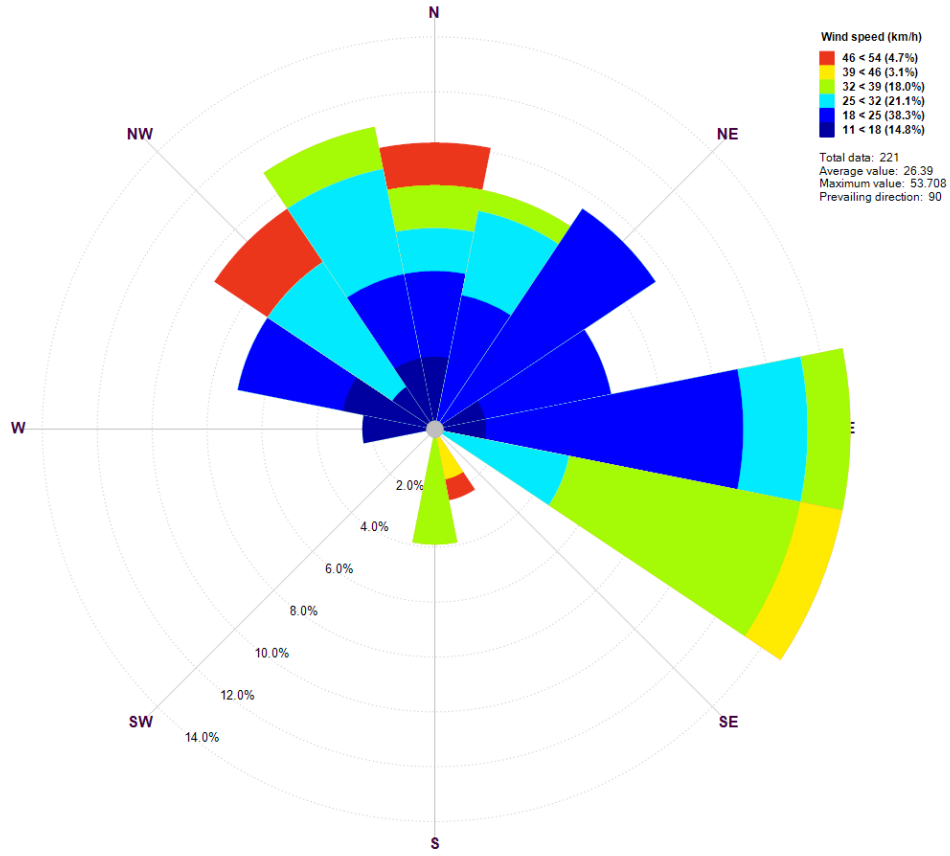

Figure 2.22. Wind rose showing speeds and bearing at St Ives Bay, January 2013.
Wind rose calculated in WindRosePRO3 (Enviroware, 2013) using Seven Stones Lightship data for January 2013.

Wind rose to show wind conditions encountered over the entire St Ives Bay study period between December 2012 to January 2013 (Figure 2.23). The slowest winds were generally easterlies (offshore), while the strongest were from northerly directions (onshore).

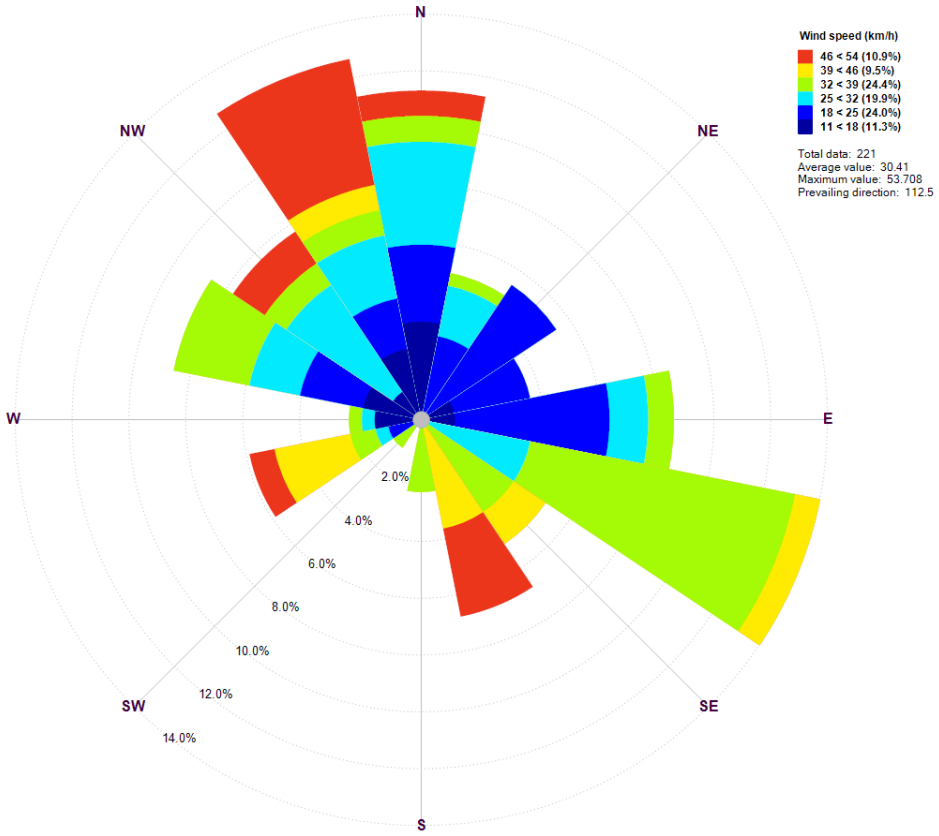

Figure 2.23. Wind rose showing speeds and bearing during all surveys at St Ives Bay, 2012-13.
Wind rose calculated in WindRosePRO3 (Enviroware, 2013) using Seven Stones Lightship data used in the analyses for December 2012 and January 2013 (n = 221 30-minute units of survey effort).

Chapter 3 Fine-scale spatio-temporal distribution of harbour porpoises in a tidally-dominated complex environment off Gwennap Head, southwest UK

A B S T R A C T

Questions remain as to how wide-ranging marine top predators preferentially use their habitat in coastal waters, particularly at fine (<1 km) scales. The high energy environment surrounding the topographically-complex Runnel Stone Reef, off southwest UK, is a regionally-important habitat for harbour porpoises *Phocoena phocoena*, listed under Annex II of the EU Habitats Directive. The horseshoe-shaped rocky reef (<20 m water depth) extends ~1.5 km south of the mainland at Gwennap Head, and falls within the recommended Marine Conservation Zone of Land's End (Runnel Stone). Between 2011-13, systematic land-based surveys were carried out to investigate fine-scale (30-minute) temporal influences on porpoise occurrence, and a theodolite used to derive precise (<50 m) surfacing locations to assess fine-scale spatial distribution. Data were collected across 55 days, totalling 404 hours of daylight-only visual survey effort (in sea states ≤ 3, and visibility >5 km), to test the hypothesis that small-scale physical processes, such as interaction between tide and topography, influence localised habitat use. This information is urgently required for management in coastal waters where human activites are increasing. Generalised additive models (GAMs) were constructed to quantify the influence of static bathymetric variables on relative density, and temporal variability on presence-absence data.

Porpoises were sighted on 49% of survey days (n = 180 recorded surfacings), while only 13.6% of 30-minute scan samples were positive for sightings. The average sightings rate was 0.35 porpoise sightings-hr^{-1} with a higher proportion of animals observed around the hours of midday. Statistical modelling indicated the survey variables cloud cover (a proxy for glare), sea state and wind conditions, significantly influenced the timing of porpoise sightings, while tidal flow direction and tidal range (a proxy for position in the spring-neap cycle) were significant hydrographic factors. Increased sightings were observed during spring tides.

Spatial analysis of gridded (600-m), relative-density data revealed depth, benthic slope, and an interaction between slope and aspect, were significant static bathymetric predictors on the fine-scale distribution of porpoise surfacing locations. There was a near-linear positive correlation between sighting density and water depth, and a marginal preference for areas of low benthic slope (<12°). The interaction term indicated low to mid-range slopes were favoured, irrespective of aspect. This was consistent with results from the kernel density estimates of core habitat, both in this study and re-analysed results from a previous study conducted at the same site using conventional visual monitoring methods, though preferences for deeper waters around the reef margins were also highlighted.

Across analyses, there was evidence of clustering around the southern and south-eastern reef margins, including adjacent areas of deeper (>35 m) water. These findings have implications for the management of this listed species, which require the designation of Special Areas of Conservation (SACs). Additionally, the tools utilised in this study may be applied at other constrained coastal locations that are amenable to shore-based observations to identify habitat use of highly mobile marine species.

3.1 Introduction

Harbour porpoises are observed off the southwest tip of the UK mainland throughout the year (Pikesley et al., 2011; Leeney et al., 2012; SeaWatch SW, 2014). They are listed under Annex II of the EU Habitats Directive (92/43/EEC) and therefore require specific measures by Member States for their protection, including the designation of Special Areas of Conservation (SACs), which will contribute to the Natura 2000 network (explained further in Chapter 1). However, the identification, management and monitoring of protected areas is challenging, and particularly problematic for wide-ranging species, such as porpoise, where their distribution and relative abundance remain poorly understood (JNCC, 2009). Sites can only be proposed where there are 'clearly identifiable areas… essential for their life and reproduction' (Article 4.1), so improved knowledge on relative density is urgently required. Additionally, according to European guidance in Annex III, a protected species may only be excluded from consideration from site selection where the 'populations are too small to be naturally viable, or where the species occur only as vagrants', i.e. outside their natural range. This highlights the importance of adequately determining a population's occurrence, or persistence, over time within a study area to usefully inform management and contribute to the scientific knowledge base required for site selection (Booth et al., 2013) at the appropriate resolution.

Improved understanding of the fine-scale drivers of porpoise distribution is clearly vital information required by the UK Government to be able to make informed proposals to the European Commission on site selection. Determining habitat selection of porpoises is ecologically-complex (Booth et al., 2013). However, fine-scale (<1 km) heterogeneity in their distribution (i.e. environmental controls that cause clustering behaviours or 'hotspots') can often be usefully quantified as a function of local static and dynamic variables (Embling et al., 2010; De Boer et al., 2014; Jones et al., 2014a), which may include bathymetric habitat, weather and tides. Close to islands and headlands, the interplay between these variables can play a particularly significant role in determining habitat selection by porpoises (Wolanski & Hamner, 1988; Franks, 1992a; Johnston et al., 2005b; Jones et al., 2014a). In nearshore (<10 km offshore) coastal environments, this information is particularly relevant, as there are increasing requirements to manage anthropogenic impacts alongside species and their habitat (Halpern et al., 2008; Bailey & Thompson, 2010), including: marine spatial planning (Witt et al., 2012b; Merchant et al., 2014; Rodrigues, 2014), wet renewables (Todd et al., 2009; Waggitt & Scott, 2014), fishing (Sonntag et al., 2012; Prado et al., 2013) and conservation (Mikkelsen et al., 2013; McClellan et al., 2014).

Due to their proximity to shore, coastal hotspots can be effectively monitored during dedicated effort-corrected surveys from land-based observation stations. Relative to boat-based surveys, which may not be practical in high energy environments, shore-based observations can be carried out at comparatively low cost (Denardo et al., 2001). Dapling et al. (2010) recommend caution be applied when observing species from a study area that is known not to encompass its entire home range, since sightings may not be a true marker of habitat preference. Instead, they may simply be recorded locations of points *along* a feeding route, as they travel between foraging grounds (Embling et al., 2010). However, where surfacings are more frequent within a study area (i.e. increased *relative* density), the habitat is likely a foraging ground and representative of higher quality habitat (Bailey & Thompson, 2010; Pirotta et al., 2013), with implications for management. Collecting visual sightings data on the surfacing locations of porpoises (Figure 3.1) is therefore considered useful to monitor fine-scale spatial and temporal distribution within constrained coastal environments (Jones et al., 2014a). Results following data analysis can contribute to urgently-required information on the interplay between controls driving this species' habitat selection, which is necessary for informing management regimes (Booth et al., 2013), e.g. fisheries and conservation.

Figure 3.1. Harbour porpoise surfacings observable from shore-based watch points.
(Photograph © D Murphy 2012).

The distribution of marine top predators is rarely uniformly distributed (Sims et al., 2008), as habitat selection is generally linked to the 'patchy' distribution of their prey (Franks, 1992a; Scott et al., 2010; Embling et al., 2012). Indeed, studies of porpoise distribution provide evidence of some areas of clustering and others of notable absences within a survey region

(Sveegaard et al., 2011b; De Boer et al., 2014; Jones et al., 2014a). Observed patchiness can also be linked to habitat heterogeneity (and areas of increased relative prey availability) in marine species (Georges et al., 2000; Guinet et al., 2001; Sims et al., 2006), where favoured areas may share topographically-distinctive characteristics (Wilson et al., 1997; Booth et al., 2013), e.g. topography, substrate, hydrodynamics, relative to the more homogenous environment of the open ocean (Sims et al., 2008). Free-ranging marine species may therefore exhibit clustering behaviours, as a response to the changing characteristics of their environment, in terms of both density and group size (Cañadas & Hammond, 2006).

Depth and slope specifically have been shown as significant predictors of harbour porpoise distribution (Watts & Gaskin, 1985; Raum-Suryan & Harvey, 1998; Johnston et al., 2005b), with animals generally found within the relatively deeper waters of their home range (Watts & Gaskin, 1985; Jones et al., 2014a). Other studies have also highlighted water depth as a significant factor driving the distribution of air breathing mammal species (Raum-Suryan & Harvey, 1998; Cañadas et al., 2002; Ingram & Rogan, 2002; Hastie et al., 2005; De Boer et al., 2014; Jones et al., 2014a). In northeast Scotland, porpoises concentrated in areas of their home range with water depths between 10 and 35 m (Bailey & Thompson, 2009). In conditions and sites that promote foraging, opposed to resting, for example, many of these studies relate water depth to the availability of prey.

Porpoise distribution is often reported as closely linked to habitat, but literature on the underlying (mechanistic) functions of the preferred habitats remains unclear (Hastie et al., 2004) although, during foraging, it is likely prey distribution is the primary driver of spatio-temporal preferences at a fine-scale. Recent studies have attempted to elucidate the bio-physical coupling responsible for these complex ecological relationships by presenting quantitative data between marine species and their environment, often reported as the interaction of tidal flow with bathymetric variables (Genin, 2004; Embling et al., 2013; Scott et al., 2013; Sharples et al., 2013a; Sharples et al., 2013b; Jones et al., 2014a). These studies provide evidence that small-scale physical processes in marine ecosystems, such as coastally-trapped Kelvin waves or internal wave activity, physically concentrate plankton into patches, which drive the spatial distribution of zooplankton and their fish prey, e.g. anchoveta (Bertrand et al., 2008). These processes are shown to trigger a bottom-up cascade that propagates through the food web, inevitably influencing the habitat preferences of larger mobile marine species (Sharples et al., 2013b). For these reasons, top predators are often

considered 'indicators' of localised zones of productivity within a survey region (Montevecchi, 1993; Votier et al., 2010).

Temporally, sightings rates of cetacean species have been related to the tidal cycle (Mendes et al., 2002; Calderan, 2003; Pierpoint, 2008; Embling et al., 2010; De Boer et al., 2014; Jones et al., 2014a) with studies reporting the association between tides and the movements of small cetaceans, such as porpoise, in particular, is due to the fact these species reflect changes in prey distribution (Mendes et al., 2002; Lopez et al., 2004; Johnston et al., 2005b; Booth et al., 2013). Several studies have linked the relationship with tidal flow to tidal-topographic forcing mechanisms of lower level prey species, which can result in regular and predictable foraging opportunities (Baumgartner et al., 2003; Johnston et al., 2005b; Pierpoint, 2008; Embling et al., 2013; Sharples et al., 2013b). Marubini (2009), for example, predicted more sightings occur in high tidal streams off northwest Scotland, as well as during times of high water. This may indicate increased shearing and turbulent mixing in coastal waters (Nash & Moum, 2001), a feature that aggregates prey (Sharples et al., 2013b), as tidal current speeds increase and interact with bathymetry, thus aiding foraging and prey capture.

Relationships between predators and prey are particularly complex in the marine environment (Cañadas & Hammond, 2006), so the value of developing a suite a complementary techniques to aid in determining the interplay of fine-scale drivers of distribution is clear, particularly when improved knowledge of habitat use in the coastal zone is urgently required by management.

Precise visual survey techniques using a theodolite enabled accurate surfacing locations to be recorded thus revealing extremely fine-scale (<20 m) habitat associations of this species where they existed. Additionally, given the range of bathymetric features in the tidally-dominated study area, the fine-scale results from the theodolite survey were used to test the hypothesis proposed in Jones et al. (2014a) that tidal-topographic forcing is a significant influence on porpoise distribution within a complex study site. Using the Runnel Stone Reef as an ideal model system, theodolite survey data were used to explore the mechanisms underpinning habitat use at a more highly-resolved spatial scale than was possible in previous work.

Porpoise data used in the Jones et al. (2014a) study were collected using conventional visual monitoring survey techniques at the same site in previous years (see Chapter 2). However, because of the positional error (~250 m) in the visually-estimated data, surfacing locations could not be constrained at a scale comparable to the high resolution static covariate data.

Therefore, although their analyses of gridded relative density revealed preferences for steep benthic slope around the reef margins, finer scale associations with smaller (<50 m) features of topographic highs, which were hypothesised, could not be identified using their survey methods.

This study therefore aimed to further explore the fine-scale spatio-temporal preferences of harbour porpoises hypothesised in previous work but at an improved spatial resolution that was only possible because of the complimentary suite of survey techniques used in this study (see Chapter 2). Testing the data collection methods to describe distribution of a highly-mobile marine species in such a physically-challenging environment, as encountered at the study site, is of considerable applied value. The methods could be used at other similarly-constrained coastal locations where appropriately-resolved covariate data are available. Patterns of porpoise habitat use revealed contributes to knowledge on the coupling of fine-scale physical processes (which likely drive prey distribution and/or availability) with locations of wide-ranging species at the top of the food web. This information specifically improves understanding on how porpoises use the coastal zone and tests the methods to do so, which are aspects needed in equal measure for their effective conservation management.

3.2 Methods

3.2.1 Survey Methodology

To detect porpoises from shore, an observation team comprising at least two observers were equipped with 10x binoculars and 30x telescopes. One observer operated the theodolite (Leica FlexLine TS02 Total Station), equipped with a 30x monocular eyepiece. The theodolite records angles to a precision of 0.0018° of arc. The instrument's tripod was set up each day directly over a precisely-surveyed point, measured at the beginning of the study using a Trimble Differential GPS (DGPS). During every hour of survey (see details below), the horizontal measurement was zeroed and the theodolite level checked. Measurements of tidal changes in the instrument's height above sea level were also recorded every 30 minutes, and necessary tidal height corrections were carried out during data processing (see Section 2.1.2 for calculation details).

Every 30 minutes, an intensive scan of ~10-12 minutes duration was conducted concurrently by members of the observation team, using telescope, binoculars and naked eye. This ensured

thorough and consistent coverage of the near- and far-fields throughout the survey period. Firstly, two observers would use their telescopes and carefully scan the distant Field of View (FoV) from east to west for five minutes (with the horizon at the top) calling out distinct, non-target objects at the sea surface, such as boats or buoys, to ensure similar scan speeds (this facilitated double-observer trials, as outlined in Section 3.2.2). Secondly, the observers would drop down one FoV and scan west to east for a further five minutes. Thirdly, the observers would scan using binoculars in the same way but with a focus on the near-field (<2 km distance) with the Runnel Stone cardinal mark in the centre of the FoV during the first sweep and at the top of the FoV during the second sweep (Figure 2.9). The final search covered the nearshore area out to 1 km with the naked eye.

When animals were sighted, the theodolite eyepiece crosshairs were centred at the waterline on the animal and, using the instrument's 'record' button, precise angles were saved onto an internal data file, automatically time- and date-stamped, having pre-installed an instrument-specific (.frt) format file for this purpose. The theodolite record number, "Point ID", along with species and group size, were noted on standardised recording sheets (Appendix D). Each recorded surfacing of an animal, or group of animals, was allocated a "Sighting ID"; the same IDs were only confirmed in the field if they had been tracked by a nominated observer engaged in a dedicated "focal follow". This observer continued to visually track the marked animal(s) with scope or binoculars to ensure that when the theodolite operator returned to record the location again (e.g. after time spent recording positions of other species), the ID could be confirmed. Observers would resume scanning immediately after foraging events were recorded to ensure consistent effort.

All visible areas of the sea surface were therefore methodically scanned in the same way for at least ten minutes every 30 minutes, ensuring a consistent and repeatable sampling strategy. Data for *in situ* weather conditions and other environmental variables, e.g. sea state, wind, visibility, cloud cover and glare (see Appendix C for descriptors), were collected every 30 minutes at the start of each scan and recorded on the same standardised recording forms (Appendix D). Survey units of 30-minute duration were selected to ensure the dedicated ~10-minute searches (conducted at the start of each 30-minute survey unit) were considered independent, and that changes in environmental parameters, e.g. weather, were recorded at a temporal resolution that allowed comparison with sightings data.

Although the observation site provided a wide FoV of the study area, the exposed location meant that observations were impacted by high winds and other inclement weather events,

e.g. rain and sea fog. Fieldwork was therefore only conducted during periods of good visibility (>5 km) or sea state ≤3. Observation periods ranged between 4 and 12 hours.

3.2.2 Distance Sampling and Double-Observer Trials

Sightings of various mobile species (including seabirds, cetaceans, and basking sharks *Cetorhinus maximus*) were recorded up to distances of 8 km from the survey watch point. The probability of detecting and confidently identify these animals, particularly smaller and less conspicuous species such as porpoises, will diminish with increasing distance from the observer, even when using high-quality optics (Thomas et al., 2012). One approach to estimate the proportion of 'items' missed by a survey is to model a detection function to the observed (and accurate) distances of recorded sightings (Buckland et al., 2001, 2010; Thomas et al., 2012).

However, surveys conducted from a single site observation station do not meet the assumptions of conventional distance sampling (CDS). These violations include the fact the observer is not distributed randomly in relation to the animals, and/or that the animals are likely not distributed randomly in relation to the observer (Buckland et al., 2010; Thomas et al., 2012). The latter violation can occur where there exists a particular environmental feature within a study area, such as a reef, that impacts on a species' otherwise random distribution. To deal with detection issues for a survey that violates the standard assumptions of CDS, independent, double-observer trials were conducted during scans to collect the necessary data to fit an acceptable detection function (Buckland et al., 2010; pers. comm. L. Thomas, 2012).

Using an adapted, 'mark-recapture' methodology (Borchers et al., 1998a; Borchers et al., 1998b; Buckland et al., 2001, 2010), whichever observer first saw a porpoise effectively initiated a 'trial' and, giving the other observer sufficient time to detect the same animal (normally a few seconds), it would then be called out loud. If the 'marked' animal had been 'recaptured' by the second observer, the sighting trial would be noted as a success (a score of 1); if not, it would be noted as a failure (a score of 0). Each sighting therefore corresponds to a binary trail under this adapted, mark-recapture distance sampling process. Scans would resume immediately after trials were recorded to ensure consistent effort.

The location of each marked porpoise sighting, whether success or failure, was fixed and recorded by the theodolite, so that accurate distances, also an assumption of CDS (Buckland et al., 2010; Thomas et al., 2012), could be calculated and attributed to the trial data. This viable

and practical method to correct for missed observations has been retrospectively applied to harbour porpoise sightings data collected at the same site in previous years (pers. comm. L. Thomas, 2012) by the SWSW survey (see Section 2.1.3). The trial data from this study were successfully applied to the visually-estimated SWSW porpoise data that were published in Jones et al. (2014a); see Appendix A.

3.2.3 Analytical Methods

3.2.3.1 Spatial Analysis

Initial data exploration was carried out to gain an overall impression of the theodolite data, post-processing in FlexOffice, v.2 (Leica Geosystems). Maps were produced in ArcGIS® v.10 (ESRI, 2012) combining the raw sightings data with the bathymetry layer. This enabled preliminary visual analysis at a very fine-scale (<20 m), including comparing exact foraging locations according to tidal state. If appropriate, tracks connecting data points of the same animal, or group of animals, by "Sighting ID" were constructed (see Section 3.2.1 for details on ID allocation). Tracks were created using the 'Point to Line' tool in GIS. To analyse the spatial data, the survey area was delineated at 3 km from the watch point. The delineation distance was selected based on: 1) evidence from the distribution of other key species at the study site (e.g. basking sharks, ocean sunfish, dolphins), and 2) standard line transect data on basking sharks and porpoises collected by boat-based surveys operating in the wider study area. Further details can be found in Jones et al. (2014a, pp. 22-3), given in Appendix A.

The delineated survey area was divided by radial bearing lines at 010° intervals, originating at the watch point, and chosen to account for positional error (see Section 2.2.2). The area was further subdivided into grid cells along concentric distance bands at 600-m, and 300-m intervals (Figure 3.2) for relative density analysis. The finer, 300-m cell size was selected as a compromise between the maximum positional error in the recorded sightings data at farther distances from the watch point and to maximise use of the high resolution bathymetry. After clipping areas of affected grid cells that were obscured from view due to land topography, precisely measured in the field with the theodolite, as depicted by the greyed-out polygon (Figure 3.2), the visible survey area encompassed 13.83 km^2.

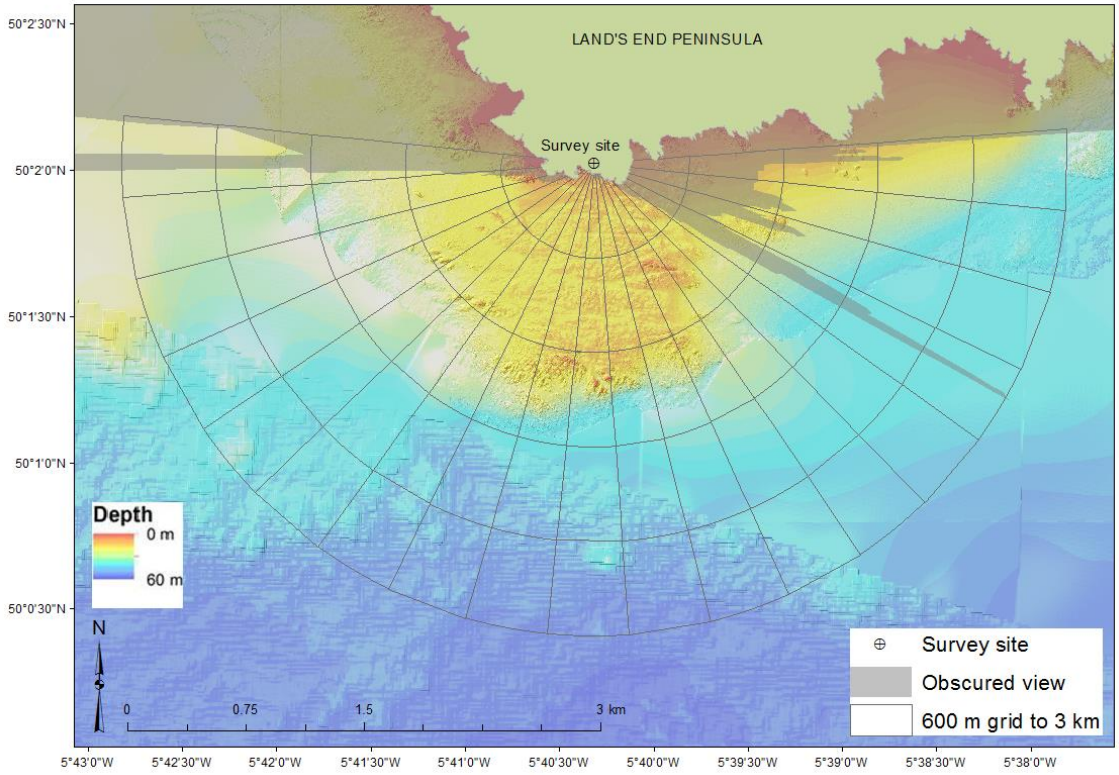

Figure 3.2. Radial grid delineated at 3 km from the watch point covering an area of 13.83 km².
Grid mapped onto high resolution (1 m) bathymetry data (courtesy of CCO/MCA © Crown copyright). Obscured areas due to land topography (greyed-out polygon) were precisely traced in the field by the theodolite and accounted for per grid cell in the analyses.

Sightings data were filtered by time and space to avoid successive measurements of the same animal, e.g. whilst being tracked, so only one sighting was retained in the spatial dataset per grid cell per 30-minute survey unit. A re-sighting was therefore discarded if recorded in the same grid cell within the same 30-minute period. However, if an animal passed into a different grid cell within the same 30-minute period, it was retained in the dataset, so all sightings were spaced by a minimum of one grid cell and one 30-minute survey unit. The density grid based on these data therefore represents *relative* habitat use across the survey area, as the values per grid cell symbolise porpoise-visit frequency within any particular cell relative to its neighbour, i.e. the intensity with which a particular area was visited.

In ArcGIS®, the sightings data were summarised per grid cell by joining the sightings point layer to the polygon grid using the Spatial Joins tool. The static covariates, depth, slope and aspect (see Section 2.3.1), were also summarised per grid cell using the Zonal Statistics tool (Spatial Analyst > Zonal Statistics) and took into account the differing grid cell areas. Extracted values The relevant values from Table 3.1, extracted from the model predictions in R, were attributed

to the centre (x,y) coordinate of every grid cell to systematically-correct porpoise counts per grid cell, and therefore account for missed observations with increasing distance from the watch point. This method was used retrospectively by Jones et al. (2014a), with this porpoise detection function applied to their subsequently published data.per variable were maximum, minimum, mean and standard deviation (s.d.).

3.2.3.2 Detection Function Calculations

In total, the position of 16 porpoise trials were successfully fixed by the theodolite using the adapted 'mark-recapture' methodology. Using a generalised linear model (GLM), with a binomial distribution and logit link function in R, the binary data from the trials were modelled in a logistic regression as a function of distance from the observer (Figure 3.3). The response variable was the trial result (i.e. success or failure) and the model covariate was distance of the animal from the observer (see also supplementary material in Jones et al., 2014a). No additional covariates that may have affected detectability, such as sea state or visibility, as recommended by Cañadas et al. (2004), were included in the model because the sample size was already small (n = 16). Similarly, individual observers were not included as a covariate, though only experienced observers collected trial data and the theodolite operator was the same across the entire study.

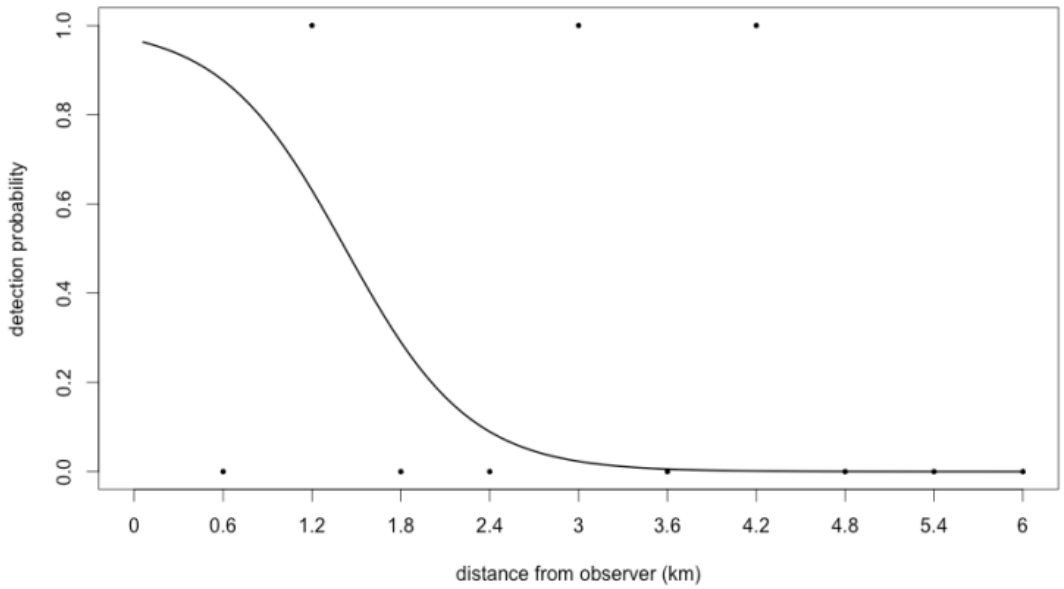

Figure 3.3. Detection function for harbour porpoises at the Runnel Stone Reef study site.
Estimated detection function was modelled from a logistic regression on binary data collected from independent double-observer trials (n = 16), as a function of distance from the observer (km).

The modelled detection function (Figure 3.3) was used to estimate porpoise detection probabilities for any given distance band from the watch point. The relevant values from Table 3.1, extracted from the model predictions in R, were attributed to the centre (x,y) coordinate of every grid cell to systematically-correct porpoise counts per grid cell, and therefore account for missed observations with increasing distance from the watch point. This method was used retrospectively by Jones et al. (2014a), with this porpoise detection function applied to their subsequently published data.

Table 3.1. Harbour porpoise detection probabilities per distance band of the radial survey grid.
Calculating a detection function enables data to be systematically-corrected for the proportion of missed animals with increasing distance from a survey watch point. Detection probabilities were extracted from the modelled logistic regression on the binary porpoise trial data (Figure 3.3), and subsequently applied to the centre point of grid cells used in the spatial analyses.

Distance band (m)	Estimated detection probability
0-600	0.95
600-1200	0.89
1200-1800	0.78
1800-2400	0.6
2400-3000	0.39

The formula for calculating detection-corrected density values km^{-2} per grid cell was:

$$\frac{(number\ of\ porpoise\ counts\ \div\ detection\ probability)}{(grid\ cell\ area\ -\ area\ of\ obscured\ view)}$$

Using these corrected counts, whilst accounting for obscured areas of the survey area from land topography and differing cell areas, a detection-corrected density value per grid cell could be calculated for relative density analyses.

3.2.3.3 Cluster Analysis

To determine if observations exhibit a systematic spatial pattern over the survey area, as opposed to complete spatial randomness (CSR), intensity images were produced using the 'density' function on an object of class "ppp" (point process pattern) within the Spatstat package in R (Baddeley & Turner, 2005). The average point intensity of the sightings data was also calculated (using the 'intensity' function on the same ppp object), and the Pearson

goodness-of-fit statistic, χ^2, given, which indicates solely whether the points are distributed completely randomly within the survey area or not. These first-order estimates of spatial patterns therefore do not provide information on the way spatial distribution changes within an area, only whether the point pattern fails to satisfy the properties of CSR or not (Baddeley, 2010).

Kernel Density Estimation

Estimating the home ranges of individual animals is a useful measure to visually estimate how the intensity of a point pattern varies over an area during a specified time (Worton, 1995). Kernel Density Estimation (KDE) is used to identify and compare areas used by individual animals, i.e. their utilisation distribution (UD), or 'home range'. A KDE measures the density of records within each grid cell that covers a study area, and uses this to estimate the probability that an individual will use neighbouring cells (Kernohan et al., 2001; Horne & Garton, 2006). It therefore provides an estimate of which areas an individual uses most frequently, i.e. it is a raster dataset that represents a probability density surface that can be used to predict where an animal is likely to occur, though it was not necessarily observed (Horne & Garton, 2006). KDE rasters can be converted to isopleth lines that contain a specified volume of the probability surface, in doughnut polygons, for example, which identify areas where an individual is likely to occur. The 0.5 isopleth represents the line containing 50% of the volume of the surface, i.e. the individual is likely to occur in that area 50% of the time. The 50% volume contour is often taken to define "core" usage area (Atwood et al., 2004; McFarlane Tranquilla et al., 2013).

For this study, Beyer's (2012) Geospatial Modelling Environment software (GME) was used within GIS to perform the kernel density analyses on the spatial data, using the KDE and Isopleth tools ('kde' and 'isopleth' commands in GME). It should be noted that the GME does not permit the creation of a KDE with "barriers", i.e. barriers to an animal's movements, such as land, in the case of marine species. In areas where such barriers exist, the creation of KDEs may not be particularly well suited, so Beyer (2012) recommends caution when interpreting any observable patterns in probability surfaces for target species of a nearshore population.

The KDE tool calculates probability density estimates based on a set of input points, and can implement three types of kernel. Depending on which kernel is used in the calculation, the bandwidth will be different. The default, Gaussian kernel was selected. Since this is a bivariate normal kernel, the bandwidth is the covariance matrix (for a bivariate normal distribution).

Various bandwidth estimation algorithms, the 'selectors', can be specified, which estimate an optimised bandwidth matrix given the specific data, calculated in R using the Kernel smoothing package, 'ks'. These are 2×2 matrices, though only three parameters need be provided for the KDE: the standard deviation for x, the standard deviation for y, and the covariance. Both the plug-in ('Hpi') and least-squares cross-validation ('Hlscv') bandwidth estimators were calculated, and entered into the KDE separately for later comparison. The final parameter required was cell size; using Beyer's recommended 'rule of thumb' (Beyer, 2012), a cell size of 20 was calculated, based on the cell size of the point data source raster.

The resultant KDEs from both the plug-in and LSCV bandwidth estimators were converted to doughnut polygons with the Isopleth tool, and specified to contain the 25%, 50% and 75% quantiles. Based on field experience, outputs from the different bandwidth estimators were visually compared to determine which of the KDEs were the most ecologically-relevant. However, observable spatial differences between the kernels were negligible, so kernels from the plug-in algorithm were selected. Beyer (2012) also notes that the 'Hpi' performs particularly well compared to other bandwidth estimators.

Porpoise sightings filtered by the 600-m grid were also split into tidal flow groups 1 and 2 for 'westward', 4 for 'eastward', and 3 for 'slack'. KDEs were computed, and the 50% isopleths entered into GIS for comparison of core habitat areas by current direction. This analysis would determine any fine-scale spatial preferences over short timescales, i.e. spatial preferences within a tidal cycle.

K Function

Second-order properties of a spatial point process describe how spatial patterns in the distribution of the sightings data change through space (i.e. over what spatial scales do the patterns exist) and were explored under a Ripley's *K* function test (using the 'Kest' package within Spatstat) to analyse the observed distribution of sightings against CSR. An estimate of the cluster statistic, *K*, was calculated relative to the true value of *K* for a completely random (Poisson) point process, given the total number of (sightings) points within the survey area. Resultant deviations between the empirical and theoretical *K* curves suggest either spatial clustering or spatial regularity. Where clustering occurs, $K(d) > \pi d^2$, where *d* is a distance between an expected number of points within a distance of an arbitrary point (i.e. we expect an excess of points at short distances). Since the estimation of *K* is biased by edge effects,

consequent on the un-observability of points of the random pattern outside the survey area, a "best" edge correction was applied.

The pair correlation function (pcf) was also computed and is a derivative of the estimated cluster statistic, *K*. Since the pcf is the probability of observing a pair of points separated by a given distance, *d*, divided by the corresponding probability for a Poisson point process, CSR occurs where *g(r)* = 1. It is a non-centred correlation and may therefore take any non-negative value.

3.2.3.4 Temporal Analysis

For the temporal dataset, sighting IDs (see Section 3.2.1 for details on ID allocation) were filtered by 30-minute units of survey. Distinct IDs were retained each 30-minute unit, with re-sightings discarded. The same ID was retained if re-sighted in the next 30-minute unit of survey effort. This was considered representative of how the porpoises used the survey area *relatively* through time, even if it was the same animal(s).

3.2.3.5 Statistical Modelling Methods

Using the 'mgcv' package in R (Wood, 2006a), generalised additive models (GAMs) were constructed to model spatial and temporal patterns in the theodolite sightings data, according to the general structure specified by Hastie and Tibshirani (1999). GAMs are useful where the relationship between the response and a continuous variable exhibits a complicated shape, i.e. where it cannot be specified by an explicit functional form (Crawley, 2012), e.g. linear or quadratic. Rather, non-parametric 'smoothers' are used to describe the data and fitted during model selection. Collinearity between candidate predictor variables may affect estimation of both the model's standard errors and associated p values, so was investigated prior to running the models using Spearman's pairwise rank correlation tests. If correlation coefficients revealed strong collinearity between variables, using $r \geq 0.8$ as the threshold (Zuur et al., 2009; De Boer et al., 2014; Jones et al., 2014a), only one or other of the collinear terms was retained in further analysis, depending on which was retained first in the model selection process, as described below.

For the spatial model of gridded sightings data, a negative binomial family structure was specified, since it is appropriate for count data with many zero's, i.e. over-dispersion, though not zero-inflated data (Zuur et al., 2007). For the temporal model, the response was the absence or presence of a porpoise per unit time, i.e. 0's and 1's, so a binomial family was used.

A log link was specified as the functional relationship between the response and predictor variables in both models.

Default thin plate regression splines (bs = "tp") were specified for all non-cyclic variables, as they allow a smooth function to be fitted to noisy data with multiple explanatory variables without the requirement of knowing where the different splines join, i.e. the "knots" (Wood, 2006b). Cyclic smoothers (bs = "cc") were specified for metrics whose first and last values are adjacent, i.e. covariates with degrees or hours as units where 359° and 0°, or 23-hrs and 0-hrs, are next to each other, for example. Two-way interaction terms were fitted using "te" tensor product smooths, which are effective for modelling smooth interactions of variables with differing units (Wood, 2006b; Crawley, 2012).

The maximum degrees of freedom ("k") for each smooth were manually limited to 4 for most covariates to prevent model over-fitting and to minimise excessive flexibility (Embling et al., 2010). Tidal variables were limited by k = 6 to allow for expected sinusoidal relationships with the response (sightings). To reduce model over-fitting in the automatic parameter smoothing process, the penalty ("gamma") given to each degree of freedom was increased from the default of 1 to 1.4 (Wood, 2006b).

Akaike's AIC score ('An Information Criterion') is a measure of a model's efficiency in explaining the data (i.e. model simplicity vs. model fit). AIC is negatively affected by the number of parameters included in a model, so helps to determine whether additional parameters are justified (Crawley, 2012). The best performing model of significant terms is that which gives the best 'fit' in terms of lowest residual deviance, and lowest AIC score. Using a manual, step-wise forward approach (adding variables iteratively at each stage), according to the selection criteria detailed in the paragraph below, models were built as a function of the explanatory variables. For the spatial model, static bathymetric covariates, mean depth, mean slope and mean aspect (listed in Table 3.2 on page 73) were modelled first, and the two-way interaction terms only specified once the main terms had been selected. For the temporal model (covariates listed in Table 3.5 on page 81), survey variables (significant wave height, sea state, cloud cover, wind speed, wind direction) were added first. Tidal variables (tide direction, tide speed, tide height, tidal range, tidal hour, tidal flow group) were added second, and the temporal variables (month and daylight hour) added last.

First, individual GAMs were run for each of the predictor variables. The significant variable with the best AIC was then selected as the first term to be included in the model. Second,

other variables were added iteratively, as a second term in the GAM, and the combination of significant variables with the best AIC was then used in the next round of selection. Variables were only selected if they were significant ($p < 0.05$), added explanatory power to the model, i.e. ≥1% increase on the previous model to 'deviance' in the data, and had a lower AIC score of at least 2, compared to the previous model, as recommended by Burnham and Anderson (2002). Third, remaining variables were added iteratively to the first two significant terms, and this process repeated until no further covariates could be added, according to the criteria specified.

3.3 Results

3.3.1 Spatial Analyses

A total of 469 theodolite fixes of porpoise were recorded over 404 hours of active survey (Figure 3.4). Surfacings with the same ID (n = 166, where an individual was sighted more than once) are joined by a dashed line, and were only confirmed in the field if they had been tracked by a nominated observer engaged in a dedicated "focal follow" (see Section 3.2.1). Some lines may appear unrealistically straight (Figure 3.4); this is a consequence of the overall aims of the study, as other target species were often recorded with the theodolite *in between* recording porpoise surfacings of the same individual(s).

Initial visual inspection of the raw data indicated a marked absence of porpoise sightings from the shallower inshore waters of Runnel Stone Reef (Figure 3.4). This was true both for individual sightings and tracked animals, with the latter often appearing to move parallel to the reef margin. There were visible clusters of sightings in deeper water areas (>20 m water depth) adjacent to the reef margin (Figure 3.4), with particular concentrations adjacent to reef-margin topographic highs, such as the Runnel Stone on the southern reef margin.

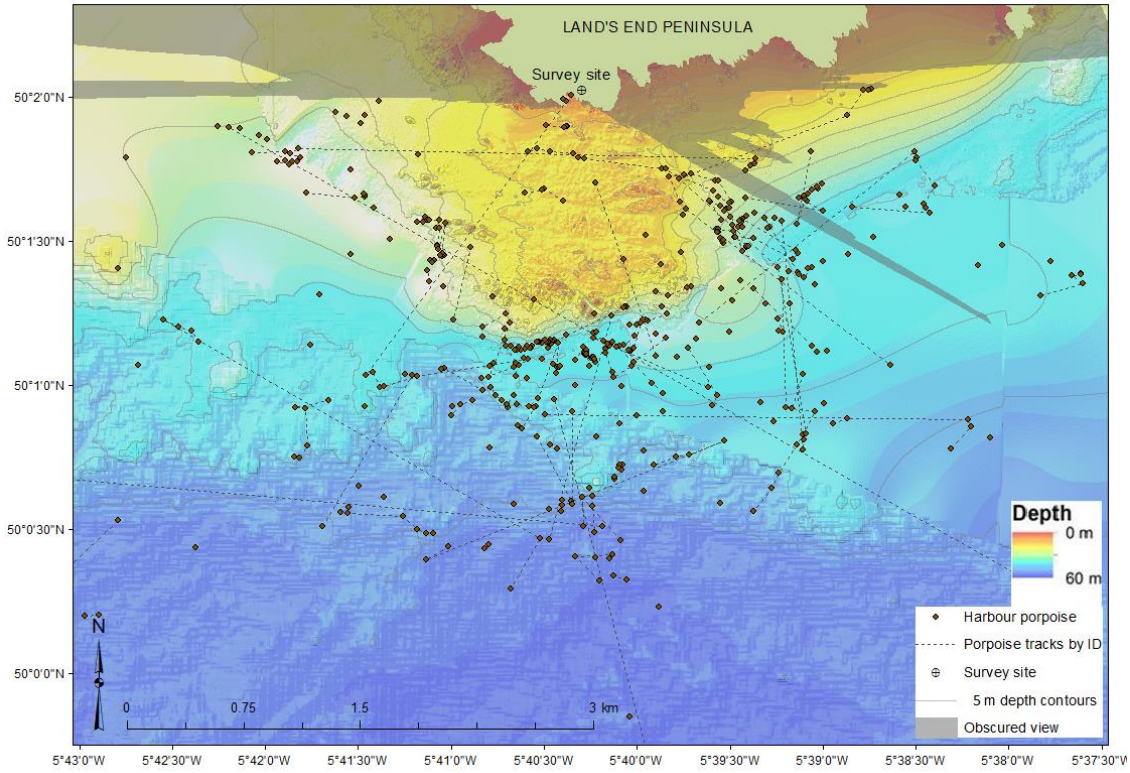

Figure 3.4. Runnel Stone Reef study site showing unfiltered harbour porpoise theodolite data.
Black dots represent all recorded surface observations (n = 469) over 55 survey days across years 2011-13. Surfacings with the same "Sighting ID" (n = 180) joined by dashed lines (n = 166). Locations mapped onto high resolution (1 m) bathymetry data (courtesy of CCO/MCA © Crown copyright) with 5 m depth contours. Observation team located at survey site 'crosshairs'. Areas of sea surface obscured from view due to land topography depicted by greyed-out polygon.

3.3.1.1 Spatial Clustering

To determine whether observations exhibited a systematic pattern over the survey area, as opposed to CSR, a Ripley's *K* analysis, with "best" edge correction, was performed on the porpoise sightings dataset. Observations were not homogenously distributed in the survey area according to CSR (Appendix H.1) but were significantly clustered ($p < 0.01$) at all spatial scales from 0 to 900 m (Appendix H.2) due to either non-uniform intensity or dependence between points. However, the most intense clustering was shown in the first 100 m (Appendix H.3). So, while it is possible that dependence between points as a result of the filtering method could be the cause of some clustering (i.e. retaining an ID if it passed into another grid cell, rather than only retaining a single position of an ID across an entire track), the filtering method implies this would only be likely if intense clustering was occurring at distances ≥cell sizes, which is not the case here. Non-uniform intensity was therefore more likely the cause of genuinely clustered data.

To investigate patterns in non-random point intensity, KDEs were calculated on surfacing data filtered by both the finer 300-m (Appendix K.1) and coarser 600-m (Figure 3.5) grids to visually test whether there were differences in core habitat areas dependent on grid cell size.

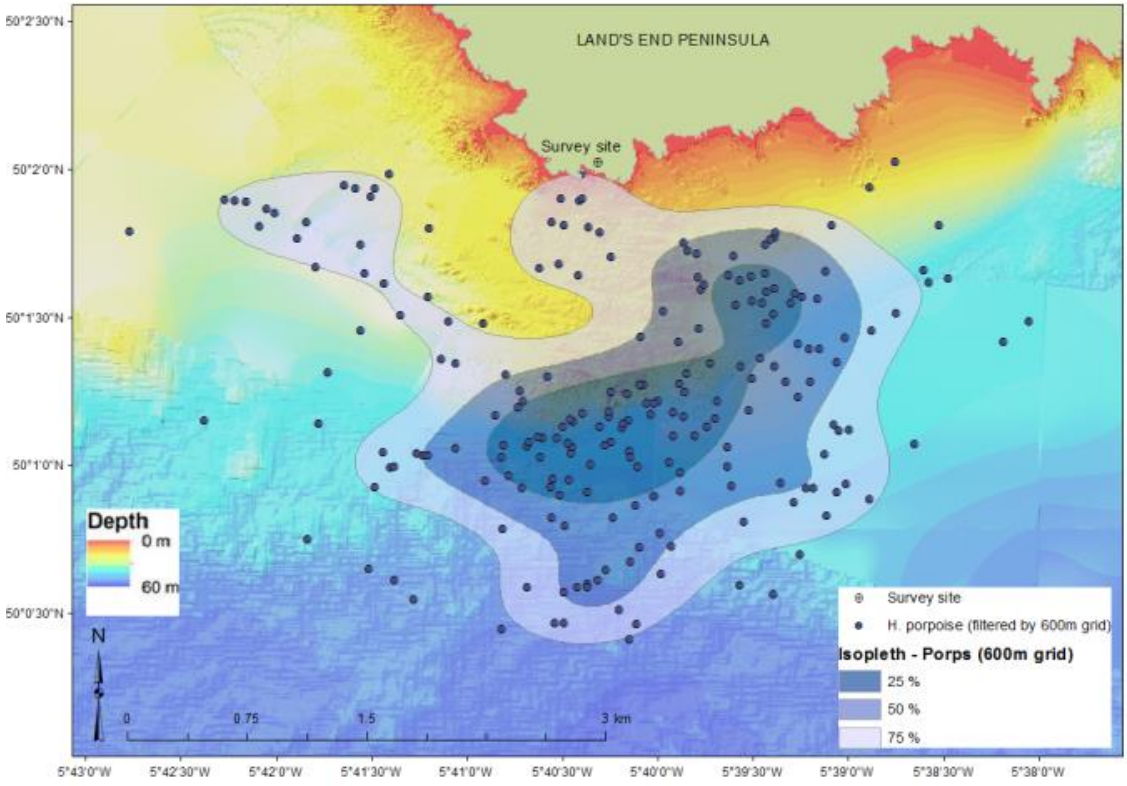

Figure 3.5. Percentage volume isopleths of filtered harbour porpoise surfacing locations.
Kernel density estimations (25%, 50%, 75%) calculated from surfacing locations (blue dots) filtered by the 600-m radial grid (n = 217) within Beyer's (2012) Geospatial Modelling Environment (bandwidth = 400 m; plug-in), mapped onto high resolution (1 m) bathymetry data (courtesy of CCO/MCA © Crown copyright). Observation team located at survey site 'crosshairs'. Theodolite data collected across years 2011-13.

There was no notable spatial difference between the 50% utility distribution (UD) kernel isopleths with different grid size, despite an additional 15 porpoise locations included in the first estimation with a 300 m grid. Core habitat areas are clearly distributed around the south and southeast reef margins and adjacent deeper water areas (Figure 3.5). The 50% UD from the 600-m grid covers an area of roughly 3.5 km² (25% of the survey area). So, although this kernel represents just 25% of the survey area, it contains approximately 50% of the sightings, indicative of clustering behaviour. The 75% isopleth extends around the reef margin to the northwest, but does not encompass deeper or shallower waters in this area; this suggests it is

the reef *margin* in general that is important habit within the study site, particularly the southern and southeastern margins.

To determine whether data collected by different survey methods (i.e. visually-estimated vs. more accurate theodolite) affects the spatial extent of core habitat, and whether there were spatial differences over time, the 50% UD kernels calculated from two independent datasets were plotted on the same base map (Figure 3.6). One kernel was calculated from the locational data collected in this study using a theodolite (n = 217; Figure 3.5) and the other from the SWSW visual sightings data collected in preceding years (n = 255), published in Jones et al. (2014a), Appendix A. Both datasets were filtered by the same, 3-km delimited, 600-m radial grid.

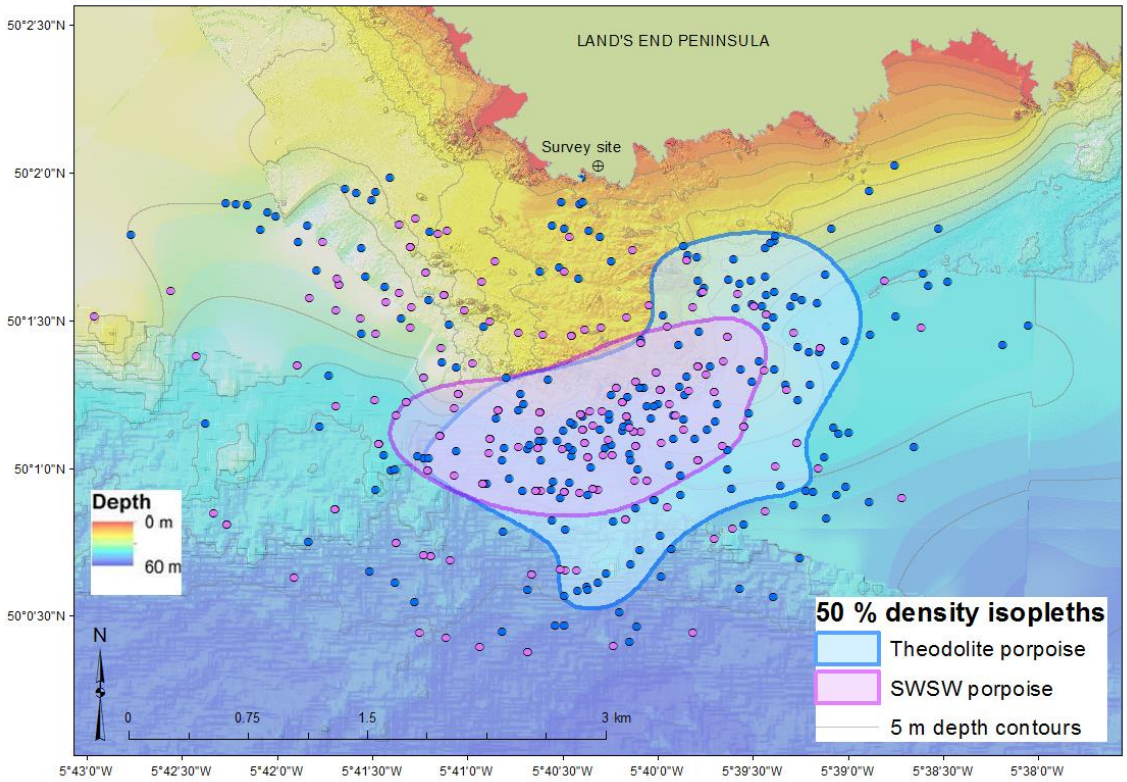

Figure 3.6. Comparison of harbour porpoise core habitat (theodolite vs. visually-estimated data). Kernel density isopleths representing core habitat calculated using theodolite surfacings (blue dots; n = 217) vs. SeaWatch South West ('SWSW') visually-estimated sightings data used in Jones et al. (2014a) (pink dots; n = 255), both filtered by the 600-m radial survey grid. Isopleths calculated from kernel density estimations within Beyer's (2012) Geospatial Modelling Environment (bandwidth = 400 m; plug-in), mapped onto high resolution (1 m) bathymetry data (courtesy of CCO/MCA © Crown copyright). Observation team located at survey site 'crosshairs'. Theodolite data collected across years 2011-13; data in Jones et al. (2014a) collected daily over summers 2007-10.

Figure 3.6, based on the two datasets collected over a seven-year period, reinforces the pattern observed in this study, whereby the southern and southeastern reef margins and adjacent deeper water areas are local 'porpoise' hotspots. The 50% UD derived from visual sightings data covers an area of 1.8 km^2, 13% of the study site, whereas that derived from theodolite observations covers an area twice the size (3.46 km^2), despite there being a similar number of observations in each dataset (n = 255 vs. n = 217, respectively). However, despite these differences in areal extent, the overall patterns, including a relative lack of sightings from the shallow reef plateau, are highly consistent.

To visualise how porpoise sightings distributions were influenced by tidal flow direction, i.e. spatial differences at a fine temporal scale, density isopleths on the filtered data were estimated according to current direction, or flow group (see Section 2.3.2 for details), and plotted with the raw sightings dataset (Figure 3.7).

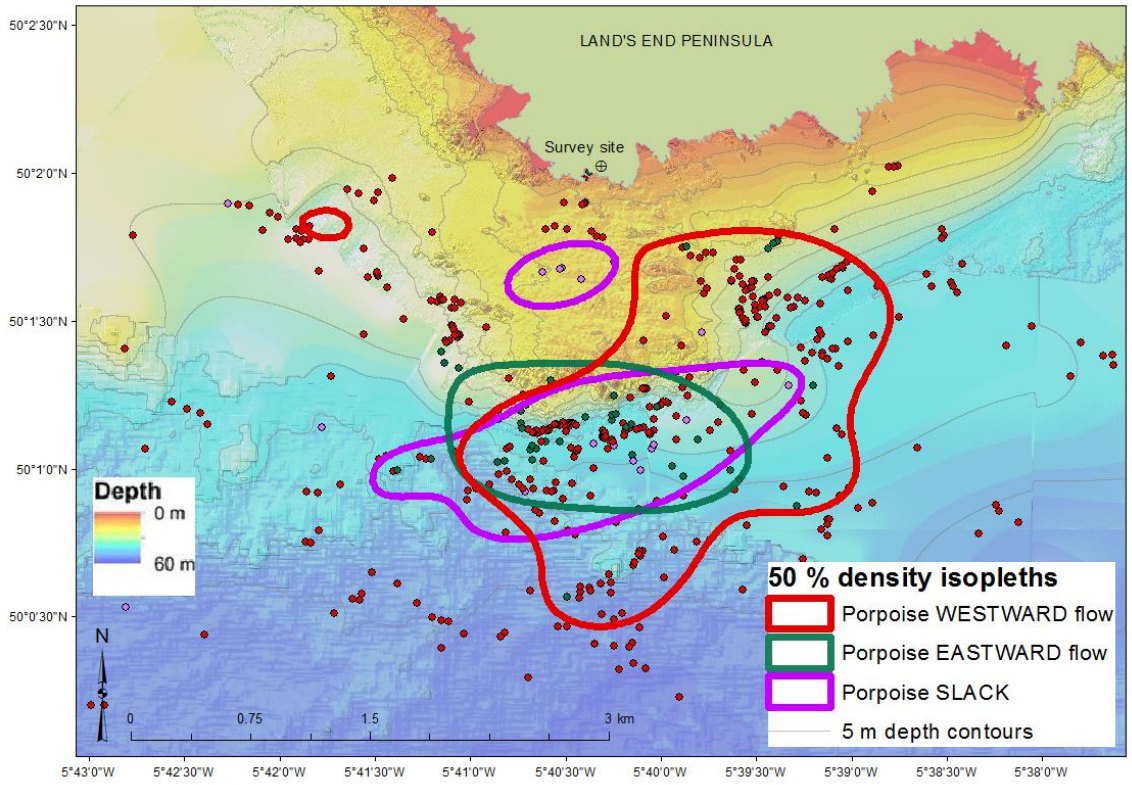

Figure 3.7. Density isopleths representing harbour porpoise core habitat according to tidal state. Raw, unfiltered porpoise locations (n = 255) colour-coded according to tidal flow group. Kernels calculated from data filtered by the 600-m radial grid (n = 217) were split by tidal flow group: westward, flow groups 1 and 2 (red, n = 163); eastward, flow group 4 (green, n = 32); slack, flow group 3 (pink, n = 22). Isopleths calculated from kernel density estimations within Beyer's (2012) Geospatial Modelling Environment (bandwidth = 400 m; plug-in), mapped onto high resolution (1 m) bathymetry data (courtesy of CCO/MCA © Crown copyright) with 5 m depth contours. Observation team located at survey site 'crosshairs'. Theodolite data collected over 55 days across years 2011-13.

Despite different sample sizes per flow direction, the core habitat areas overlap considerably, with the three UDs sharing a concentrated 1.1 km^2 area (8% of the total survey region) adjacent to the southern reef margin (Figure 3.7). This clustering behaviour is reinforced by the fact that many of the sightings within this core area represent distinct IDs. Since they are located very near to each other (≤600 m apart), i.e. within the area of individual cells, this is not indicative of pseudo-replication, as sightings with the same ID in such short proximity of one another would not have been retained in the filtered dataset.

As the current flows westwards for at least 8 hours of the 12-hour tidal cycle, it is not surprising the number of observations for this flow group is highest (n = 163), with the largest area of core habitat, approximately 4 km^2 or ~30% of the total survey area. The raw sightings data during westwards flow are also more spread out, particularly compared to sightings recorded during eastwards flow, which are concentrated at the southern reef margin (Figure 3.7). The eastwards and slack flow groups have comparable sample sizes (n = 32 and n = 22, respectively) while their UDs cover similarly sized areas of 1.5 km^2 and 1.9 km^2. Though both of these kernels identify waters adjacent to the southern reef margin as core habitat, it is interesting that although the slack sample size is smaller by ~30%, its UD covers a larger area, indicating the recorded surfacings at this flow state are more scattered.

The kernel analyses described above highlight a notable absence of core habitat in the western quadrant of the study area (e.g. Figure 3.6). However, an area of seafloor be.d.f.orms (probably sand bars,) visible in the underlying bathymetry (see annotation in Figure 2.3), has been selected as core habitat by a small part of the 'westwards flow' kernel, driven by <10 individual filtered sightings in close proximity (Figure 3.7).

3.3.1.2 Spatial Gridded Analysis

The detection-corrected relative densities of porpoise sightings per km^2 (filtered by the 600-m radial grid) were calculated for each grid cell, and accounted for differing cell areas, including obscured areas of the field of view from land topography (Figure 3.8-A). Average values of the static bathymetric variables, aspect (Figure 3.8-B), depth (Figure 3.8-C) and slope (Figure 3.8-D), are summarised per grid cell.

A)

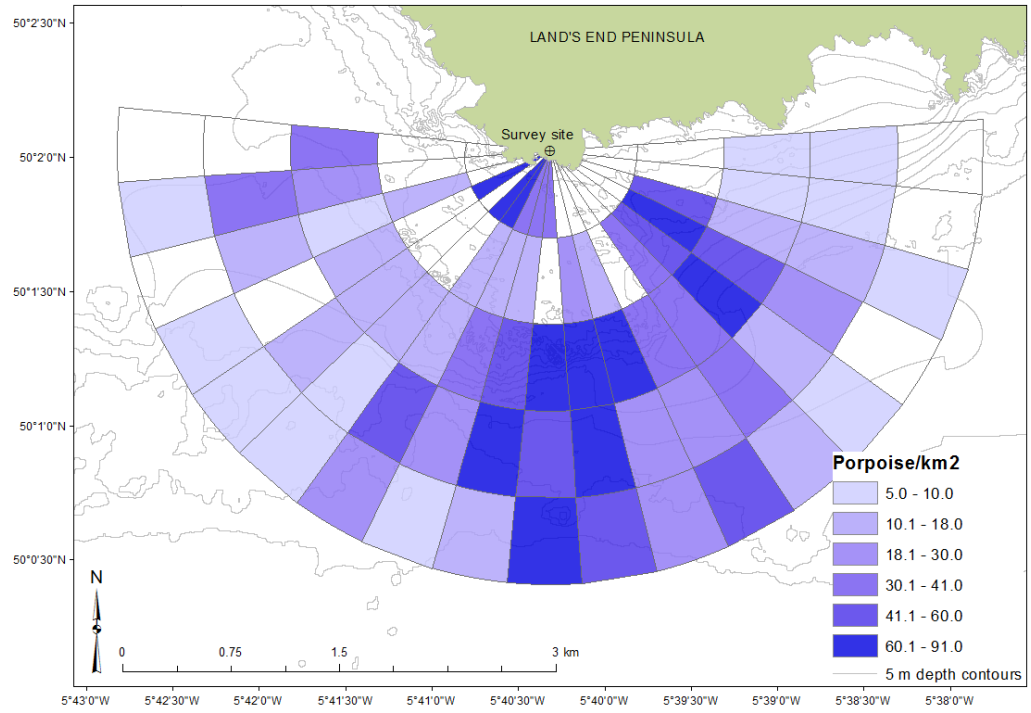
LAND'S END PENINSULA
Survey site
50°2'30"N
50°2'0"N
50°1'30"N
50°1'0"N
50°0'30"N
5°43'0"W
5°42'30"W
5°42'0"W
5°41'30"W
5°41'0"W
5°40'30"W
5°40'0"W
5°39'30"W
5°39'0"W
5°38'30"W
5°38'0"W
N
0
0.75
1.5
3 km
Porpoise/km2
5.0 - 10.0
10.1 - 18.0
18.1 - 30.0
30.1 - 41.0
41.1 - 60.0
60.1 - 91.0
5 m depth contours

B)

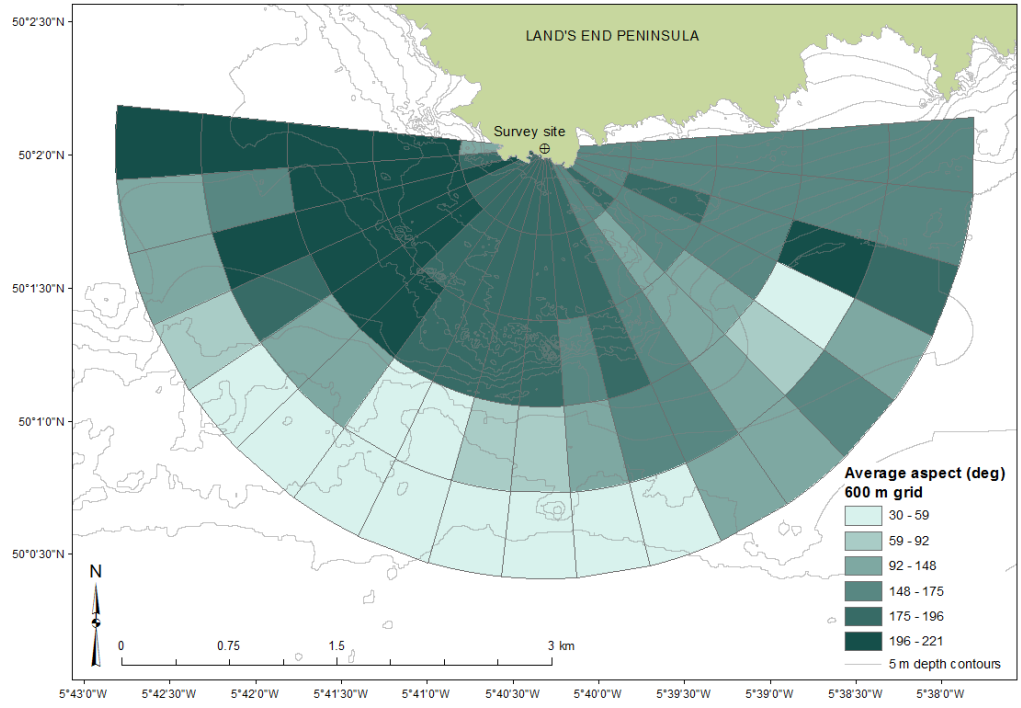
LAND'S END PENINSULA
Survey site
50°2'30"N
50°2'0"N
50°1'30"N
50°1'0"N
50°0'30"N
5°43'0"W
5°42'30"W
5°42'0"W
5°41'30"W
5°41'0"W
5°40'30"W
5°40'0"W
5°39'30"W
5°39'0"W
5°38'30"W
5°38'0"W
N
0
0.75
1.5
3 km
Average aspect (deg)
600 m grid
30 - 59
59 - 92
92 - 148
148 - 175
175 - 196
196 - 221
5 m depth contours

C)

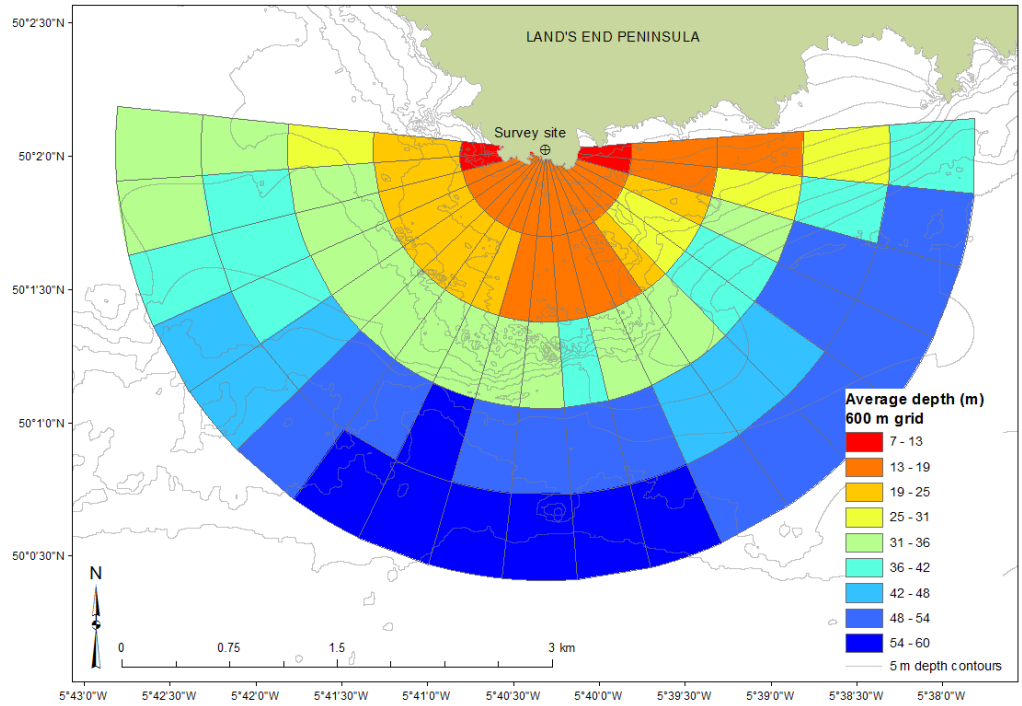

D)

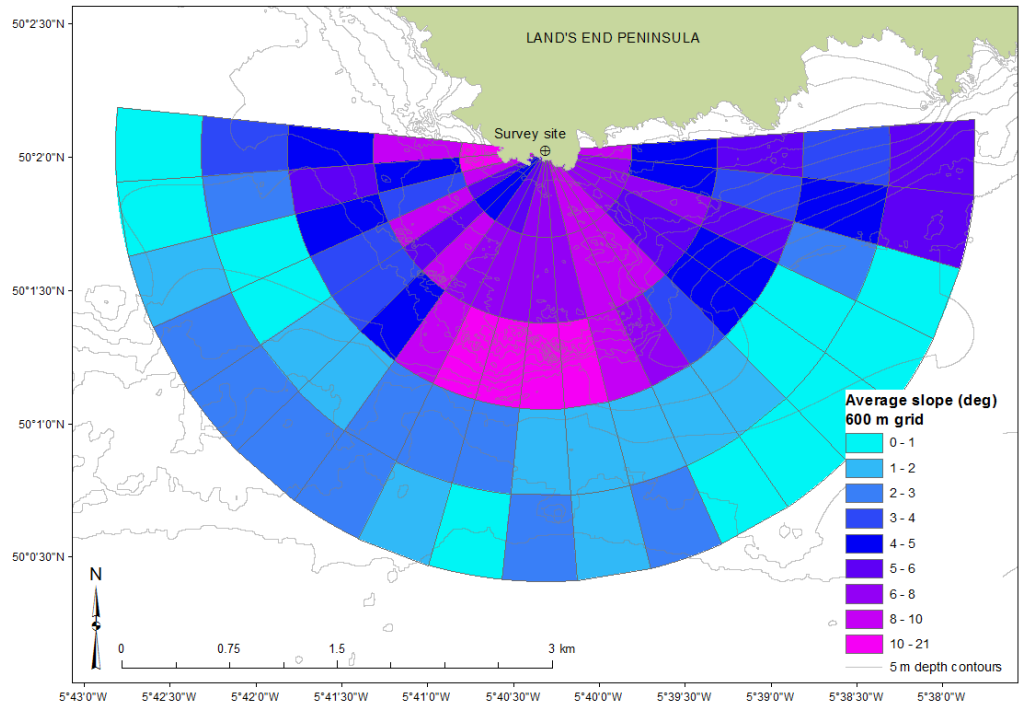

Figure 3.8. Summarised variables per 600-m radial grid cell of the 13.83 km^2 survey area.
A): Detection-corrected relative densities of porpoise surfacings per km^2 per grid cell (n = 217 sightings; n = 95 cells). Gridded values of B): mean aspect (degrees), C): mean depth (m), and D): mean slope (degrees). Static bathymetric variables derived in ArcGIS® from high resolution (1 m) bathymetry data (courtesy of CCO/MCA © Crown copyright), shown here with 5 m depth contours. Observation team located at survey site 'crosshairs'. Theodolite data collected across years 2011-13.

The map of relative sightings density per grid cell shows the highest values are located at the southern reef margin (Figure 3.8-A), which is consistent with the kernel density data (Figure 3.5). There are additional high-density values in some of the deeper water grid cells beyond the southern reef margin, areas also indicated as core habitat in the kernel density plots (Figure 3.5). Other cells with high-density values are at the south-eastern reef margin, and close inshore southwest of the watchpoint. Relationships between sightings data and static environmental variables will be explored in the statistical analysis.

Summaries of the sightings data and static environmental variables filtered by the 600-m radial grid are given in Table 3.2. (See Appendix H.5 for summary of covariates and gridded sightings filtered by the 300-m grid, for comparison). There were no notable differences in high density areas, although there were 41% of absene cells when filtering by the finer grid, and 27% when filtering by the coarser grid.

Table 3.2. Summary of gridded harbour porpoise sightings with static covariate data per grid cell.

Parameter	Value
Number of (600-m) grid cells (after removing missing values)	95 (91)
Number of 'absence' cells (%) (from 91-cell dataset)	25 (27%)
Number of (filtered) sightings: Harbour porpoise	217
Range of sightings per grid cell	0 – 10
Mean sightings per cell (s.d.)	2.4 (2.69)
Static physical variables	
Depth (m)	
Range	7.0 – 59.9
Mean (s.d.)	32.8 (14.8)
Aspect (degrees)	
Range	29.5 – 220.5
Mean (s.d.)	154.3 (51.8)
Slope (degrees)	
Range	0.2 – 21.4
Mean (s.d.)	5.0 (3.9)
Distance from shore to centre of grid cell (m)	
Range	57.2 – 2591.5
Mean (s.d.)	1126.5 (775.1)
Grid cell area (m^2)	
Range	1849 – 285623
Mean (s.d.)	151988 (92420)

3.3.1.3 Spatial Model

To improve statistical robustness during modelling, the spatial model was constructed for porpoise sightings data filtered by the 600-m radial grid, since it contained fewer cells of zero observations (Table 3.2). A disproportionately high slope value (21.4°) relative to the next highest (15.7°) was identified in one grid cell of a very small area nearest the watch point, so was removed from further analysis. Cells with missing data (n = 4) were also removed. The final dataset contained 90 grid cells.

A thorough data exploration was carried out on the spatial data (Appendix H.6). Collinearity between model covariates (Table 3.2) was investigated prior to the model selection process using Spearman's pairwise rank correlation tests (Appendix H.7). Distance from shore and mean depth were highly collinear (r = 0.88). Mean depth was more correlated with the response, and considered more ecologically-relevant, given the topographic complexity of the study site, so distance was removed from further analysis.

A GAM with a negative binomial logit-link distribution was constructed with an offset term, log area, to correct for differing grid cell sizes. The response variable (detection-corrected porpoise counts per grid cell) was modelled using a step-wise forward selection procedure (see Section 3.2.3.5), as a function of the candidate static covariates (Table 3.2). Two-way interaction terms were specified between all three candidate variables.

The final model explained 50.8% of deviance (Table 3.3) in the relative density of porpoise sightings per grid cell across years 2011-13.

Table 3.3. Results of forward GAM model selection for harbour porpoise density per grid cell.
Variables are shown in order of importance. Smooths are shown with the number of estimated degrees of freedom (e.d.f.) in parentheses; AIC_{Δ} is the reduction in AIC score caused by the addition of the significant variable to the model, with the first score in bold showing the starting AIC; % Dev is the additional deviation (%) in the data explained by adding the selected variable to the model. Surveys conducted over 55 days between years 2011-13 at the Runnel Stone Reef.

	Detection-corrected porpoise counts per grid cell		
Order	Smooth (e.d.f.)	% Dev	AIC_{Δ}
1	s(MeanDep, 1)	4.11	**397.6**
2	s(MeanSlp, 2.1)	+14.1	-9.97
3	te(MeanSlp:MeanAsp, 15.48)	+32.6	-8.57
Total		50.8	

The spatial model took the form:

Corrected porpoise counts ~ s(MeanDep) + s(MeanSlp) + te(MeanSlp:MeanAsp) + offset(LArea)

The interaction term explained the majority of deviance (33%; Table 3.3), followed by benthic slope (14%), then depth (4%). All terms were highly significant ($p < 0.01$). Model smooths are shown in Figure 3.9, along with a 3D visualisation of the interaction term. Model validation plots are provided in Appendix H.8.

The fitted smoothing function for mean depth (Figure 3.9-A) shows a near-linear positive relationship with the response, with more animals recorded in grid cells of intermediate to high average depths (>25 m). Given the width of the confidence interval for the smooth function of mean slope (Figure 3.9-B), there seems limited preference for any particular value, with possible avoidance of areas with higher slope (>10°). Although aspect as a main term is not significant, when modelled with slope, the interaction was a significant predictor on the number of sightings in any given cell. Figure 3.9-C and D show possible preference for lower slopes (<10°) regardless of aspect.

A)

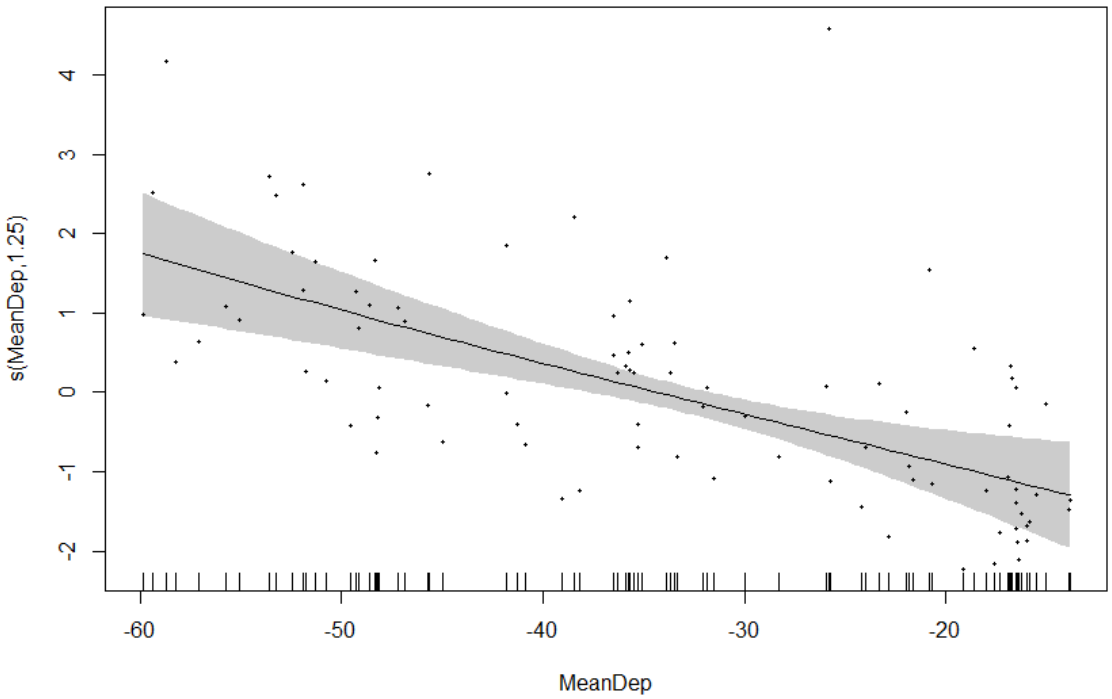
s(MeanDep,1.25)
4
3
2
1
0
-1
-2
-60
-50
-40
-30
-20
MeanDep

B)

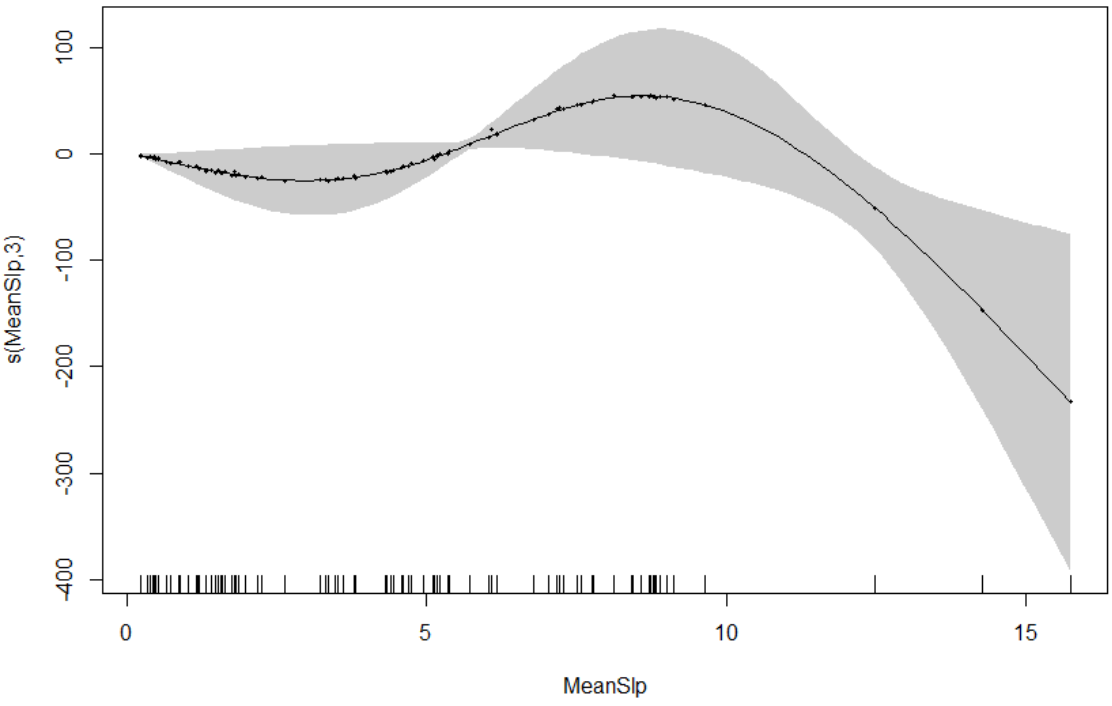
s(MeanSlp,3)
100
0
-100
-200
-300
-400
0
5
10
15
MeanSlp

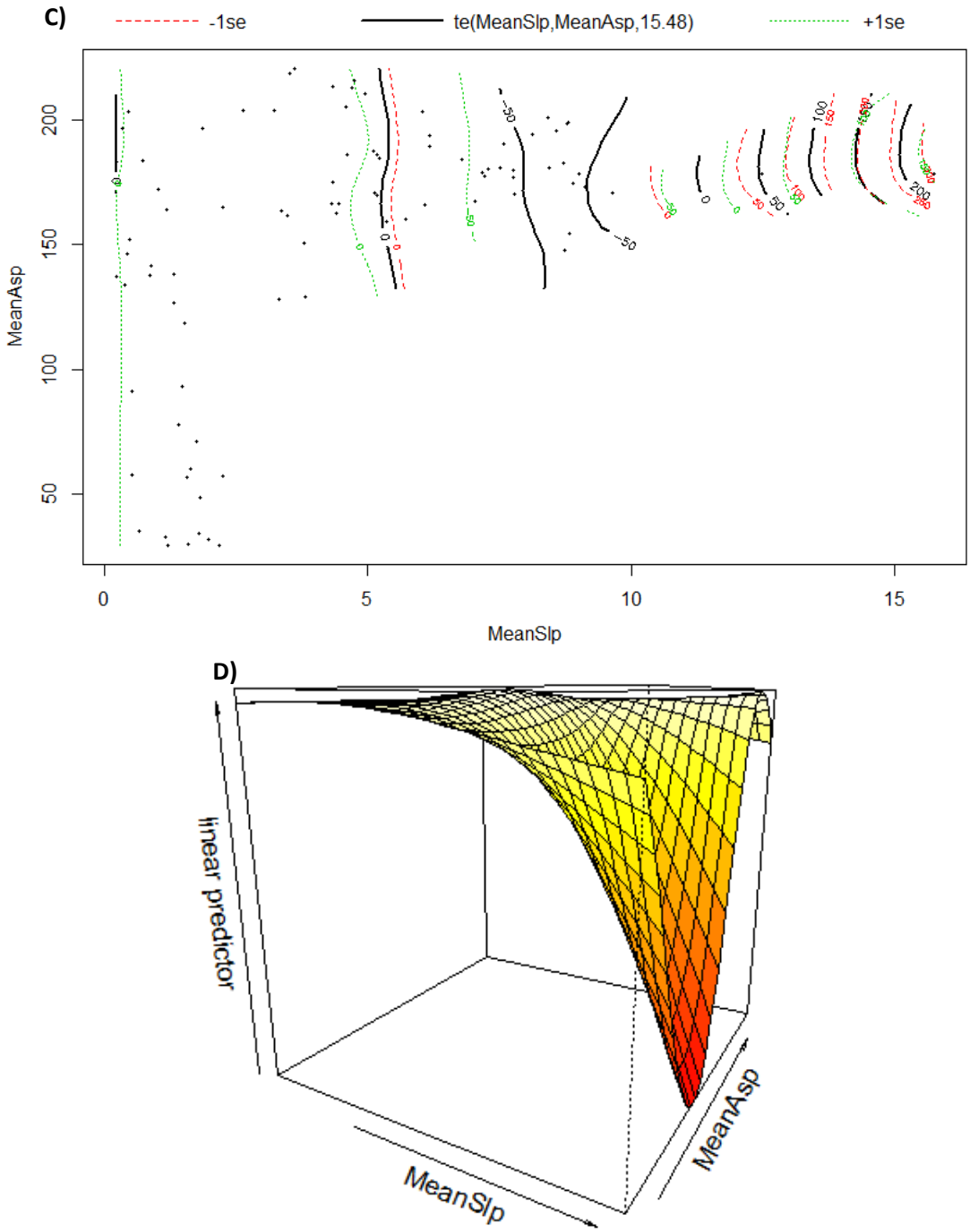

Figure 3.9. Smooths from the final spatial model for harbour porpoise sightings at Gwennap Head. Relationships between detection-corrected counts of porpoise filtered by the 600-m grid (n = 90) and the significant predictor variables, as selected by the final negative binomial GAM. A): Mean depth (e.d.f. = 1.25), B): Mean slope (e.d.f. = 3), C) and D): MeanSlp:MeanAsp (e.d.f. = 15.48). Results reported on scale of the linear predictor. Numbers in y-axis captions are e.d.f. (estimated degrees of freedom) of the smooths. In A) and B), Pearson's residuals are plotted as dots, and the shaded regions around the smooths represent 95% confidence intervals. Rug plots at bottom of A) and B), and the dots in C), are covariate values.

3.3.1.4 Model Predictions

The plot of gridded porpoise density, as predicted by the final GAM (Figure 3.10), shows the lowest values are located in cells over the reef plateau, and in the western quadrant of the survey area, observations also apparent in the gridded sightings data (Figure 3.8-A). The model predicts relatively higher porpoise densities along the southern and south-eastern reef margins, areas also identified as core habitat in the kernel density estimations (Figure 3.5). The model predicts higher than average densities (>3.66 porpoise per km^2) in the majority of cells in deeper water south of the reef (>36 m depth, see Figure 3.8-C).

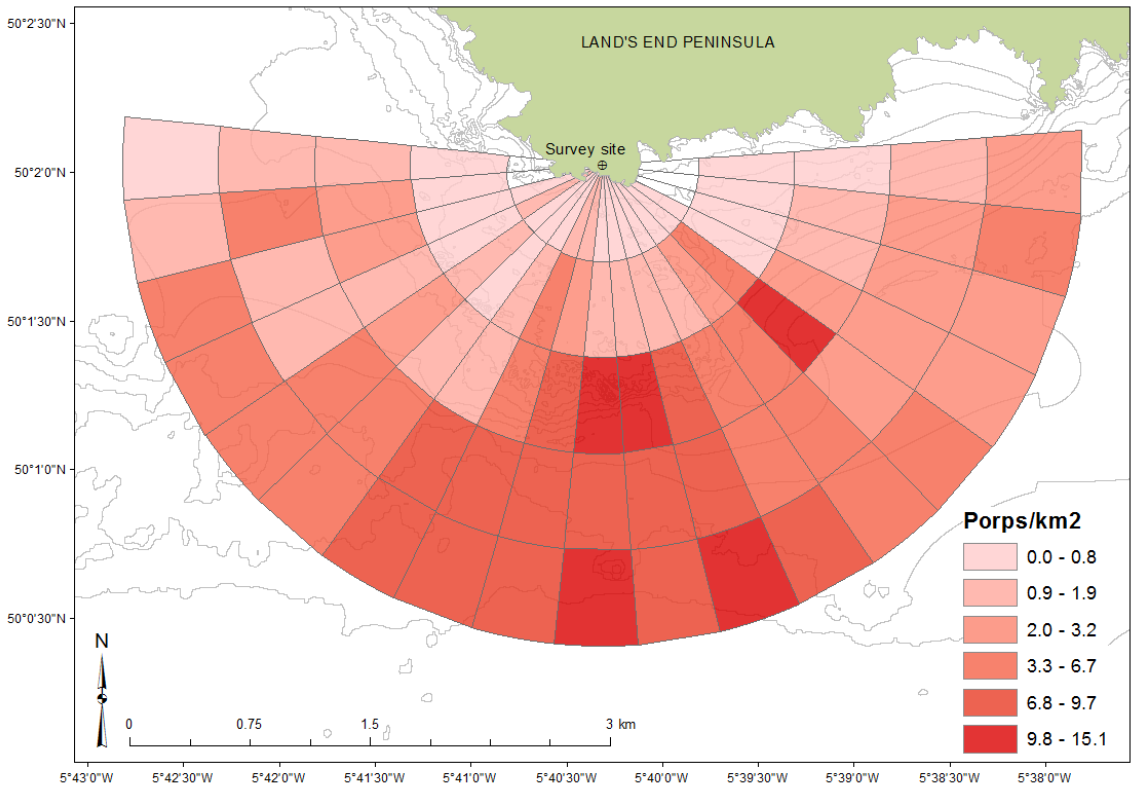

Figure 3.10. Model predictions of harbour porpoise sightings per km^2 per grid cell.
Predictions based on model covariates of mean depth and mean slope, an interaction between mean aspect and mean slope, and an area offset. Density grid mapped onto high resolution (1 m) bathymetry data (courtesy of CCO/MCA © Crown copyright) with 5 m depth contours.

3.3.1.5 Model Performance

To visually represent how the model performed, relative to sightings data collected *in situ*, the difference between model-predicted density values, and observed densities, were calculated

per grid cell (*observed density – predicted density*). Negative densities represent model over-prediction, while positive densities under-prediction (Figure 3.11).

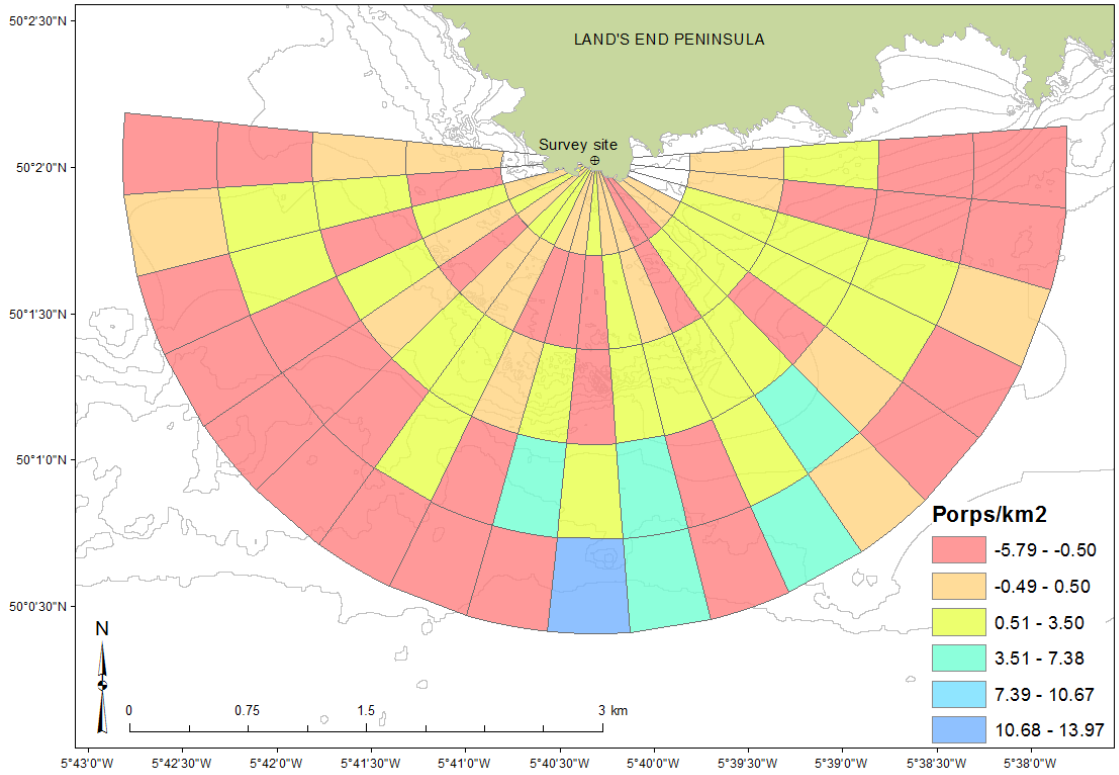

Figure 3.11. Model performance showing the difference between observed and model-predicted harbour porpoise sightings density per km^2 per grid cell.
Predictions based on model covariates of mean depth and mean slope, an interaction between mean aspect and mean slope, and an area offset. Density grid mapped onto high resolution (1 m) bathymetry data (courtesy of CCO/MCA © Crown copyright) with 5 m depth contours. Theodolite data collected across years 2011-13 (n = 217). Negative densities represent model over-prediction, while positive densities under-prediction. Orange represents good model performance with a difference of ±1 porpoise per km^2.

Maximum over-prediction by the model for porpoise sightings per km^2 within a single cell is -5.8, while the maximum under-prediction is +14. Some of the highest over-predictions (dark pink) are located in cells over the reef plateau and in waters > 36 m deep, particularly to the south-west of the watch point. Under-predictions (green-blue shaded cells) occurred in only 6.6% of the grid cells in the deeper waters to the south. The model performed well across 24.4% (n = 22) of the survey grid (orange-shaded cells representing a difference of ±1 porpoise per km^2 between predicted and observed density values). Since the average difference between the model predictions and observed densities across the radial grid is only -0.009 sightings per km^2, with a median value of -0.019 (mean s.e. = 1.1), this suggests good model performance, based on a final GAM that explained 50% of deviance in the data.

3.3.2 Temporal Analyses

Over 55 days, 808 30-minute units of survey effort were conducted across years 2011-13, averaging seven hours of active survey effort per day. A total of 469 individual porpoise surfacings were recorded, of which 180 were the same Sighting ID, i.e. an individual animal, or group of animals (see Section 3.2.1).

Table 3.4. Summary of harbour porpoise sightings from theodolite surveys, 2011-13.
'Positive' hours/days are periods during surveys when a porpoise was sighted and recorded. Data filtered by 30-minute survey units.

Year	Survey days	30-minute observations	Sightings (individual IDs)	Animals (individuals)	Positive 30-min units (%)	Positive days (%)
2011	36	492	79	190	54 (11)	14 (38.9)
2012	18	303	62	175	44 (14.5)	12 (66.7)
2013	1	13	39	64	12 (92.3)	1 (100)
All years	**55**	**808**	**180**	**429**	**110 (13.6%)**	**27 (49%)**

Porpoises were sighted in 110 (13.6%) 30-minute samples, while 49% of survey days were positive for sightings (Table 3.4). The average pod size per sighting was 2.75 animals (s.d. = 2.09), though single individuals were observed most frequently (n = 44; 40% of all porpoise sightings). The maximum pod consisted of 12 porpoises (median = 2). The number of theodolite-recorded porpoise sightings per 30-minute observation unit was scaled-up to give annual hourly sightings rates. These rates were 0.32 in 2011, 0.41 in 2012 and 6.0 in 2013. Note that there was only one survey day in 2013, which would give a falsely-inflated value if included in a multi-annual average; the average sightings rate in 2011-12 was 0.35 porpoise sightings-hr^{-1} (n = 397.5 hours of survey effort).

For analysis of the temporal sightings dataset, samples with missing covariate data were removed. The final dataset contained 157 porpoise IDs (5% data loss) over 737 30-minute samples (91% of total survey effort). Table 3.5 summarises the 30-minute unit porpoise occurrence dataset and associated environmental covariates, which were measured, extrapolated, or observed *in situ* during survey effort (see Section 2.3.2).

Table 3.5. Summary of covariates used in the temporal analysis.
Filtered harbour porpoise sightings data (157 IDs) collected over 55 days (n = 737 30-minute survey units) across three years of theodolite surveys in 2011-13 (missing data removed). Abbreviation: IQR = inter-quartile range.

Parameter	Value
30-minute sampling units of survey effort (hours)	737 (368.5)
Number of sighting IDs	157
Survey variables	
Significant wave height (m)	
Range	0.12 – 0.8
Median (IQR)	0.32 (0.23 – 0.45)
Sea state (BFT)	
Range	0 – 4
Median (IQR)	2 (2 – 3)
Cloud cover (oktas)	
Range	0 – 8
Median (IQR)	4 (1 – 7)
Wind speed (km h^{-1})	
Range	0 – 15.8
Median (IQR)	7.2 (4.0 – 9.7)
Wind direction (degrees)	
Range	1 – 360
Median (IQR)	240 (130 – 305)
Tidal variables	
Tide direction (degrees)	
Range	38 – 334
Median (IQR)	270 (111 – 289)
Tide speed (m s^{-1})	
Range	0.09 – 1.46
Median (IQR)	0.59 (0.36 – 0.84)
Tide range (m)	
Range	2.1 – 5.73
Median (IQR)	3.9 (3.27 – 4.3)
Tidal hour (relative to HW)	
Range	-6.2 to +6.3
Median (IQR)	-0.4 (-3.5 to +3.3)
Tide height (m)	
Range	0.13 – 5.83
Median (IQR)	2.65 (1.6 – 4.07)
Tidal flow group (as factor)	
Range	1 – 4
Median (IQR)	2 (1 – 4)
Temporal variables	
Month (as factor)	
Range	1 – 12
Daylight hour (ratio between sunrise and sunset)	
Range	0.02 – 0.97
Mean (IQR)	0.58 (0.42 – 0.73)

A thorough data exploration was carried out on the temporal sightings data prior to modelling (see Appendix I.1 for additional plots and interpretation). Preliminary analysis indicates that increasing sea state (Figure 3.12-A) negatively impacts on sightings rate after a threshold value where it drops dramatically. Increasing cloud cover (inversely proportional to glare) is associated with increased porpoise sightings in the survey area (Figure 3.12-B). There is a 0.01 probability of sighting animals during periods of clear skies (0 oktas), which steadily increases to 0.35 when completely overcast (8 oktas).

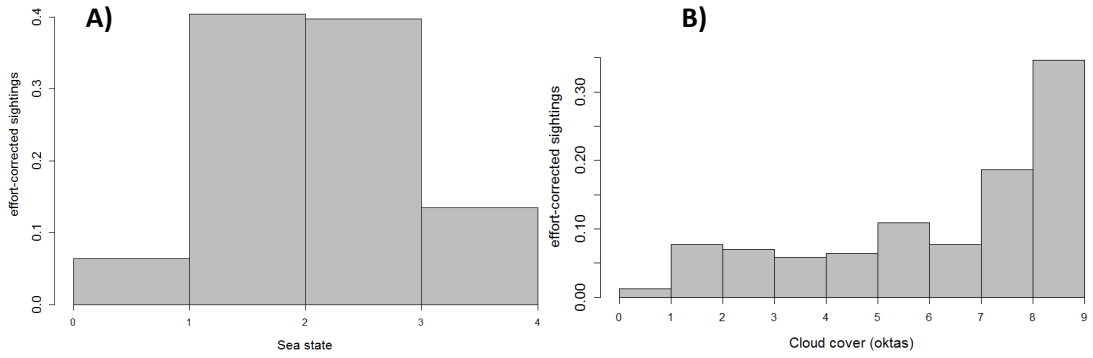

Figure 3.12. Effort-corrected harbour porpoise sightings (n = 157) as a function of survey conditions. A): Sea state (BFT), and B): Cloud cover (oktas). Histograms calculated over 737 30-minute units of survey effort across years 2011-13.

Sightings rate as a function of daylight hour indicates the highest probability of sighting a porpoise occurs between mid-morning and mid-afternoon, with fewer seen in the early morning and late afternoon (Figure 3.13-A). Porpoise occurrence is strongly associated with tidal flow direction (Figure 3.13-B) where there is a six-fold increase in the probability of sighting a porpoise during westward flows than during eastward. Although there are not equal periods of eastward and westward tidal flows in the survey area (Appendix F), the frequency density histogram accounts for this. Westward flow at the study site occurs both during the ebb tide (tidal hours HW+3 to HW+6) and the initial part of the flood tide (HW-6 to HW-2), which explains the bi-modality in the distribution of porpoise sightings relative to tidal state (Figure 3.13-C), irrespective of tidal hour.

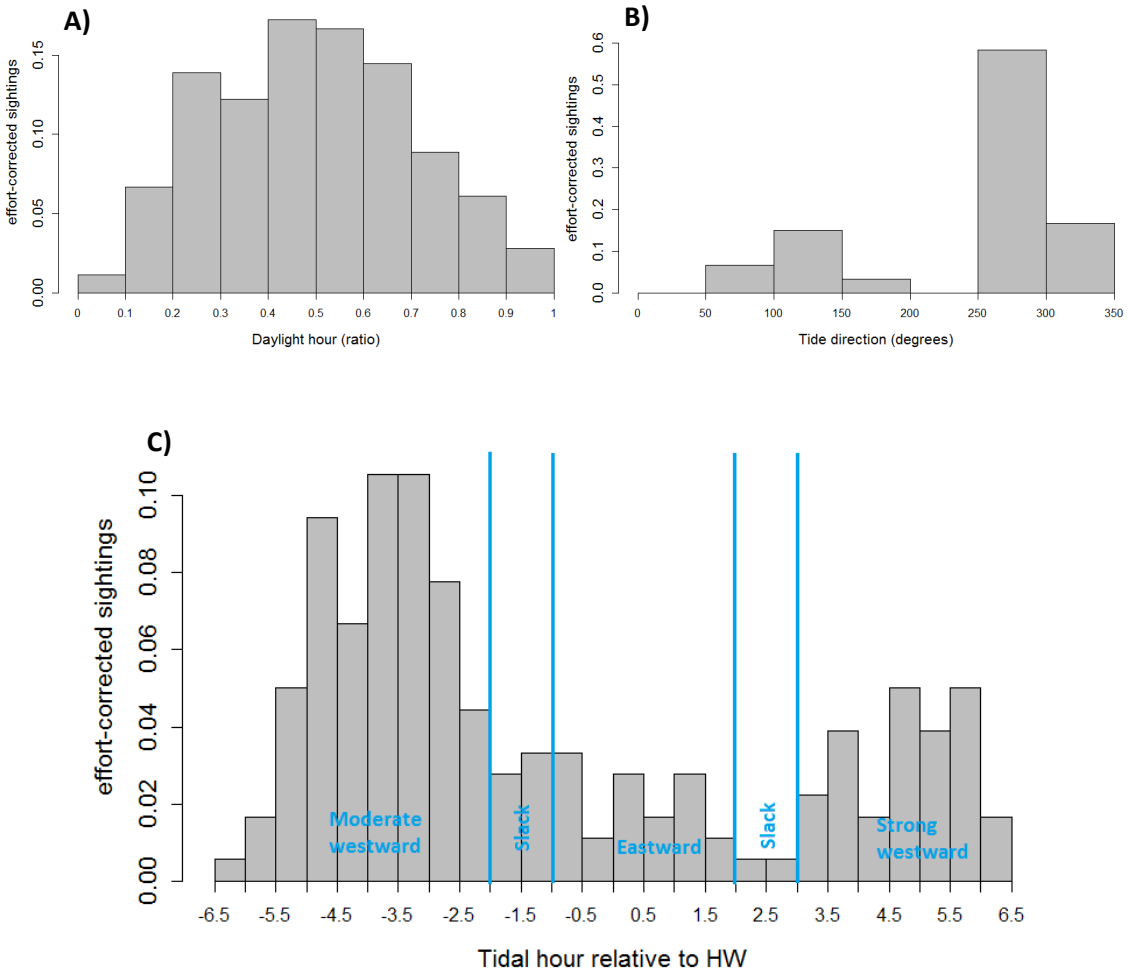

Figure 3.13. Effort-corrected harbour porpoise sightings (n = 157) as a function of temporal variables. A): Daylight hour (ratio, sunrise:sunset), B): Tidal flow direction (degrees), and C): Tidal hour (relative to HW, where HW = 0). Histograms calculated over 737 30-minute units of survey effort across years 2011-13.

Boxplots for the effect of continuous environmental variables on the presence or absence of porpoise indicate a strong influence of wind conditions. Wind speeds (Figure 3.14-A) are significantly lower during presence hours than absence hours, with no porpoise sighted in speeds >10 km h^{-1}. More sampling units were positive for sightings during east/northeast winds (which result in lower sea states at the study site), than onshore-blowing southwest winds (Figure 3.14-B), which blow directly at the watch point.

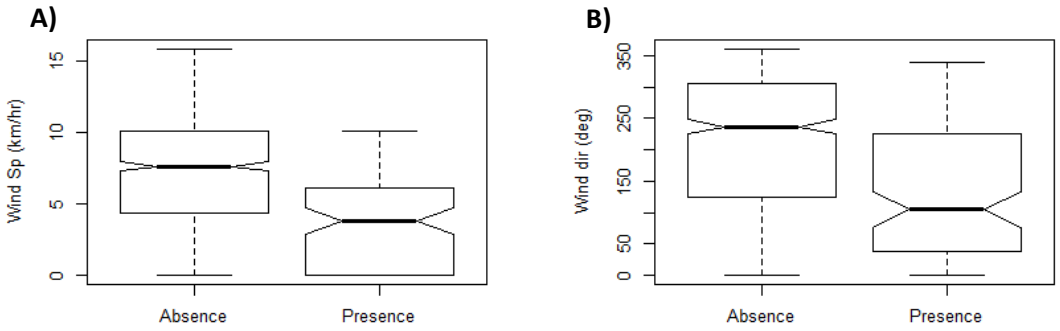

Figure 3.14. Boxplots to show effect of continuous covariates on harbour porpoise occurrence.
A): Wind speed (km h^{-1}), B): Wind direction (degrees). Boxplots calculated over 737 30-minute units of survey effort across years 2011-13.

3.3.2.1 Temporal Model

To explain temporal patterns of porpoise occurrence, the presence or absence of animals per 30-minute sample was modelled using a binomial GAM with a logit-link function (see Section 3.2.3.5). Collinearity between the candidate variables (given in Table 3.5) was explored using a pairplot (Appendix I.4). Tide height and tidal flow group were highly collinear (r = 0.81), though neither were retained during model selection. Through step-wise forwards selection, the modelling process first compensated for survey effects, then tidal variables and finally temporal variables. Model results are given in Table 3.6.

Table 3.6. Results of forward GAM model selection for harbour porpoise surfacing occurrence.
Variables are shown in order of importance, first compensating for survey effects (wind and sea conditions, cloud cover). Smooths are shown with the number of estimated degrees of freedom (e.d.f.) in parentheses; AIC_{Δ} is the reduction in AIC score caused by the addition of the significant variable to the model, with the first score in bold showing the starting AIC; % Dev is the additional deviation (%) in the data explained by adding the selected variable to the model. Surveys conducted over 55 days between years 2011-13 at the Runnel Stone Reef (n = 368.5 hours).

	Porpoise presence-absence per 30-minutes		
Order	Smooth (e.d.f.)	% Dev	AIC_{Δ}
1	s(WindSp, 1.6)	14.0	**472.25**
2	s(Cloud, 2.1)	+3.0	-12.33
3	s(Hs, 2.89)	+4.6	-17.99
4	s(WindDir, 1.4)	+1.3	-4.28
5	s(TideRng, 1.6)	+1.5	-5.7
6	s(TideDir, 1.1)	+1.2	-4.51
Total		25.6	

The final GAM explained 25.6% of deviance (Table 3.6) over 368.5 hours of survey effort across years 2011-13. The model explained 25.6% of the deviance in the occurrence of porpoise over 737 30-minute units of survey effort across years 2011-2013. Wind speed and cloud cover were the most significant predictor variables ($p < 0.001$) explaining 14% and 3% of deviance, respectively. The remaining variables were significant to $p < 0.01$. It took the form:

Porpoise sightings occurrence ~ s(WindSp) + s(Cloud) + s(Hs) + s(WindDir) + s(TideRng) + s(TideDir)

Figure 3.15 shows the model smooths. The auto-correlation function (ACF) of model residuals (Appendix I.4) shows significant residual correlation of 30-minutes that the model has not accounted for. (This is perhaps suggestive of the 30-minute sampling window being too narrow or that the model requires an auto-correlation structure to be built in; though the overall patterns are unlikely to change).

The fitted smooth for cloud cover (Figure 3.15-A) shows a near-linear positive correlation with porpoise sightings. Figure 3.15-B shows a clear decrease in porpoise occurrence where significant wave height >0.5 m. It is evident from Figure 3.15-C that porpoise sightings peaked during offshore-blowing northerly winds (350° to 080°), which lead to low sea states in the survey area. The fewest sightings occur during onshore-blowing south-west winds (~230°). The effect of wind speed on the presence of porpoise per 30-minute units shows significantly fewer sightings are recorded as wind speed increases (Figure 3.15-D), particularly where speed >10 km hr^{-1}.

The smooth for tide direction (Figure 3.15-E) has a wide confidence interval suggesting little relationship with the response, though it is marginally narrower during periods of westward tidal flow (260° to 330°) where sightings rates are higher. The smooth for tidal range (Figure 3.15-F) is positively correlated with the response, showing increased porpoise occurrence with increasing tidal range, which is a proxy for time in the spring-neap cycle, i.e. increased sightings during springs.

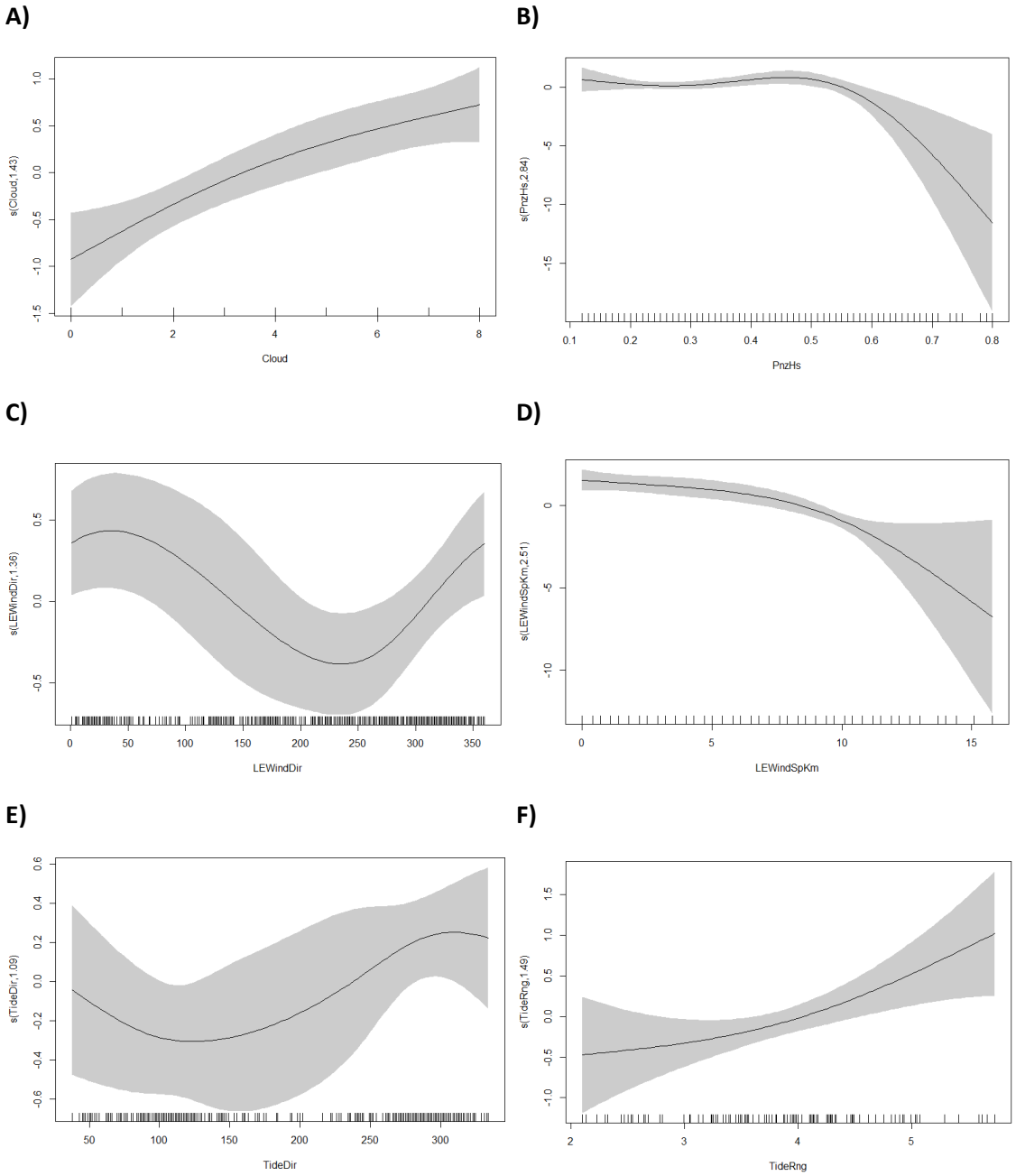

Figure 3.15. Relationships between harbour porpoise occurrence and temporal variables.
As selected by the final binomial GAM (n = 737 samples) A): Cloud (e.d.f. = 1.4), B): Wave height (e.d.f. = 2.84), C): Wind direction (e.d.f. = 1.37), D): Wind speed (e.d.f. = 2.51), E): Tide direction (e.d.f. = 1.09), and F): Tidal range (e.d.f. = 1.49). Results reported on the scale of the linear predictor. Numbers in brackets in y-axis captions are estimated degrees of freedom (e.d.f.) of the smooths. Rug plots at bottom of figures are covariate values. Shaded regions around smooths represent 95% confidence intervals.

3.4 Discussion

At fine-scales (<1 km resolution), questions remains as to how free-ranging marine animals, such as porpoises, preferentially use their habitat in coastal waters (Booth et al., 2013); areas where anthropogenic activites continue to increase (Waggitt & Scott, 2014). Quantifying the interplay between multiple environmental drivers of distribution remains complex but is information urgently required for their appropriate conservation and management (Embling et al., 2010). Dedicated land-based surveys were therefore carried out using a theodolite at a constrained coastal location off the tip of southwest UK to not only build on previous work in the area (see Jones et al., 2014a), but contribute to the knowledge base identifying fine-scale habitat preferences of harbour porpoises within tidally-dominated, complex bathymetric environments.

Generalised additive models (GAMs) were constructed to determine significant environmental controls on the spatio-temporal distribution of this Annex II species, through integration of static bathymetric and persistent hydrographic variables. Across analyses, spatial and temporal clustering behaviours were apparent in the porpoise data, and results were consistent with findings from the conventional visual monitoring survey conducted at the same site in previous years (Jones et al., 2014a). However, precise theodolite mapping enabled novel visual analysis at a very fine-scale (<50 m) and results convincingly indicated the localised influence of tidal-topographic interactions on porpoise distribution that had been hypothesised in Jones et al (2014a).

The extremely fine-scale habitat associations revealed in this study reinforces the utility of a multi-disciplinary approach for determining physical controls on the distribution of highly mobile marine species in the coastal zone. Improved knowledge on habitat use, combined with testing the suite of complementary techniques, have implications for conservation management. Applying a similar suite of methodological tools at other constrained coastal locations (that are amenable to shore-based observations, and where appropriately resolved covariate data exist) may be used to help in the identification and monitoring of SACs for porpoises in the future.

Spatial Distribution

Clustering in the porpoise sightings data was most pronounced at the southern and eastern reef margins (Figure 3.5). Modelled spatial distribution was best explained by depth and slope,

and an interaction between slope and aspect (Figure 3.9), with higher relative densities predicted in areas of deeper water and low slope (<15 °). The use of spatial models to identify habitat preferences is a valid approach that has been previously applied during other studies of harbour porpoises (Skov & Thomsen, 2008; Marubini et al., 2009; Embling et al., 2010; Booth et al., 2013; Mikkelsen et al., 2013; De Boer et al., 2014; Jones et al., 2014a).

To challenge the validity of the core habitat areas determined by the kernel density estimates (Figure 3.5), results were spatially compared to those obtained not only at the same site using different survey methods, but for the same data using a grid-based method with model-predicted densities. Both methods identified similar high density areas at the southern and south-eastern reef margins that extended into deeper water (Figure 3.10). Sveegaard et al. (2011b) also used this approach, comparing results from kernel estimates and gridded analyses, and found them to be in close agreement. The same relative high density areas were highlighted by a previous study in the survey area (Jones et al., 2014a), though results from their analysis and others at different sites (e.g. Bailey & Thompson, 2009) revealed porpoise preference for 'steeply' sloping topography, opposed to 'low' slope found in this study. Though slope was an important predictor on porpoise distribution in both studies, the difference in gradient preferences may be a result of the survey methods. Visual location estimates were underestimating by ~300 m (Figure 2.5), relative to more accurate theodolite locations, thus positioning more sightings directly over the steeper reef edge itself, rather than in the adjacent waters just offshore, where slope values are lower. Even by gridding their sightings data to account for positional error, this underestimation may have affected the reported preference for higher slope values compared to those found in this study. During the gridding process, more sightings may have fallen in cells directly over the reef margins, rather than in those of deeper water with a flatter seafloor. Raum-Suryan (1998) did observe porpoises in areas of low slope, but these were extreme values (<0.5°), associated with deep (>125 m) waters and flat bottom topography.

Results have identified waters adjacent to the reef margin as favoured habitat perhaps due to specific hydrodynamic features that influence prey density and/or availability (Le Fevre, 1986; Franks, 1992b; Jones et al., 2014a), relative to more homogenous offshore waters (Guinet et al., 2001; Scott et al., 2010; Embling et al., 2013; Sharples et al., 2013a). Although prey densities may at times be higher over the shallow reef plateau and directly at the inner reef margin, e.g. within eddies and tide races (Wolanski & Hamner, 1988; Mikkelsen et al., 2013), these highly turbulent zones would require excessive energy expenditure by porpoises. Indeed,

Maravelias (1999) observed that Atlantic herring *Clupea harengus* clusters were located either directly *on* plankton patches or, at their edge, *adjacent* to the paths of strong currents. As a free-ranging species, the harbour porpoise is therefore likely to exploit the moderately turbulent, yet (probably) prey-denser areas around the outer reef margins to effectively increase their prey encounter rates (Sims et al., 2006; Skov & Thomsen, 2008), while utilising the marginally less turbulent areas adjacent to the reef edge itself.

Depth has often been suggested as a significant driver of cetacean distribution (Watts & Gaskin, 1985; Raum-Suryan & Harvey, 1998; Johnston et al., 2005b), with studies reporting porpoise associated with the relatively deeper waters of their home range (Watts & Gaskin, 1985; Goodwin & Speedie, 2008; Booth et al., 2013; Jones et al., 2014a). However, many early studies lacked quantification, only qualitatively linking water depth to the availability of prey (Hastie et al., 2004). Sveegaard et al. (2012b) were the first authors to show a significant correlation between porpoise and herring densities in their spatial analyses of the Norwegian Trench. Porpoise distribution was best explained 'solely' by the distribution of herring, while herring densities were positively related to water depth. Their study was the first demonstration of a direct relationship between porpoises and a specific prey species that was linked to the static covariate, depth.

Temporal Distribution

After compensating for survey effects, porpoise occurrence was best explained by the tidal variables, flow direction and amplitude, which is a proxy for time in the lunar cycle, i.e. springs or neaps. Sightings rates of cetaceans have previously been related to time in the tidal cycle (Mendes et al., 2002; Calderan, 2003; Pierpoint, 2008; Embling et al., 2010; De Boer et al., 2014; Jones et al., 2014a) with distribution in the smaller species, such as porpoises, explained by the association between tides and tidal impact on prey distribution (Mendes et al., 2002; Lopez et al., 2004; Johnston et al., 2005b; Booth et al., 2013).

There was a positive correlation between porpoise sightings and tidal range in this study (Figure 3.15-F), i.e. higher occurrence during spring tides. The increase in sightings during springs may be due to a more concentrated foraging distribution, reflecting changes in behaviour of their fish prey (Embling et al. 2010). During other times in the lunar cycle, i.e. during periods of smaller tidal range, porpoises and prey may be more dispersed (Genin, 2004; Embling et al., 2013). It may therefore be that during springs, high density areas are more

important to resident porpoise populations than at other times, which may help to inform more temporally-managed protected areas for the species.

There was a six-fold increase in the porpoise sightings rate during westward flows in the survey area rather than eastward (Figure 3.13-B), a result supported by the statistical analysis (Figure 3.15-E). The sightings rate accounted for the fact there are approximately seven hours of westward flow in the survey area (during tidal hours HW-6 to HW-2, and HW+3 to HW+6) where tidal currents are strongly deflected by the eastern reef margin and pass around the southern reef margin. Jones et al. (2014a) also found an association between sightings rate and their metric, 'tidal flow group' ('flow group' in this study) at the survey site. The authors reported increased observations during strong westward flows, and fewer during hours HW-2 to HW+3, i.e. slack and eastward flows.

Neither this study or previous work found time in the tidal cycle to be a significant predictor on porpoise occurrence, which suggests that the animals were not responding to time in the tidal cycle *per se*, but rather, current flow direction; this is plausible given the non-typical nature of the tidal flow regime in the survey area (Appendix E). Since there was no correlation between flow speed and flow direction, this provides further evidence it is flow direction and resultant tidal-topographic interactions that influence porpoise distribution temporally, rather than flow speed itself (in the context of the tidal cycle). Further details of the physical oceanography and results of the ADCP survey conducted at the site can be found in Jones et al. (2014a) but, essentially, it seems that it is the relationship between increased shear instability and turbulence that occurs post- the formation of lee waves when the tide reverses from an eastward to westward flow that likely results in increased prey aggregation in areas near the steep-sloping eastern reef edge during these times (which therefore attract higher numbers of porpoises).

Although the model did not retain time of day as a significant covariate affecting absence-presence sightings data, it did appear to influence porpoise abundance, with a higher proportion of animals observed around the hours of midday (Figure 3.13-A). Dolman et al. (2013) also found numbers sighted in their survey in The Minch, northwest Scotland, rose from an early morning low, to a clear peak just after 1100 hrs, which then declined towards 1600 hrs. Diel preferences in porpoise have been recorded in both their surfacing (Otani et al., 1998) and vocalisation (acoustic) behaviours (Todd et al., 2009; Embling et al., 2010; Mikkelsen et al., 2013), although the latter studies of acoustic activity report increased echolocation during the hours of darkness. This is likely due to the diel migratory pattern of fish between deep and

shallow water, which porpoises may follow (Ohizumi et al., 2000), as they are opportunistic feeders with a limited ability to store energy (Koopman et al., 2002). This would explain reports of more recordings in the shallower areas of a survey region at night where data loggers are normally deployed. However, Westgate et al. (1995) only reported two cases of seven animals in which diving behaviour mirrored the migrations of their prey; similarly, Otani et al. (1998) suggested diel patterns of porpoise diving behaviour are not determinate for the species. It therefore seems plausible that porpoises require maximum daylight when visually-orienting towards prey in the dynamic (and acoustically-noisy) reef margin environment but, as it gets darker, periods during which they rely increasingly on their echolocation abilities to forage, they avoid noisy environments. This may explain increased sightings during maximum light at the noisiest areas of the survey site, i.e. the reef margin.

Sightings rate differed between years of survey (39% and 67 % between years 2011-12), which may be a reflection of the comparatively few, randomly spread, survey days relative to an effort-based monitoring programme that collects data on a daily basis, such as that from the SeaWatch SW reported in Jones (2012) and Jones et al. (2014a). Data from this comprehensive survey show relative consistency amongst porpoise occurrence each year, with animals being sighted on 36% of survey days on average, with an annual range of 33-42% over years 2007-10. However, other studies have found considerable inter-annual differences in numbers of cetacean sightings, with four-fold changes in abundance between consecutive years for porpoises (Marubini et al., 2009), and bottlenose dolphins *Tursiops truncatus* (Cañadas & Hammond, 2006). Nevertheless, it is clear from the seven consecutive years of data collected from the Runnel Stone Reef, as presented here and in Jones et al. (2014a), that this site is a consistently important area for harbour porpoises.

Non-spatial variables, such as time in the tidal cycle, did not change the location of the high density areas, as seen in the kernel estimates according to flow direction (Figure 3.7), providing additional confidence in marked preferences of porpoises for waters adjacent to the southern reef margin. The kernels also suggested that animals only use the reef plateau during periods of slack water, which is consistent with Watts and Gaskin (1985) who proposed porpoise avoid highly turbulent flows. Results from ADCP surveys at the site showed that, as tidal flow was pushed up and over the shoaling seabed, there was a notable increase in flow speed over the shallower, topographically-complex reef plateau (Jones et al., 2014a). This may explain why the reef top is only highlighted as a core habitat area during the two hours of slower flow speeds around the site-specific hours of slack tide, i.e. hours of HW-2 and HW+2.

Tidal-topographic Interactions

Precise theodolite mapping techniques provided evidence for spatio-temporal clustering of sightings adjacent to topographic features during westward flows (Figure 3.7). Though the kernel estimates did not indicate a shift in the primary areas of core density at the survey site, during periods of westward flow there were increased sightings (raw data) located near the pinnacles on the reef margin, near to the sand bar and, most notably, around the eastern reef edge where the reef slope inflects (Figure 3.7). These patterns are likely linked to local upwelling events, or physical forcing processes associated with enhanced turbulence (Farmer et al., 1995; Genin, 2004). Strong westward tidal flows are possibly forcing prey species into concentrated patches, especially along the eastern reef edge, which drives porpoise distribution resulting in increased observations in these areas. This is consistent with the explanation by Jones et al. (2014a), based on detailed ADCP data over the reef, that lee waves form along the sloping reef margins, as a result of the influence of bathymetric features on tidal currents, i.e. tidal-topographic interaction. These interactions lead to baroclinic flow, hydraulic jumps and lee waves, which form on the downstream side of a topographic feature (Nash & Moum, 2001), and result in enhanced shear and associated turbulent mixing. These 'lee eddies' may be those depicted in Figure 2.13 (p. 35), labelled as 'tide races' and 'shear boundaries'.

The 'western tide race' is seen around HW+2.5, during site-specific eastward flow (i.e. water flowing into the channel), while the eastern tide races are seen during HW+6, during site-specific westward flows (i.e. flows against the eastern reef edge). It is possible these features visible at the sea surface are therefore a consequence of increased vorticity and flow separation (Jones et al., 2014a). Although there were increased sightings apparently associated with areas of topographic highs during westward flows (Figure 3.15-E), it may be that changes in current direction are influencing the behaviour of porpoises at the surface, which in turn affects their detectability (Marubini et al., 2009). For example, if they are foraging rather than travelling, these different activities are likely to affect their surface behaviours, including time spent at the surface and their potential to be detected. The fact sightings are clustered in concentrated areas during strong flows against the reef edge, suggests the animals were foraging, as they were more likely to be detected. This provides further evidence that during westward flows, prey species are potentially trapped against the steep slopes of the eastern reef edge, which is a process seemingly less likely to occur along the western reef edge, where it is less steep. Therefore, during eastward flows, any influence of tidal-topographic interaction

is assumed to be minimal along this area of reef margin, hence fewer observed sightings. During eastward flows, sightings are restricted to areas just offshore of the largest pinnacles at the southern reef edge (Figure 3.7), which are features probably strongly interacting with tidal flow. The tidal-topographic boundaries identified in this study are likely zones of increased prey density, given increased sightings recorded in these areas, though studies attempting to evidence the mechanistic links between fine-scale physical oceanography and top predator distribution remain few.

Recent work is beginning to demonstrate the previously missing links between the underlying physical processes, such as internal wave activity (Embling et al., 2013; Scott et al., 2013; Sharples et al., 2013a; Sharples et al., 2013b; Jones et al., 2014a), and their interaction with bathymetric features. These interactions are proposed to drive the spatial distribution of zooplankton and their fish predators, which are the prey species of many top predators of conservation interest, e.g. cetaceans and seabirds (Maravelias, 1999; Bertrand et al., 2008; Sveegaard et al., 2011b). Therefore, work in this area is attempting to better explain how underlying physical processes influence the distribution of top predators by quantifying the (often missing) links between physics, zooplankton and fish. Porpoises have been observed preferentially utilising areas within survey regions that contain irregular topographic features, such as gullies, with waters depths between 10 m and 30 m (Calderan, 2003; De Boer et al., 2014). When strong tidal currents flow into these areas, it is hypothesised that restricted channels interrupt the water flow, slowing it down, leading to aggregations of zooplankton in these small-scale convergence zones (Le Fevre, 1986; Franks, 1992b, 1992a).

Furthermore, fish may also take shelter from the strong currents, or become trapped between two dominating tidal flows, possibly explaining higher porpoise occurrence in these areas, which may be intensified by complex topography. In productive areas of small-scale tidal-topographic fronts (Wolanski & Hamner, 1988; Hao et al., 2003; Scott et al., 2010; McPhee-Shaw et al., 2011), it is therefore plausible that porpoise and their prey fish avoid the areas of highest current speeds, where turbulent water is often visible at the sea surface, and instead distribute themselves *adjacent* to the shear zones (Maravelias, 1999). This means they can benefit from higher food availability, while remaining themselves in more favourable habitat conditions, where there is a trade-off between energy expenditure and optimised foraging opportunity (Sims et al., 2006; Witt et al., 2012a). It is possible the animals wait just outside these fast flowing tidal races, scan for prey, and then enter for a short burst to (probably) capture fish (pers. comm. S. Ingram, 2015).

Capes and headlands have been reported as 'anchor-points' (Booth et al., 2013) for upwelling and fronts that lead to potentially higher densities of prey near to these features (Yen, 2004; Scott et al., 2010), which in turn attracts higher trophic level species to the area, such as porpoises. In these localised zones of tidal-topographic interaction, aggregations of prey species are predictable at a range of spatial and temporal scales (Genin 2004; Embling et al. 2013; Sharples et al. 2013a). These habitat-species associations that are both predictable, and spatially-constrained, have important and practical implications for ecosystem-based approaches to marine spatial planning and intelligent MPA management, which is increasingly required (Sveegaard et al., 2011b) by management in the nearshore zone.

Survey Bias

The staged modelling process accounted for survey covariates in the first round of selection to remove survey bias before other habitat/temporal variables were added. They were found to account for 23% (of 26%) of deviation in the temporal data between them (Table 3.6), highlighting their influence on the 'occurrence' or, rather, detectability of porpoises. Wind speed accounted for 14% of deviation. The study site was very exposed to high winds that would affect sea state (see Section 2.4.1). Many studies have shown sea state to negatively impact on the detection of small cetacean species, particularly porpoises (Palka, 1996; Forney, 2000; Embling et al., 2010; Dolman et al., 2013; Jones et al., 2014a). Environmental variables have been shown to explain a higher amount of model deviation in years with good sea states (Forney, 2000; Embling et al., 2010), which means that during poor sea states, associated with reduced sightings, adequately modelling the habitat preferences of porpoise becomes problematic. De Boer et al. (2014), for example, reported a five-fold decrease in the probability detection in a sea state 2, compared to 0. It is clearly imperative that survey conditions are accounted for in visual surveys, particularly abundance estimates.

Conclusions

Currently, no standardised methods for analysing land-based sightings data exist for cetaceans, so direct (quantitative) comparisons between this study and results of previous work, or studies in other areas, may not be possible. Standardising methods of data collection and analysis would be useful for nationwide, accurate comparative studies across species, with associated benefits for management regimes. However, this study has highlighted the utility of the theodolite method, which enabled visual analysis at very fine-scale and thus highlighted the likely influence of localised tidal-topographic interactions, that would otherwise be

impossible for conventional visual monitoring data given the error in the positional estimates of animals' locations. On the other hand, the theodolite method does validate conventional visual monitoring surveys to some extent, as when the sightings data are gridded, similar relative high use areas were revealed. This suggests that if extremely fine-scale (<50 m) habitat associations are not a research objective, then conventional visual survey techniques would be more than adequate to describe overall patterns of habitat use in an area, particularly as they are relatively inexpensive and non-specialised, except that observers must be experienced in detection of target species.

In both cases, i.e. using theodolite or visually-estimated locational data, the complimentary techniques developed in this study reinforce the utility of a coherent set of tools in order to analyse fine-scale patterns of distribution for highly mobile marine species in the nearshore zone. Improved knowledge on the fine-scale environmental drivers of porpoise distribution is urgently required for their management in coastal waters, as not only are populations particularly vulnerable near shore but, given the increasing number of anthropogenic impacts, this information will be increasingly needed for effective EIAs of wet renewables and other proposed marine spatial planning activities. The results presented in this study therefore successfully builds on previous work, contributes to knowledge on this species, and improves understanding of some of the complex interactions between animal distribution and static and dynamic habitat variables.

Chapter 4 Using acoustic detectors to assess fine-scale temporal variations in cetacean activity within a tidally-dominated environment in southwest UK

A B S T R A C T

Questions remain as to how different cetacean species respond to fine-scale (30-minute) temporal drivers of distribution over time, and whether (species-specific) habitat use is variable between sites within a relatively constrained (<14 km^2) spatial area. Three static acoustic data loggers (CPODs) were deployed over consecutive summer/autumn (July-October) periods between 2010-12 at the Runnel Stone Reef off southwest UK. The horseshoe-shaped rocky reef (<20 m water depth) extends ~1.5 km south off the mainland at Gwennap Head, and falls within the recommended Marine Conservation Zone of Land's End (Runnel Stone). Waters in the area are known, regionally-important habitat for a variety of species protected under the EU Habitats Directive, including harbour porpoises *Phocoena phocoena*, bottlenose dolphins *Tursiops truncatus* and common dolphins *Delphinus delphis*.

Acoustic surveys provided continuous subsurface presence information on cetaceans under all weather conditions to test the broader assertion that interaction between tide and topography can influence their fine-scale distribution. Two CPODs were deployed along the Runnel Stone Reef's eastern edge, fully exposed to tidal action: one at the southern reef edge and, the other, in lee of the reef during eastward tidal flows. A third CPOD was deployed nearby, in the gently-sloping sandy bay of Penberth. A total of 15,974 hours of echolocation data were collected between the three CPODs. Analysis of acoustic noise revealed Penberth is less tidally-dominated, whilst noise at the two reef sites is high, and primarily caused by sediment transport that is strongly associated with the tidal cycle.

Generalised additive models (GAMs) were constructed to determine the influence of survey, tidal and temporal variability on acoustic detections; marked differences were found between species. For porpoises, deployment site was significant, so models were constructed for each. Year, month and acoustic noise significantly influenced detections across sites. At Penberth, there was also a strong diel pattern, with increased nocturnal activity, while porpoise presence was negatively correlated with increasing dolphin detections. The influence of tidal hour was different between the two reef sites, with increased detections recorded at one site during eastward flows, where the CPOD was sheltered from tidal currents in lee of the reef. Marked temporal variability in the porpoise data was apparent.

There was a strong diel pattern in dolphin activity across sites, with detections peaking around midnight and decreasing towards early afternoon. Fewer dolphins were recorded approaching spring tides. Though acoustic noise is contributed to by dolphin clicks, increased noise negatively influenced their overall detection. No significant effect of site, year or month was found on dolphin occurrence during the summer-only survey periods, indicating less inter- and intra-annual temporal variability in the species' distribution within the survey area, relative to porpoises, with implications for management.

4.1 Introduction

Harbour porpoises and other cetaceans are observed off the southwest tip of the UK mainland throughout the year (Pikesley et al., 2011), and include species such as bottlenose, common and Risso's *Grampus griseus* dolphin (Leeney et al., 2012; SeaWatch SW, 2014). Risso's are protected under Annex IV of the EC Habitats Directive (92/43/EEC), while porpoises, bottlenose and common dolphins are also listed under Annex II. As species of Community interest, Annex II species require specific measures by Member States for their protection, such as Special Areas of Conservation (SACs). One of the main aims of the Habitats Directive is to 'maintain or restore, at favourable conservation status, natural habitats and species of wild fauna and flora of Community interest' (Article 2.2) by creating a coherent ecological network of protected areas across the EU, known as 'Natura 2000' (see Chapter 1).

The designation of SACs will contribute to this network, so acquiring sufficient scientific evidence on the fine-scale distributions of protected species is vital for management for make informed decisions on site selection. This can be problematic for wide-ranging species, as sites can only be proposed where there are 'clearly identifiable areas…essential for their life and reproduction' (Article 4.1) but the distribution and relative abundance of many listed species remain poorly understood (JNCC, 2009). Additionally, according to European guidance in Annex III, a protected species may only be excluded from consideration from site selection where the 'populations are too small to be naturally viable, or where the species occur only as vagrants', i.e. outside their natural range. It is clearly essential to adequately determine a population's occurrence, or persistence, over time within an area to contribute to the evidence base required for the site selection process.

Acoustic monitoring of small cetaceans

To thoroughly interpret behaviour, feeding ecology and habitat use of cetacean species, visual sightings data collected by land- or boat-based observation teams can be usefully supplemented by acoustic datasets in coastal waters (Pikesley et al., 2011). Visual survey methods typically cover a large spatial area, but only snapshots in time during daylight hours. Continous, long-term data collected from stationary, moored acoustic devices are therefore invaluable for understanding species distributions and behaviour throughout the daily cycle. It is clear that complimentary datasets, combining effort-based visual sightings with acoustic data, are urgently needed to support the conservation and management of vulnerable populations (MacLeod & Zuur, 2005), e.g. Annex II species. This information is particularly

relevant in nearshore (<10 km offshore) environments, where there are increasing requirements to manage anthropogenic activities alongside species and their habitat (Halpern et al., 2008), e.g. marine spatial planning (Merchant et al., 2014; Rodrigues, 2014), offshore renewable energy devices (Todd et al., 2009), and conservation (Mikkelsen et al., 2013). Additionally, entanglement in nets remains a significant problem that has not been resolved (Gannon et al., 2005), which is particularly surprising given the ability of small cetaceans to use echolocation, and vision, to detect and avoid objects in controlled trials (Au, 1993). Furthermore, in most cases, attempts to enhance the acoustic reflectivity of nets to reduce bycatch in the wild have been unsuccessful (Cox & Read, 2004). This highlights the complexity of acoustic behaviours, and the importance of understanding fine-scale habitat use of local cetacean populations that may be environment-specific, i.e. the necessity of interpreting results *in context*.

Autonomous data loggers have been increasingly used over the past decade to detect and record echolocation click data for a variety of highly vocal cetacean species (Sostres Alonso & Nuuttila, 2014), including porpoises (Carlström, 2005; Kastelein et al., 2008; Koschinski et al., 2008 395; Deruiter et al., 2009; Bailey et al., 2010; Kyhn et al., 2012; Mikkelsen et al., 2013; Rodrigues, 2014), dolphins (Au et al., 2007; Philpott et al., 2007; Bailey et al., 2010; Nuuttila et al., 2013; Pirotta et al., 2013; Sostres Alonso & Nuuttila, 2014) and whales (Marques et al., 2009; Marques et al., 2011; Martin et al., 2013). Knowing when and where wide-ranging marine species, such as coastal populations of cetaceans, preferentially spend their time, is challenging (Redfern et al., 2006), as is evaluating the distribution of prey resources (Sveegaard et al., 2012a). However, it is generally assumed that areas of greatest usage by predators reflect higher quality habitat (Bailey & Thompson, 2010; Pirotta et al., 2013), so determining fine-scale temporal preferences will help explain when the animals preferentially visit certain areas within their home range. This is useful for further understanding their ecology, and for informing management of the species and their environment on which they depend (Bailey & Thompson, 2009; Embling et al., 2012), particularly in areas that are persistently used by the animals through time. Indeed, monitoring temporal variation in cetacean distribution has helped identify appropriate sites for marine protected area (MPA) designation (Hooker et al., 2001; Cañadas et al., 2002; Cañadas et al., 2005) and develop management plans within protected areas (Hastie et al., 2004), so the importance of collecting time series, continuous datasets is clear.

Acoustic surveys are particularly useful where assessing habitat use is constrained by the limited availability of fine-scale presence data, such as in low density areas (Kyhn et al., 2012) and for marine species that do not generally meet the assumptions of standard distance sampling, i.e. guaranteed detectability at zero distance from the observation station, *g(0)*, discussed further in Section 3.2.2. Additionally, when carrying out visual surveys, variations in sea state and light conditions can lead to variable, often low, detection probabilities (Buckland et al., 2010), which is compounded by the fact air-breathing marine mammals spend much of their time (~70% for porpoises; Otani et al., 1998) subsurface (Bailey et al., 2010). Therefore, acoustic survey methods not only offer the potential to overcome this problem (Marques et al., 2009; Bailey et al., 2010), but they can collect 24-hour continuous, long-term baseline data at reduced effort, and relatively low cost. The primary considerations that affect deployment and data retrieval are battery life and weather conditions, though the click detectors used in this study, CPODs (Chelonia Ltd, Mousehole, UK), can normally record for extended time periods, e.g. up to months (Chelonia, 2013).

Echolocation in small cetaceans

Toothed cetaceans (odontocetes), such as porpoises and dolphins, produce echolocation click 'trains', or clusters of clicks, i.e. regular sequences of similar events, to communicate, navigate and forage (Verfuß et al., 2009). Porpoises are included in the group that produce narrowband high frequency (NBHF) clicks (>117 kHz) with a peak frequency of ~128 kHz and a mean source level (sound pressure level 1 m from the animal) of 157 dB re 1µPa (Philpott et al., 2007). In contrast, dolphins emit short, broadband echolocation clicks in the range of 100-130 kHz with a mean source level of 220 dB re 1µPa (Au, 1993), though some studies have reported peak frequencies in bottlenose of ~70 kHz (e.g. Dos Santos & Almada, 2004). There are few marine noise sources that have frequency components overlapping with the narrowband high frequencies of porpoise echolocation (Au et al., 2007), initially making them ideal candidates for automatic detection by acoustic data loggers (Philpott et al., 2007). This was only possible later for dolphins, as technology was adapted to identify their low frequency but higher energy, broadband clicks (Dos Santos & Almada, 2004; Philpott et al., 2007). Recognising the clicks produced in trains is therefore a powerful tool to identify the presence of cetaceans in different time periods (Marques et al., 2009; Bailey et al., 2010).

CPODs are self-contained ultrasound monitors that identify and record up to 4GB of selected 'tonal' clicks at a 5-microseconds resolution (Chelonia, 2013). The CPOD-specific SD cards are formatted by the manufacturer (.CHE files) and designed to allow the on-board filtering

mechanism to only select those periods of sounds when a narrow band of frequencies (20-160 kHz) contain more energy than the rest of that frequency range. The data loggers can detect porpoises within a ~300-m radius (Chelonia, 2013), while Philpott et al. (2007) confirmed the CPOD's predecessor, the TPOD, could detect bottlenose dolphins up to distances of 1246 m. Through the application of quality-filtered click train data, a measure of habitat use can be inferred, referred to as 'detection positive minutes' (DPM) or 'time present' (Kyhn et al., 2012).

Cetaceans and acoustic noise in the nearshore marine environment

Echolocating marine mammals are vulnerable to excessive acoustic noise (Kastelein et al., 2005), both naturally-occurring and pollution (e.g. from the development of wet renewables), as sounds outside their frequency range may impact on any prevailing behaviours, such as foraging (Miller & Wahlberg, 2013). Acoustic noise originating from natural sources can therefore be particularly high in tidally-dominated environments (Rodrigues, 2014) where currents interact with sediment and topographic features, e.g. rocky reefs and headlands. This may have implications for vocalising species under certain conditions, such as time in the tidal cycle and/or season. Noise in the coastal environment can also influence cetacean activity generally; rainfall, for example, contributes to high frequency background noise, which can 'irritate' NBHF species like porpoise (Miller & Wahlberg, 2013), causing them to swim rapidly and/or 'porpoise' (break the surface) more often. Significant wave height has also been found to correlate with noise levels in coastal seas (Wenz, 1962).

Echolocating marine mammals therefore have to continually deal with a multitude of unwanted clutter echoes from objects other than their prey, including bottom structures in relatively shallow water. Porpoises overcome this by extracting echoes from the additional noise using their narrow band auditory filters (see Miller & Wahlberg, 2013, for further explanation). Interestingly, Gannon et al. (2005) suggested bottlenose dolphins in fact use their echolocation system sparingly in the wild, as they detect their prey by 'passive listening', and only vocalise to track their target during the pursuit and capture phases. The authors even hypothesised this may be due to the significant energetic, or ecological (e.g. advertising their location to potential prey or competitors), costs of utilising this sensory system. Dolphin echolocation rates have also been found to correlate with pod size, where lone foraging animals produced a variety of sounds at significantly higher rates than animals foraging in groups (Nowacek, 2005).

Temporal variations in cetacean acoustic activity

Analyses of acoustic data have revealed temporal distribution patterns in porpoises, and other cetacean species, however, these appear to be site specific. Todd et al. (2009), for example, found a pronounced diel pattern in porpoise echolocation activity around a North Sea offshore gas installation, with more detections at night than during the day, which the authors linked to foraging behaviour. Their inference was based on the inter-click intervals in the data, which decrease when porpoises target an object (e.g. prey fish) at short (<few metres) distances, relative to when the animals are simply navigating their environment or investigating objects further away (Carlström, 2005; Verfuß et al., 2009). Mikkelsen (2013) also found marked diel patterns in porpoise activity around a re-established stony reef (<18 m water depth) in the northern Kattegat, Denmark, which the authors suggested was due to a new food source occurring at night that was exploited by the porpoises. However, there were increased acoustic detections during the day at the reference site in their study, which was located on a relatively flatter plateau. The authors indicated this reverse pattern in activity between the two sites is likely a response to the diel migratory pattern of fish between deep and shallow water, which may be more pronounced closer to the reef's slopes. They also found the number of daily DPM varied by year, so acknowledged that additional data collection would be required to determine whether these changes were caused by natural variation or a continuing trend. Jones and Sayigh (2002) observed that dolphins have different vocal and activity patterns at different sites and therefore recommend that caution should be used when extrapolating results from one study area to another. This highlights the importance of obtaining site-specific datasets over time within a study area to more fully determine habitat use of local cetacean populations, particularly when protected area designation requires valid, long-term baseline information on their activity.

Previous work and aims of this study

Waters in the study area around the Runnel Stone Reef are a known, regionally-important habitat for a variety of toothed cetaceans (Leeney et al., 2012; SeaWatch SW, 2014), including harbour porpoises, and bottlenose, common and Risso's dolphins, which are frequently observed in the survey area throughout the year (Pikesley et al., 2011). Results from a land-based visual survey (see Chapter 3), carried out at the same site as the acoustic survey, also evidence the diversity of cetacean species visiting these waters (Figure 4.1). Across 404 hours of survey effort over 55 days, during similar years (2011-13) as the CPOD deployments, a total of 1756 surfacing marine mammal locations were recorded with a theodolite; of these, 250

were the same animal, or group of animals. This averages 0.6 sightings-hr^{-1} or 4.5 observations of a surfacing cetacean each day of survey.

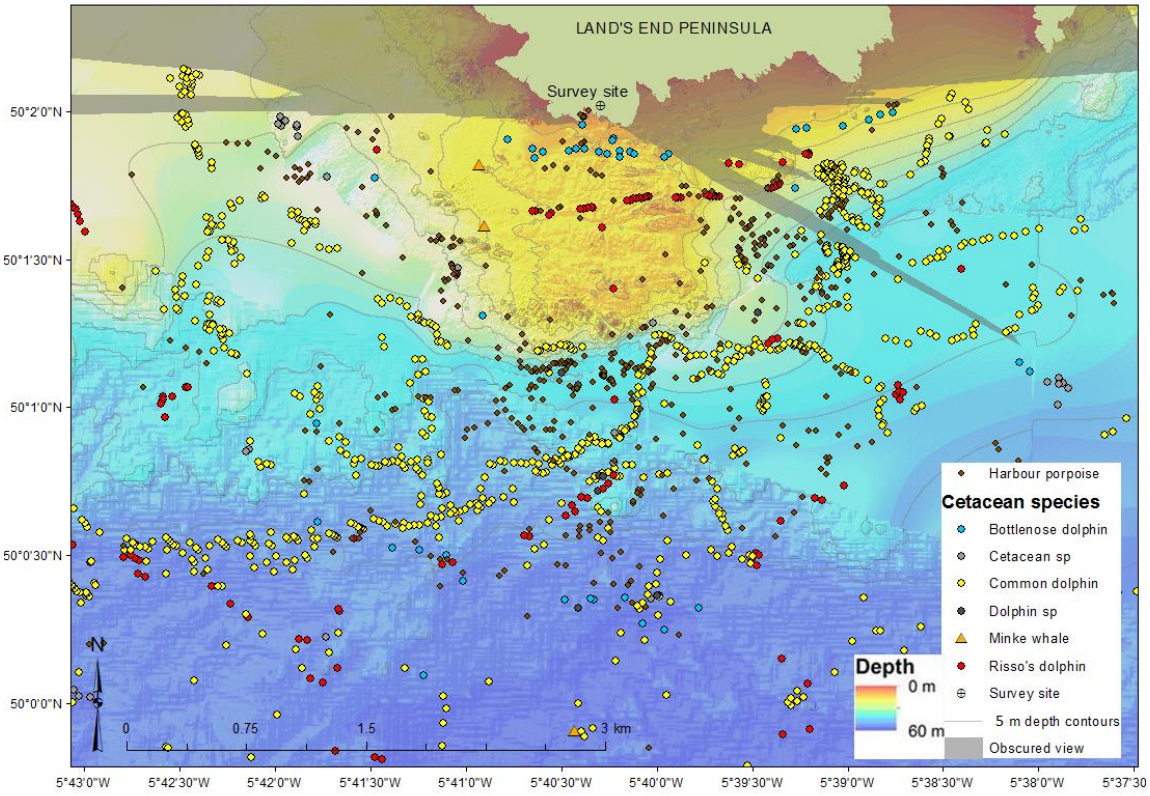

Figure 4.1. Surfacings of multiple cetacean spp. recorded at the Runnel Stone Reef by a theodolite. A visual survey carried out over 55 days across years 2011-2013 recorded accurate cetacean surfacing locations using a theodolite (n = 1756). Locations mapped onto high resolution (1 m) bathymetry data (courtesy of CCO/MCA © Crown copyright) with 5 m depth contours. Visual survey observation team located at survey site 'crosshairs'. Areas of sea surface obscured from view due to land topography are greyed-out.

A previous study deployed three acoustic data loggers at this study site (Jones, 2012) between July and October, 2010. Although only harbour porpoise detections were analysed, the author reported a consistent baseline level of acoustic activity over the survey period. The study showed a strong effect of month on porpoise detections, and also a diel effect, with increased nocturnal activity recorded across sites. However, detections were not corrected for 'effort', i.e. periods during which the CPODs maxed out and stopped recording, nor were detections of other dolphin species considered.

An additional study that aimed to assess the response of cetaceans to acoustic pingers (acoustic deterrent devices) set on gillnets, with the aim of reducing entanglement bycatch

incidents, was also carried out at the Runnel Stone Reef over a 12-month period between April 2009-10 (Hardy et al., 2012). The study focused solely on CPOD-recorded porpoise detections, as only 170 minutes of dolphin encounters were logged by the detectors, though the authors noted these were likely bottlenose or common (Hardy et al., 2012). The trial revealed the pingers had a much reduced effect on porpoise detections at the noisier Runnel Stone Reef site, compared to the quiet site in their study, which was attributed to higher levels of ambient noise associated with strong tides in the area. No further analysis of their porpoise data in relation to temporal variables has been published.

The overall aim of this study was therefore to measure acoustic activity of porpoises and dolphins in a tidally-dominated, topographically-complex environment around the Runnel Stone Reef. Comparing acoustic activity, and a range of tidal and temporal variables, between two closely-located sites (~1 km apart) along the rocky reef margin with activity at a 'control' site nearby (~3 km away), selected for its very different habitat (i.e. a sandy, gently sloping, tidally-sheltered bay), will determine small-scale temporal preferences. CPOD sites located on both the southern and eastern reef margins were selected to reveal whether there were any temporal differences in acoustic behaviour between the study site's two highest-density areas for porpoises (based on visual sightings data collected from a land-based observation station; see Section 3.3.2). Results are interpreted in light of high resolution (1-m) bathymetry data and radar-derived hourly tidal flow metrics (see Section 2.3).

This chapter has three main aims: 1) determine and compare fine-scale temporal variations in acoustic activity of dolphins and porpoises in a high energy environment within a recommended Marine Conservation Zone, relative to a sheltered 'control' site; 2) compare results from the acoustic dataset with visual sightings data collected by a land-based survey (reported in Chapter 3) to enable discussion on the same species at the same location but with data collected by different survey methods, i.e. visual vs. acoustic; and 3) use a multi-year acoustic dataset (and more reliable, sensitive processing software) to test the hypotheses proposed by Jones (2012) that porpoises exhibit strong diel patterns of acoustic activity, and that detection variability is linked to month, while the relationship with time in the tidal cycle is specific to deployment site.

4.2 Methods

4.2.1 Acoustic Data Collection

Three CPODs (Chelonia Ltd) were used to detect and record echolocation click train data around the Runnel Stone Reef in the period July-Oct, 2010-12. The CPODs were deployed in the same location each year to build on, and compare, results from previous work (Jones, 2012) (Figure 4.2).

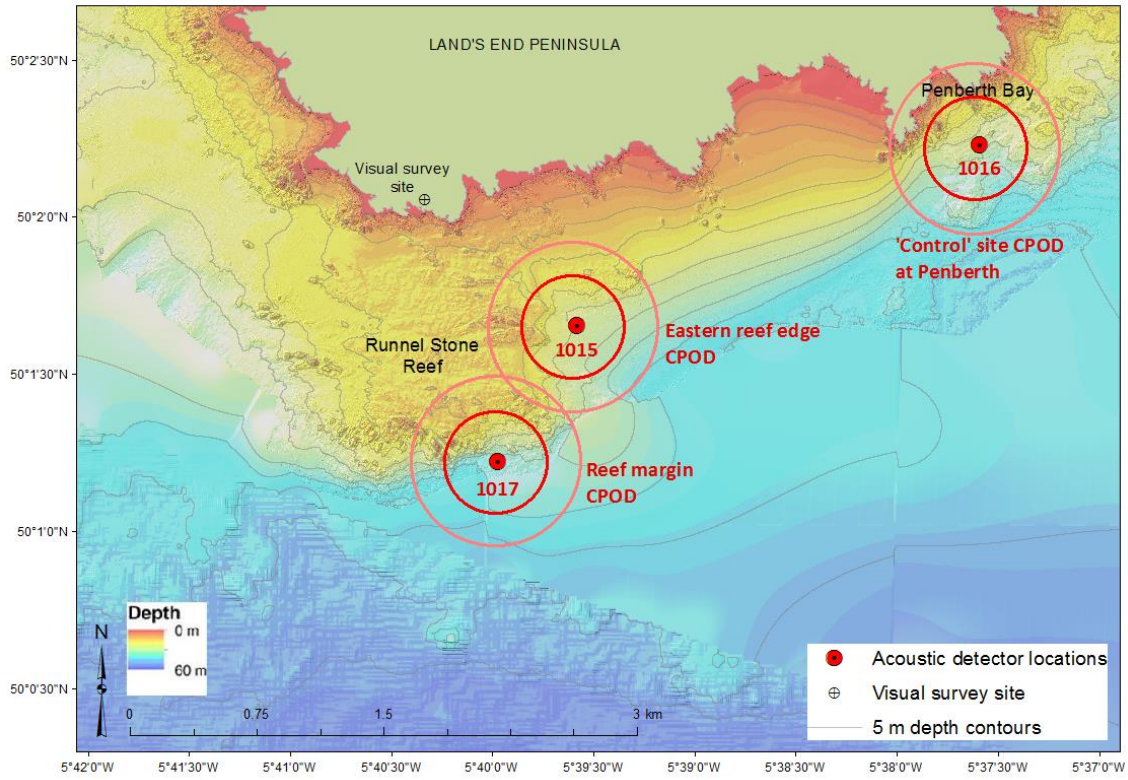

Figure 4.2. Acoustic detector (CPOD) deployment locations at the Runnel Stone Reef study site. Three detectors were deployed in the survey area: CPOD 1015 at the eastern reef edge, CPOD 1016 at Penberth, and CPOD 1017 at the southern reef margin. Detectors collected continuous daily acoustic data during July-Oct 2010-12. Red dots mark deployment locations; circles represent approximate 300-m and 500-m detection radii (for porpoise and other cetaceans, respectively). High resolution (1 m) bathymetry data (courtesy of CCO/MCA © Crown copyright) with 5 m depth contours.

Two CPODs were deployed along the Runnel Stone Reef margin, 1 km apart but associated with different bathymetric habitats (e.g. aspect), while the third device was deployed at a sheltered 'control' site, 3.5 km away from the reef (Figure 4.2). CPOD 1015 was anchored at the eastern reef edge on a sloping area of reef margin in 30 m water depth. CPOD 1017 was

deployed at the southern reef margin in 41 m water depth, near to the upstanding rocky pinnacle of the Runnel Stone. The third detector, CPOD 1016 was moored in 33 m water depth at a control site off Penberth Bay, characterised by a gently sloping, sandy substrate.

Figure 4.3. Fisherman, Ted Chappell, deploying an acoustic detector at the Runnel Stone reef edge. Acoustic data loggers (CPODs) were attached with a surface buoy to a modified, lobster pot mooring line and 35 kg of iron chain. (Photograph © A Jones 2010).

Prior to deployment, the CPOD batteries and timer were set, and internal memory cards inserted to collect data on time, duration and click characteristics. The CPODs were deployed by Mr Ted Chappell, an experienced local fisherman operating out of Penberth, using approximately 35 kg of iron chain attached to a modified, lobster pot mooring line running through the centre of the instrument with a small, surface buoy at the end (Figure 4.3). In a tidal stream, the forces on the upper and lower halves of the CPOD are balanced, so the lighter, hydrophone end necessarily floats upwards. The moorings were designed for the detectors to float several metres off the seabed to minimise any effects on data quality from the 'noisy' sea surface, often noted as a source of tonal ultrasound from rain and breaking waves, and to avoid noise from saltating sediment at the seabed (Chelonia, 2013).

4.2.2 Raw Data Processing and Validation

Data were extracted and processed using the manufacturer's dedicated software, CPOD.exe v. 2.043 (Chelonia, 2013), which carries out objective, automated analyses to find click trains in the data. Using the GENENC encounter classifier, which automatically selects the Quality filters when a particular species is checked, the software identifies those clicks produced by: 1) NBHF species (of which porpoises are the only ones in UK waters); 2) "Other cet" species (non-NBHF toothed whales, except for sperm whales), i.e. dolphins; and 3) "Sonar".

The GENENC encounter classifier was selected as an improved algorithm over the earlier KERNOW classifier (used for analysis in Jones 2012), as it considers a wider time span, which generates more reliable results in difficult situations, e.g. where some dolphins are classified as NBHF species (thereby reducing false NBHF positives), and/or where some porpoises are classified as other cetaceans, during periods of strong background noise, for example (thus reducing false NBHF negatives). The GENENC classifier is also useful where NBHF species occur with substantial sediment transport noise, which can be particularly problematic in tidally-dominated high energy environments. (For further information on how the encounter classifier discriminates between and identifies different cetacean species, see Chelonia's website; Chelonia, 2013).

To investigate sediment transport noise, the "Detections and Environment" noise level measurement export option was used (see 'Noise' auto-correlation functions in Section 4.3.1, Acoustic Environment). Sediment transport-generated noise is at the mid to low end of the NBHF frequency range, and can be so intense it saturates the data buffer quickly, which is set at 4096 clicks per minute (Chelonia, 2013), thus preventing the CPOD from detecting any additional click trains. This is problematic in terms of sampling effort, i.e. increased "%TimeLost" values per minute of data, as observed during data processing, where cetacean species go undetected. This is particularly relevant at sites with high tidal flow rates, e.g. the Runnel Stone Reef, especially during the 'noisier' spring phase of the tidal cycle (Figure 4.4). The spring phase is clearly reflected in the middle portion of the 19-day sub-sample, where increased acoustic noise is represented by the solid black line in the lower panel.

Filtered acoustic data in the upper panel (Figure 4.4) showed more cetaceans were detected by the software during neap tides, and fewer during springs, where noise levels were high and cetacean detection was low. Elevated noise levels impair cetacean identification, as they not only mask initial click detection but also subsequent train detection (Chelonia, 2013); high

levels of background noise can therefore make filtered data interpretation problematic. Though fewer click train data were detected during periods of high noise, it may be a consequence of three scenarios: animals were 1) truly absent during these periods; 2) they simply did not echolocate; or 3) true cetacean-sourced activity could not be detected, i.e. issues of 'false negatives'. It is clear that determining sources of marine noise at specific marine sites may therefore be highly relevant to better understanding the fine-scale spatial behaviours, and temporal acoustic activity, of cetacean species between CPOD locations.

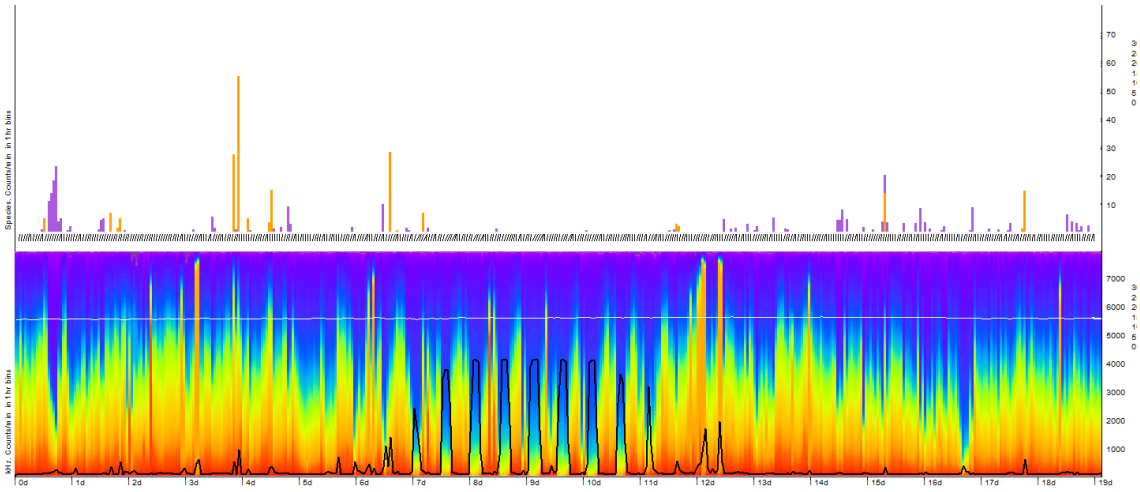

Figure 4.4. Screen shot during data processing using CPOD.exe (Chelonia, 2013).
Panels show a 19-day subset of data from the eastern Runnel Stone reef edge data logger (CPOD 1015) in 2011. Lower panel shows raw acoustic data; solid black line represents mean numbers of tonal, high frequency ultrasound clicks per minute. Spring phase of tidal cycle is clearly reflected in middle portion of this acoustic subsample where black line flattens during periods of data overload. Upper panel shows filtered click train data using GENENC classifier; purple bars = porpoise, orange bars = other cetacean species.

Increased sonar frequency detections, including ADCP, can also cause a decline in porpoise detection positive minutes, as they make pulse trains at porpoise frequencies (Chelonia, 2013). Sonars produce 'blocks' of single colour when their narrowband emissions dominate the sound spectrum, so it is difficult to reliably identify the click trains of NBHF species. This means the CPOD may not be able to detect dolphins or porpoises in a high noise environment, such as high volume sonar clicks or high tidal sediment noise, and/or the detectors may simply max out and stop recording on reaching the maximum number of clicks (pers. comm. N. Tregenza, 2014).

4.2.3 Data Filtering

CPOD data were filtered in the following ways: 1) removing any hours that had not logged a full 60-minute period ("MinsON"); 2) cropping data files by year, so that for each annual survey period, the dates and times matched between between the detectors at each site; and 3) from the filtered and cropped dataset, *either* a) only retaining for analysis those hours in which the CPODs had not maxed out (i.e. those hours with 0 %TimeLost), *or* b) correcting sampling effort for any hours in which the CPODs had maxed out by calculating a corrected, detection positive minute value (cDPM) per hour, following:

$$cDPM\ per\ hour = \frac{DPM\ per\ hour}{\%TimeLost\ as\ a\ decimal}$$

So, if the CPOD topped out after 30 minutes (i.e. 50 %TimeLost), the DPM for that hour was doubled. Corrections on DPM were based on the assumption that the number of detections per hour of data was constant across that hour.

Table 4.1. Summary of acoustic data logger detection data.
Acoustic data loggers (CPODs) were deployed at three sites in the region of the Runnel Stone Reef during July-Oct 2010-12. (Abbreviations: HP = harbour porpoise; Cet = other cetaceans, i.e. dolphins; cDPM = 'corrected' Detection Positive Minutes). No data at Penberth in 2012.

Year	Start date (Time GMT)	End date (Time GMT)	Survey days (full hours)	Site	HP cDPM	Cet cDPM	HP DPM only 0% TimeLost (data loss)	Cet DPM only 0% TimeLost (data loss)
2010	18/08 (11:00)	13/10 (12:00)	56 (1345)	Eastern	382	182	332 (-13%)	51 (-72%)
				Margin	830	213	813 (-2%)	115 (-46%)
				Penberth	654	321	619 (-5%)	149 (-54%)
2011	04/07 (06:00)	09/10 (08:00)	98 (2328)	Eastern	2649	592	2160 (-18%)	176 (-70%)
				Margin	1615	380	1523 (- 6%)	195 (-49%)
				Penberth	3367	515	3282 (-3%)	231 (-55%)
2012	15/07 (07:00)	30/10 (10:00)	106 (2570)	Eastern	5238	547	4501 (-14%)	357 (-35%)
				Margin	2887	456	2759 (-4%)	257 (-44%)
			Total:		(20,828)	17,622	3,206	
			% by	species:		85%	15%	

Table 4.1 provides information on data loss between porpoise (HP) and other dolphin species (Cet) if only 0 %TimeLost hours were retained, i.e. simply excluding data where topping out had occurred (final two columns), rather than correcting DPM according to sampling effort

("cDPM"), as presented in the preceding two columns. Since removing %TimeLost data excluded a lot of dolphins, it is likely it was the dolphin sonar that caused the CPODs to top out (also see Appendix J.1, which provides frequency density histograms of DPM by hour of the day, and how the observed patterns changed dependent on the value of %TimeLost selected as the threshold value to exclude data). Compensating for sampling effort each hour, and using calculated cDPM in the analyses, was considered more viable than altogether excluding hours that contained topped out minutes, as this would exclude all the periods during which the CPODs were overloaded, and exclude potentially important data.

4.2.4 Data Processing

Hourly time series objects ('ts') were created in R (R Development Core Team, 2012) on the cDPM dataset for each species (porpoises and dolphins), at each site, and each year of survey.

Time series objects were also created on the hourly totals of unfiltered clicks (i.e. all acoustic noise: "Nall") at each CPOD site each year of survey. 'Nall' is a useful index of acoustic noise and detections were extracted during data processing in CPOD.exe from the CP1 files (see Chelonia 2013 for further details on the manufacturer-specific CPOD data files).

Using the auto-correlation 'acf' function in R, ACF plots of the hourly time series were calculated, using a maximum lag ('lag.max') of 50 hours to show association with smaller timescales over the survey period, i.e. tidal and/or diurnal, and extended to 700 hours (~55 days) to show association with two spring-neap cycles.

4.2.5 Statistical Modelling

Using the 'mgcv' package in R (Wood, 2006a), generalised additive models (GAMs) were constructed to model temporal patterns in the acoustic data, according to the general structure specified by Hastie and Tibshirani (1999). GAMs are useful where the relationship between the response and a continuous variable exhibits a complicated shape, i.e. where it cannot be specified by an explicit functional form (Crawley, 2012), e.g. linear or quadratic. Rather, non-parametric 'smoothers' are used to describe the data and fitted during model selection. Collinearity between candidate predictor variables may affect estimation of both the model's standard errors and associated p values, so was investigated prior to running the models using Spearman's pairwise rank correlation tests. If correlation coefficients revealed strong collinearity between variables, using $r \geq 0.8$ as the threshold (Zuur et al., 2009; De Boer

et al., 2014; Jones et al., 2014a), only one or other of the collinear terms was retained in further analysis, depending on which was retained first in the model selection process, as described below.

The response variable used in both the porpoise and dolphin acoustic models, was the presence or absence of detections per hour. A GAM with a binomial error distribution ("family = binomial") was therefore specified as the model structure with a logit-link function (Marques et al., 2009). Converting the response into positive or negative detection periods was considered more sensible than modelling the number of cDPM per hour, as it would not only reduce the effect of possible false negatives or positives, but also the total number of clicks may have been produced (echoed) by a single animal, i.e. the absolute number of clicks are not likely representative of density within the sensed areas of the detectors.

Default thin plate regression splines (bs = "tp") were specified for all non-cyclic variables, as they allow a smooth function to be fitted to noisy data with multiple explanatory variables without the requirement of knowing where the different splines join, i.e. the "knots" (Wood, 2006b). Cyclic smoothers (bs = "cc") were specified for metrics whose first and last values are adjacent, i.e. covariates with degrees or hours as units where 359° and 0°, or 23-hrs and 0-hrs, are next to each other, for example.

The maximum degrees of freedom ("k") for each smooth were manually limited to 4 for most covariates to prevent model over-fitting and to minimise excessive flexibility (Embling et al., 2010). Tidal variables were limited by k = 6 to allow for expected sinusoidal relationships with the response (acoustic detections). To reduce model over-fitting in the automatic parameter smoothing process, the penalty ("gamma") given to each degree of freedom was increased from the default of 1 to 1.4 (Wood, 2006b).

Akaike's AIC score ('An Information Criterion') is a measure of a model's efficiency in explaining the data (i.e. model simplicity vs. model fit). AIC is negatively affected by the number of parameters included in a model, so helps to determine whether additional parameters are justified (Crawley, 2012). The best performing model of significant terms is that which gives the best 'fit' in terms of lowest residual deviance, and lowest AIC score. Using a manual, step-wise forward approach (adding variables iteratively at each stage), according to the selection criteria detailed in the paragraph below, models were built as a function of the explanatory variables. For the temporal models (listed in Table 4.5 on page 125), survey variables (site, wave height, wave direction, and acoustic noise "Nall") were added first. Tidal variables (tide

direction, tide speed, tide height, tidal range, tidal hour, tidal flow group) were added second, and temporal variables (year, month, hour; and dolphin cDPM for the porpoise models) added last.

First, individual GAMs were run for each of the predictor variables. The significant variable with the best AIC was then selected as the first term to be included in the model. Second, other variables were added iteratively, as a second term in the GAM, and the combination of significant variables with the best AIC was then used in the next round of selection. Variables were only selected if they were significant ($p < 0.05$), added explanatory power to the model, i.e. ≥1% increase on the previous model to 'deviance' in the data, and had a lower AIC score of at least 2, compared to the previous model, as recommended by Burnham and Anderson (2002). Third, remaining variables were added iteratively to the first two significant terms, and this process repeated until no further covariates could be added, according to the criteria specified.

4.3 Results

After cropping the CPOD data files by matching the hours of survey effort each year, retaining only complete hours of data collection, i.e. 60 "MinsOn" per hour, and correcting DPM by "%TimeLost" (i.e. the sampling effort per hour caused by memory overload), the final dataset comprised a total of 16,159 hours (674 days) of acoustic data collected by three data loggers over 260 separate days across years 2010-12 (Table 4.1). The number of survey days varied by year with 56 days in 2010, 98 in 2011, and 106 in 2012. The control site CPOD at Penberth did not record in 2012, so there are no data.

Across 404 hours of visual survey at a watch point monitoring waters around the Runnel Stone Reef, 1756 individual theodolite fixes of mixed cetacean species were recorded, of which 250 were individual "Sighting IDs", which denoted the same animal or group of animals (see 3.2.1 on page 54 for further details on Sighting ID allocation). Harbour porpoise comprised 66% of the total visual dataset (n = 165 IDs). Of the other cetacean species (n = 85), common dolphin were the most frequently observed (48%), followed by Risso's (17%) and bottlenose (12%). Other dolphin sightings are given in Table 4.2.

Table 4.2. Cetacean sightings recorded at the Runnel Stone Reef during visual surveys.
A visual survey monitoring waters around the acoustic data logger (CPOD) deployment locations collected position data on all cetacean species, including harbour porpoise, using a theodolite (n = 1756) over 55 days between years 2011-13.

Cetacean species	Individual theodolite surfacing locations	Number of Sighting IDs	Proportion of total visual dataset, n = 250	Proportion of visual dataset of 'other dolphins', n = 85
Harbour porpoise	*469*	*165*	*66%*	--
Common dolphin	1003	41	16%	48%
Risso's dolphin	186	14	6%	17%
Bottlenose dolphin	46	10	4%	12%
Unidentified cetacean spp.	29	11	4%	13%
Unidentified dolphin spp.	16	5	2%	6%
Minke whale	7	4	2%	5%

The acoustic dataset (Table 4.1 on page 109) shows a broadly similar proportion of recordings attributed to each group of cetaceans (porpoises = 85% of the total DPM; dolphins = 15%) as the visual sightings dataset (66% porpoise to 34% dolphins). Of the dolphin species, almost half of sightings were of common dolphins (Table 4.2), meaning only ~7% of detections were likely to be species other than porpoises and common dolphins.

4.3.1 Acoustic Environment

In a tidally-dominated environment, unfiltered clicks ("Nall") exported from the CP1 data files represent acoustic noise caused by sediment transport. To investigate the sediment transport-noise relationship with the tidal cycle at each site, i.e. site-specific 'sediment signatures', auto-correlations functions on the unfiltered clicks were calculated, shown in Figure 4.5.

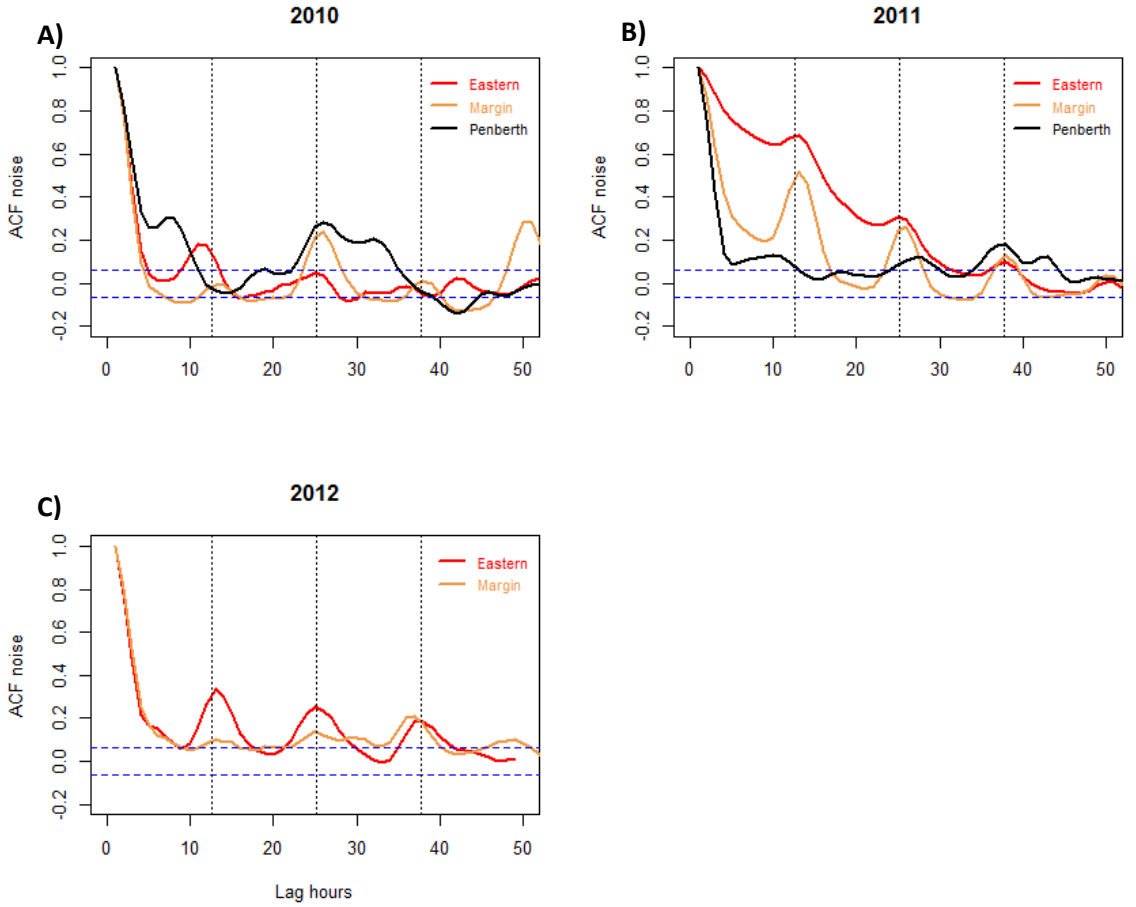

Figure 4.5. Tidal cycle auto-correlation functions (ACFs) of acoustic noise for each CPOD by year. ACFs on total unfiltered clicks ("Nall": 'noise all') extracted from the CP1 files for each CPOD, as an index of noise levels, for years A): 2010, B): 2011, and C): 2012. Red line = eastern reef edge; orange line = reef margin; black line = Penberth 'control' site. Dashed blue lines represent significance thresholds; points outside them are 95% likely to indicate true temporal correlation between the values (hours) separated by the time difference ("lag-hours"). Dotted black lines placed every 12.6 hours represent HW's of the semi-diurnal tidal cycle at the study site. Time lag extends to 50 lag-hours to encompass noise auto-correlation at each site over two full tidal cycles. No data collected at Penberth in 2012.

At the two reef sites, there was clear ebb and flood tide asymmetry, with significant auto-correlations every ~12.4 hours (i.e. synchronicity with time in the tidal cycle), though these observations vary across years (Figure 4.5). The strongest correlations ('sediment signatures') appeared where the curves are most pronounced, arguably, during 2011 (Figure 4.5-B) where the eastern CPOD recorded particularly high noise levels, though this may be due to a period of rough sea lasting two or three days, which is reflected in the tidal ACF (pers. comm. N. Tregenza, 2014). When the number of lag-hours used in the ACF was extended (Figure 4.6), the correlation became significantly negative, as the time differences increased, until the offset data were at the opposite tidal phase, i.e. springs and neaps.

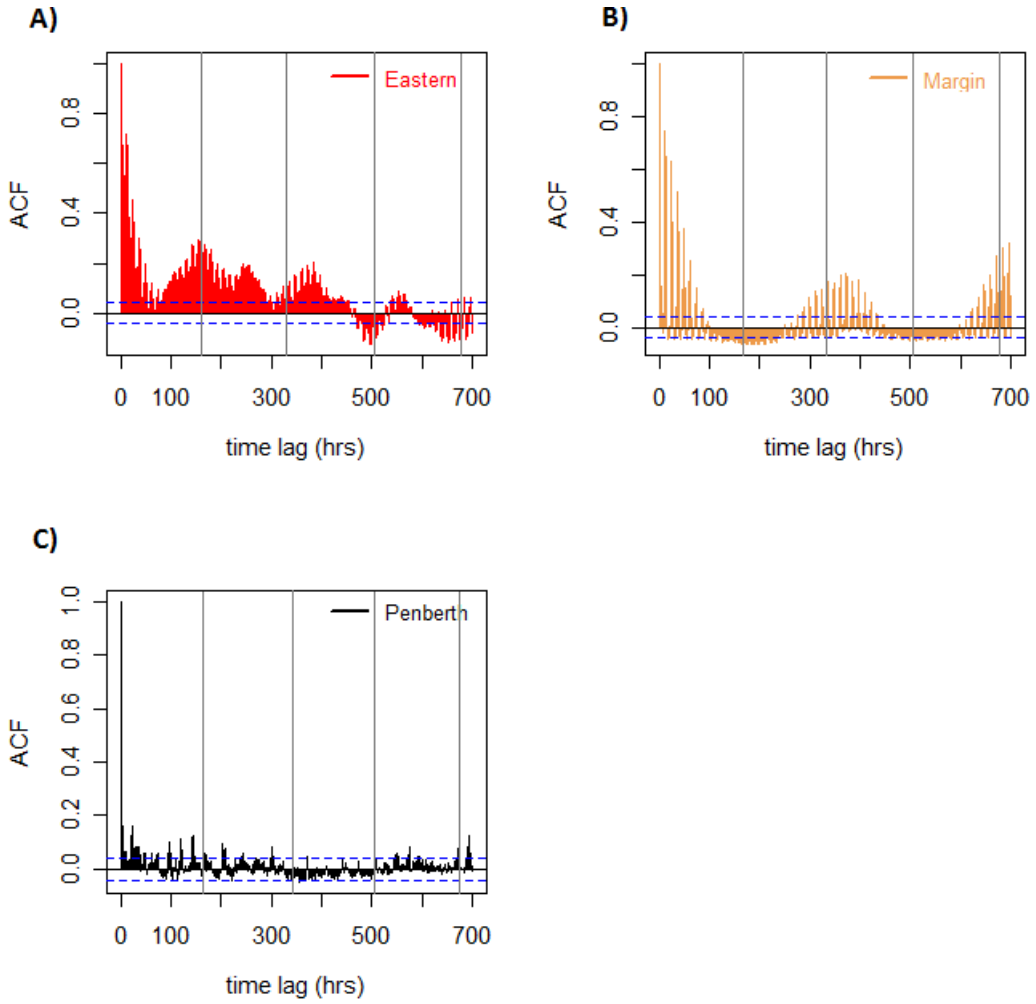

Figure 4.6. Spring-neap cycle auto-correlation functions of acoustic noise for each CPOD, 2011. Auto-correlation funcitons (ACFs) on total unfiltered clicks ("Nall") extracted from the CP1 files, as an index of noise levels, calculated per site, A): eastern reef edge (red line), B): reef margin (orange line), and C): Penberth 'control' site (black line). Dashed blue lines represent significance thresholds; points outside them are 95% likely to indicate true temporal correlation between the values (hours) separated by the time difference ("lag-hours"). Time lag extends to 700 lag-hours (~29 days) to encompass noise auto-correlation at each site within an entire lunar (spring-neap) cycle. Grey lines placed every 168 hours (~7 days) represent approximate occurrences of alternate spring and neap tides.

Figure 4.6 demonstrates the influence of the lunar cycle on acoustic noise/sediment transport at each CPOD location, using 2011 data as an example, as sediment signatures in that year were strongest. The lunar cycle (tidal range) appeared to have the least influence at Penberth (Figure 4.6-C), which is relatively sheltered from tidal streams, compared to the reef sites. The influence of spring and neap tides is most obvious at the reef margin (Figure 4.6-B), which is fully exposed to prevailing tidal currents (east to west orientation across the survey area) and less impacted by any tidal-topographic interactions during certain flow directions. This latter scenario is more likely the case at the reef edge (see ADCP results in Jones et al., 2014a,

Appendix A), where the lunar/tidal range influence on acoustic noise (sediment transport) was more complex (Figure 4.6-A).

4.3.2 Harbour Porpoises

There was considerable inter-annual and inter-site variability in the acoustic porpoise data, shown in Table 4.3. The largest range of detection positive hours (DPH) were recorded at the eastern reef edge and varied from 6% (2010) to 29% (2012). The proportion of detection positive days ranged between 64% (2010) and 98% (2012), with both values recorded at the eastern reef edge. In 2010, at the reef margin, there was 13% DPH, while at Penberth there was only 7% DPH. The following year, however, there was no difference between sites (17% DPH).

Table 4.3. Harbour porpoise acoustic detection data in the Runnel Stone Reef study area.
Acoustic data loggers (CPODs) deployed at three sites collected data over three summer periods between 2010-12. Abbreviations: HP = harbour porpoise; cDPM = 'corrected' Detection Positive Minutes. No data collected at Penberth in 2012.

Year	Site	Survey days (full hours)	Detection positive days (%)	Detection positive hours (%)	HP cDPM
2010	Eastern	56 (1345)	36 (64%)	85 (6%)	382
	Margin		45 (80%)	170 (13%)	830
	Penberth		42 (75%)	98 (7%)	654
2011	Eastern	98 (2328)	85 (87%)	423 (18%)	2649
	Margin		93 (95%)	385 (17%)	1615
	Penberth		87 (89%)	395 (17%)	3367
2012	Eastern	106 (2570)	104 (98%)	743 (29%)	5238
	Margin		102 (96%)	624 (24%)	2887

Summary data in Table 4.4 show considerable variability in acoustic activity between sites, which increases over increasing timescales. The average cDPM per hour ranged from 0.9 at the southern reef margin (near the southern pinnacles) to a high of 1.3 at the eastern reef edge. Over a 24-hour period, the southern reef margin recorded the lowest average cDPM of 20.5, the sandy bay at Penberth averaged 26.1, while the highest number of detections were, again, at the eastern reef edge (31.8 cDPM per day). However, Penberth recorded the highest porpoise DPH over a 24-hour period, averaging 8.9 hours, the reef margin site averaged 4.6 DPH, while the lowest was at the eastern reef edge, with only 1.4 DPH. These results show

porpoise were detected at the eastern reef edge less frequently than at the other sites (<6% of the day) but, when they did visit, they echolocated intensively (highest average cDPM per hour and per day). Conversely, though porpoise spent more hours of the day at Penberth (~40%), the animals did not echolocate intensively whilst at this site, particularly compared to the eastern reef edge (where there was ~30% more DPM per day). The number of positive hours does not necessarily relate to the total number of positive minutes per day at any given location, i.e. detection occurrence is not related to frequency.

Table 4.4. Harbour porpoise acoustic detection data summarised by site.
Acoustic data loggers (CPODs) deployed at three sites in the Runnel Stone Reef survey area collected data over three summer periods between 2010-12. Abbreviations: cDPM = 'corrected' Detection Positive Minutes; DPH = Detection Positive Hours, s.d. = standard deviation. Data is pooled by site across years. No data collected at Penberth in 2012.

Site	Survey days (full hours)	Average cDPM per hour (s.d.)	Average cDPM per day	Average DPH per day	% DPH per day
Eastern	260 (6243)	1.3 (4.2)	31.8	1.4	5.7
Margin	260 (6243)	0.9 (2.6)	20.5	4.6	19.3
Penberth	154 (3673)	1.1 (4.4)	26.1	8.9	37.2

Daily time series of porpiose cDPM at each site across years show a consistent baseline level of acoustic activity (Figure 4.7). However, there was considerable inter-annual and intra-site variation with higher, more frequent peaks in activity each subsequent year. In 2010 (Figure 4.7-A), there was a low level of detection acrosss sites, which, by 2012 (Figure 4.7-C), had increased to frequent high peaks, with observable maximums occurring at the eastern reef edge. Importantly, there were concurrent peaks and troughs in activity at two or three sites throughout the survey period (Figure 4.7).

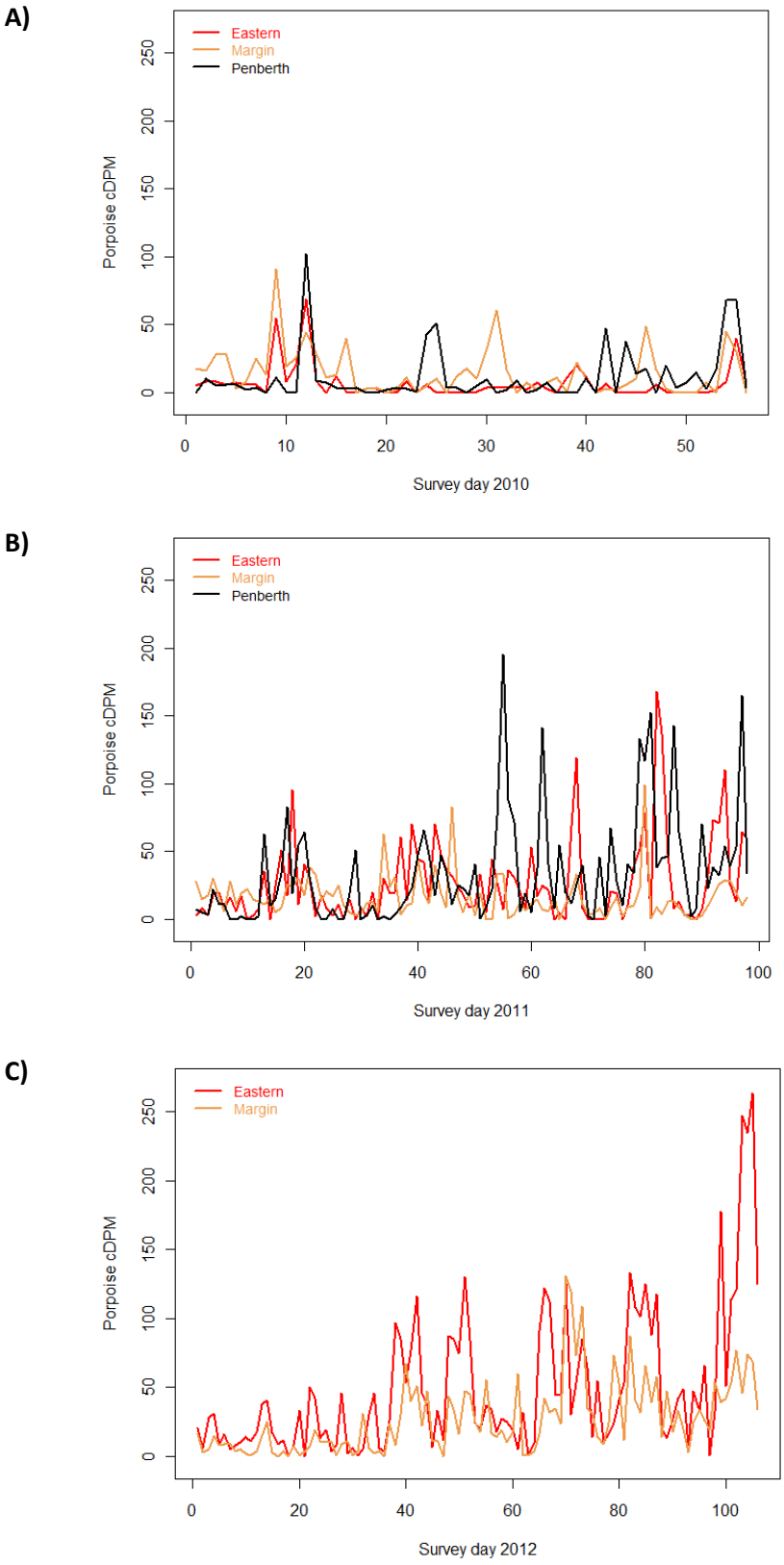

Figure 4.7. Harbour porpoise corrected Detection Positive Minutes (cDPM) per survey day, per year. Acoustic data loggers (CPODs) deployed at three sites collected data during three summer periods across years A): 2010 (n = 56 days), B): 2011 (n = 98 days), and C): 2012 (n = 106 days). Time series show consistent, though variable, baseline levels of acoustic activity across sites and years. Red line = eastern reef edge; orange line = reef margin; black line = Penberth. No data collected at Penberth in 2012.

There was a notable day-night split in the proportion of cDPM by hour of the day in years 2010 and 2011 across all three CPOD locations (Figure 4.8, Figure 4.9, Figure 4.10) which was not apparent in the 2012 data recorded at the two reef sites (Figure 4.8-C and Figure 4.9-C).

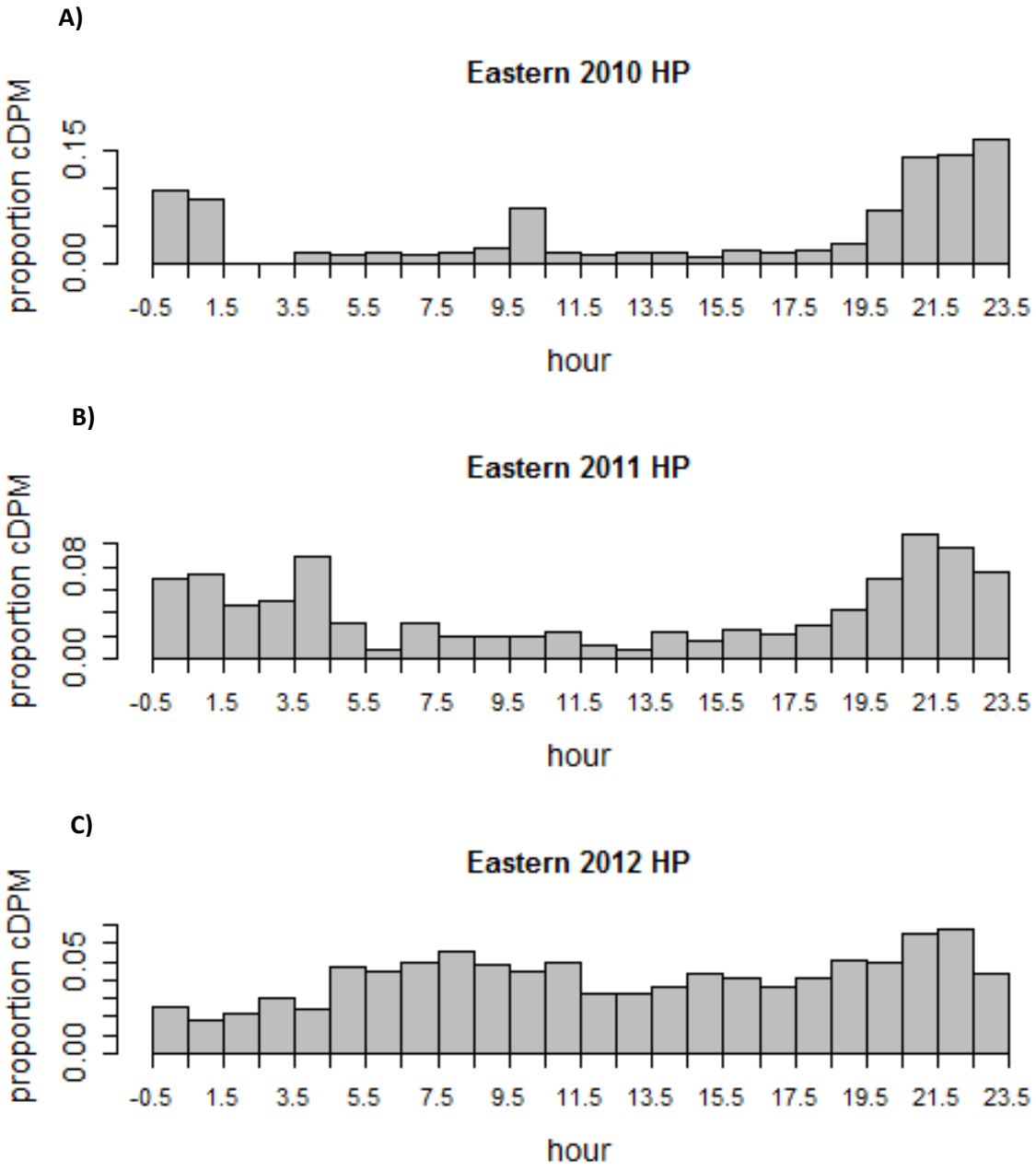

Figure 4.8. Frequency density distributions of harbour porpoise cDPM at the eastern reef edge. Acoustic data loggers (CPODs) deployed at the eastern reef edge collected data over three summer periods across years A): 2010 (n = 56 days), B): 2011 (n = 98 days), and C): 2012 (n = 106 days). Abbreviations: cDPM = 'corrected' Detection Positive Minutes; HP = harbour porpoise.

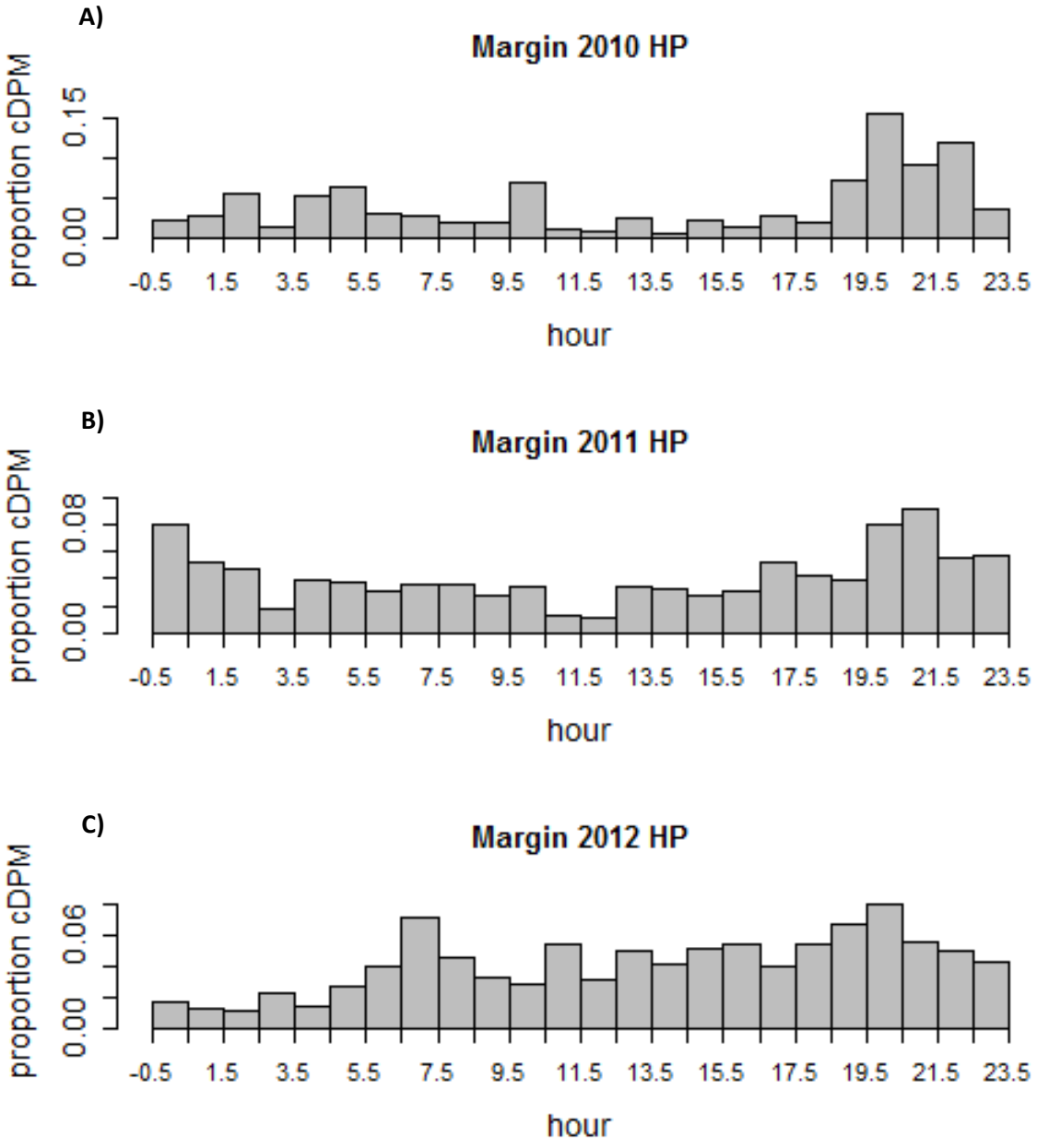

Figure 4.9. Frequency density distributions of harbour porpoise cDPM at the reef margin.
Acoustic data loggers (CPODs) deployed at the reef margin collected data over three summer periods across years A): 2010 (n = 56 days), B): 2011 (n = 98 days), and C): 2012 (n = 106 days). Abbreviations: cDPM = 'corrected' Detection Positive Minutes; HP = harbour porpoise.

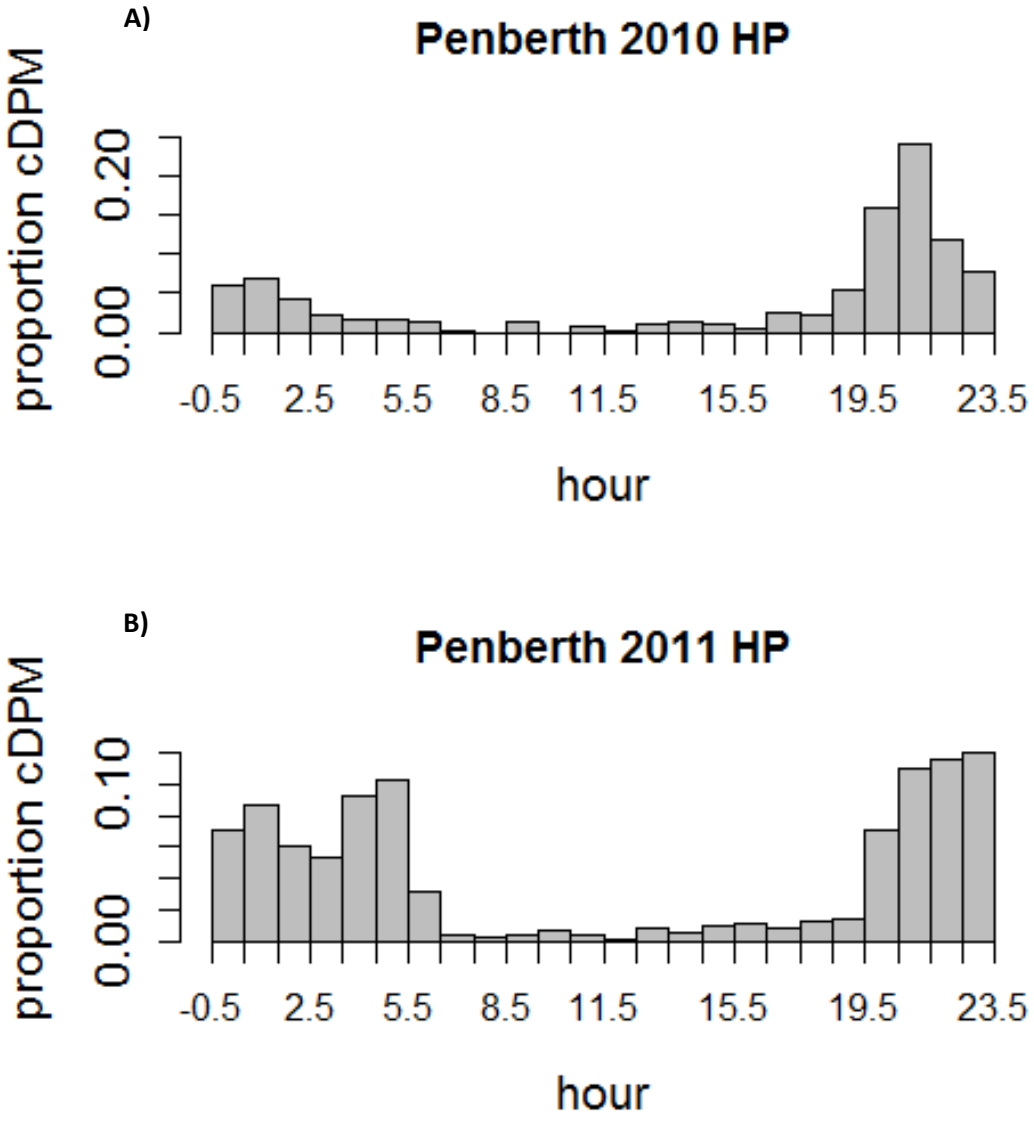

Figure 4.10. Frequency density distributions of harbour porpoise cDPM at Penberth.
Acoustic data loggers deployed at Penberth collected data over two summer periods between years A): 2010 (n = 56 days) and B): 2011 (n = 98 days). Abbreviations: cDPM = 'corrected' Detection Positive Minutes; HP = harbour porpoise.

There was more variability in the distribution of cDPM throughout the 24-hr cycle at the two reef sites, whereas the day-night split was most obvious at Penberth (Figure 4.10). There were increased detections between 2000 hrs and 0600 hrs, which, in 2010, rose towards midnight then fell in subsequent hours. In 2011, however, there was more consistent activity across the range of night time hours.

At the eastern reef edge (Figure 4.8), there was a day-night split in years 2010 and 2011, with increased detections between 2100 hrs and 0100 hrs, and between 2100 hrs and 0500 hrs,

respectively. In 2012, there was fairly consistent distribution of cDPM throughout the 24-hr period, though lower detections were recorded in the early hours between 0000 and 0500 hrs. At the reef margin (Figure 4.9), there were similar patterns although, in 2010, the peak was between 2000 and 2300 hrs, with a less marked day-night split in 2011, when compared to the eastern reef edge. The difference lies in the proportion of detections in the 3 hours after midnight between years 2011 and 2012, with a clear decrease.

Auto-correlation functions calculated on the hourly cDPM time series (Figure 4.11) show the data are significantly correlated at differing lag-hours depending on location and year, suggesting varying clustering of porpoise activity and non-activity (i.e. residency times). The series of regular peaks represent the interval the animals returned to a site on a repeated basis. In 2010 and 2011, they returned to the same site every 24 hours (i.e. diurnally) at all locations. In 2012, the re-visit times shifted to around 12 hours at both reef sites, representing an additional association with the tidal cycle, particularly at the eastern reef edge.

Though there was inconsistency between sites and inter-annually, in 2010 (Figure 4.11-A) there was a 3-hour lag at all three sites and a recurrent positive correlation at 24-hour intervals. In 2011 (Figure 4.11-B) there was an 8-hour lag at the eastern reef edge, a 6-hour lag in the sandy bay at Penberth and only 3 hours at the reef margin. All three sites show a recurrent positive auto-correlation at around 24 lag-hours, i.e. diurnal patterns, while at Penberth, the 12-hour time lag auto-correlation indicates there was an association with each tidal cycle, where 12 hours later the correlation goes negative. In 2012 (Figure 4.11-C), there was a lag of 18 hours at the eastern reef edge and 6 hours at the reef margin (no data collected at Penberth). These correlations indicate that porpoises at both reef locations showed association with each phase of the tidal cycle (ebb and flood), and also between alternate cycles (where peaks recurred every 12 hours).

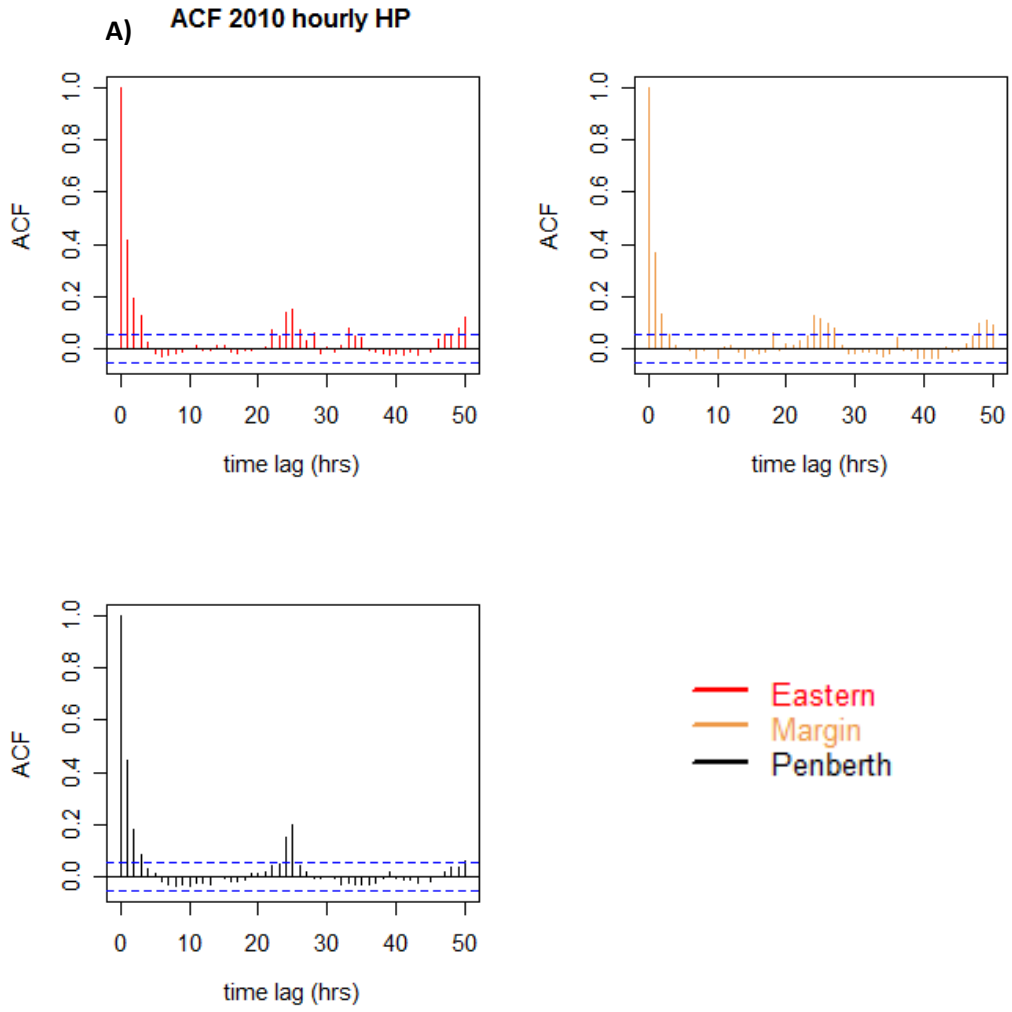
A)
ACF 2010 hourly HP
ACF
time lag (hrs)
Eastern
Margin
Penberth

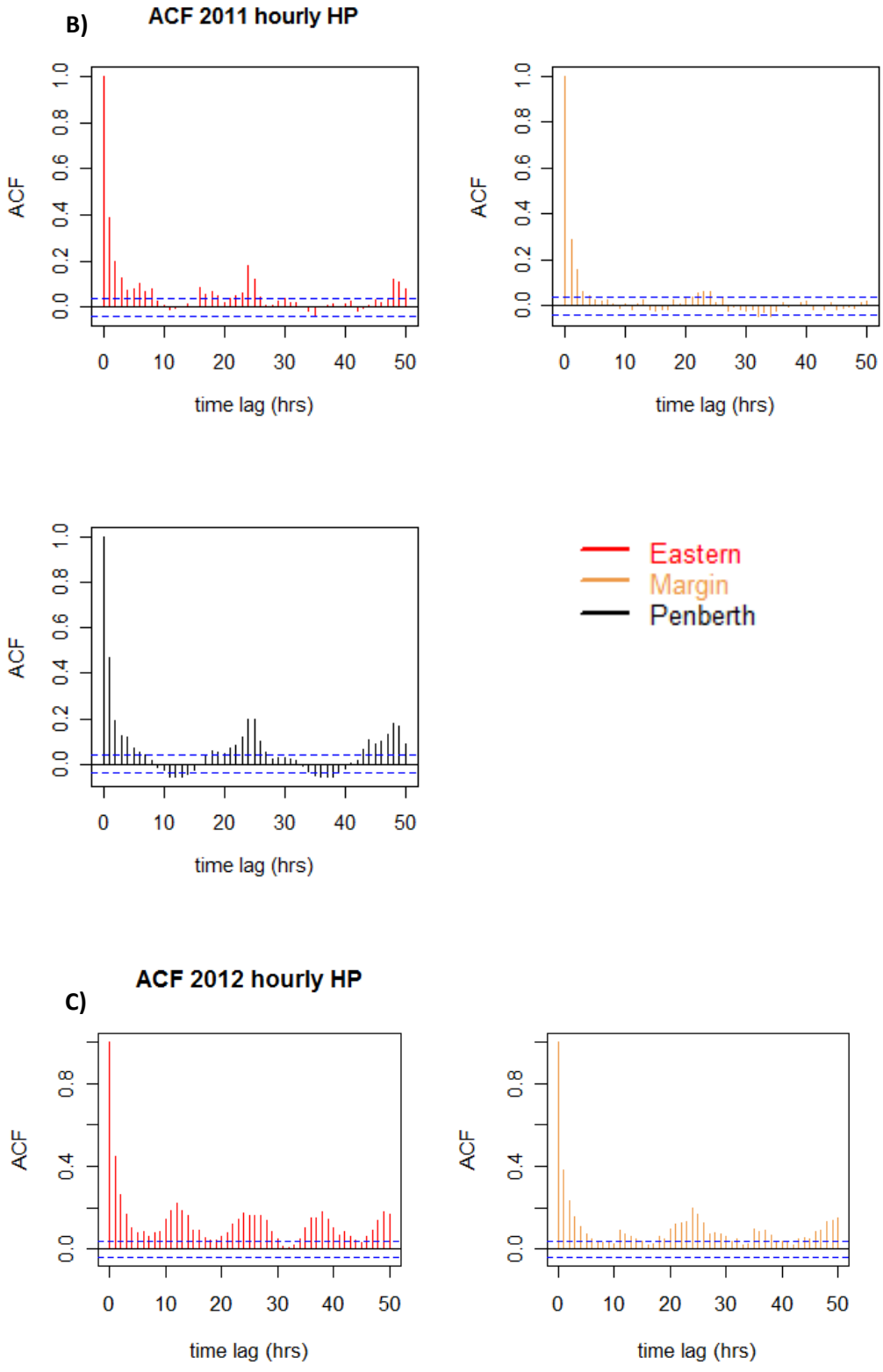

Figure 4.11. ACFs of hourly harbour porpoise corrected Detection Positive Minutes (cDPM).
Acoustic data loggers (CPODs) deployed at three sites collected data during three summer periods across years A): 2010 (n = 56 days), B): 2011 (n = 98 days), and C): 2012 (n = 106 days). Peaks represent the interval porpoises returned to a site on a repeated basis. Red line = eastern reef edge; orange line = reef margin; black line = Penberth 'control' site. Blue dashed lines indicate 95% threshold values for significant correlation. No data collected at Penberth in 2012.

4.3.2.1 Temporal Analyses (porpoises)

Where no covariate data were available for some hours of survey, sampling units were removed from further analysis (n = 185). The final dataset contained 15,974 hours (98.9% of total survey effort). Table 4.5 summarises the hourly porpoise acoustic dataset and associated environmental covariates, which were measured or extrapolated (see Chapter 2, Section 2.3.2, Environmental Data, on page 24).

Table 4.5. Summary of covariates used in hourly analysis of harbour porpoise acoustic data.
Acoustic data loggers (CPODs) deployed at three sites in the Runnel Stone Reef survey area collected data over three summer periods between 2010-12. Missing data removed (n = 15,974 hours). No data collected at Penberth in 2012. Abbreviation: IQR = inter-quartile range.

Parameter	Eastern	Margin	Penberth
Hours of data per year: 2010, 2011, 2012 (total)	1335, 2292, 2546 (6173)	1335, 2291, 2546 (6172)	1335, 2294 (3629)
Number of 'presence' hours (%)	1233 (20%)	1166 (19%)	485 (13%)
Survey variables			
Wave direction (degrees)			
Range	4 – 356	4 – 356	98 – 311
Median (IQR)	185 (179 – 190)	185 (179 – 190)	185 (179 – 190)
Wave height (m)			
Range	0.08 – 3.62	0.08 – 3.62	0.08 – 1.94
Median (IQR)	0.44 (0.27 – 0.67)	0.44 (0.27 – 0.67)	0.44 (0.27 – 0.64)
Acoustic noise ("Nall"; total clicks)			
Range	64 – 245,760	440 – 245,760	318 – 199,029
Median (IQR)	41,509 (1608 – 31,293)	15,149 (2082 – 5920)	2600 (1439 – 4224)
Tidal variables			
Tide direction (degrees)			
Range	27 – 333	27 – 333	27 – 333
Median (IQR)	207 (110 – 287)	207 (110 – 287)	203 (110 – 287)
Tide speed (m s^{-1})			
Range	0.07 – 1.56	0.07 – 1.56	0.07 – 1.56
Median (IQR)	0.56 (0.33 – 0.86)	0.56 (0.33 – 0.86)	0.56 (0.33 – 0.86)
Tide height (m from LAT)			
Range	0.14 – 5.8	0.14 – 5.8	0.14 – 5.8
Median (IQR)	2.89 (1.75 – 4.1)	2.89 (1.75 – 4.1)	2.9 (1.75 – 4.1)
Tide range (m)			
Range	2.06 – 5.77	2.06 – 5.77	2.06 – 5.77
Median (IQR)	3.8 (3 – 4.47)	3.8 (3 – 4.47)	3.8 (2.9 – 4.37)
Tidal hour (hours relative to HW)			
Range	-6.28 to +6.32	-6.28 to +6.32	-6.28 to +6.32
Median (IQR)	0.0 (-3.08 to +3.12)	0.0 (-3.08 to +3.12)	0.0 (-3.1 to +3.1)
Tidal flow group (as factor)			
Range	1 – 4	1 – 4	1 – 4
Median (IQR)	2 (1 – 3)	2 (1 – 3)	2 (1 – 3)
Temporal variables			
Year (as factor)			
Range	2010 – 2012	2010 – 2012	2010 – 2011
Month (as factor)			
Range	7 – 10	7 – 10	7 – 10
Hour (GMT)			
Range	0 – 23	0 – 23	0 – 23
Dolphin activity (cDPM)			
Range	0 – 46	0 – 59	0 – 47
Mean (s.d.)	0.21 (1.78)	0.17 (1.64)	0.23 (2.02)

Analyses of the effort-corrected dataset indicates there was increased porpoise acoustic activity during eastward flows compared to westward (Figure 4.12-A), while the rate of acoustic activity decreased with increasing tidal speeds (Figure 4.12-B) and range (Figure 4.12-D), which is a proxy for time in the spring-neap cycle. This suggests there were reduced rates of acoustic detections during spring tides, and when flow speeds in the survey region exceeded a threshold value of ~0.9 m s^{-1}.

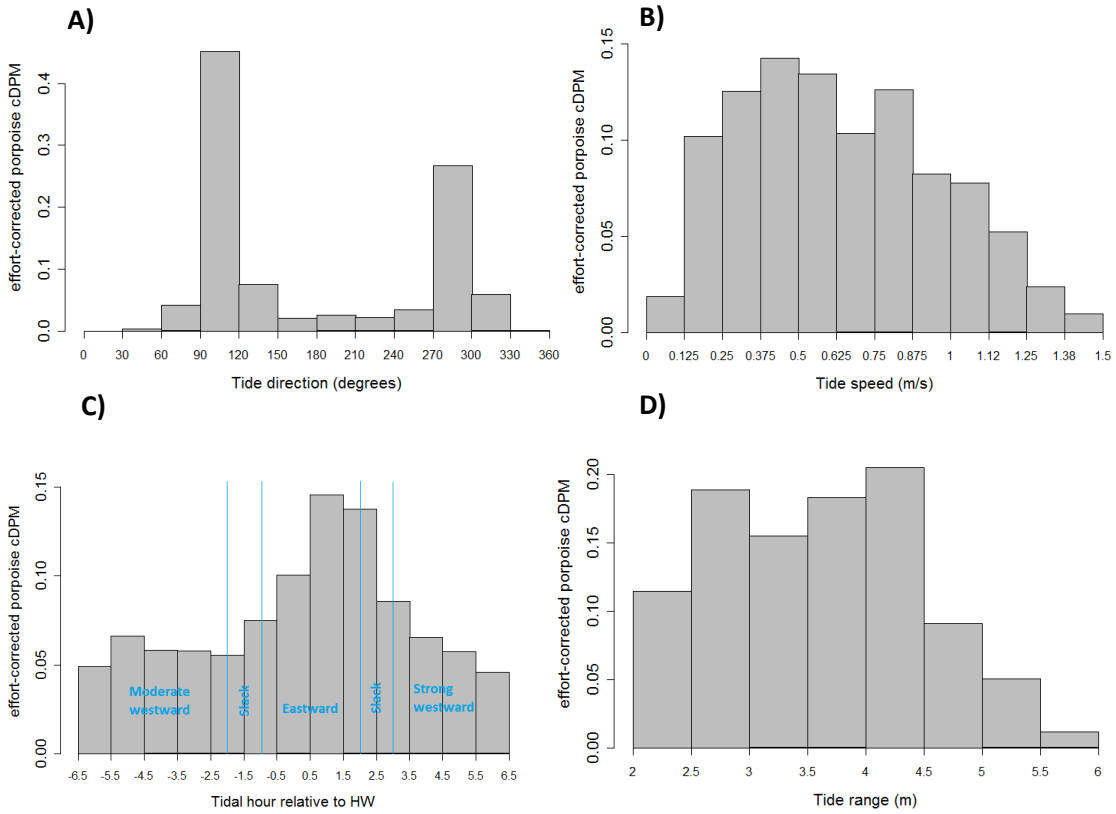

Figure 4.12. Effort-corrected harbour porpoise cDPM as a function of tidal variables.
Acoustic data collected by three data loggers (CPODs) in the survey area, over 15,974 hours of survey effort across years 2010-12. Data were pooled across sites and years. A): Tidal flow direction (degrees), B): Tide speed (m s^{-1}), C): Tidal hour (relative to HW, where HW = 0), and D): Tidal range (m).

There was minimal variability in the rate of acoustic detection throughout most of the tidal cycle (Figure 4.12-C), but a clear increase in activity, from ~0.06 cDPM hr^{-1} to ~0.15 cDPM hr^{-1}, between the hours of HW-1 and HW+2 , i.e. site-specific eastward flow (see Appendix F for schematics of local tidal flow regime).

4.3.2.2 Temporal Model (porpoises)

To determine the influence of tidal and temporal variables on porpoise acoustic activity at each site, the hourly presence-absence of detections was modelled with a range of candidate survey, tidal and temporal covariates (Table 4.5) using a binomial GAM with a logit-link function. Collinearity between the candidate variables was explored using a pairplot (Appendix J.2). Tide height and flow group were highly collinear (r = 0.81), which was dealt with during model selection, according to the procedure to deal with collinearity (Section 4.2.5). Through forward step-wise selection, the modelling process first compensated for survey effects (including 'site'), then tidal variables, and finally temporal variables (Section 4.2.5). Modelling data that were pooled across sites showed location was significant for porpoises, so relationships between the response and the other covariates would be masked if 'site' were not included as a variable in the model. (Results from the site-pooled model are provided in Appendix J.4).

Results of the forward GAMs modelled for each site are provided in Table 4.6, and relationships with the significant variables shown in Figure 4.13 (Eastern), Figure 4.14 (Margin), and Figure 4.15 (Penberth). See Appendix J.3 for ACFs of models' residuals. The Eastern model explained 13.6% of deviance in the occurrence of porpoise detections each hour of survey (n = 6173), the Margin model explained 9.87% (n = 6172), and the Penberth model explained 23.5% (n = 3629).

Table 4.6. Results of forward GAM model selection for presence-absence of porpoise detections.
Variables are shown in order of importance, first compensating for survey effects (acoustic noise "Nall", wave direction, wave height). Smooths are shown with the number of estimated degrees of freedom (e.d.f.) in parentheses; AIC_{Δ} is the reduction in AIC score caused by the addition of the significant variable to the model, with the first score in bold showing the starting AIC; % Dev is the additional deviation (%) in the data explained by adding the selected variable to the model. Surveys conducted across summer periods at the Runnel Stone Reef (Eastern: years 2010-12, n = 6173 hours; Margin: years 2010-12, n = 6172; Penberth: years 2010-11, n = 3629).

	Eastern (reef edge)			Margin (southern pinnacles)			Penberth		
Order	Smooth (e.d.f.)	% Dev	AIC_{Δ}	Smooth (e.d.f.)	% Dev	AIC_{Δ}	Smooth (e.d.f.)	% Dev	AIC_{Δ}
1	s(Nall, 4.5)	6.27	**5797.64**	s(Nall, 3.9)	4.86	**5701.82**	s(Nall, 3.9)	8.4	**2624.27**
2	s(TideHr, 4.4)	+1.02	-54.55	s(TideHt, 4.5)	+2.23	-122.47	s(WaveHt, 2.2)	+1.37	-34.5
3	factor(Year)	+4.01	-241.16	s(TideHr, 4.1)	+1.38	-75.36	s(Hour, 2.0)	+7.73	-215.51
4	factor(Month)	+2.3	-136.87	factor(Year)	+1.4	-79.45	factor(Year)	+3.6	-101.43
5							s(Cet_cDPM, 2.9)	+1.4	-33.44
6							factor(Month)	+1.0	-22.95
Total		13.6			9.87			23.5	

Of the survey variables, acoustic noise was the most important predictor of harbour porpoise detection rates in all models, explaining between 4.9% (Margin) and 8.4% (Penberth) of the deviance (Table 4.6). Detection occurrence decreases with increasing noise at the Eastern and Margin sites (Figure 4.13-A and Figure 4.14-A, respectively). Interestingly, at the Margin site, where noise levels were high, detection rates start to rise again, which suggests that as the environment at this particular location gets noisier, total noise is contributed to by porpoise clicks. The noise-detection relationship is not as clear at Penberth, where there are fewer covariate data points (Figure 4.15-A), particularly where Nall > 100,000. However, wave height was also a significant influence on detection rates in the sandy bay, which explained 1.4% of deviance (Table 4.6), though the relationship is also variable where wave heights were higher (Figure 4.15-B), indicating more variable detection rates in choppier seas.

Acoustic noise detected by the CPODs was contributed to by different sources depending on location (Table 4.7); wave height contributed the most at the eastern reef edge (9.7%), tidal range at the reef margin (34.3%), and dolphin clicks at Penberth (6.7%). Table 4.7 shows that all tidal variables, including time in the spring-neap cycle, and tidal hour, heavily contributed to noise levels at the reef margin (24-34%), and to a lesser extent at the reef edge (1.3-6%), while tidal influence had the least impact at Penberth (0.4-3%).

Table 4.7. Acoustic noise at each site explained by significant variables as % deviance.
Total number of clicks ("Nall") modelled as a function of individual variables in a negative binomial GAM with a logit-link. Superscript numbers indicate the order of variables relative to amount of deviance explained. Bold values indicate the variable explaining most deviation in the noise data. Where no value is given, the variable is not significant. Surveys conducted across summer periods at the Runnel Stone Reef (Eastern: years 2010-12, n = 6173 hours; Margin: years 2010-12, n = 6172; Penberth: years 2010-11, n = 3629).

	Eastern	S. Margin	Penberth
Noise explained by:			
Tidal hour	1.27%^{5}	24.2%^{3}	--
Tidal range	5.39%^{2}	**34.3%^{1}**	2.8%^{2}
Tide height	1.79%^{4}	28.8%^{2}	0.35%^{5}
Wave height	**9.74%^{1}**	6.81%^{4}	2.28%^{4}
Dolphin cDPM	0.08%^{6}	--	**6.67%^{1}**
Porpoise cDPM	2.96%^{3}	2.79%^{5}	2.47%^{3}

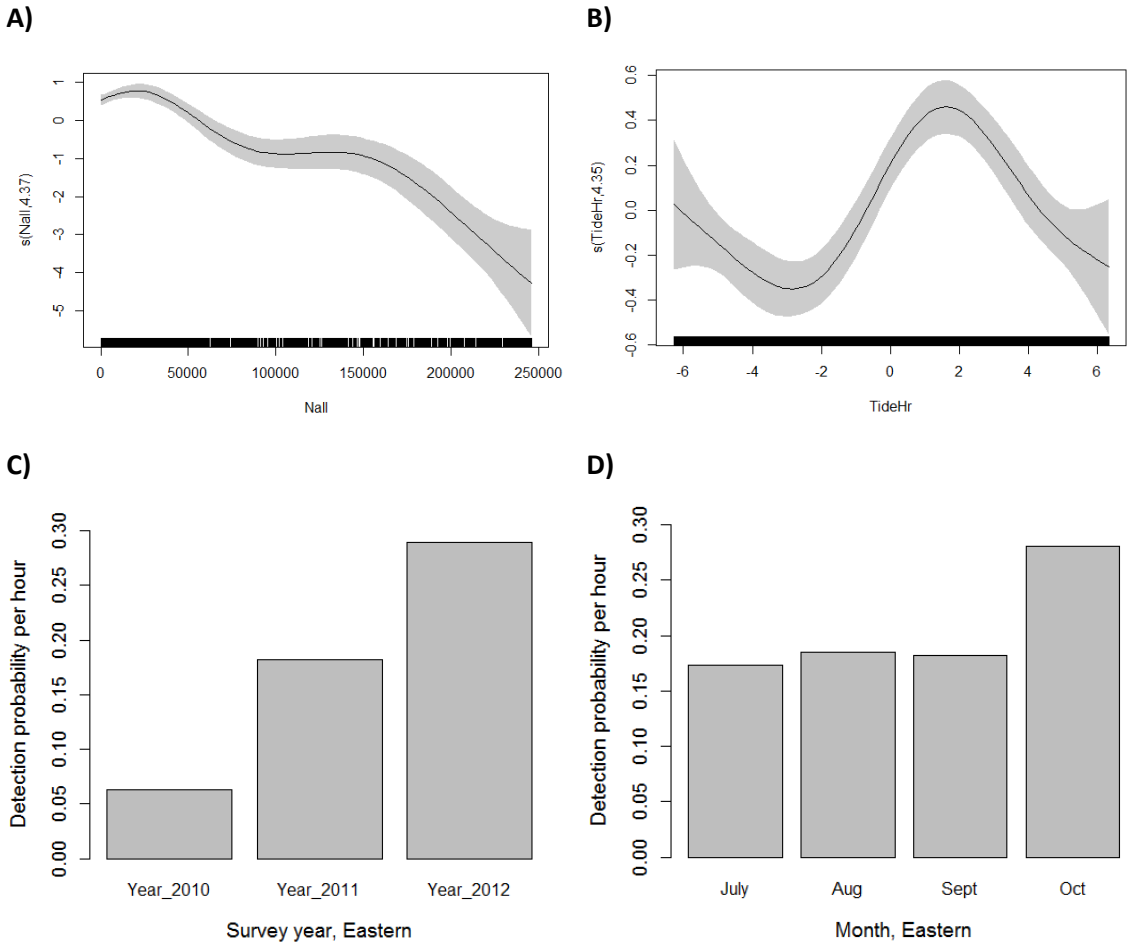

Figure 4.13. Significant predictors of harbour porpoise detections at the eastern reef edge.
As selected by the final binomial GAM (n = 6173 samples), A): Acoustic noise (e.d.f. = 4.37), B): Tidal hour (e.d.f. = 4.35), C): Year, and D): Month. Figures A) and B), smooths reported on the scale of the linear predictor, numbers in brackets in y-axis captions are e.d.f. (estimated degrees of freedom) of the smooths, rug plots at bottom of figures are covariate values, and shaded regions around the smooths represent 95% confidence intervals.

Tidal hour was selected as a significant predictor on porpoise detection at the two reef sites, Eastern and Margin, but only explaining 1% and 1.4% in deviance, respectively (Table 4.6); the relationships also vary. At the eastern reef edge (Figure 4.13-B), detection rates peak between tidal hours HW0 and HW+3, i.e. hours of strong eastward and HW slack (just before the current switches flow direction to westward), and clearly decrease around HW-3 (middle of westward flow). At the reef margin, there are also decreased detections around HW-2, but no obvious peak (Figure 4.14-C).

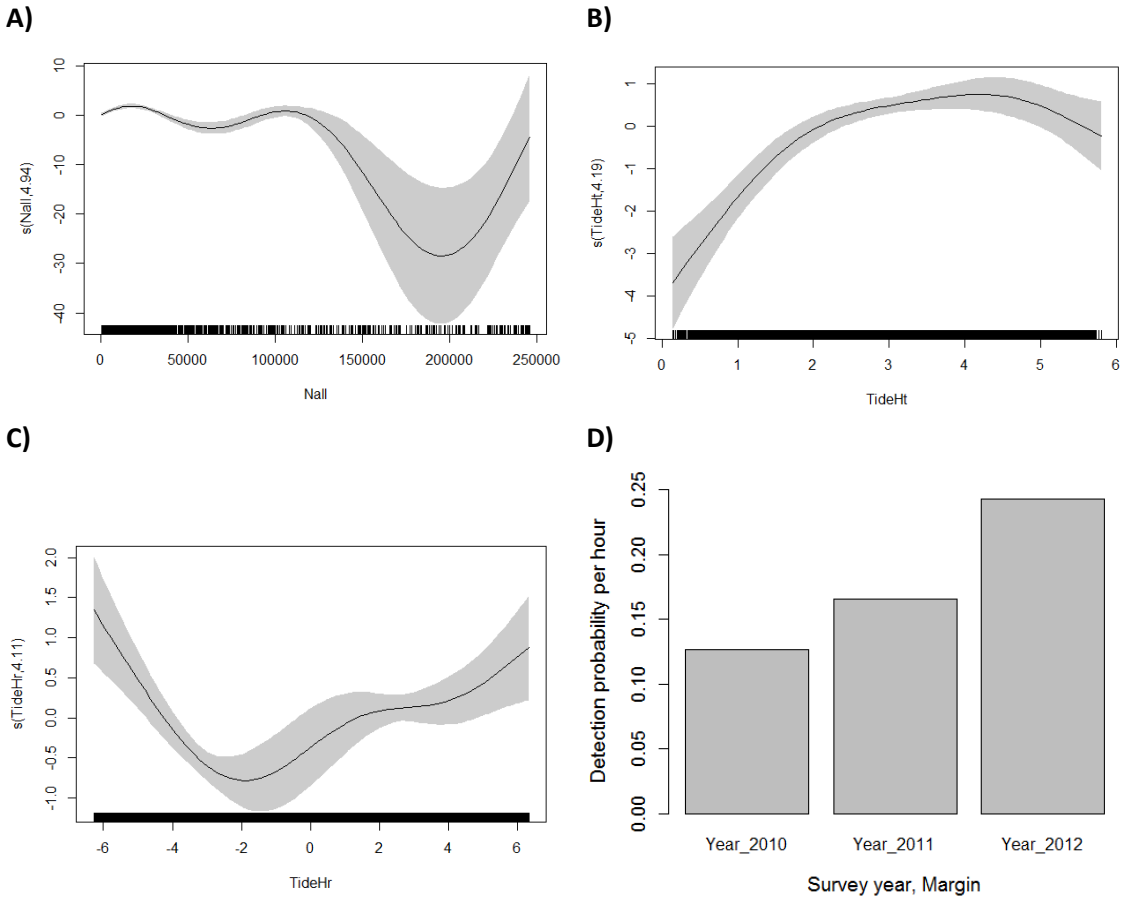

Figure 4.14. Significant predictors of harbour porpoise detections at the southern reef margin.
As selected by the final binomial GAM (n = 6172 samples), A): Noise (e.d.f. = 4.94), B): Tide height (e.d.f. = 4.19), C): Tidal hour (e.d.f. = 4.11), and D): Year. Figures A) – C), smooths reported on the scale of the linear predictor, numbers in brackets in y-axis captions are e.d.f. (estimated degrees of freedom) of the smooths, rug plots at bottom of figures are covariate values, and shaded regions around the smooths represent 95% confidence intervals.

Tide height was only selected as an important predictor of porpoise detection occurrence at the Margin site, explaining 2.2% of deviance (Table 4.6). The positive correlation between detection rate and tide height indicates detections increase towards the hours of HW, i.e. on a flood tide, when tidal current flows eastward past the reef into the Channel. Additional analysis that explored the relationship between total noise and tide height (Appendix J.5), revealed decreasing noise levels with increasing tide heights, i.e. a quieter acoustic environment towards HW.

Penberth was the only site where a significant (negative) relationship was found between porpoise detection and increasing acoustic activity of other cetacean species (Figure 4.15-D), explaining 1.4% of the variation (Table 4.6).

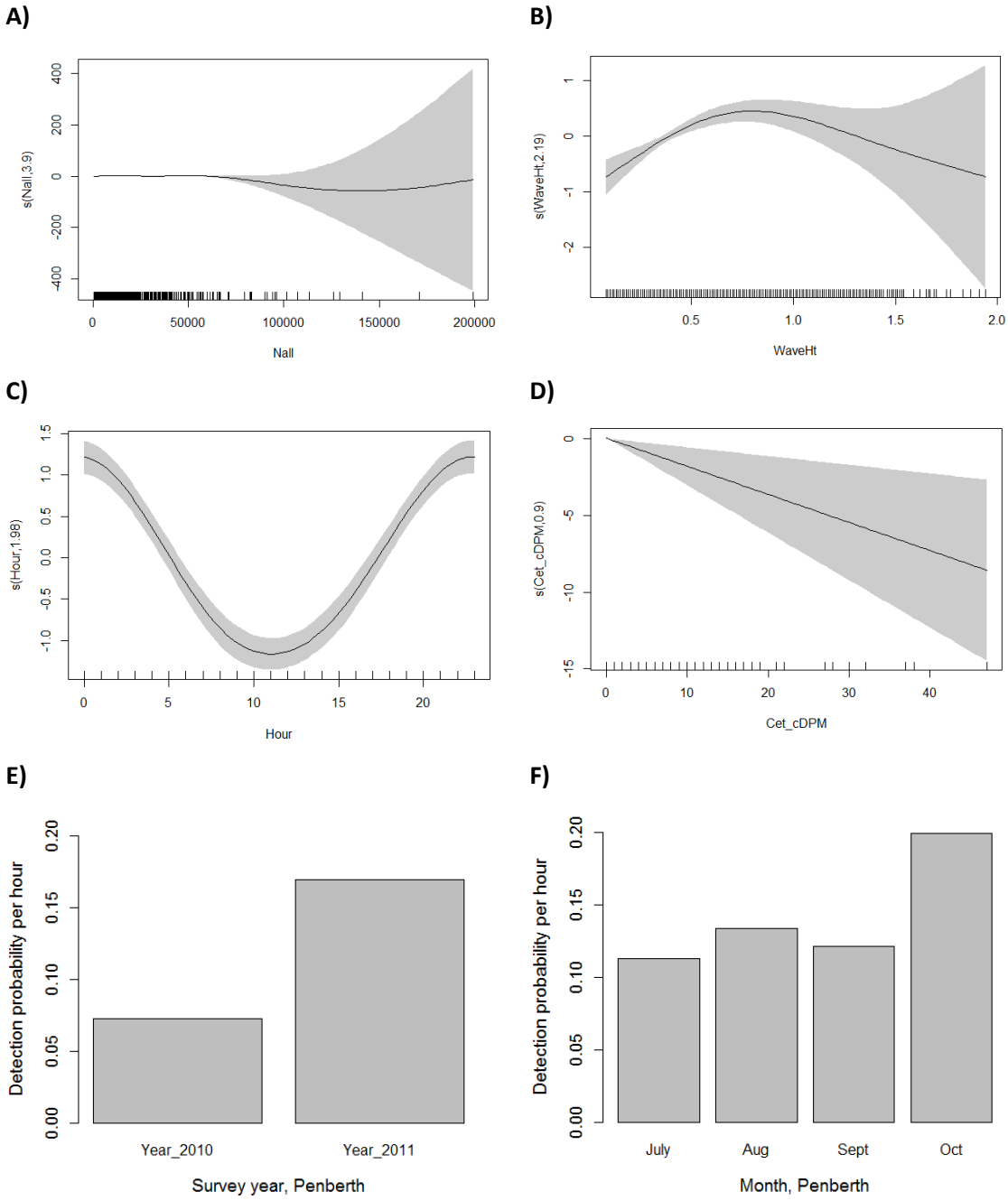

Figure 4.15. Significant predictors of harbour porpoise detections at Penberth.
As selected by the final binomial GAM (n = 3629 samples), A): Noise (e.d.f. = 3.9), B): Wave height (e.d.f. = 2.19), C): Hour (e.d.f. = 1.98), D): Dolphin cDPM (e.d.f. = 0.9), E): Year, and F): Month. Figures A) – D), smooths reported on the scale of the linear predictor, numbers in brackets in y-axis captions are e.d.f. (estimated degrees of freedom) of the smooths, rug plots at bottom of figures are covariate values, and shaded regions around the smooths represent 95% confidence intervals.

Year was a significant predictor on porpoise detections across all three CPOD locations, explaining between 1.4% (Margin) and 4% (Eastern) of deviance (Table 4.6), with increased detection rates each year of survey (Figure 4.13-C, Figure 4.14-D, and Figure 4.15-E). Month

was also an important predictor on occurrence at the Eastern (2.3%) and Penberth (1%) sites, with consistent rates between July and September each year, and marked increases in October (Figure 4.13-D and Figure 4.15-F). Penberth was the only site that exhibited a strong diel pattern in porpoise occurrence where hour of the day explained 7% of deviance (Table 4.6). Detections peaked around midnight and decreased around 1100 hrs (Figure 4.15-C).

4.3.3 Dolphins

There was minimal variability between sites and years in the acoustic dolphin data (see Table 4.8), as the proportion of detection positive days only ranged between 30% and 43%, and only marginally higher rates recorded by the reef margin CPOD each year (near the southern pinnacles). The proportions of DPH were also consistent (2-3%) across the three-year survey period.

Table 4.8. Dolphin acoustic detection data in the Runnel Stone Reef study area.
Acoustic data loggers (CPODs) deployed at three sites collected data over three summer periods between 2010-12. (Abbreviations: Cet = cetaceans excluding porpoise, i.e. dolphin species; cDPM = 'corrected' Detection Positive Minutes). No data collected at Penberth in 2012.

Year	Site	Survey days (full hours)	Detection positive days (%)	Detection positive hours (%)	Cet cDPM
2010	Eastern	56 (1345)	19 (34%)	28 (2%)	182
	Margin		24 (43%)	36 (3%)	213
	Penberth		19 (34%)	34 (3%)	321
2011	Eastern	98 (2328)	35 (36%)	69 (3%)	592
	Margin		37 (38%)	63 (3%)	380
	Penberth		36 (37%)	64 (3%)	515
2012	Eastern	106 (2570)	38 (36%)	80 (3%)	547
	Margin		32 (30%)	65 (3%)	456

Summary data in Table 4.9 shows minimal variability in dolphin echolocation activity between sites. The average cDPM hr^{-1} was the same (0.2) for each CPOD, indicating the animals echolocated at similar intensities irrespective of site. The average number of DPH per 24-hr period was also similar at each site (0.63 – 0.68), suggesting dolphins visited each location with similar frequencies (~2.7% of the day spent visiting each site).

Table 4.9. Dolphin acoustic detection data summarised over different timescales by site.
Acoustic data loggers (CPODs) deployed at three sites in the Runnel Stone Reef survey area collected data over three summer periods between 2010-12. Abbreviations: cDPM = 'corrected' Detection Positive Minutes; DPH = Detection Positive Hours, s.d. = standard deviation. Data is pooled by site across years. No data collected at Penberth in 2012.

Site	Survey days (full hours)	Average cDPM per hour (s.d.)	Average cDPM per day	Average DPH per day	% DPH per day
Eastern	260 (6243)	0.2 (1.8)	5.08	0.68	2.83
Margin	260 (6243)	0.2 (1.6)	4.85	0.63	2.63
Penberth	154 (3673)	0.2 (2.0)	5.43	0.64	2.67

There was a low level of baseline acoustic activity in the dolphin data across years and site, seen in the daily time series (Figure 4.16). There are similar peaks and troughs in the data each year, which again suggests dolphin echolocation activity was consistent over time, with perhaps more regular intensive activity during 2011 (Figure 4.16-B), indicated by more 'peak' events. The peaks at each site, though fairly sporadic each survey period, tended to coincide with peaks at other sites, particularly at the two reef sites (denoted by the red and orange lines in the figures).

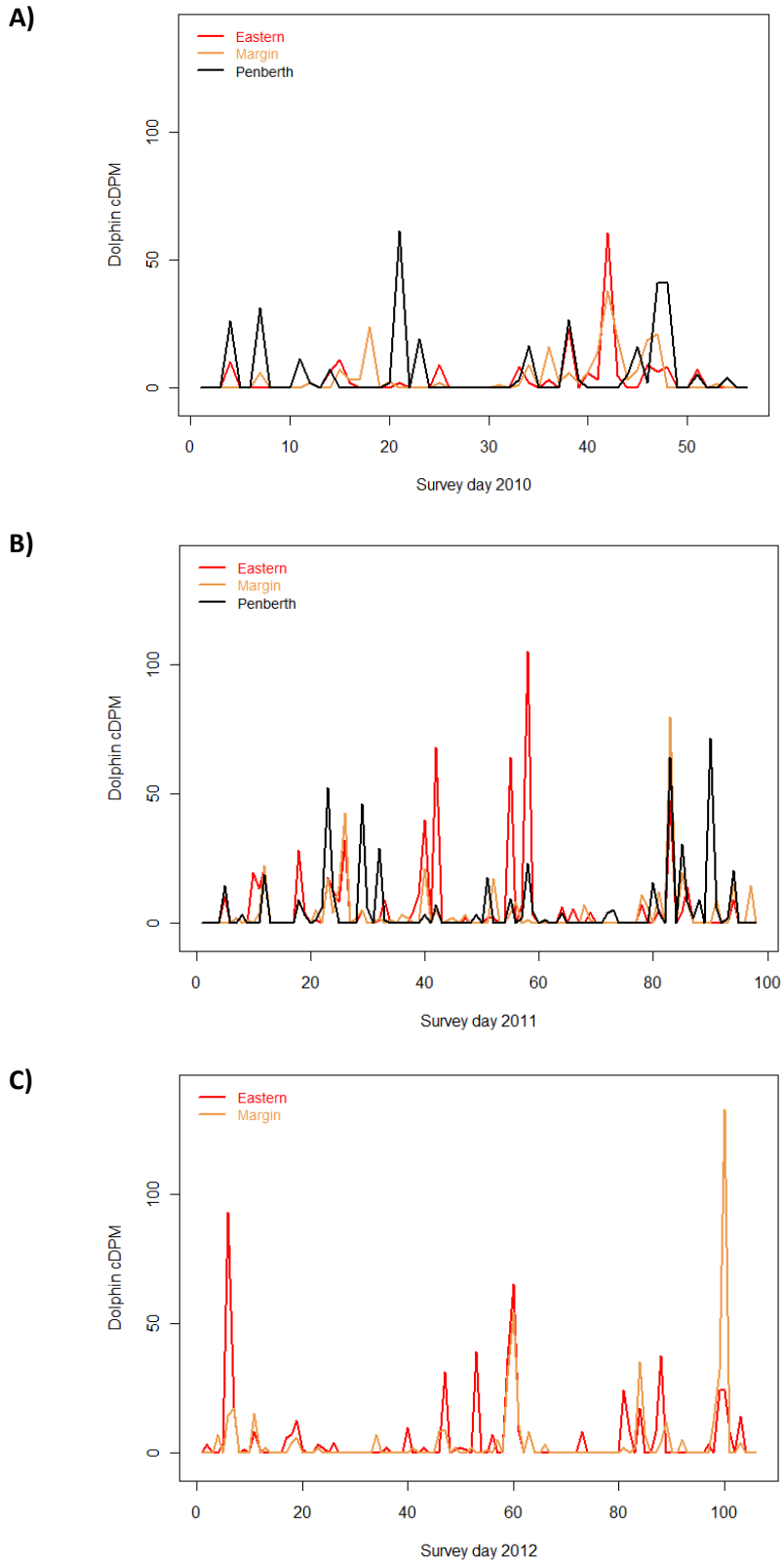

Figure 4.16. Dolphin corrected Detection Positive Minutes (cDPM) per survey day, by year.
Acoustic data loggers (CPODs) deployed at three sites collected data during three summer periods across years A): 2010 (n = 56 days), B): 2011 (n = 98 days), and C): 2012 (n = 106 days). Time series show low levels of baseline acoustic activity across years and sites, with similar peaks and troughs in each year's data. Red line = eastern reef edge; orange line = reef margin; black line = Penberth 'control' site. No data collected at Penberth in 2012.

There was a notable day-night split in the proportion of cDPM by hour of the day across all sites and years (Figure 4.17, Figure 4.18, Figure 4.19). Additionally, the patterns were consistent each year of survey at each site, though marginally less marked at the reef margin in 2011 (Figure 4.18-B) although, in 2012 (Figure 4.18-C), there was a clear absence of dolphin activity between 0830 hrs and 1730 hrs.

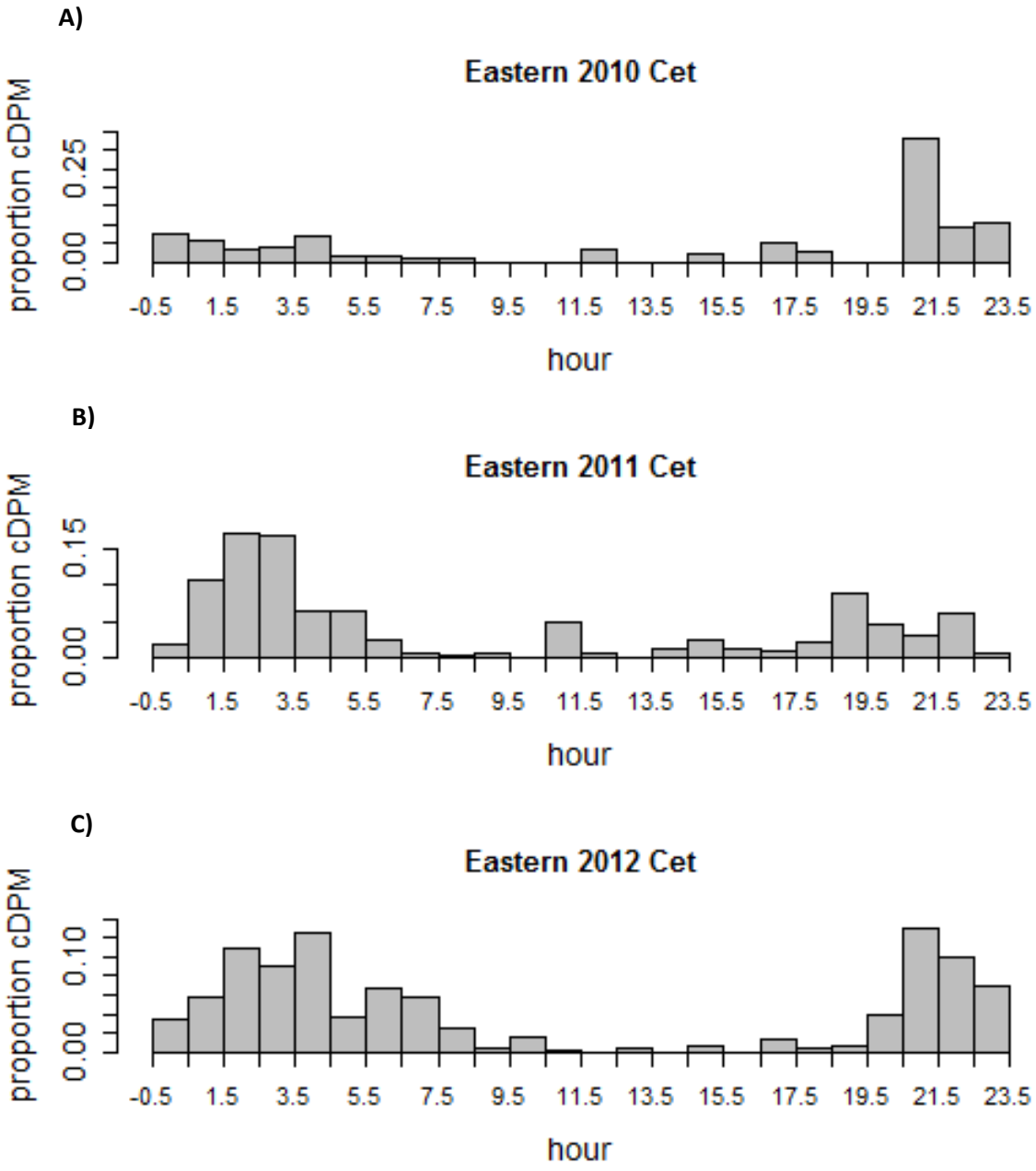

Figure 4.17. Frequency density distributions of dolphin cDPM at the eastern reef edge.
Acoustic data loggers (CPODs) deployed at the eastern reef edge collected data over three summer periods across years A): 2010 (n = 56 days), B): 2011 (n = 98 days), and C): 2012 (n = 106 days). Abbreviations: cDPM = 'corrected' Detection Positive Minutes; Cet = cetaceans, excluding porpoise.

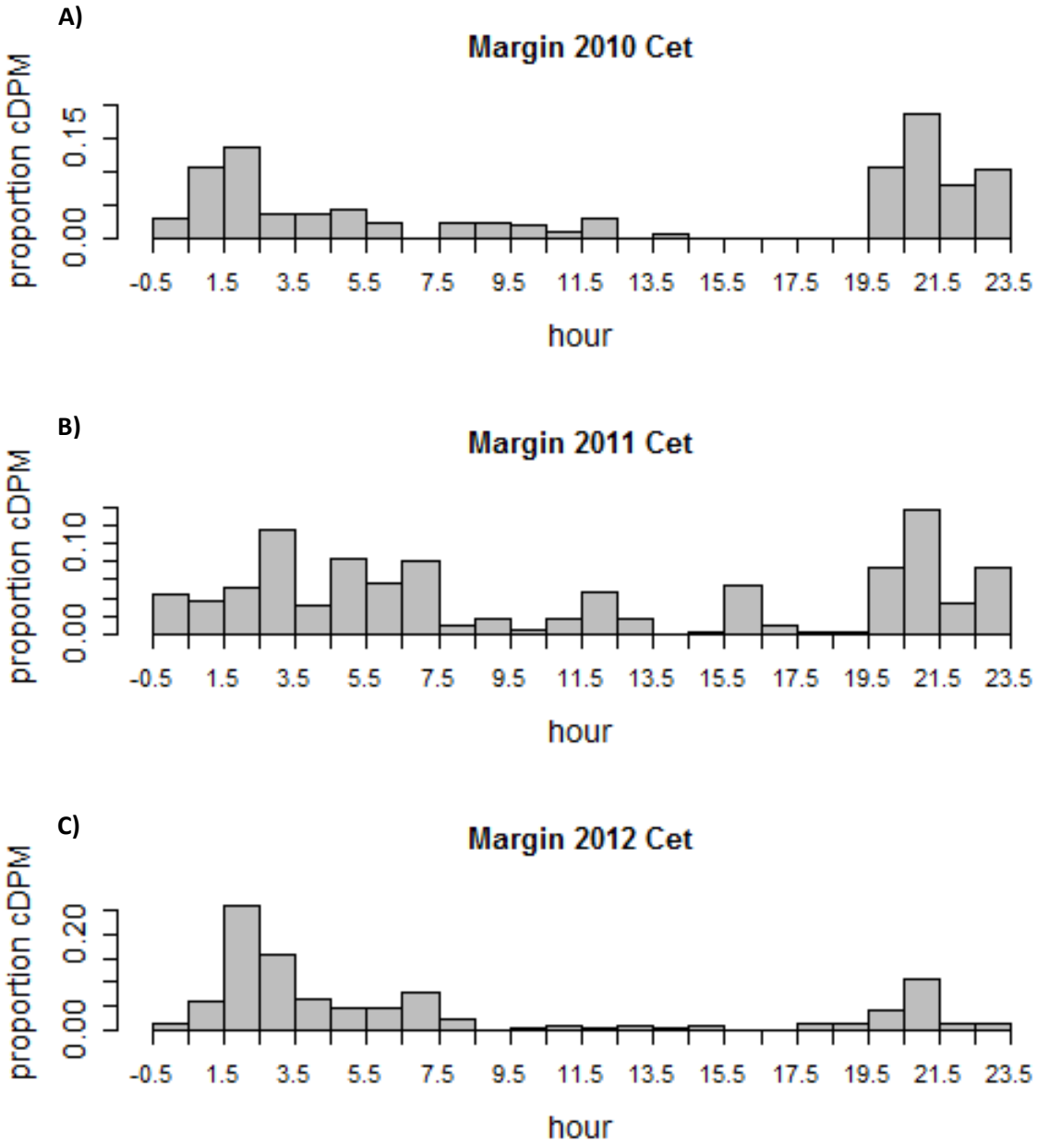

Figure 4.18. Frequency density distributions of dolphin cDPM at the reef margin.
Acoustic data loggers (CPODs) deployed at the reef margin collected data over three summer periods across years A): 2010 (n = 56 days), B): 2011 (n = 98 days), and C): 2012 (n = 106 days). Abbreviations: cDPM = 'corrected' Detection Positive Minutes; Cet = cetaceans, excluding porpoise.

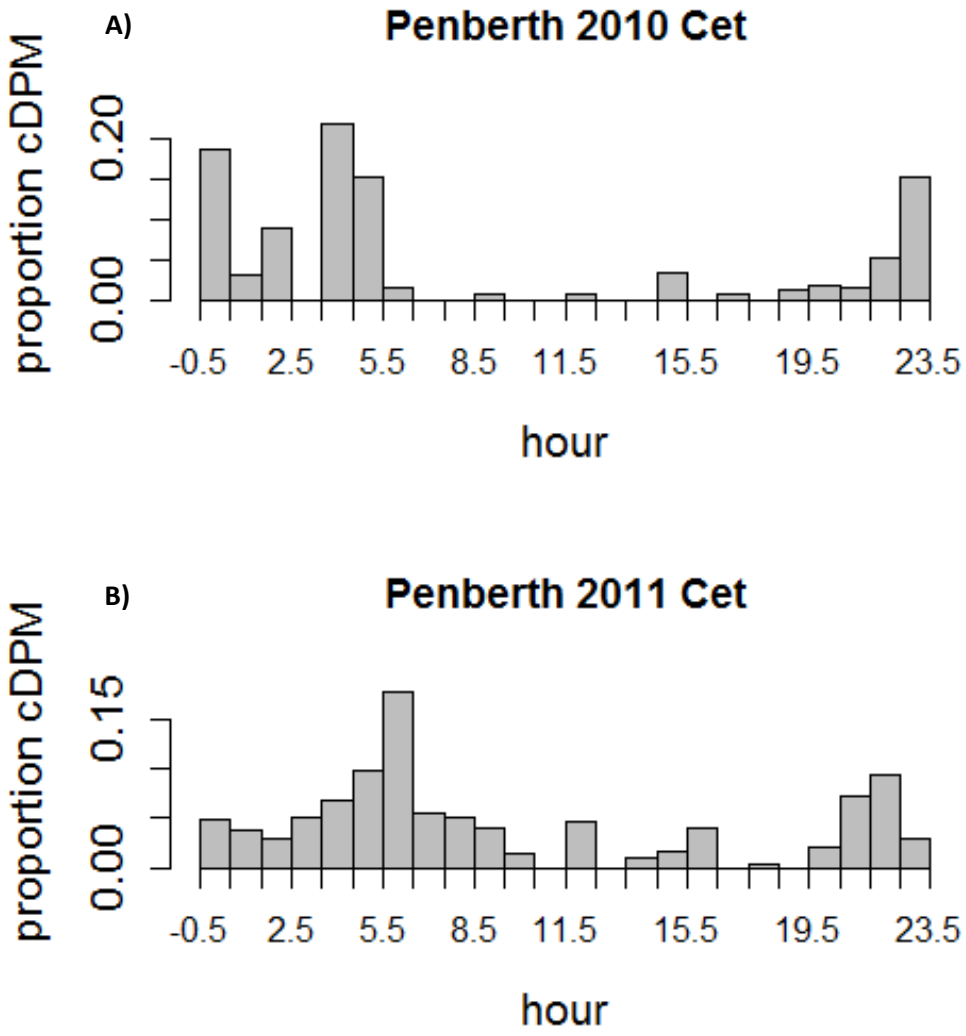

Figure 4.19. Frequency density distributions of dolphin cDPM at Penberth.
Acoustic data loggers deployed at Penberth collected data over two summer periods between years A): 2010 (n = 56 days) and B): 2011 (n = 98 days). Abbreviations: cDPM = 'corrected' Detection Positive Minutes; Cet = cetaceans, excluding porpoise.

The day-night split was particularly clear at Penberth in 2010 (Figure 4.19-A), though less so in 2011 (Figure 4.19-B). Early morning (before 0600 hrs) echolocation activity appeared to increase in 2011-12 at the eastern reef edge (Figure 4.17-B and C), compared to 2010 (Figure 4.17-A) when there were relatively very low rates of detection during the same hours.

4.3.3.1 Temporal Analyses (dolphins)

Where no covariate data were available for some hours of survey, sampling units were removed from further analysis (n = 185). The final dataset contained 15,974 hours (98.9% of total survey effort). Table 4.10 summarises the hourly dolphin acoustic dataset and associated

environmental covariates, which were measured or extrapolated (see Chapter 2, Section 2.3.2, Environmental Data, on page 24).

Table 4.10. Summary of covariates used in hourly analysis of dolphin acoustic data.
Acoustic data loggers (CPODs) deployed at three sites in the Runnel Stone Reef survey area collected data over three summer periods between 2010-12. Missing data removed (n = 15,974 hours). No data collected at Penberth in 2012. Abbreviation: IQR = inter-quartile range.

Parameter	Value
Hours of data per year: 2010, 2011, 2012 (total)	4005, 6877, 5092 (15,974)
Hours of data per site: Eastern, Margin, Penberth (total)	6173, 6172, 3629 (15,974)
Number of 'presence' hours: Eastern, Margin, Penberth (%)	177 (2.9%), 164 (2.7%), 98 (2.7%)
Survey variables	
Site (as nominal)	East, Marg, Pen
Wave direction (degrees)	
Range	4 – 356
Median (IQR)	185 (179 – 190)
Wave height (m)	
Range	0.08 – 3.62
Median (IQR)	0.44 (0.27 – 0.66)
Tidal variables	
Tide direction (degrees)	
Range	27 – 333
Median (IQR)	207 (110 – 287)
Tide speed (m s^{-1})	
Range	0.07 – 1.56
Median (IQR)	0.56 (0.33 – 0.86)
Tide height (m from LAT)	
Range	0.14 – 5.8
Median (IQR)	2.89 (1.75 – 4.1)
Tide range (m)	
Range	2.06 – 5.77
Median (IQR)	3.8 (2.99 – 4.45)
Tidal hour (hours relative to HW)	
Range	-6.28 to +6.32
Median (IQR)	0.0 (-3.08 to +3.12)
Tidal flow group (as factor)	
Range	1 – 4
Median (IQR)	2 (1 – 3)
Temporal variables	
Year (as factor)	
Range	2010 – 2012
Month (as factor)	
Range	7 – 10
Hour (GMT)	
Range	0 – 23

Preliminary analysis on the effort-corrected dataset indicates dolphin acoustic activity was not influenced by tidal flow direction (Figure 4.12-A), with an even distribution of detection rates

across eastward and westward flow. The rate of acoustic activity decreased with increasing tidal speeds (Figure 4.12-B), particularly when flow streams in the survey region exceeded a threshold value of ~0.9 m s^{-1}.

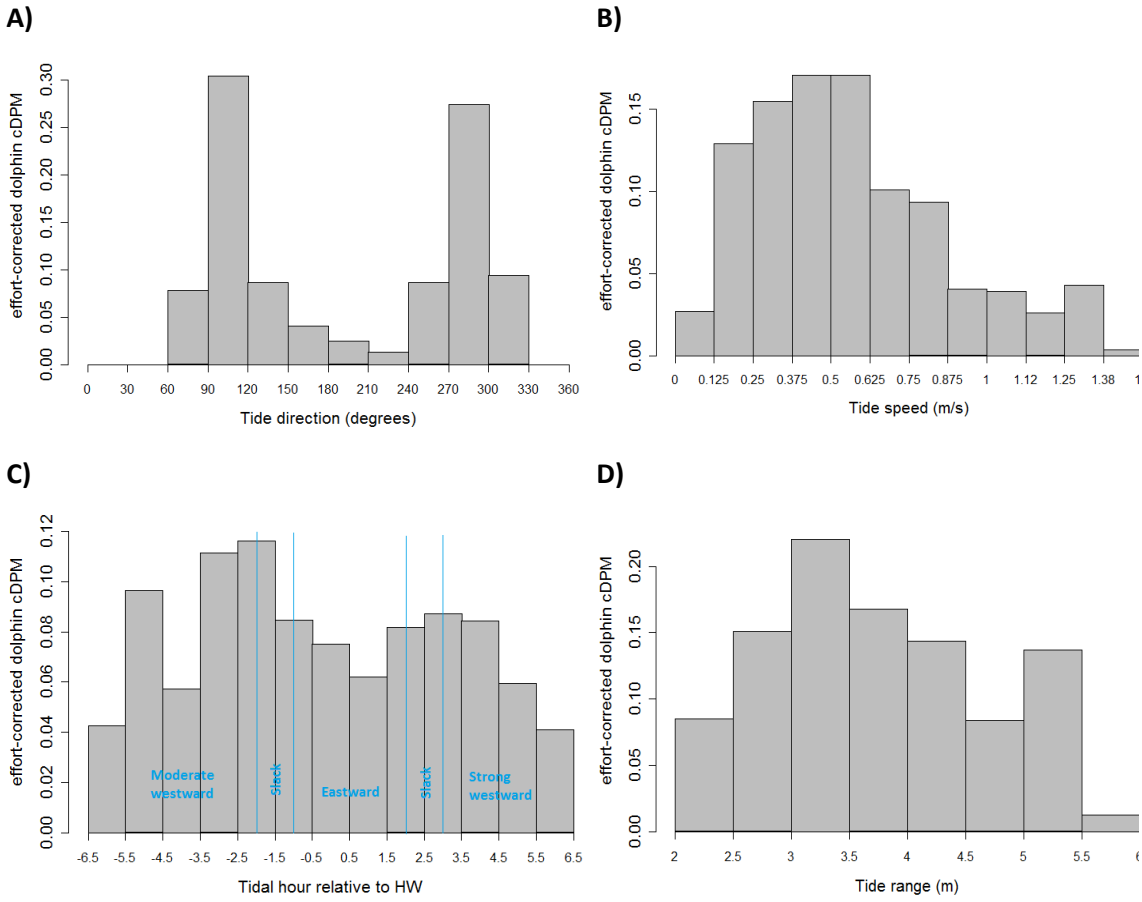

Figure 4.20. Effort-corrected dolphin cDPM as a function of tidal variables.
Acoustic data collected by three data loggers (CPODs) in the survey area, over 15,974 hours of survey effort across years 2010-12. Data were pooled across sites and years. A): Tidal flow direction (degrees), B): Tide speed (m s^{-1}), C): Tidal hour (relative to HW, where HW = 0), and D): Tidal range (m).

Rates of dolphin echolocation appeared to have little relationship with time in the tidal cycle (Figure 4.12-C), though there was increased activity around periods of slack water (HW-3 to HW-1, and HW+2 to HW+4) and a decrease during eastward flows (local HW-1 to HW+2). Tidal range (Figure 4.12-D), a proxy for phase in the lunar cycle, had little influence on dolphin acoustic activity, although there was an increase that peaks nearly half way through, i.e. just before neap tides, between 3-3.5 m (where the tidal range was 2-6 m).

4.3.3.2 Temporal Model (dolphins)

To investigate temporal patterns of dolphin acoustic activity, the presence-absence of cDPM hr^{-1} was modelled with a range of candidate survey, tidal and temporal variables measured each hour of acoustic survey effort (Table 4.10) using a binomial GAM with a logit-link function. Collinearity between the candidate variables was explored using a pairplot (Appendix J.2). Tide height and flow group were highly collinear (r = 0.81), with the latter removed from further analysis, according to the procedure to deal with collinearity (see Section 4.2.5). Through forward step-wise selection, the modelling process first compensated for survey effects (site, wave direction, wave height, and acoustic noise), then tidal variables and finally temporal variables. Site was not significant, which justified pooling the dolphin data.

The final model selected acoustic noise ("Nall"), tidal range, and hour of the day, as significant predictors (all $p < 0.001$) on the presence or absence of dolphin detections at the Runnel Stone Reef (Table 4.11). The model explained 17.4% of deviance over 15,974 hours of survey effort across years 2010-12, and took the form:

Dolphin detection occurrence ~ s(Nall) + s(TideRng) + s(Hour)

Figure 4.21 shows the model smooths. The ACF of model residuals (Appendix J.3) shows significant residual correlation of ~6 hours that the model has not accounted for.

Table 4.11. Results of forward GAM model selection for presence-absence of dolphin detections.
Variables are shown in order of importance, first compensating for survey effects (acoustic noise "Nall", wave direction, wave height, site). Smooths are shown with the number of estimated degrees of freedom (e.d.f.) in parentheses; AIC_{Δ} is the reduction in AIC score caused by the addition of the significant variable to the model, with the first score in bold showing the starting AIC; % Dev is the additional deviation (%) in the data explained by adding the selected variable to the model. Surveys conducted across summer periods 2010-12 at the Runnel Stone Reef (n = 15, 974 hours).

	Dolphin detections pooled across sites		
Order	Smooth (e.d.f.)	% Dev	AIC_{Δ}
1	s(Nall, 4.9)	12.3	**3521.55**
2	s(TideRng, 4.5)	+1.2	-40.47
3	s(Hour, 2.0)	+3.9	-153.94
Total		17.4	

Of the survey variables, acoustic noise was the only important predictor of dolphin detection occurrence, explaining 12.3% of deviance (Table 4.11). Detection rate decreased significantly

with increasing noise (Figure 4.21-A), which was contributed to by a variety of possible sources (Table 4.12), primarily tidal range (8.2%) and wave height (7.7%), with dolphin clicks contributing the least (0.08%).

Table 4.12. Acoustic noise across sites explained by significant variables as % deviance.
Noise (total number of detected clicks) modelled as a function of individual variables in a negative binomial GAM with a logit-link. Superscript numbers indicate the order of variables relative to amount of deviance explained. Bold value indicates the variable explaining most deviation in the noise data. Surveys conducted across summer periods 2010-12 at the Runnel Stone Reef (n = 15,974 hours).

	Across sites
Noise explained by:	
Tidal range	**8.19%**[1]
Wave height	7.66%[2]
Tide height	4.76%[3]
Tidal hour	3.48%[4]
Porpoise cDPM	1.88%[5]
Dolphin cDPM	0.08%[6]

Position in the spring-neap cycle (represented by the proxy covariate, tidal range) was the only significant tidal predictor, explaining 1.2% of the deviance (Table 4.11), with fewer detections recorded towards springs (Figure 4.21-B). Additional analysis on the pooled data revealed a significant relationship ($p < 0.001$) between acoustic noise and tidal range (Appendix J.6), where noise levels increase with increasing tidal range, i.e. approaching springs.

There was a significant diel pattern (Figure 4.21-C), peaking around midnight and decreasing towards early afternoon (~1400 hrs), which explained 3.9% of deviance (Table 4.11). Hour was the only temporal variable retained in the model; year and month were not significant predictors on dolphin detections during the summer-only survey periods.

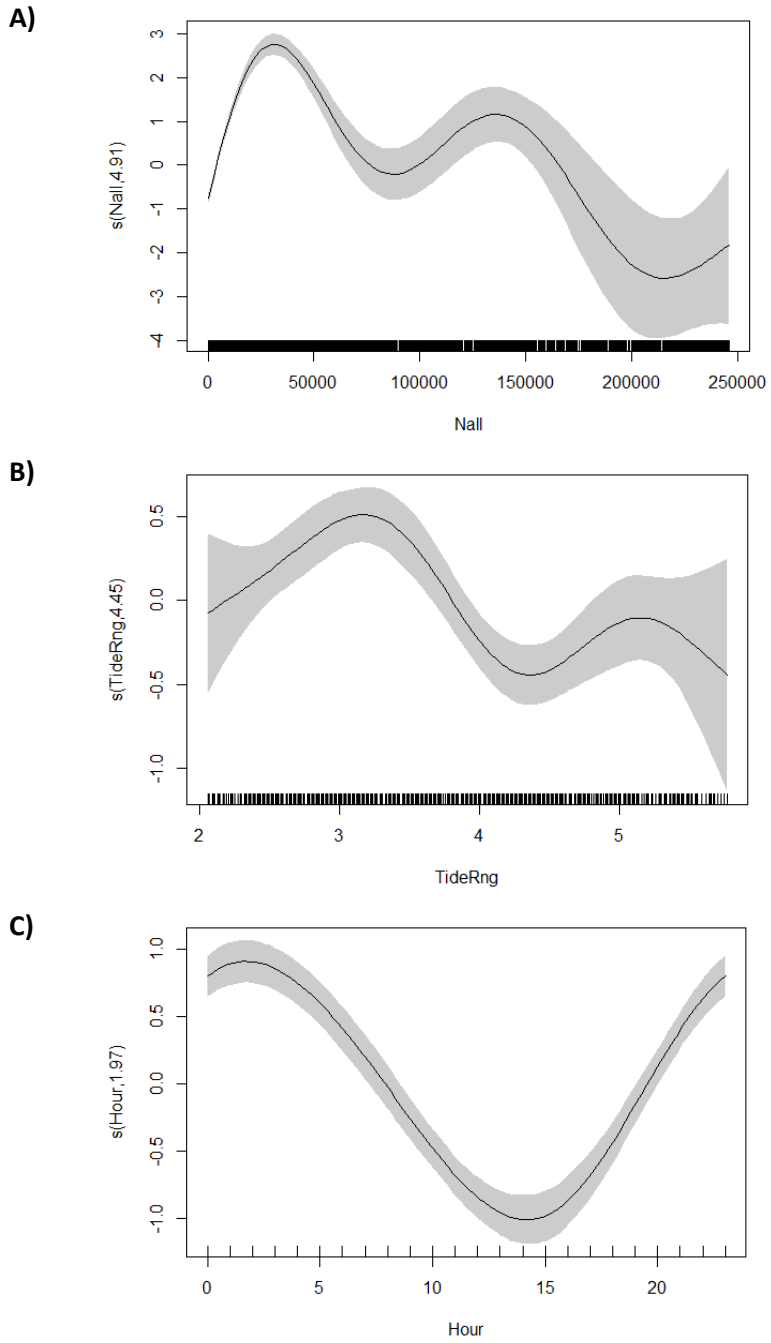

Figure 4.21. Smoothed relationships between dolphin cDPM occurrence and predictor variables.
As selected by the final binomial GAM (n = 15,974 samples), A): Acoustic noise (e.d.f. = 4.91), B): Tidal range (e.d.f. = 4.45), and C): Hour (e.d.f. = 1.97). Figures A) – C), smooths reported on the scale of the linear predictor, numbers in brackets in y-axis captions are e.d.f. (estimated degrees of freedom) of the smooths, rug plots at bottom of figures are covariate values, and shaded regions around the smooths represent 95% confidence intervals.

4.4 Discussion

Questions remain as to how different cetacean species respond to fine-scale (30-minute) temporal drivers of distribution over time, and whether (species-specific) habitat use is variable between sites within a constrained (<14 km^2) area. Three acoustic data loggers were deployed off southwest UK within the Runnel Stone Reef survey area over three consecutive summer periods to collect echolocation data on harbour porpoises and dolphin species. Since cetaceans only spend a small portion (~30%) of their time at the surface (Otani et al., 1998), it is possible that visual surveys may not accurately represent habitat use (Kyhn et al., 2012), as they only record snapshots in time during daylight hours. Additionally, the influence of variable survey conditions on cetacean detectability by land- or boat-based observation teams (Buckland et al., 2010) can affect the reliability of sightings-only datasets.

Acoustic survey methods, though spatially-constrained, can help overcome some of these issues, as they offer the possibility of collecting continuous, long-term datasets on subsurface presence with reduced effort and at comparatively low cost (Marques et al., 2009; Bailey et al., 2010). The acquisition of complimentary datasets that combine acoustic and visual sightings data is urgently needed (Booth et al., 2013) to better understand and explain the fine-scale distributions of vulnerable species that require effective conservation measures (such as SACs for Annex II species of Community interest; Directive 92/43/EC) aimed at the restoration and protection of the habitat on which they depend (Pirotta et al., 2013). This is particularly challenging for wide-ranging species (Roff, 2014), such as porpoises and dolphins, as their habitat preferences at very fine-scales remain poorly understood (Embling et al., 2012; Scales et al., 2014), yet knowing when and where these animals preferentially spend their time, and which environmental drivers (and the interplay between them) are responsible, is vital for informing management efforts (Redfern et al., 2006; Bailey & Thompson, 2009).

Detections

Analyses in this study have revealed a consistent level of baseline acoustic activity each year of survey for both porpoises (Table 4.3) and dolphins (Table 4.8), which indicates the area is locally-important for both species throughout the year, at least during the summer/autumn periods. This is consistent with results from other surveys, which highlight waters off Gwennap Head as host to a variety of cetaceans across seasons (e.g. Pikesley et al., 2011; Hardy et al., 2012; Leeney et al., 2012). Discreet peaks in the absolute number of detections for porpoises and dolphins, seen in the time series data (Figure 4.7 and Figure 4.16, respectively), often

corresponded between two or sometimes three of the sites, indicative of temporal clustering. This clustering suggests that if the animals visit one site, they are likely to visit another site in the study area within a short timeframe, i.e. within a few days. This is unsurprising, as regular sightings of porpoises were observed in the area on ~49% of days during an effort-based visual survey (see Chapter 3), while waters off southwest UK (apart from a variety of other cetaceans, as referenced above) also host a well-recognised, resident group of bottlenose dolphins (Hardy et al., 2012), which are known to regularly travel the ~50 km section of coastline (see Marine Discovery Penzance, and the Cornwall Wildlife Trust for public sightings data).

Dolphin detections were generally lower and more sporadic than those of porpoises, which may indicate the animals are primarily on transit through the study area and out of range of the detectors, except during irregular (perhaps more opportunistic) foraging events. Futhermore, travelling dolphins are less likely to be detected than foraging ones (Jones & Sayigh, 2002; Nuuttila et al., 2013), so the lower echolocation rates may also indicate travelling behaviours (Philpott et al., 2007) rather than prey pursuit, for example.

Results from the visual survey (Chapter 3) found peak numbers of dolphins in the area were regularly (>15 sightings) seen in pods of between 20 and 85 individuals, which contrasts to a peak of just 12 animals on one occasion for porpoises. These observed group sizes may account for the difference in the number of echolocation detections between species, as they are engaged in varying activities in the survey area. Additionally, Gannon et al. (2005) suggest bottlenose use their echolocation systems sparingly in the wild, as they detect their prey by 'passive listening', and only vocalise to track their target during the pursuit and capture phases. Conversely, porpoises need to be within high density areas for prey species throughout most of their life cycle, due to their limited echolocation range (Kastelein et al., 2005).

Since bottlenose dolphins can detect prey up to seven times further away than porpoises, they can survive in relatively less prey-dense environments (Au et al., 2007) further offshore and plausibly only come in to feed in higher energy, nearshore waters when necessary. This may be advantageous at the Runnel Stone study site considering the likely, higher energetic costs of travelling within the more dynamic environment around the reef itself. The ability of dolphins being able to detect prey at further distances than porpoises possibly provides an explanation of the different ecological niches occupied by these species in the survey area, indicated in the acoustic data. Dolphins perhaps only forage within the dynamic waters surrounding the reef

(where the detectors were located) on an more opportunistic and less frequent basis than porpoises.

A study monitoring dolphins and porpoises in Cardigan Bay, Wales, also reported habitat partitioning between the species within some parts of the study area (Simon et al., 2010), while Thompson et al. (2004) confirm that fine-scale segregation of the two species occurs where their ranges overlap. A contributing factor to this may be avoidance behaviours by porpoises in the presence of bottlenose dolphins that are known to attack them in the wild (Ross & Wilson, 1996; Bailey et al., 2010). However, the depth of the detectors and species' detectability should also be borne in mind when making inferences about possible habitat partitioning between the species, as Sostres Alonso and Nuuttila (2014) showed significantly more porpoise clicks were detected at loggers moored in the water column closer to the surface relative to those near the seabed, whereas no differences were recorded for bottlenose. Furthermore, the actual position of CPODs in the water can affect the vertical detection range of the loggers, and there is evidence to show that this vertical range is not as effective as the horizontal (Todd et al., 2009; Tougaard et al., 2009). For example, in water depth of 48 m, at a range of 70 m an animal's 16° vertical beam would only provide an acoustic footprint 20 m high (Todd et al., 2009). This has obvious implications for drawing conclusions between species, where their acoustic beam widths vary, and from data collected by only a handful of detectors at a study site.

Temporal variability

In the porpoise data, there was marked intra- and inter-annual variability in the number of detections. Small-scale variations in porpoise presence has also been noted by Booth (2013), Goodwin and Speedie (2008) and Hamazaki (2002), where seasonal shifts in habitat use were observed. Such fine-scale variability suggests the animals use the survey area for foraging, as they are more likely influenced by short-term fluctuations in their environment, which affect prey distribution and availability (Johnston et al., 2005b; Verfuß et al., 2007). This is particularly vital for porpoises given their daily, high energy requirements (Read & Westgate, 1997; Koopman et al., 2002; Sveegaard et al., 2012a).

Year and month were significant predictors on detection rates, with increased occurrence during the last month of surveys (October). Studies that surveyed across the year have found similar results (e.g. Pikesley et al., 2011; Sveegaard et al., 2011a; Leeney et al., 2012; Rodrigues, 2014), where higher numbers of cetacean sightings were observed in autumn and

winter. Simon et al. (2010) also reported peak porpoise detections during the winter months in Cardigan Bay but, at a location just 30 km away (at Bardsey Island), De Boer (2014) found porpoise numbers peaked during the summer. These reports, and the data presented in this study, seem to reinforce the idea that porpoises are more sensitive to fine-scale temporal fluctuations in the environment than dolphins, and will respond to changes on relatively short timescales, which is reflected by the inter- and intra-annual variability in the occurrence data. These findings have implications for coastal zone management regimes, particularly with regard to carrying out effective EIAs for wet renewable projects, or establishing fixed marine protected areas for the species.

This contrasts to the dolphin data, where neither year or month were significant predictors on detection, which highlights the more stable presence of dolphin activity through time. Indeed, Pirotta et al. (2013) indicated dolphins respond to coarser scale temporal dynamics (i.e. seasonality in prey abundance), where foraging is best predicted at daily scales, rather than hourly. Their study and others (e.g. Bailey & Thompson, 2006) found dolphins to have a detailed understanding of the finer-scale spatial distribution of resources, but acknowledge that it may be more profitable for dolphins to concentrate on relatively higher prey-dense areas within their home range, rather than attempt to develop a detailed understanding of temporal dynamics and/or small-scale patches of increased prey density. This may be a particularly relevant explanation to the findings reported in this study, where these dynamics may be so uncertain, or small-scale, that predicting food availability at such a fine-scale may not be beneficial for the animals (Pirotta et al., 2013).

Physical habitat

When the porpoise data were pooled across sites and modelled, site was selected as a significant predictor on detection occurrence, which was not the case in the pooled dolphin data. This suggests the animals are not using the survey area for foraging but, rather, as a passageway. The significant influence of deployment site on porpoise detection, even within a fairly spatially-constrained (<14 km^2) survey area, necessitated running the models for porpoises at each site separately, which, again, highlights porpoise susceptibility to fine-scale temporal and environmental variations. Due to the physical habitat differences between sites, the influence of tidal flows will be different at each location, as evidenced in the noise auto-correlation functions (Figure 4.5). The bay at Penberth is less tidally-dominated, while there is clear ebb and flood tide asymmetry at the two reef sites. The differing acoustic environments have implications for fine-scale spatio-temporal preferences and echolocation behaviours of

porpoises, as there were marked differences in the absolute number of detections between sites for the species that were not apparent in the dolphin data (Table 4.1).

The radar-derived current vectors (Figure 2.17) clearly show that during certain periods of strong westward flows, currents interact with steep slopes along the eastern reef edge (identified by the closely-spaced depth contours in the high resolution bathymetry data; Figure 4.2) and reach speeds of up to 2 m s^{-1}, as tidal streams are forced over and around the reef top. It is theorised that these slope-driven upwelling events cause patches of increased prey density (McPhee-Shaw et al., 2011), so it would be useful for future work in the area to focus on data collection of these 'missing links' to better explain the relationship between underlying physical processes and the distribution of top predators at these locations. Since these phenomena are temporally and spatially predictable (Franks, 1992b), and often focused around headlands or other protruding land features (Wolanski & Hamner, 1988; Embling et al., 2013), it is suggested that topographic features within tidally-dominated environments therefore serve as 'anchor points' for eddies and island wakes, and thus localised zones of enhanced prey density (Hao et al., 2003; Yen, 2004; Embling et al., 2013; Scott et al., 2013; Sharples et al., 2013a) and/or increased availability to predation.

During certain times of the tidal cycle, it seems likely that these localised zones of increased prey densities will attract porpoises for short time periods, and cause the animals to echolocate more during the prey-capture phases (Gannon et al., 2005). However, during the night, the noisy, topographically-complex environment may not be as suitable for acoustic foraging when the animals' use of vision is ineffective, and a quieter, less complex habitat may be preferred. Increased porpoise detections (~30% more) were recorded at the two reef sites, particularly the eastern reef edge, relative to the quieter, sandy bay at Penberth, though the number of hours spent there was considerably higher (~9 hours per day, compared to only 1.4 at the eastern reef edge, and 4.6 at the reef margin). This suggests the animals are using the sites in different ways, and choosing to spend the hours of darkness in an acoustically-quieter location. Jones (2012) also found the longest encounter durations were recorded at Penberth (54 minutes, compared to 25 and 14 minutes at the reef sites), where the diel pattern was also more pronounced. Interestingly, Penberth was the only site where the number of dolphin detections was a significant (negative) influence on porpoise presence, which suggests this is one area within the study region where the animals' spatial habitat preferences may overlap. The negative relationship may be explained by porpoise avoidance of dolphins, given the

known occurrences of aggression between the species (Ross & Wilson, 1996; Bailey et al., 2010).

Diel activity

Penberth was the only location with a significant diel pattern in porpoise detections (Figure 4.15-C), with a clear increase in nocturnal activity, suggesting the animals use this area for nocturnal feeding, most probably related to the diel activity of their prey (Todd et al., 2009). Carlström (2005) also indicated that porpoises increase their echolocation rates and/or visit the depth of the data logger more often at night than during the day, explaining that, given the decreased inter-click intervals in the train data, the animals are likely foraging. This seems plausible, as, during the day, cetaceans may preferentially utilise vision to forage, given the metabolic costs of echolocation (Gannon et al., 2005), so, for successful foraging in the darkness, poor levels of ambient light would necessitate increasing echolocation rates, thus justifying the strong diel pattern observed at the less acoustically-noisy site of Penberth. Equally, it is likely porpoises do not visit the noisy reef sites as much at night, as they would not be able to reliably use their echolocation senses to forage, given the louder, acoustic environment encountered there. Additionally, results from the visual sightings data for porpoises (Chapter 3) indicate these areas of the reef margin are core habitat within the survey region during daylight hours, which further indicates the animals do visit regularly, but perhaps use their vision in preference to echolocation for foraging.

There was a strong diel pattern in dolphin detections (Figure 4.21-C), with increased activity recorded in the hours just after midnight, decreasing towards the early afternoon. Allen et al. (2001) reported feeding frequency associated with diel state in bottlenose dolphins, where increased foraging peaked at dawn and decreased throughout the day. A study on the south side of the Shannon Estuary in Ireland (Ingram et al., 2005) also found that 79% of detections were recorded at night during one month of survey. However, Philpott et al. (2007) found no diel patterns in their study, which was carried out on the north side of the Shannon over a two-month period. Without taking into account the static habitat variables and other tidal influences at these study sites that may have impacted acoustic activity, caution should be applied extrapolating the findings to other areas or attempting to make more general inferences about the species' diel preferences.

Tidal influence

Tidal range was a significant predictor on dolphin detections, which decreased approaching spring tides (Figure 4.21-B). Embling et al. (2010) found increased detection rates during spring tides for visual sightings of porpoises, which the authors proposed may be due to an increase in visible feeding cues during such periods. By the same token, this may explain the reduced dolphin echolocation rates found in this study during springs, as there may be less need for energy-expensive acoustic foraging methods.

Porpoises were acoustically more active during eastward flows (double the rate of cDPM) than during westward (Figure 4.12-A), though this pattern is reversed in the visual sightings data (Chapter 3), where the rate was six times higher during westward flows. In this study, the reef sites are in lee of the eastward tidal streams flowing over the plateau. This points to the impact of tidal-topographic interactions in the survey area where, following tidal flow reversal, westward flows interact with the steep, eastern reef edge leading to the formation of a lee wave with associated hydraulic jump; these conditions are evidenced in the ADCP data presented in Jones et al. (2014a). Resultant increased shear instability and turbulence may therefore contribute to acoustic noise on this side of the reef, either making it difficult for the animals to echolocate during these noisy periods or compromising the ability of the data loggers to continue recording if the data buffer saturates from too many detections (pers. comm. N. Tregenza, 2013). In fact, these tidal-topogrpahic interations are indirectly evidenced in the strong sediment signatures revealed in the noise auto-correlation plots at the reef sites (Figure 4.5), which are indicative of tidally-dominated environments (Chelonia, 2013). Since there was no difference in the absolute number of dolphin clicks with tide direction, this again suggests that dolphins are not using the area to forage, but rather as a passageway.

The reef sites in lee of eastward tidal flows are thus relatively sheltered and less noisy during these periods, which may likely be more conducive to acoustic foraging than during westward flows. Rodrigues (2014) also reported increased porpoise acoustic presence during weaker tidal flows in the Netherlands, though noted that the animals vocalised more during noisy periods. However, given marine mammals' vulnerability to sound pollution (Kastelein et al., 2005), and naturally-occurring noise, this may reach a threshold value at which the animals would choose to avoid an area. The influence of noise on porpoise detection occurrence has been frequently reported in other studies (Kastelein et al., 2005), including undesired 'clutter' echoes from bottom structures and rainfall (Miller & Wahlberg, 2013). High acoustic background noise can not only irritate porpoises, but also interfere with communication and

prey detection (Au, 1993), which may explain avoidance of the noisier reef sites during certain times of the tidal cycle.

Conclusions

This study analysed a three-year (summer-only) acoustic dataset to compare fine-scale temporal preferences between porpoises and dolphins within a recommended Marine Conservation Zone. Time series comparisons highlighted the intra-annual variability that was more marked in porpoises than in dolphins, but provided evidence of a consistent level of acoustic activity, and therefore likely cetacean presence throughout the survey region.

Though questions remain regarding quantifiable predator-prey interactions at fine-scales (Embling et al., 2012), recent work is attempting to elucidate these relationships to better explain the interaction of environmental drivers of top predator distribution (Embling et al., 2013; Scott et al., 2013; Sharples et al., 2013a). The studies collected concurrent data on physical habitat, physics, and fish distribution (acoustics) within survey areas, and ensured sampling across tidal and lunar cycles for more complete temporal coverage. Findings presented in this study were discussed in light of results from the visual dataset collected by a land-based survey (see Chapter 3). Using results from two complimentary datasets to better understand cetacean distribution in the study area also highlights the importance of acquiring more than one type of occurrence dataset for species that spend much of their life cycle subsurface, and demonstrates the value of using a complementary suite of techniques to collect and analyse observation data (Embling et al., 2013; Sharples et al., 2013a).

Whilst the study is limited by the seasonal nature of the survey design, it has provided detailed information on between site and inter-annual patterns in the subsurface presence of protected species, thus building on previous work presented in Jones (2012). Temporal preferences revealed in this study are based on only three summers of data, so caution should be applied when making inferences or extrapolating results to draw wider conclusions, particularly as echolocating marine mammals exhibit different vocal and activity patterns between sites (Jones & Sayigh, 2002). However, the study revealed considerable differences in environmental predictors on the distribution of harbour porpoises and dolphins within a relatively confined survey area, that are also site-specific. These findings may have implications for effective marine protected area site selection, which is urgently required for their protection, particularly as the differences were exhibited by local populations within the same survey area.

Chapter 5 Fine-scale spatio-temporal distribution of plunge-diving seabirds in a tidally-dominated complex environment in southwest UK

A B S T R A C T

Questions remain as to how wide-ranging marine top predators preferentially use their habitat in coastal waters, particularly at fine (<1 km) scales. Waters off the headland at Gwennap Head, southwest UK, are a known, regionally-important habitat for aggregations of foraging seabirds, primarily northern gannets *Morus bassanus* and black-legged kittiwakes *Rissa tridactyla*, which target areas around the topographically-complex Runnel Stone Reef (<20 m water depth). The horseshoe-shaped rocky reef extends ~1.5 km south off the mainland, and falls within the recommended Marine Conservation Zone of Land's End (Runnel Stone). Between 2011-13, systematic land-based surveys were carried out using a theodolite to derive precise locations in order to assess fine-scale (<20 m) spatial distribution, and determine fine-scale (30-minute) environmental variability in occurrence; information currently lacking for these species at such scales. Sightings of harbour porpoises *Phocoena phocoena* and fishing vessels were also recorded for comparison of habitat use. Data were collected across 55 days, and 404 hours of daylight-only survey effort (in sea states ≤ 3, and visibility >5 km). Generalised additive models (GAMs) were constructed to determine the influence of static bathymetric variables on relative density, and temporal variability on presence-absence data.

Foraging aggregations were sighted on 58% of survey days (n = 119 individual events); only 11.3% of 30-minute scan samples were positive for sightings. The average sightings rate was 0.29 sightings of aggregations-hr^{-1}. Statistical modelling indicated the survey variables, wind speed and cloud cover (suggested to affect flight and foraging ability), had a significant negative influence on the timing of foraging events. Tidal range (a proxy for position in the spring-neap cycle) was the only significant hydrographic influence, with increased sightings towards spring tides. Daylight hour was the only significant temporal variable, with fewer foraging events around midday.

Analysis of gridded (600-m) relative-density data revealed benthic slope, depth, aspect, and an interaction between slope and depth, were significant bathymetric predictors of distribution, with slope explaining 38% of variation. There was a positive correlation with (east-facing) slope, and decreased preference for areas ~40 m water depth. The interaction suggests areas of high slope were favoured in shallower (<30 m) water depths. This was consistent with results from the kernel density analyses, which highlighted the steeply-sloping eastern reef edge, particularly near areas of topographic highs (e.g. pinnacles) identified in the raw theodolite data. Core habitat was not influenced by tidal flow direction. Spatial clustering significantly overlapped with artisanal line fishing ($r = 0.83$, $p < 0.001$).

This study proposes the influence of tidal-topographic interaction on predictable (and spatially-constrained) prey availability based on a novel dataset, including: 1-m resolved bathymetry, radar-derived tidal flow metrics, ADCP survey data and theodolite-derived locational data. Identifying extremely fine-scale habitat associations between foraging seabirds and their environment has implications for management of vulnerable species, such as wet renewables.

5.1 Introduction

Seabirds live and forage in the marine environment (Schreiber & Burger, 2002), which includes pelagic and coastal areas. The focal species in this study, northern gannets *Morus bassanus* and black-legged kittiwakes *Rissa tridactyla*, are true seabirds, since they feed at sea (Nelson, 1978) for extended periods of time (Croxall et al., 2012). Relative to land birds, they experience late maturity, low fecundity and are long-lived (Schreiber & Burger, 2002). Furness and Camphuysen (1997) suggest seabirds should not be regarded as 'monitors' of the marine environment but, rather, potential 'indicators' of prey availability (Montevecchi, 1993), e.g. schooling fish, and, by association, localised zones of productivity (Votier et al., 2010). Additionally, seabirds have a high and constant energy requirement, so, given their high mobility, they can be expected to show a strong aggregative response towards prey concentrations (Fauchald, 2009).

Monitoring changes in seabird foraging ranges and patterns of distribution are therefore clearly useful tools for marine spatial planning (Ronconi et al., 2012) and their position as top predators means their response to climate change is a good index of its effect on the whole food web (Durant et al., 2004). Seabirds are likely highly effective proxies for identifying priority sites for the conservation of other taxa for which data are deficient (Hooker & Gerber, 2004; Lascelles et al., 2012), though such indirect links should not be used in isolation (Thaxter et al., 2012). Furthermore, predicting the response of local marine organisms to possible climate variability or climate change scenarios remains a 'highly speculative exercise' (Frank et al., 1990; Ottersen et al., 2004). However, the coastal seas are not a homogenous environment (Franks, 1992a; Sims & Quayle, 1998), so analysing the fine-scale spatial distribution of foraging seabirds, as a proxy of prey availability (Hunt et al., 1998; Diamond & Devlin, 2003; Lewis et al., 2004), can provide important information on the influences of tidal, temporal and static habitat (e.g. depth, slope) variables that drive productive zones (Schneider, 1997; Diamond & Devlin, 2003; Sveegaard et al., 2012b; Sharples et al., 2013a; Sharples et al., 2013b). This is particularly useful in the absence of appropriately-resolved remote sensing data on productivity, and/or quantifiable data on fish distribution (which may also be difficult to acquire in challenging, high energy environments).

Studies attempting to statistically correlate water mass parameters (e.g. salinity, SST, water depth), productivity and the distribution of pelagic seabirds for assessing the value of their presence as environmental predictors across wide oceanic zones began in the early 1970s

(Dunn, 1973; Pocklington, 1979; Abrams & Griffiths, 1981; Schneider & Piatt, 1986). The tentative hypothesis was that local seabird distribution is mainly a function of prey availability and the species' attributes (i.e. their ecology and phenology) for prey location and capture (Gaston & Nettleship, 1982; Ainley & Boekelheide, 1983; Hunt, 1991a). Abrams and Griffiths (1981) noted that subsets of parameters for water masses and weather (barometric pressure, air temperature, wind and wave metrics) also correlated with seabird distribution, so relevant behaviours (such as foraging) may therefore reflect changes in the marine ecosystem (Haney, 1986; Hunt, 1991b; Elkins, 1995), which is of particular interest to studies of marine ecology (Montevecchi, 1993; Furness & Camphuysen, 1997; Barrett, 2002; Wilson et al., 2002; Diamond & Devlin, 2003).

In more recent years, studies combining geostatistical interpolation methods with environmental, hydrographic and ecological parameters (such as abundance estimates) have attempted to delineate sea areas of potential importance for seabirds (DiGiacomo et al., 2002; Burger & Shaffer, 2008; Wakefield et al., 2009a) needed to inform a variety of marine activities. These include the designation and effectiveness of marine protected areas (MPAs), vital for population persistence (Grecian et al., 2012; Lascelles et al., 2012; Ronconi et al., 2012; Thaxter et al., 2012; Pollet et al., 2014), mitigating seabird bycatch in gillnet fisheries (Melvin et al., 1999; Bull, 2007; Munilla et al., 2007; Sonntag et al., 2012; Žydelis et al., 2013), and to inform environmental impact assessments (Garthe & Hüppop, 2004; Guilford et al., 2012; McFarlane Tranquilla et al., 2013; Bogdanova et al., 2014; Soanes et al., 2014).

During the third national quantitative review of Birds of Conservation Concern (BoCC 3), 246 bird species were assessed against a set of objective criteria (Eaton et al., 2009). The target seabird species in this study, northern gannets and black-legged kittiwakes, comprise two of 126 species that are included on the BoCC 3's 'amber' list (see Appendix G for assessment criteria), reflecting their conservation status at the UK, European and global levels. The urgency to identify, designate and effectively manage MPAs for highly mobile seabirds is increasing (Grecian et al., 2012), so the need to better understand the ecological significance of certain concentrations of animals is vital, and their potential for interaction with human activites (Waggitt & Scott, 2014).

Studies should not only collect presence-absence data (for relative density analyses) but also behavioural information (Camphuysen et al., 2012), including foraging locations, so that variation in seabird distribution can be better understood and explained in context. More integrated survey approaches will help explain the most significant environmental drivers on

distribution, and improve knowledge required for MPA designation for the species. Gannets and kittiwakes are plunge divers that visually locate prey from the air (Nelson, 1978), so the number of dives may be considered a suitable proxy for prey-encounter rate (Lewis et al., 2004). Kittiwakes are surface feeders, but also make shallow plunge dives up to ~1 m (Camphuysen et al., 2006), while gannets typically make high, vertical dives to between 5 and 20 m water depth (Garthe et al., 2000; Brierley & Fernandes, 2001). Apart from shallow-diving kittiwakes, gannets are the only deep plunge divers in the North Atlantic (Nelson, 1978). Since they commonly fish in flocks of tens or hundreds (Garthe et al., 2000) in the cold, nutrient-rich waters overlying continental shelves and fishing banks, this is often a signal to fishermen and other marine species (e.g. cetaceans) that there are shoals of fish near the surface in sufficient concentrations (Barrett, 2002; Camphuysen et al., 2006). In the northeast Atlantic, studies have shown these fish include: sprat and herring (family Clupeidae), mackerel (family Scombridae), schools of capelin *Mallotus villosus*, deeper in the water column (Garthe et al., 2000), and sandeels *Ammodytes* spp., a principal prey fish of seabirds (Camphuysen et al., 2006; Daunt et al., 2006; MacLeod et al., 2007a; Wanless et al., 2007; Embling et al., 2012), either settled in the seafloor or foraging mid-water (Camphuysen et al., 2006).

In tidally-dominated environments, small-scale physical processes, such as localised convergence zones (e.g. island wakes, eddies, tidal-topographic fronts) are important for seabirds to locate prey resources (Hunt et al., 1999; Wilson et al., 2002; Genin, 2004). For example, tidal currents have been shown to influence sandeel schooling making them more accessible to surface-feeding kittiwakes (Embling et al., 2012). The same study hypothesised that this was topographically-driven, leading to spatially-focused foraging by top predators (Stevick et al., 2008). Indeed, Genin (2004) showed that currents interacting with abrupt topographies, such as seamounts, led to daily accumulations of zooplankton that become trapped in relatively small confined areas, a mechanism the author terms ‘trophic focusing’, which support aggregations of higher predators (MacLeod & Zuur, 2005; Bertrand et al., 2008; Skov et al., 2008).

Physical processes are potentially more regular and predictable than biological phenomena over a long time span (Shealer, 1996) and, at the smallest scales, can result in greater prey availability, relative to biotic interactions (Hunt, 1991b; DiGiacomo et al., 2002). However, although a strong or persistent pycnocline (density gradient) may concentrate prey at particular depths in the vertical dimension, the processes are not static (Franks, 1992b, 1992a; Shealer, 1996; Hunt et al., 1999). Environmental conditions (e.g. wind, sea state, air

temperature) can induce changes in the physical structure of a water mass (Lynch et al., 1992; Sharples, 2007), which alters localised concentrations of lower trophic level prey in the short term (<14 days; Haney, 1986; Hao et al., 2003; Bertrand et al., 2008). This variability can influence the 'patchiness' (Georges et al., 2000; Guinet et al., 2001) of prey fish and therefore the spatio-temporal distribution of seabird foraging (Wilson et al., 2002; Adams & Flora, 2009) at similar scales. Additionally, oceanographic variables (internal wave activity, shear fluxes, position in the spring-neap cycle) also impact on fish schooling behaviour (Sharples et al., 2013b), which influences their availability to predation (Embling et al., 2013), again highlighting the importance of seabirds as indicators of sites of elevated trophic transfer (Yen, 2004). Understanding the drivers of their distribution is clearly important for ecosystem-level conservation plans (Yen, 2004; Embling et al., 2012).

Information downloaded from satellite transmitters and data loggers, technologies that have been developed over the last decade (Daunt et al., 2006), have been successfully used to identify areas of potential importance for seabirds (Camphuysen et al., 2012).

Figure 5.1. Photograph showing a seabird foraging aggregation at the Runnel Stone Reef study site. A foraging event was defined where >5 gannets or >20 kittiwakes plunge-dive in obvious association with each other within a concentrated area, which varied depending on the number of birds present. (Photograph © R Wynn 2011).

Camphuysen (2012) cited several studies that describe distribution patterns based on ship-based surveys within the North Sea but noted the lack of precision in spatial foraging patterns. The author suggested this information can only be collected effectively during visual observations, which reinforces the value of the precise theodolite method used in this study to reveal fine-scale associations with bathymetric (static) variables that may be used as proxies to characterise habitat suitability (e.g. fine-scale frontal systems; Le Fevre, 1986; Franks, 1992b; Farmer et al., 1995; Yen, 2004 and tidal-topographic interaction; Wolanski & Hamner, 1988; Scott et al., 2010; McPhee-Shaw et al., 2011; Jones et al., 2014a) and better explain foraging preferences. Although the majority of their life cycle is spent at sea (Croxall et al., 2012) where seabirds may be hard to study, nearshore foraging flocks (Figure 5.1) can be monitored effectively from land-based observation stations, which is often a more cost-effective (Denardo et al., 2001) and practical method in tidally-dominated environments, relative to boat-based surveys.

Waters off the land-based watch point at Gwennap Head, southwest UK, are characterised by strong tidal flows but amenable to shore observations of a variety of foraging seabirds that are known to visit the area in high numbers (Collins, 2011; SeaWatch SW, 2014). Given the complex topography of the Runnel Stone Reef, with its areas of bathymetric highs (e.g. pinnacles), relative to the more homogenous environment of waters surrounding it (Figure 2.13 on page 35), the survey area was selected to test the hypothesis presented by Collins (2011) that fine-scale physical processes, possibly caused by tidal-topographic interaction, result in increased numbers of foraging seabird aggregations associated with these features (primarily steep seabed gradients). Spatial and temporal variability in distribution patterns was hypothesised to vary at similar scales at the study site, and tested using gannets and kittiwakes as model species.

This study aimed to: 1) explain which static habitat variables drive the spatial distribution of foraging aggregations of gannets and/or kittiwakes; 2) explain temporal drivers of foraging distribution, including the influence of survey and tidal variability; and 3) identify features within the survey area that host increased numbers of foraging aggregations and determine whether these overlap with human activity, such as fishing effort, or the presence of other marine top predators, such as harbour porpoises *Phocoena phocoena*, which would highlight their wider importance to a variety of top predators. These objectives were met by combining novel survey data (of precise locations of foraging seabird aggregations, fishing vessels and porpoises, collected using a theodolite during surveys) with co-located high resolution

bathymetry, a suite of temporal variables (collected at a similar resolution as the sightings data), and interpreted in light of radar-derived current flow imagery and ADCP analysis from Jones et al. (2014a). By gridding the visual sightings data, a spatial model was constructed to explain significant patterns in the relative density of foraging locations within the study area, and predicted distribution was compared to the observation data. Additionally, by modelling the effort-based sightings data together with dynamic hydrographic and temporal variables, contrasts in fine-scale foraging patterns, that are tide- or time-dependent, and variable at short (<14 days) timescales, were revealed.

This study provides extremely fine-scale qualitative and quantitative assessment of bathymetric and temporal foraging preferences exhibited by the focal seabird species, and compares these to porpoise distribution and human activity in the area. Significant environmental drivers explaining their distribution at this site may be used to inform marine spatial planning in areas that have similar bathymetric or tidal flow characteristics, and contribute to the knowledge base for more effective, ecosystem-level MPA management in the future (Yen, 2004). Appropriate management is vital for their persistence, particularly in the face of climate change (Wanless et al., 2007; Wynn et al., 2008) and ever-increasing anthropogenic stressors in coastal waters (Grecian et al., 2012; Pollet et al., 2014; Waggitt & Scott, 2014).

5.2 Methods

5.2.1 Survey Methodology

Visual surveys to detect and record seabird foraging aggregations were carried out over 55 days during years 2011 to 2013. A foraging aggregation was defined as a group of >5 gannets or >20 kittiwakes actively foraging (plunge-diving) in obvious association with each other within a concentrated area, which varied depending on the number of birds present.

To detect aggregations from shore, an observation team comprising at least two observers were equipped with 10x binoculars and 30x telescopes. One observer operated the theodolite (Leica FlexLine TS02 Total Station), equipped with a 30x monocular eyepiece. The theodolite records angles to a precision of 0.0018° of arc. The instrument's tripod was set up each day directly over a precisely-surveyed point, measured at the beginning of the study using a Trimble Differential GPS (DGPS). During every hour of survey (see details below), the horizontal

measurement was zeroed and the theodolite level checked. Measurements of tidal changes in the instrument's height above sea level were also recorded every 30 minutes, and necessary tidal height corrections were carried out during data processing (see Section 2.1.2 for calculation details).

Every 30 minutes, an intensive scan of ~10-12 minutes duration was conducted concurrently by members of the observation team, using telescope, binoculars and naked eye. This ensured thorough and consistent coverage of the near- and far-fields throughout the survey period. Firstly, two observers would use their telescopes and carefully scan the distant Field of View (FoV) from east to west for five minutes (with the horizon at the top). Secondly, the observers would drop down a FoV and scan west to east for a further five minutes. Thirdly, the observers would scan using binoculars in the same way but with a focus on the near-field (<2 km distance) with the Runnel Stone cardinal mark in the centre of the FoV during the first sweep, and at the top of the FoV during the second sweep (Figure 2.9). The final search covered the nearshore area out to 1 km with the naked eye.

When aggregations were sighted, the theodolite eyepiece crosshairs were centred at the waterline on an animal in the centre of the group and, using the instrument's 'record' button, precise angles were saved onto an internal data file, automatically time- and date-stamped, having pre-installed an instrument-specific (.frt) format file for this purpose. The theodolite record number, "Point ID", along with species composition and group size, were noted on standardised recording sheets (Appendix D). Each recording of a foraging aggregation was allocated a "Sighting ID"; the same IDs were only confirmed in the field if they had been tracked by a nominated observer engaged in a dedicated "focal follow". This observer continued to visually track the marked group with scope or binoculars to ensure that when the theodolite operator returned to record the location again (e.g. after time spent recording positions of other species), the ID could be confirmed. Observers would resume scanning immediately after foraging events were recorded to ensure consistent effort.

All visible areas of the sea surface were therefore methodically scanned in the same way for at least ten minutes every 30 minutes, ensuring a consistent and repeatable sampling strategy. Data for *in situ* weather conditions and other environmental variables, e.g. sea state, wind, visibility, cloud cover and glare (see Appendix C for descriptors), were collected every 30 minutes at the start of each scan and recorded on the same standardised recording forms (Appendix D). Various forms of fishing activity were also recorded, taking a single theodolite fix of each vessel every 30 minutes, to visualise any correspondence with seabird foraging, in

terms of spatial preferences within the survey region. Survey units of 30-minute duration were selected to ensure the dedicated ~10-minute searches (conducted at the start of each 30-minute survey unit) were considered independent, and that changes in environmental parameters, e.g. weather, were recorded at a temporal resolution that allowed comparison with sightings data.

Locations of surfacing harbour porpoises were also recorded during surveys (see Chapter 3) to analyse spatial overlap of core density areas with those of seabirds at the study site to test whether preferred habitat is shared across species (with implications for management). Various forms of fishing activity were also recorded, taking a single theodolite fix of each vessel every 30 minutes, to quantify spatial overlap with seabird foraging areas and identify any potential for interaction. Notes were taken on fishing vessel activity, e.g. handlining, recreational, tourist, netting.

Although the observation site provided a wide FoV of the study area, the exposed location meant that observations were impacted by high winds and other inclement weather events, e.g. rain and sea fog. Fieldwork was therefore only conducted during periods of good visibility (>5 km) or sea state ≤3. Observation periods ranged between 4 and 12 hours.

5.2.2 Analytical Methods

5.2.2.1 Spatial Analysis

Initial data exploration was carried out to gain an overall impression of the theodolite data, post-processing in FlexOffice, v.2 (Leica Geosystems), see Section 2.1.2 for details. Maps were produced in ArcGIS® (ESRI, 2012) combining the raw sightings data with the bathymetry layer. This enabled preliminary visual analysis at a very fine-scale (<20 m), including comparing exact foraging locations according to tidal state. To analyse the spatial data, the survey area was delineated at 3 km from the watch point, for multiple reasons detailed in Jones et al. (2014a, pp. 22-3), Appendix A.

To analyse the spatial data, the survey area was delineated at 3 km from the watch point, so results could be compared with those of other species in the same survey area for which delineation at this distance was required (see Section 3.2.3.1 in Chapter 3 for further details on the rationale behind this decision). Issues of visibility were also considered at further distances, as more sightings would be missed beyond 3 km from the watch point, although it should be noted that seabird foraging aggregations could be spotted in the field up to 3 km

with the naked eye, given the criteria that defined a (very conspicuous) foraging event in this study, i.e. >5 gannets or >20 kittiwakes in clear association with each other.

The survey area (out to 3 km) was divided by radial bearing lines at 010° intervals, originating at the watch point, and chosen to account for positional error (see Section 2.2.2). The area was further subdivided into grid cells along concentric distance bands at 600-m, and 300-m intervals (Figure 5.2) for relative density analysis. The finer, 300-m cell size was selected as a compromise between the maximum positional error in the recorded sightings data at farther distances from the watch point (again, see Section 2.2.2) and to maximise use of the high resolution bathymetry. After clipping areas of affected grid cells that were obscured from view due to land topography, precisely measured in the field with the theodolite, as depicted by the greyed-out polygon (Figure 5.2), the visible survey area encompassed 13.83 km^2.

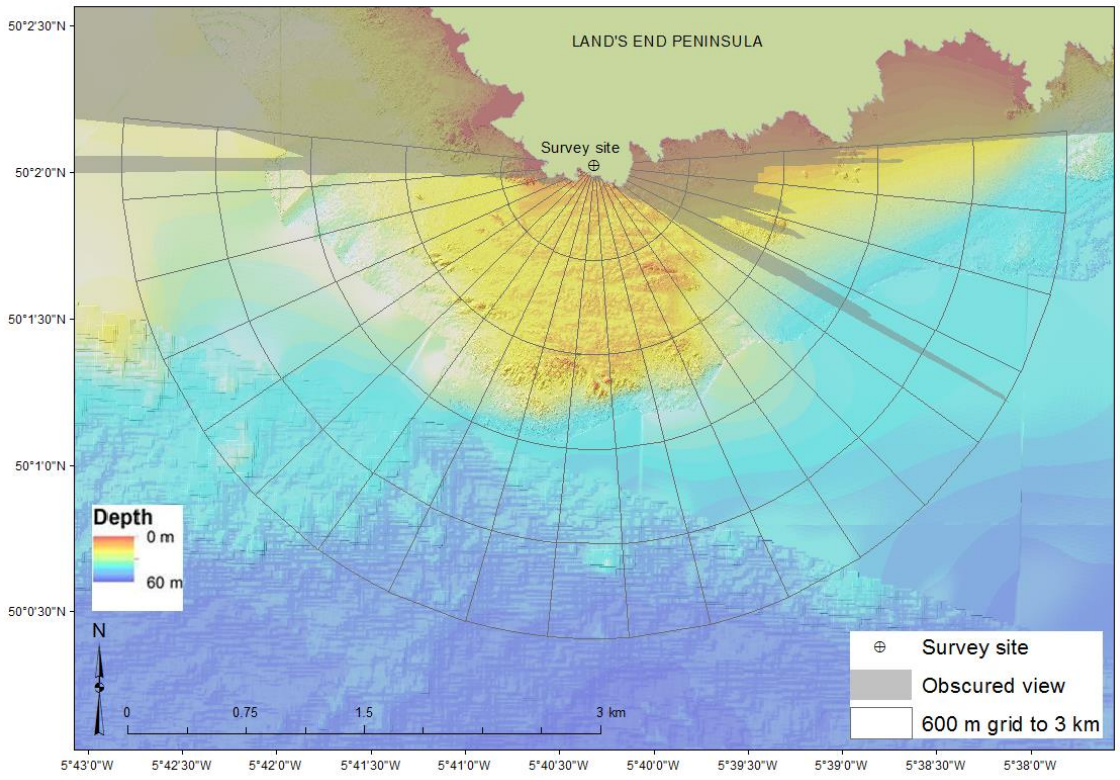

Figure 5.2. Radial grid delineated at 3 km from the watch point covering an area of 13.83 km².
Grid mapped onto high resolution (1 m) bathymetry data (courtesy of CCO/MCA © Crown copyright). Obscured areas due to land topography (greyed-out polygon) were precisely traced in the field by the theodolite and accounted for per grid cell in the analyses.

Sightings data were filtered by time and space to avoid successive measurements of the same aggregation, e.g. whilst being tracked, so only one sighting was retained in the spatial dataset

per grid cell per 30-minute survey unit. A re-sighting was therefore discarded if recorded in the same grid cell within the same 30-minute period. However, if an aggregation passed into a different grid cell within the same 30-minute period, it was retained in the dataset, so all sightings were spaced by a minimum of one grid cell and one 30-minute survey unit. The aggregation density grid based on these data therefore represents *relative* habitat use across the survey area, as the values per grid cell symbolise seabird foraging-visit frequency within any particular cell relative to its neighbour, i.e. the intensity with which a particular area was visited.

In ArcGIS®, the seabird sightings data (and fishing vessel locations recorded each 30 minutes) were summarised per grid cell by joining the sightings point layer to the polygon grid using the Spatial Joins tool. The static covariates, depth, slope and aspect (see Section 2.3.1), were also summarised per grid cell using the Zonal Statistics tool (Spatial Analyst > Zonal Statistics), taking into account differing grid cell areas. Extracted values per variable included: maximum, minimum, mean and standard deviation (s.d.).

5.2.2.2 Cluster Analysis

Kernel Density Estimation

Estimating the home ranges of individual animals is a useful measure to visually estimate how the intensity of a point pattern varies over an area during a specified time (Worton, 1995). Kernel Density Estimation (KDE) is used to identify and compare areas used by individual animals, i.e. their utilisation distribution (UD) or 'home range'. A KDE measures the density of records within each grid cell that covers a study area, and uses this to estimate the probability that an individual will use neighbouring cells (Kernohan et al., 2001; Horne & Garton, 2006). It therefore provides an estimate of which areas an individual uses most frequently, i.e. it is a raster dataset that represents a probability density surface that can be used to predict where an animal is likely to occur, though it was not necessarily observed (Horne & Garton, 2006). KDE rasters can be converted to isopleth lines that contain a specified volume of the probability surface, in doughnut polygons, for example, which identify areas where an individual is likely to occur. The isopleths are located where a shape with the shortest perimeter encloses a specified percentage of the positional records, which helps to identify areas of core habitat within a species' home range, i.e. 'hotspots'. The 0.5 isopleth represents the line containing 50% of the volume of the surface, i.e. the individual is likely to occur in that

area 50% of the time, and is often taken to define "core" usage area (Atwood et al., 2004; McFarlane Tranquilla et al., 2013).

For this study, Beyer's (2012) Geospatial Modelling Environment software (GME) was used within GIS to perform the kernel density analyses on the spatial data, using the KDE and Isopleth tools ('kde' and 'isopleth' commands in GME). It should be noted that the GME does not permit the creation of a KDE with "barriers", i.e. barriers to an animal's movements, such as land, in the case of marine species. In areas where such barriers exist, the creation of KDEs may not be particularly well suited, so Beyer (2012) recommends caution when interpreting any observable patterns in probability surfaces for target species of a nearshore population.

The KDE tool calculates probability density estimates based on a set of input points, and can implement three types of kernel. Depending on which kernel is used in the calculation, the bandwidth will be different. The default, Gaussian kernel was selected. Since this is a bivariate normal kernel, the bandwidth is the covariance matrix (for a bivariate normal distribution). Various bandwidth estimation algorithms, the 'selectors', can be specified, which estimate an optimised bandwidth matrix given the specific data, calculated in R using the Kernel smoothing package ('ks'). These are 2×2 matrices, though only three parameters need be provided for the KDE: the standard deviation for x, the standard deviation for y, and the covariance. Both the plug-in ('Hpi') and least-squares cross-validation ('Hlscv') bandwidth estimators were calculated, and entered into the KDE separately for later comparison. The final parameter required was cell size. Using Beyer's recommended 'rule of thumb' (Beyer, 2012), a cell size of 20 was calculated, based on the cell size of the point data source raster.

The resultant KDEs from both the plug-in and LSCV bandwidth estimators were converted to doughnut polygons with the Isopleth tool, and specified to contain the 25%, 50% and 75% quantiles. Based on field experience, outputs from the different bandwidth estimators were visually compared to determine which of the KDEs were the most ecologically-relevant. However, observable spatial differences between the kernels were negligible, so kernels from the plug-in algorithm were selected. Beyer (2012) also notes that the 'Hpi' performs particularly well compared to other bandwidth estimators.

The KDEs of porpoise sightings were calculated in the same way; see Chapter 3 (Section 3.2.3.3).

Seabird aggregation sightings filtered by the 600-m grid were also split into tidal flow groups: 1 and 2 for 'westward', 4 for 'eastward', and 3 for 'slack'. KDEs were computed, and the 50%

isopleths inputted into GIS for comparison of core habitat areas by tidal flow direction. This analysis would determine any fine-scale spatial preferences over short timescales, i.e. spatial preferences within a tidal cycle.

5.2.2.3 Temporal Analysis

For the temporal dataset, sighting IDs (see Section 5.2.1 for details on ID allocation) were filtered by 30-minute units of survey. Distinct IDs were retained each 30-minute unit, with re-sightings discarded. The same ID was retained if re-sighted in the next 30-minute unit of survey effort. This was considered representative of how the birds used the survey area *relatively* through time, even if it was the same feeding aggregation.

5.2.2.4 Statistical Modelling Methods

Using the 'mgcv' package in R (Wood, 2006a), generalised additive models (GAMs) were constructed to model spatial and temporal patterns in the seabird aggregation data, according to the general structure specified by Hastie and Tibshirani (1999). GAMs are useful where the relationship between the response and a continuous variable exhibits a complicated shape, i.e. where it cannot be specified by an explicit functional form (Crawley, 2012), e.g. linear or quadratic. Rather, non-parametric 'smoothers' are used to describe the data and fitted during model selection. Collinearity between candidate predictor variables may affect estimation of both the model's standard errors and associated p values, so was investigated prior to running the models using Spearman's pairwise rank correlation tests. If correlation coefficients revealed strong collinearity between variables, using $r \geq 0.8$ as the threshold (Zuur et al., 2009; De Boer et al., 2014; Jones et al., 2014a), only one or other of the collinear terms was retained in further analysis, depending on which was retained first in the model selection process, as described below.

For the spatial model of gridded sightings data, a negative binomial family structure was specified, since it is appropriate for count data with many zero's, i.e. over-dispersion, though not zero-inflated data (Zuur et al., 2007). For the temporal model, the response was the absence or presence of a foraging aggregation per unit time, i.e. 0's and 1's, so a binomial family was used. A log link was specified as the functional relationship between the response and predictor variables in both models.

Default thin plate regression splines (bs = "tp") were specified for all non-cyclic variables, as they allow a smooth function to be fitted to noisy data with multiple explanatory variables

without the requirement of knowing where the different splines join, i.e. the "knots" (Wood, 2006b). Cyclic smoothers (bs = "cc") were specified for metrics whose first and last values are adjacent, i.e. covariates with degrees or hours as units where 359° and 0°, or 23-hrs and 0-hrs, are next to each other, for example. Two-way interaction terms were fitted using "te" tensor product smooths, which are effective for modelling smooth interactions of variables with differing units (Wood, 2006b; Crawley, 2012).

The maximum degrees of freedom ("k") for each smooth were manually limited to 4 for most covariates to prevent model over-fitting and to minimise excessive flexibility (Embling et al., 2010). Tidal variables were limited by k = 6 to allow for expected sinusoidal relationships with the response (sightings). To reduce model over-fitting in the automatic parameter smoothing process, the penalty ("gamma") given to each degree of freedom was increased from the default of 1 to 1.4 (Wood, 2006b).

Akaike's AIC score ('An Information Criterion') is a measure of a model's efficiency in explaining the data (i.e. model simplicity vs. model fit). AIC is negatively affected by the number of parameters included in a model, so helps to determine whether additional parameters are justified (Crawley, 2012). The best performing model of significant terms is that which gives the best 'fit' in terms of lowest residual deviance, and lowest AIC score. Using a manual, step-wise forward approach (adding variables iteratively at each stage), according to the selection criteria detailed in the paragraph below, models were built as a function of the explanatory variables. For the spatial model, static bathymetric covariates, mean depth, mean slope and mean aspect (listed in Table 5.1 on page 177) were modelled first, and the two-way interaction terms only specified once the main terms had been selected. For the temporal model (covariates listed in Table 5.4 on page 185), survey variables (significant wave height, sea state, cloud cover, wind speed, wind direction) were added first. Tidal variables (tide direction, tide speed, tide height, tidal range, tidal hour, tidal flow group) were added second, and temporal variables (month and daylight hour) added last.

First, individual GAMs were run for each of the predictor variables. The significant variable with the best AIC was then selected as the first term to be included in the model. Second, other variables were added iteratively, as a second term in the GAM, and the combination of significant variables with the best AIC was then used in the next round of selection. Variables were only selected if they were significant ($p < 0.05$), added explanatory power to the model, i.e. ≥1% increase on the previous model to 'deviance' in the data, and had a lower AIC score of at least 2, compared to the previous model, as recommended by Burnham and Anderson

(2002). Third, remaining variables were added iteratively to the first two significant terms, and this process repeated until no further covariates could be added, according to the criteria specified.

5.3 Results

5.3.1 Spatial Analyses

A total of 556 theodolite fixes of seabird foraging aggregations were recorded over 404 hours of active survey (Figure 5.3). There were 109 individual foraging aggregation events (of the same Sighting ID), confirmed in the field through dedicated "focal follows", and tracked while the birds continued to engage in foraging activity, i.e. feeding in close association with one another.

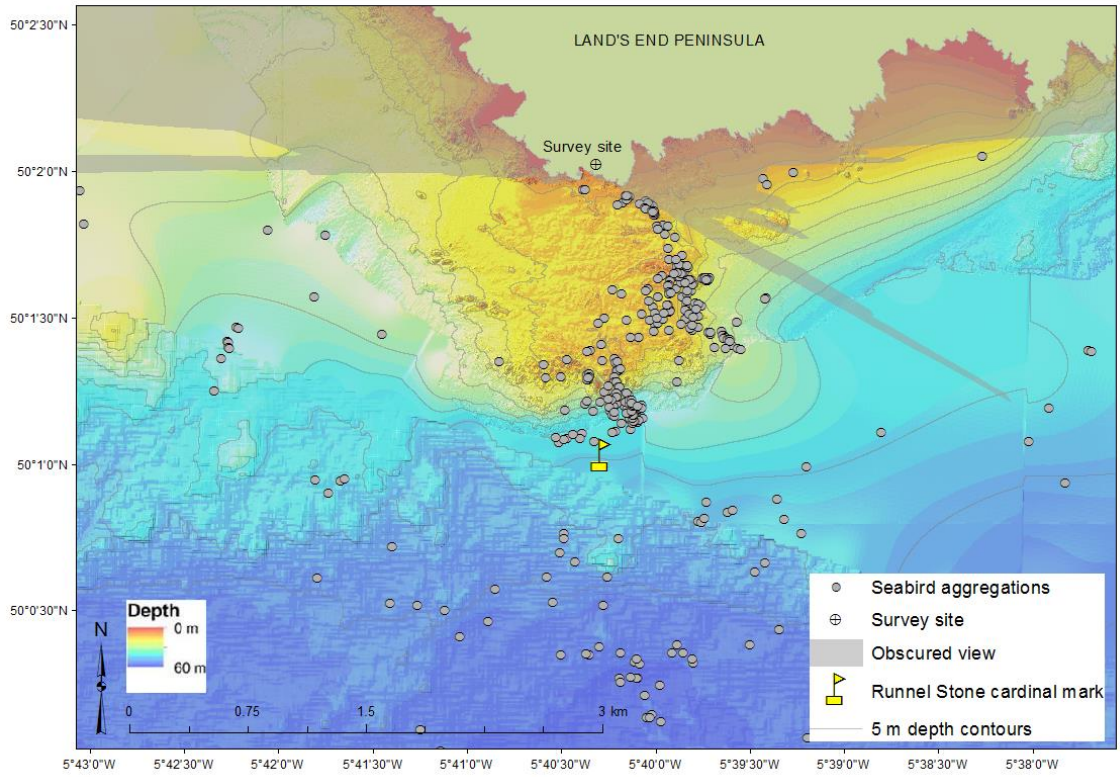

Figure 5.3. Runnel Stone Reef study site showing unfiltered (raw) foraging seabird aggregations. Grey dots represent a zoomed-in portion of the 556 total recorded observations (109 individual events) that were located within the survey region. Locations mapped onto high resolution (1 m) bathymetry data (courtesy of CCO/MCA © Crown copyright) with 5 m depth contours. Observation team located at survey site 'crosshairs'. Areas of sea surface obscured from view due to land topography depicted by greyed-out polygon. Theodolite data collected over 55 days across years 2011-13.

Initial visual inspection of the raw data indicated most seabird foraging aggregations were associated with topographic highs on the outer Runnel Stone Reef, denoted by the darker orange shading (Figure 5.3), particularly around pinnacles on the southern and easten reef margin; very few observations were recorded outside of these areas.

Of all the fishing activity in the survey area, 492 recorded positions of line fishers actively engaged in their work, matched closely with the locations of foraging seabirds (Figure 5.4), with clear clustering around topographic highs at the reef margin and few observations in waters deeper than ~30 m. The fishers were most commonly observed working alone or in pairs on small vessels using traditional handline fishing methods in pursuit of mackerel *Scomber scombrus*, pollack *P. pollachius/P. virens*, bass *Dicentrarchus labrax* and/or using small pots for lobsters (family Nephropidae) and crab *Cancer pagurus*. There was minimal interaction/impact observed between these artisanal fishermen and seabirds, or other cetaceans.

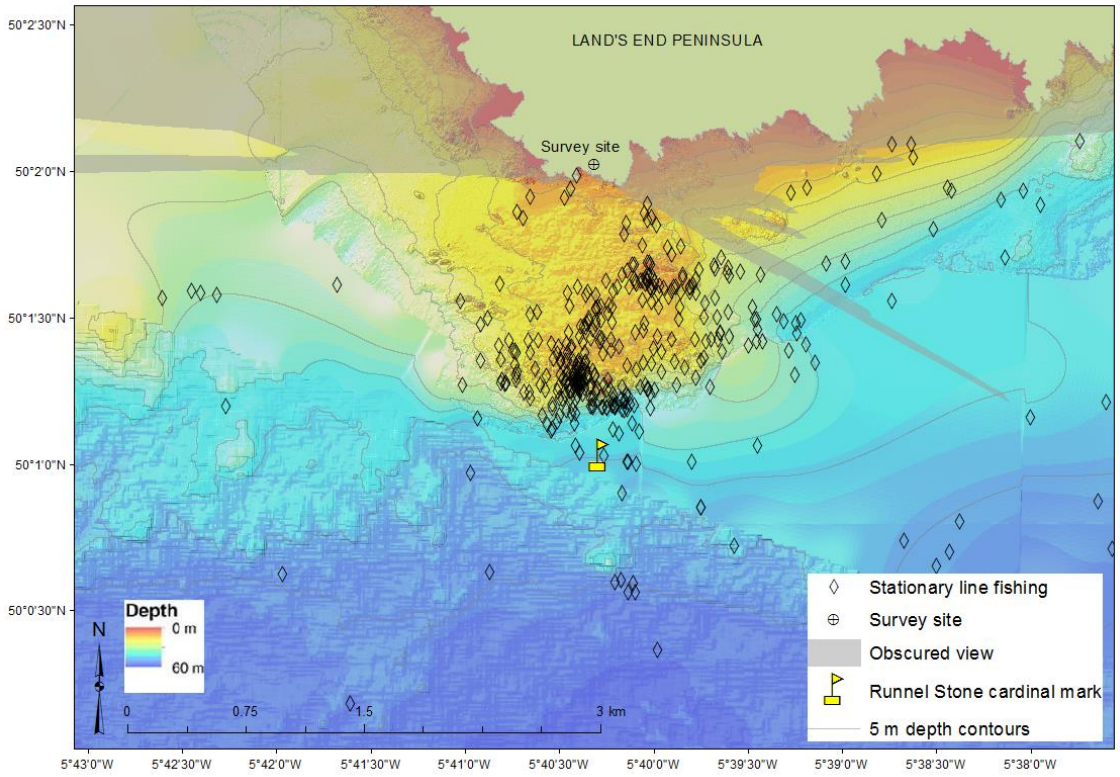

Figure 5.4. Stationary line fishing vessels recorded each 30-minute unit of survey effort.
Locations (n = 492) mapped onto high resolution (1 m) bathymetry data (courtesy of CCO/MCA © Crown copyright) with 5 m depth contours. Observation team located at survey site 'crosshairs'. Areas of sea surface obscured from view due to land topography depicted by hashed polygon. Theodolite data collected over 55 days across years 2011-13.

To compare seabird foraging activity at the study site using data collected with different survey methods (Figure 5.5), and at a different time (one year earlier than the start of the theodolite survey), locations of visually-estimated seabird aggregations (n = 110) filtered by Collins (2011) using data from the SeaWatch SW survey (see Section 2.1.3 for details) were plotted on the same map as the filtered theodolite observations (n = 109). Results from both visual datasets highlight some clustering of foraging activity around the southern, and to a lesser extent the eastern, reef margins, but the more precise theodolite mapping has clearly identified fine-scale associations with particular areas of topographic highs, which are not apparent in the conventional visual monitoring data.

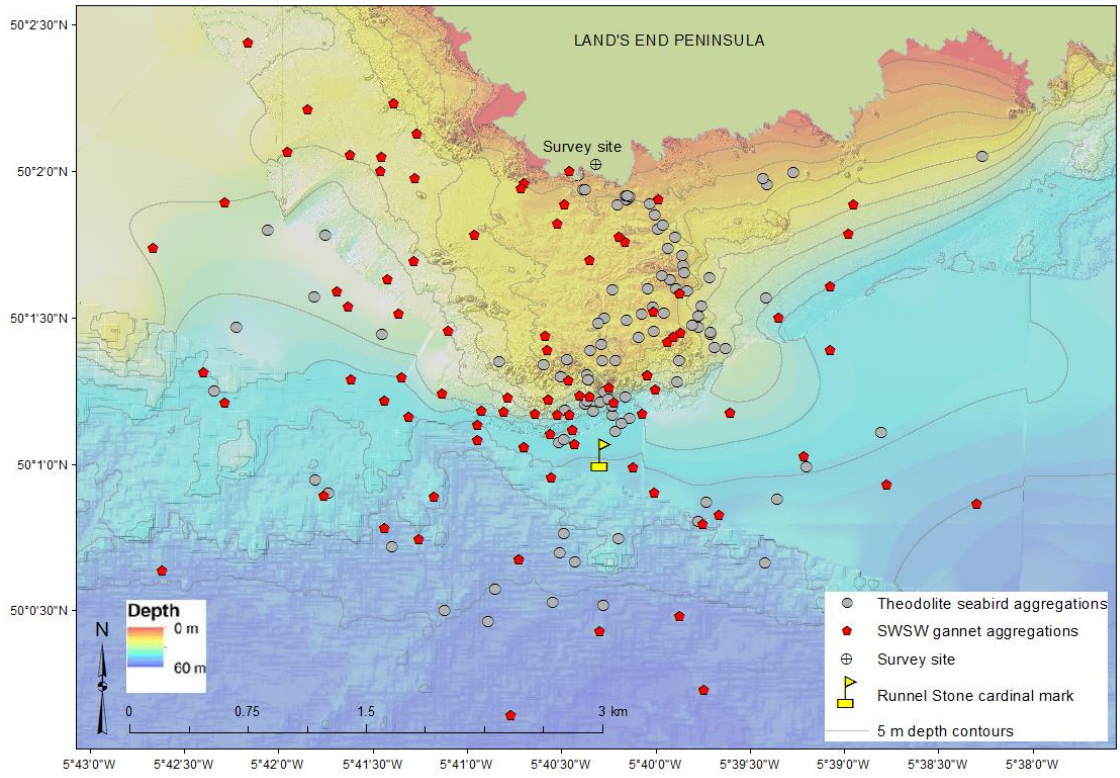

Figure 5.5. Seabird aggregation locations (theodolite vs. conventional visually-estimated sightings). Grey dots represent filtered theodolite observations (n = 109 individual events) by 30-minute survey units; red dots represent hourly-filtered sightings data from the SeaWatch SW survey (n = 110). Theodolite data collected over 55 days across years 2011-13; SeaWatch SW data collected daily over 93 days in summer 2010. Locations mapped onto high resolution (1 m) bathymetry data (courtesy of CCO/MCA © Crown copyright) with 5 m depth contours. Observation team located at survey site 'crosshairs'. Areas of sea surface obscured from view due to land topography depicted by greyed-out polygon.

The SeaWatch SW data show notably more events recorded in the western quadrant of the survey area, although results from both datasets show those aggregations that occured in

deeper waters (~50 m water depth) were located at a similar range from the watch point (~2.5-3 km offshore), with an absence around 2 km in all directions (i.e. just beyond the distance of the Runnel Stone cardinal mark; yellow flag in Figure 5.5). Fewer sightings at this range appear to be associated with the southern edge of the substantial wake that is created by the prevailing westward tidal flows interacting with the Runnel Stone pinnacles (see the radar-derived current vectors in Figure 5.6). During periods of sufficiently high tidal flow streams, this interaction can result in a significant patch of water, sheltered from the currents, that extends >2 km northwest, in lee of the shallow pinnacles.

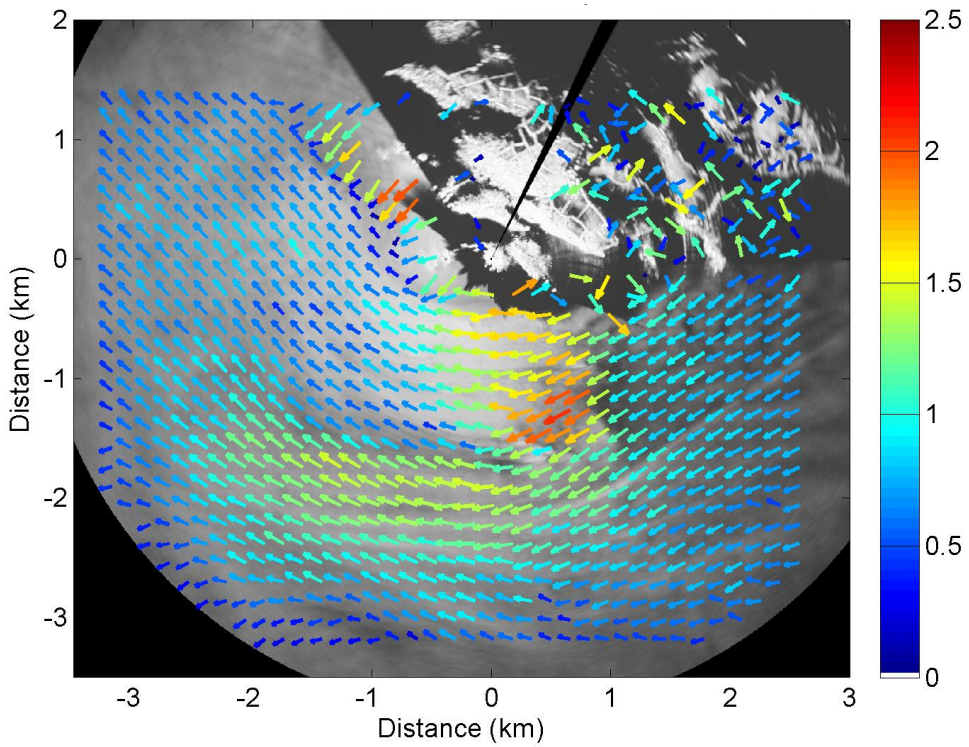

Figure 5.6. Radar-derived current vectors covering the Runnel Stone Reef survey area out to 3.8 km. Radar was mounted on the National Coastwatch Institution at Gwennap Head (at 0, 0). Black and white area in the top right corner is the headland; the image is oriented North; bright spot at 0.3 km, -1.5 km, is the Runnel Stone cardinal mark; colour scale is m s^{-1}; current vectors scale logarithmically with speed. Image taken during a spring tide on 16/09/2011 at 1100 hrs (HW+4).

5.3.1.1 Spatial Clustering

Spatial clustering on the seabird foraging aggregation data was investigated using KDEs calculated on sightings data filtered by both the finer 300-m (Appendix K.1) and coarser 600-m (Figure 5.7) grids to visually compare if there were spatial differences in the core habitat areas identified for seabird foraging, dependent on grid cell size. The kernels show little difference in

spatial distribution of the core density areas (50% isopleths), which are strongly associated with the eastern half of the reef plateau, particularly at the eastern reef margin.

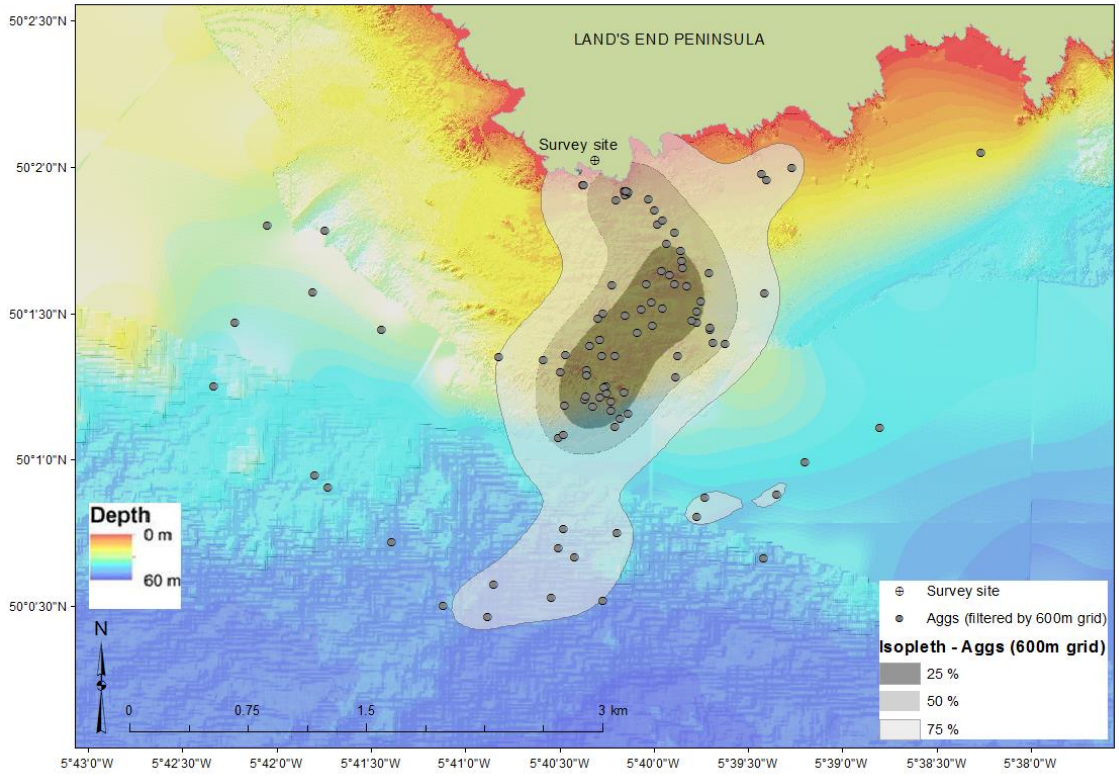

Figure 5.7. Percentage volume isopleths of foraging seabird aggregations.
Kernel density estimations (25%, 50%, 75%) calculated from locations (grey dots) filtered by the 600-m radial grid (n = 109) within Beyer's (2012) Geospatial Modelling Environment (bandwidth = 400 m; plug-in), mapped onto high resolution (1 m) bathymetry data (courtesy of CCO/MCA © Crown copyright). Observation team located at survey site 'crosshairs'. Theodolite data collected across years 2011-13.

To visualise how core density areas compared between seabird foraging activity and harbour porpoises, a species commonly observed in the survey region on 49% of days (see Chapter 3), the 50% kernels are displayed in Figure 5.8. The porpoise core habitat covers a much larger area of 3.46 km^2, and only overlaps with seabird foraging habitat by 0.86 km^2. This represents a shared core utility distribution (UD) within the total (13.83 km^2) survey region of just 6.22%. Though no significant correlation ($p = 0.9$) was found between the relative densities of seabirds and porpoises per grid cell, where the 50% kernels do overlap, they are convincingly located along the southern and south-eastern reef margins.

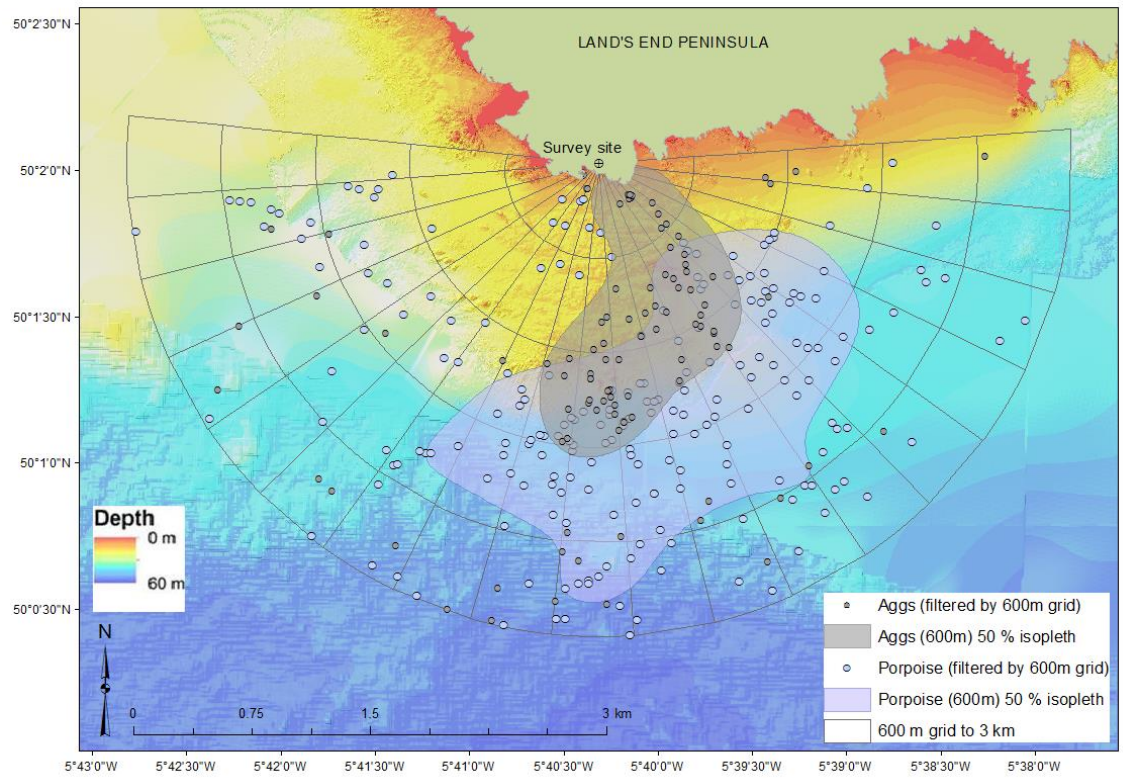

Figure 5.8. Comparison of seabird foraging and harbour porpoise core habitat areas.
Kernel density isopleths representing core habitat (50% kernels) calculated using theodolite locations of harbour porpoise (blue dots; n = 217) and seabird aggregations (grey dots; n = 100), both filtered by the coarser 600-m radial grid. Isopleths calculated from kernel density estimations within Beyer's (2012) Geospatial Modelling Environment (bandwidth = 400 m; plug-in), mapped onto high resolution (1 m) bathymetry data (courtesy of CCO/MCA © Crown copyright). Observation team located at survey site 'crosshairs'. Theodolite data collected across years 2011-13.

To visualise how tidal flow direction influenced sightings' distributions, i.e. spatial differences at a fine temporal scale, density isopleths on the filtered sightings data were estimated according to tidal direction (see Section 2.3.2), and plotted with the raw sightings dataset (Figure 5.9).

Despite different sample sizes per tidal flow direction, Figure 5.9 shows the westward UD (group with largest sample size, n = 53) covers an area of 1.3 km^2 and is clearly associated with the shallowest areas of the eastern reef margin (<10 m). The fact that the westward (ebb tide) kernel was calculated based on double the number of filtered sightings compared to the slack kernel (n = 27) but covers an area the same size (1.3 km^2), suggests aggregations were more clustered during westward flows (~7 hours of the tidal cycle at this site). Similarly, the eastward (flood) kernel was calculated using the fewest number of filtered sightings (n = 20)

but covers the largest area (2.5 km^2), suggesting aggregations were more dispersed during eastward flows (~3 hours of the tidal cycle at this site).

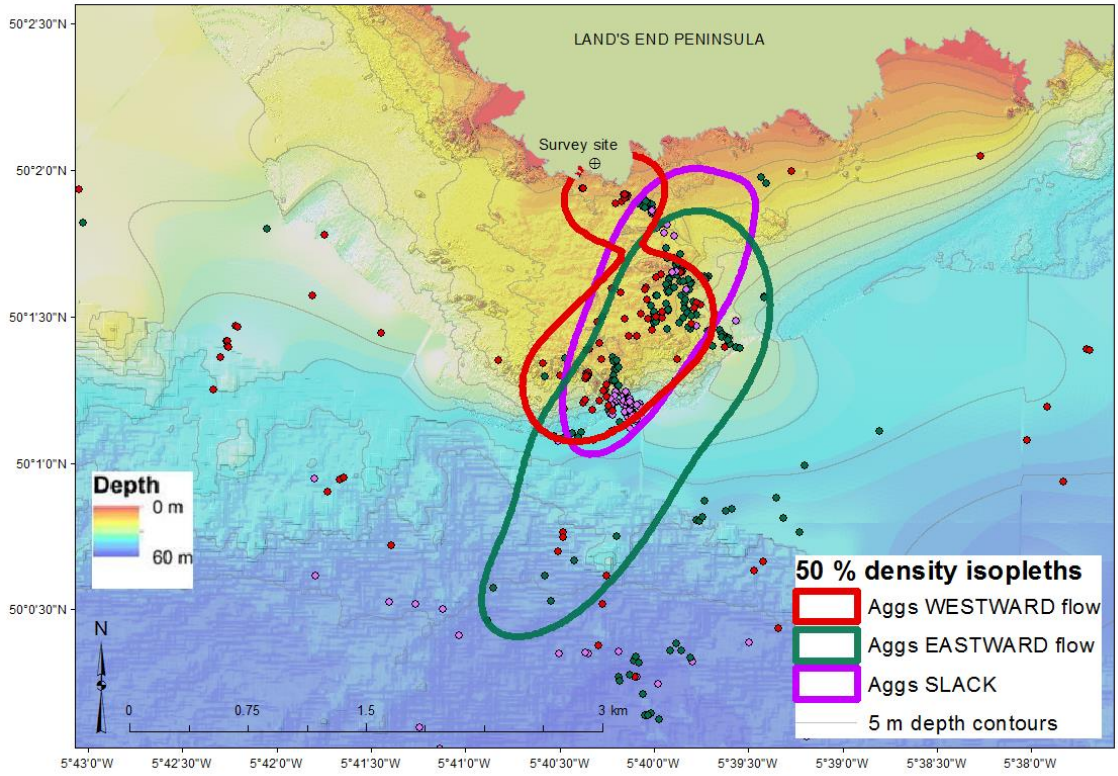

Figure 5.9. Core habitat of foraging seabirds according to tidal state.
Raw, unfiltered aggregation locations denoted by filled circles (n = 566) colour-coded according to tidal flow group. Kernel density isopleths calculated from data filtered by the 600-m radial grid (n = 100) were split by tidal flow group: westward, flow groups 1 and 2 (red, n = 53); eastward, flow group 4 (green, n = 20); slack, flow group 3 (pink, n = 27). Isopleths calculated from kernel density estimations within Beyer's (2012) Geospatial Modelling Environment (bandwidth = 400 m; plug-in), mapped onto high resolution (1 m) bathymetry data (courtesy of CCO/MCA © Crown copyright) with 5 m depth contours. Observation team located at survey site 'crosshairs'. Theodolite data collected across years 2011-13.

The slack and eastward flow groups had comparable sample sizes, yet the kernel distributions are very different. They are both located convincingly along the eastern reef margin but the eastward UD extends south into deeper (>60 m) waters by nearly 2 km. Although the kernel density isopleths only overlap by 0.69 km^2, the eastern reef plateau is identified as core habitat during all three tidal states, which strongly indicates clustering behaviour. No UD's cover the western reef margin.

By focusing in on the reef plateau, additional fine-scale analysis was possible. Figure 5.10 evidences how foraging seabirds associated themselves with different topographic features

according to tidal state. Feeding events appeared more dispersed along the entire extent of the eastern reef margin during eastward flows, while sightings during westward flows seemed restricted to the shallower (<20 m) areas of the reef plateau, and more strongly associated with areas of topographic highs, including the southern pinnacles and the lee ore pinnacle (near where the reef inflects, indicated by the arrow; Figure 5.10). During slack tide, sightings were clustered in an extremely concentrated area adjacent to the southern reef edge, south of the pinnacles, in slightly deeper water (~40 m depth).

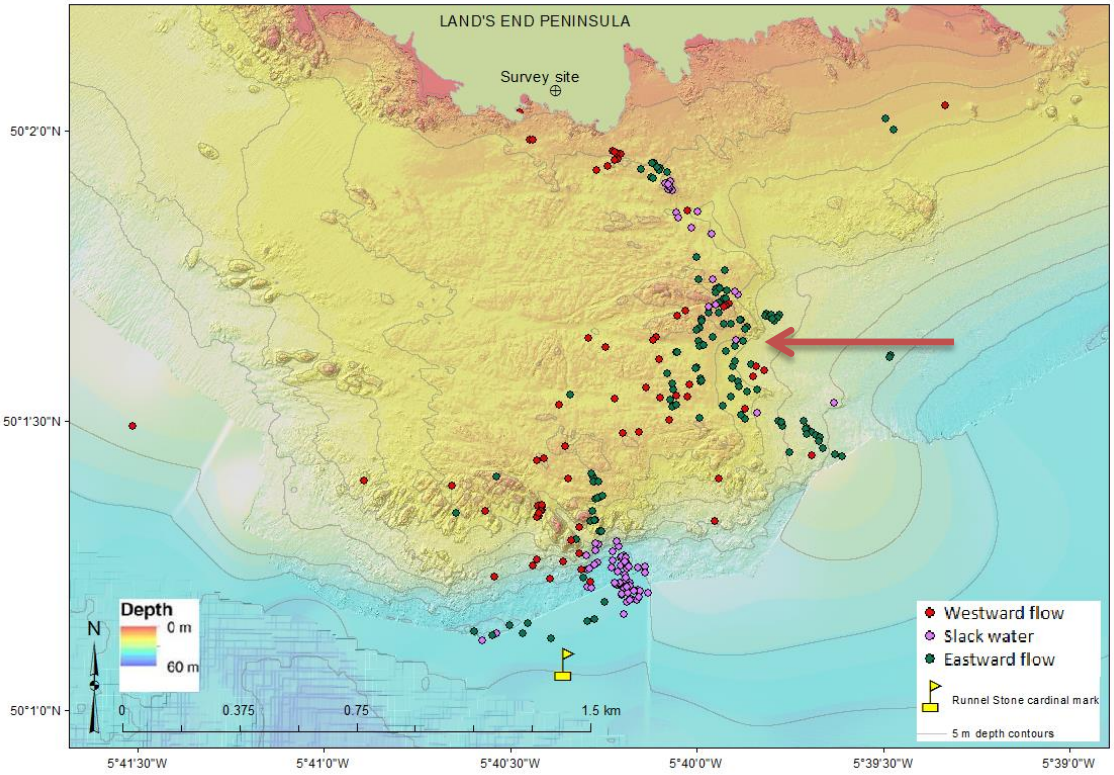

Figure 5.10. Runnel Stone Reef foraging seabird aggregations plotted according to tidal state.
Filtered sightings data denoted by filled circles (n = 110) colour-coded according to tidal flow group: westward, flow groups 1 and 2 (red); eastward, flow group 4 (green); slack, flow group 3 (pink). Locations mapped onto high resolution (1 m) bathymetry data (courtesy of CCO/MCA © Crown copyright) with 5 m depth contours. Observation team located at survey site 'crosshairs'. Theodolite data collected across years 2011-13. Arrow indicates area of reef margin near the lee ore pinnacle.

5.3.1.2 Spatial Gridded Analysis

The density of line fishing vessels per km^2 was calculated for each 600-m grid cell, and accounted for differing cell areas, including obscured areas of the field of view from land topography (Figure 5.11). Effort is concentrated around the southern pinnacles and eastern

reef edge, including the plateau. There is a notable absence of fishing effort in the western quadrant of the survey area.

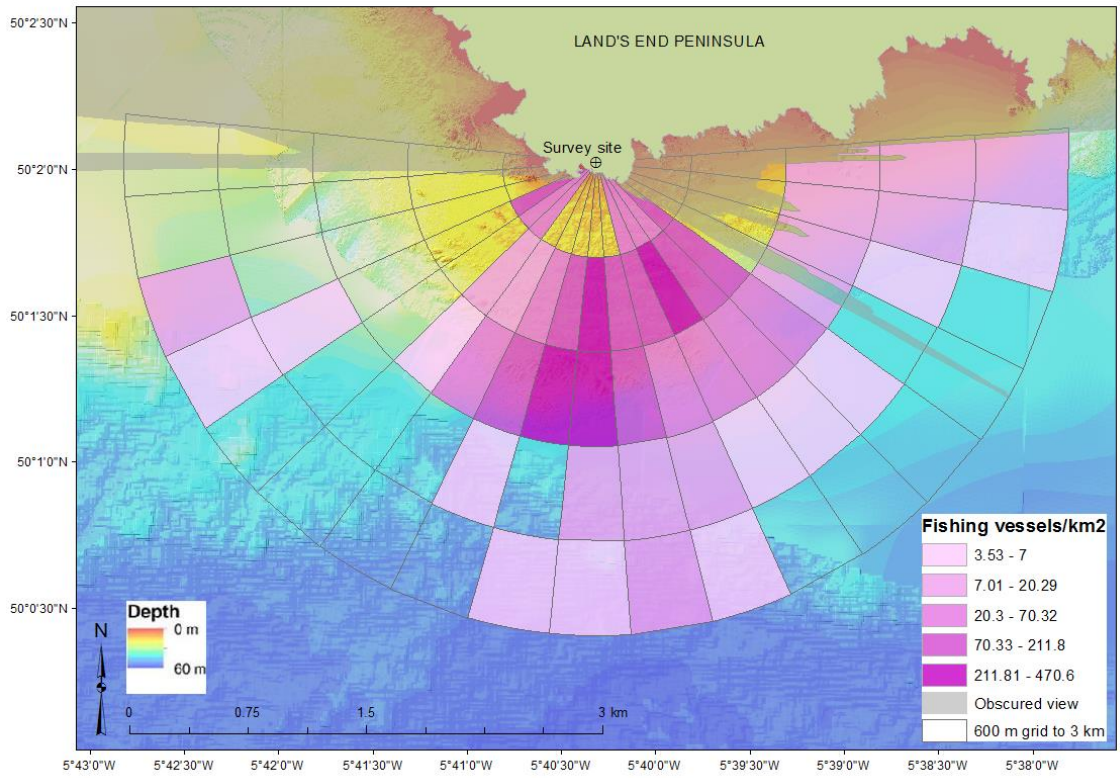

Figure 5.11. Area-corrected densities of line fishing vessels per km^2 per grid cell.
Grid mapped onto high resolution (1 m) bathymetry data (courtesy of CCO/MCA © Crown copyright). Theodolite data collected across years 2011-13.

The relative density of seabird aggregations per km^2 were calculated for each 600-m grid cell, and corrected for differing cell areas (Figure 5.12-A). Average values of the static variables, aspect (Figure 5.12-B), depth (Figure 5.12-C) and slope (Figure 5.12-D), are summarised.

A)

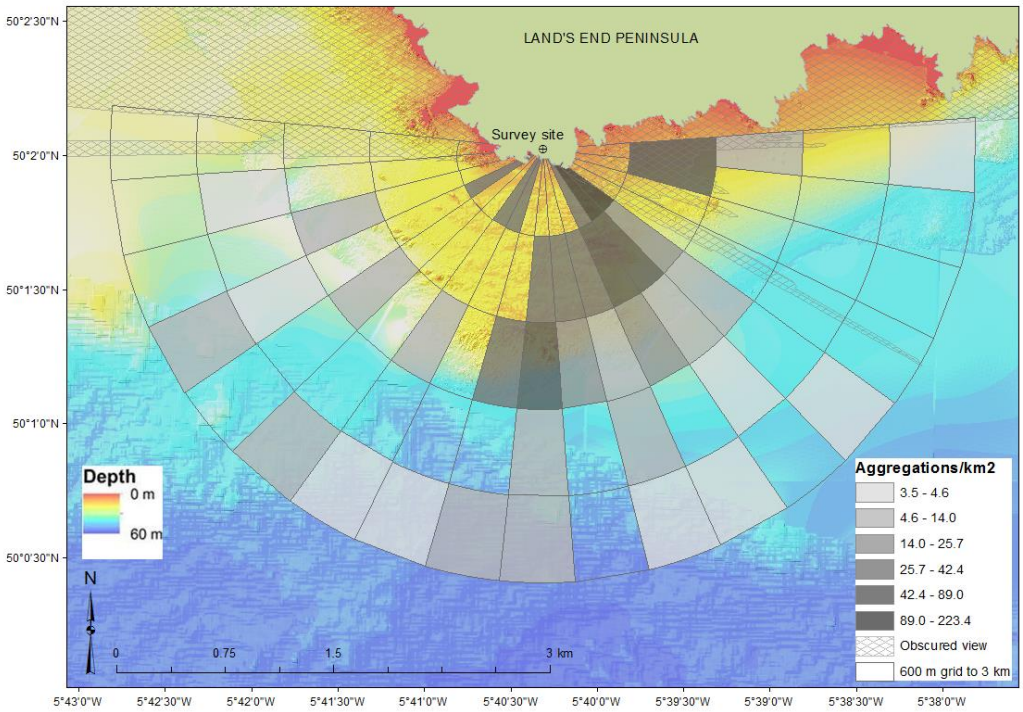
LAND'S END PENINSULA
Survey site
Depth
0 m
60 m
N
0
0.75
1.5
3 km
Aggregations/km2
3.5 - 4.6
4.6 - 14.0
14.0 - 25.7
25.7 - 42.4
42.4 - 89.0
89.0 - 223.4
Obscured view
600 m grid to 3 km
50°2'30"N
50°2'0"N
50°1'30"N
50°1'0"N
50°0'30"N
5°43'0"W
5°42'30"W
5°42'0"W
5°41'30"W
5°41'0"W
5°40'30"W
5°40'0"W
5°39'30"W
5°39'0"W
5°38'30"W
5°38'0"W

B)

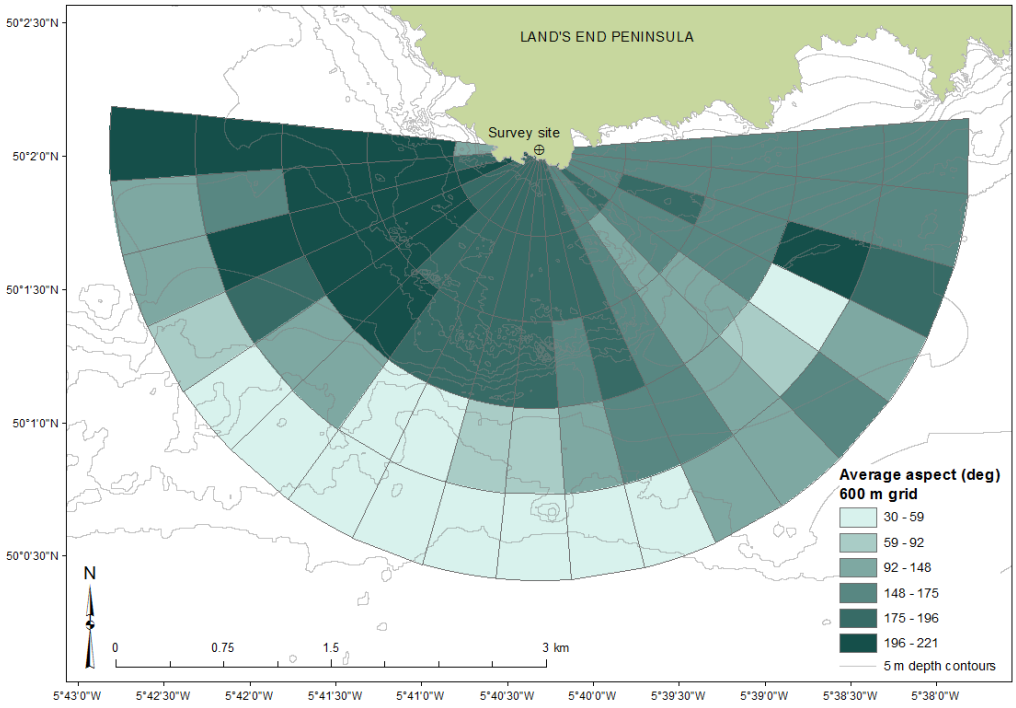
LAND'S END PENINSULA
Survey site
N
0
0.75
1.5
3 km
Average aspect (deg)
600 m grid
30 - 59
59 - 92
92 - 148
148 - 175
175 - 196
196 - 221
5 m depth contours
50°2'30"N
50°2'0"N
50°1'30"N
50°1'0"N
50°0'30"N
5°43'0"W
5°42'30"W
5°42'0"W
5°41'30"W
5°41'0"W
5°40'30"W
5°40'0"W
5°39'30"W
5°39'0"W
5°38'30"W
5°38'0"W

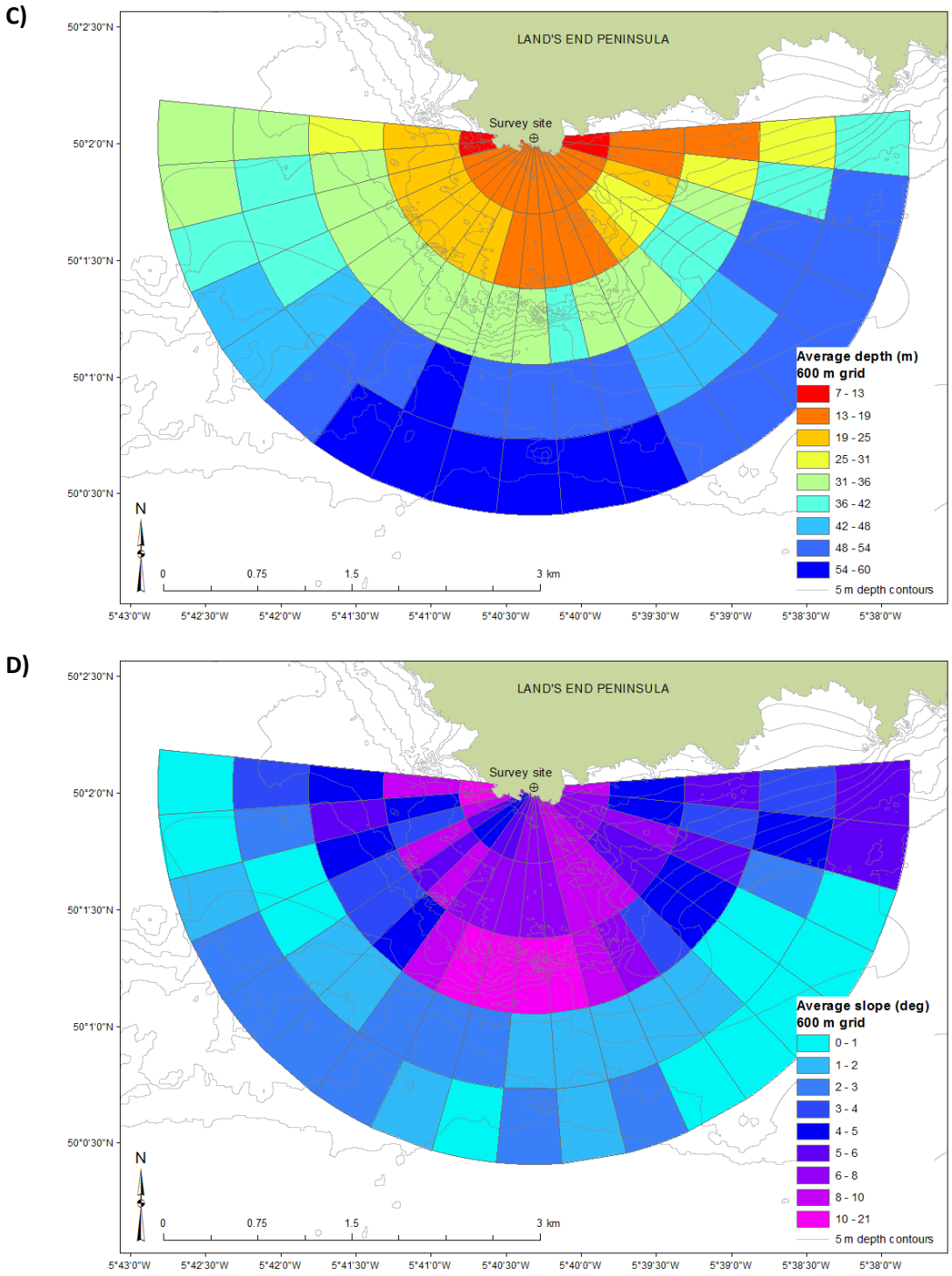

Figure 5.12. Summarised variables per 600-m radial grid cell of the 13.83 km^2 survey area.
A): Area-corrected relative densities of seabird aggregations per km^2 per grid cell (n = 95 cells; n = 100 sightings). Gridded values of B): mean aspect (degrees), C): mean depth (m), and D): mean slope (degrees). Static bathymetric variables derived in ArcGIS® from high resolution (1 m) bathymetry data (courtesy of CCO/MCA © Crown copyright), shown here with 5 m depth contours. Observation team located at survey site 'crosshairs'. Theodolite data collected across years 2011-13.

The map of relative sightings density per grid cell (Figure 5.12-A) shows grid cells in the eastern quadrant contain the majority of high density values in relatively shallow water depths (<20 m). There are also high values (~200 aggregation km^{-2}) within 600-m of the headland directly to the east, in cells of higher slope (>6°) compared to others in the survey region (Figure 5.12-D). Grid cells over the southern pinnacles contain high densities (~89 aggregations km^{-2}), where slope values are highest (~10-21°), and higher than other areas of reef margin. These cells contain the only highly-dense areas in deeper waters (>30 m; Figure 5.12-D). There is a notable absence of sightings ~2 km range from the watch point.

There was a significant positive relationship between the number of 30-minute line fishing vessels per grid cell and the number of (filtered) seabird aggregations ($r = 0.83$, $p < 0.001$). There was also a positive correlation between the density of line fishing activity and aggregation density per grid cell ($r = 0.52$, $p < 0.05$).

Summaries of the sightings data and static environmental variables filtered by the 600-m radial grid are given in Table 5.1. (For comparison, summarised covariate and gridded data filtered by the 300-m grid are provided in Appendix K.2. There were no notable differences in high density areas, but 10% more 'absence' data when sightings were filtered by the finer grid). A thorough data exploration and analysis was carried out on the spatial data prior to modelling, which can be found in Appendix K.3.

Table 5.1. Summary of gridded seabird aggregation data with static covariates per grid cell.
Missing data removed (n = 91). Abbreviation: s.d. = standard deviation.

Parameter	Value
Number of (600-m) grid cells (after removing missing values)	95 (91)
Number of 'absence' cells (%) (from 91-cell dataset): seabird aggregations	51 (56%)
Number of (filtered) sightings	100
Range of sightings per grid cell	0 – 14
Mean sightings per cell (s.d.)	1.1 (2.05)
Number of 'absence' cells (%) (from 91-cell dataset): line fishing vessels	41 (45%)
Number of (30-minute) sightings	376
Range of sightings per grid cell	0 – 74
Mean sightings per cell (s.d.)	4.1 (10.1)
Static physical variables	
Depth (m)	
Range	59.9 – 7.0
Mean (s.d.)	32.8 (14.8)
Aspect (degrees)	
Range	29.5 – 220.5
Mean (s.d.)	154.3 (51.8)
Slope (degrees)	
Range	0.2 – 21.4
Mean (s.d.)	5.0 (3.9)
Distance from shore to centre of grid cell (m)	
Range	57.2 – 2591.5
Mean (s.d.)	1126.5 (775.1)
Grid cell area (m^2)	
Range	1849 – 285623
Mean (s.d.)	151988 (92420)

5.3.1.3 Spatial Model

The spatial model for foraging seabird aggregations was constructed for sightings filtered by the coarser 600-m grid, as there were fewer cells of zero observations for improved robustness. A disproportionately high slope value (21.4°) relative to the next highest (15.7°) was identified in one grid cell of a very small area nearest the watch point, so removed from further analysis. Cells with missing data (n = 4) were also removed. The final dataset contained 90 grid cells.

Collinearity between model covariates (Table 5.1) was investigated prior to the model selection process using Spearman's pairwise rank correlation tests (Appendix K.4). Distance from shore and mean depth were highly collinear (r = 0.88). Mean depth was more correlated with the response, and considered more ecologically-relevant given the topographic complexity of the study site, so distance was removed from further analysis.

A GAM with a negative binomial logit-link distribution was constructed with an offset term, log area, to correct for differing grid cell sizes. The response variable (area-corrected counts of foraging aggregations per grid cell) was modelled using a step-wise forward selection procedure (see Section 5.2.2.4), as a function of the candidate static covariates (Table 5.1). Two-way interaction terms were specified between all three candidate variables.

The final GAM explained 63.4% of deviance (Table 5.2) in the relative density of foraging events per grid cell across years 2011-13, and took the form:

Seabird aggregation counts ~ MeanSlp + s(MeanDep) + s(MeanAsp)
+ te(MeanSlp:MeanDep) + offset(LArea)

Benthic slope explained most deviance (38.3%), followed by depth (7.1%) and aspect (5.7%). The interaction term, slope and depth, explained a further 12.3% when added to the significant main terms during model selection (Table 5.2). All covariates were significant to $p < 0.01$.

Table 5.2. Results of forward GAM model selection for seabird foraging events per grid cell.
Variables are shown in order of importance. Smooths are shown with the number of estimated degrees of freedom (e.d.f.) in parentheses; AIC_{Δ} is the reduction in AIC score caused by the addition of the significant variable to the model, with the first score in bold showing the starting AIC; % Dev is the additional deviation (%) in the data explained by adding the selected variable to the model. Surveys conducted over 55 days between years 2011-13 at the Runnel Stone Reef, n = 90 grid cells.

	Area-corrected aggregation counts per grid cell		
Order	Smooth (e.d.f.)	% Dev	AIC_{Δ}
1	s(MeanSlp, 2.5)	38.3	**244.99**
2	s(MeanDep, 2.2)	+7.1	-8.23
3	s(MeanAsp, 1.6)	+5.7	-4.27
4	te(MeanSlp:MeanDep, 5.7)	+12.3	-4.43
Total		63.4	

Model smooths are shown in Figure 5.13, along with a 3D visualisation of the interaction term. (Model validation plots are provided in Appendix K.5). There is a strong correlation between slope and the response (Figure 5.13-A), with more aggregations in grid cells of higher slope (up to 15°). There are increased sightings in east-facing cells, i.e. at the eastern reef margin, and a decrease in those of south-westerly aspect (Figure 5.13-B). There is preference for shallow (<20 m) and deeper (>50 m) water, with less observations in between (Figure 5.13-C) (e.g. the

isobaths along the reef margin; Figure 2.9). The interaction term, between depth and slope (Figure 5.13-C and D), suggests a preference for higher slope (>8°) in shallow water (<35 m).

A)

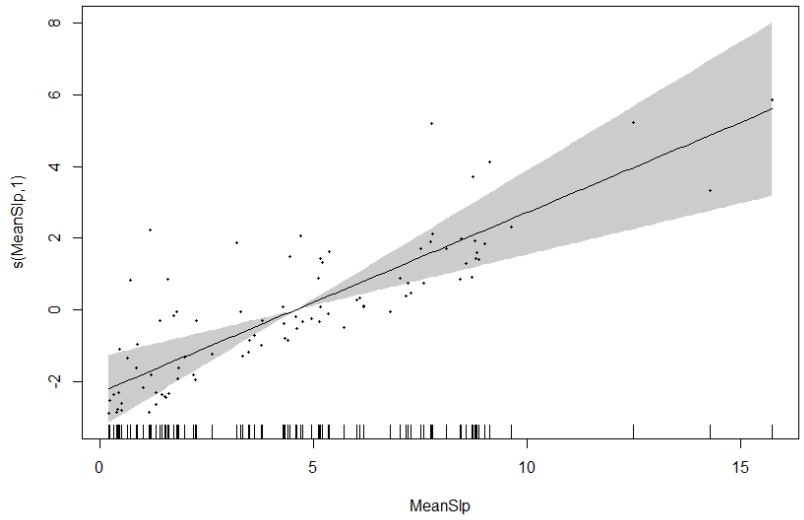
s(MeanSlp,1)
8
6
4
2
0
-2
0
5
10
15
MeanSlp

B)

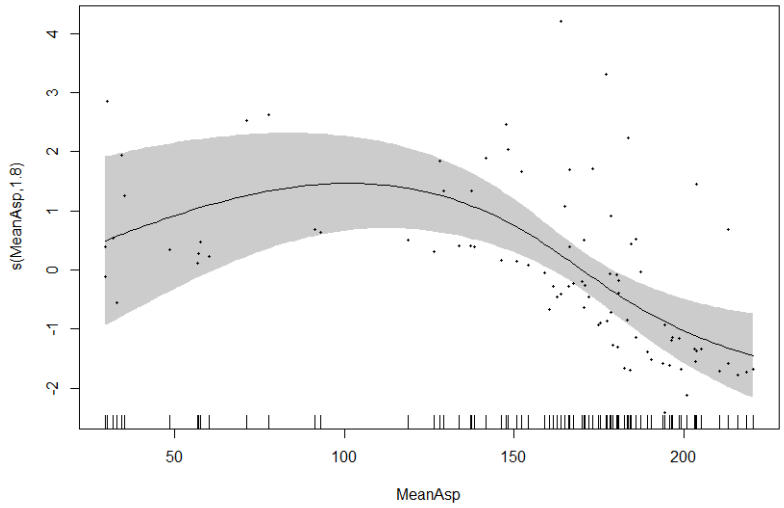
s(MeanAsp,1.8)
4
3
2
1
0
-1
-2
50
100
150
200
MeanAsp

C)

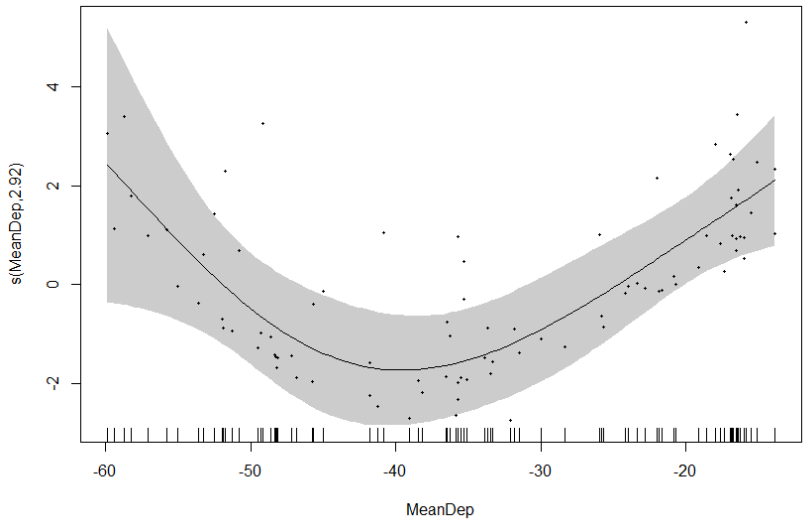
s(MeanDep,2.92)
4
2
0
-2
-60
-50
-40
-30
-20
MeanDep

D)

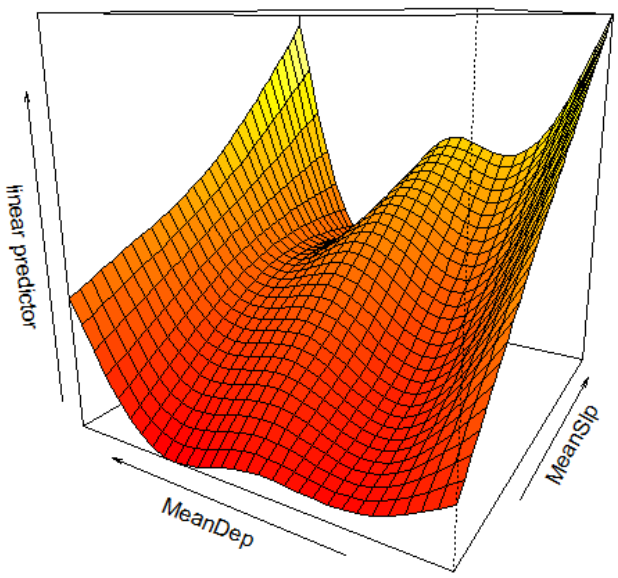

E)

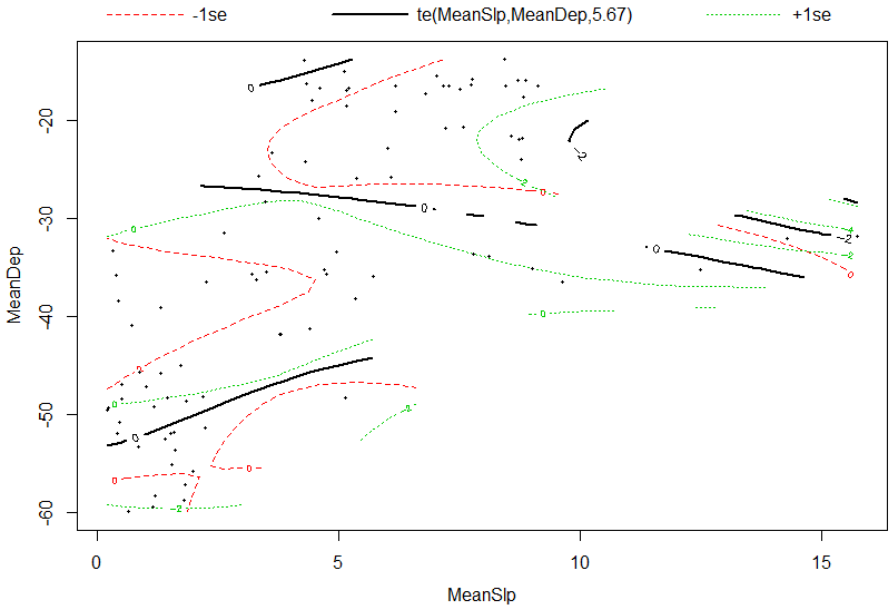

Figure 5.13. Smooths from the final spatial model for foraging seabirds at the Runnel Stone Reef. Relationships between area-corrected counts of seabird aggregations filtered by the 600-m grid (n = 90) and the significant predictor variables, as selected by the final negative binomial GAM. A): Mean slope (linear), B): Mean aspect (e.d.f. = 1.8), C): Mean depth (e.d.f. = 2.92) and, D): 3D visualisation of the interaction term MeanSlp:MeanDep, and E): smooth of interaction term MeanSlp:MeanDep (e.d.f. = 5.67). Results reported on scale of the linear predictor. Numbers in y-axis captions are e.d.f. (estimated degrees of freedom) of the smooths. In A), B) and C), Pearson's residuals are plotted as dots, the shaded regions around the smooths represent 95% confidence intervals, and the rug plots at the bottom are the covariate values.

5.3.1.4 Model Predictions

The plot of gridded seabird aggregation density, as predicted by the final GAM (Figure 5.14), shows the highest values located in cells over the southern pinnacles and at the eastern reef margin, where the slope inflects, including some areas of the reef plateau.

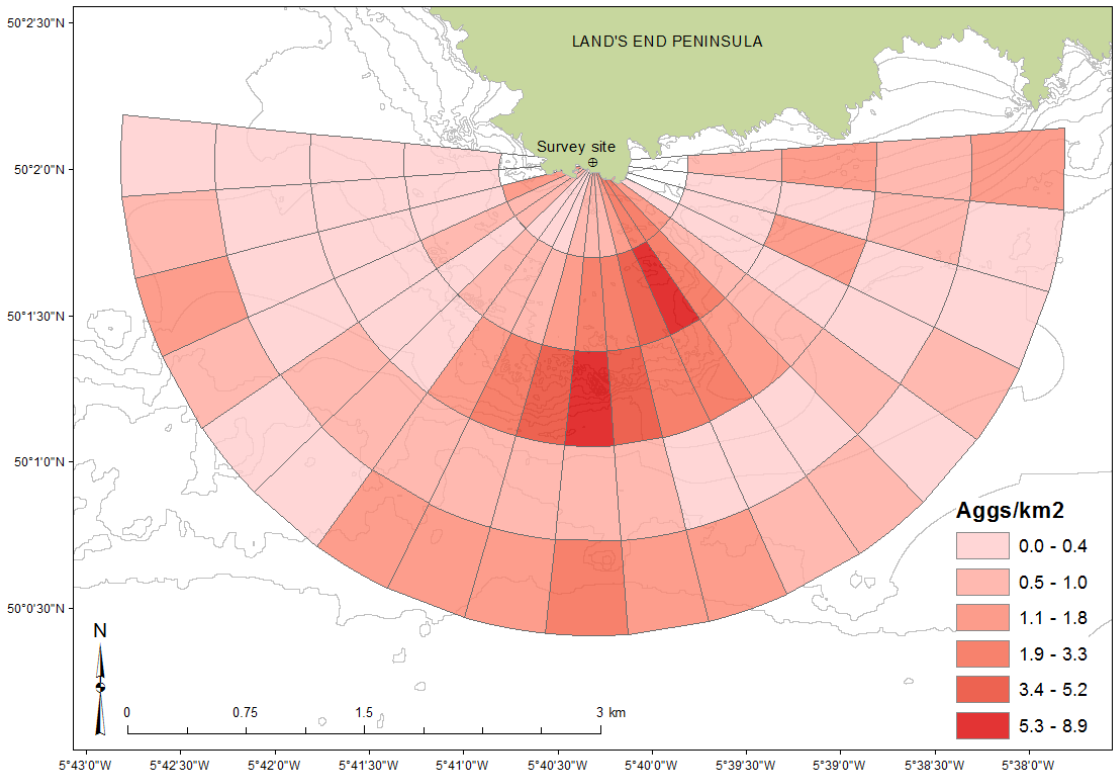

Figure 5.14. Model predictions of foraging seabird aggregations per km^2 per grid cell.
Predictions based on model covariates of average slope, aspect and depth, an interaction between average depth and slope, and an area offset. Density grid mapped onto high resolution (1 m) bathymetry data (courtesy of CCO/MCA © Crown copyright) with 5 m depth contours.

5.3.1.5 Model Performance

To visually represent how the model performed, relative to sightings data collected *in situ*, the difference between model-predicted density values, and observed densities, were calculated per grid cell (*observed density – predicted density*). Negative densities therefore represent model over-prediction, while positive densities under-prediction (Figure 5.15).

Maximum over-prediction by the model for seabird aggregations per km^2 within a single cell is -3.2, while the maximum under-prediction is +5.1. The majority of over-predictions are located in cells of mid-water depths (shaded orange) >1.8 km from the watch point. The model

performed well across 41% (n = 37) of the survey grid (yellow-shaded cells representing a difference of ±1 aggregation-km^{-2} between predicted and observed density values). The average difference between the model predictions and observed densities across the radial grid is only 0.016 sightings per km^2 (mean s.e. = 0.41), suggesting good model performance, based on a final GAM that explained 63.4% of deviance in the data.

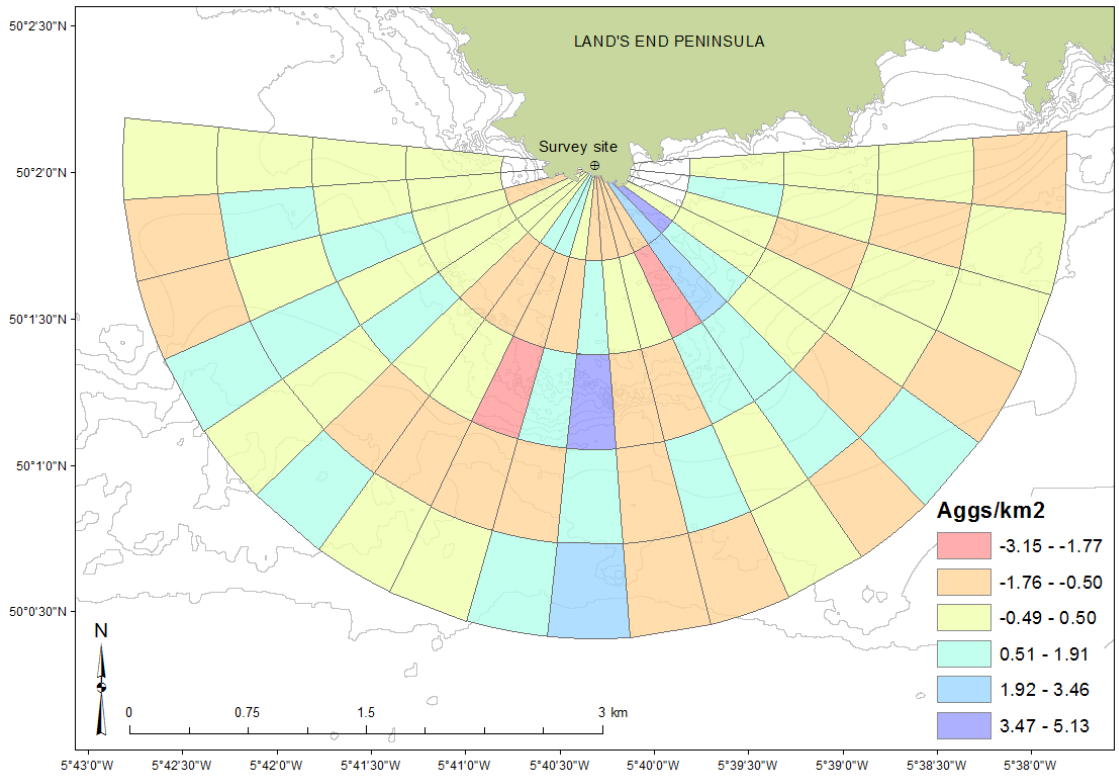

Figure 5.15. Model performance showing the difference between observed and model-predicted numbers of foraging seabird aggregations per km^2 per grid cell.
Predictions based on model covariates of average slope, aspect and depth, an interaction between average depth and slope, and an area offset. Density grid mapped onto high resolution (1 m) bathymetry data (courtesy of CCO/MCA © Crown copyright) with 5 m depth contours. Theodolite data collected across years 2011-13 (n = 100). Negative densities represent model over-prediction, while positive densities under-prediction. Yellow represents good model performance with a difference of ±1 aggregation per km^2.

5.3.2 Temporal Analyses

Over 55 days, 808 30-minute units of survey effort were conducted across years 2011-13, averaging seven hours of active survey effort per day. A total of 556 locations of seabird foraging aggregations were recorded, of which 530 recordings consisted of ≥5 gannets, while 22 recordings consisted of ≥20 kittiwakes. Though many of those observations will have represented the same feeding event, the criteria defining a foraging aggregation was normally (>80%) met due to the presence of >5 gannets. Theodolite recordings were filtered by 30-minute units of survey effort, leaving 119 IDs in the final temporal dataset (removing 437 observations from the raw dataset).

Table 5.3. Summary of seabird foraging events from theodolite surveys, 2011-13.
'Positive' hours/days are periods during surveys when a seabird foraging aggregation was sighted and recorded. Data filtered by 30-minute survey units.

Year	Survey days	30-minute observations	Foraging events (individual IDs)	Positive 30-min units (%)	Positive days (%)
2011	36	492	58	43 (8.7)	16 (44.4)
2012	18	303	58	45 (14.9)	15 (83.3)
2013	1	13	3	3 (23.1)	1 (100)
All years	**55**	**808**	**119**	**91 (11.3%)**	**32 (58.2%)**

Aggregations were sighted in 91 (11.3%) 30-minute survey units, while 58% of survey days were positive for sightings (Table 2.1). Discounting the single survey day in 2013, the average annual sightings rate was 0.29 aggregations-hr^{-1} (n = 397.5 hours of survey effort) and the average sighting composed of 33.7 birds (s.d. = 34.9). In October 2012, both the largest single aggregation was observed, composed of >200 birds and, across two aggregations, >320 birds were present in one 30-minute survey unit.

Samples with missing covariate data were removed. The final dataset contained 100 seabird aggregation IDs (16% data loss) over 737 30-minute survey units (91% of total effort). Table 5.4 summarises the foraging seabird aggregation dataset and environmental covariates (see Section 2.3.2). A thorough data exploration was carried out on the aggregation sightings data prior to modelling (Appendix L.1), including effort-corrected histograms of the number of sightings each 30-minutes as a function of the temporal covariates.

Table 5.4. Summary of covariates used in temporal analysis of foraging seabird aggregations.
Filtered seabird aggregation data (100 IDs) collected over 55 days (n = 737 30-minute survey units) across years 2011-13 (missing data removed). Abbreviation: IQR = inter-quartile range.

Parameter	Value
30-minute units of survey effort (hours)	737 (368.5)
Number of sighting IDs	100
Survey variables	
Significant wave height (m)	
Range	0.12 – 0.8
Median (IQR)	0.32 (0.23 – 0.45)
Sea state (Beaufort)	
Range	0 – 4
Median (IQR)	2 (2 – 3)
Cloud cover (oktas)	
Range	0 – 8
Median (IQR)	4 (1 – 7)
Wind speed (km hr^{-1})	
Range	0 – 15.8
Median (IQR)	7.2 (4.0 – 9.7)
Wind direction (degrees)	
Range	1 – 360
Median (IQR)	240 (130 – 305)
Tidal variables	
Tide direction (degrees)	
Range	38 – 334
Median (IQR)	270 (111 – 289)
Tide speed (m s^{-1})	
Range	0.09 – 1.46
Median (IQR)	0.59 (0.36 – 0.84)
Tide range (m)	
Range	2.1 – 5.73
Median (IQR)	3.9 (3.27 – 4.3)
Tidal hour (hour relative to HW)	
Range	-6.2 to +6.3
Median (IQR)	-0.4 (-3.5 to +3.3)
Tide height (m)	
Range	0.13 – 5.83
Median (IQR)	2.65 (1.6 – 4.07)
Tidal flow group (as factor)	
Range	1 – 4
Median (IQR)	2 (1 – 4)
Temporal variables	
Month (as factor)	
Range	1 – 12
Daylight hour (ratio between sunrise and sunset)	
Range	0.02 – 0.97
Mean (IQR)	0.58 (0.42 – 0.73)

5.3.2.1 Temporal Model

To explain temporal patterns in the occurrence of seabird foraging events, the presence or absence of an aggregation per 30-minute survey unit was modelled using a binomial GAM with a logit-link function (see Section 5.2.2.4). Collinearity between candidate variables (Table 5.4) was explored using a pairplot (Appendix I.4). Tide height and tidal flow group were highly collinear (r = 0.81), though neither were retained during model selection. Through step-wise forwards selection, the modelling process first compensated for survey effects, then tidal variables and finally temporal variables. Model results are given in Table 5.5.

Table 5.5. Results of forward GAM model selection for presence-absence of foraging events.
Variables are shown in order of importance, first compensating for survey effects (wind and sea conditions, cloud cover). Smooths are shown with the number of estimated degrees of freedom (e.d.f.) in parentheses; AIC_{Δ} is the reduction in AIC score caused by the addition of the significant variable to the model, with the first score in bold showing the starting AIC; % Dev is the additional deviation (%) in the data explained by adding the selected variable to the model. Surveys conducted over 55 days between years 2011-13 at the Runnel Stone Reef (n = 368.5 hours).

	Aggregation presence-absence per 30-minutes		
Order	Smooth (e.d.f.)	% Dev	AIC_{Δ}
1	s(WindSp, 1)	3.38	**476.66**
2	s(Cloud, 1)	+1.48	-5.22
3	s(TideRng, 3)	+4.5	-16.13
4	s(DayHr, 1.8)	+1.34	-3.08
Total		10.7	

The final GAM explained 10.7% of deviance (Table 5.5) over 368.5 hours of survey effort across years 2011-13. Wind speed and tidal range were the most significant predictor variables ($p < 0.001$), followed by daylight hour ($p < 0.05$) and cloud cover ($p = 0.05$). It took the form:

Seabird foraging occurrence ~ WindSp + Cloud + s(TideRng) + s(DayHr)

Figure 5.16 shows the model smooths. The ACF of model residuals (Appendix L.3) shows significant residual correlation of 30 minutes that the model has not accounted for.

Of the survey variables, wind speed was the most significant predictor of seabird foraging events in the survey area, explaining 3.4% of deviance (Table 5.5), with decreased sightings as wind speeds increased (Figure 5.16-A). Cloud cover explained 1.5% of deviance, with more sightings during periods of clear skies (Figure 5.16-B).

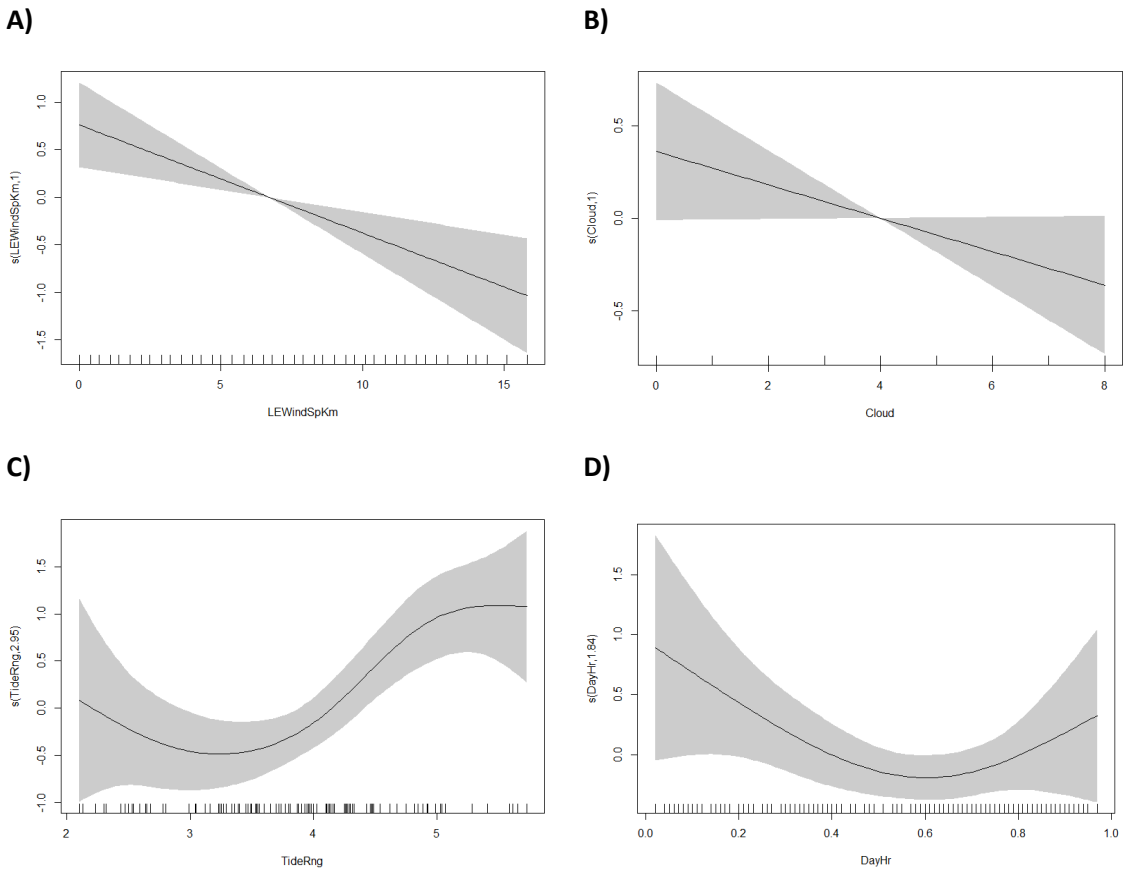

Figure 5.16. Relationships between foraging aggregation occurrence and temporal variables.
As selected by the final binomial GAM (n = 737 samples), A): Wind speed (e.d.f. = 1), B): Cloud cover (e.d.f. = 1), C): Tidal range (e.d.f. = 2.9), and D): Daylight hour (e.d.f. = 1.8). Results reported on the scale of the linear predictor. Numbers in brackets in y-axis captions are estimated degrees of freedom (e.d.f.) of the smooths. Rug plots at bottom of figures are covariate values. Shaded regions around smooths represent 95% confidence intervals.

Tidal range (a proxy for position in the spring-neap cycle) was the most important, and only tidal, predictor of foraging seabird aggregation occurrence, explaining 4.5% of deviance (Table 5.5). The smooth (Figure 5.16-C) shows an increase in sightings towards spring tides, where tidal range is larger. Daylight hour explained an additional 1.3% of deviance, with a dip in sightings just after midday (Figure 5.16-D). Marginally more foraging events are associated with the hours immediately after sunrise, relative to the hours preceding sunset.

5.4 Discussion

Questions remain as to how wide-ranging marine top predators preferentially use their habitat in coastal waters, particularly at fine (<1 km) scales. To identify fine-scale habitat preferences of foraging seabird aggregations, dedicated land-based surveys were carried out using a theodolite at a constrained coastal location off the tip of southwest UK that falls within an rMCZ. Surveys focused on two amber-listed seabirds of conservation concern, gannets and kittiwakes, used as model species to test the hypothesis proposed in previous work (Collins, 2011) that tidal-topographic interactions drive distribution at fine-scales in tidally-dominated environments.

Precise theodolite mapping revealed clustering associated with areas of topographic highs and steep slopes, across tidal states, and evidenced significant spatial overlap with fishing effort, indicating the localised influence of tidal-topographic interactions on prey availability (Votier et al., 2010). Improved knowledge on the fine-scale habitat use of foraging seabirds, as a proxy for localised zones of enhanced prey density (Sharples et al., 2013a), combined with the multi-disciplinary approaches used in this study, have implications for conservation management regimes that require robust scientific evidence on species' distribution in coastal waters (Guilford et al., 2012). The suite of methodological tools may be applied elsewhere at similarly constrained coastal locations amenable to shore-based observations (where appropriately-resolved covariate data exist) to help identify controls on foraging seabird distributon, needed to designate and effectively monitor MPAs for the species.

Survey variability

Modelling temporal variability, including survey conditions and tidal influence, in the distribution of foraging aggregations at the Runnel Stone Reef explained 11% of variation in the data. Cloud cover significantly influenced the number of observed foraging events, explaining 1.5% of deviance, with more sightings during periods of clearer skies. This indicates the importance of visibility to the birds during prey capture, which influences seabird foraging decisions (Hunt et al., 1999), as the amount of light available at depth will affect the distance at which prey are visible, and thus the rate at which diving seabirds encounter prey (Thetmeyer & Kils, 1995; Van Eerden & Voslamber, 1995). Indeed, Katzir (1993), discusses the multiple, instantaneous calculations that must be made by plunge-diving seabirds while still above the water, including: accounting for prey position, anticipating their movement, underwater depth and distance to the seafloor, their own height above the water, and their

strike speed through the water during prey-capture. In a complex visual environment, which is dominated by ambient light reflected from the sea surface, refracted after penetrating the water (Lythgoe, 1979), the importance of optimal light conditions is clear. Additionally, since gannets and kittiwakes are highly mobile species, free to move among habitat patches (Fauchald, 2009), the ability to quickly assess a potential area for sufficient concentrations of prey during flight is vital to maximise foraging efficiency (Fretwell & Lucas, 1969). Furthermore, the significance of cloud cover highlights the need to account for survey variability in temporal analyses of visual predators at sea, such as plunge-diving seabirds.

Wind speed explained a further 3.4% of deviance; as speeds increased, the numbers of foraging aggregations decreased. It therefore seems plausible that wind conditions may affect sea state, as described previously, by impacting on the seabirds' ability to detect prey beneath the surface (although this variable was not retained during model selection). Furthermore, since plunge-diving seabirds have high energy demands (Gabrielsen et al., 1987), they need to continually minimise the costs of long-foraging trips (Furness & Bryant, 1996). This suggests that seabirds will preferentially use flyways that provide favourable wind conditions. During periods of strong winds, seabirds may respond in two ways: either spend less time foraging, observed in breeding shags *Phalacrocorax aristotelis* off northeast Scotland (Daunt et al., 2006) or, choose to avoid areas heavily impacted by strong winds, and forage elsewhere (Furness & Bryant, 1996).

Fritz et al. (2003) demonstrated that wandering albatross *Diomedea exulans* continually adjust for wind at small scales (<100 m) through zigzag movements but, at medium scales between 100 m and 10 km (e.g. during prey-searching), their movements corresponded to food-rich areas that are restricted in space, such as upwelling zones that concentrate prey itno patches (Hunt & Schneider, 1987). The study proposed that the third, and final, spatial scale at which flight behaviour is influenced is during the longest flights (>10 km), which are likely foraging trips. However, Dehnhard et al. (2013) noted that wind-induced patterns in prey availability on foraging success have often been neglected in seabird studies, though they often indicate the potential influence of large-scale weather systems on the occurrence of seabird foraging aggregations within a study area. These variables may need to be accounted for during analyses, and are potential effects likely to become increasingly important with changes in climatic variability (Lehodey et al., 2006; MacLeod et al., 2007a).

Time of day

After controlling for survey variables, daylight hour, a metric calculated to represent time between sunrise and sunset, had a significant effect on temporal distribution, with reduced numbers of foraging events observed around midday. Garthe et al. (2003) also found that gannet flight and diving activity off Newfoundland was concentrated during the early morning and late afternoon, with decreased activity during midday. Although results were for different species, Paiva et al. (2010) reported Cory's shearwaters *Calonectris borealis* using the period around noon for resting, and concentrating their flying periods during the morning and afternoon, while Hedd et al. (2001) observed a similar pattern in the shy albatross *Thalassarche cauta*, where birds were increasingly active after sunrise, and a second peak near dusk. In their study, the albatross were feeding on schooling mackerel, which follow swarms of krill *Nyctiphanes* spp. that come close to the surface just after sunrise, disperse to depth throughout the day in bright sunshine, and form again during the last few hours of daylight, i.e. diel vertical migration (DVM; Forward, 1988). However, it is unlikely this is the case at the Runnel Stone Reef study site, due to the highly dynamic tides (Appendix E); the daily patterns are more likely reflecting periods of seabird peak passage (Collins, 2011).

The reduced number of foraging aggregations around the hours of midday have been reported in studies of a variety of seabird species observed off Gwennap Head (e.g. Collins, 2011; Jones, 2012; SeaWatch SW, 2014) and in gannets on Funk Island, Newfoundland, using data loggers (Garthe et al., 2003). The clear diel rhythm exhibited in gannet foraging is likely a consequence of the pelagic seabirds transiting to and from their roosting sites (or colonies) during the day (Camphuysen et al., 2012), as they are inactive at night (Garthe et al., 2003). Periods of peak passage (in flight and diving activity) occur in the hours of first light when the birds awake and need to feed, and again in the hours preceding roosting. The decrease in foraging concentrations observed around midday is therefore attributable to the fact there is no urgent need to feed at this time, and thus reflects their diurnal pattern.

Tidal influence

Of all the tidal variables included in the modelling process, only tidal range was a significant variable on the occurrence of seabird aggregations. This was unexpected given the well-documented influence of tidal currents on ecosystem dynamics in temperate coastal systems (Hunt et al., 1998; Embling et al., 2012; Embling et al., 2013). These interactions result in patchy distributions of prey that are predictable in space and time (Scott et al., 2010),

significantly affecting everything from primary productivity and zooplankton (Decker & Hunt, 1996), to fish and other top predators (Mendes et al., 2002; Johnston et al., 2005a; Bertrand et al., 2008). Until recently, the mechanisms linking fish schooling behaviour to bio-physical oceanography in tidal ecosystems had not been quantified (e.g. Sharples, 2007), but had long been regarded as the missing link needed to better understand top predator distribution (Embling et al., 2013) urgently required for their effective conservation, e.g. the establishment of MPAs. However, recent studies have attempted to fill this gap (Scott et al., 2010; McPhee-Shaw et al., 2011; Embling et al., 2012; Sharples et al., 2013a; Sharples et al., 2013b), for example, by combining novel fine-scale survey data of fish behaviour using acoustics, with co-located oceanographic data at contrasting topographical study sites (e.g. Embling et al., 2013).

In this study, tidal range, a proxy for position in the spring-neap cycle, explained the largest amount of variation in the temporal dataset (4.5%), relative to the other selected variables in the model (Table 5.5), with increased foraging aggregations observed towards spring tides. Scott et al. (2013) also found the most significant driver of foraging gannets, at Jones Bank in the Celtic Sea, was the spring-neap cycle, but higher densities were observed during neaps, rather than springs, though the authors acknowledge theirs was possibly the first study to have identified that. However, their results indicated that different locations within the study site were preferentially used for foraging by the gannets, with higher numbers targeting the top of the bank during spring tides.

Embling et al. (2013) found the behaviour of fish schools close to the bottom of Jones Bank, i.e. in deeper water, were also most strongly influenced by the spring-neap cycle, relative to other oceanographic variables in their study (e.g. current speed, current direction, thermocline gradient). The deep schools were larger, closer to the bottom, and less dense during neap tides, whereas shallow, pelagic schools were more concentrated over the bank, and closer to the surface during times of high internal wave activity (during springs). Higher plankton density was also recorded above and within the thermocline during these periods, which likely explains the shallow fish distribution and therefore why, during springs, gannets preferentially targeted the top of the bank, as observed by Scott et al. (2013). Although there were generally more fish schools during neap tides than during springs (plausibly explaining the overall preference of gannets to feed during neaps at the bank), the highest number of shallow fish schools was indeed found over the top of the bank, opposed to over the bank slopes, which were areas that tended to host increased concentrations of zooplanktivorous fish above the thermocline, regardless of the spring-neap cycle (Embling et al., 2013). This possibly suggests a

response by the gannets to increased prey availability, or visibility by the vertical movement of water (Sharples et al., 2013b) caused by higher hydraulic jump activity and associated shear (due to the higher amplitude of internal waves), which occur during spring tides and concentrate plankton into patches (Embling et al., 2013).

Given that a majority of foraging aggregations in this study were located over the Runnel Stone Reef itself (Figure 5.3), these theories seem applicable here, as not only were the foraging events observed taking place in similar, highly focused locations over time, possibly due to increased plankton densities in these areas (attracting prey fish of foraging seabirds) but, Jones et al. (2014a), also reported increased hydraulic jump activity and associated shear instability during the hours of strongest tidal flows, which may enhance prey availability by concentrating plankton into patches (Bertrand et al., 2008), i.e. enabling top predators to maximise their foraging efficiency in these highly mixed areas. Although limited to only one day at sea, the ADCP survey conducted by Jones et al. (2014a) did cover an entire tidal cycle over the survey area to show variations in localised physics, dependent on changing flow direction and speed. Given that shear instability increases with increasing tidal flow speeds, it seems a reasonable assumption that shear instability would be highest during spring tides (Lwiza et al., 1991), rather than neaps, when flows are faster, therefore contributing to increased prey availability during these periods within affected areas, i.e. near topographic features.

Spatial clustering

Seabirds have been shown to forage preferentially in areas that hold predictable, localised aggregations of prey, including plankton and other marine organisms (Wolanski & Hamner, 1988; Franks, 1992b, 1992a). Crucially, Hunt (1999) notes that it is the tightness of the spatial and temporal association between seabirds and hydrographic features (particularly in the vicinity of shallow topographic features) that determines whether the mechanism responsible for increased prey abundance in these very specific areas (highlighted by the precise theodolite locational data) is straightforward production, or physically-forced aggregation.

Given that non-spatial variables, such as tidal state, did not change the location of the high density areas within the Runnel Stone Reef study site (Figure 5.9), it seems reasonable to suggest that fine-scale physical forcing mechanisms are responsible for the extremely fine-scale spatial clustering of seabird foraging activity associated with certain topographic features (e.g. pinnacles), rather than production theories alone. In the highly dynamic Runnel Stone Reef environment, the water column is fully mixed (Jones et al., 2014a), so small-scale physical

processes (e.g. tidal-topographic interactions) are going to be the dominant factor influencing prey availability.

However, Embling et al. (2013) qualitatively evidenced increased zooplankton concentrations over the bank in their study and suggest that both fish and fishing are supported by primary productivity, rather than tidal dynamics *per se*. This perhaps points to the fact that the reef feature itself is an area of increased production generally, within the otherwise homogeneous ocean environment off the mainland peninsula but, within this relatively more productive reef area, there are very fine-scale zones of increased prey availability, likely caused by equally small-scale physical-forcing mechanisms, making these zones particularly attractive, and predictable, to top predators. This is evidenced not only by the fact the core foraging areas of piscivorous seabirds were important during all tidal states, but that the small shifts in location (<50 m) of the raw data points are likely a result of schooling forage fish, and/or their plankton prey, being physically pushed into slightly different areas dependent on current flow direction, or taking refuge in lee of certain areas of topographic highs (i.e. the influence of fine-scale physical forcing). Additionally, the increased density of foraging aggregations in these areas (Figure 5.12-A) in close proximity to shallow topographic features (e.g. the pinnacles) and/or the steep slopes of the eastern reef edge, points to the localised and significant influence of tidal-topographic interactions. These small-scale processes are known to host increased densities of marine organisms at their boundary (Wolanski & Hamner, 1988; Franks, 1992a, 1992b; Baumgartner et al., 2003; Hao et al., 2003; Genin, 2004; Yen, 2004).

Tidal-topographic interaction

After modelling relative-density of foraging aggregations, it was unsurprising that the static bathymetric variables explained 63% of spatial distribution, of which benthic slope explained 38%. The map of model predictions (Figure 5.14) clearly shows increased foraging predicted along the steep, eastern reef edge particularly near areas of topographic highs. However, model results also show a reduced preference for waters of intermediate depth within the study site (30-50 m water depth), which, in most areas, are the isobaths running along the reef margin itself (Figure 2.9). This suggests that, although depth is a significant influence, foraging seabirds are perhaps avoiding diving into areas over the reef slope itself, where prey may not be as visible, or their movements may not be sufficiently predictable in these precise locations. Although the highest densities of foraging events were found in cells with higher slope values (up to 15°) that are located near to, and over, the steep reef margin, this again points to the

fact there is likely increased prey availability in these areas, but perhaps indicates the prey is not as accessible over the actual slope, along the 30-50 m isobaths.

The significant interaction between depth and slope on foraging occurrence explained 12% of variation, and indicated that in areas of shallow water (<35 m), there is a preference for higher slope (<8°), which could plausibly describe features such as the pinnacles. It is therefore likely that small-scale physical forcing mechanisms, e.g. topographically-driven internal waves (Jones et al., 2014a), can help explain spatial distribution of foraging events by accumulating debris and organisms in these spatially-predictable convergence zones (Wolanski & Hamner, 1988; Franks, 1992a; Genin, 2004). Scott et al. (2013) also discuss predator-prey encounter rates, in the context of bio-physical coupling mechanisms, and note that, often, the simplest explanation is that prey are easier to catch when internal wave activity actively aggregates and/or brings prey closer to the surface, i.e. straightforward topographical-forcing, rather than a result of complex trophic interactions. This is clearly important for visually-orienting seabirds. Indeed, Hunt et al. (1998) found that strong tidal currents passing over a submerged reef in the Aleutian Islands caused upwelling on the upstream side of the reef, and zones of convergence on the downstream side. Three species of auklet (family Alcidae) partitioned foraging habitat along this gradient, demonstrating that the strength of the tidal current was positively related to the number of birds present and that, when the tide reversed, so did the sides of the reef occupied by the auklet species.

Apart from tidally-induced convergence zones, tidal flows can also contribute to the formation of internal waves and hydraulic jumps, which are often caused when stratified water interacts with steep-sloping topography (e.g. Nash & Moum, 2001). Internal waves and associated shear were evidenced at the Runnel Stone Reef by Jones et al. (2014a) during periods of strong westward flow along slopes near the eastern reef margin. Tidal current vectors in the radar-derived images (Figure 2.17) reflected similar patterns, showing increased tidal flow speeds at the eastern reef edge (red arrows) during westward flows (Figure 2.17-A) but, during eastward flows (Figure 2.17-B), currents were relatively unaffected on interaction with the western reef edge (green arrows across survey area), indicating that it is the interaction between strong westward flows against the steep, eastern reef edge that is more significant than eastward flows against the western reef edge. It should be noted that the only feature to exert an influence on interaction with either flow direction is the highest pinnacle of the Runnel Stone itself, at the southern reef edge, which can create a substantial wake in lee of the prevailing tidal currents that runs for several kilometres, particularly during westward flows (Figure 2.17-

A). Cells of lowest foraging aggregation density were found in these sheltered areas, where fewer fine-scale physical-forcing mechanisms are likely at play, which suggests reduced prey availability. However, the spatial correlation between these areas has not been quantified. Future work on these data could focus on deriving quantitative, highly-resolved (~160-m; pers. comm. P. Bell, 2015) hourly metrics of the radar-derived current flows (speed and direction) across the survey area. Data for each hour of the tidal cycle, taking the temporally-restricted coverage samples as representative across tidal conditions, could then be incorporated into the temporal model process as a covariate and/or used in spatio-temporal analysis of tracking data. Interestingly though, the data as they are clearly show the effect of the headland reef, which is felt over a range of at least double the extent of the feature itself, as tidal flow is pushed offshore and concentrated around the outside of the rocky outcrop. Furthermore, the largest eddies seem to form during periods of slack water (Figure 2.17-C; see also Appendix E), which may also have implications for prey availability during certain periods of the tidal cycle, though determining these correlations was beyond the scope of this study.

Fishing and other cetaceans

To successfully implement effective management plans, understanding key areas of habitat use by all users of the marine environment is essential. This not only includes the distribution and spatial overlap of top predators, as indicators of sites worthy of protection (Georges et al., 1997; Wilson et al., 2009), but also possible interaction with local fisheries. At the Runnel Stone Reef, there was significant spatial overlap between line fishing and seabird foraging (Figure 5.11), which again suggests that seabirds and schooling fish or, rather, fish in sufficient concentrations (to warrant being targeted by fishers or plunge-diving seabirds) are highly aggregated within the vicinity of the reef, despite not having been monitored directly. Schneider and Piatt (1986) also found high correlation between seabirds and schooling fish in a coastal ecosystem, though the correlations were scale-dependent. The fact that the high density areas for both fishing and seabird foraging significantly overlap indicates that the same physical processes, i.e. topographic features interacting with tidal flow, are responsible for causing increased prey availability in identifiable, and predictable, areas, and that they are perhaps worthy of protection in their own right. Scott et al. (2010) suggest that these 'hotspot' areas may represent a 'newly identified class' of spatially-important location that, despite comprising a small percentage of the marine environment (5% in their study), hosts a significant proportion of apex predators (50% of foraging animals monitored in their study), including species such as gannet, kittiwake and porpoise.

Surprisingly, given the relatively small survey area, and the association between the identified features and foraging, and between cetaceans and seabirds in the area (Collins, 2011) and elsewhere (Camphuysen, 2011), there was no significant spatial overlap between the gridded seabird and porpoise data, despite the core habitat of both species sharing certain areas of the reef margin (Figure 5.8). The lack of core spatial correspondence between the species may be because the animals use the features in different ways; the seabirds actively foraged in close association with these features (Figure 5.10), whereas the porpoise surfacings were located *adjacent* to the reef edge in slightly deeper water (see Discussion in Chapter 3 for further detail). Additionally, not only does the porpoise dataset not represent foraging-only sightings data (for fair comparison) but 70% of the animal's time is spent subsurface, so their habitat use and, in particular, their foraging preferences may not be adequately represented by the data. Similarly, Camphuysen (2011) found the association of gannets with marine mammals, off Bass Rock in the North Sea, was typically an offshore-only (>60 km from the colony) phenomenon, despite noting an abundance of cetaceans in inshore waters (~45% of sightings). The author suggests the seabirds were simply using the cetaceans as cues to begin their search, and rarely (~15%) plunge-dived with them.

Conclusions

Finding appropriate and adaptable conservation and monitoring methods of dynamic systems is a key component of an ecosystem-based approach to management (Lascelles et al., 2012; Ronconi et al., 2012). The survey methods, and analyses, used in this study have demonstrated their utility by revealing fine-scale foraging patterns of plunge-diving seabirds, which is information much-needed by fisheries and conservation management in the coastal zone in the face of increasing anthropogenic threats, and the need for effective EIAs (Waggitt & Scott, 2014). Developing a cost-effective suite of complimentary techniques that can be successfully applied at other constrained coastal locations has implications for the monitoring of these species further afield. The methodological toolbox developed in this study can therefore be applied elsewhere where necessary, subject to the availability of appropriately-resolved covariate data and locations that are amenable to shore-based observations.

This study only collected data across one area over 55 non-consecutive days, but the focus was solely on the foraging locations of the seabirds, which has enabled detailed spatial analyses of static habitat variables that may drive their distribution. Results have clearly evidenced important physical areas within the study site, although collecting a longer time series dataset would consolidate the findings and provide additional context. However, results indicated a

degree of temporal and tidal variability in the occurrence of foraging aggregations that may be predictable in space and time. Top marine predators, such as seabirds, depend upon specific environmental conditions at a limited number of suitable locations for successful prey capture (Scott et al., 2010), so identifying features that are predictable and if possible static would be helpful for conservation purposes. Data collected by a theodolite have enabled very fine-scale visual analysis of those features within the study area that host increased numbers of foraging seabirds, most notably the spatially-constrained areas of tidal-topographic interaction, which points to the critical and useful role they should perhaps play in the designation of protected areas. Results in this study have therefore contributed to knowledge of the potential importance of features such as topographic highs (in the presence of high tidal flows) for foraging seabirds, whilst highlighting the importance of accounting for survey variability during analyses.

Chapter 6 Fine-scale distribution of foraging wintering seabirds in St Ives Bay, southwest UK, with implications for local fisheries' management

A B S T R A C T

Incidental fisheries bycatch is one of the principle causes of seabird population decline globally, accounting for ~half a million deaths. Bycatch events in a gently-sloping sandy bay off southwest UK at St Ives triggered a local Gillnet Fishery byelaw in January 2012, as >100 birds were found drowned in nets. The byelaw prohibits fishing in certain areas of the bay, which impacts on the economy of local fishers. However, detailed information on localised fine-scale spatial and temporal distribution of wintering seabirds is currently lacking, though urgently needed to better inform fisheries' management. A joint partnership between the National Oceanography Centre, Southampton (NOCS), the charitable organisation, Royal Society for the Protection of Birds (RSPB), and the Cornish Inshore Fisheries Conservation Authority (CIFCA), was initiated that same year, and a land-based pilot study carried out over 19 days between December 2012-January 2013 from a strategic watch point on St Ives Island.

Data on spatial distribution were collected using a theodolite to derive precise locations of foraging aggregations, and high resolution (30-minute) temporal information collected to quantify the influence of tidal and temporal variability on foraging occurrence. Sightings of cetaceans and fishing vessels were also recorded for comparison of habitat use and to elucidate any potential for interaction. More than 110 hours of daylight-only survey effort data (in sea states ≤ 3, and visibility >5 km) were acquired. Generalised additive models (GAMs) were constructed to determine the influence of static bathymetric variables on relative density, and temporal variability on count data.

Foraging aggregations were sighted on 84% of survey days (n = 118 individual events); only 38.9% of 30-minute scan samples were positive for sightings. The average sightings rate was 0.39 sightings of aggregations-hr^{-1}. Statistical modelling indicated the survey variables, wind speed, wind vector and significant wave height (suggested to affect flight and foraging ability), had a significant influence on the timing of foraging events. Increased aggregations were recorded during offshore winds, periods during which the bay is more sheltered. Tidal range (a proxy for position in the spring-neap cycle) was the only significant hydrographic influence, with decreased sightings around neap tides. Daylight hour was not found to significantly affect the number of foraging events recorded in the bay during surveys.

Analysis of gridded (500-m) relative-density data revealed distance from shore was negatively correlated, and explained 43% of variation in the data. This was consistent with results from the kernel density analyses, which highlighted the nearshore zone of the southern bay. Benthic slope explained a further 3% of deviation, though the relationship was less clear. The raw theodolite data and density grid identified the association of foraging seabirds with areas of topographic highs (e.g. pinnacles), indicating the possible influence of tidal-topographic interaction on prey availability, which is both predictable and spatially-constrained, with implications for management. Spatial clustering appears to overlap with higher use areas of fishing activity and cetaceans, including bottlenose dolphin *Tursiops truncatus* and harbour porpoise *Phocoena phocoena*, so time-area fishing restrictions may not be appropriate in the long-term; voluntary gear modification or nighttime-only gillnet deployment should be (re-)considered.

6.1 Introduction

Breeding seabird numbers in the UK are generally in decline for many species (Hayhow et al., 2014), including kittiwakes *Rissa* spp. (-61%) and herring gulls *Larus argentatus* (-30%). Threats range from: marine spatial planning (Garthe & Hüppop, 2004), climate change (Durant et al., 2004; Chambers et al., 2011), pollution (Croxall et al., 2012) and incidental capture ('bycatch') in fisheries (Žydelis et al., 2013). Since the 1970s, increasing attention has been paid to the issue of mortality in gillnets worldwide, and the possible impact at population level for some species (Sonntag et al., 2012; Žydelis et al., 2013), including pelagic seabirds (e.g. albatross; family Diomedeidae) and cetaceans (e.g. harbour porpoise *Phocoena phocoena*). There is an urgent need for adequate protection policies and realistic, yet innovative, conservation measures that are easy to monitor and enforce (Lascelles et al., 2012), and straightforward for fishers to follow.

Seabirds have the potential as 'indicators' of prey availability (Montevecchi, 1993; Diamond & Devlin, 2003), e.g. schooling fish, and therefore localised zones of productivity (Votier et al., 2010), but knowledge of their winter distribution remains limited (McFarlane Tranquilla et al., 2013). True seabirds, such as gannets *Morus bassanus*, kittiwakes and shearwaters (family Procellariidae), experience late maturity, low fecundity and are long-lived (Schreiber & Burger, 2002). They live and forage in the pelagic environment for extended periods of time (Nelson, 1978), so may be hard to study. However, when feeding nearshore or along coastlines (Croxall et al., 2012) seabird foraging flocks can be monitored (Figure 6.1), and are often co-located with shorebirds, such as gulls (family Laridae).

Explaining environmental drivers of seabird distribution is required to better understand the links between habitat use and habitat perturbations (Webster et al., 2002) on the species, which may help mitigate mortality in nets. Consequently, monitoring changes in foraging ranges and patterns of distribution is a useful tool in marine spatial planning (Ronconi et al., 2012) and for informing local fisheries (Lascelles et al., 2012). Thaxter et al. (2012) recommend foraging range estimates should be used by management to initially help identify potentially-important foraging areas. Improving knowledge on the fine-scale distribution of seabirds (and other top predators at risk of incidental capture where they co-exist, e.g. cetaceans), which includes assessment of their potential for spatial interaction with fishing effort, and developing appropriate methods to monitor them, is therefore essential to provide effective and

scientifically-robust information for management, based on an ecosystem approach; see the UN Convention on Biological Diversity ('CBD'), 2000, for more information.

Figure 6.1. Foraging seabird aggregation observed from a land-based watch point at St Ives Bay. (Photograph © D Murphy 2012)

This is particularly important where management decisions require political advocacy to balance the interests of multiple users of the marine environment with sustainable conservation efforts.

Bycatch Issues Affecting Coastal Marine Species

A recent global review on incidental catch of seabirds estimates a minimum annual mortality of 400,000 birds in gillnet fisheries (Žydelis et al., 2013). Monofilament gillnets in coastal areas are common gear in artisanal fisheries and, though bycatch is considered one of the principle causes of seabird population decline (Croxall et al., 2012), quantitative data on both fishing effort and catch of non-target species, which also includes other megafauna (e.g. cetaceans and sharks), remain few. Bird species most at risk to gillnet entanglement are plunge- and pursuit-divers foraging for prey fish or other benthic fauna in the water column. Žydelis (2013) identified 19 of 23 auk species (family Alcidae) that are particularly susceptible to bycatch in gillnets, and 13 of 22 shearwater species. In the northeast Atlantic, both these families are commonly found, with millions of auks breeding on islands and along rocky coasts.

Shearwaters (family Procellariidae) are also seasonally abundant in both nearshore and offshore waters (BirdLife International, 2004).

Bycatch in gillnet fisheries in the UK does not appear as a significant threat to seabirds at a regional scale (Žydelis et al., 2013), but there may be local colony impacts from these mortality events. A single incident or, more certainly, a series of sporadic incidents within a season or over consecutive years, is likely to affect the global population of a critically-endangered species, even if only a handful are caught. The Balearic shearwater *Puffinus mauretanicus*, for example, as Europe's only critically-endangered seabird (IUCN, 2014), means a bycatch event that kills any number of them would have a significant carry-over effect on breeding performance at the population level (McFarlane Tranquilla et al., 2013).

Bycatch in St Ives Bay

St Ives Bay (SIB) off the north Cornish coast is an important winter foraging area for the Balearic shearwater (Wynn, 2009), as well as several species of auk, including common guillemots *Uria aalge* and razorbills *Alca torda* (see Appendix B; also RSPB, 2012). During the first week of January 2012, an estimated 100 seabirds were found drowned in a gillnet north of the town, west of Porthmeor, approximately 100 m from the shore in shallow water (Figure 6.2). Another 200 birds were also found washed up on local beaches (RSPB, 2012).

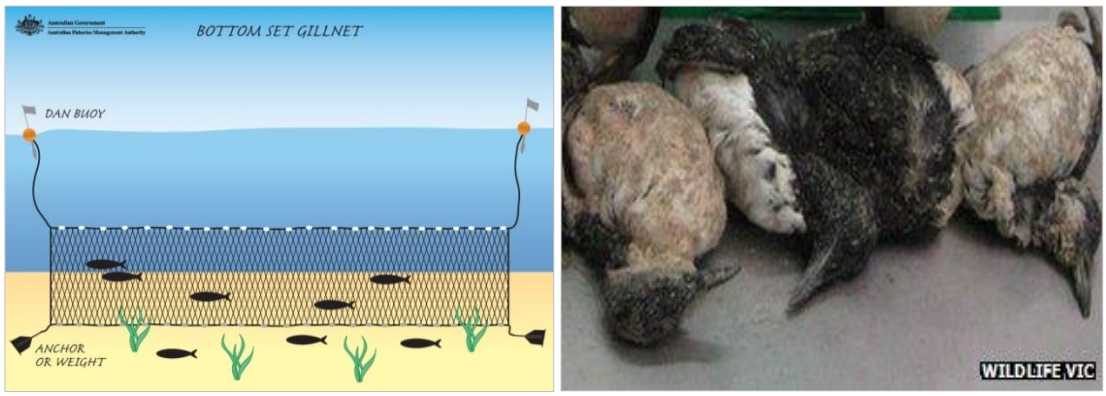

Figure 6.2. Bottom set gillnet (left); incidental seabird bycatch (right).
Graphic shows a typical, bottom set monofilament gillnet used by fishermen local to the St Ives Bay area; photograph shows some of the birds killed in the reported 2012 gillnet entanglement incident. (Photographs: left © Australian Fisheries Management Authority, 2015; right © RSPB, 2012).

These bycatch incidents triggered a threat to the wintering seabirds in SIB, including the Balearic shearwater, and also to cetacean species that are known to visit these waters (Leeney et al., 2012), e.g. porpoises and bottlenose dolphins *Tursiops truncatus*.

The set nets target seabass *Dicentrarchus labrax*, which are attracted to areas visited by their prey fish, sprats (family Clupeidae). Sprats are also primary prey for guillemots and razorbills in the area, so, as the birds were pursuit-diving for their prey, they were incidentally caught in the nets. It was suggested strong westerly winds may have conspired with the annual movement of sprats nearer to shore, bringing higher-than-normal numbers of feeding birds, and their prey, into greater proximity of gillnet fishing areas (pers. comm. P. St Pierre, 2012). This sequence of events resulted in the unusually high numbers of birds being trapped in the nets and drowning.

Mitigation Measures and the St Ives Bay Gillnet Fishery

The Cornish Inshore Fisheries and Conservation Authority (CIFCA), formerly the Cornwall Sea Fisheries Committee, is responsible for managing fishing activities within the six nautical mile limit around the coast of Cornwall, including rivers and estuaries within tidal limits (Figure 6.3). It was fully vested on 1st April 2011, under the Marine and Coastal Access Act 2009.

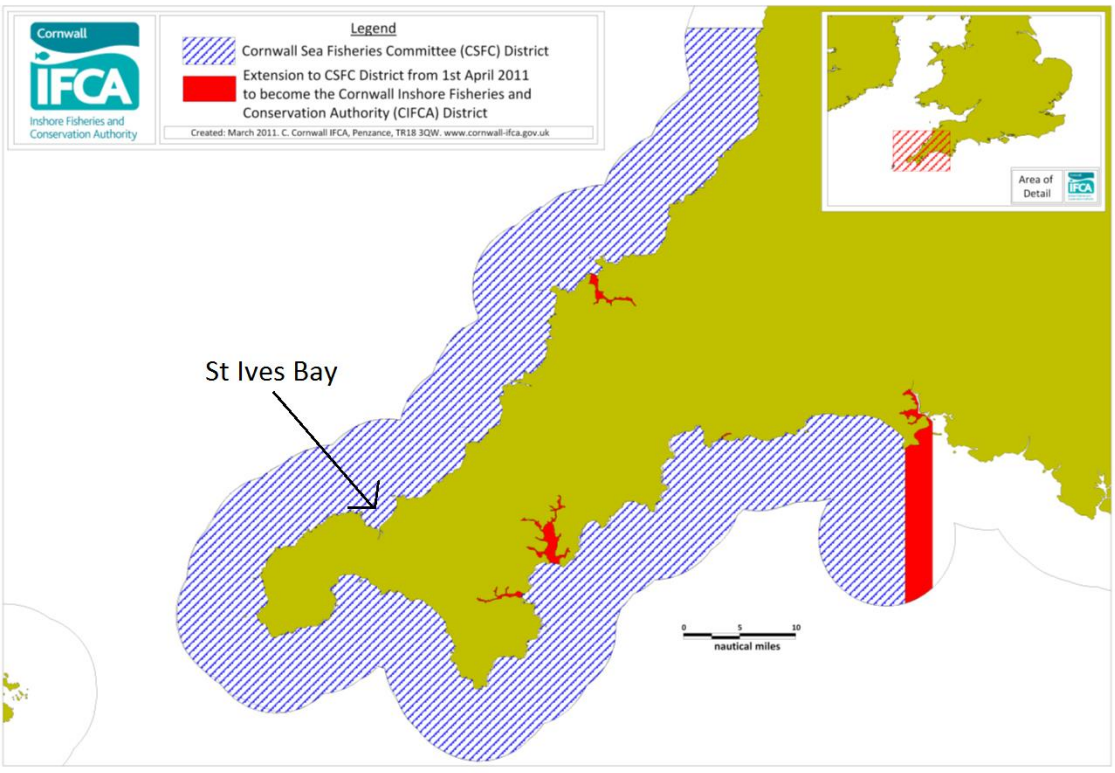

Figure 6.3. Cornish IFCA (Inshore Fisheries and Conservation Authority) District Chart.
Chart delimits the six nautical mile limit around the coast of Cornwall for which the Cornish Inshore Fisheries Conservation Authority (CIFCA) is responsible for managing fishing activities, including rivers and estuaries within tidal limits. CIFCA was fully vested on 01/04/2011.

The current SIB Gillnet Fishery byelaw, originally enacted in 1999 (Appendix M.1), is triggered once more than 100 birds have been killed in nets, and results in a time-area restriction for the local gillnet fishery. The closure enforced by the first-time use of this byelaw is the only one of its kind in the country, and affects an arbitrarily-defined area of the bay on the landward side of a theoretical line between St Ives Head and the northern extremity of the Black Cliffs, east of the Hayle Estuary (see map in the CIFCA closure notice, Appendix M.2). This equates to an area encompassing ~25% of SIB. Since the bycatch incidents occurred within a single week in January 2012, the byelaw imposed a temporary three-week fishing exclusion zone preventing fishermen from deploying gillnets between 5th and 26th January that same year.

The closure notice was backed up by fines of up to £50,000, under the IFCA's option to issue Financial Administrative Penalties (FAPs), as detailed in Section 2.11 of the 2012 to 2013 Enforcement Plan (CIFCA, 2012). FAPs are an alternative to criminal prosecution and considered essential to discourage serious non-compliance. The Enforcement Plan sets out its description of netting methods, with the main regulatory concerns highlighting, amongst other requirements, that fixed nets must not be set within three metres of the sea surface in many coastal areas (Section 3.5 of the document). The Plan, however, notes that enforcement is primarily for the protection of migrating salmonids to and from river systems around the coast, rather than as a bycatch mitigation measure aimed at protecting seabirds.

The Cornwall Wildlife Trust suggested the 'very small' exclusion zone defined by the byelaw could be widened, in order to give adequate protection to the foraging seabirds. CIFCA, however, suggested this may not be necessary, and explained that fishermen had simply 'misjudged' the tides and were therefore unable to haul in the nets before daylight (RSPB, 2012), which are the hours when diving birds feed. It seems plausible that a simple time restriction may be one of several effective short-term solutions, e.g. restricting net-shooting to the hours of darkness when birds are roosting, and enforcing pre-daylight retrieval. Indeed, subsequent to the reported incidents in January 2012, a majority of the local fishers in SIB did agree to a Fishing Nets Code of Practice (Appendix M.3), which applies beyond the extent of the byelaw-enforced closure areas. Fishers agreed to ensure nets are not deployed during daylight hours, and endeavour to recover them by first light, with the aim of reducing the likelihood of future seabird deaths caused by accidental capture in nets.

The local byelaw does not provide a solution to the problem outside the geographical area that it covers. Nevertheless, it is unique to the UK, in terms of the type of event by which it is triggered, i.e. seabird fatalities due to fisheries' bycatch, as well as by the measures taken for

its implementation, e.g. closures to certain fishing activity, including financial penalties for non-compliance. However, it should be noted that the bycatch issue around SIB points to a wider issue at the European level where, to date, there has been no clear or coherent plan to tackle the incidental bycatch of seabirds in European waters. This contrasts with notable achievements that have taken place in the Southern Ocean, for example, where measures were implemented with the aim of preventing albatross fatalities (e.g. the 2001 international treaty, *Agreement on the Conservation of Albatrosses and Petrels,* which entered into force in 2004, the same year during which it was ratified by the UK).

Rationale and aims

During the third quantitative review of Birds of Conservation Concern (BoCC 3), the UK's leading bird conservation organisations, including the RSPB, assessed 246 bird species against a set of objective criteria (Eaton et al., 2009). Species of conservation concern were assigned to one of three lists (green, amber or red), with each list representing an increasing level of concern, which reflects their status at the UK, European and global levels. In SIB, foraging aggregations are composed primarily of surface-feeding shorebirds, typically herring gulls, which are red-listed. Other species commonly sighted are plunge-diving seabirds, including northern gannets, black-legged kittiwakes *Rissa tridactyla*, and two species of auk, guillemots and razorbills. These comprise four of 126 species on the BoCC 3's amber list (see Appendix G for assessment criteria).

The Balearic shearwater comprises ~2-3000 breeding pairs (Guilford et al., 2012) and is known to visit waters off southwest UK in internationally-important (>1 %) numbers (Jones et al., 2014b), including SIB, where peak numbers of up to 100 birds were recorded during winter 2012-13. This is equivalent to ~0.5% of the world population (Wynn, 2009). Recent studies have indicated this species in shifting its inter-breeding range northwards (Wynn et al., 2007; Darlaston & Wynn, 2012), so numbers may continue to rise in southwest waters. The value of the at-risk Balearics given their conservation status, coupled with the bycatch events of other listed-seabirds, triggered a renewed interest in this issue at SIB, and resulted in high-profile national media coverage (Figure 6.4).

Figure 6.4. Media coverage of seabird bycatch incidents off southwest UK, January 2012.

Clearly, there is therefore a strong policy driver to effectively manage the nearshore environment in this area, to balance both local fisheries' interests with adequate conservation measures for these species to avoid such events in the future. However, before mitigation measures are modified or developed to tackle the problem, detailed evidence on both their spatial distribution (where they are feeding) and temporal preferences (when they feed) is needed, as records of these species in SIB have previously been sporadic and typically based upon casual observations by ornithologists. This is particularly relevant during periods of peak counts in mid-winter (Abrams & Griffiths, 1981; Sonntag et al., 2012), as sprats embark on their annual movement into the bay to shelter from stormier weather further offshore (RSPB, 2012).

To obtain robust baseline data on the distributions of feeding seabirds, and cetaceans (which, as frequent visitors to the bay, are also at risk of entanglement), the National Oceanography Centre (NOC) initiated a three-year land-based survey in partnership with CIFCA, Natural England, RSPB and Marinelife (http://www.marine-life.org.uk/). The work presented in this chapter represents results from the first year's pilot study. The aims of the study were to: 1) accurately map locations of foraging aggregations within SIB, in combination with high resolution seafloor imagery, 2) analyse these data to construct a predictive spatial model of hotspot areas, and 3) analyse the time series sightings data with a suite of dynamic environmental (survey, tidal and temporal) variables to reveal patterns in the timing of seabird foraging. This information will aid interpretation of the processes driving observed distributions within the bay.

The potential of bird mortality from gillnet entanglement underscores the importance of monitoring the foraging locations of these species to better inform local policy, while

developing cost-effective and practical survey methods is vital for sustainable monitoring in the future. Analyses presented in this chapter can therefore be used as a template for future work in the area, and at other at-risk locations with similar issues.

6.2 Methods

6.2.1 Survey Methodology

Visual surveys to detect and record winter seabird foraging aggregations in St Ives Bay were carried out over 19 days in two sessions between December and January 2012-13 (Table 6.1).

Table 6.1. Schedule of St Ives Bay pilot study carried out in two sessions between 2012-13.

Field session ID	Fieldwork session description	Date range	Number of observation days	Total number of observation hours
1	December 2012	07 Dec – 15 Dec	8	46.5
2	January 2013	13 Jan – 24 Jan	11	64

A foraging aggregation was defined as a group of >5 of any one seabird species actively foraging in obvious association with each other in a concentrated area, which varied depending on the number of birds present.

To detect aggregations from shore, an observation team comprising at least two observers were equipped with 10x binoculars and 30x telescopes. One observer operated the theodolite (Leica FlexLine TS02 Total Station), equipped with a 30x monocular eyepiece. The theodolite records angles to a precision of 0.0018° of arc. The instrument's tripod was set up each day directly over a precisely-surveyed point, measured at the beginning of the study using a Trimble Differential GPS (DGPS). During every hour of survey (see details below), the horizontal measurement was zeroed and the theodolite level checked. Measurements of tidal changes in the instrument's height above sea level were also recorded every 30 minutes, and necessary tidal height corrections were carried out during data processing (see Section 2.1.2 for calculation details).

Every 30 minutes, an intensive scan of ~15 minutes duration was conducted concurrently by members of the observation team, using telescope, binoculars and naked eye. This ensured thorough and consistent coverage of the near- and far-fields throughout the survey period. The Field of View (FoV) within the bay was searched methodically. Firstly, observers would use

their telescopes and carefully scan the distant FoV from left to right (with Godrevy Island in the centre; Figure 2.20). Secondly, the observers would drop down a FoV and scan right to left (with Gwithian Beach at the top). The final search covered the nearshore areas out to ~2 km with binoculars and the naked eye.

When aggregations were sighted, the theodolite eyepiece crosshairs were centred at the waterline on an animal in the centre of the group and, using the instrument's 'record' button, precise angles were saved onto an internal data file, automatically time- and date-stamped, having pre-installed an instrument-specific (.frt) format file for this purpose. The theodolite record number, "Point ID", along with species composition and group size, were noted on standardised recording sheets (Appendix D). Each recording of a foraging aggregation was allocated a "Sighting ID"; the same IDs were only confirmed in the field if they had been tracked by a nominated observer engaged in a dedicated "focal follow". This observer continued to visually track the marked group with scope or binoculars to ensure that when the theodolite operator returned to record the location again (e.g. after time spent recording positions of other species), the ID could be confirmed. Observers would resume scanning immediately after foraging events were recorded to ensure consistent effort.

All visible areas of the sea surface were therefore methodically scanned in the same way for at least 15 minutes every 30 minutes, ensuring a consistent and repeatable sampling strategy. Data for *in situ* weather conditions and other environmental variables, e.g. sea state, wind, visibility, cloud cover and glare (see Appendix C for descriptors), were collected every 30 minutes at the start of each scan and recorded on the same standardised recording forms (Appendix D). Survey units of 30-minute duration were selected to ensure the dedicated ~15-minute searches (conducted at the start of each 30-minute survey unit) were considered independent, and that changes in environmental parameters, e.g. weather, were recorded at a temporal resolution that allowed comparison with sightings data.

Locations of surfacing cetacean species (Figure 6.5), including harbour porpoise and bottlenose dolphin, were also recorded, to qualitatively analyse spatial overlap with seabird hotspot areas, as they are vulnerable species also potentially at risk from entanglement in nets.

Figure 6.5. Surfacing cetacean species visiting the waters of St Ives Bay.
Left: harbour porpoise *Phocoena phocoena*; right: bottlenose dolphins *Tursiops truncatus*. (Photographs © R Wynn 2013).

Various forms of fishing activity were also recorded, taking a single theodolite fix of each vessel every 30 minutes for a more thorough picture of how the waters of St Ives Bay are used and to qualitatively analyse any spatial overlap between fishing effort and seabird foraging to assess the potential for interaction. Notes were taken whether the fishing vessel was 'large', i.e. with a wheelhouse, or a 'handline' vessel, generally one or two fishers (Figure 6.6).

Figure 6.6. Typical fishing vessels utilising the waters of St Ives Bay.
Left: vessel defined as 'large', i.e. with a wheelhouse; right: 'large' vessel with wheelhouse in foreground, yellow 'handline' vessel in background.

Although the observation site provided a wide FoV of the study area (Figure 2.19), the exposed location meant that observations were impacted by high winds and other inclement weather events, e.g. rain and sea fog. Fieldwork was abandoned when the far side of the bay could not be seen, i.e. <6 km range. Observation periods ranged between 3 and 8 hours.

6.2.2 Analytical Methods

6.2.2.1 Spatial Analysis

Initial data exploration was carried out to gain an overall impression of the theodolite data, post-processing in FlexOffice, v.2 (Leica Geosystems), see Section 2.1.2 for details. Maps were produced in ArcGIS® (ESRI, 2012) combining the raw sightings data with the bathymetry layer. This enabled preliminary visual analysis at a very fine-scale (<20 m), including comparing exact foraging locations according to tidal state and wind vector. For cetaceans, tracks connecting data points of the same animal, or group of animals, by "Sighting ID" were constructed (see 6.2.1 for details on ID allocation). Tracks were created using the 'Point to Line' tool in GIS.

To analyse the spatial data, the survey area was delineated at 6 km from the watch point, as conspicuous seabird foraging aggregations could be detected in the field up to 5 km with binoculars and 6 km with telescopes. The 6 km survey extent was gridded with 500-m cells for relative density analysis to account for the maximum positional error in the recorded theodolite data (see Section 2.2.1 on accuracy) and to maximise use of the high resolution bathymetry. After clipping areas of affected grid cells that were obscured from view due to land topography, precisely measured in the field with the theodolite, as depicted by the greyed-out polygon (Figure 6.7), the visible survey area encompassed 33.24 km^2.

Sightings data were filtered by time and space to avoid successive measurements of the same aggregation (or group of cetaceans), e.g. whilst being tracked, so only one sighting was retained in the spatial dataset per grid cell per 30-minute survey unit. A re-sighting was therefore discarded if recorded in the same grid cell within the same 30-minute period. However, if an aggregation passed into a different grid cell within the same 30-minute period, it was retained in the dataset, so all sightings were spaced by a minimum of one grid cell and one 30-minute survey unit. The sightings density grid based on these data therefore represents *relative* habitat use across the survey area, as the values per grid cell symbolise seabird foraging-visit frequency (or cetacean sightings) within any particular cell relative to its neighbour, i.e. the intensity with which a particular area was visited.

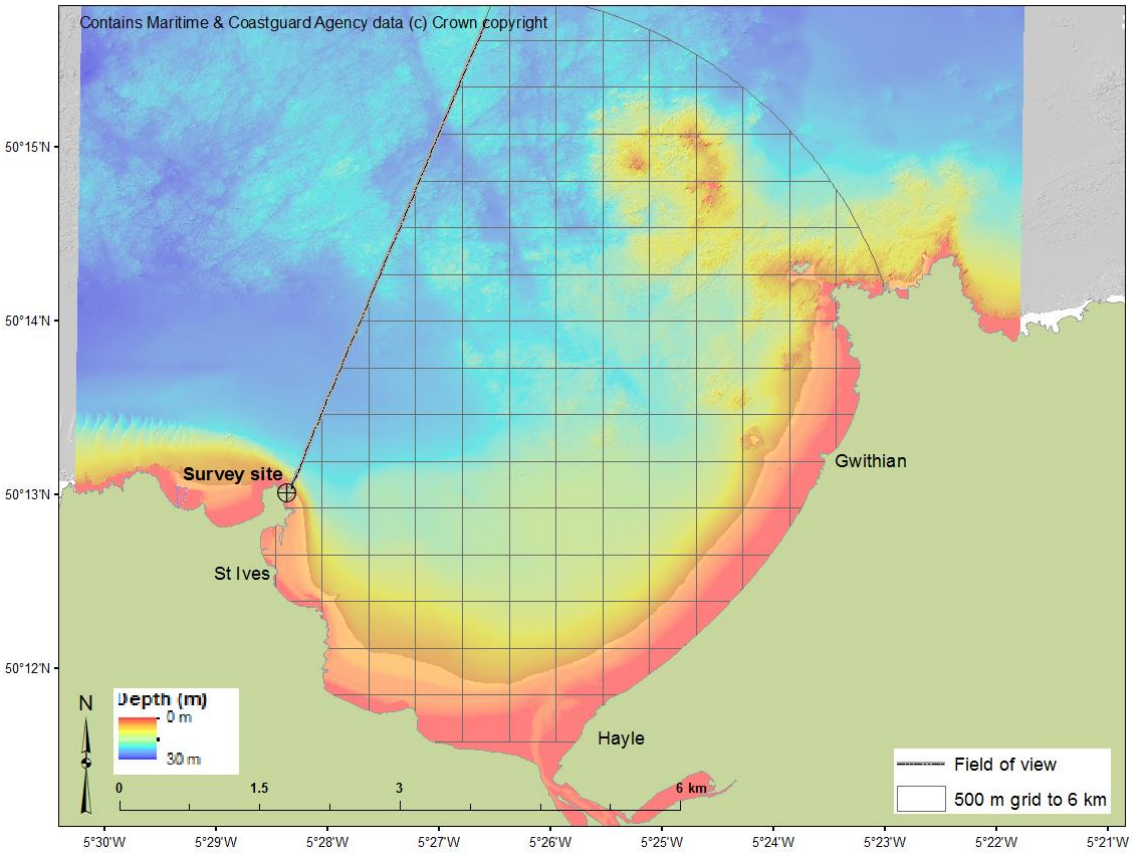

Figure 6.7. St Ives Bay 500-m survey grid delineated at 6 km covering an area 33.24 km².
Survey grid mapped onto high resolution (1 m) bathymetry data (courtesy of CCO/MCA © Crown copyright). Field of view due to land topography (east of the grey line) was accurately measured in the field by the theodolite, and used to precisely clip the survey grid.

In ArcGIS®, the sightings data were summarised per grid cell by joining the sightings point layer to the polygon grid using the Spatial Joins tool. The static covariates, depth, slope and aspect (see Section 2.3.1), were also summarised per grid cell using the Zonal Statistics tool (Spatial Analyst > Zonal Statistics), taking into account differing grid cell areas. Extracted values per variable included: maximum, minimum, mean and standard deviation (s.d.).

6.2.2.2 Cluster Analysis

Kernel Density Estimation

Estimating the home ranges of individual animals is a useful measure to visually estimate how the intensity of a point pattern varies over an area during a specified time (Worton, 1995). Kernel Density Estimation (KDE) is used to identify and compare areas used by individual animals, i.e. their utilisation distribution (UD) or 'home range'. A KDE measures the density of records within each grid cell that covers a study area, and uses this to estimate the probability

that an individual will use neighbouring cells (Kernohan et al., 2001; Horne & Garton, 2006). It therefore provides an estimate of which areas an individual uses most frequently, i.e. it is a raster dataset that represents a probability density surface that can be used to predict where an animal is likely to occur, though it was not necessarily observed (Horne & Garton, 2006). KDE rasters can be converted to isopleth lines that contain a specified volume of the probability surface, in doughnut polygons, for example, which identify areas where an individual is likely to occur. The isopleths are located where a shape with the shortest perimeter encloses a specified percentage of the positional records, which helps to identify areas of core habitat within a species' home range, i.e. 'hotspots'. The 0.5 isopleth represents the line containing 50% of the volume of the surface, i.e. the individual is likely to occur in that area 50% of the time, and is often taken to define "core" usage area (Atwood et al., 2004; McFarlane Tranquilla et al., 2013).

For this study, Beyer's (2012) Geospatial Modelling Environment software (GME) was used within GIS to perform the kernel density analyses on the spatial data, using the KDE and Isopleth tools ('kde' and 'isopleth' commands in GME). It should be noted that the GME does not permit the creation of a KDE with "barriers", i.e. barriers to an animal's movements, such as land, in the case of marine species. In areas where such barriers exist, the creation of KDEs may not be particularly well suited, so Beyer (2012) recommends caution when interpreting any observable patterns in probability surfaces for target species of a nearshore population.

The KDE tool calculates probability density estimates based on a set of input points, and can implement three types of kernel. Depending on which kernel is used in the calculation, the bandwidth will be different. The default, Gaussian kernel was selected. Since this is a bivariate normal kernel, the bandwidth is the covariance matrix (for a bivariate normal distribution). Various bandwidth estimation algorithms, the 'selectors', can be specified, which estimate an optimised bandwidth matrix given the specific data, calculated in R using the Kernel smoothing package ('ks'). These are 2×2 matrices, though only three parameters need be provided for the KDE: the standard deviation for x, the standard deviation for y, and the covariance. Both the plug-in ('Hpi') and least-squares cross-validation ('Hlscv') bandwidth estimators were calculated, and entered into the KDE separately for later comparison. The final parameter required was cell size. Using Beyer's recommended 'rule of thumb' (Beyer, 2012), a cell size of 20 was calculated, based on the cell size of the point data source raster.

The resultant KDEs from both the plug-in and LSCV bandwidth estimators were converted to doughnut polygons with the Isopleth tool, and specified to contain the 25%, 50% and 75%

quantiles. Based on field experience, outputs from the different bandwidth estimators were visually compared to determine which of the KDEs were the most ecologically-relevant. However, observable spatial differences between the kernels were negligible, so kernels from the plug-in algorithm were selected. Beyer (2012) also notes that the 'Hpi' performs particularly well compared to other bandwidth estimators.

6.2.2.3 Temporal Analysis

For the temporal dataset, sighting IDs (see Section 6.2.1 for details on ID allocation) were filtered by 30-minute units of survey. Distinct IDs were retained each 30-minute unit, with re-sightings discarded. The same ID was retained if re-sighted in the next 30-minute unit of survey effort. This was considered representative of how the birds used the survey area *relatively* through time, even if it was the same feeding aggregation.

6.2.2.4 Statistical Modelling Methods

Using the 'mgcv' package in R (Wood, 2006a), generalised additive models (GAMs) were constructed to model spatial and temporal patterns in the seabird aggregation data, according to the general structure specified by Hastie and Tibshirani (1999). GAMs are useful where the relationship between the response and a continuous variable exhibits a complicated shape, i.e. where it cannot be specified by an explicit functional form (Crawley, 2012), e.g. linear or quadratic. Rather, non-parametric 'smoothers' are used to describe the data and fitted during model selection. Collinearity between candidate predictor variables may affect estimation of both the model's standard errors and associated p values, so was investigated prior to running the models using Spearman's pairwise rank correlation tests. If correlation coefficients revealed strong collinearity between variables, using $r \geq 0.8$ as the threshold (Zuur et al., 2009; De Boer et al., 2014; Jones et al., 2014a), only one or other of the collinear terms was retained in further analysis, depending on which was retained first in the model selection process, as described below.

For the spatial model of gridded sightings data, a negative binomial family structure was specified, since it is appropriate for count data with many zero's, i.e. over-dispersion, though not zero-inflated data (Zuur et al., 2007). Two models were constructed for the temporal dataset: one response was the absence or presence of a foraging aggregation per 30-minute survey unit, i.e. 0's and 1's, so a binomial family was used; the other response was the absolute

number of filtered foraging aggregations per survey unit. A log link was specified as the functional relationship between the response and predictor variables in both models.

Default thin plate regression splines (bs = "tp") were specified for all non-cyclic variables, as they allow a smooth function to be fitted to noisy data with multiple explanatory variables without the requirement of knowing where the different splines join, i.e. the "knots" (Wood, 2006b). Cyclic smoothers (bs = "cc") were specified for metrics whose first and last values are adjacent, i.e. covariates with degrees or hours as units where 359° and 0°, or 23-hrs and 0-hrs, are next to each other, for example. Two-way interaction terms were fitted using "te" tensor product smooths, which are effective for modelling smooth interactions of variables with differing units (Wood, 2006b; Crawley, 2012).

The maximum degrees of freedom ("k") for each smooth were manually limited to 4 for most covariates to prevent model over-fitting and to minimise excessive flexibility (Embling et al., 2010). Tidal variables were limited by k = 6 to allow for expected sinusoidal relationships with the response (sightings). To reduce model over-fitting in the automatic parameter smoothing process, the penalty ("gamma") given to each degree of freedom was increased from the default of 1 to 1.4 (Wood, 2006b).

Akaike's AIC score ('An Information Criterion') is a measure of a model's efficiency in explaining the data (i.e. model simplicity vs. model fit). AIC is negatively affected by the number of parameters included in a model, so helps to determine whether additional parameters are justified (Crawley, 2012). The best performing model of significant terms is that which gives the best 'fit' in terms of lowest residual deviance, and lowest AIC score. Using a manual, step-wise forward approach (adding variables iteratively at each stage), according to the selection criteria detailed in the paragraph below, models were built as a function of the explanatory variables. For the spatial model, static bathymetric covariates, maximum depth, mean slope and mean aspect (listed in Table 6.3 on page 225) were modelled first, and the two-way interaction terms only specified once the main terms had been selected. For the temporal model (covariates listed in Table 6.6 on page 231), survey variables (significant wave height, sea state, cloud cover, wind speed, wind direction) were added first. Tidal variables (wave direction, tidal range, tidal hour) were added second, and temporal variables (month and daylight hour) added last.

First, individual GAMs were run for each of the predictor variables. The significant variable with the best AIC was then selected as the first term to be included in the model. Second,

other variables were added iteratively, as a second term in the GAM, and the combination of significant variables with the best AIC was then used in the next round of selection. Variables were only selected if they were significant ($p < 0.05$), added explanatory power to the model, i.e. ≥1% increase on the previous model to 'deviance' in the data, and had a lower AIC score of at least 2, compared to the previous model, as recommended by Burnham and Anderson (2002). Third, remaining variables were added iteratively to the first two significant terms, and this process repeated until no further covariates could be added, according to the criteria specified.

6.3 Results

A total of 176 theodolite fixes of seabird foraging aggregations were recorded over 110.5 hours of active survey in St Ives Bay across 19 days between December 2012 and January 2013. There were 118 individual foraging aggregation events (of the same Sighting ID), confirmed in the field through dedicated "focal follows", and tracked while the birds continued to engage in foraging activity, i.e. feeding in close association with one another.

Aggregations were primarily composed of herring gulls (68%) and shags *Phalacrocorax aristotelis* (11%) (Figure 6.8), while a peak count of 15 Balearic shearwaters was observed on 14/01/2013. A week later (22/01/2013), a peak count of auks was observed resting on the water (>300 individuals) identified as ~80-90% razorbills and ~10% guillemots.

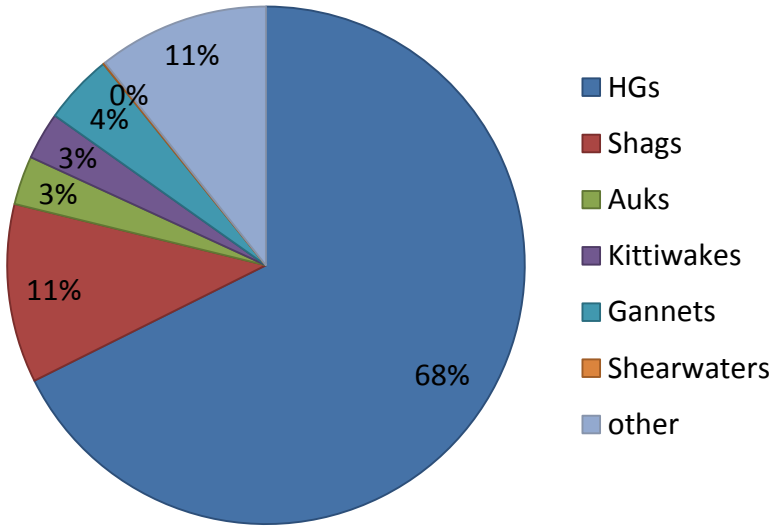

Figure 6.8. Chart showing species composition (%) of seabird foraging aggregations in St Ives Bay. Abbreviation: HG = herring gull.

Though the dominant species forming foraging aggregations was herring gull, group composition varied by month (Table 6.2), with notably more shags observed in December (23%) than in January (3%). Other key species seen in theodolite-recorded foraging aggregations included gannet (4%), auks and kittiwakes (both 3%). There were 324 theodolite fixes of cetacean species, which comprised 281 bottlenose dolphin and 43 harbour porpoise. Of these, 45 had the same Sighting ID. Bottlenose dolphin (n = 32 IDs) were the most frequently observed (71%), while 13 IDs were allocated to porpoise (29%).

Table 6.2. Species composition (%) of foraging seabird aggregations in St Ives Bay by month.

	HGs	Shags	Auks	Kittiwakes	Gannets	Shearwaters	other
December 2012	63	23	4	5	4	<1	1
January 2013	71	3	2	1	5	<1	18
Total (%)	**68**	**11**	**3**	**3**	**4**	**<1**	**11**

6.3.1 Spatial Analyses

Data with erroneous spatial coordinates, collected on 13/01/2013 (nine aggregation IDs, and four bottlenose dolphin IDs), were removed. After filtering, the final spatial dataset consisted of 136 foraging aggregations (109 IDs), and 110 surfacing cetaceans (41 IDs). Seabird foraging events were plotted according to the number of birds present per aggregation (Figure 6.9).

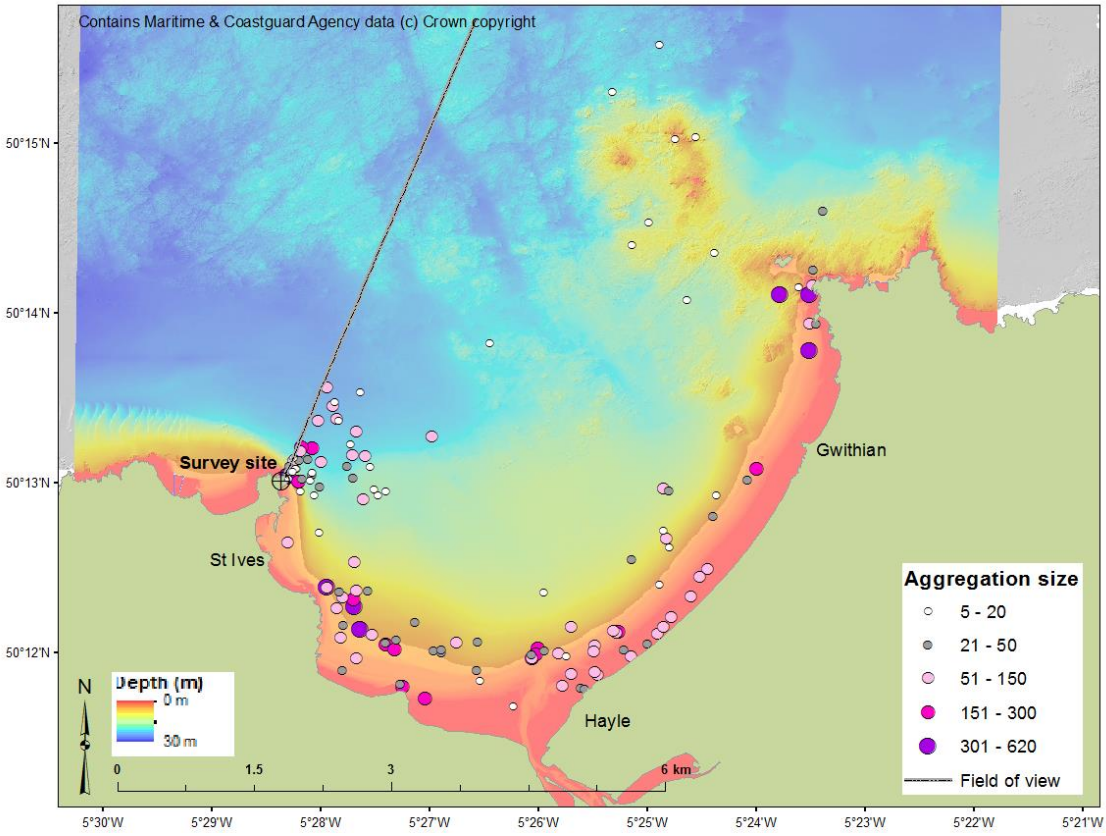

Figure 6.9. St Ives Bay study site showing filtered foraging seabird aggregations by group size. Filled circles are scaled according to number of birds present and represent 136 recorded observations (109 individual events). Locations mapped onto high resolution (1 m) bathymetry data (courtesy of CCO/MCA © Crown copyright). Observation team located at survey site 'crosshairs'. Field of view (east of the grey line) as a result of land topography measured precisely in the field using a theodolite. Theodolite data collected over 19 days across winter 2012-13.

Within the bay, aggregations were recorded along the shallow, sandy shoreline in all directions, reaching group sizes of up to 620 individuals, including around the headland near Godrevy, in the northwest extent of the survey area (Figure 6.9). At these further distances, aggregations were sporadically recorded around the pinnacles, which are areas of topographic highs associated with the shallow reef (<10 m water depth) ~2 km northwest of Godrevy Island. A concentration of sightings were located immediately beneath the watch point on St Ives Island (survey site 'crosshairs'), closely associated with an area of turbulent water often visible at the sea surface near the steep slopes of the headland (labelled 'tide race' in Figure 2.4, Chapter 2).

Where possible, the 90 bottlenose dolphin and 21 porpoise fixes with the same ID (n = 28 and n = 13, respectively), were connected by their tracks (Figure 6.10).

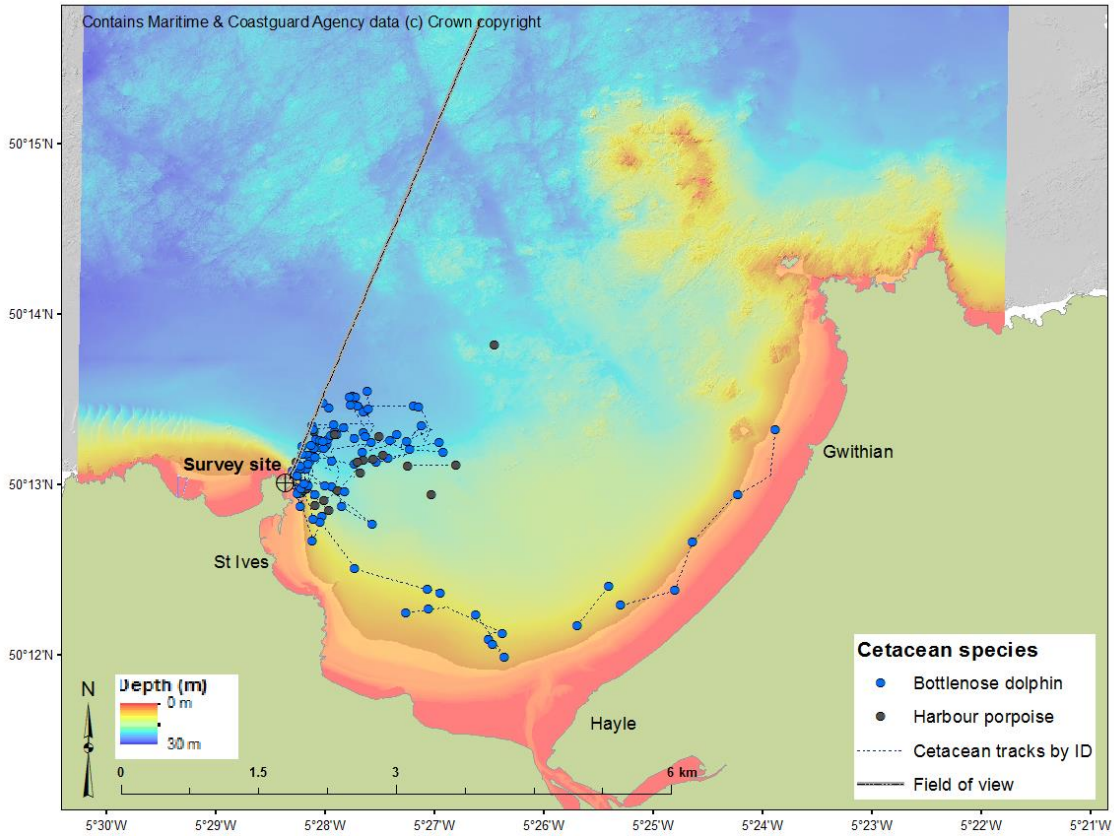

Figure 6.10. St Ives Bay study site showing surfacing locations of cetacean species.
Filled circles represent filtered cetacean sightings (n = 110) colour-coded according to species: blue = bottlenose dolphin (n = 90, 28 IDs); grey = harbour porpoise (n = 21, 13 IDs). Where an observation with the same "Sighting ID" was tracked (n = 41), positions are joined by dotted lines. Locations mapped onto high resolution (1 m) bathymetry data (courtesy of CCO/MCA © Crown copyright). Observation team located at survey site 'crosshairs'. Field of view (east of the grey line) due to land topography measured precisely in the field using a theodolite. Theodolite data collected over 19 days across winter 2012-13.

The area immediately offshore of St Ives Island, near the steep slopes of the headland, held the highest number of cetacean sightings, where animals, mainly bottlenose dolphin (71%), were seen in pods of up to seven individuals. When porpoise were sighted, locations were confined to this area. Bottlenose dolphin however were tracked surfacing all along the nearshore zone, though there is a clear absence of sightings in the slightly deeper (<20 m water depth) central bay area. Additionally, dolphin pods tended to stay in the area for several hours at a time (~2-4 hours) and were frequently observed playing, fighting/mating, and tossing fish.

6.3.1.1 Spatial Clustering

Spatial clustering on the seabird foraging aggregation data was investigated using KDEs calculated on the filtered sightings data (Figure 6.11).

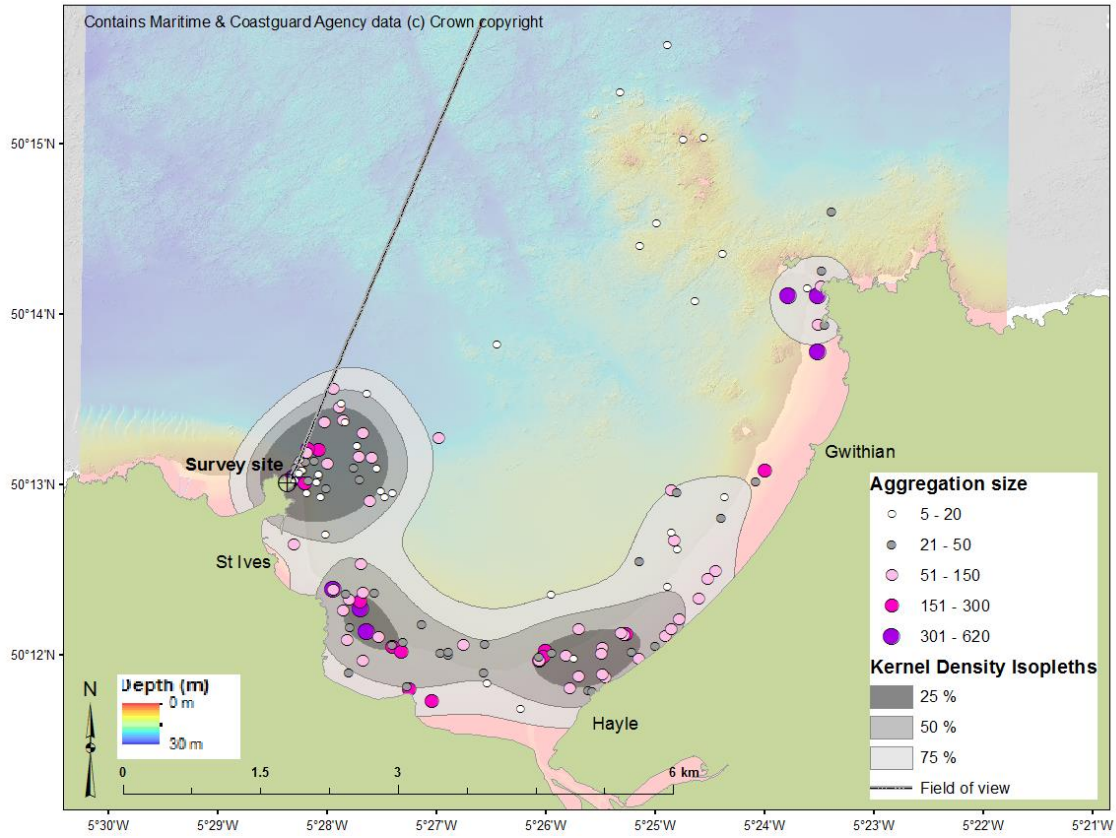

Figure 6.11. Percentage volume isopleths of foraging seabird aggregations with sightings locations. Kernel density estimations (25%, 50%, 75%) calculated within Beyer's (2012) Geospatial Modelling Environment (bandwidth = 400 m; plug-in) from filtered sightings data (n = 136), scaled according to group size. Locations mapped onto high resolution (1 m) bathymetry data (courtesy of CCO/MCA © Crown copyright). Observation team located at survey site 'crosshairs'. Field of view (east of the grey line) due to land topography measured precisely in the field using a theodolite. Theodolite data collected over 19 days across winter 2012-13.

The core density areas identified by the 50% kernel shows clustering around steep slopes beneath the watch point, and along the shallow, sandy nearshore zone of the southern bay. The kernel covers 5.61 km2 (~20% of the 33.24 km2 delimited survey area), suggesting the importance of this site and these hotspots for foraging seabirds. The 75% isopleth also encompasses areas around Godrevy Island, where the fine-scale bathymetry shows areas of steep benthic slope and topographic highs.

Figure 6.12 shows seabird foraging hotspot areas closely connected with observed cetacean distribution in the study area. Of the cetacean sightings near the watch point, only seven surfacings were not located within core seabird habitat. Even as the animals were tracked travelling along the shoreline, surfacing locations perfectly match the 50% and 70% seabird kernels, evidencing areas of favoured habitat are shared by both species within the bay.

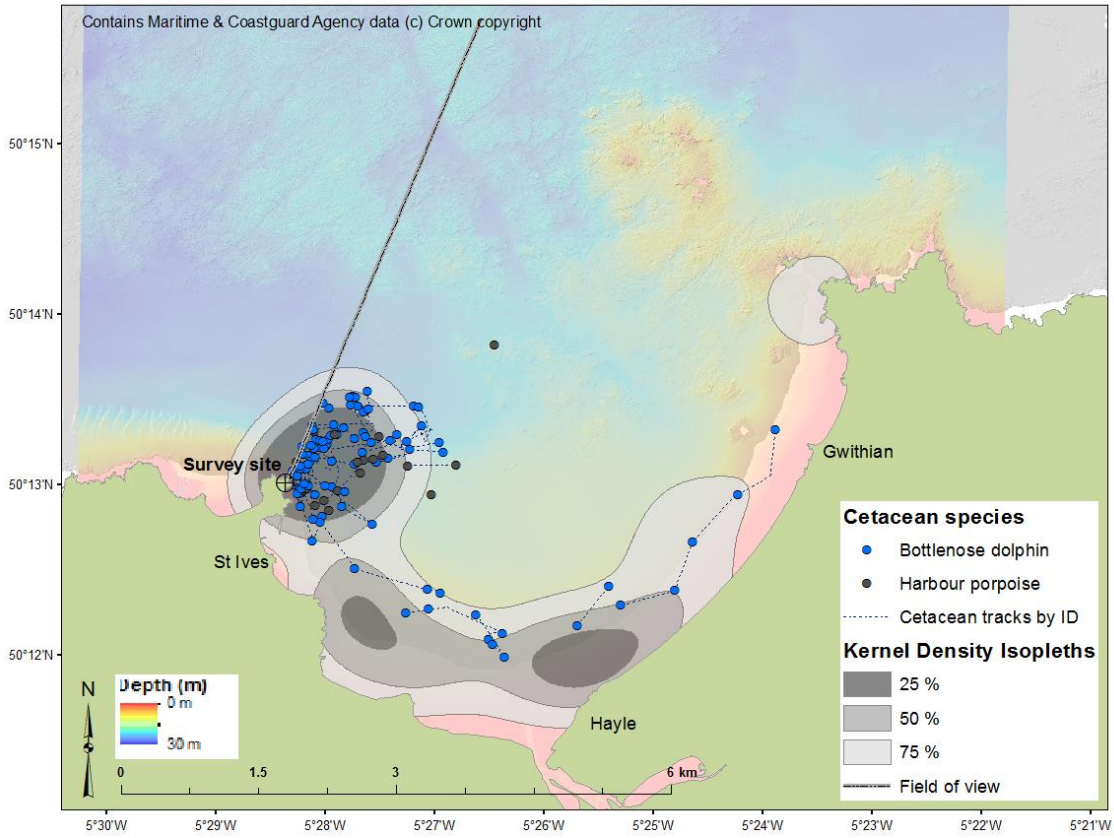

Figure 6.12. Percentage volume isopleths of foraging seabird aggregations with cetacean tracks. Kernel density estimations (25%, 50%, 75%) calculated within Beyer's (2012) Geospatial Modelling Environment (bandwidth = 400 m; plug-in) from filtered seabird aggregation data (n = 136), shown with surfacing cetacean locations (n = 110) joined by dotted lines representing tracks between observations of the same Sighting ID (n = 41). Locations mapped onto high resolution (1 m) bathymetry data (courtesy of CCO/MCA © Crown copyright). Observation team located at survey site 'crosshairs'. Field of view (east of the grey line) due to land topography measured precisely in the field using a theodolite. Theodolite data collected over 19 days across winter 2012-13.

To visualise the influence of wind direction on the fine-scale spatial distribution of foraging seabird aggregations, the filtered sightings (filled circles) were colour-coded according to four wind categories and overlain on the high resolution bathymetry layer (Figure 6.13). Increased observations were recorded during offshore-blowing southerly winds (38%). The positions (red circles) suggest foraging seabirds are focused in the more sheltered nearshore areas, beneath the headland and cliffs around Hayle. During westerly winds, the aggregations (white-filled circles) were solely located in the eastern quadrant of the survey area, again indicating birds are focussing in sheltered areas. Foraging events were notably absent from the southern, south-eastern nearshore zones during northerlies (black circles), indicating birds actively avoided areas facing onshore winds.

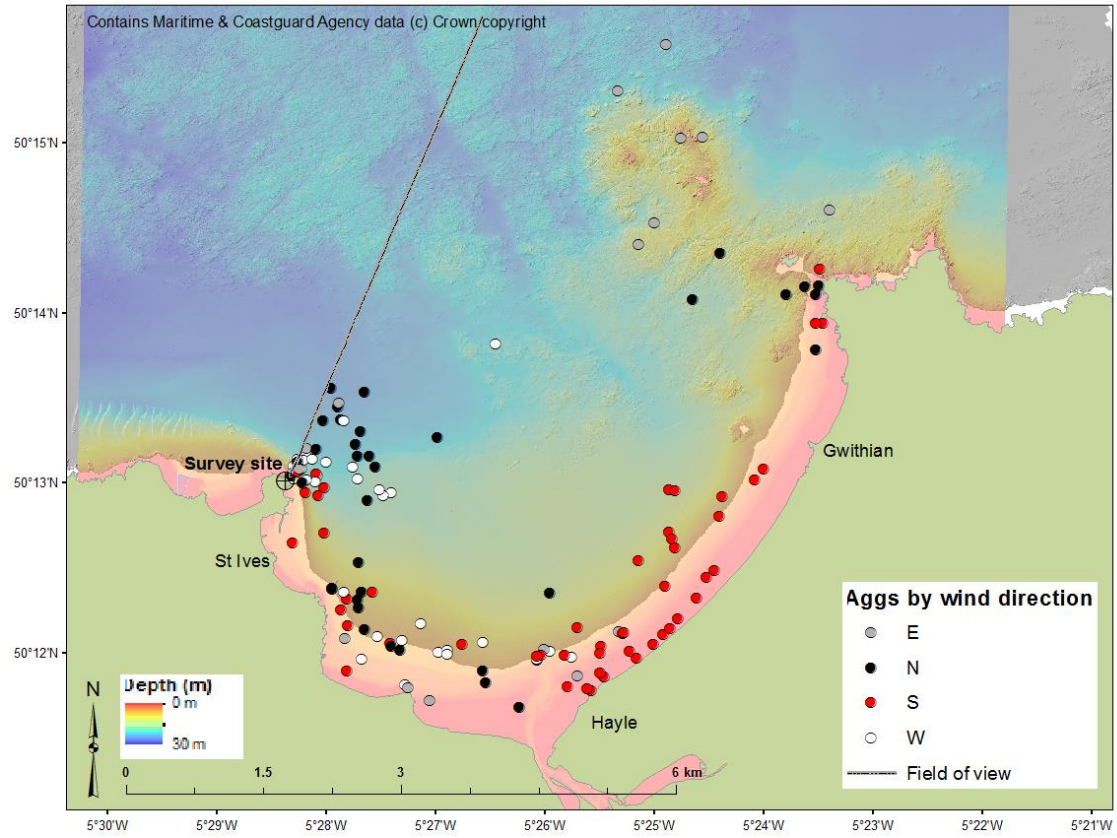

Figure 6.13. St Ives Bay foraging seabird aggregations plotted according to wind direction.
Filtered sightings denoted by filled circles (n = 136) colour-coded according to wind direction during the observation: easterly (grey, n = 16); northerly (black, n = 36); southerly (red, n = 51); westerly (white, n = 33). Locations mapped onto high resolution (1 m) bathymetry data (courtesy of CCO/MCA © Crown copyright). Observation team located at survey site 'crosshairs'. Field of view (east of the grey line) due to land topography measured precisely in the field using a theodolite. Theodolite data collected over 19 days across winter 2012-13.

To visualise how tidal state influenced sightings' distributions, i.e. spatial differences at a fine temporal scale, the filtered sightings (filled circles in Figure 6.14) were colour-coded according to tidal hour (where black = LW slack, pale blue = flood tide, red = HW slack, and pink = ebb tide). Around the beaches at Hayle, aggregations during low water were generally further (~30 m) offshore relative to those during high water. Notably, aggregations clustered near the tide race, beneath the survey site (see Figure 2.4), are prominently those recorded during a flood tide, i.e. when waters are flowing fastest into the bay around the headland of St Ives Island. Conversely, observations associated with the pinnacles, northwest of Godrevy Island, were only recorded during an ebb tide.

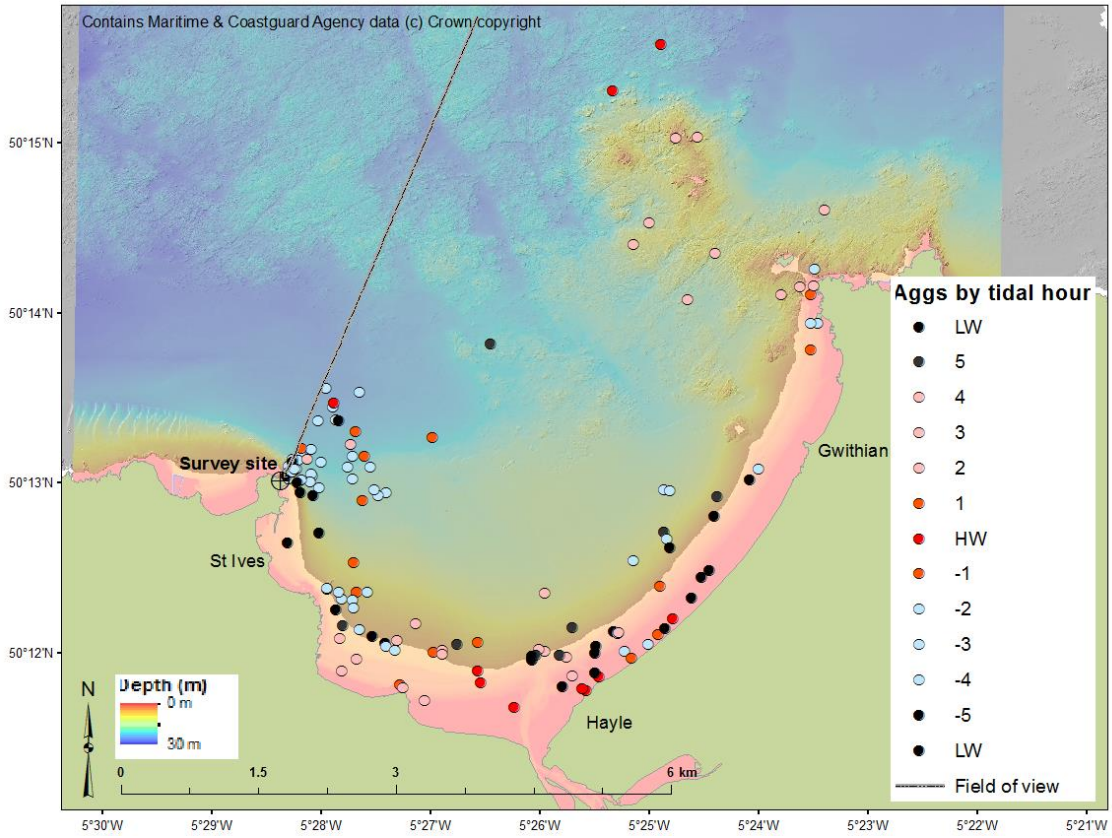

Figure 6.14. St Ives Bay foraging seabird aggregations plotted according to tidal hour.
Filtered sightings denoted by filled circles (n = 136) colour-coded according to tidal hour during the observation: low water 'LW' slack (black, n = 35); flood tide (pale blue, n = 49); high water 'HW' slack (red, n = 25); ebb tide (pink, n = 27). Locations mapped onto high resolution (1 m) bathymetry data (courtesy of CCO/MCA © Crown copyright). Observation team located at survey site 'crosshairs'. Field of view (east of the grey line) due to land topography measured precisely in the field using a theodolite. Theodolite data collected over 19 days across winter 2012-13.

6.3.1.2 Spatial Gridded Analysis

The relative-densities of seabird aggregations per km^2 (filtered by the 500 m survey grid) were calculated for each grid cell, and corrected for differing cell areas (Figure 6.15-A). Values of the static bathymetric variables, mean aspect (Figure 6.15-B), maximum depth (Figure 6.15-C) and mean slope (Figure 6.15-D), are summarised. (The gridded relative-densities of cetaceans per km^2 are provided in Appendix N.1).

A)

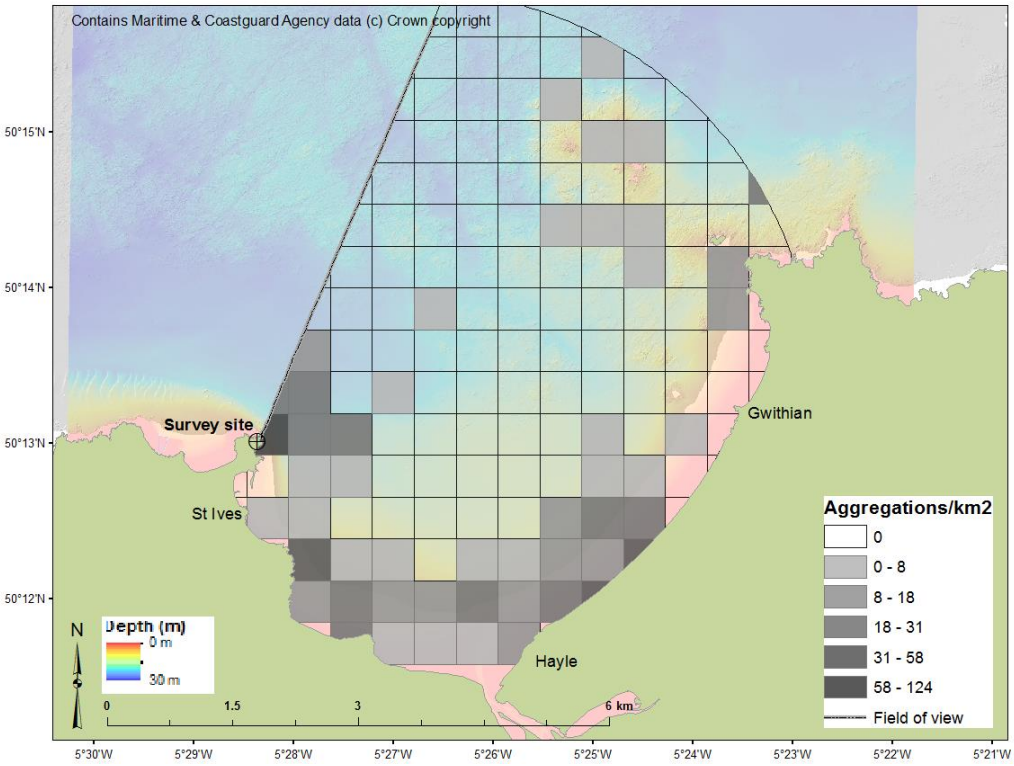
Contains Maritime & Coastguard Agency data (c) Crown copyright
50°15'N
50°14'N
50°13'N
50°12'N
Survey site
St Ives
Gwithian
Hayle
Depth (m)
0 m
30 m
N
0
1.5
3
6 km
5°30'W
5°29'W
5°28'W
5°27'W
5°26'W
5°25'W
5°24'W
5°23'W
5°22'W
5°21'W
Aggregations/km2
0
0 - 8
8 - 18
18 - 31
31 - 58
58 - 124
Field of view

B)

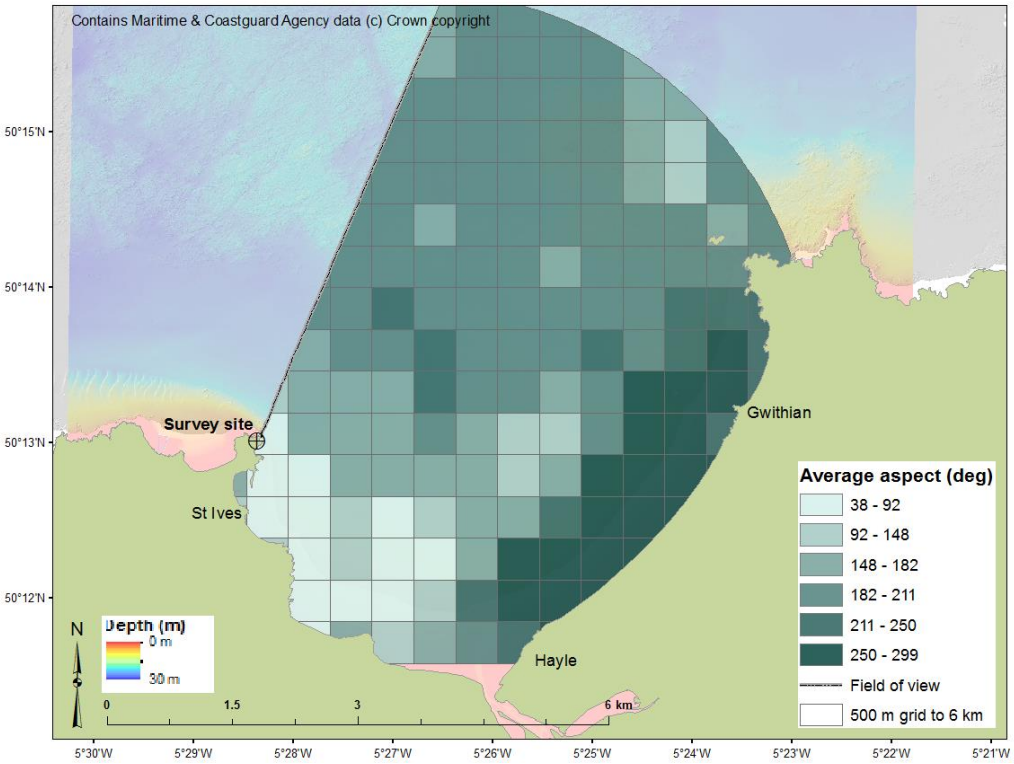
Contains Maritime & Coastguard Agency data (c) Crown copyright
50°15'N
50°14'N
50°13'N
50°12'N
Survey site
St Ives
Gwithian
Hayle
Depth (m)
0 m
30 m
N
0
1.5
3
6 km
5°30'W
5°29'W
5°28'W
5°27'W
5°26'W
5°25'W
5°24'W
5°23'W
5°22'W
5°21'W
Average aspect (deg)
38 - 92
92 - 148
148 - 182
182 - 211
211 - 250
250 - 299
Field of view
500 m grid to 6 km

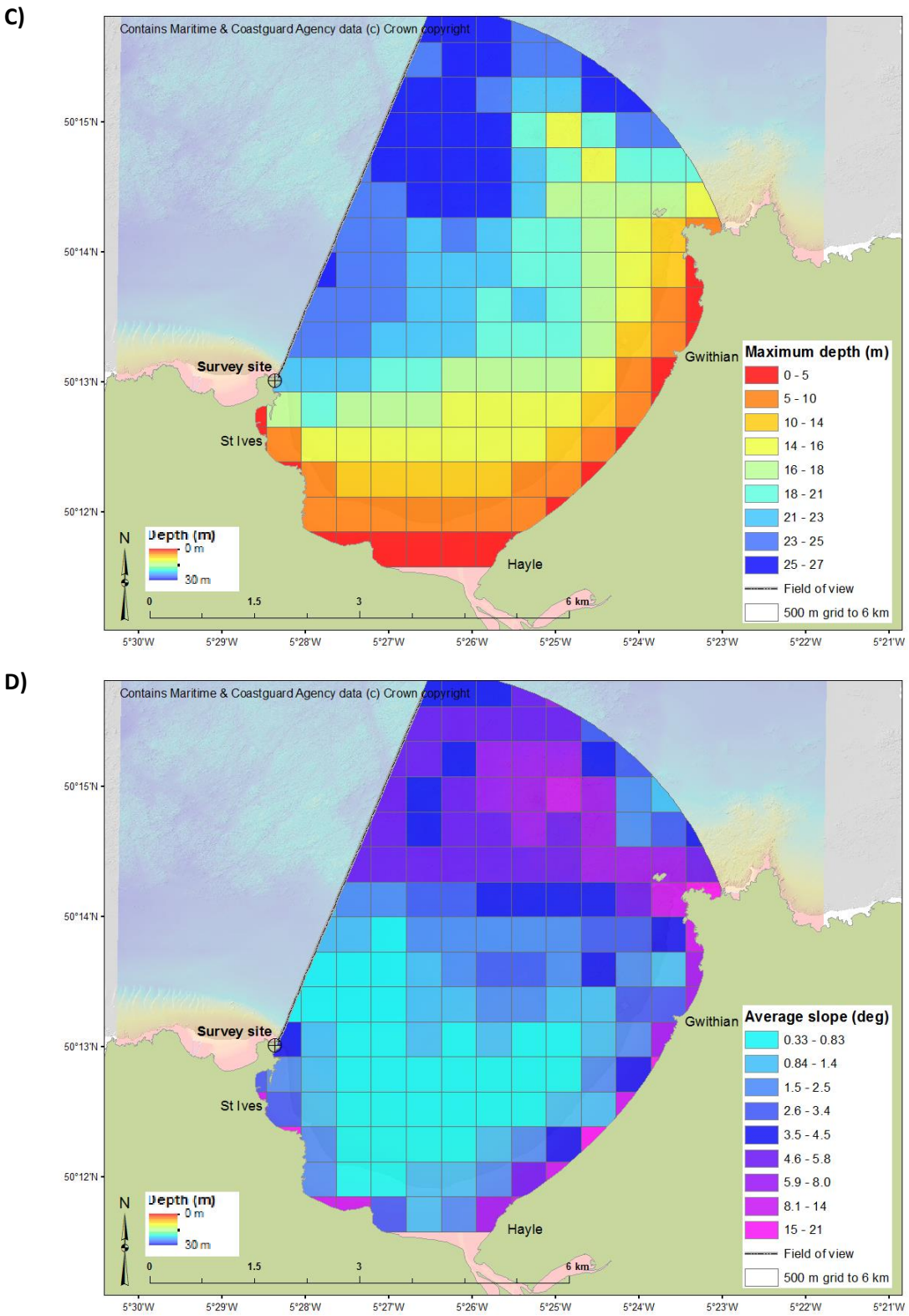

Figure 6.15. Summarised variables per 500-m grid cell of the 33.24 km^2 survey area.
A): Area-corrected relative densities of seabird aggregations per km^2 per grid cell (n = 136 sightings; n = 164 cells). Gridded values of B): mean aspect (degrees), C): maximum depth (m), and D): mean slope (degrees). Static bathymetric variables derived in ArcGIS® from high resolution (1 m) bathymetry data (courtesy of CCO/MCA © Crown copyright). Observation team located at survey site 'crosshairs'. Field of view (east of the grey line) due to land topography measured precisely in the field using a theodolite. Theodolite data collected over 19 days across winter 2012-13.

Figure 6.15-A shows the highest densities are located in the cell closest to the watch point. Other high density areas are located within ~1.5 km of the shoreline, in the southern areas of the bay near St Ives and Hayle. Areas near the headland north of Gwithian Beach are also relatively high density. There is an absence of sightings in the flatter areas of the bay (depicted by the turquoise shading in Figure 6.15-D). Some of the highest relative-density areas for seabird foraging aggregations are located along the shoreline with slope values >8°, e.g. near Hayle and Godrevy Island.

Summaries of the sightings data and static environmental variables are provided in Table 6.3. A thorough data exploration was carried out prior to statistical modelling, and is appended (Appendix N.2).

Table 6.3. Summary of gridded seabird aggregation (and cetacean surfacing) data per grid cell.
Abbreviation: s.d. = standard deviation.

Parameter	Value
Number of (500-m) grid cells	164
Number of 'absence' cells (%): seabird aggregations	113 (69%)
Number of (filtered) sightings	136
Range of sightings per grid cell	0 – 20
Mean sightings per cell (s.d.)	0.82 (2.08)
Number of 'absence' cells (%): cetaceans	135 (82%)
Number of (filtered) sightings	110
Range of sightings per grid cell	0 – 21
Mean sightings per cell (s.d.)	0.67 (2.48)
Static physical variables	
Maximum Depth (m)	
Range	2.05 – 26.3
Mean (s.d.)	16.4 (7.6)
Mean Aspect (degrees)	
Range	38.3 – 299.4
Mean (s.d.)	186.9 (50.8)
Mean Slope (degrees)	
Range	0.3 – 21.0
Mean (s.d.)	3.7 (3.6)
Distance from shore to centre of grid cell (m)	
Range	1.7 – 4118.7
Mean (s.d.)	1492.0 (1112.8)
Grid cell area (m^2)	
Range	32.7 – 249815.7
Mean (s.d.)	202658.7 (79520)

6.3.1.3 Spatial Model

All 164 grid cells were used in the spatial model, as there were no missing covariate data. Collinearity between candidate variables (Table 6.3) was investigated prior to the model selection process using Spearman's pairwise rank correlation tests (Appendix N.3). Distance from shore was highly collinear with maximum depth (r = 0.85). Following the procedure to deal with collinearity (see Section 6.2.2.4), depth was removed from further analysis.

A GAM with a negative binomial logit-link distribution was constructed with an offset term, log area, to correct for varying grid cell sizes. The response variable (area-corrected counts of foraging aggregations per grid cell) was modelled using a step-wise forward selection procedure (see Section 6.2.2.4), as a function of the candidate static covariates (Table 6.3).

Results from the final model are provided below. It retained the terms distance from shore, and mean slope, and took the form:

Seabird aggregation counts ~ Dist_km + s(MeanSlp) + offset(LArea)

The final GAM explained 46.1% of deviance (Table 6.4) in the relative density of seabird foraging aggregations in St Ives Bay between December 2012 and January 2013. Distance from shore was the most significant predictor variable ($p < 0.001$) and explained 43% of deviation. Mean slope was significant at the $p < 0.05$ level and explained a further 3% of deviation. Model smooths are shown in Figure 6.16. (Model validation plots are provided in Appendix N.4).

Table 6.4. Results of forward GAM model selection for seabird foraging events per grid cell.
Variables are shown in order of importance. Smooths are shown with the number of estimated degrees of freedom (e.d.f.) in parentheses; AIC_{Δ} is the reduction in AIC score caused by the addition of the significant variable to the model, with the first score in bold showing the starting AIC; % Dev is the additional deviation (%) in the data explained by adding the selected variable to the model. Surveys conducted over 19 days between December 2012 and January 2013 at St Ives, n = 164 grid cells.

	Area-corrected aggregation counts per grid cell		
Order	Smooth (e.d.f.)	% Dev	AIC_{Δ}
1	s(Dist_km, 1.5)	42.7	**301.11**
2	s(MeanSlp, 2.5)	+3.4	-2.52
Total		46.1	

There are significantly more sightings nearer to shore (Figure 6.16-A). The model smooth for slope is less convincing (Figure 6.16-B).

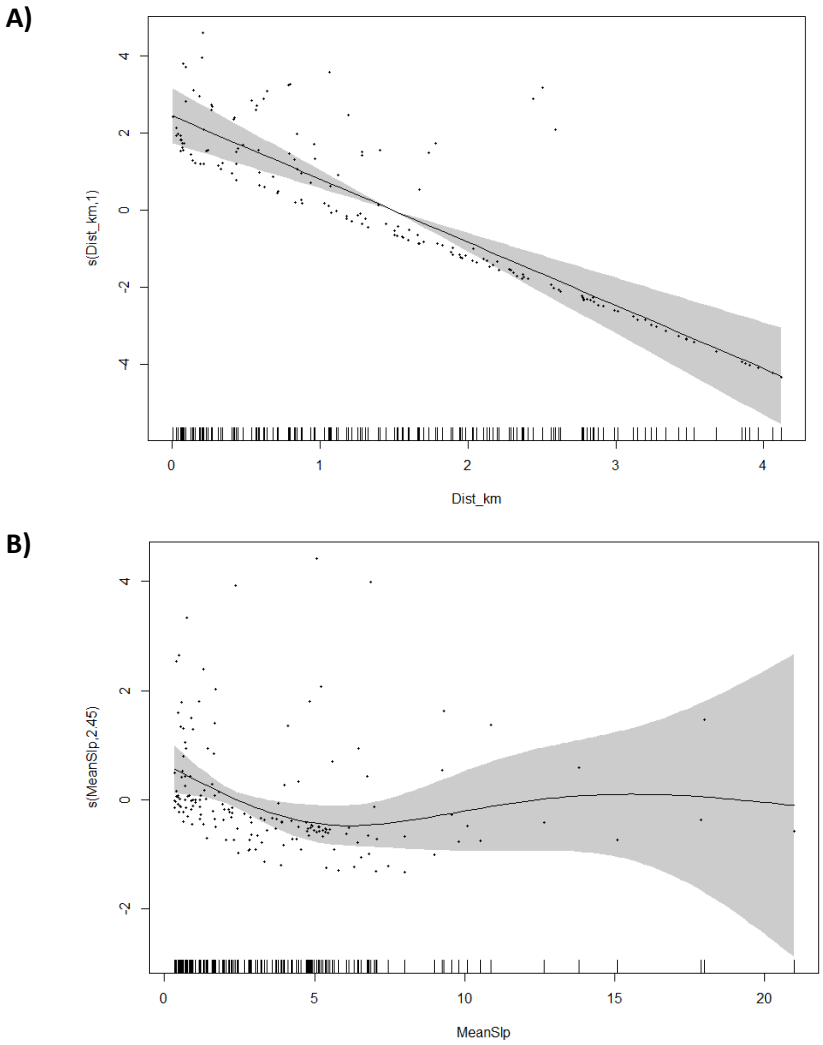

Figure 6.16. Smooths from the final spatial model for foraging seabirds St Ives Bay.
Relationships between area-corrected counts of seabird aggregations filtered by the 500 m grid (n = 164) and the significant predictor variables, as selected by the final negative binomial GAM. A): Distance from shore (linear), and B): Mean slope (e.d.f. = 2.45). Results reported on the scale of the linear predictor. Numbers in y-axis captions are e.d.f. (estimated degrees of freedom) of the smooths. Pearson's residuals are plotted as dots, the shaded regions around the smooths represent the 95% confidence intervals, and the rug plots at the bottom are the covariate values.

6.3.1.4 Model Predictions

The plot of gridded seabird aggregation density, as predicted by the final GAM (Figure 6.17), shows the highest values near the shoreline in the southern bay. There are some moderately high density areas predicted around Godrevy Island, near the pinnacles. There are low numbers of sightings predicted in the central flat areas of the bay.

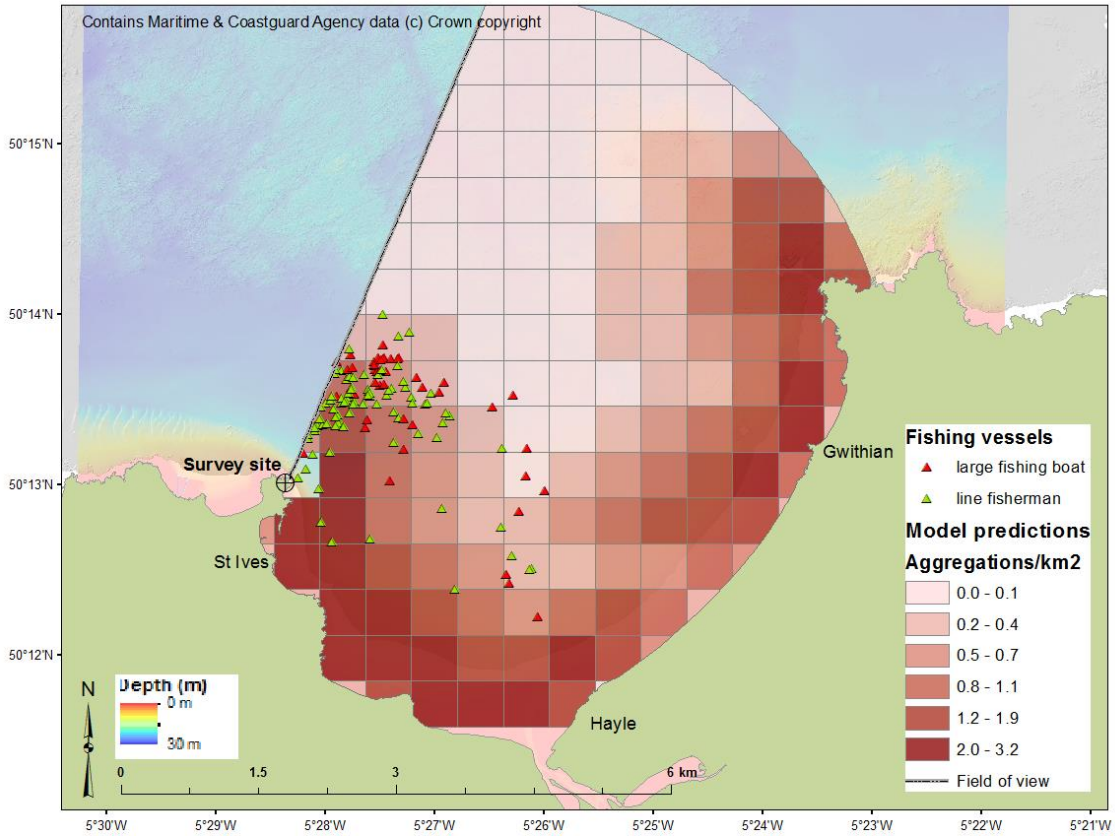

Figure 6.17. Model predictions of foraging seabird aggregation density and fishing activity.
Predictions based on model covariates of average slope, distance from shore, and an area offset. Filled triangles represent fishing vessel locations (n = 130) every 30 minutes colour-coded according to boat size: red = 'large' fishing boat with wheelhouse (n = 44); green = handline fishing boat (n = 86). Density grid mapped onto high resolution (1 m) bathymetry data (courtesy of CCO/MCA © Crown copyright).

Thirty-minute recordings of fishing vessel locations are mapped onto the grid of predicted relative densities (Figure 6.17). It should be noted that not all vessels were actively engaged in fishing activity when their positions were recorded, most obviously those in the centre of the bay, as these represent steaming boats leaving and returning from Hayle. However, the high concentration of vessels located within 1.5 km of the watch point, overlaps with the high density areas for foraging seabirds, as predicted by the model (Figure 6.17) and evidenced in the kernel density analysis (Figure 6.11). This zone, associated with the tide race (labelled in Figure 2.4), also hosted high numbers of cetaceans (Figure 6.10), where they were frequently observed at the surface during their visit to the bay.

6.3.1.5 Model Performance

To visually represent how the model performed, relative to sightings data collected *in situ*, the difference between model-predicted density values, and observed densities, were calculated per grid cell (*predicted density – observed density*). Positive densities represent model over-prediction, while negative densities under-prediction (Figure 6.18).

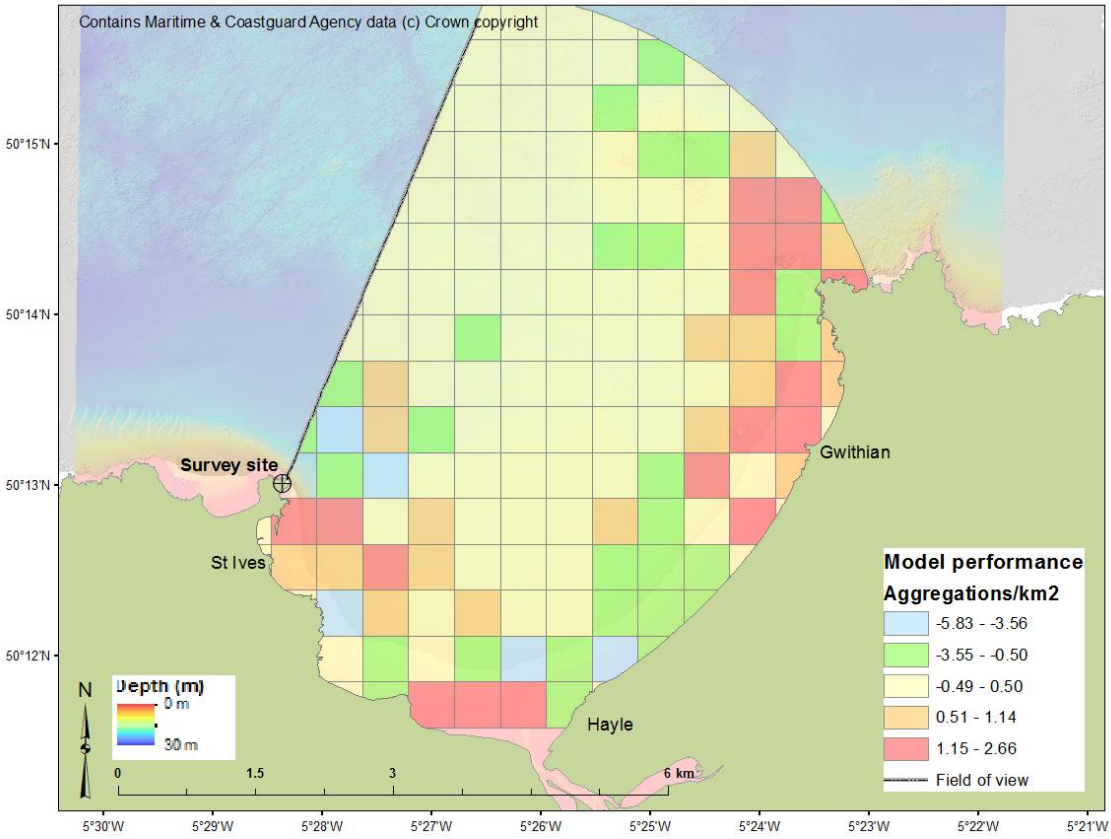

Figure 6.18. Model performance showing the difference between observed and model-predicted numbers of foraging seabird aggregations per km^2 per grid cell.
Predictions based on model covariates of average slope, distance from shore, and an area offset. Density grid mapped onto high resolution (1 m) bathymetry data (courtesy of CCO/MCA © Crown copyright). Theodolite data collected over 19 days across winter 2012-13. Negative densities represent model under-prediction, while positive densities over-prediction. Yellow represents good model performance with a difference of ±1 aggregation per km^2.

Maximum over-prediction by the model for seabird aggregations per km^2 within a single cell is 2.66, while the maximum under prediction is -5.83. Some of the highest over predictions (red shade) are located within 1.5 km of the shoreline near Gwithian, and in the area between Godrevy headland and the pinnacles. The model also over-predicted near the shore at Hayle, though this area is heavily impacted by boat traffic leaving and returning from the estuary, which may explain the lower number of observed sightings than would otherwise be the case.

The model under-predicted in several nearshore areas between Hayle and Gwithian, and directly over the pinnacles near Godrevy. The model performed well across 68% (n = 111) of the survey grid (yellow-shaded cells representing a difference of ±1 aggregation-km^{-2} between predicted and observed density values). The average difference between the model predictions and observed densities across the grid is only -0.005 sightings per km^2 (mean s.e. = 0.16), suggesting good model performance, based on a final GAM that explained 46.1% of variation in the data.

6.3.2 Temporal Analyses

Over 19 days between December 2012 and January 2013, 110.5 hours of survey effort were conducted, averaging six hours of survey effort per day (Table 6.5). A total of 176 foraging seabird aggregations were recorded, with numbers per group ranging between 5 and 620. Theodolite recordings were filtered by 30-minute units of survey effort, leaving 118 IDs in the final temporal dataset (removing 58 observations from the raw dataset). There were no missing covariate data.

Table 6.5. Summary of seabird foraging events during theodolite surveys between 2012-13.
Sightings filtered by 30-minute survey units. 'Positive' hours/days are periods during surveys when an aggregation was sighted and recorded.

Session	Survey days	30-min observations	Foraging events (individual IDs)	Total number of birds (daily average)	Positive 30-min units (%)	Positive days (%)
12/2012	8	93	77	4453 (557)	52 (56)	8 (100)
01/2013	11	128	41	6758 (614)	34 (27)	8 (73)
Total	**19**	**221**	**118**	**11211 (590)**	**86 (38.9%)**	**16 (84%)**

Aggregations were sighted in 86 (39%) 30-minute survey units, while 84% of survey days were positive for sightings (Table 6.5). The average sightings rate was 0.39 aggregations-hr^{-1} (n = 110.5 hours of survey effort) and the average sighting composed of 50.7 birds (s.d. = 143.9; median = 85). The 17 largest foraging flocks occurred in January's session, with peak numbers ranging between 115-620. Aggregations were sighted with cetaceans in 50 30-minute units (23%), though there was no particular time of day when co-sightings were recorded (average daylight hour = 4.1).

Table 6.6 summarises the 30-minute foraging seabird aggregation occurrence dataset and associated environmental covariates (see Section 2.3.2).

Table 6.6. Summary of covariates used in the temporal analysis of foraging seabird aggregations. Filtered seabird aggregation data (118 IDs) collected over 19 days of survey effort (n = 221 30-minute survey units) between 12/2012 and 01/2013. Abbreviation: IQR = inter-quartile range.

Parameter	Value
30-minute units of survey effort (hours)	221 (110.5)
Number of sighting IDs	118
Survey variables	
Significant wave height (m)	
Range	0.45 – 4.15
Median (IQR)	1.61 (1.05 – 1.99)
Sea state (Beaufort)	
Range	1 – 7
Median (IQR)	2 (2 – 3)
Cloud cover (oktas)	
Range	0 – 8
Median (IQR)	7 (4 – 8)
Wind speed (km hr^{-1})	
Range	11.1 – 53.7
Median (IQR)	29.6 (22.2 – 37.0)
Wind direction (degrees)	
Range	10 – 360
Median (IQR)	160 (100 – 320)
Tidal variables	
Wave direction (degrees)	
Range	233 – 336
Median (IQR)	288 (280 – 297)
Tide range (m)	
Range	2.67 – 6.96
Median (IQR)	4.98 (3.58 – 6.5)
Tidal hour (relative to HW)	
Range	-6.0 to +6.0
Median (IQR)	+1.0 (-3.0 to +3.0)
Temporal variables	
Month (as factor)	
Range	12 – 1
Daylight hour (hours post-sunrise)	
Range	0 – 8
Mean (IQR)	4 (2 – 6)

A thorough data exploration was carried out on the temporal aggregation sightings data prior to modelling. Preliminary analysis indicates more sightings were observed with increasing cloud cover (Figure 6.19-A). Increasing sea state wa associated with a marked decline in

foraging events in the survey area (Figure 6.19-B). There were reduced sightings rates during south-westerly winds and north-easterly onshore winds (Figure 6.19-C). Sightings rates appears to increase with increasing wind speeds until a threshold value (Figure 6.19-D), after which the rate falls dramatically. (Further analysis revealed that when offshore wind speeds reached ~28 km hr^{-1} sea state in the bay was affected).

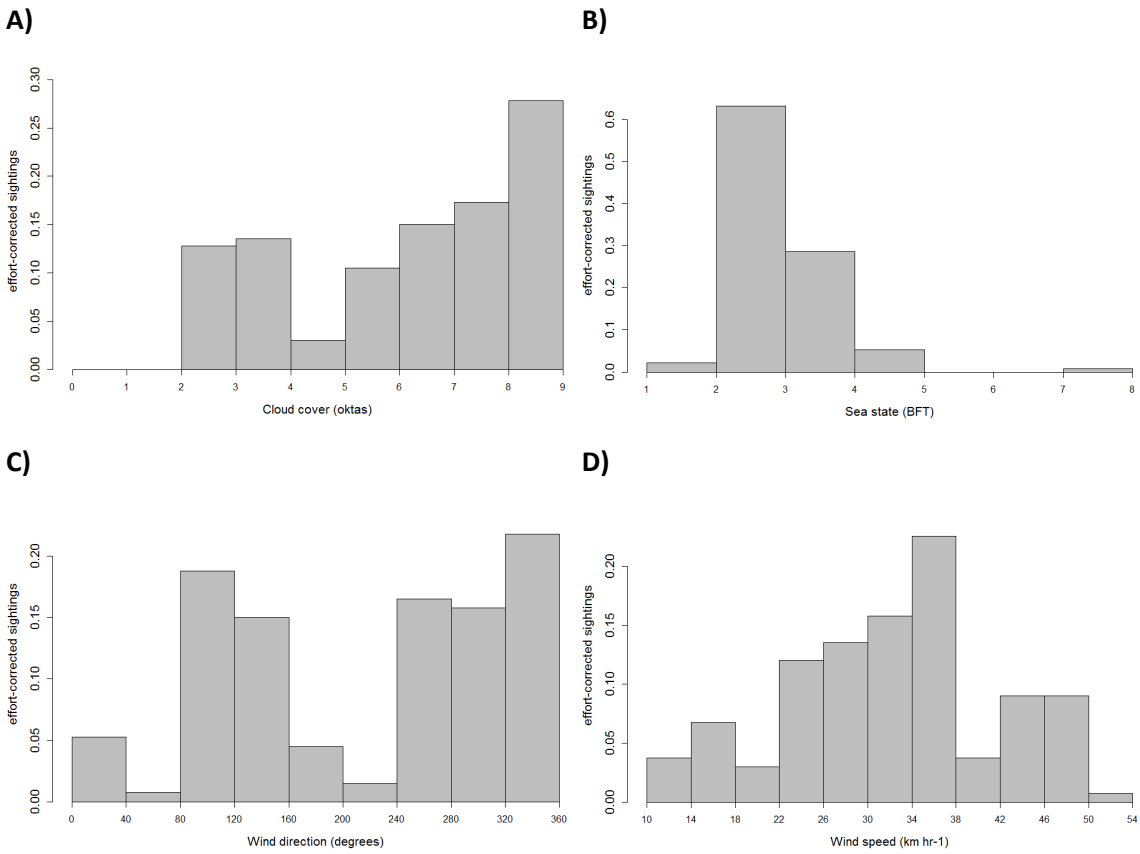

Figure 6.19. Effort-corrected seabird foraging events as a function of survey conditions.
A): Cloud cover (oktas), B): Sea state (BFT), C): Wind direction (degrees), and D): Wind speed (km hr^{-1}). Histograms calculated over 221 30-minute units of survey effort between 12/2012 and 01/2013, (n = 118 foraging events).

Figure 6.20-A shows marginally increasing sightings rates with increasing tidal range, a proxy for time in the spring-neap cycle. There were increased probabilities of observing foraging events during hours of flood tide (Figure 6.20-B), relative to ebb tide, but notably reduced sightings rates around HW slack (tidal hour 0) of ~0.03 aggregations-hr^{-1}.

Daylight hour appeared to exert limited influence on the number of observations (Figure 6.20-D), though there were decreased observations around midday, particularly during the last hour.

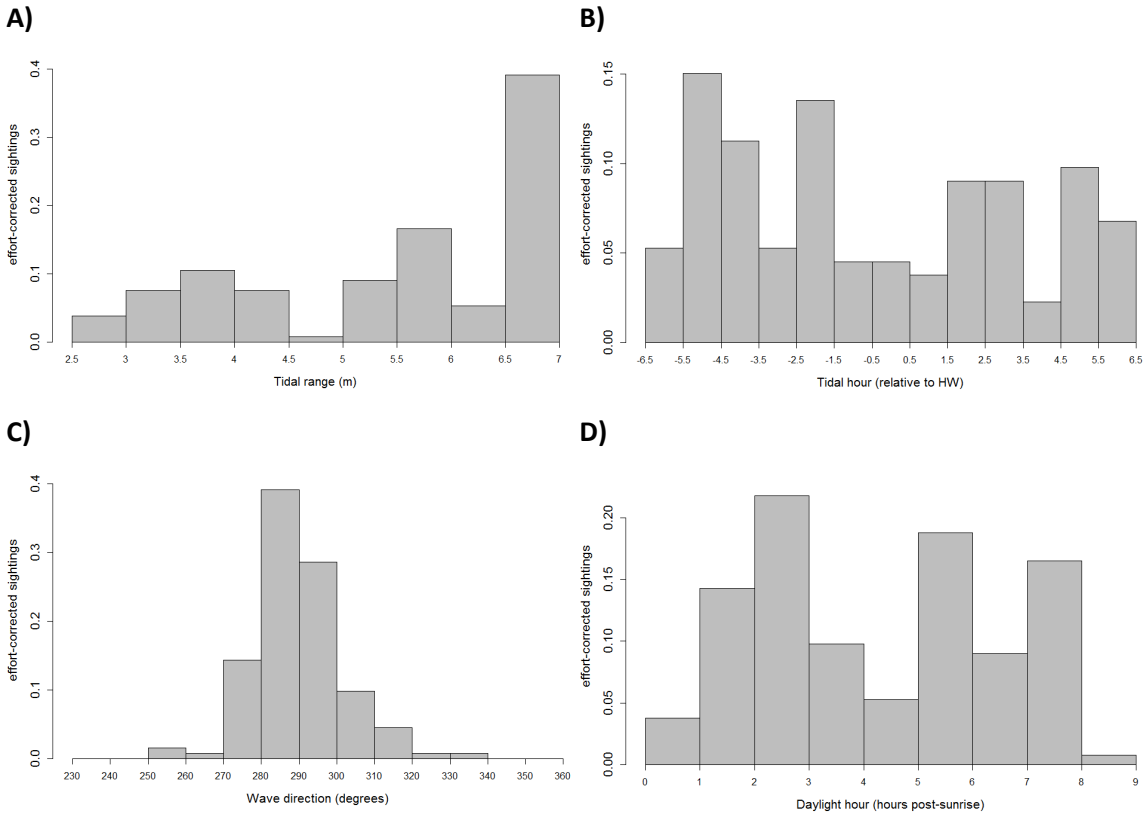

Figure 6.20. Effort-corrected seabird foraging events as a function of temporal variables.
A): Tidal range (m), B): Tidal hour (relative to HW, where HW = 0), C): Wave direction (degrees), and D): Daylight hour (where 0 is sunrise). Histograms calculated over 221 30-minute units of survey between 12/2012 and 01/2013 (n = 118 foraging events).

Further analysis on the presence-absence seabird data, as a function of the covariates is presented in Appendix O.1. (For reference, cetacean sightings rates in the survey area as a function of the temporal variables are also provided, see Appendix O.2).

6.3.2.1 Temporal Model

To explain temporal patterns in seabird foraging events, the numbers of sightings per 30-minute survey unit were modelled using a negative binomial GAM with a logit-link function (see Section 6.2.2.4). Collinearity between candidate variables (Table 6.6) was explored using a pairplot (Appendix O.3) though none was found. Through step-wise forwards selection, the modelling process first compensated for survey effects, then tidal variables and finally

temporal variables. Model results are given in Table 6.7. (The presence or absence of foraging events were also modelled for comparison, and results provided in Appendix O.4). Figure 6.21 shows the model smooths. (The auto-correlation function of model residuals is provided in Appendix O.5).

Table 6.7. Results of forward GAM model selection for the number of foraging events.
Variables are shown in order of importance, first compensating for survey effects (wind and sea conditions, cloud cover). Smooths are shown with the number of estimated degrees of freedom (e.d.f.) in parentheses; AIC_{Δ} is the reduction in AIC score caused by the addition of the significant variable to the model, with the first score in bold showing the starting AIC; % Dev is the additional deviation (%) in the data explained by adding the selected variable to the model. Surveys conducted over 19 days between December 2012 and January 2013 at St Ives (n = 110.5 h).

	Aggregation count per 30-minutes		
Order	Smooth (e.d.f.)	% Dev	AIC_{Δ}
1	s(WindSp, 2.8)	7.48	**460.54**
2	s(Hs, 2.2)	+6.32	-9.67
3	s(WindDir, 1.4)	+3.6	-6.15
4	s(TideRng, 4.7)	+8.7	-10.74
Total		26.1	

The final GAM explained 26.1% of deviance (Table 6.7) over 110.5 hours of survey effort between December 2012 and January 2013 at St Ives Bay. Wind speed and tidal range were the most important predictor variables explaining 7% and 9% of deviance. All variables were significant to $p < 0.05$. It took the form:

Numbers of foraging events ~ s(WindSp) + s(Hs) + s(WindDir) + s(TideRng)

The fitted model for wind speed (Figure 6.21-A) shows increased sightings until a threshold value (~35 km hr^{-1}) after which numbers of aggregations fall. There is a negative relationship between sightings and significant wave height (Figure 6.21-B); more foraging events occur during calmer seas. The smooth for wind direction (Figure 6.21-C) shows a marked decrease in foraging seabird aggregations during onshore-blowing north/north-easterly winds (~90°) and an increase during offshore-blowing south-westerlies (~250°). The numbers of aggregations are lowest around neap tides (Figure 6.21-D), where tidal range is proxy for time in the spring-neap cycle.

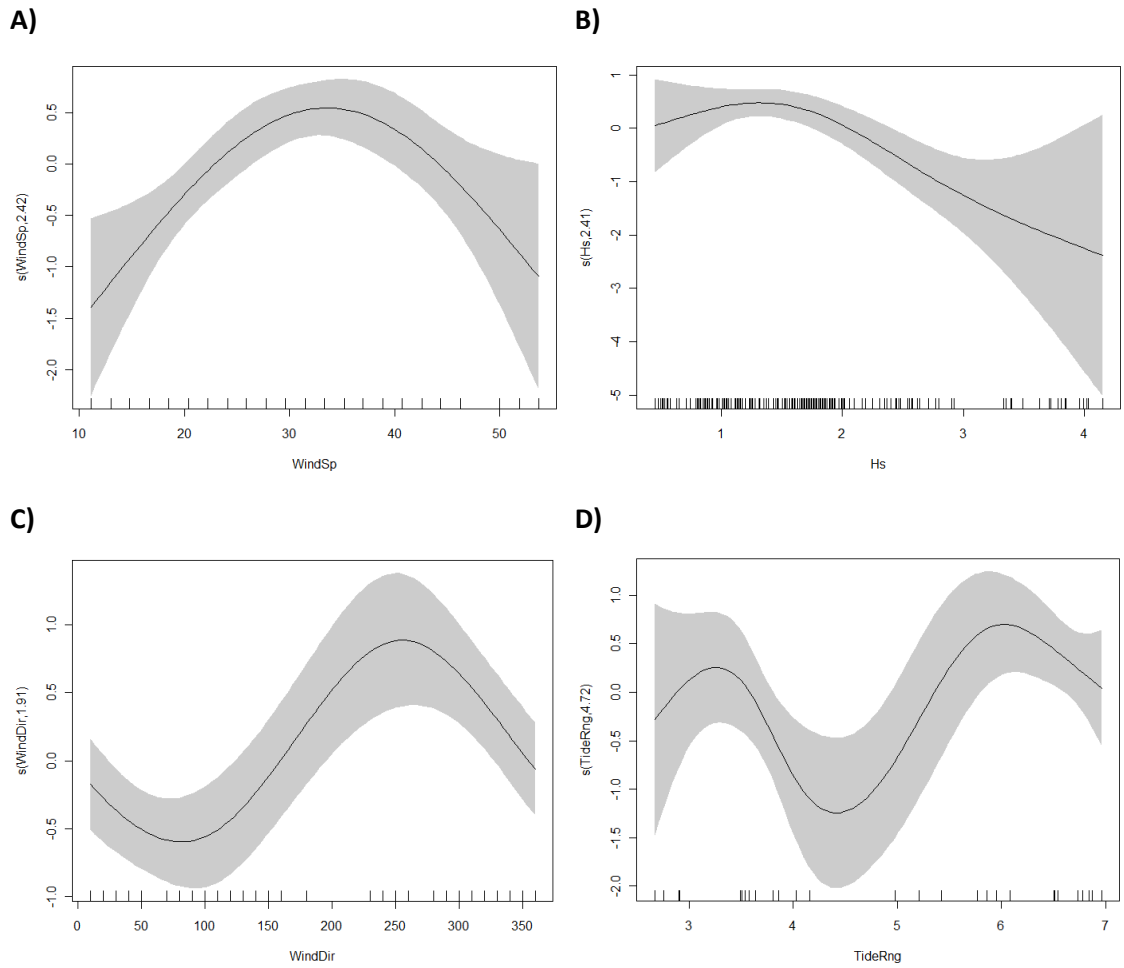

Figure 6.21. Relationships between number of foraging seabird aggregations and temporal variables. Significant variables, as selected by the final negative binomial GAM (n = 221 30-minute survey units), A): Wind speed (e.d.f. = 2.47), B): Significant wave height (e.d.f. = 2.41), C): Wind direction (e.d.f. = 1.91), and D): Tidal range (e.d.f. = 4.72). Results reported on the scale of the linear predictor. Numbers in brackets in y-axis captions are estimated degrees of freedom (e.d.f.) of the smooths. Rug plots at bottom of figures are covariate values. Shaded regions around smooths represent 95% confidence intervals.

6.4 Discussion

Incidental capture in nets is a principle cause of seabird mortality globally (Žydelis et al., 2013). Across scales, bycatch incidents can impact vulnerable species at the population level (Garthe & Hüppop, 2004; McFarlane Tranquilla et al., 2013), though questions remain as to when and where seabirds preferentially forage at fine spatial (<6 km) and temporal (30-minute) scales within relatively constrained coastal environments. This high resolution information is needed to more effectively inform local fisheries management regimes concerned with mitigating bycatch incidents of marine megafauna, which include both seabirds and cetaceans (Hardy et al., 2012; Senko et al., 2013) and reducing any unnecessary economic impacts on fishers.

A total of 110.5 hours of theodolite mapping data were collected from St Ives Bay on 19 dates in mid-winter 2012-13 with the aim of improving understanding of the distribution of foraging seabirds; an interest triggered by recent bycatch events. The results of this pilot study support previous observations that indicated SIB as a regionally-important foraging area for a variety of seabird species (RSPB, 2012), several of which were concentrated in aggregations of >500 birds. Aggregations were focused along the shallow, sandy, nearshore zone of the southern bay, and shared considerable spatial overlap with cetaceans and line fishing effort, particularly near the visible tide race immediately northeast of St Ives Island. There was a notable absence of seabirds in the flat, central bay area. Spatial and temporal models (GAMs) were constructed to explain the distribution of foraging locations based on co-located bathymetric, and dynamic hydrographic and temporal variables. In addition to nearshore areas of core habitat, the spatial model predicted foraging hotspots around the shallow reef features near Godrevy, indicating increased prey availability likely due to tidal-topographic interaction (steep slopes and hydrodynamic processes in the water column) (Wolanski & Hamner, 1988; Franks, 1992b, 1992a). Tidal range significantly influenced the number of aggregations, with a decrease during neap tides, while sea state and wind conditions were also significant. Wind vector appeared to exert some control, with seabird foraging focused in more sheltered areas of the bay. Such fine-scale (10s m), cost-effective survey methods combined with (predictive) analyses demonstrate the utility of this type of study for informing fisheries' management, and as a possible methodological 'toolbox' to be applied at other constrained coastal locations amenable to shore-based observations and where appropriately-resolved covariate data exist.

Rationale

The identification of ecologically-relevant areas warranting seabird protection, typically by highlighting 'hotspots' based on abundance data (Ronconi et al., 2012), i.e. simple presence-absence, may not be sufficiently accurate, and even misleading (Camphuysen et al., 2012). For this study, it was necessary to collect the most pertinent information relevant to mitigation of bycatch, i.e. the exact locations and timings of foraging seabird aggregations, opposed to resting, roosting or general count data, since it is during foraging that birds are at risk to mortality in set nets (Munilla et al., 2007).

Spatial distribution

The kernel isopleths (Figure 6.11) and gridded relative density analysis (Figure 6.15-A) indicate increased numbers of feeding events focused on the shallow, sandy, nearshore zone of the southern bay, whilst the grid cell with the highest density was located over the area of steepest slope beneath the watch point on St Ives Island. Further offshore, foraging is associated with the shallow reef feature (pinnacles) near Godrevy, while there is a notable absence of feeding events within the flat, central bay area. These patterns were backed up by the statistical analysis, whereby the density of foraging aggregations was most significantly influenced by distance from shore (collinear with depth), and explained 43% of variation in the data, while slope explained an additional 3%. Interaction terms were specified between all three static habitat variables (distance, slope and aspect) during model selection, but none were significant.

The spatial model predicted areas of increased relative density close to shore (Figure 6.17), particularly around the south-western parts of the bay, and off the headland at Godrevy, over the reef. Garthe and Hüppop (2004) also found that seabird density decreased with distance from shore in their study throughout the year in the south-eastern North Sea. Similarly, Sonntag et al. (2012) reported a decline in seabird numbers with increasing depth in their eight-year study in the southern Baltic Sea. It is likely that in the gently-sloping bay at St Ives prey species are fairly dispersed thoughout the study area in the absence of any complex topography but, near the shoreline, tidal flows physically concentrate smaller organisms further up the beaches in the shallower, southern areas, explaining the increased relative densities of foraging seabirds evidenced in Figure 6.15-A. Sonntag et al. (2012) also discussed increased seabird vulnerability and potential conflict with gillnet fishing during winter and spring in the shallow coastal waters (<10 m water depth), which decreased further (<12 nM)

offshore and during other seasons. Notably, the shallow offshore grounds of Odra Bank in the southern Baltic (relative to the surrounding deeper, flatter areas in their survey region) were considered a hotspot all year.

The areas of high relative density near Odra Bank highlighted in the Baltic study (Sonntag et al., 2012), the topographic features off Godrevy headland in this study, along with the steep cliff feature near the watch point, all suggest the influence of tidal-topographic interaction on prey availability in these areas (indicated by seabirds actively plunge- or pursuit-diving; Montevecchi, 1993), relative to the more homogenous environments that characterise the surrounds (Scott et al., 2010). These interactions can occur where topography interacts with tidal flows, causing secondary currents (Genin, 2004) and convergence zones (McPhee-Shaw et al., 2011) that lead to predictable (Stevick et al., 2008), localised aggregations of prey (Wolanski & Hamner, 1988; Franks, 1992b, 1992a). The small-scale physical features in SIB, apparent in the high resolution bathymetry (Figure 2.20), may therefore be locally important to foraging seabirds in the area. Knowledge of these locations (Irons, 1998; Hunt et al., 1999) would enable the birds to maximise their foraging efficiency (Fretwell & Lucas, 1969), which is a strategy clearly important for highly mobile marine species (Fauchald, 2009) with high energy demands (Gabrielsen et al., 1987).

The influence of wind

There is an indication that, during foraging, wind vector exerts some control on the spatial distribution of seabird aggregations, which appear to be located in more sheltered areas of the bay, in lee of offshore winds (Figure 6.13). This preference is reflected in the statistical model, which revealed a significant influence of wind vector on the number of aggregations, explaining 4% of deviation. The model smooth (Figure 6.21-C) indicates increased foraging during south-westerly winds, i.e. offshore, periods during which the bay is more sheltered. It should also be noted that during surveys, offshore winds were more moderate than onshore (Figure 2.23). There is limited literature relating seabird foraging locations *per se* to wind vector, though more exists correlating it with flight behaviour and track-line trajectories during prey search (Furness & Bryant, 1996; Pennycuick, 2002; Fritz et al., 2003; Adams & Flora, 2009; Wakefield et al., 2009b; Paiva et al., 2010).

However, it seems likely there are less foraging aggregations in rough weather due to decreased prey visibility through increased sea state (significant wave height was significant in this study) and water column turbidity, though some studies of other species on passageways

(e.g. Cory's shearwaters *Calonectris diomedea;* Paiva et al., 2010 and wandering albatrosses *Diomedea exulans*; Weimerskirch et al., 2000), suggest seabirds may preferentially forage in more sheltered areas where they can, as this would save energy. Since onshore winds were also those recording the highest wind speeds during surveys (Figure 2.23) and the importance of visibility to seabirds (Hunt et al., 1999), it is likely birds will preferentially forage where they are able to more quickly assess an area's potential for sufficient concentrations of prey, i.e. areas of good visibility, worthy of energy expenditure. It seems reasonable to assume that during periods of onshore winds and higher significant wave height, wide-ranging seabirds will simply forage in other coastal areas rather than SIB, thereby explaining the observed relationships between both wind vector and wave height on the number of foraging events.

Tidal influence on the timing of seabird foraging

Tidal range, a proxy for position in the spring-neap cycle, was the only significant tidal variable influencing the number of foraging aggregations (Table 6.7). Tidal range explained the most variation in the temporal dataset (9%) with clearly decreased numbers of aggregations around neap tides, and slight increases towards springs. In a study at Jones Bank (a feature in ~80 m water depth) in the Celtic Sea, Embling et al. (2013) found fish schooling behaviour to change with the spring-neap cycle. Fish schools in the upper water column, containing gannet prey species, such as horse mackerel *Trachurus trachurus*, were more diffuse during neaps, despite being shallower and containing higher numbers of fish (likely a consequence of less turbulent mixing during lower tidal speeds). If these findings are extrapolated to SIB, the tentative implication is that during neaps, aggregations of prey species are less visible to predation, potentially explaining the decreased observations.

Spatial overlap

Spatial data collected using a theodolite have enabled fine-scale visual analysis of foraging seabird aggregations at a comparable resolution as the bathymetry. During surveys, data were also collected on fishing vessel locations and surfacing marine mammals, which comprised bottlenose dolphins and harbour porpoises, in groups of up to seven individuals, to identify potential areas of conflict within SIB (e.g. Figure 6.22). Indeed, Ronconi et al. (2012) highlight the need to identify areas most in need of action by assessing threats and risks of interactions to mitigate bycatch (Cooper et al., 2001). Spatial overlap is a useful tool that serves this purpose, and has been previously applied to indicate potential interactions between fisheries and marine mammals (Herr et al., 2009; Prado et al., 2013) and seabirds (Sonntag et al., 2012).

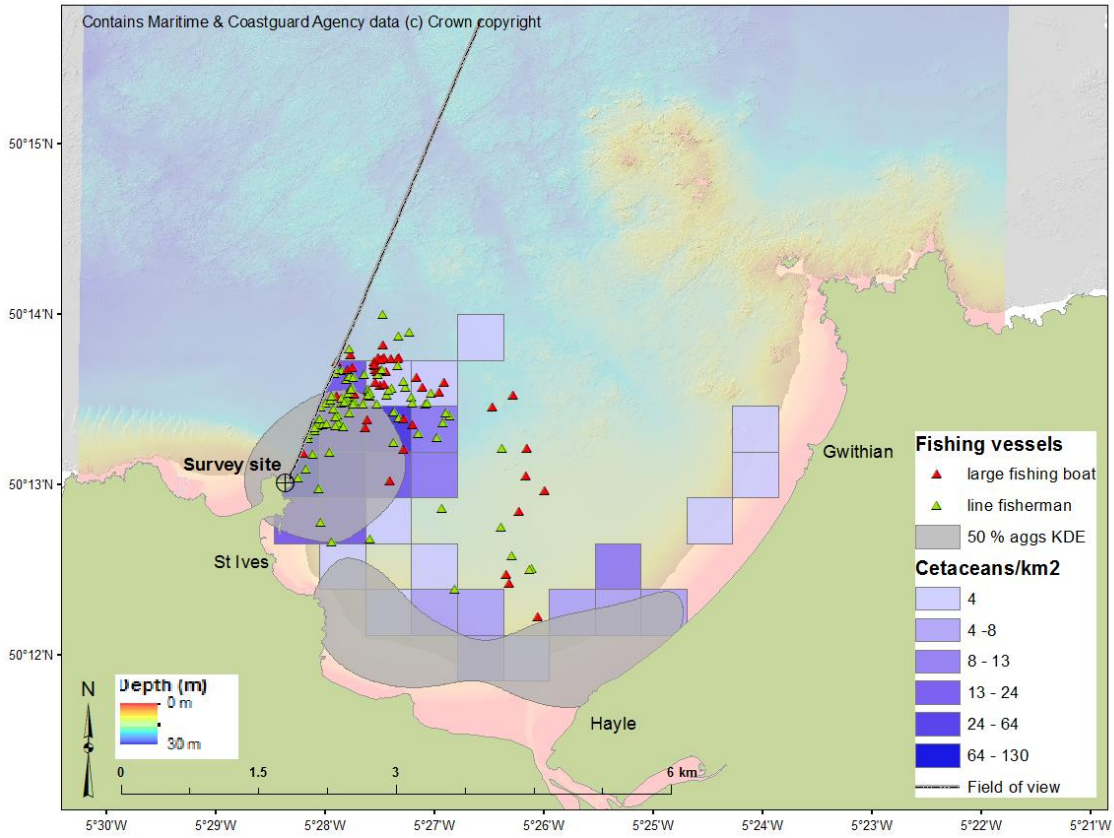

Figure 6.22. Fishing, cetacean and seabird spatial interaction in St Ives Bay.
Relative densities of cetaceans per km^2 per grid cell (shaded blue squares); 50% kernel represents core density areas of foraging seabirds (grey polygon); filled triangles represent fishing vessel locations (red = 'large' fishing boat, n = 44; green = small fishing boat, n = 86) every 30 minutes. Locations mapped onto high resolution (1 m) bathymetry data (courtesy of CCO/MCA © Crown copyright). Theodolite data collected over 19 days across winter 2012-13.

In this study, the core density areas of foraging aggregations, indicated by the 50% kernel isopleths, contain 52% (n = 45) of the smaller fishing vessels, possibly gill-netters, although this information was not recorded. Spatial overlap between fishing and seabirds was not quantified due to insufficient information on vessel activity, but, visually, it does indicate possible interaction with foraging seabirds, under the assumptions that bycatch is proportional to spatial overlap (Sonntag et al., 2012) and the vessels would engage in gill-netting in the locations recorded. Sonntag et al. (2012) also found that diving birds and fisheries were concentrated in the same areas in the Baltic Sea, and that vulnerability and potential conflict were highest during the winter and spring in coastal waters, and the shallow grounds offshore. The density of foraging gannet aggregations has also been shown to significantly overlap with artisanal line fishing activity off a rocky reef in southwest UK (see Chapter 5), where the target

fish species are likely shared by both the birds and the fishers, though there is no risk of entanglement with line fishing.

Core areas of foraging seabirds also overlapped with the highest densities of cetaceans recorded in the survey area, which, for coastal populations, are species at risk of entanglement in nets (Tregenza et al., 1997; Cox & Read, 2004; Gannon et al., 2005; Hardy et al., 2012). The main threat to the conservation of the endangered franciscana dolphin *Pontoporia blainvillei* in Brazil, for example, is bycatch in gillnets (Secchi, 2010), largely due to the fact its coastal distribution greatly overlaps with fishing activities (Prado et al., 2013). In SIB, where foraging locations for both seabirds and cetaceans share considerable overlap, this indicates cetaceans are at increased risk in these areas, as they represent increased prey availability, relative to the rest of the bay, since it is generally assumed that areas of greatest usage by predators reflect higher quality habitat (Bailey & Thompson, 2010; Pirotta et al., 2013). This may also explain why the fishers were recorded in similar locations.

Implications for management

Identifying areas of spatial overlap has implications for fisheries' management in SIB. The bycatch events in January 2012 evidenced interactions between the gillnet fishery and foraging seabirds with fatal consequences. The events triggered a time-area restriction for the local gillnet fishery that was enforced for a three-week period following the drowning of >100 seabirds trapped in nets. Sonntag et al. (2012) combined the vulnerability indices of seabirds with spatial density analyses, and highlight the fact that temporal-spatial restrictions can be derived from visual observation data, despite a lack of real information on bycatch rates. The authors also suggest this method is particularly useful in situations where mortality cannot be properly addressed or monitored, as in artisanal gillnet fisheries, thus justifying the approaches used in this study for informing fisheries. Additionally, Senko et al. (2013) stress the importance of adaptive management, whereby mitigation measures should ideally be developed and implemented in a bottom-up approach, as fishers are more likely to comply with measures that work well from an economic and operational standpoint. Socio-politically, mitigation measures are also more likely to be effective if they are cost-effective and voluntary (Senko et al., 2013). This reinforces the importance of on-going consultation with fishers, and also the usefulness of voluntary agreements, such as the Fishing Nets Code of Practice (Appendix M.3). Although Senko et al. (2013) discussed the limited effectiveness of time-area closures for species such as leatherback turtles *Dermochelys coriacea* and vaquita porpoise *Phocoena sinus*, they showed that timing, size and enforcement did influence their efficacy.

This points to the applicability of time-area restrictions on a case-by-case basis, which may need modification over time.

During this pilot study, no seabird or cetacean bycatch incidents were observed. However, two apparently freshly-dead razorbills were seen drifting into the bay from the northwest in December 2012, another was seen to die upon surfacing close to the watch point in January 2013, and, on the same day, another found fairly freshly-dead and un-oiled on St Ives beach. Nevertheless, given the very large numbers of this species using the area, it is possible that the birds died of natural causes. A cautious approach to attribution of seabird deaths is therefore required, unless the direct cause is witnessed. It should also be noted that no relationship between the number of multi-species foraging events with time of day was found in SIB during the statistical analysis, in contrast to foraging gannet aggregations off southwest UK (see Chapter 5) where there was a clear lull in observations around noon. This may be useful information for fisheries in the area, as the birds actively forage throughout the daily cycle, with no apparent focus for hours around dawn and dusk, as was expected.

Conclusions

At St Ives, there was a critical need to identify the fine-scale foraging distribution of seabirds in the bay, spatially and temporally, to inform fisheries' management. This pilot study aimed to improve knowledge of the controls on distribution, required by management, and, if successful, follow-on surveys over subsequent years would be carried out to collect a more robust dataset. A longer term dataset means drivers of distribution can be identified with higher confidence, and therefore used to better predict areas of interaction with gillnet fisheries. This would enable management to make more confident decisions on policy aimed at mitigating bycatch. However, precise theodolite mapping has been demonstrated as an effective and practical survey method for the sustainable monitoring of coastal environments where potential seabird mortality exists. Combined with statistical modelling, and a suite of highly resolved environmental data, the multi-disciplinary approaches developed in this study have successfully described extremely fine-scale habitat patterns of ephemeral aggregations of seabirds at St Ives where there was a strong policy driver to do. This 'toolbox' of complimentary methods could be applied elsewhere at similarly constrained coastal locations where information on small-scale drivers of distribution for highly mobile marine species is lacking, and where a coherent set of tools for data collection and analyses would be useful for informing management regimes, such as local fisheries and/or conservation.

Chapter 7 Overall Conclusions

The primary aim of this thesis was to describe the fine-scale spatial and temporal patterns of mobile marine top predators in two contrasting coastal locations. A secondary aim was to collect data (evidence) that would help inform policymakers currently engaged in management activities at these locations. Fine-scale drivers of distribution were explained by integrating a suite of highly resolved environmental data with multi-disciplinary survey and analytical techniques, including the use of a theodolite, static acoustic data loggers and statistical (predictive) modelling. As a result, a methodological 'toolbox' was developed, that can potentially be applied at other constrained coastal environments where appropriately-resolved covariate data can be acquired and incorporated into analyses. Results from this project successfully demonstrated the utility of this toolbox, and its application for studying a variety of focal species that are amenable to shore-based observations for conservation, fisheries management, and marine planning purposes.

Although the focal species are unrelated, harbour porpoises, dolphins and certain species of seabirds are all of conservation concern within the UK and EU and, as such, require improved understanding of their habitat use to more effectively inform conservation, management and fisheries. The underlying drivers controlling habitat associations are relatively well-understood across species at varying scales (i.e. suitable environmental conditions and prey abundance). However, questions remains regarding the fine-scale interplay between these drivers in complex, dynamic environments nearshore, and their influence on the distribution and behaviour of top marine predators (which likely reflect the varying influence of these processes on the distribution and availability of preferred prey). Furthermore, environmental parameters controlling habitat use at fine-scales may be site-specific.

The four results chapters in this thesis have attempted to identify common environmental drivers on distribution across target species. By incorporating observation and environmental data at similar scales across sites and species, a range of common and differing controls of habitat use were revealed. A key aspect of this research was the mapping of precise theodolite data for target species onto high resolution bathymetry maps, enabling extremely fine-scale visual analyses of species distribution; this highlighted the influence of various topographic features within the survey areas, and also revealed the influence of dynamic variables, such as wind vector and/or tidal flow direction.

New theodolite survey data were compared to archive datasets collected using conventional visual monitoring techniques, to determine any similarities or differences between methods and years. Static acoustic data loggers were also deployed over three years within a single survey area, which not only enabled comparison with sightings data of the same species (harbour porpoises) at the same site, but provided information on continuous, subsurface cetacean presence in all weather conditions, and for 24-hours a day, opposed to daylight-only visual sightings data collected during periods of fair weather. The acoustic data loggers were strategically deployed at three different locations within the study site, so that location-specific temporal patterns of distribution could be identified, compared between two species (harbour porpoises and dolphins), and explained within the context of different bathymetric and tidal habitats. This created an additional opportunity to test the methodological toolbox; this time using animal response data collected by a different survey method (subsurface acoustic) and on other top predators (dolphins), opposed to visual sightings of seabirds or porpoises.

Cetaceans

Results from the porpoise distribution study (Chapter 3) tested the hypothesis from previous work that fine-scale tidal-topographic interactions result in ephemeral hydrodynamic features that are attractive to this species, although these features are predictable and spatially-constrained. Precise theodolite data provided further evidence of these fine-scale habitat associations, at a resolution that was previously not possible due to the error in visually-estimated sightings data collected using conventional monitoring techniques.

Analyses of cetacean acoustic data (Chapter 4) indicated similar environmental drivers on distribution, though results revealed high inter- and intra-annual variability in distribution for porpoises. This suggests the animals are more susceptible to fine-scale fluctuations in their environment, which may have implications for the conservation of this species in the context of (static) marine protected area designation and/or the mitigation of potential conflict with human activity in coastal waters, such as fishing or the development of wet renewables. Results were compared to the temporal drivers of dolphin distribution, which showed more consistency across years and no significant influence of small-scale habitat variability. The studies contributed to knowledge on when and where cetaceans interacted with their environment within a complex study site, including the influence of acoustic background noise and the day-night cycle.

Increased coverage of current flow dynamics and evidence of prey distribution would better elucidate how exactly physical habitat interactions, and predator-prey dynamics, influence cetacean habitat use, i.e. trophic coupling (discussed further below). Although the multi-year surveys indicate a consistent baseline level of activity across species, acoustic data logger deployments were only made during three summer periods, and have very localised detection radii, so animals may have been missed and/or observed patterns may be season-specific. Similarly, visual surveys only collected data on sporadic days, and some sightings would have been missed across the survey area (a detection issue that increases with distance from the watch point, discussed in Section 3.2.2), so extrapolating key findings to other study sites or predicting future trends is likely not possible or, should be done cautiously, bearing these limitations in mind.

Seabirds

Results from the seabird distribution study (Chapter 5) at the Runnel Stone Reef tested whether the hypothesis for porpoises held true for a different species at the same study site to better determine any influence of fine-scale physical processes, i.e. whether they exert similar control across species. This study was particularly relevant to the scientific question, given the fact that observations were only recorded of those seabird aggregations engaged in foraging activity (opposed to simple presence data where the activity is not defined). This means recorded locations and timings of foraging events represented the spatio-temporal distribution of prey availability, rather than seabird habitat use *per se*. Although analyses were carried out on gridded density data, as with the porpoise study, the raw theodolite observations demonstrated the utility of the field method to highlight extremely fine-scale habitat associations that would not be possible with any other low-cost technique. So, although other at-sea data collection methods exist to provide high resolution behavioural data (e.g. GPS loggers or satellite tracking), they are (often prohibitively) expensive. The theodolite data successfully revealed the predictability of tidal-topographic interactions on prey availability, which is suggested by the increased numbers of foraging aggregations that were associated with identifiable bathymetric features. These findings also point to seabirds' memory and knowledge of an area, which highlight the potential importance of protecting these features within a conservation/management framework.

The study on foraging seabird aggregations at St Ives Bay (Chapter 6) provided an opportunity to test methods developed at Gwennap Head at a different location, to determine their applicability for monitoring similar highly mobile marine species but at a physically contrasting

site with different management issues. Although seabird foraging activity and cetacean sightings were largely focussed on shallow nearshore sedimentary environments of the inner bay, upstanding rocky pinnacles and areas of tidally-swept steep slopes off a prominent headland were also shown to be local foraging 'hotspots'. On-going work from data collected over subsequent winters will further elucidate the environmental controls on distribution indicated in this study, and will be used to inform fisheries management to help mitigate future seabird bycatch in nets. Since the timing of foraging aggregations will be analysed at fine-scale (30-minute) intervals, and the precise locations of foraging seabirds mapped at a resolution suitable for practical purposes (i.e. identifying those areas most likely to host higher relative densities of foraging seabirds that may conflict with fisheries), these data will provide valuable information that are robust enough for fisheries management in the bay. Furthermore, the complimentary techniques employed could be applied elsewhere where similar policy drivers exist. However, it may be worthwhile to not only consider ecological variables during future analyses, as this study has done, but also integrate economic and socio-political factors, which will ensure management measures are both appropriate and proportionate.

Future research

Until recently, relatively few studies quantified trophic interactions that may be responsible for the distribution of top marine predators in tidally-dominated environments nearshore (up to 6 km offshore) at fine spatial and temporal scales. However, recent work has found internal waves and associated hydraulic jumps (causing enhanced turbulent mixing triggered by current flows interacting with topography) to be possible mechanisms for bio-physical coupling, which may lead to enhanced foraging opportunities for top predators. This highlights the need to collect concurrent (appropriately-resolved) ADCP data at each site of interest, to provide evidence of any physical processes at work within a study area. To improve understanding of the effect of these processes on distribution (prey availability) of both cetaceans and seabirds, it would also be useful to collect data on lower trophic levels, e.g. zooplankton and fish. For example, 1) current data could be collected from bottom-mounted ADCPs moored in strategic locations across the study site, sampling equally between the spring-neap cycle, including at any 'control' sites; 2) zooplankton samples could be collected using bongo nets deployed during vertical boat tows; 3) a keel-mounted EK60 scientific echosounder would provide acoustic data on fish schooling behaviours; 4) acoustic telemetry methods could be employed to track the fish themselves; and 5) potential prey fish from the study site, captured by local

fishers, could be investigated. These data would provide key information on prey species and their distribution/availability to predators given any hydrodynamic processes at work, thereby providing evidence of the 'missing link' between static habitat, environmental variables and species distribution, i.e. bio-physical trophic coupling.

It should be borne in mind that the work presented in this thesis only considers fine-scale nearshore habitat associations of the focal species at two constrained locations, and not broader-scale preferences or behaviours *per se* (although see Appendix P for initial results of theodolite-tracking of basking sharks at the Runnel Stone Reef that may provide insights into behavioural information). Specific results from this project should be extrapolated to other sites with caution, although key findings may help to explain habitat use at other (larger) scales when interpreted in context, e.g. interpreting results from tracking studies or vessel-based observations. Additionally, the potentially-important physical features identified in this study, and the methods developed to do so, may provide context to results from studies of other marine species in constrained coastal environments further afield, particularly where complex topographic and tidal features are present.

Questions remain, however, as to why and how free-ranging marine species, including those studied for this thesis, 'choose' one (predictable) productive feature over another. At what time-scales do they make these decisions? Do they exhibit foresight (within the context of Ideal Free Distribution theories) or, do they exploit prey-dense patches randomly? Answering these questions will require improved, multi-disciplinary approaches to research that involves not only empirical data on prey fields, but fully-integrated collaborations between behavioural ecologists, biologists and physical oceanographers, as well as incorporating remotely-sensed and meteorological datasets. Free-ranging 'knowledgeable' top predators make complex decisions in highly dynamic environments, so data collection and analyses need to be conducted at similarly complex levels across disciplines. It is vital for conservation and (inter)national management regimes to more fully understand ecosystem-wide (often whole ocean) habitat preferences, particularly as waters further offshore become increasingly subject to anthropogenic disturbances, such as large-scale commercial fishing, seismic surveys, telecommunications, and the development of renewables.

Analyses used in this study can be used to highlight areas of core habitat use that may suggest the need for increased monitoring or management of certain hotspot areas. Conversely, when bathymetric features of a particular location are considered, it may be that management is in fact little needed at current levels of human activity, and finite resources may be better

allocated elsewhere. For example, the topographic or hydrographic features present at the Runnel Stone Reef may serve to protect the ecosystem itself, as an area of extreme tidal forcing in the presence of shallow, rocky substrate. This contrasts with a location such as St Ives Bay where anthropogenic impacts are in potential conflict with the environment and species therein. At this location, or similar, where the physical habitat cannot 'protect' itself or any dependent species, it may be necessary to carry out regular surveys to provide relevant scientific evidence on the spatio-temporal distribution of at-risk marine animals to ensure that management is making informed decisions based on current, best-available knowledge. On the other hand, protecting potentially-important hotspot areas that may not need management at current levels of human activity would be useful for future-proofing them against any negative impacts that are, as yet, unknown or unquantified.

The ability to identify and predict spatially-constrained hotspot areas is clearly useful within the complex realm of site designation and management for mobile marine species. Provided there is access to sufficiently-resolved covariate data, an appropriate land-based observation point, and/or suitable mooring sites for acoustic detectors, the cost-effective field methods presented in this study could be applied to other distribution studies of top marine predators at similarly-constrained coastal locations. These multi-disciplinary approaches are particularly useful in high energy, tidally-dominated environments where other types of at-sea surveys, such as boat-based or aerial, may be practically too difficult. Although the use of a theodolite is not necessary to assess temporal variability in species distribution, it is a particularly informative and cost-effective tool to identify extremely fine-scale spatial habitat associations in the nearshore zone (if the scientific question requires this), relative to expensive GPS loggers or satellite tags, for example. Some recommendations for future theodolite use, and precautions, arising from this study are presented in Appendix Q.

In summary, this research has identified significant relationships between a variety of focal species and highly resolved environmental variables, integrating data from both visual and acoustic surveys at two contrasting locations. The different species each exhibited a clear spatial and temporal 'signature', which advances knowledge on their fine-scale distribution in complex tidally-dominated environments. Results from field surveys using a theodolite supported the view that tidal-topographic interactions are potentially important features worthy of protection. The complimentary suite of techniques presented in this thesis can be applied at other locations where mobile marine species are amenable to land-based

observations, and used to help identify fine-scale habitat preferences, as required by policy for the sustainable management of the marine environment.

Appendices

Appendix A Co-authored paper: Jones et al. (2014a) "Fine-scale hydrodynamics influence the spatio-temporal distribution of harbour porpoises at a coastal hotspot."

Progress in Oceanography 128 (2014) 30–48

Contents lists available at ScienceDirect

Progress in Oceanography

journal homepage: www.elsevier.com/locate/pocean

Fine-scale hydrodynamics influence the spatio-temporal distribution of harbour porpoises at a coastal hotspot

A.R. Jones [a,*], P. Hosegood [b], R.B. Wynn [a], M.N. De Boer [c,d], S. Butler-Cowdry [a], C.B. Embling [e,f]

[a] National Oceanography Centre – Southampton, European Way, Southampton SO14 3ZH, UK
[b] University of Plymouth, School of Marine Science and Engineering (Faculty of Science and Technology), Reynolds Building, Drake Circus PL4 8AA, UK
[c] Wageningen IMARES, Institute for Marine Resources and Ecosystem Studies, PO Box 167, 1790 AD Den Burg, The Netherlands
[d] Marine Discovery Penzance, Shed 5, Albert Pier, Penzance Harbour, Penzance TR18 2LL, UK
[e] Centre for Ecology and Conservation, University of Exeter, Cornwall Campus, Penryn TR10 9EZ, UK
[f] Marine Institute, University of Plymouth, Marine Building, Drake Circus PL4 8AA, UK

ARTICLE INFO

Article history:
Received 23 August 2013
Received in revised form 29 June 2014
Accepted 4 August 2014
Available online 11 August 2014

ABSTRACT

The coastal Runnelstone Reef, off southwest Cornwall (UK), is characterised by complex topography and strong tidal flows and is a known high-density site for harbour porpoise (*Phocoena phocoena*); a European protected species. Using a multidisciplinary dataset including: porpoise sightings from a multi-year land-based survey, Acoustic Doppler Current Profiling (ADCP), vertical profiling of water properties and high-resolution bathymetry; we investigate how interactions between tidal flow and topography drive the fine-scale porpoise spatio-temporal distribution at the site. Porpoise sightings were distributed non-uniformly within the survey area with highest sighting density recorded in areas with steep slopes and moderate depths. Greater numbers of sightings were recorded during strong westward (ebbing) tidal flows compared to strong eastward (flooding) flows and slack water periods. ADCP and Conductivity Temperature Depth (CTD) data identified fine-scale hydrodynamic features, associated with cross-reef tidal flows in the sections of the survey area with the highest recorded densities of porpoises. We observed layered, vertically sheared flows that were susceptible to the generation of turbulence by shear instability. Additionally, the intense, oscillatory near surface currents led to hydraulically controlled flow that transitioned from subcritical to supercritical conditions; indicating that highly turbulent and energetic hydraulic jumps were generated along the eastern and western slopes of the reef. The depression and release of isopycnals in the lee of the reef during cross-reef flows revealed that the flow released lee waves during upslope currents at specific phases of the tidal cycle when the highest sighting rates were recorded. The results of this unique, fine-scale field study provide new insights into specific hydrodynamic features, produced through tidal forcing, that may be important for creating predictable foraging opportunities for porpoises at a local scale. Information on the functional mechanisms linking porpoise distribution to static and dynamic physical habitat variables is extremely valuable to the monitoring and management of the species within the context of European conservation policies and marine renewable energy infrastructure development.

Introduction

Marine megavertebrates are noted for their wide-ranging behaviour, but often concentrate within spatially constrained areas (e.g. Sims, 2003; Kai et al., 2009), referred to as 'hotspots' (Myers, 1990). The mechanism driving animal aggregations at hotspots is likely to be based on foraging decisions made in response to meso- and fine-scale environmental cues (Stephens and Krebs, 1986; Russell et al., 1992; Sims et al., 2008). By examining the distribution of a species in time and space, at a range of scales, we can improve our understanding of the species' interaction with its environment (Fauchald and Erikstad, 2002; Bertrand et al., 2008; Embling et al., 2012). This is particularly important for spatial management and conservation of threatened marine megavertebrates, such as the harbour porpoise *Phocoena phocoena*. A better understanding of the mechanisms underlying the links between porpoise distribution and physical habitat will aid in protected area site selection, as well as improving our understanding of potential anthropogenic impacts, e.g. proposed marine renewable energy infrastructure (Dolman and Simmonds, 2010; Witt et al., 2012).

* Corresponding author. Current address: The Environment Institute & School Earth and Environmental Sciences, University of Adelaide, South Australia 5005, Australia. Tel.: +61 (0)8 8313 2243.
E-mail address: alice.jones01@adelaide.edu.au (A.R. Jones).

http://dx.doi.org/10.1016/j.pocean.2014.08.002
0079-6611/

Harbour porpoises are small cetaceans, which must feed regularly in order to fulfil their energetic requirements. As a result they cannot stray far from areas containing reliable prey resources (Brodie, 1995; Koopman, 1998; Santos et al., 2004; Lockyer, 2007), and the ability to react to predictable oceanographic and hydrodynamic drivers of prey availability will greatly reduce foraging costs. Broad-scale studies show that the distribution of harbour porpoises is directly influenced by the distribution of prey (e.g. Read and Westgate, 1997; Herr et al., 2009; Sveegaard, 2011) and indirectly affected by both static and dynamic environmental variables that are hypothesised to predictably influence prey distribution or foraging efficiency, such as water depth, topography, substrate, tidal flow, fronts, stratification, turbulence, and time of day (e.g. Watts and Gaskin, 1985; Johnston et al., 2005; Embling et al., 2010; Scott et al., 2010; Mikkelsen et al., 2013). However, there are no known studies investigating the fine-scale bio-physical mechanisms linking physical habitat variables to increased harbour porpoise densities, due to the rarity of the quantitative, fine-scale physical and biological data required to carry out robust investigations of these links.

Harbour porpoises have a wide coastal distribution around the UK (Reid et al., 2003; Hammond et al., 2013), making them a suitable focus species for land-based surveys. Sites around the coast of southwest England have previously been identified as hotspots for harbour porpoise (Northridge et al., 1995; Hammond, 2006; Brereton et al., 2007), with a number of studies specifically highlighting the regional importance of the Runnelstone Reef in southwest Cornwall (Leeney et al., 2008; Pikesley et al., 2012); not only in the summer months, but also throughout the winter (Evans et al., 2003; De Boer and Saulino, 2008). Using new high-resolution bathymetric data, we have been able to identify that the Runnelstone Reef site is a regionally unique bathymetric feature.

In light of the potential bio-physical links suggested by previous research, and the conservation and management policies pertaining to the species in the UK; this multidisciplinary study examines the effect of fine-scale physical habitat on harbour porpoise distribution. We investigate the drivers of porpoise distribution patterns using sightings recorded in an effort-based visual survey from a land-based watchpoint overlooking the Runnelstone Reef. The collection of co-located, high-resolution data on static and dynamic physical habitat variables, such as Acoustic Doppler Current Profiling (ADCP), water property profiles, and 1-m resolution bathymetry data, has provided a unique and timely opportunity to investigate the fine-scale spatial (~600 m resolution) and temporal (hourly resolution) distribution of harbour porpoises at a known hotspot in relation to hydrodynamics and interactions between tide and topography at the site. The main aims of the study were threefold: (1) to examine whether the spatial distribution of harbour porpoise sightings was linked to topographic features within the study area, (2) to collect high-resolution data on the physical marine environment at the study site, and (3) to investigate the spatio-temporal distribution of porpoise sightings in relation to tidal flow regime and fine-scale hydrodynamics.

Materials and methods

Study area

Survey data were collected from a land-based watchpoint on a south-facing headland (Gwennap Head) at ~30 m above mean sea level, at the southwest tip of the UK mainland (50°02′ 06.29″N 005°40′ 45.66″W). The watchpoint has an almost 180° field of view from east to west, directly overlooking the tidally dominated Runnelstone Reef (Fig. 1). The characteristics of the Runnelstone Reef create a challenging environment for data collection. Commercial fishing activities in the area restrict the strategic mooring of large arrays of acoustic monitoring equipment, and the site is wind exposed and tidally dominated, which precludes regular boat-based transect surveys at an appropriately fine scale. This results in land-based observation surveys being the most effective, and practical, method for intensive fine-scale monitoring of the distribution of porpoises at this regionally important site.

The Runnelstone Reef is a roughly horseshoe-shaped bedrock platform with an average depth of approximately 15 m out to 1.6 km, where it shallows at its southern edge, forming several upstanding pinnacles that come to within a few metres of the surface. Beyond the pinnacles, water depth drops sharply to >60 m (Fig. 1). To the east and west sides of the reef the seafloor slopes away gently and depth increases gradually. Two high-resolution multi-beam bathymetry datasets were combined to create a full bathymetric map of the survey area (Fig. 1). Inshore data (up to ~2 km offshore), at a resolution of 1 m, were collected by the Plymouth Coastal Observatory as part of the Southwest Regional Coastal Monitoring Programme (© Teignbridge District Council), and provided by the Channel Coastal Observatory. Data from further offshore (12 m resolution) were collected as part of the Maritime and Coastguard Agency (MCA) Civil Hydrography Programme (CHP) (© Crown Copyright) and are released under the Open Government Licence.

Broad-scale tidal data from Admiralty Charts show that water is driven around the headland reef by the tidal current as it enters and exits the western English Channel during the semi-diurnal tidal regime. The tidal flow through the survey area is westward (i.e. flowing out of the Channel) for the majority of the semi-diurnal cycle. Eastwards flow (i.e. into the Channel) occurs for only ~3 h per tidal cycle, between approximately 1 h before, to 2 h after high water (HW). Tidal range varies from ~1.5 m during neap tides to ~5.5 m during spring tides.

Visual surveys

Visual monitoring data were collected between 15th July and 15th October 2007–2010. The survey period was defined by the migration season of seabirds and other marine megavertebrates, which were also monitored in the multi-species survey. Observations were carried out through the full daylight period each day; this intensive constant-effort design enabled investigation of fine-scale temporal patterns in the survey data. A 2-h break was taken each day between 1200 and 1400 h, to prevent observer fatigue and avoid the period of highest glare. Observers working in pairs, with one core observer and one supporting observer. The core observers ($N = 29$ over the 4-year period) were skilled in surveying for seabirds and cetaceans, with prior field experience of identifying the target species. Selection priority was given to supporting observers who had previous marine wildlife survey experience.

Observers applied continuous search effort using 8× or 10× magnification binoculars, with naked-eye and telescope (20–30× magnification) scans of the survey area to ensure even surveillance of the near and far fields. Telescopes were also used to ensure species ID and record group size. There was rotation of survey effort between observers and regular breaks were encouraged, whilst always maintaining at least two observers 'on watch'.

Harbour porpoise sighting records always included date, time, number of animals, movement direction and an estimate of distance and direction from the watchpoint to the point of first sighting (with subsequent sighting positions also recorded where possible). Best practice was to record direction using a compass, but on occasion a cardinal direction was used. The Runnelstone buoy was an obvious reference point, at approximately 1.6 km from the observation watchpoint, on a bearing of 170° (Fig. 1). Data

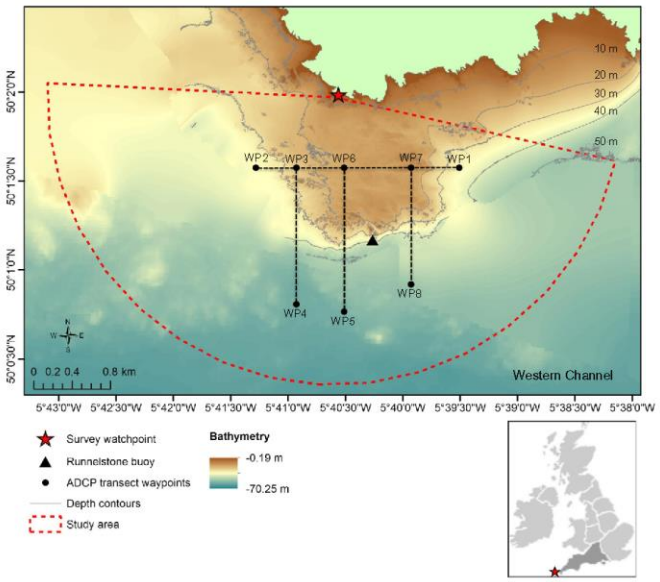

Fig. 1. Overview map of the study site off southwest Cornwall (UK) showing survey area extent and ADCP survey tracklines and waypoints. The bathymetry data has been re-gridded at a resolution of 12-m. Waypoints where CTD data were collected are indicated by red filled circles. Note the steep southern margin of the reef, and associated pinnacles immediately inshore of the Runnel Stone buoy (filled black triangle). (For interpretation of the references to colour in this figure legend, the reader is referred to the web version of this article.)

on survey conditions were recorded hourly, these included Beaufort sea state, visibility, cloud cover and glare.

Estimating error in sighting position estimates

Distance estimation was tested for two of the primary observers (jointly responsible for ~40% of total survey effort), in an attempt to constrain potential location errors associated with visually estimating positions of porpoises. Error tests were undertaken on two occasions, in October 2010 and January 2011. In the first test, observer-estimated positions of a boat were compared to the true position collected with an onboard GPS (2 observers, $N = 60$). During the second test (one observer, $N = 22$), visual estimates of the position of porpoises were compared to positions recorded using a surveyor's theodolite (Leica FlexLine TS02 Total Station). In both cases, observer estimates and 'true' positions were plotted in a GIS and the distance between them was calculated. The mean error across all tests ($N = 82$ position estimates by 2 observers) was 281 m (test 1 mean error = 320 m, SD = 141; test 2 mean error = 242 m, SD = 144). The mean error estimate from these tests was used to constrain analyses of the spatial dataset, including the smoothing bandwidth of kernel density estimates (300-m) and grid cell size for spatial modelling (600-m).

Detection of porpoises

It is not possible to use Conventional Distance Sampling (CDS) methods on data collected in single point, land-based observation surveys, because of violation of the assumptions of Distance Sampling theory (Buckland et al., 2001). As a result, there is no way to estimate the effect of distance on the ability of observers to detect animals recorded in this survey using CDS methods. Instead, a series of independent double-observer trials were carried out at the same site using a surveyor's theodolite, and the results were modelled in a logistic regression in order to estimate a detection function (Nichols et al., 2000; Buckland et al., 2008). The detection function was then used to systematically correct for the proportion of missed animals with increasing distance (Buckland et al., 2004).

The double-observer trials were undertaken retrospectively, during 2012 and 2013, in an attempt to better constrain the impact of detection bias on the results of the monitoring survey carried out in previous years (2007–2010). Although the trials were collected at a different time to the original survey data, the overall survey conditions and observer experience were comparable; therefore it is deemed valid to use the resulting detection function to correct the dataset that was previously collected at the site (personal communication: Dr. Len Thomas, Centre for Research into Ecological and Environmental Modelling). If both of the observers independently detected the same animal(s), the trial was recorded as successful; if only one observer detected the animal(s), the trial was a failure (detailed methods are provided in Section S1.1. of the Supplementary Material). 16 double observer trials on porpoise sightings were carried out during the limited data collection period at the survey site in 2012–13. Although the sample size is acknowledged to be small, in the absence of a more powerful dataset, the trials data were modelled using a logistic regression to estimate the probability of detection as a function of distance from the observer. The standard Distance Sampling assumption of $g(0) = 1$ was used, i.e. the probability of detection at a distance of 0 km from the observer equals 1 (Buckland et al., 2001), and the model-estimated detection function is presented in Fig. S1 of the Supplementary Material. The detection function was used to predict the probability of detection within each grid cell, based on the distance of the grid cell centre from the observer's position.

The sightings within each grid cell were then corrected using the model-predicted detection probabilities. The detection-corrected data were supplied as the response variable in the subsequent model of the spatial distribution of porpoises within the survey area.

Because of the low sample size for the double observer trials, additional measures were also used to ensure the visual survey methods had not been affected by bias related to detectability, and to support the robustness of the dataset and analyses. These included analysis of (1) distance distribution data for other species recorded during visual surveys, and (2) an additional boat-based survey dataset collected within the survey area (details of these analyses are provided in Sections S1.2. and S1.3. of the Supplementary Material). The boat-based data showed a similar spatial pattern in relative density of porpoise sightings as the land-based survey data; therefore we are confident that detection bias did not significantly affect the observed spatial distribution pattern of porpoise sightings (Supplementary Material, Figs. S3 and S4). On the basis of the outcome of these investigations, the effective survey area was delineated at a distance of 3 km from the survey watchpoint on Gwennap Head (Fig. 1).

Data analysis

Harbour porpoise sightings data treatment

Data filters were applied to the 4020 h of total survey effort (containing a total of 736 porpoise sightings) in order to remove effort and sightings recorded during poor survey conditions, defined as visibility <5 km and/or Beaufort sea-state of >3. Sightings recorded outside of the delineated survey area (100–270° and out to 3 km) were also removed, as were known or suspected re-sightings of the same individuals or groups. The final filtered-sightings dataset contained 2413 h of survey effort, and 418 sightings of harbour porpoise (Table 1). All sighting records retained in the dataset had associated distance estimates (in order to ensure they were within the delineated survey area), but only those sightings that also had precise bearings recorded (as opposed to cardinal directions) were used in the spatial analyses. The spatial dataset contained 255 sighting records.

The visually estimated locations of the filtered spatial sightings dataset ($N = 255$) were transformed from bearing and distance to decimal degree coordinates (Veness, 2012) and imported into a GIS where they were mapped over the high-resolution bathymetry map. Mapping was carried out in ArcGIS v.10 and all statistical analyses were performed using the R software (R Development Core Team, 2011).

Cluster analysis

The spatial distribution of porpoise sightings within the survey area (un-corrected for detection bias) was explored using a Ripley's K analysis in the R package 'spatstat' (function 'kest', Baddeley and Turner, 2005). The test is a second order analysis of spatial point processes that examines the distribution of distances between points over various scales to look for scale-dependent patterns. The cluster statistic, $K(d)$, represents the intensity of points within specified distances bands (d) from other points, and is compared to an expected K value based on 999 simulations of complete spatial randomness.

Kernel density

Utility distributions (UD) (Powell, 2000), describing the pattern of porpoise sighting intensity in the raw sightings data (uncorrected for detection bias) within the survey area, were estimated using un-weighted fixed kernel density estimation (KDE) and kernel isopleths, calculated in the Geospatial Modelling Environment software (Beyer, 2012). The X and Y coordinate data for the porpoise sightings were normally distributed; therefore a quartic approximation of the Gaussian kernel was used, which gives a uni-modal kernel that is symmetrical around the origin (the estimated sighting position).

Bandwidth (h) optimisation was carried out using functions in the R package 'sm' (Bowman and Azzalini, 2010). Selection of h was based on visual comparison of performance and minimisation of the mean square error. A value of $h = 300$ m (estimated using an un-weighted normal smoothing method) was used in the kernel density estimate calculations. Powell (2000) recommends using a smoothing bandwidth that is at least equal to the uncertainty in the location estimates, therefore the selected value of 300 m is appropriate considering the error on the sighting position estimates. The 50% KDE isopleth was selected to define a core-use area within the survey area; on the basis that this will delineate the area of 50% probability of sightings, which contains approximately 50% of the observations (Börger et al., 2006).

Generalised Additive Modelling (GAM) methods

Generalised additive models (GAMs), with Poisson or negative binomial error structure (dependent on presence of overdispersion), were used to model spatial and temporal patterns in the porpoise sighting data. The GAMs take the general structure specified by Hastie and Tibshirani (1990) and were carried out in the R package 'mgcv' (function 'gam', Wood, 2006), which contains integrated smoothness estimation. Smooth functions for model covariates were specified using thin plate regression splines with shrinkage (Wood, 2006). For most model covariates, the dimension, k, representing maximum degrees of freedom of each smooth, was manually limited by $k = 4$ to avoid excessive flexibility and model overfitting. The smoother of time to high water (TtHW) in the temporal model was given maximum $k = 6$, to allow for the expected sinusoidal patterns in sightings with respect to tide. The penalty (*gamma*), given to each degree of freedom in the automatic smoothing parameter selection process, was increased from the default of 1 to 1.4, as recommended by Wood (2006) to reduce the potential for model over-fitting. Interactions between covariates were modelled using tensor product (te) smooths. Aspect and TtHW were modelled with cyclic smoothers to account for the circular nature of the degree unit of aspect (where 0 and 359

Table 1
Summary of survey effort and harbour porpoise sightings from the visual monitoring survey, 2007–2010 (after filtering for poor survey conditions and quality control). 'Positive' hours/days are defined as periods during which one or more porpoises were recorded.

Year	Hrs obs	Sightings	% Positive hrs	% Positive days	% Survey effort by Beaufort sea state (% sightings)			
					0	1	2	3
2007	608	86	11.35	35	3 (12)	21 (12)	46 (59)	30 (17)
2008	538	124	16.54	34	2 (5)	17 (46)	41 (25)	40 (24)
2009	569	128	18.10	42	2 (4)	25 (54)	45 (28)	28 (14)
2010	698	81	9.17	33	1 (2)	19 (41)	47 (51)	33 (6)
All Years	2413	419	13.47	36	2 (6)	20 (40)	45 (38)	33 (16)

Table 2
Names and definitions of all explanatory variables used in the analyses of spatial and temporal patterns in the distribution of porpoise sightings.

Variable	Model	Description of variable
Av. Depth	Spatial	The average depth value for each grid cell, calculated from the mosaic of 1 m and 12 m resolution bathymetry data. Measured in metres below the surface
Av. Slope	Spatial	Slope of the seabed, derived from the bathymetry data using using the maximum change in elevation of each of the bathymetry layer cells and its 8 neighbours (i.e. a 3 × 3 cell window). The value used in the model was the average slope value (gradient in degrees) for each of the survey area grid cells
Av. Aspect	Spatial	Aspect was derived from the bathymetry data and identifies the downslope direction of maximum rate of change in value from each of the bathymetry layer cells and its 8 neighbours (i.e. a 3 × 3 cell window). This metric can be thought of as the direction of the slope, and is measured in clockwise degrees from 0 (due north). Flat areas are given a value of −1. The value used in the model was the average aspect value for each of the survey area grid cells
Slope:Aspect	Spatial	The interaction term between the slope and aspect covariates for each grid cell
Depth:Slope	Spatial	The interaction term between the depth and slope covariates for each grid cell
Depth:Aspect	Spatial	The interaction term between the depth and aspect covariates for each grid cell
Year	Temporal	Year of the survey. Factor variable with 4 levels (2007, 2008, 2009, 2010)
Month	Temporal	Month of the survey. Factor variable with 4 levels (July, August, September, October)
Beaufort sea state	Temporal	From the hourly observations of survey conditions collected by observers at the watchpoint, using the Beaufort scale. Factor variable with 4 levels (0, 1, 2, 3)
TtHW	Temporal	Time to high water. In decimal hours relative to HW time, where HW = 0. Values range from −6.33 to +6.33. Calculated using HW times from the POLPRED CS20 model for location within survey area (Proctor, Bell et al., 2004)

are adjacent values) and the cyclic nature of the tidal cycle (+6.3 to −6.3 h relative to HW time).

Retention of collinear variables in a model can lead to poor estimation of standard errors and p-values. To avoid the problems introduced by correlation between covariates, pairwise Spearman's rank correlation tests and Variance Inflation Factors (VIF) (R 'AED' package, function 'corvif', Zuur et al., 2009) were calculated for all of the candidate model covariates. Pairs of variables with high levels of correlation (Rho = ⩾0.6) or VIF values exceeding the conservative threshold of 3 (Zuur et al., 2009) were identified. For collinear pairs, the covariate that was selected first during the stepwise selection process was retained, while the other was discarded.

Predictor variables were selected through manual stepwise forwards selection, using the model fit score (AIC) to select the best model at each step. At each step, the significant ($p < 0.05$) covariate that added most explanatory power (⩾1% increase on previous model iterations) and resulted in the lowest AIC was selected. The AIC score must have been reduced by a value of 2 or more for a covariate to be considered for addition to the model (Burnham and Andersen, 2002). The updated model was then taken forward into the next round of selection, where the effect of adding the remaining predictor variables was tested again using the same method; and so on until no more covariates could be added, according to the above criteria.

Gridded relative density analysis

A radial grid was defined by the extent of the survey area (100–270° out to a distance of 3 km from the observer's location on Gwennap Head) and divided into cells along concentric distance bands from the watchpoint location at 600-m intervals, and radial bearing lines at 10° intervals (representing ± the mean error on visual position estimates, see Section 'Estimating error in sighting position estimates'). Number of porpoise sightings and area (km^2) were calculated for each grid cell, along with associated values for mean depth, slope and aspect in each cell.

The detection function, created using a logistic regression on binary data from independent double observer trials collected at the survey site in 2012/13, was used to correct the data for missed sightings. For further information on the double observer trials and modelling methods see Sections 'Detection of porpoises' and S1.1. The sightings recorded within each grid cell were then corrected for detection using:

$$D_{sightings(i)} = N_{sightings(i)} / P_{(i)}$$

where $D_{sightings(i)}$ is the detection corrected sighting density in the ith grid cell, $N_{sightings(i)}$ is the number of sightings observed within the ith grid cell, and P is the modelled detection probability for the distance from the observer to the centre of the ith grid cell.

The detection-corrected counts of porpoise sightings per grid cell were then modelled as a function of static physical covariates within a Generalised Additive Model (GAM) framework. Models had a negative binomial error distribution (to account for overdispersion) and all candidate covariates are presented in Table 2. The models included an offset of (logged) grid cell area, to account for differences in the area of the radial grid cells.

Standard model validation was carried out (as outlined by Wood, 2006; and Zuur et al., 2007), and spatial autocorrelation was checked using the residuals from the final model in a Mantel test (R package 'Vegan', Oksanen et al., 2013). The test calculates Pearson correlations from dissimilarity matrices of (1) the distance between pairs of points (locations of grid cell centroids) and (2) the differences in model residual values between pairs of points. The calculated correlation of the modelled data is then compared to correlation calculated on 999 random reassignments of residual values to location points (retaining the spatial structure of the data, Legendre and Legendre, 2012).

Effect of tidal flow on the temporal distribution of porpoise sightings

The number of porpoise sightings per hour was modelled using a GAM with Poisson error distribution and log-link. Candidate model covariates are listed in Table 2. Standard GAM validation was carried out, and an assessment of dependence structure in the residuals of the final model was undertaken using an autocorrelation function ('acf') in R.

Oceanographic survey

A fine-scale ADCP survey was undertaken within the survey area over a semi-diurnal tidal cycle on 11th July 2011 (2 days after neap tide). The aim of the survey was to identify flow features, driven by the interaction with topography, which may be relevant in the context of fine-scale harbour porpoise distribution. The survey was carried out aboard the University of Southampton inshore vessel, *RV Callista*, using a hull-mounted RDI Workhorse Mariner in bottom tracking mode. The ADCP frequency was 600 kHz and ping rate was 2 Hz (2 cycles per second). Vertical bin size was 1-m and ensemble interval was set at 2 s (4 pings per ensemble). The ADCP transect route (Fig. 1) was repeated nine times over a 12.6 h tidal cycle. The vessel's average speed of travel throughout the survey

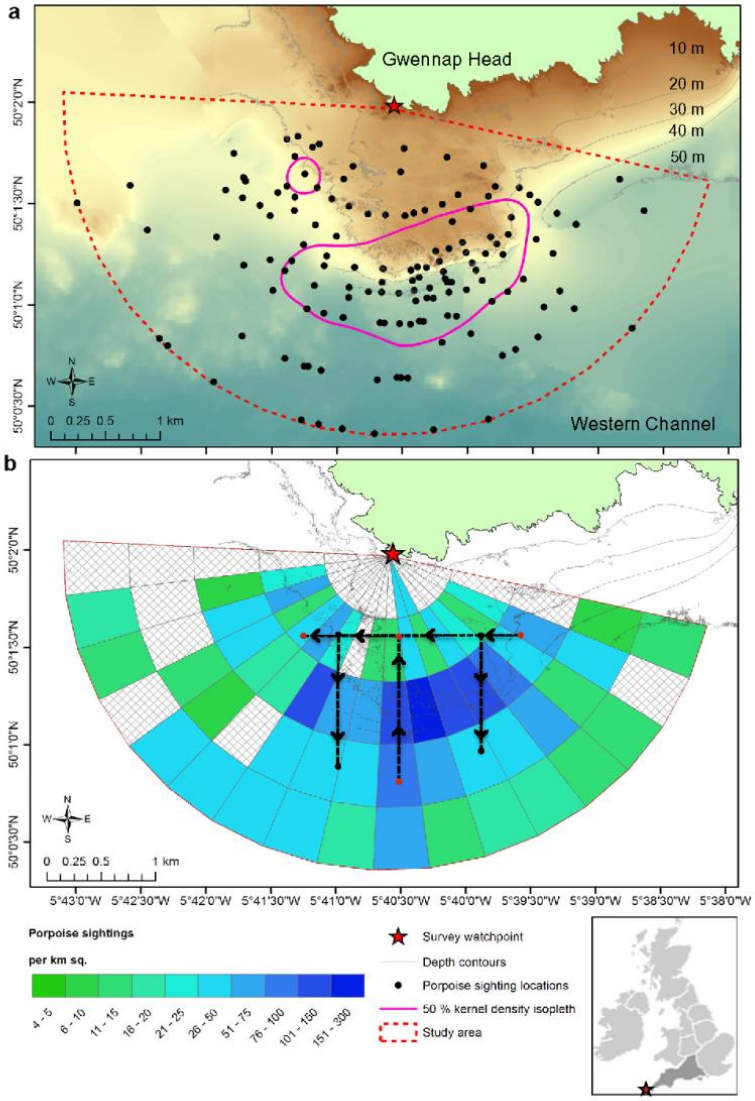

Fig. 2. (a) Raw data: filtered harbour porpoise sightings ($N = 255$) and 50% kernel density estimate isopleth (smoothing bandwidth = 300 m). (b) Detection-corrected porpoise sighting density by grid cell ($N = 85$), corrected for cell area and presented as sightings per km^2. Hatched cells contained 0 sightings. Reef contours (10 m intervals) are shown. Oceanographic survey transect route is overlain (for detailed transect route map see Fig. 1).

was 5.14 knots, and average sea state was Beaufort 1.5 (SD = 0.5). Vertical shear, S, in the horizontal velocity across 1-m vertical intervals was calculated as:

$$S = ((\partial U/\partial z)^2 + (\partial V/\partial z)^2)^{1/2}$$

where $\partial U/\partial z$, $\partial V/\partial z$ are the vertical gradients in the east and north velocity components, respectively. Shear was computed over 1-min intervals (average of 30 × 2-s ensembles).

Conductivity Temperature Depth (CTD) and fluorescence data were collected throughout the ADCP survey at waypoints (WP) 1, 2, 5, and 6 (Fig. 1) using an FSI CTD with fluorometer, mounted on a 12-bottle CTD rosette. Data were processed using FSIpost and have been used to investigate patterns in density and fluorescence through the tidal cycle at key sample sites and to calculate a Richardson Number depth profile during tidal periods associated with high and low porpoise sightings. The Richardson number (Ri) indicates the susceptibility of a stratified fluid to the generation of turbulence by shear-instability. Ri, computed over 1-m vertical intervals, was calculated as:

$$Ri = N^2/S^2$$

where $N = \{-g/\rho_o \partial\rho/\partial z)^{1/2}$ is the buoyancy frequency and dependent on the vertical density gradient, $\partial\rho/\partial z$. $Ri < 0.25$ is indicative of transition from laminar to turbulent flow (Miles, 1961). An estimate of Ri was calculated using data from, firstly, WP5 because this was the

Table 3
Summary of negative binomial GAM of detection-corrected porpoise sightings per grid cell (N = 85 cells). See Table 2 for description of variables and full list of candidate covariates that were considered during model selection. Variables are shown in the order of selection, with terms being selected sequentially based on reduction in AIC score compared to the previous model (with the starting AIC score given in bold in top row) and the amount of deviance explained by each term addition. All selected terms were significant to at least p = 0.05. The degrees of freedom of the estimated smooth functions are given as 'edf'.

Order	Linear term/smooth (df)	% Deviance	Adjusted R	AIC	Chisq.	Estimated p-value
Null	**Intercept = 3.36**	**0**	0.1	**381.9**		
1	S(average slope), edf = 1.1	17.8	0.4	397.4	9.5	<0.001
2	S(average depth), edf = 1.1	13.8	0.5	382.1	47.1	<0.001
3	S(average depth: average aspect), edf = 8.2	14.9	0.5	379.8	16.0	0.024
Final	S(average depth) + S(average slope) + S(average depth: average aspect)	***46.5***	*0.5*	***379.8***		

Dispersion (sum(resid^2)/residual degrees of freedom) = 1.02.
Total model degrees of freedom = 11.47.
K = 2.919.

closest CTD sampling point to the porpoise sightings core density area, as defined by a 50% kernel density isopleth. Secondly, Ri was computed for WP1 and WP2 on either side of the reef to assess the impact of the observed lee wave in promoting critical conditions for shear instability and the generation of turbulence.

Results

Harbour porpoise survey

Harbour porpoises were sighted on 135 of the 372 survey days between 15th July and 15th Oct 2007–2010. The highest rate of sightings was recorded in 2009 and the lowest in 2010 (Table 1). Group sizes of up to 20 porpoises were recorded, though single animals were most frequently observed (41%). The average pod size per sighting was 2.33 animals (SD = 2.02). The proportion of survey effort during each sea state (0–3) was similar throughout all four years of the survey (Table 1); therefore it is unlikely that changes in survey effort with relation to sea state would account for the inter-annual variability in the recorded numbers of sightings.

Sea state conditions had a considerable effect on the number of harbour porpoise sightings recorded per hour. As sea state increased, there was a corresponding decrease in the rate of sightings per hour of effort; therefore sea state was included as a covariate in the model of the temporal distribution of porpoise sightings (see Section 'Fine-scale temporal distribution of porpoise sightings in relation to temporal variables'). The highest sighting rate was 0.48 porpoises per hour in sea state 0, although this sea state was very rarely observed (Table 1). The sighting rate reduced to 0.38 in sea state 1 and 0.15 in sea state 2. During sea state 3, the sighting rate was only 0.08, which represents a 6-fold decrease compared to the rate in sea state 0.

A two-sample Kolmogorov–Smirnoff test was carried out on pairwise comparisons of the density distribution of porpoise sightings by distance from observer, under each sea state (0–3). Although sea state was shown to clearly affect sighting rate at the study site, the comparison of the spatial distribution of sightings showed no significant difference in the density-by-distance curves in all pairwise tests (p = >0.08, with correction for multiple testing, see Fig. S5 and Table S1 in Supplementary Material Section S2). This suggests no systematic bias caused by sea state on the observed spatial distribution of sightings.

Spatial clustering of porpoise sightings

Porpoise sighting locations (N = 225), uncorrected for detection, are shown in Fig. 2a. Results of Ripley's K analysis showed that porpoise sightings were significantly clustered (p = <0.001, N = 255 sighting locations). The 50% UD kernel isopleth (N = 255 sighting locations) had an area of 1.87 km^2, representing just 14% of the full survey area of 13.3 km^2, but containing approximately 50% of

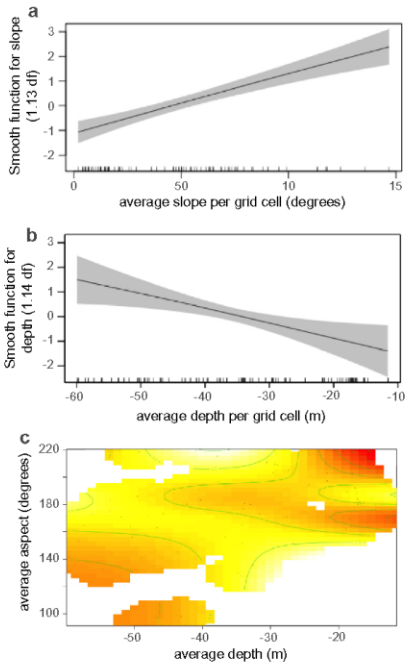

Fig. 3. Spatial distribution of harbour porpoise sightings modelled using a GAM with negative binomial error structure. (a) Smooth function of average slope within grid cells and (b) Smooth function of average depth within grid cells. Shaded areas represent 95% CIs and rug plot along x axis shows observed data values. (c) Heat plot with overlaid contours for the smooth interaction term of depth and aspect within each grid cell. Strength of interaction effect is colour scaled, with warmer colours indicating combinations of depth and aspect with greatest effect on porpoise sightings. (For interpretation of the references to colour in this figure legend, the reader is referred to the web version of this article.)

porpoise sightings. The position of the 50% UD isopleth indicates that clustering of porpoise sightings occurs around the southern and south-eastern margins of the Runnelstone Reef (Fig. 2a). There was no notable change in the location of the 50% isopleth when kernels were calculated for subsets of sighting locations collected in different years or under different flow conditions.

The survey area was divided into a total of 85 grid cells, 58 of which had at least one porpoise sighting recorded within them

Table 4
Summary of Poisson GAM of porpoise sightings per hour of survey effort (N = 4019 h). See Table 2 for description of variables and full list of candidate covariates that were considered in model selection. Variables are shown in the order of selection, with terms being selected sequentially based on the reduction in AIC score compared to the previous model (with the starting AIC score in top row in bold) and the amount of deviance explained. All selected terms were significant to at least p = 0.05. Degrees of freedom for estimated smooth functions are given as 'edf'.

Order	Linear term/smooth (df)	% Deviance	Adjusted R	AIC	L (df)	Estimated p-value
Null	**Intercept = −1.75**	**0**	**0**	**2465.8**		
1	Beaufort sea state (factor with 4 levels)	7.9	0.04	2346.4	195 (3)	<0.001
2	Month (factor with 4 levels)	7.1	0.1	2213.9	137 (3)	<0.001
3	Year (factor with 4 levels)	2	0.12	2184.7	35 (3)	<0.001
4	Smooth (TtHW), edf = 3.5	2	0.13	2158.1	34 (3.5)	<0.001
Final	Month + Beaufort sea state + Year + s(TtHW)	**19**	**0.132**	**2158.1**		

Dispersion (sum(resid^2)/residual degrees of freedom) = 1.15.
Total model degrees of freedom = 13.49.

(Fig. 2b). Grid cells containing the highest numbers of detection-corrected porpoise sightings per km^2 were located in a radial band along the reef edge, between 1.2 and 1.8 km from the survey watchpoint location (Fig. 2b).

Spatial model of porpoise relative density

The best model of the detection-corrected porpoise sightings per grid cell explained 46.5% of the deviance in the fine-scale spatial distribution of harbour porpoise sightings as a function of the covariates slope, depth, and an interaction of depth and aspect (Table 3). Slope was the most significant predictor variable (p = <0.001), explaining 17.8% of the deviance, with depth and the interaction between depth and aspect explaining another 13.8% (p = 0.01) and 14.9% (p = <0.001) of the deviance respectively (Table 3). Porpoises were more frequently recorded within areas of high average slope and intermediate to high average depth (Fig. 3a and b). The interaction term indicates a preference for areas where shallow to moderate depth is combined with slopes of southerly and south-westerly aspect (Fig. 3c). These conditions predominate around the southern Runnelstone Reef margins and the steep pinnacles. There was no spatial autocorrelation in the model residuals (Mantel statistic r = −0.043, significance based on 999 permutations = 0.175), which justifies the use of a GAM model structure that does not include an autocorrelation parameter to account for spatial dependence.

Fine-scale temporal distribution of porpoise sightings in relation to temporal variables

GAM analysis found the covariates TtHW, Beaufort sea state, year and month as significant explanatory variables; explaining 19% of the temporal variability in porpoise sightings (Table 4). Highest numbers of sightings were recorded in 2008 and 2009 (Fig. 4a). Sighting rates reduced as sea state increased (Fig. 4c) and there were higher sightings per hour recorded in July and October compared to August and September (Fig. 4b). Greater numbers of sightings were recorded during hours when the tide was flowing to the west (ebbing), particularly between 2 and 6 h after HW (Fig. 5), corresponding to the period of strongest west-

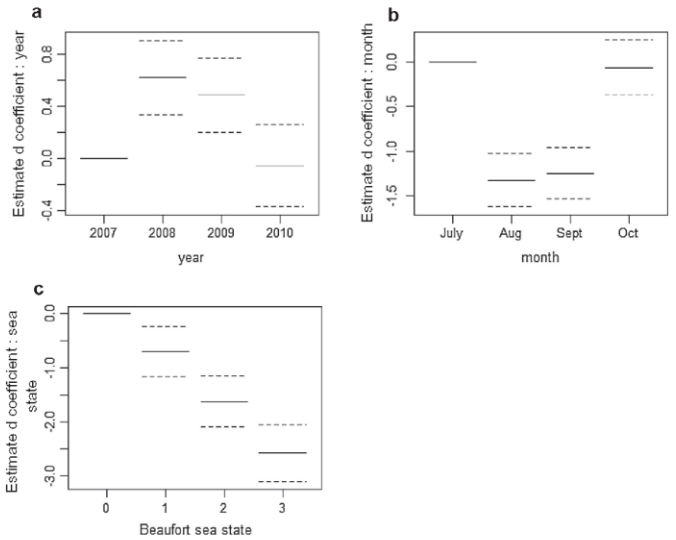

Fig. 4. Termplots showing estimated partial coefficients for parametric explanatory variables in the Poisson GAM of harbor porpoise sightings per hour: (a) year of survey, (b) month of survey, (c) Beaufort sea state. Base level of each factor variable is centered at 0.95% confidence intervals are shown by dashed lines.

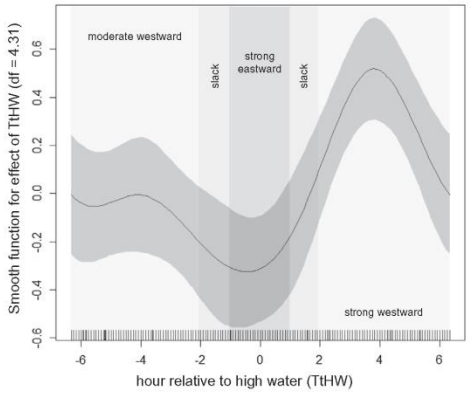

Fig. 5. Harbour porpoise sightings temporal distribution modelled using a GAM with Poisson error structure: estimated smoother for the effect of time to high water (TtHW) on harbour porpoise sightings per hour. Shading around line indicates 95% confidence interval. Vertical shading bands on plot show predominant flow direction in the survey area during each hour of the tidal cycle. Rug plot of observed TtHW values is also shown.

ward flow. Much lower sighting rates were recorded between −2 and +1 h relative to HW, which are characterised by eastward flow and slack water periods (Fig. 5). The rug plot along the bottom of Fig. 5 indicates all observed values of TtHW, showing a good spread of effort throughout the full tidal cycle. A non-parametric two-sample Kolmogorov–Smirnov test (2-sided) indicated significant differences in the temporal distribution of porpoise sightings with reference to tidal flow, when compared to the overall distribution of effort; indicating that the results are not simply a function of the distribution of survey effort ($D = 0.1161$, $p = <0.001$). There was no significant temporal correlation structure in the final model residuals, therefore no requirement to use a mixed model to account for temporal autocorrelation.

Oceanographic survey

Current and density fields

Images showing the ADCP data (flow velocity and shear) from a selection of periods throughout the surveyed tidal cycle are given in Figs. 6 and 7, with further ADCP transect data in the Supplementary Material (Figs. S6 and S7). The ADCP survey recorded relatively strong tidal flows at the site during the survey (up to 1 m s^{-1}), as well as complex fine-scale flow patterns and hydrodynamic features (Figs. 6 and 7, S6 and S7). Flow over the shallower reef top area was generally faster than in the deeper water at the reef edges and beyond (by between 0.2 and 0.6 m s^{-1}; Fig. S6a). Tidal asymmetry was apparent in the eastward velocity component, *U*; currents were directed to the east only during groups 5 and 6 and were otherwise directed to the west (Fig. 7a and b). Similarly the weaker northward current component, *V*, exhibited a brief reversal along leg 3 from northward to southward (Fig. 7a). A significant difference was apparent in *V* between legs 3 and 4, both of which were orientated north to south, as shown on the transect route

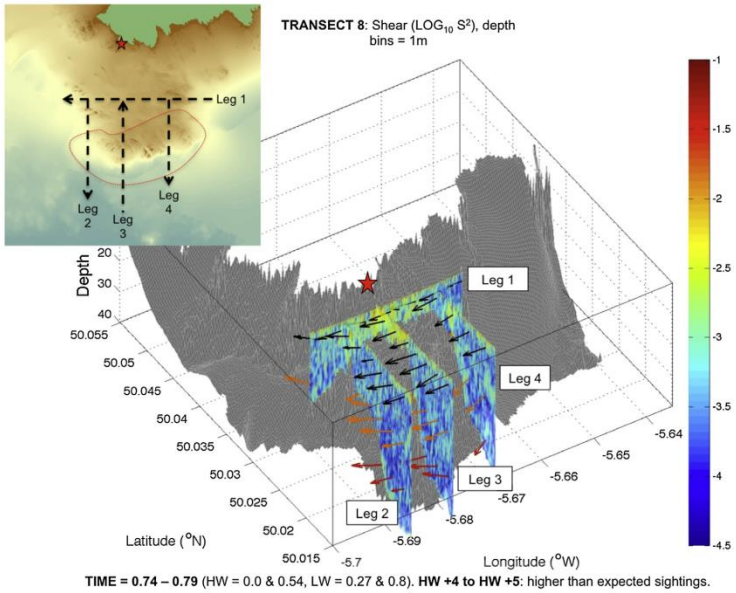

Fig. 6. Shear squared ($\log_{10} S^2$) computed over 1-m vertical intervals for the eighth transect run (approximately HW +4 to HW +5). Velocity vectors (indicated by arrows) are plotted at 90-s intervals along each leg at depths of 5 (black), 15 (orange) and 30 m (red). Current profile data were collected as 2-s ensembles in 1- m depth bins from a hull mounted ADCP on the *RV Callista*. Insert identifies transect line location with reference to the 50% UD of the visual porpoise sightings. Red star shows position of visual survey watchpoint on Gwennap Head and gray background is bathymetry. (For interpretation of the references to colour in this figure legend, the reader is referred to the web version of this article.)

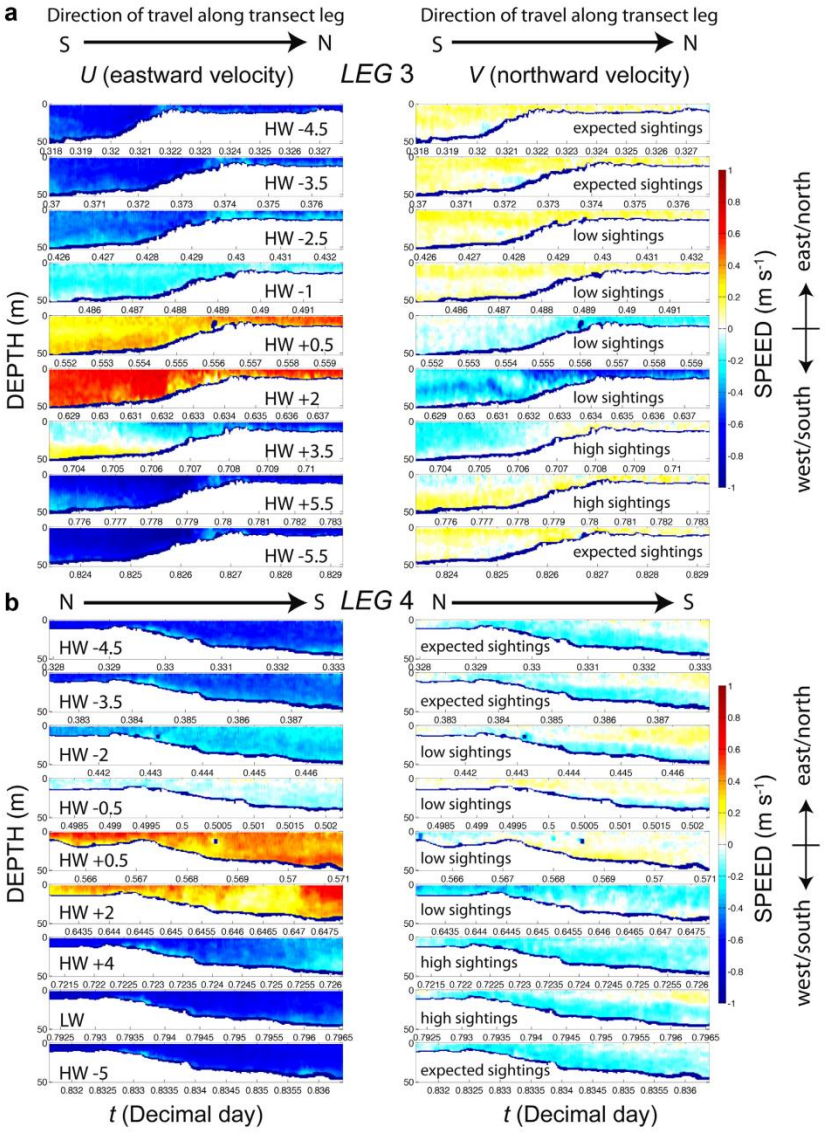

Fig. 7. Current velocity profiles from transect groups (G) 1–9 of the ADCP survey in the study area, carried out on 11th July 2011 from *RV Callista*: (a) leg 3 (travelling south to north) and (b) along leg 4 (travelling north to south) Data are from a full tidal cycle. Decimal time relative to HW (0 and 0.5) is given along the *x* axes and water depth along the *y* axes. Current velocity is colour scaled with (a) the eastward velocity component, from east in red to west in dark blue and (b) the northward velocity component, from north in red to south in dark blue. The timing of each profile relative to HW and to relative density of porpoise sightings is labelled. (For interpretation of the references to colour in this figure legend, the reader is referred to the web version of this article.)

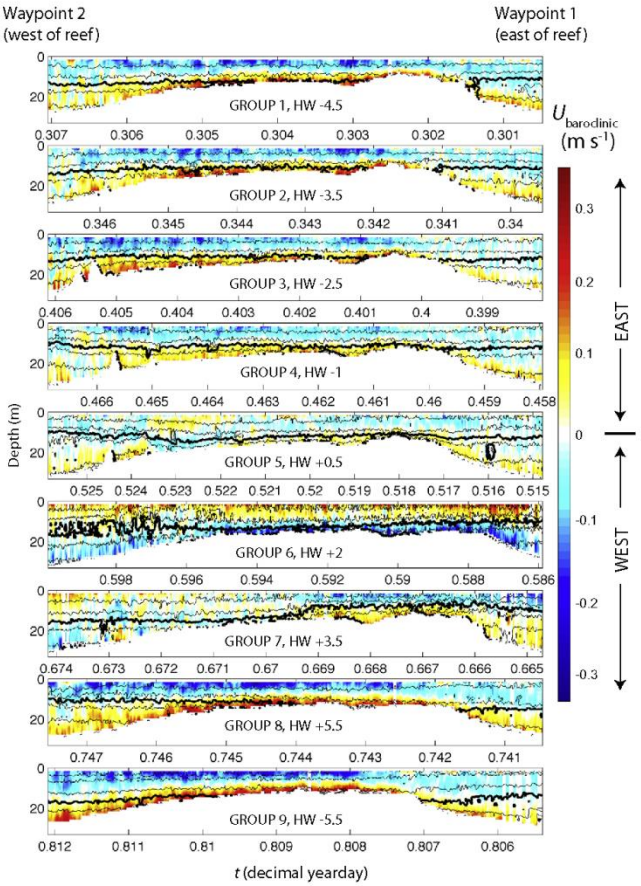

Fig. 8. Leg 1 baroclinic eastward velocities, $U_{baroclinic}$, computed as the total velocity following subtraction of the depth-mean component. Overlain are contours of echo intensity from the ADCP at 10 db intervals with the 110 db contour indicated by the heavy black line. The panels are reversed in time such that WP2 on the western side of the reef is on the left side of the figure; each leg began at WP1 and crossed the reef to WP2, i.e. from right to left when looking at the figure.

map in Fig. 1. Leg 3 was located centrally across the reef where depth contours started to turn northwards with respect to a westward flow. Leg 4 crossed the reef on its eastern edge where depth contours headed south for a current flowing in a westward direction. During leg 3, *V* was predominantly northward whereas within the same groups flow during leg 4 was predominantly southward (Fig. 7). Thus, flow followed depth contours around the outer flank of the reef and indicates a pronounced curvature in the velocity field in response to local bathymetry, as depicted by the velocity vectors in Fig. 6.

The flow is two-layered, manifested by flow reversal over depth in *U* during leg 3 around HW +3.5 (Fig. 7a), and exhibits a significant baroclinic component, estimated as the observed current following subtraction of the depth-mean barotropic component (Fig. 8). At times, these two-layered flows were associated with the formation of a mid-depth layer of elevated shear at a height above bed (HAB) of ~25 m, within which $S^2 > 10^{-4}\ s^{-2}$. This shear layer can be seen along legs 3 and 4 during the period HW +4 to HW +5 as a mid-depth layer of lighter blue/green in Fig. 6. Two-layered flows were also observed during the westward ebbing tide in the northward velocity component along leg 4 from HW −4.5 to HW −2 and again at LW (Fig 7b).

The CTD and fluorescence data collected through the tidal cycle at four of the waypoints indicate that there was also a tidal asymmetry in water properties. The overall pattern is represented in Fig 9 by the data from waypoint 5 on the outer edge of the reef at the end of leg 3 (see location in Fig. 1). Fig. 9a shows that a body of warmer (less dense) surface water was advected along the coast through the end of the westwards ebbing tide (HW −3.5 to HW +0.5) and the period of the eastward flooding tide (HW +0.5 to HW +2). Cooler water was then flushed back through the survey site as the tide turned westward again (after HW +2) and through-

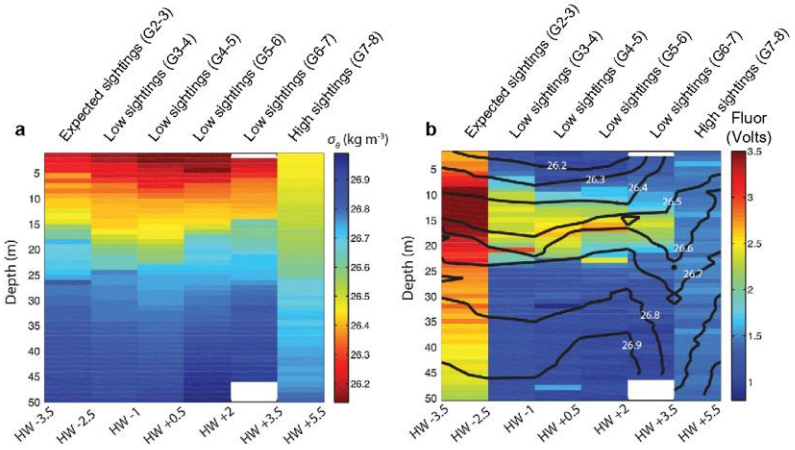

Fig. 9. (a) Density (σ_θ) and (b) fluorescence obtained from CTD casts at Waypoint 5 between transect groups 2 and 8. Labels at top relate to modelled porpoise sightings and are consistent with those in Fig. 7a, as are the times relative to HW. Fluorescence is indicated as Volts and overlain with isopycnals. Changes in density were due almost entirely to temperature, which decreased at the surface from a maximum of 15C at HW +0.5 to a minimum of 13 at HW +5.5.

out the following period of westward dominated current flow during transect groups 7–8 (HW +3 to HW −5.5). A mid-depth peak in fluorescence also occurred during the ebbing westward tidal flow and the following eastward flood between HW −3.5 to HW +3.5 (Fig. 9b); although this result is only representative of the sampling period and may not be consistent across all tidal cycles at the site. The overall pattern in the CTD data, from all four waypoints, showed cooler water and less thermal structure throughout the Runnelstone Reef survey during the westward ebbing tide (between HW +3 and HW −1); suggesting that regional-scale variations in water properties are advected past the reef during different phases of the tide (note the full CTD dataset from the entire survey area is not presented).

Internal shear and boundary layer turbulence

The pronounced vertical shear in the currents and the accompanying stratification (Figs. 6 and 7) suggest that shear-instabilities may play a role in promoting the development of turbulence throughout the water column. In the absence of direct measurements of turbulence, we firstly consider ADCP echo intensity as an indication of suspended material within the water column or stratified turbulence (van Haren, 2009). Echo intensity |E| varied strongly throughout the 12 h of observation but also with position relative to the reef (Fig. 10). During leg 4, which was the leg furthest to the east, |E| reached maximum values at each depth during groups 8 and 9 (Fig. 10) when the 110db contour (arbitrarily selected for indicative purposes) descended below the reef crest (Fig. 10). At this time currents had reversed from eastward to westward (Fig. 7a) and we propose that this deepening of 110db contour during the westward flow (Fig. 10, G8 and 9) indicates an increase in turbulence through shear instabilities attributable to the release of a lee wave generated during the eastward flood tide (G5 and 6); this is discussed in Section 'Internal lee waves and hydraulic jumps' with specific reference to the observed deepening of isopycnals on either side of the reef.

Further evidence for the role played by shear in promoting turbulence is found in the ADCP echo intensity data collected along leg 4 shown in Fig. 10. At $t = 0.7955$ (G8, HW +5.5), 5 cusps extended downwards from the near surface layer (highlighted by black box in Fig. 10, G8) as the upper layer was flowing to the northwest, corresponding to an upstream but on-slope direction. The cusps closely resemble the form of Kelvin Helmholtz billows observed in oceanic conditions (van Haren and Gostiaux, 2010), and are strongly suggestive of shear-induced instabilities at moderate depths (~30 m).

To assess the likelihood that shear was elevated to the level required for shear instability in the region of highest sightings and the formation of the observed billows, we computed the Richardson number at adjacent WP5 (Fig. 11). Lowest values of *Ri* were observed at the times of highest porpoise sighting rates; during groups 7 and 8 (indicated by bold lines in Fig. 11). During group 7 critical *Ri* (<0.25) occurred in the lower half of the water column (below ~30 m) and the top half was only marginally stable ($0.25 < Ri < 1$). Conversely, the following group (G8) exhibited critical conditions indicative of shear instability and the generation of turbulence in the top half of the water column (above ~30 m), and marginally stable conditions below (Fig. 11), corresponding well with the depth where the billows were formed (~30 m depth, Fig. 10 G8). Importantly, during the tidal periods associated with reduced rates of porpoise sightings (G2–G6), *Ri* was significantly higher at WP 5 (Fig. 11); indicating a greater degree of stability and the reduced likelihood of shear-driven turbulence being generated in the core sightings area during these periods.

In addition to the generation of turbulence by shear instabilities in a two-layered flow (as observed in the ADCP data), frictional effects near the bed can also promote shear and turbulence. Analysis of the physics suggests that, for the maximum observed velocity of $O(1\ m\ s^{-1})$ recorded at HW +5.5, the corresponding Bottom Boundary Layer (BBL) would extend to HAB ~9 m (based on the calculation for height of BBL in a tidal flow proposed by (Lueck and Lu, 1997)). This provides evidence that the mid-depth shear layer evident along legs 3 and 4 between HW +4 and HW +5 (G7 and 8 in Fig. 7) at ~25 m HAB is not associated with frictional effects at the bed leading to an increase in the thickness of the BBL; but instead results from the baroclinic flow (Fig. 8, G7 and 8) and potentially the influence of topographic steering of flow

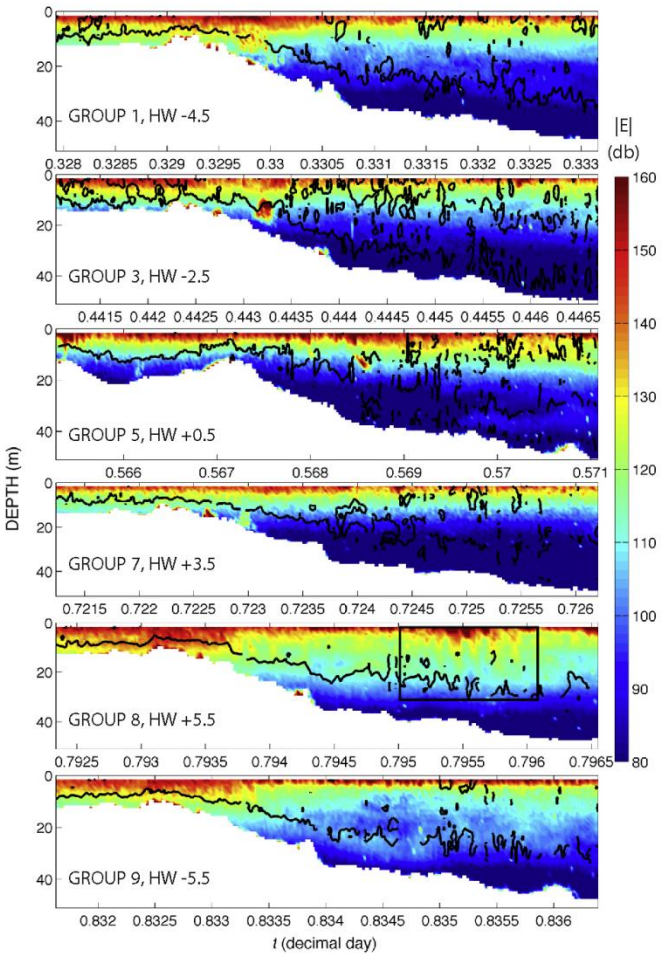

Fig. 10. Echo intensity |E| (db) during leg 4, which started on the reef and progressed offshore. The $U_{\text{barocliniic}} = 0$ contour is overlain on each panel. The black box in the profile for transect group 8 highlights the Kelvin Helmholtz instabilities that are strongly suggestive of shear-induced instabilities. Higher values of |E| indicate stronger turbulence and/or resuspended material. As the increase in |E| is clearly related to surface and interior processes rather than bed-processes, we consider that in this location |E| acts as a proxy for stratified turbulence.

around the reef (see velocity vectors in Fig. 6) and the larger scale hydrographic structure.

Internal lee waves and hydraulic jumps

Fig. 7 demonstrates that the primary flow direction at Runnelstone Reef was east/west, perpendicular to the subsurface ridge, suggesting that some of the water encountering the reef is forced over, rather than around, the reef. Lee waves can be formed under such circumstances, as the flow is forced over topographic irregularities (Geyer, 1993; Nash and Moum, 2001; Roughan et al., 2005). Despite the three-dimensionality of the Runnelstone Reef bank, a continuously stratified flow will pass over a gently varying two-dimensional bottom as long as the height of the reef (~25 m) is less than U/N, where U is the free stream velocity and N is a representative buoyancy frequency (Hunt and Snyder, 1980). Here $U = 0.5$ m s^{-1} and $N = 0.01$ s^{-1}, such that $U/N = 50$ m. However, the validity of the 2-dimensional assumption fails at peak observed flow speeds of $O(1$ m s$^{-1})$. Under such circumstances the flow may be blocked by the reef and be forced to travel around it, inducing strong vorticity at the reef edge.

Flow directed over the reef is implicated in the mechanism driving the vertical excursion of the density surface contours (isopycnals) on either side of the reef throughout the tidal cycle. Isopycnals descended rapidly on both sides of the reef in response

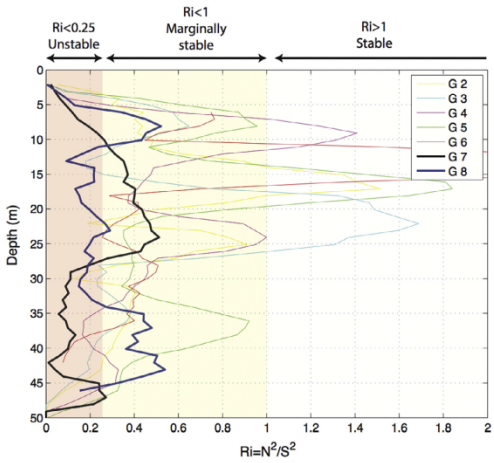

Fig. 11. Vertical profiles of the Richardson number, $Ri = N^2/S^2$, during groups 2–8 at waypoint 5 (to the south of the reef where highest sightings were recorded). The profiles obtained during groups 7 and 8, when the highest sightings were recorded, are indicated by the bold lines. Red shading represents conditions for which shear instability is expected at $Ri < 0.25$ and the yellow shading for which conditions are marginally stable ($Ri < 1$). The profiles were smoothed with a 5 point running average filter. (For interpretation of the references to colour in this figure legend, the reader is referred to the web version of this article.)

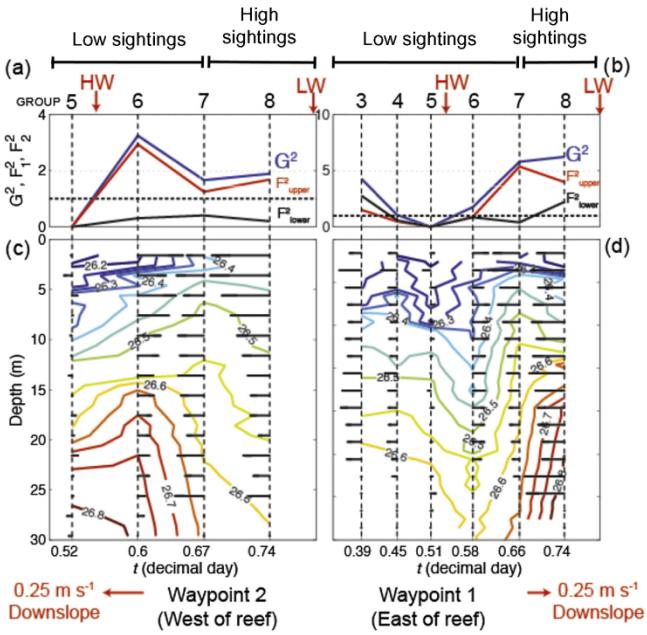

Fig. 12. (a,b) Froude numbers and (c,d) isopycnals (coloured lines) and mean U velocity vectors (black lines) at waypoints 2 and 1 on the western and eastern side of the reef respectively. Isopycnal depths are estimated from the CTD profiles conducted at the beginning and end of leg 1 for groups 3–8 (WP 1) and 5–8 (WP 2). Velocity vectors were calculated from ADCP data as mean eastward velocities over a 1-min period corresponding to the time of the CTD profile. The vectors show westward velocities when directed to the left, and eastward velocities when directed to the right. (For interpretation of the references to colour in this figure legend, the reader is referred to the web version of this article.)

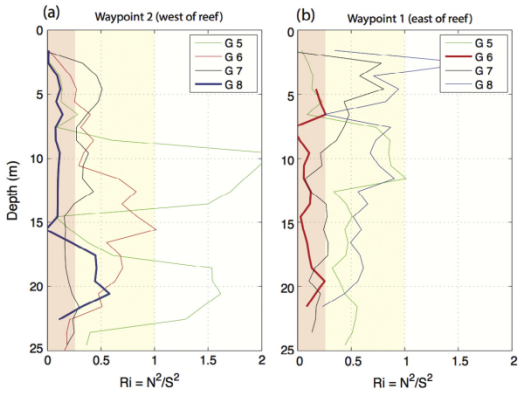

Fig. 13. Richardson number profiles during groups 5–8 for (a) WP 2 on the western side of the reef and (b) WP 1 on the eastern side. Shading is as in Fig. 11. Bold lines indicate profiles corresponding to times when isopycnals were observed to deepen rapidly on either side of the reef (group 8 at WP2, group 6 at WP1). These time periods also correspond to shear-induced instabilities detected in echo intensity, as highlighted by the black box in Fig. 8.

to currents directed down the respective side of the reef (Fig. 12). At WP1, on the eastern side of the reef, a pronounced (>10 m) depression of isopycnals occurred during group 6 as the flow was briefly (~2 h) directed off the reef to the east (Fig. 12d). At WP2 on the western side of the reef, isopycnals similarly descended >10 m over less than 2 h between groups 7 and 8 when the currents reversed from eastward (up-slope) during the preceding groups to westward (down-slope; Fig. 12c). Thus isopycnals were depressed in the lee of the reef when defined by the orientation of the current but, following relaxation or reversal of that current, returned and even overshot by a considerable distance their initial depth. During the same period, baroclinic velocities in the upper and lower layers increased in magnitude on both sides of the reef but were orientated in opposite directions, indicating the generation of significant shear (Fig. 8). Note that black horizontal lines in Fig. 12c and d indicate the velocity measured at the end of the cross-reef section; velocities over the bank itself were significantly greater by up to a factor of 2 (Fig. S6a).

Vertical profiles of *Ri* provide strong evidence for the criticality of the flow to shear instability and thus the generation of turbulence at the times when the lee waves were observed on both sides of the reef (Fig. 13). CTD data were collected at both WP 1 and 2 throughout transect groups 5–8. These data show that *Ri* was typically <1, indicating marginal stability. However, during group 8 at WP 2 on the western side of the reef (Fig. 13a) and during group 6 at WP 1 on the eastern side (Fig. 13b); $Ri < 0.25$ throughout the water column indicating widespread shear instability. These times of minimum *Ri* correspond exactly to the period during which isopycnals were rapidly depressed on either side of the reef (Fig. 12c and d) and represent the minimum values of *Ri* observed throughout the survey. At WP 2 at the western side of the reef, *Ri* decreased continuously from group 5 until group 8 (Fig. 13a) as the lee wave was formed (Fig. 12c). Similarly at WP 1 to the east of the reef, *Ri* increased following group 6 (Fig. 13b) as the lee wave passed (Fig. 12d).

Cross-reef currents, estimated as *U*, were maximal at WP1 during group 6 and directed to the east (velocity vectors in Fig. 12c and d), thereby constituting a down-slope flow. Previous observations over isolated sills and ledges have demonstrated the generation of lee waves and, under strong flows, hydraulically supercritical conditions (e.g. Klymak and Gregg, 2004; McCabe et al., 2006). Having potentially identified hydraulic jumps occurring at the site, we estimated the composite internal Froude number in order to assess the extent to which the flow at the reef was hydraulically controlled over the slopes to the east and west sides. Froude number was estimated as:

$$G^2 = F_1^2 + F_2^2$$

where $F^2_i = u^2_i / g' h_i$ are the internal Froude for each layer, $i = 1$ and 2, corresponding to the upper and lower layer respectively and $g' = \Delta\rho/\rho$ is the reduced gravitational acceleration(Armi, 1986). The interface between the two layers is defined by the position of the 1026.55 kg m^{-3} isopycnal. For $G^2 > 1$ the flow is supercritical and kinetic energy dominates the flow such that waves cannot propagate away, whereas for $G^2 < 1$, potential energy dominates and waves can propagate in any direction. For a given layer, supercritical flows ($F > 1$) tend to be fast and shallow, whereas subcritical flows ($F < 1$) are usually slower and deeper. When the flow changes between supercritical and subcritical regimes (e.g. when tidal currents change or flow interacts with local topography), a hydraulic jump can occur (Farmer and Armi, 1999). This is characterised by a sudden change in the layer depth and associated changes from potential to kinetic energy, usually accompanied by shear instability (Lawrence, 1990) and turbulent mixing (Moum and Nash, 2000).

Flow became supercritical (hydraulically controlled) at WP 1 at precisely the time that the depression of isopycnals was observed (G6-7, Fig. 12b and d). As the flow was previously subcritical (i.e. $G^2 < 1$) during transect groups 4 and 5, the transition to supercritical conditions is likely to have occurred in the form of a hydraulic jump as the current was briefly reversed to a downslope direction (see velocity vectors in Fig. 12d). The upper layer appears to exert the dominant hydraulic control with the corresponding Froude number, *F*, always larger than the lower layer *F*; which reached supercritical values only during groups 3 and 8 at WP 1 (Fig. 12b, black line). The rationale for the upper layer control is clear when considering the current magnitude; velocities are intensified at the surface and decrease towards the bed (as indicated by velocity vectors in Fig. 6 and 12c and d) in much the same way as depicted in Cummins et al. (2006). At WP 2 (on the western side of the reef) the lower layer *F* remains subcritical throughout the survey, but the upper layer flow becomes supercritical between groups 6 and

7 (Fig. 12a), approximately 1.5 h before the isopycnal depression occurs (Fig. 12c). Note that at WP2 the isopycnals deepened at the same time as the current reversed to a downslope orientation (at ~HW +2; see velocity vectors for G6-7 in Fig. 12c). The flow around the reef thus appears to be hydraulically controlled and transitions from sub- to supercritical as it reverses to a downslope orientation on either side of the reef. The depression of isopycnals occurs at both WP 1 and 2 during tidal flows associated with low sightings (G5 & 6, Fig. 12c and d). However the subsequent recovery of the isopycnals, associated with maximum baroclinic velocities (Fig. 8), flow reversal and release of a lee wave, occurred during the tidal period with greatest porpoise sighting rates. This is particularly evident at WP1 on the eastern side of the reef, where greatest porpoise densities were recorded (Figs. 12b and d, 2).

Summary of the fine scale spatial distribution of porpoise sightings in relation to hydrodynamic features

Our findings show that porpoise sightings were clustered (Fig. 2), with greatest numbers observed in parts of study area with a south-westerly aspect, combined with moderate depth and steep topography (Fig. 3). The sighting rates were highest during periods of westward tidal flow, peaking during the strongest westward flows between approximately 2 and 6 h after HW (Figs. 5 and 7). This period of the tidal cycle is represented during groups G7 and G8 of the oceanographic survey, and was characterised by cooler (denser) water moving through the survey area and a drop in fluorescence (Fig. 9). Intriguingly, we recorded development of layered flows and water column instabilities within the area of highest porpoise sighting density (legs 3 and 4 of the ADCP transect, Fig. 1) during G7 and G8 of the oceanographic survey. The specific hydrodynamic features identified in the physical data include:

(1) Layered flow (e.g. between HW +3.5 and LW: see profiles G7 and G8 in Fig. 7a, and G8 in Fig. 7b) likely to be created by tidal-topographic interactions at the steeply sloping reef edge (velocity vectors in Fig. 6) and driven by baroclinic currents (Fig. 8).
(2) The layered flows described above were associated with mid-depth shear boundaries, for example the line of lighter colouring at mid-depth along legs 3 and 4 in Fig 6.
(3) Mid-depth shear induced instability is further evidenced during G7 and G8 by the 'billows' in the echo intensity along leg 4 of the ADCP transect (Fig. 10), and low Richardson numbers recorded at WP5 (located at the southern end of leg 4, within the core porpoise sightings area; Fig. 11). These features suggest susceptibility to shear-induced turbulence during the periods of the tidal cycle characterised by strong westward flows, when highest sighting rates were recorded throughout the visual survey.
(4) Peak sightings are closely related to the timing of hydraulically critical conditions on either side of the reef and the generation of lee waves. The waves are initially formed by the down-slope flow and then subsequently radiate away from the reef as the current reverses to an up-slope orientation. On the eastern side of the reef (at WP 1 in the core sightings area), the hydraulic jump occurs on the eastward flow, evidenced by the transition from sub- to super-critical flow during the down-slope current (Fig. 12b). The hydraulically controlled flow is associated with a depression of the isopycnals (G5-6, Fig. 12d) during the period of lowest sighting rates recorded on the eastward flood tide (~HW −1 to HW +1, Fig. 5). The isopycnals on the eastern side of the reef were subsequently released as the tide turned back westwards (i.e. up-slope; G7-8, Fig. 12b and d). This timing corresponds to the tidal flows associated with the greatest porpoise sightings (~HW +2 to LW, Fig. 5). We propose the return of the isopycnals represents the release of the lee wave at the eastern side of the reef as the flow returned to an up-slope direction.

Discussion

This study is the first to examine fine-scale (up to ~600 m) habitat associations of harbour porpoises with reference to quantitative high-resolution hydrodynamic data (1-m vertical resolution and 2-s ensemble interval) collected within an identified hotspot for the species. Harbour porpoise sightings recorded at the Runnelstone Reef during this study were not distributed uniformly across the survey area (Fig. 2). Higher relative densities were associated with moderate depths and steeply sloping topography, in particular around the southeastern reef margins (Fig. 3). The importance of this part of the survey area has also been identified in boat-based studies (Fig. S3), and in passive acoustic data collected at three sites within the survey area using CPODs deployed during the 2010 survey season (Jones, 2012). We have linked the fine-scale spatio-temporal variability in porpoise surface sightings to hydrodynamic features associated with predictable tidal timescales. These include tidal flow velocity (Figs. 7 and 8), shear (Fig. 6), shear-induced instabilities (Figs. 10, 11 and 13) and changes in water column properties (Figs. 9 and 12).

Our results provide insights into the fine-scale functional mechanisms driving the physical habitat associations that are often reported in broader extent and coarser scale studies on this species. Previous studies have identified links between porpoise sightings and areas of specific physical habitat, such as moderate depth (Northridge et al., 1995; Goodwin and Speedie, 2008; Marubini et al., 2009), high slope (Pierpoint, 2008; Booth et al., 2013) and tidal variables (Johnston et al., 2005; Embling et al., 2010; Isojunno et al., 2012). However, the physical variables identified in these studies are generally recognised as proxies for underlying drivers (e.g. Isojunno et al., 2012; Booth et al., 2013) and few studies have been able to provide quantitative data on the potential physical mechanisms at the root of these habitat associations (De Boer et al., 2014).

We have demonstrated that the current regime at the Runnelstone Reef was sufficient to generate hydraulic jumps during across-reef flows. Specifically there was transition from subcritical to supercritical hydraulic flow at the eastern side of the reef, just prior to the time of maximum sightings which was associated with the subsequent development of a lee wave as the flow reversed up-slope (westwards). Estimates of the Richardson number from WP1 (at the east side of the reef) confirm that the water column was highly susceptible to shear instability during the periods of upper layer supercritical flow, experienced at times of the tidal cycle associated with greatest numbers of sightings. Our results suggest that the high numbers of porpoises sighted during westward flows were exploiting periods during which lee waves were formed along the sloping margins of the Runnelstone Reef, and that these aspects of the flow field arose as a result of the influence of bathymetric features on the tidal currents (tidal-topographic interaction); leading to baroclinic flow, hydraulic jumps and lee waves.

Given the oscillatory nature of the flow and the wide range of current speeds and stratification experienced at the site, we consider that the flow field is most likely to generate all of the above hydrodynamic features, depending primarily on the strength of the currents. The regime appears to be similar to that depicted in Nash and Moum (2001, their Fig. 5), for which hydraulic jumps and lee waves form on the downstream side of the ridge and low Richardson number shear instabilities form over the ridge due to the highly sheared currents. Our observations, taken from a single

tidal cycle in the middle of the spring-neap phase, suggest that lee waves are a common feature at the reef and lead to enhanced shear and associated turbulent mixing. Pronounced curvature in the flow field offshore of the reef further indicates an increase in vorticity and likely flow separation, which other studies have shown will produce a lee eddy on the downstream side of the headland. The definitive link between these well-defined processes and the porpoise activity requires further targeted research but the timing of the hydrodynamic processes and porpoise sightings appears not to be coincidental.

We only recorded the simultaneous velocity and CTD measurements required for the computation of Froude number (F) on either side of the Runnelstone Reef (at WP1 and 2 on the east and west sides respectively). Velocities over the shallower reef top are much higher (Fig. S6) and as a result we would expect significantly higher values of F in these areas, where turbulence generation is more pronounced (Fig. 6, leg 1). Therefore, the values of F we present can be considered a lower limit.

We expect that the localised oceanographic features identified in our study area lead to improved foraging opportunities for prey fish, and subsequently porpoises, at specific areas within the Runnelstone Reef survey site at temporal scales of hours to days. Johnston and Read (2007) identified meso-scale bio-physical links between porpoises and hydrodynamics in the Bay of Fundy, where the evolution of tidally induced vertical shear boundaries around small eddies created by an island wake was associated with high concentrations of sound-scatterers (zooplankton and fish). They thus provide direct evidence for increased porpoise foraging opportunities associated with shear; however it should be noted that their study was over a larger spatial scale than our study; and different physical processes, such as secondary flows, may have influenced their findings (Johnston and Read, 2007). The small scale of Runnelstone Reef compared to the Bay of Fundy, and the short (tidal) timescales of variability in the current field suggest that the influence of the topography may be more relevant to prey availability rather than prey abundance (Embling et al., 2013; Thorne and Read, 2013). Such a distinction may also explain why the highest sightings were made at a time during the oceanographic survey when chlorophyll reached minimum values (Fig. 9), thereby suggesting that the factors other than the abundance of phytoplankton are important in driving porpoise foraging distribution at the site.

How higher predators key into prey aggregations is not well understood but is assumed to be associated with maximising foraging efficiency as described by Houghton et al. (2006) and Sims et al. (2008). It has also been noted that the distribution of top predators at a fine-scale may be more influenced by the predictability or energy value of prey, rather than prey abundance *per se* (Grémillet et al., 2008; Benoit-Bird et al., 2013), and that memory of profitable areas can also play an important role in deterministic selection of foraging habitat (Nabe-Nielsen et al., 2013; Regular et al., 2013).

Recent studies by Scott et al. (2010, 2013) and Embling et al. (2012, 2013) have attempted to elucidate the biophysical links between current flow and marine species distribution at a small-scale in shelf seas. Their studies provide empirical evidence of links between tidal forcing, chlorophyll, fish and seabirds. Specifically, Embling et al. (2013) studied fish behaviour in response to hydrodynamics at Jones Bank in the Celtic Sea. They found that internal waves created during hydraulically controlled flows over the shallow sea bank (see also Palmer et al., 2013) acted to concentrate both zooplankton and zooplanktivorous fish close to the surface. Similar results were also reported in Embling et al. (2012). Such biophysical links may also be acting within our study area, leading to prey fish aggregation and favourable foraging conditions for porpoises.

The spatial and temporal consistency of the flow features identified in the ADCP survey, as well as the causative biophysical links between them and the distribution of porpoises, require further investigation. A repeated ADCP survey over the transect route, carried out at a variety of periods within the spring-neap cycle, would provide more robust characterisation of tidal-topographically controlled hydrodynamics at the site. Collection of bio-acoustic data, using hydroacoustic tools such as the EK60 echosounder, along with collection of plankton samples during the ADCP transect would add valuable direct biological evidence of spatial and/or temporal concentration of prey at the survey site, which is missing from this analysis.

The links that we have identified between fine-scale porpoise distribution and ephemeral, but predictable, tidal-topographic flow features are likely to be overlooked in studies covering a larger area and with less intensive temporal survey coverage (Wiens, 1989; Isojunno et al., 2012). However, the results must be taken in the context of the limited spatial and temporal coverage of the visual survey data. In addition, as with all visual survey data, the distribution of surface sightings of porpoises is assumed to be representative of habitat usage throughout the water column.

Conservation applications

UK waters are home to a significant number of Europe's harbour porpoises (Hammond et al., 1995, 2002; Hammond, 2006), but there is currently only a single SAC in UK waters where the species is identified as a 'qualifying feature' (N.I.E.A., 2010, 2011). The guidelines for site selection of proposed porpoise SACs state that the area should contain key sites that are used regularly by high numbers of the species, and they "must be clearly identifiable areas representing the physical and biological factors essential to the species' life and reproduction" (Article 4 of the Council Directive 92/43/EEC). In order for these sites to be identified, the species' interactions with their physical and biological environment must be better understood. Our research, and other recent studies, indicate that there are complex interactions between static and dynamic environmental variables in the marine environment, and that sole reliance on static physical features for the identification of key habitats may not accurately capture the complexities of the biophysical interactions involved in habitat selection (e.g. Johnston et al., 2005; Scott et al., 2010, 2013; Embling et al., 2012; Isojunno et al., 2012; Embling et al., 2013; Thorne and Read, 2013; De Boer et al., 2014). In addition, information on the interaction of porpoises with fine-scale flow features is necessary in order to understand the possible effects of the installation of tidal turbines or wave energy arrays, which may have the potential to exclude porpoises from areas of key foraging habitat in tidally dynamic areas, or alter localised flows (Dolman and Simmonds, 2010; Simmonds and Brown, 2010; Shields et al., 2011).

Conclusion

In line with our stated aims, the data presented in this study build upon the limited research into the underlying biophysical drivers of fine-scale porpoise distribution within a known hotspot. We provide new insights into specific hydrodynamic features, produced through tidal forcing, that may be important for creating foraging opportunities at a local scale. These spatially and temporally predictable dynamic habitats are likely to be especially important for porpoises due to their small size, high metabolism and requirement for regular feeding. Although aspects of the fine-scale biophysical interactions between harbour porpoises and their immediate environment remain unanswered, this study represents an increase in knowledge, and highlights the complexities of the relationship between the animals and their physical habitat.

Increasing our understanding of habitat associations and, perhaps more importantly, the mechanistic links between oceanographic variables and top predator distribution, is a key research area within the context of vulnerable marine species protection. Description of fine-scale species distributions can provide important information on key habitats, trends in variation of habitat use, and animal-environment interactions, which give insight into potential drivers of distribution. In addition, our research highlights the value of visual monitoring at key hotspot locations where regular boat-based transect surveys are excluded by conditions, other users of the sea, or prohibitive costs. It is hoped that the data presented here will help to direct future multidisciplinary research, focussed on the fine-scale biophysical drivers of marine vertebrate distribution within hotspot areas, in order to better understand why these particular sites prove especially attractive.

Acknowledgments

This research was funded by a NERC PhD studentship to A. Jones, with CASE support from the Sir Alister Hardy Foundation of Ocean Science (SAHFOS). Additional funding was received from MAREMAP (the Marine Environmental Mapping Programme). The Total Foundation provided funding for the oceanographic survey, which was undertaken with the support of the crew of the *RV Callista*, S. Ingram, L. Suberg and T. Horton. We thank all funders and volunteers of the SeaWatch SW wildlife-monitoring project, in particular assistant co-ordinator John Swann. Thanks also to Duncan and Hannah Jones of Marine Discovery Penzance for kindly providing the boat-based survey data. Thanks to the Channel Coastal Observatory, Plymouth Coastal Observatory, National Coastwatch Institute, UK Hydrographic Office and National Oceanography Centre Liverpool for providing covariate data. Thanks to Ted and John Chappell for sharing their knowledge of local fine-scale tidal dynamics in the study area; and to the two anonymous reviewers whose comments greatly improved the manuscript.

Appendix A. Supplementary material

Supplementary data associated with this article can be found, in the online version, at http://dx.doi.org/10.1016/j.pocean.2014.08.002.

References

Armi, L., 1986. The hydraulics of two flowing layers with different densities. Journal of Fluid Mechanics 163, 27–58.
Baddeley, A., Turner, R., 2005. Spatstat: an R package for analyzing spatial point patterns. Journal of Statistical Software 12, 1548–7760.
Benoit-Bird, K.J., Battaile, B.C., Heppell, S.A., Hoover, B., Irons, D., Jones, N., Kuletz, K.J., Nordstrom, C.A., Paredes, R., Suryan, R.M., Waluk, C.M., Trites, A.W., 2013. Prey patch patterns predict habitat use by top marine predators with diverse foraging strategies. PLoS ONE 8.
Bertrand, A., Gerlotto, F., Bertrand, S., Gutiérrez, M., Alza, L., Chipollini, A., Díaz, E., Espinoza, P., Ledesma, J., Quesquén, R., Peraltilla, S., Chavez, F., 2008. Schooling behaviour and environmental forcing in relation to anchoveta distribution: an analysis across multiple spatial scales. Progress in Oceanography 79, 264–277.
Beyer, H., 2012. Geospatial Modelling Environment (version 0.6.0.0). Spatial Ecology LLC.
Booth, C.G., Embling, C., Gordon, J., Calderan, S.V., Hammond, P.S., 2013. Habitat preferences and distribution of the harbour porpoise *Phocoena phocoena* west of Scotland. Marine Ecology Progress Series 478, 273–285.
Börger, L., Franconi, N., De Michele, G., Gantz, A., Meschi, F., Manica, A., Lovari, S., Coulson, T.I.M., 2006. Effects of sampling regime on the mean and variance of home range size estimates. Journal of Animal Ecology 75, 1393–1405.
Bowman, A.W., Azzalini, A., 2010. R package 'sm': nonparametric smoothing methods (version 2.2-4).
Brereton, T., MacLeod, C.D., Wall, D., MacLeod, K., Cermeno, P., Curtis, D., Zanderink, F., Benson, C., Osinga, N., Martin, C., Pinn, E., 2007. Monitoring Cetaceans in UK and Adjacent Waters: Current and Potential Uses of Atlantic Research Coalition (ARC) Data. Atlantic Research Coalition.
Brodie, P.F., 1995. The Bay of Fundy/Gulf of Maine harbour porpoise (Phocoena phocoena): some considerations regarding species interactions, energetics density dependence and by-catch. In: Bjorge, A., Donovan, G.P. (Eds.), Special Issue, 16: Biology of Phocoenids. International Whaling Commission, Cambridge, pp. 181–187.
Buckland, S.T., Anderson, D.R., Burnham, K.P., Laake, J.L., Borchers, D.L., Thomas, L., 2001. Introduction to Distance Sampling: Estimating Abundance of Biological Populations. Oxford University Press, Oxford, UK.
Buckland, S.T., Anderson, D.R., Burnham, K.P., Laake, J.L., Borchers, D.L., Thomas, L., 2004. Advanced Distance Sampling. Oxford University Press, Oxford, UK.
Buckland, S.T., Marsden, S.J., Green, R.E., 2008. Estimating bird abundance: making methods work. Bird Conservation International 18, S91–S108.
Burnham, K.P., Andersen, D.R., 2002. Model Selection and Multimodel Inference. A Practical Information-theoretic Approach. Springer-Verlag, New York.
Cummins, P.F., Armi, L., Vagle, S., 2006. Upstream internal hydraulic jumps. Journal of Physical Oceanography 36, 753–769.
De Boer, M.N., Saulino, J.T., 2008. Winter distribution and density of small cetaceans in the inshore fishing grounds off southwest England. Annual Conference of the European Cetacean Society. Egmond aan Zee, The Netherlands, pp. 229 (Abstract S-206).
De Boer, M.N., Simmonds, M.P., Reijnders, P.J.H., Aarts, G., 2014. The influence of topographic and dynamic cyclic variables on the distribution of small cetaceans in a shallow coastal system. PLoS ONE 9, e86331.
Development Core Team, R., 2011. R: A Language and Environment for Statistical Computing. R Foundation for Statistical Computing, Vienna, Austria.
Dolman, S., Simmonds, M., 2010. Towards best environmental practice for cetacean conservation in developing Scotland's marine renewable energy. Marine Policy 34, 1021–1027.
Embling, C.B., Gillibrand, P.A., Gordon, J., Shrimpton, J., Stevick, P.T., Hammond, P.S., 2010. Using habitat models to identify suitable sites for marine protected areas for harbour porpoises (Phocoena phocoena). Biological Conservation 143, 267–279.
Embling, C.B., Illian, J., Armstrong, E., van der Kooij, J., Sharples, J., Camphuysen, C.J., Scott, B.E., 2012. Investigating fine-scale spatio-temporal predator-pey patterns in dynamic marine ecosystems: a functional data analysis approach. Journal of Applied Ecology 49, 481–492.
Embling, C.B., Sharples, J., Armstrong, E., Palmer, M.R., Scott, B.E., 2013. Fish behaviour in response to tidal variability and internal waves over a shelf sea bank. Progress in Oceanography.
Evans, P., Anderwald, P., Baines, M.E., 2003. UK Cetacean Status Review. Report to English Nature and Countryside Council for Wales. Oxford: Seawatch Foundation, p. 160.
Farmer, D.M., Armi, L., 1999. Stratified flow over topography: the role of small scale entrainment and mixing in flow reestablishment. Proceedings of the Royal Society of London, Series A 455, 3221–3258.
Fauchald, P., Erikstad, K.E., 2002. Scale-dependent predator-prey interactions: the aggregative response of seabirds to prey under variable prey abundance and patchiness. Marine Ecology Progress Series 231, 279–291.
Geyer, W.R., 1993. Three-dimensional tidal flow around headlands. Journal of Geophysical Research: Oceans 98, 955–966.
Goodwin, L., Speedie, C., 2008. Relative abundance, density and distribution of the harbour porpoise (Phocoena phocoena) along the west coast of the UK. Journal of the Marine Biological Association of the United Kingdom 88, 1221–1228.
Grémillet, D., Lewis, S., Drapeau, L., Van Der Lingen, C.D., Huggett, J.A., Coetzee, J.C., Verheye, H.M., Daunt, F., Wanless, S., Ryan, P.G., 2008. Spatial match–mismatch in the Benguela upwelling zone: should we expect chlorophyll and sea-surface temperature to predict marine predator distributions? Journal of Applied Ecology 45, 610–621.
Hammond, P., 2006. Small Cetaceans in the European Atlantic and North Sea. In P. Hammond (Ed.), LIFE Project. St. Andrews: Sea Mammal Research Unit, University of St. Andrews, p. 55.
Hammond, P.S., Benke, H., Berggren, P., Borchers, P., Buckland, S.T., Collet, A., Heide-Jorgensen, M.P., Heimlich-Boran, S., Hiby, A.R., Leopold, M.F., Oien, N., 1995. Distribution and Abundance of the Harbour Porpoise and Other Small Cetaceans in the North Sea and Adjacent Waters. SCANS, p. 240.
Hammond, P.S., Berggren, P., Benke, H., Borchers, D.L., Collet, A., Heide-Jorgensen, M.P., Heimlich, S., Hiby, A.R., Leopold, M.F., Oien, N., 2002. Abundance of harbour porpoise and other cetaceans in the North Sea and adjacent waters. Journal of Applied Ecology 39, 361–376.
Hammond, P.S., Macleod, K., Berggren, P., Borchers, D.L., Burt, L., Cañadas, A., Desportes, G.V., Donovan, G.P., Gilles, A., Gillespie, D., Gordon, J., Hiby, L., Kuklik, I., Leaper, R., Lehnert, K., Leopold, M., Lovell, P., Øien, N., Paxton, C.G.M., Ridoux, V., Rogan, E., Samarra, F., Scheidat, M., Sequeira, M., Siebert, U., Skov, H., Swift, R., Tasker, M.L., Teilmann, J., Van Canneyt, O., VÁzquez, J.A., 2013. Cetacean abundance and distribution in European Atlantic shelf waters to inform conservation and management. Biological Conservation 164, 107–122.
Hastie, T.J., Tibshirani, R.J., 1990. Generalised Additive Models. Chapman and Hall/CRC, New York.
Herr, H., Fock, H.O., Siebert, U., 2009. Spatio-temporal associations between harbour porpoise Phocoena phocoena and specific fisheries in the German Bight. Biological Conservation 142, 2962–2972.
Houghton, J.D.R., Doyle, T.K., Wilson, M.W., Davenport, J., Hays, G.C., 2006. Jellyfish aggregations and leatherback turtle foraging patterns in a temperate coastal environment. Ecology 87, 1967–1972.
Hunt, J.C.R., Snyder, W.H., 1980. Experiments on stably and neutrally stratified flow over a model three-dimensional hill. Journal of Fluid Mechanics 96, 671–704.

Isojunno, S., Matthiopoulos, J., Evans, P.G.H., 2012. Harbour porpoise habitat preferences: robust spatio-temporal inferences from opportunistic data. Marine Ecology Progress Series 448, 155–170.
Johnston, D.W., Read, A.J., 2007. Flow-field observations of a tidally driven island wake used by marine mammals in the Bay of Fundy, Canada. Fisheries Oceanography 16, 422–435.
Johnston, D.W., Westgate, A.J., Read, A.J., 2005. Effects of fine-scale oceanographic features on the distribution and movements of harbour porpoises Phocoena phocoena in the Bay of Fundy. Marine Ecology-Progress Series 295, 279–293.
Jones, A., 2012. PhD Thesis: The spatio-temporal distribution and habitat associations of marine mega-vertebrates off southwest UK. Faculty of Natural and Earth Sciences, Ocean and Earth Science. Southampton: University of Southampton, p. 329.
Kai, E.T., Rossi, V., Sudre, J., Weimerskirch, H., Lopez, C., Hernandez-Garcia, E., Marsac, F., Garcon, V., 2009. Top marine predators track Lagrangian coherent structures. Proceedings of the National Academy of Sciences of the United States of America 106, 8245–8250.
Klymak, J.M., Gregg, M.C., 2004. Tidally generated turbulence over the knight inlet sill. Journal of Physical Oceanography 34, 1135–1151.
Koopman, H., 1998. Topographical distribution of the blubber of harbour porpoises (*Phocoena phocoena*). Journal of Mammology 79, 260–270.
Lawrence, G.A., 1990. On the hydraulics of Boussinesq and non-Boussinesq two-layered flows. Journal of Fluid Mechanics 215, 457–480.
Leeney, R.H., Amies, R., Broderick, A.C., Witt, M.J., Loveridge, J., Doyle, J., Godley, B.J., 2008. Spatio-temporal analysis of cetacean strandings and bycatch in a UK fisheries hotspot. Biodiversity and Conservation 17, 2323–2338.
Legendre, P., Legendre, L., 2012. Numerical Ecology. Elsevier.
Lockyer, C., 2007. All creatures great and smaller: a study in cetacean life history energetics. Journal of the Marine Biological Association of the UK 87, 1035–1045.
Lueck, R.G., Lu, Y., 1997. The logarithmic layer in a tidal channel. Continental Shelf Research 17, 1785–1801.
Marubini, F., Gimona, A., Evans, P.G.H., Wright, P.J., Pierce, G.J., 2009. Habitat preferences and interannual variability in occurrence of the harbour porpoise Phocoena phocoena off northwest Scotland. Marine Ecology-Progress Series 381, 297–310.
McCabe, R.M., MacCready, P., Pawlak, G., 2006. Form drag due to flow separation at a Headland. Journal of Physical Oceanography 36, 2136–2152.
Mikkelsen, L., Mouritsen, K.N., Dahl, K., Teilmann, J., Tougaard, J., 2013. Re-established stony reef attracts harbour porpoises Phocoena phocoena. Marine Ecology-Progress Series 481, 239–248.
Miles, J., 1961. On the stability of heterogeneous shear flows. Journal of Fluid Mechanics 104.
Moum, J.N., Nash, J.D., 2000. Topographically-induced drag and mixing at a small bank on the continental shelf. Journal of Physical Oceanography 30, 2049–2054.
Myers, N., 1990. The biodiversity challenge: expanded hotspots analysis. Environmentalist 8, 1–20.
N.I.E.A., 2010. Inshore Special Area of Conservation: Skerries and Causeway SAC Selection Assesment. Belfast, NI: Northern Ireland Environment Agency, p. 38.
N.I.E.A., 2011. Inshore Special Area of Conservation: Skerries and Causeway Conservation Objectives and Advice on Operations. Northern Ireland Environment Agency, p. 18.
Nabe-Nielsen, J., Tougaard, J., Teilmann, J., Lucke, K., Forchhammer, M.C., 2013. How a simple adaptive foraging strategy can lead to emergent home ranges and increased food intake. Oikos.
Nash, J.D., Moum, J.N., 2001. Internal hydraulic flows on the continental shelf: high drag states over a small bank. Journal of Geophysical Research: Oceans 106, 4593–4611.
Nichols, J.D., Hines, J.E., Sauer, J.R., Fallon, F.W., Fallon, J.E., Heglund, P.J., 2000. A Double- observer approach for estimating detection probability and abundance from point counts. The Auk 117, 393–408.
Northridge, S.P., Tasker, M.L., Webb, A., Williams, J.M., 1995. Distribution and relative abundance of harbour porpoises (*Phocoena phocoena* L.), white beaked dolphins (Lagenorhynchus albirostris Gray) and minke whales (Balaenoptera acutorostrata Lacepede) around the British Isles. ICES Journal of Marine Science 52, 55–66.
Oksanen, J., Blanchet, F.G., Kindt, R., Legendre, P., Minchin, P.R., O'Hara, R.B., Simpson, G.L., Solymos, P., Stevens, M.H.H., Wagner, H., 2013. vegan: Community Ecology Package. R Package Version 2.0-7.
Palmer, M.R., Inall, M.E., Sharples, J., 2013. The physical oceanography of Jones Bank: a mixing hotspot in the Celtic Sea. Progress in Oceanography 117, 9–24.
Pierpoint, C., 2008. Harbour porpoise (Phocoena phocoena) foraging strategy at a high energy, near-shore site in south-west Wales, UK. Journal of the Marine Biological Association of the United Kingdom 88, 1167–1173.
Pikesley, S.K., Witt, M.J., Hardy, T., Loveridge, J., Loveridge, J., Williams, R., Godley, B.J., 2012. Cetacean sightings and strandings: evidence for spatial and temporal trends? Journal of the Marine Biological Association of the UK 92, 33.
Powell, R.A., 2000. Animal Home Ranges and Territories and Home Range Estimators. In: Boitani, L., Fuller, T.K. (Eds.), Research Techniques in Animal Ecology. Columbia University Press, New York, pp. 65–110.
Proctor, R., Bell, C., Eastwood, L., Holt, J.T., Prandle, D., Young, E.F., 2004. UK Marine Renewable Energy Atlas: Phase 2 - POL contribution. Proudman Oceanographic Laboratory, Internal Document, No 163, 26 p.
Read, A.J., Westgate, A.J., 1997. Monitoring the movements of harbour porpoises (*Phocoena phocoena*) with satellite telemetry. Marine Biology 130, 315–322.
Regular, P.M., Hedd, A., Montevecchi, W.A., 2013. Must marine predators always follow scaling laws? Memory guides the foraging decisions of a pursuit-diving seabird. Animal Behaviour 86, 545–552.
Reid, J.B., Evans, P.G.H., Northridge, S.P., 2003. Atlas of Cetacean Distribution in North-west European Waters. Peterborough: JNCC, p. 75.
Roughan, M., Mace, A.J., Largier, J.L., Morgan, S.G., Fisher, J.L., Carter, M.L., 2005. Subsurface recirculation and larval retention in the lee of a small headland: a variation on the upwelling shadow theme. Journal of Geophysical Research: Oceans 110, C10027.
Russell, R.W., Hunt, G.L., Coyle, K.O., Cooney, R.T., 1992. Foraging in a fractal environment: spatial patterns in a marine predator-prey system. Landscape Ecology 7, 195–209.
Santos, M.B., Pierce, G.J., Learmonth, J.A., Reid, R.J., Ross, H.M., Patterson, I.A.P., Reid, D.G., Beare, D., 2004. Variability in the diet of harbor porpoises (Phocoena phocoena) in Scottish waters 1992–2003. Marine Mammal Science 20, 1–27.
Scott, B.E., Sharples, J., Ross, O.N., Wang, J., Pierce, G.J., Camphuysen, C.J., 2010. Sub-surface hotspots in shallow seas: fine-scale limited locations of top predator foraging habitat indicated by tidal mixing and sub-surface chlorophyll. Marine Ecology Progress Series 408, 207–226.
Scott, B.E., Webb, A., Palmer, M.R., Embling, C.B., Sharples, J., 2013. Fine scale bio-physical oceanographic characteristics predict the foraging occurrence of contrasting seabird species; Gannet (Morus bassanus) & Storm Petrel (Hydrobates pelagicus). Progress in Oceanography.
Shields, M.A., Woolf, D.K., Grist, E.P.M., Kerr, S.A., Jackson, A.C., Harris, R.E., Bell, M.C., Beharie, R., Want, A., Osalusi, E., Gibb, S.W., Side, J., 2011. Marine renewable energy: the ecological implications of altering the hydrodynamics of the marine environment. Ocean & Coastal Management 54, 2–9.
Simmonds, M.P., Brown, V.C., 2010. Is there a conflict between cetacean conservation and marine renewable-energy developments? Wildlife Research 37, 688–694.
Sims, D.W., 2003. Tractable models for testing theories about natural strategies: foraging behaviour and habitat selection of free-ranging sharks. Annual Symposium of the Fisheries-Society-of-the-British-Isles. Norwich, England, pp. 53–73.
Sims, D.W., Southall, E.J., Humphries, N.E., Hays, G.C., Bradshaw, C.J.A., Pitchford, J.W., James, A., Ahmed, M.Z., Brierley, A.S., Hindell, M.A., Morritt, D., Musyl, M.K., Righton, D., Shepard, E.L.C., Wearmouth, V.J., Wilson, R.P., Witt, M.J., Metcalfe, J.D., 2008. Scaling laws of marine predator search behaviour. Nature 451, pp. 1098–U1095.
Stephens, D.W., Krebs, J.R., 1986. Foraging Theory. Princeton University Press, Princeton, USA.
Sveegaard, S., 2011. Spatial and temporal distribution of harbour porpoises in relation to their prey. National Environment Research Institute (NERI) Department for Arctic Environment, Vol. PhD. Roskilde, Denmark: Aarhus University, p. 128.
Thorne, L.H., Read, A.J., 2013. Fine-scale biophysical interactions drive prey availability at a migratory stopover site for *Phalaropus* spp. in the Bay of Fundy, Canada. Marine Ecology Progress Series 2013, 261–273.
van Haren, H., 2009. Using high sampling-rate ADCP for observing vigorous processes above sloping [deep] ocean bottoms. Journal of Marine Systems 77, 418–427.
van Haren, H., Gostiaux, L., 2010. A deep-ocean Kelvin–Helmholtz billow train. Geophysical Research Letters 37, L03605.
Veness, C., 2012. Calculate Distance, Bearing and more Between Latitude/longitude Points, vol. 2012.
Watts, P., Gaskin, D.E., 1985. Habitat index analysis of the harbour porpoise (*Phocoena phocoena*) in the southern coastal Bay of Fundy, Canada. Journal of Mammology 66, 733–744.
Wiens, J.A., 1989. Spatial scaling in ecology. Functional Ecology 3, 385–397.
Witt, M.J., Sheehan, E.V., Bearhop, S., Broderick, A.C., Conley, D.C., Cotterell, S.P., Crow, E., Grecian, W.J., Halsband, C., Hodgson, D.J., Hosegood, P., Inger, R., Miller, P.I., Sims, D.W., Thompson, R.C., Vanstaen, K., Votier, S.C., Attrill, M.J., Godley, B.J., 2012. Assessing wave energy effects on biodiversity: the Wave Hub experience. Philosophical Transactions of the Royal Society A: Mathematical, Physical and Engineering Sciences 370, 502–529.
Wood, S.N., 2006. Generalised Additive Models: An Introduction with R. Chapman and Hall/CRC, Florida.
Zuur, A.F., Ieno, E.N., Smith, G.M., 2007. Analysing Ecological Data. Springer, New York, USA.
Zuur, A.F., Ieno, E.N., Walker, N.J., Saveliev, A.A., Smith, G.M., 2009. Mixed Effects Models and Extensions in Ecology with R. Springer, New York.

Appendix B Co-authored St Ives Bay project report delivered to NE, RSPB and CIFCA: Monitoring and mapping of seabirds and cetaceans in St Ives Bay, Cornwall, in winter 2012/13.

Year 1 SIB project report: Monitoring and mapping of seabirds and cetaceans in St Ives Bay, Cornwall, in winter 2012/13

Russell Wynn*, Sophia Butler-Cowdry and Andrew Colenutt

National Oceanography Centre, European Way, Southampton, SO14 3ZH
**Corresponding author email: rbw1@noc.ac.uk*

Cover image: Bottlenose Dolphins, Herring Gulls and fishing boat off St Ives Island (Photo: Russell Wynn)

Executive Summary

- In order to assess seabird distributions in St Ives Bay in mid-winter, a total of 107 hours of theodolite mapping data were successfully collected on 17 dates in Dec 2012 and Jan 2013, supported by visual monitoring data for the area between St Ives Island and Clodgy Point. No seabird or cetacean bycatch incidents were observed during the survey period, in contrast to widely reported incidents at this location in Jan 2012.

- The results of this pilot study support previous observations indicating that St Ives Bay is a regionally important foraging area for a variety of seabird species, with peak counts of 1000 Herring Gulls, 300 Razorbills/Guillemots, 300 Kittiwakes, 150 Gannets, 100 Shags, 16 Great Northern Divers and 15 Balearic Shearwaters. Two cetacean species (Bottlenose Dolphin and Harbour Porpoise) were also regularly recorded.

- The mapped theodolite data support field-based interpretations of foraging hotspots for seabirds and cetaceans which, within the bay, were focused on the visible tide race immediately north and northeast of St Ives Island, and the shallow, sandy, nearshore zone of the southern bay. It is notable that the majority of the flat central bay was not generally utilised by foraging seabirds.

- Balearic Shearwaters were recorded in small numbers within the study area on all but one of the survey dates, with a peak count of up to 15 on 13-14 Jan 2013. Outside of the effort-based survey, a count of 58 moving west passed St Ives Island on 30 Dec 2012 corresponded with 45 being seen in Carbis Bay, and equates to ~0.25% of the World population. This highlights the continuing importance of St Ives Bay for this species in mid-winter.

- These preliminary results provide a useful first snapshot of seabird and cetacean foraging distribution in winter 2012/13, but further work is required in subsequent winters to assess inter-annual variability in species composition, numbers and distributions. Nevertheless, the fixed bathymetric controls on megavertebrate distributions observed in this study are likely to persist between years and seasons.

1. Introduction

Commercial fisheries are a potential threat to seabirds feeding in the inshore waters of southwest UK, particularly through entanglement in fixed gear such as gillnets. Recent bycatch incidents involving tens to hundreds of auks in St Ives Bay and off Portland Bill have led to renewed interest in this issue, partly due to high-profile national media coverage (Fig. 1). However, before mitigation measures are developed or modified to tackle this problem, it is important to gather robust baseline data on seabird distributions in hotspot areas. These include both spatial distributions (where the birds are feeding), and temporal distributions (when they are feeding there). Land-based surveys can provide a cost-effective way of obtaining baseline data at key sites, and integration with environmental data, e.g. high-resolution seafloor maps, can aid interpretation of the processes controlling observed distributions.

Figure 1: Media coverage of seabird bycach incidents off southwest UK in 2012

In order to obtain improved information on distributions of feeding seabirds and cetaceans in St Ives Bay in winter, the National Oceanography Centre (NOC) initiated a land-based survey in partnership with CIFCA, Natural England, RSPB and Marinelife. This involved mapping of seabirds and cetaceans with a survey theodolite (which

provides accurate locations for seabirds and cetaceans at the sea surface) combined with visual mapping and counts of numbers of seabirds within St Ives Bay and along the adjacent coast (see Annex 1 for the original scope of work).

2. Study area

St Ives Bay (SIB; Figs 2 and 3) off northwest Cornwall is an important winter foraging area for a variety of seabirds, in particular Razorbills *Alca torda*, Guillemots *Uria aalge*, Gannets *Morus bassanus*, Kittiwakes *Rissa tridactyla* and large gulls (mostly Herring Gulls *Larus argentatus* and Great Black-backed Gulls *Larus marinus*, with smaller numbers of Lesser Black-backed Gulls *Larus fuscus*). In the last decade, there have also been increasing numbers of the Critically Endangered Balearic Shearwater *Puffinus mauretanicus* using SIB in the mid-winter period, with peak numbers of up to 100 birds recently recorded (equivalent to ~0.5% of the World population; Wynn, 2009; Paul St Pierre, *in litt*.). Recent studies have indicated that this species is shifting its inter-breeding range northwards (Wynn *et al*., 2007; Wynn and Yésou, 2007; Darlaston and Wynn, 2012), so numbers are likely to continue increasing in the future. However, records of all of these seabirds in SIB are sporadic and are typically based upon casual observations by ornithologists. Therefore, the spatial and temporal distribution of seabird foraging within SIB in the peak mid-winter period is poorly understood.

Figure 2: Location map of St Ives Bay with 1 km grid (from UK Ordnance Survey)

SIB is a crescentic embayment that is up to 6x3 km across (Fig. 2), with a mean spring tidal range of 5.8 m. High-resolution (metre-scale) multibeam bathymetry data for the SIB area were collected by the Maritime and Coastguard Agency as part of their Civil

Hydrography Programme (Fig. 3). These data were made available for this project via the Channel Coastal Observatory (CCO) as part of the UK MAREMAP partnership. Analysis of combined bathymetric and sedimentological data indicate that most of SIB is <15 m deep and is floored by smooth seabed with a layer of coarse shelly sand. The eastern and southern shore is gently sloping and sandy, whereas the western shore is steeper and rocky, with deeper water (>20 m) relatively close to shore (Fig. 3). Zones of tidal shear and enhanced turbulence are visible at surface off prominent headlands, e.g. St Ives Island, and around rock outcrops, e.g. northwest of Godrevy Island, at certain tidal states. Further offshore, north of SIB, the seabed is dominated by rock outcrops with a thin coarse sediment cover and scattered migrating bedforms (megaripples).

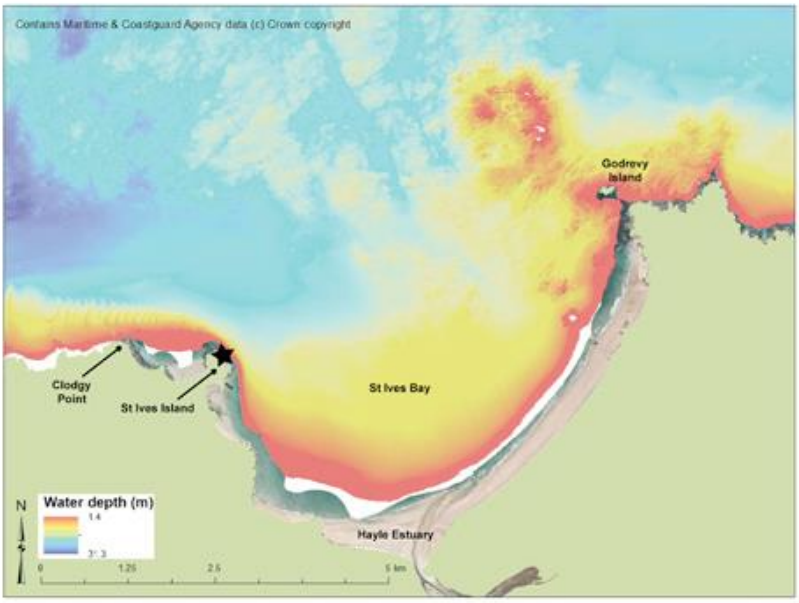

Figure 3: High-resolution multibeam bathymetry mapping of St Ives Bay. Note the presence of deep water close inshore to the St Ives Island watchpoint (marked with a black star), the shallow rocky reef and pinnacles northwest of Godrevy Island, the smooth shallow seafloor within SIB, and the migrating tidally generated sand waves northwest of St Ives Island.

3. Bycatch incidents in SIB and mitigation measures

Recent seabird bycatch incidents in the SIB area have highlighted this potential threat to wintering seabirds. For example, on 7 January 2012, approximately 100 seabirds (mostly auks) were discovered drowned in a net to the north of St Ives, while another 200 were found washed up on local beaches. This was one of several incidents that featured in national media (Fig. 1).

http://www.bbc.co.uk/news/uk-england-cornwall-16418261
http://www.bbc.co.uk/news/uk-england-cornwall-16469347
http://www.bbc.co.uk/news/uk-england-cornwall-16541924

The current St Ives Bay Gillnet Fishery byelaw, originally enacted in 1999, is triggered once more than 100 birds have been killed in nets, and results in a time-area restriction for the local gillnet fishery. The closure enforced by this byelaw is the only one of its kind in the country, and affects an arbitrarily defined area of the bay on the '*landward side of a line drawn between St Ives Head and the northern extremity of the Black Cliffs (east of Hayle Estuary)*' (see Figs. 2 and 3 for locations).

Under this byelaw, the bycatch incidents in January 2012 triggered a three-week fishing exclusion zone for gillnets between 5 and 26 January, backed up by fines of up to £50,000. Although this local byelaw does not provide a solution to the problem outside the geographical area that it covers, it is unique to the UK in terms of the type of event by which it is triggered (i.e. seabird fatalities due to fisheries' bycatch), as well as by the measures taken for its implementation (e.g. closures to certain fishing activity, and financial penalties for non-compliance). It should also be noted that a majority of local fishers using SIB have subsequently agreed to a Fishing Nets 'Code of Practice' whereby, even outside of the byelaw-affected closure areas, they would ensure their nets were not set during daylight hours and would aim to recover them by first light, when the birds start to feed on prey species adjacent to or within the nets.

4. SIB survey methods

Survey work was conducted from a single watchpoint, on a concrete platform immediately below the St Ives NCI (National Coastwatch Institution) station on St Ives Island (Figs 2 and 3). This watchpoint was selected due to its ease of access, option of shelter during harsh conditions, and because it provides an unobstructed view over the entirety of SIB. Precise GPS coordinates of the watchpoint were obtained from a differential GPS (courtesy of the CCO, Plymouth). The survey site is located 24.2 m above sea level at 05°28'31.64"W / 50°13'3.79"N.

The SIB study area, defined as the area within which marine life can be observed and recorded from the watchpoint, is approximately 35 km^2 in area. The main points of reference are 1) the Stones cardinal mark anchored to the NNE, approximately 6 km from the watchpoint, 2) Godrevy Lighthouse atop Godrevy Island, 6 km to the NE at 05°23'57.205"W / 50°14'30.691"N, and 3) Gwithian Beach and the Hayle Estuary, delimiting the eastern and southern extent of SIB, respectively (Figs 2 and 3).

Observations at SIB were carried out over two periods during winter 2012-2013. The first session, from 7-15 Dec 2012, comprised 46 hours of observation on eight dates. The second session, from 13-24 Jan, comprised 61 hours of observation on nine dates. In total, 107 hours of data were collected, split into 214 half-hour survey units. Data collection combined the use of theodolite mapping with conventional visual surveys, and was focused on seabird foraging aggregations (defined as a group of >5 birds of any one species actively feeding in close association in a concentrated area, which could vary depending on the number of birds present).

To detect foraging aggregations from shore, a team of three or more observers was equipped with 10x binoculars, 30x telescope and the 30x monocular of the theodolite (Leica FlexLine TS02 Total Station, Fig. 4).

Figure 4: Theodolite surveying at Gwenap Head, Cornwall (Photo: Russell Wynn)

The theodolite records positions to an angle measurement accuracy of 2 mgon (2 milligon = 0.0018°). The instrument tripod was set up each day directly over a known survey point measured using a differential GPS. Every hour, the 'horizontal' was zeroed and the theodolite 'level' checked. Half hourly measurements of tidal changes in the instrument's height above sea level were recorded. The target for the theodolite cross hairs was the waterline at the centre of the object, or centre of the feeding flock. Though the observation site facilitated a wide field of view (FoV) of the SIB study area, its relatively exposed location rendered it vulnerable to high winds and other extreme weather events (e.g. rain and sea fog). Fieldwork was therefore abandoned when conditions deteriorated and visibility decreased to <6 km (meaning the far side of SIB was not visible).

The scanning methodology is outlined below:

Scan at 00 and 30 minutes past each hour

1) Telescope scan from N around SIB to Carbis Bay, with horizon/shoreline at top of field of view.

2) Binocular scan from Carbis Bay back to N, with horizon/shoreline at top of field of view.

3) Binocular scan close inshore from N to S, followed by naked eye scan of shoreline.

Scan at 20 and 50 minutes past each hour

1) Telescope scan from Clodgy Point (to W) around to N with horizon at top of field of view.

2) Binocular scan from N to Clodgy Point with horizon at top of field of view.

3) Binocular scan close inshore from W to E.

Communication was maintained between observers at all times, and sightings were immediately fixed and recorded by the theodolite using the 'record' button. Positions of foraging seabirds and cetaceans were automatically date- and time-stamped, and saved to the instrument's on-board memory. For each sighting, the theodolite record number ('Point ID'), along with species composition and group size, were noted on standardised recording sheets, to be later incorporated into a database. Data on weather conditions and other environmental variables (e.g. sea state, wind vector/velocity, and cloud cover) were also collected every 30 minutes at the start of each scan, and recorded on the same record sheet. Scans resumed immediately after sightings were recorded to ensure consistent data collection and methodology.

Once scans of SIB had taken place, one observer would then scan from SIB headland out to the northwest and record any sightings using conventional visual monitoring techniques with binoculars and telescope, estimating range to the foraging aggregation and using a compass to measure bearing.

Positions of some permanent buoys and protruding topographic features were also recorded using the theodolite, so the survey methodologies (both visual and theodolite) could be calibrated against known positions and/or bathymetric features in GIS, to precisely quantify any errors in the acquired observation data.

5. SIB data analysis

Sightings data from the theodolite were uploaded onto a computer using the manufacturer's software, FlexOffice, version 2.0 (Leica Geosystems). Data were then downloaded from the program and saved as a spreadsheet via an ASCII format file that had been expressly written to extract the desired information (namely: Point ID, date, time, and the vertical and horizontal angles). Visual observation data were added to a database and merged with the corresponding Point ID data from the theodolite. Using a series of trigonometric formula in MS Excel (taking into account the curvature of the Earth, varying height of the instrument due to daily set-up and half-hourly tide changes, and the GPS locations of both the observation site and the reference point on which the horizontal angle was zeroed), the angles were converted into Eastings and Northings, so that each sighting could be assigned a set of coordinates. These data were then processed into a format compatible for loading into a GIS using ArcGIS® software, version 10.0 (ESRI, 2012). A fine-scale bathymetry layer of SIB at 1.0 m resolution is used as the base layer in all distribution maps (Fig. 3).

6. Results

A number of seabird species were recorded in aggregations within the survey area (>5 birds, mostly foraging but occasionally roosting/resting), some in regionally significant numbers (Table 1).

Species	Scientific name	Peak count
Balearic Shearwater	*Puffinus mauretanicus*	15 (14/01/13)
Northern Gannet	*Morus bassanus*	150 (13/01/13)
European Shag	*Phalacrocorax aristotelis*	100 (14/12/12)
Herring Gull	*Larus argentatus*	1000 (11/01/13)
Black-legged Kittiwake	*Rissa tridactyla*	300 (15/12/12)
Razorbill / Guillemot	*Alca torda / Uria aalge*	300 (22/01/13)

Table 1: Peak day counts of the commonest seabird species observed in foraging aggregations during SIB effort-based surveys. Note that Razorbill and Guillemot are grouped together due to issues with long-range field identification of these two species, but Razorbill was usually the commoner species (~80-90% of auks identified).

Great Northern Divers peaked at 16 on 11 Dec 2012, but these were typically widely dispersed as singles or small groups across the bay. Other species recorded in single figures within the study area during the survey period included Red-throated Diver *Gavia stellata*, Black-throated Diver *Gavia arctica*, Slavonian Grebe *Podiceps auritus*, Manx Shearwater *Puffinus puffinus*, Great Cormorant *Phalacrocorax carbo*, Common Scoter *Melanitta nigra*, Common Eider *Somateria mollissima*, Red-breasted Merganser *Mergus serrator*, Great Skua *Stercorarius skua*, Mediterranean Gull *Larus melanocephalus*, Black-headed Gull *Chroicocephalus ribundus*, Common Gull Larus *canus*, Lesser Black-backed Gull *Larus fuscus* and Glaucous Gull *Larus hyperboreus*.

The dominant species forming foraging aggregations was Herring Gull, which accounted for a total of about 70% of birds recorded in all aggregations (Table 2). Other key species seen in foraging aggregations included Shag (10%), Gannet (5%), auks (5%) and Kittiwakes (3%). On one occasion the prey fish during a foraging aggregation was positively identified as sandeel, but generally the prey species was not identified (e.g. on 11 Jan 2013 the prey fish were described as 3-4 inch fish, probably sprats).

	H. Gull	Shag	Auk	K'wake	Gannet	Other
TOTAL	**69**	**10**	**5**	**3**	**5**	**8**
Total (Dec 2012)	62	23	5	6	3	1
Total (Jan 2013)	74	2	5	1	6	12
TOTAL (visuals)	**76**	**5**	**11**	**2**	**6**	**0**
Visuals (Dec 2012)	57	24	7	11	1	0
Visuals (Jan 2013)	80	1	12	0	7	0
TOTAL (theodolite)	**68**	**11**	**3**	**3**	**4**	**11**
Theodolite (Dec 2012)	63	23	4	5	4	1
Theodolite (Jan 2013)	71	3	2	1	5	18

Table 2: Percentage totals of different seabird species recorded in foraging aggregations in SIB in winter 2012/13, separated by session (Dec 2012 and Jan 2013) and method of observation (visual vs theodolite). Results are broadly consistent between categories. HG = Herring Gull; K'wake = Kittiwake. Note that Razorbill and Guillemot are grouped together as 'Auk' due to issues with long-range field identification of these two species, but Razorbill was usually the commoner species (~80-90% of auks identified).

Not all seabird aggregations related to foraging birds. For example, up to 4000 auks (estimated to be 90% Razorbills) were widely dispersed throughout SIB from 11-14 Jan 2013, but only a small proportion of these were observed in concentrated foraging aggregations. In addition, several hundred Herring Gulls appeared to regularly commute between St Ives town and SIB, and a roost of at least 400 birds was observed on the water about 1 km northwest of the watchpoint in the late afternoon of 12 Dec 2012, with 350 there on the late afternoon of 24 Jan 2013 (mostly adults). Outside of the survey period, the small number of reports received from experienced observers between 1 Dec 2012 and 31 Jan 2103 at SIB included peak counts of 58 Balearic Shearwaters passing St Ives Island on 30 Dec 2012 (with 45 in Carbis Bay on the same date), and a foraging aggregation of 1000-1500 Gannets in the eastern sector of the bay on 23 Dec 2012.

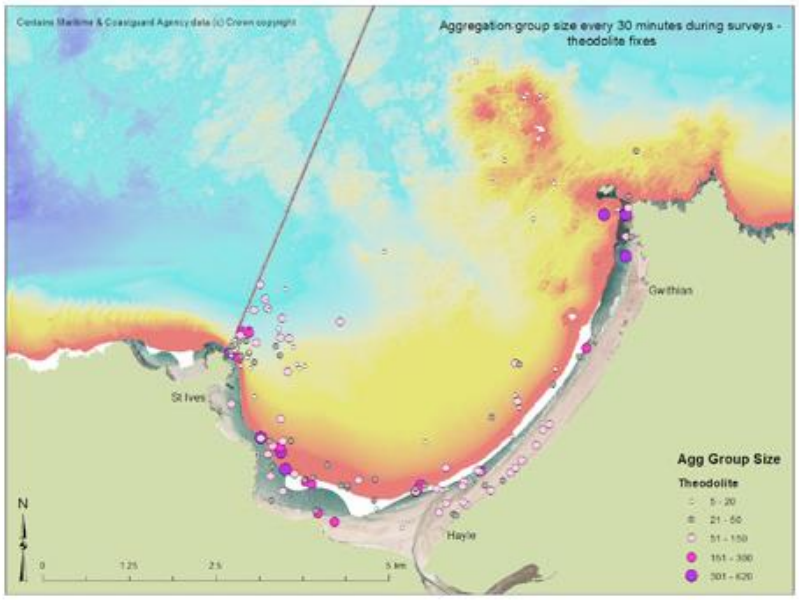

Figure 5: Map showing location and size of seabird foraging aggregations in SIB, mapped using a theodolite during effort-based observations in winter 2012/13. Field of view delimited by black line projected from the watchpoint on St Ives Island.

All seabird aggregations mapped in SIB using the theodolite have been entered into a GIS and overlain on high-resolution multibeam bathymetry of the seafloor (Figs 5, 7 and 9). It should be noted that the inshore area northwest of St Ives Island (off Porthmeor Beach) was also important for foraging seabirds, but precise mapping was challenging because birds were typically widely dispersed between St Ives Island and Clodgy Point. The largest aggregations in this area reached up to 1800 birds (mostly Herring Gulls), and sometimes drifted on the tide into the SIB recording area. Visual sightings data from northwest of SIB are therefore not included in the distribution maps.

Figure 6: A small foraging aggregation of adult and first-winter Shags in the tide race immediately offshore of St Ives Island (Photo: Russell Wynn)

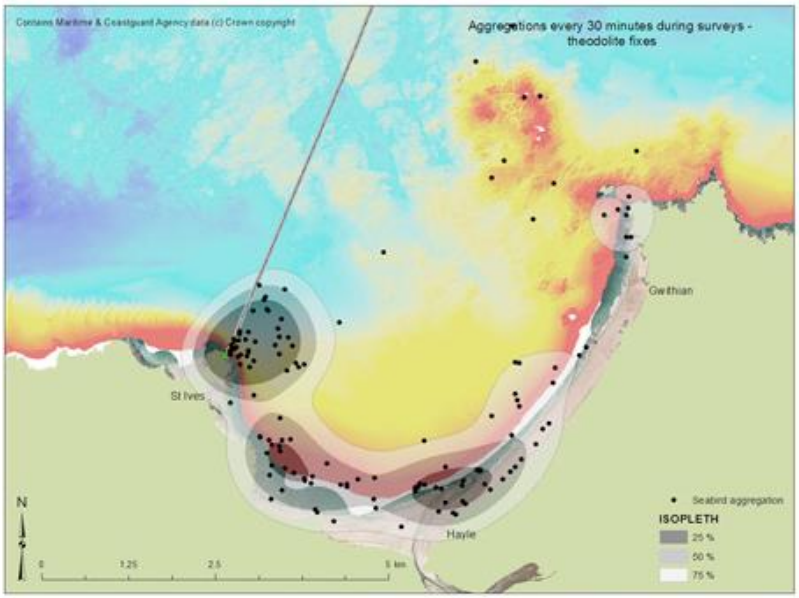

Figure 7: Kernel density plots of seabird foraging aggregations in SIB, mapped using a theodolite during effort-based observations in winter 2012/13. Field of view delimited by black line projected from the watchpoint on St Ives Island.

Figure 8: A large nearshore foraging aggregation of Herring Gulls in SIB, with small numbers of Gannets and Lesser Black-backed Gulls also present (Photo: John Swann)

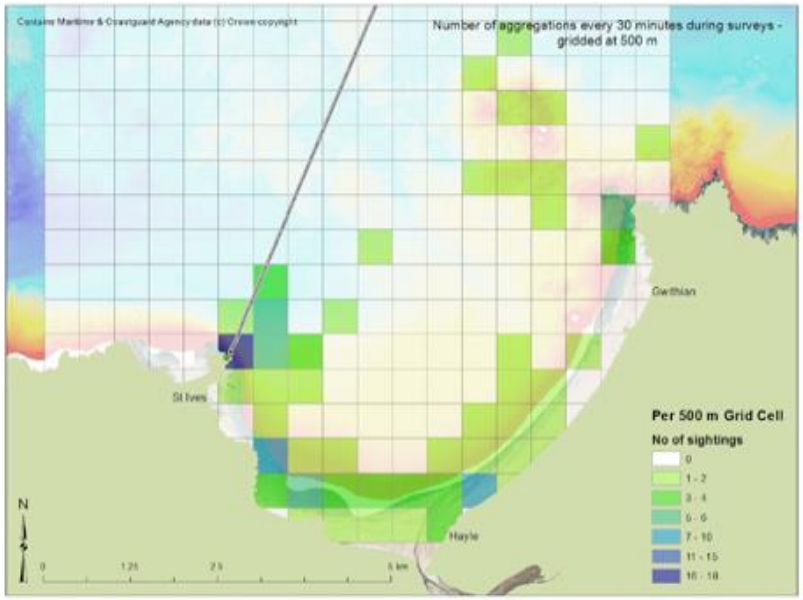

Figure 9: Gridded data showing seabird foraging aggregations in SIB, mapped using a theodolite during effort-based observations in winter 2012/13. Field of view delimited by black line projected from the watchpoint on St Ives Island.

Small groups of up to five Harbour Porpoise were regularly recorded during the survey period (often accompanied by Gannets overhead), and one or more pods of up to seven Bottlenose Dolphins were seen and tracked on several dates. The tide race immediately offshore of St Ives Island appeared to be a favoured feeding area for Harbour Porpoise and a loafing area for Bottlenose Dolphins, e.g. on 12 Dec 2012 a pod of seven dolphins was observed in this area for much of the day and on 22 Jan 2012 a group of six dolphins were also present for several hours (and were seen tossing fish and mating/fighting). Up to three Grey Seals were also seen sporadically within SIB. The marine mammal observations have also been mapped in GIS and overlain on the bathymetry and seabird data (Figs 9, 10 and 12).

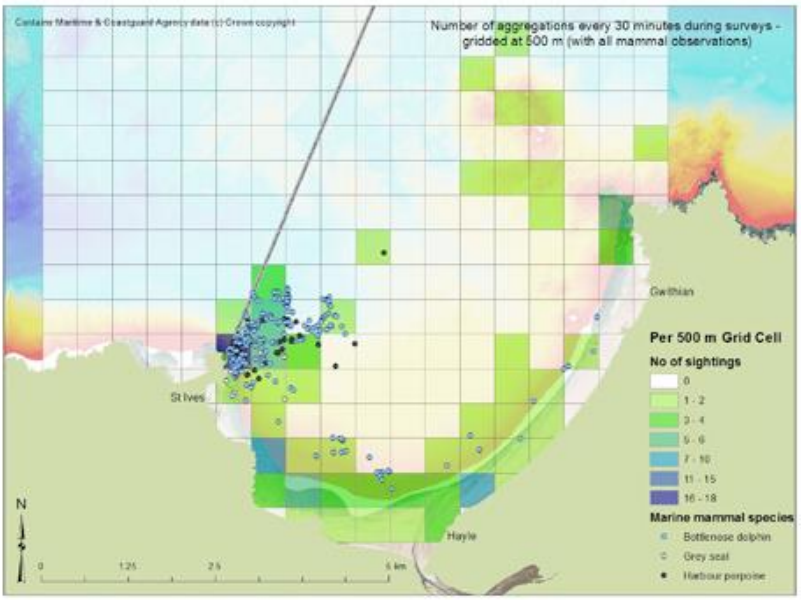

Figure 10: Map of marine mammal observations (coloured circles) overlain on gridded seabird foraging aggregation data in SIB, collected using a theodolite during effort-based observations in winter 2012/13. Field of view delimited by black line projected from the watchpoint on St Ives Island.

Figure 11: Bottlenose Dolphins loafing in the tide race immediately offshore of St Ives Island (Photo: Russell Wynn)

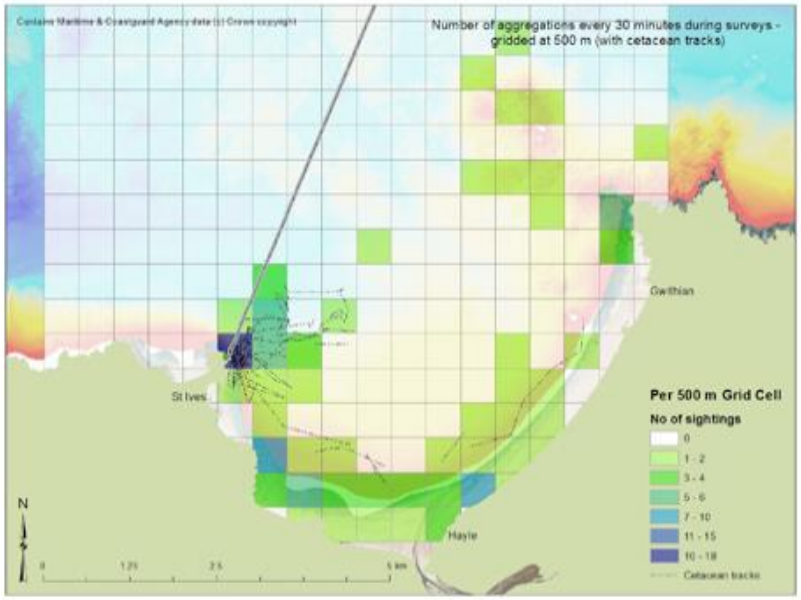

Figure 12: Map of cetacean tracks (Bottlenose Dolphins and Harbour Porpoises) overlain on gridded seabird foraging aggregation data in SIB, collected using a theodolite during effort-based observations in winter 2012/13. Field of view delimited by black line projected from the watchpoint on St Ives Island.

Figure 13: Harbour Porpoise in the tide race immediately offshore of St Ives Island (Photo: Russell Wynn)

7. Conclusions

A total of 107 hours of theodolite mapping data were collected from SIB on 17 dates in mid-winter 2012/13, supported by visual monitoring data for the area between St Ives Island and Clodgy Point. The results of this pilot study support previous observations indicating that SIB is a regionally important foraging area for a variety of seabird species, several of which were concentrated in aggregations of >100 birds. This study also highlights the potential importance of the site for two cetacean species: Bottlenose Dolphin and Harbour Porpoise.

The mapped theodolite data support field-based interpretations of foraging hotspots for seabirds and cetaceans which, within the bay, were focused on the visible tide race immediately north and northeast of St Ives Island, and the shallow, sandy, nearshore zone of the southern bay. The shallow reef northwest of Godrevy Island also sporadically held foraging seabird aggregations. All of these habitats are likely to hold enhanced numbers and/or increase the availability of prey fish due to tidal-topographic interactions and hydrodynamic processes in the water column. It is notable that the majority of the flat central bay was not utilized by foraging seabirds, although non-foraging auks, gulls and kittiwakes were occasionally dispersed in large numbers as individuals or groups of <5 birds across this area. Great Northern Divers were the only species to be widely dispersed across the whole bay when foraging, and were presumed to be accessing demersal species at the seabed (flatfish were identified as prey species on several occasions).

Balearic Shearwaters were recorded in small numbers within the study area on all but one of the survey dates, with a peak count of up to 15 on 13-14 Jan 2013. Birds were either recorded moving west through St Ives Bay and/or associating with foraging aggregations. Outside of the effort-based survey, a count of 58 moving west passed St Ives Island on 30 Dec 2012 corresponded with 45 being seen in Carbis Bay, and equates to ~0.25% of the World population. This highlights the continuing importance of St Ives Bay for this species in mid-winter.

These preliminary results provide a useful first snapshot of seabird foraging distribution in winter 2012/13, but further work is required in subsequent winters to assess inter-annual variability in species composition, numbers and distributions. Nevertheless, the fixed bathymetric controls on megavertebrate distributions observed in this study are likely to persist between years and seasons. Ongoing data analysis is investigating the

influence of tidal state and weather conditions on seabird distribution in SIB, e.g. wind vector appeared to exert some control, with seabird aggregations often apparently focused in shelter areas of the bay.

No seabird or cetacean bycatch incidents were observed during the survey period. However, two apparently freshly dead Razorbills were seen drifting into the bay from the northwest on 10 Dec 2012 (attended by Great Black-backed Gulls), and one Razorbill was seen to die upon surfacing close to the watchpoint on 24 Jan 2013; the same day one was found fairly freshly dead and un-oiled on St Ives Beach. Given the very large numbers of Razorbills using the area, it is possible (and perhaps unsurprising) that all these birds died of natural causes. A cautious approach to attribution of seabird deaths is therefore required unless the direct cause is witnessed.

Acknowledgements
We are grateful to all observers who assisted with fieldwork in winter 2012/13, especially Kevin Bainbridge, Phillip Dutt, Dan Murphy and Teresa Donohue. Fieldwork costs were supported by CIFCA and the UK Marine Environmental Mapping Programme (MAREMAP). Natural England, Cornwall Wildlife Trust and RSPB are also thanked for their support of this project.

References

Wynn, R.B. (2009) Balearic Shearwaters in UK and Irish waters from 2004 to 2006. *British Birds*, 102, 350-354.

Wynn, R.B., Josey, S.A., Martin, A.P., Johns, D.J. and Yésou, P. (2007) Climate-driven range expansion of a critically endangered top predator in northeast Atlantic waters, *Biology Letters*, 3, 529-532.

Wynn, R.B. and Yésou, P. (2007) Changing status of the Balearic Shearwater *Puffinus mauretanicus* in northwest European waters. *British Birds*, 100, 392-406.

Darlaston, M. and Wynn, R.B. (2012) A record influx of Balearic Shearwaters off Devon and Cornwall. *British Birds*, 105, 37-38.

Annex 1: Original scope of work for the project

The aim of the proposed project is to undertake a nested approach to monitoring and mapping of seabird foraging aggregations in SIB in the mid-winter period for three successive winters (2012/13, 2013/14 and 2014/15). The project will have three components:

1) Through the successful SeaWatch SW project (www.seawatch-sw.org), we i) will inform the wider birding community of the current initiative (e.g. by advertising on the Birdguides webzine; www.birdguides.com), ii) encourage local and visiting observers to focus effort on SIB in the Dec-Jan period, and iii) request that all records are submitted to the project co-ordinator (RBW) for inclusion in this project. Records will be in the form of date, location of observer, number of birds, species composition, behaviour (including any interactions with fisheries) and the approximate location of the birds within SIB.

2) We will, in collaboration with experienced local volunteer observers and RSPB staff, also undertake effort-based visual monitoring to monitor and map seabird foraging aggregations. Our recent experience at Gwennap Head (where we undertook 5000 hours of effort-based visual observations between 2007-11) is that visual mapping with compass and estimated distance has an error of ±300 m. This recording will be undertaken within a meteorological context, to assess the influence of weather conditions on seabird foraging in SIB. Meteorological data will be collected on site and calibrated with data from the Land's End weather station.

3) In order to obtain high-resolution maps of foraging hotspots, we will also undertake theodolite mapping on selected dates in the Dec-Jan period. Theodolite mapping is typically an order of magnitude more accurate than visual mapping, i.e. with an error of <20-30 m for animal locations up to 2 km offshore. Theodolite mapping can also calibrate distance to fixed markers, e.g. permanent buoys, headlands, that will improve distance estimates undertaken when visual monitoring. We are already successfully applying theodolite mapping to cetacean and seabird foraging aggregations (Gannets and Kittiwakes) off Gwennap Head, where high-resolution multibeam bathymetry data allow the sightings to be put into a bathymetric context. We hope to be able to access recently collected high-resolution bathymetry data from the SIB area (from our MAREMAP partners at the MCA) for use in this project.

The above recording methods will particularly focus on Balearic Shearwaters, but will also include all other seabirds whenever possible. It is planned that RBW and SBC will be on site for two two-week periods either side of Christmas and New Year, which appears to be the peak period for seabird foraging aggregations in SIB. In suitable weather conditions (light winds and good visibility) we will undertake theodolite mapping during all daylight hours; in periods of inclement weather we will undertake visual monitoring only. The main watchpoint to be used will be on St Ives Island; observations from this watchpoint will cover the whole of SIB. Exact details of methodology will be determined in the coming months, through dialogue with RSPB, NE, JNCC, and CIFCA.

Appendix C Weather classifications used in fieldwork.

Sea State codes (SSC)

Universal SSC	Description	Characteristics	Wave Height (feet)
0	Calm	Glassy sea like a mirror	0
1	Smooth	Ripples, no foam	0-1
2	Slight	Small wavelets	1-2
3	Moderate	Large wavelets, crests begin to break	2-4
4	Rough	Moderate waves, many crests break, whitecaps, some wind blown spray	4-8
5	Very Rough	Waves heap up, forming foam streaks and spindrift	8-13

Beaufort Wind Force Scale

Wind Force	Description	Speed (mph)	Sea Conditions	Land Observations
0	Calm	0-1	Flat	Smoke rises vertically
1	Light Air	1-3	Ripples without crests	Smoke drifts slowly
2	Slight Breeze	4-7	Small wavelets. Crests of glassy appearance, not breaking	Wind felt on face; leaves rustle; flags stir
3	Gentle Breeze	8-12	Large wavelets. Crests begin to break; scattered whitecaps	Leaves and twigs in constant motion; wind extends light flags
4	Moderate Breeze	13-18	Small waves breaking crests. Fairly frequent whitecaps	Dust and small branches move; flags flap
5	Fresh Breeze	19-24	Moderate waves of some length. Many whitecaps. Small amounts of spray	Small trees with leaves begin to sway; flags ripple
6	Strong Breeze	25-31	Long waves begin to form. White foam crests are very frequent	Large branches move; flags beat
7	Moderate Gale	32-38	Sea heaps up. Some foam from breaking waves is blown into streaks along wind direction. Moderate amounts of airborne spray	Whole trees move; flags extended

Cloud cover (in oktas): eighths of the sky covered in cloud

0 – completely clear

8 – completely overcast

Glare (0-5): strength of glare from sea

0 – no glare

5 – maximum glare (sea watching becomes impossible)

Appendix D Standardised recording forms.

Fieldwork recording form: Watch log sheet

Date	Site / Height of instrument	Watch no.	Start time	End time	No. of scans	Time of LW	Time of HW

Fieldwork recording form: Scan log sheet

Watch no./Scan no./Time		Tide (Hz)	(V)
Sea State code		Wind Force (BFT)	
Wind direction		Wind speed (mph)	
Cloud cover (0-8 oktas)		Glare (0-5)	
Glare arc (start Hz)		Glare arc (end Hz)	
Precipitation		Other / Viz	

Pt ID	**Hz**	**V**	**Species**	**No**	**Direction**	**Behaviour**	**Sighting**

Appendix E Radar-derived and predicted current vectors at the Runnel Stone Reef.

Radar-derived plots and Polpred-predicted schematics are provided to highlight some of the key tidal flow features around the Runnel Stone Reef, and evidence flow complexity in the region for each hour of the tidal cycle, outlined in the table below.

Tidal hour (relative to nearest HW, where HW = 0)	**Flow group**	**Flow description**
-6 (LW) to -5	1	Strong westward – full strength (full)
-5 to -4	2	Westward – gradually slowing (moderate)
-4 to -3	2	Westward – gradually slowing (moderate)
-3 to -2	2	Westward – gradually slowing (moderate)
-2 to -1	3	slackening – starting to turn W to E
-1 to 0	4	Eastward – slowly increasing (moderate)
0 to +1	4	Eastward – full strength (full)
+1 to +2	4	Eastward – full strength (full)
+2 to +3	3	slackening – tide quickly turns E to W
+3 to +4	1	Strong westward – full strength (full)
+4 to +5	1	Strong westward – full strength (full)
+5 to +6 (LW)	1	Strong westward – full strength (full)

Radar-derived surface flows: current vectors scale logarithmically with speed; vectors coloured according to colour scale in m s^{-1} (blue = 0 m s^{-1}, red = 2.5 m s^{-1}). Black and white area in the top right corner is the headland; the image is oriented North; bright spot at ~0.3 km, -1.5 km, is the Runnel Stone cardinal mark. Flows calculated for each hour of the tidal cycle during a spring tide on 16/09/2011 (top plot each tidal hour) and during a neap tide on 05/10/2011 (bottom plot each tidal hour). The images at ~160-m resolution are instantaneous results to be used as examples of currents for any particular tidal state.

Polpred tidal flows: size of arrows is proportional to current speed, and coloured according to speeds shown in the legend (red = 0.2 m s^{-1}, pink = 1.8 m s^{-1}). Speed and flow direction shown is for the location at the base of the arrow. Polpred output calculated using Sigma 31 and Sigma 16 (middle and right columns, respectively) for each half an hour during the day of the ADCP survey (11/07/2011), two days after a neap tide.

	RADAR-derived surface flows (springs and neaps for each tidal hour)	Surface flows (Sig 31) (images each half tidal hour)	Mid-water column (Sig 16) (images each half tidal hour)
HW-6	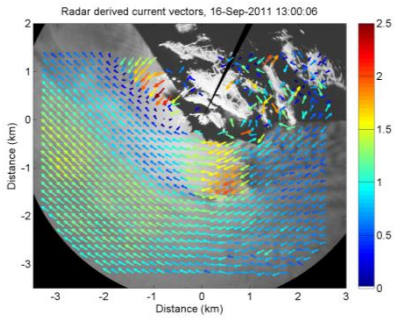	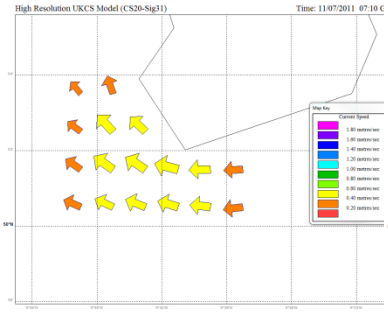	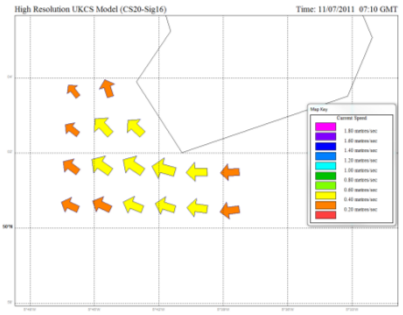
spring			
HW-5	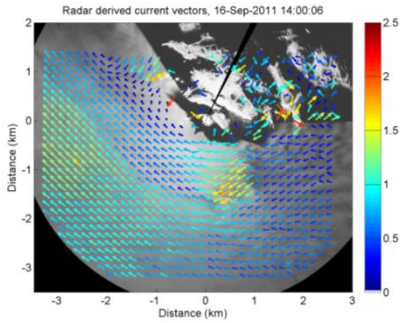	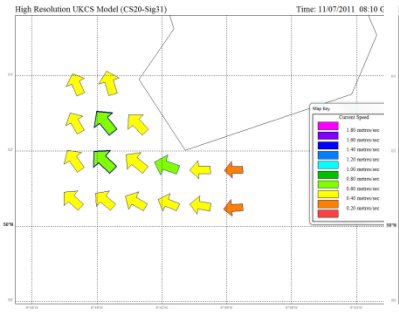	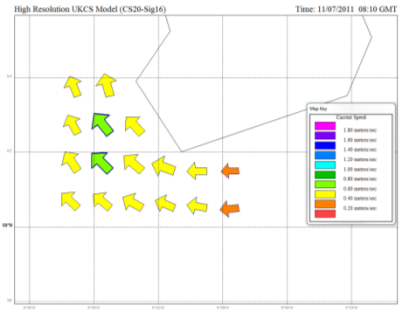
	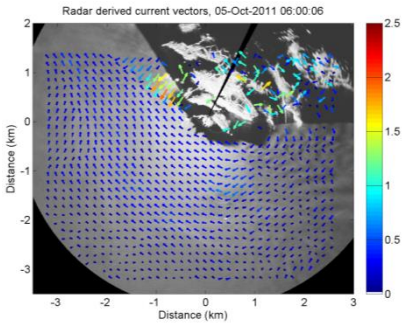	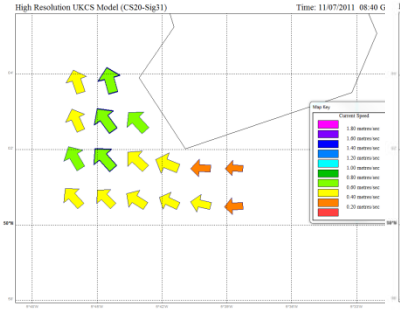	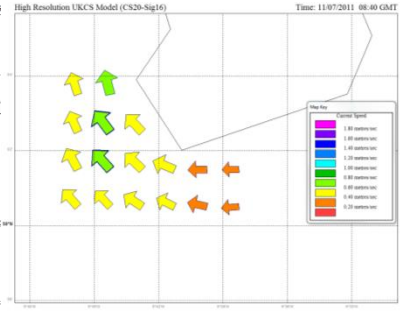
HW-4	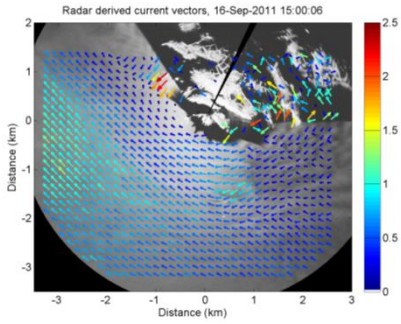	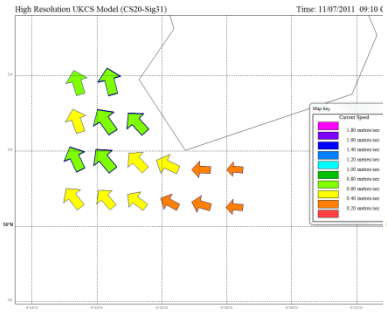	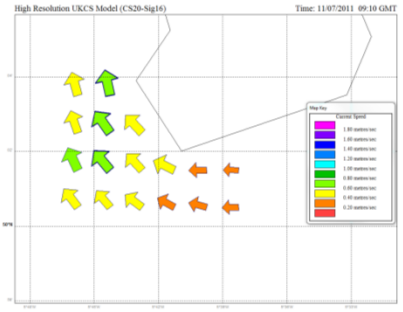

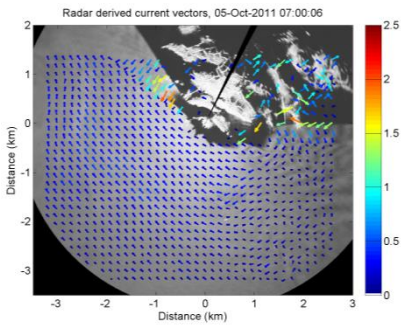
Radar derived current vectors, 05-Oct-2011 07:00:06
Distance (km)
Distance (km)

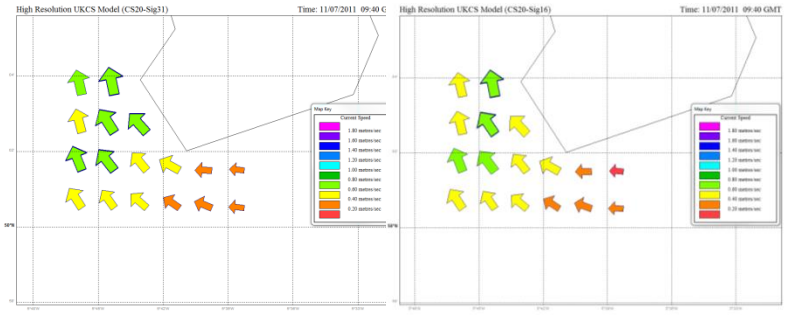
High Resolution UKCS Model (CS20-Sig31)
High Resolution UKCS Model (CS20-Sig16)

HW-3

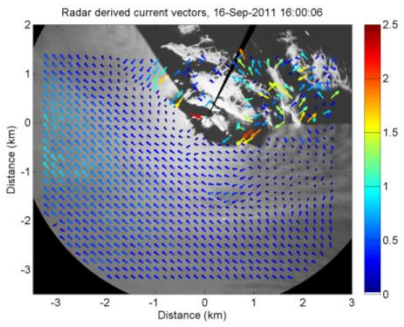
Radar derived current vectors, 16-Sep-2011 16:00:06
Distance (km)
Distance (km)

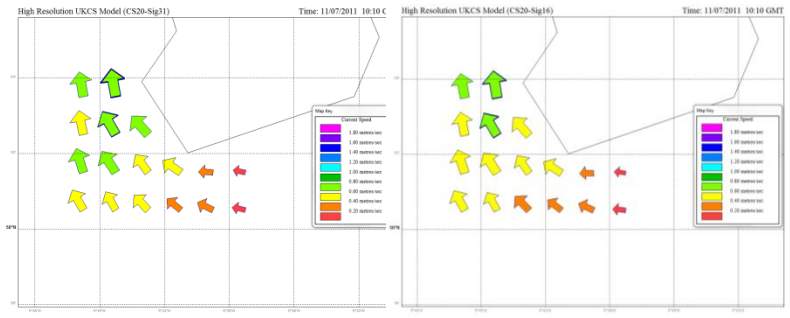
High Resolution UKCS Model (CS20-Sig31)
High Resolution UKCS Model (CS20-Sig16)

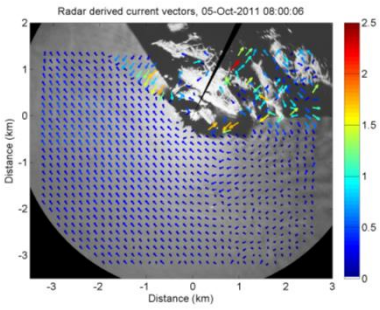
Radar derived current vectors, 05-Oct-2011 08:00:06
Distance (km)
Distance (km)

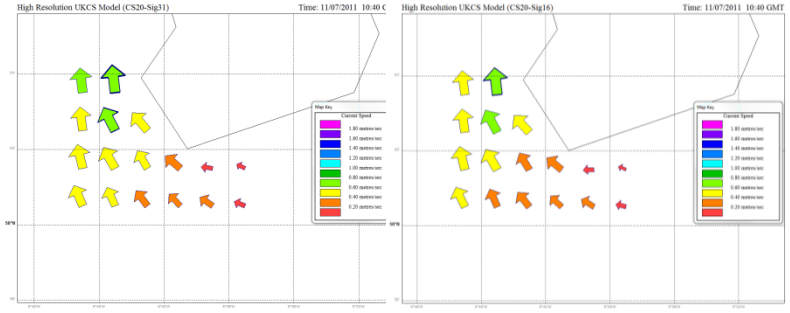
High Resolution UKCS Model (CS20-Sig31)
High Resolution UKCS Model (CS20-Sig16)

HW-2

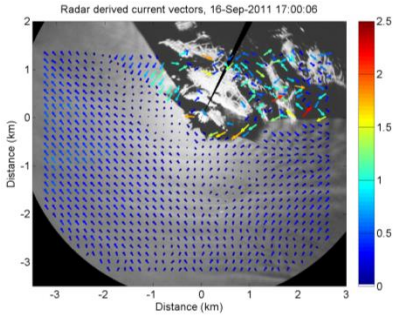
Radar derived current vectors, 16-Sep-2011 17:00:06
Distance (km)
Distance (km)

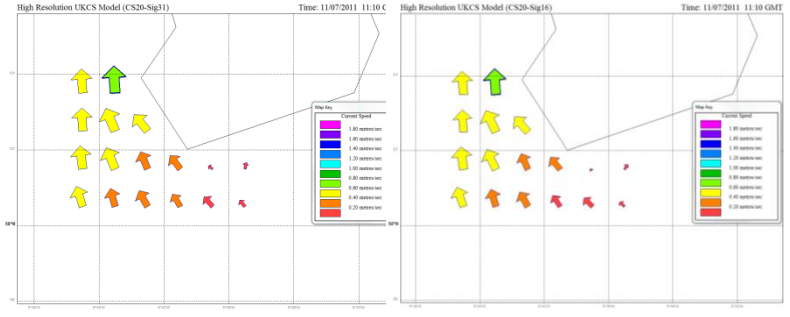
High Resolution UKCS Model (CS20-Sig31)
High Resolution UKCS Model (CS20-Sig16)

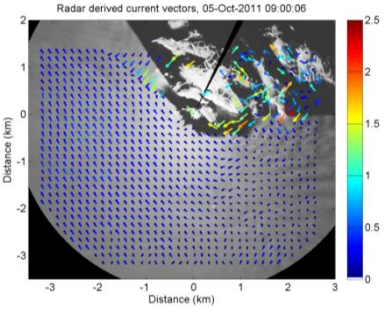
Radar derived current vectors, 05-Oct-2011 09:00:06
Distance (km)
Distance (km)

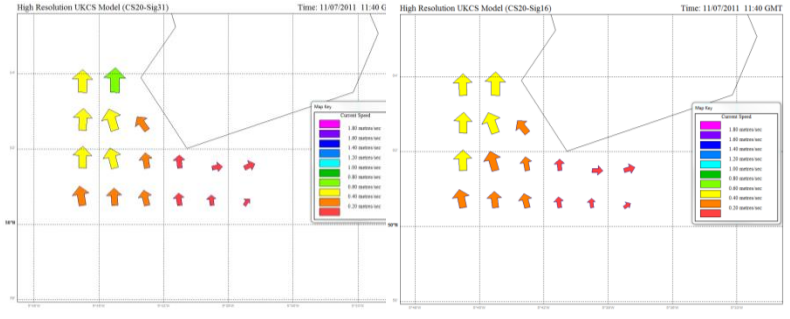
High Resolution UKCS Model (CS20-Sig31)
High Resolution UKCS Model (CS20-Sig16)

HW-1

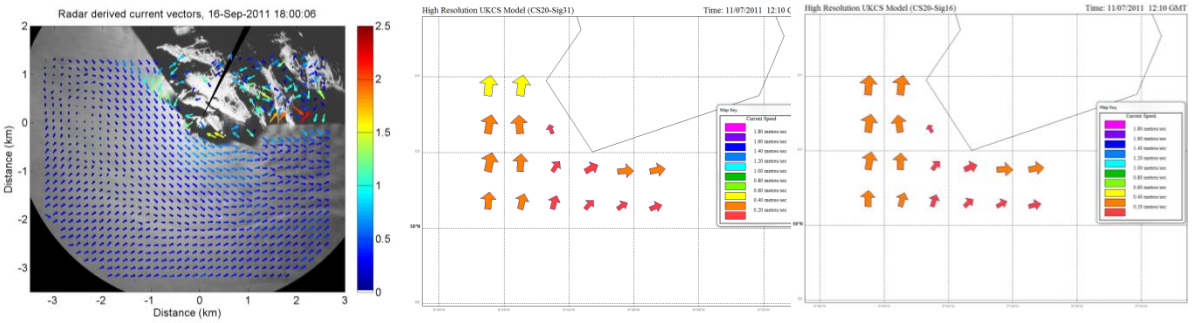
Radar derived current vectors, 16-Sep-2011 18:00:06
High Resolution UKCS Model (CS20-Sig31)
Time: 11/07/2011 12:10 G
High Resolution UKCS Model (CS20-Sig16)
Time: 11/07/2011 12:10 GMT
Distance (km)
Distance (km)

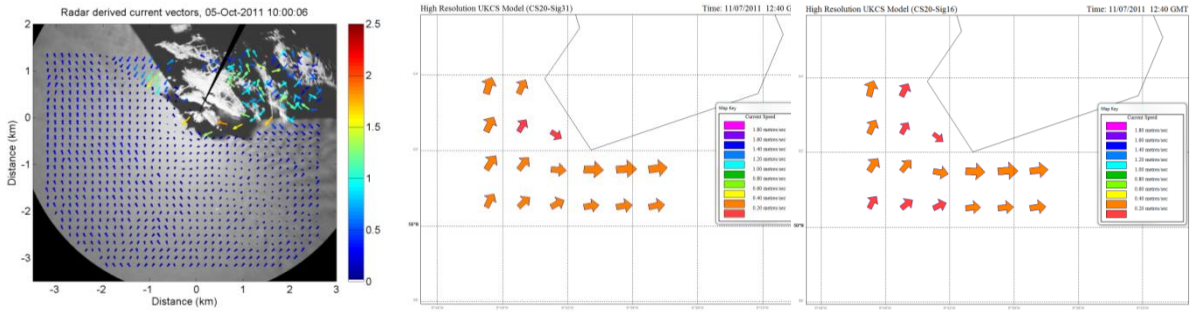
Radar derived current vectors, 05-Oct-2011 10:00:06
High Resolution UKCS Model (CS20-Sig31)
Time: 11/07/2011 12:40 G
High Resolution UKCS Model (CS20-Sig16)
Time: 11/07/2011 12:40 GMT
Distance (km)
Distance (km)

HW

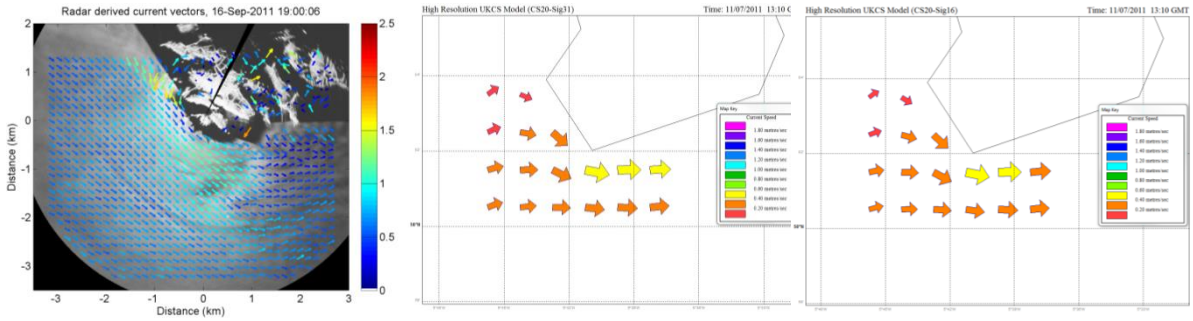
Radar derived current vectors, 16-Sep-2011 19:00:06
High Resolution UKCS Model (CS20-Sig31)
Time: 11/07/2011 13:10 G
High Resolution UKCS Model (CS20-Sig16)
Time: 11/07/2011 13:10 GMT
Distance (km)
Distance (km)

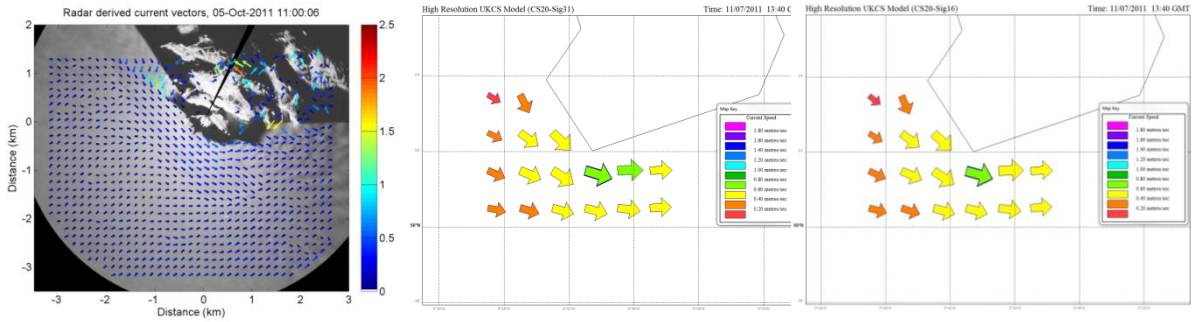
Radar derived current vectors, 05-Oct-2011 11:00:06
High Resolution UKCS Model (CS20-Sig31)
Time: 11/07/2011 13:40 G
High Resolution UKCS Model (CS20-Sig16)
Time: 11/07/2011 13:40 GMT
Distance (km)
Distance (km)

HW+1

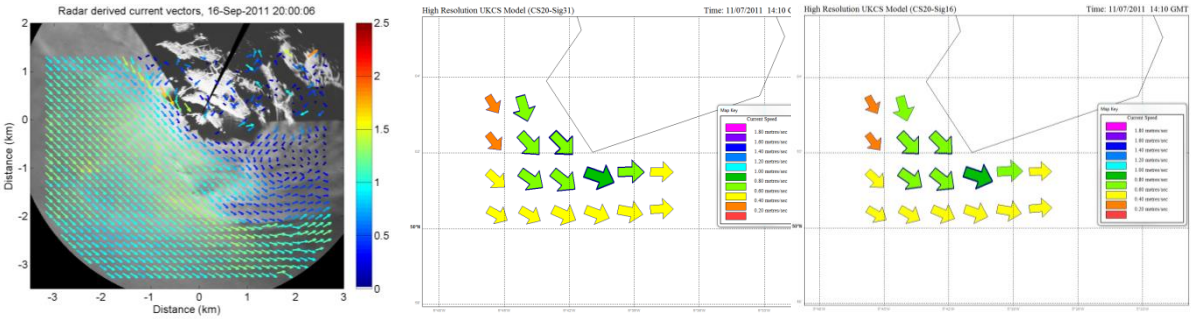
Radar derived current vectors, 16-Sep-2011 20:00:06
High Resolution UKCS Model (CS20-Sig31)
Time: 11/07/2011 14:10 G
High Resolution UKCS Model (CS20-Sig16)
Time: 11/07/2011 14:10 GMT
Distance (km)
Distance (km)

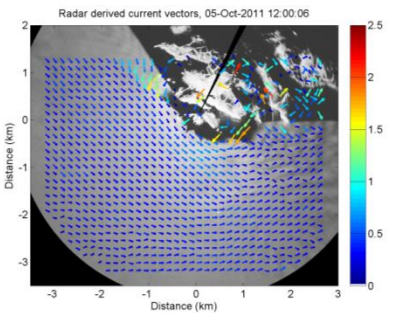
Radar derived current vectors, 05-Oct-2011 12:00:06
Distance (km)
Distance (km)

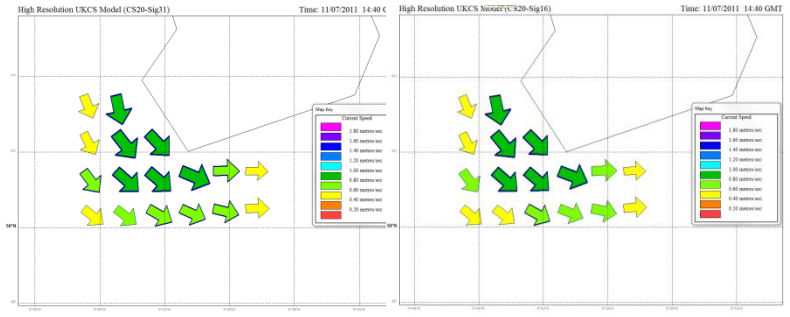
High Resolution UKCS Model (CS20-Sig31)
High Resolution UKCS Model (CS20-Sig16)

HW+2

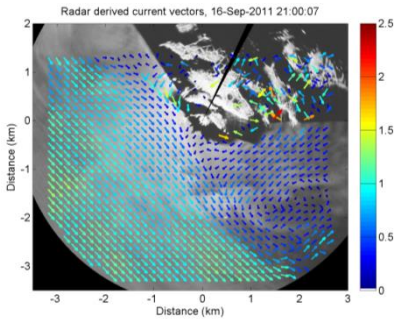
Radar derived current vectors, 16-Sep-2011 21:00:07
Distance (km)
Distance (km)

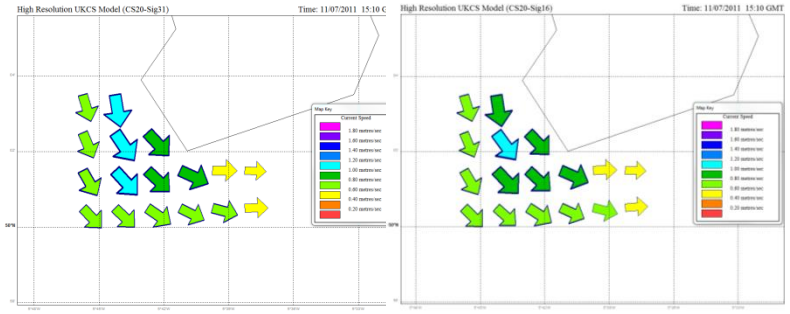
High Resolution UKCS Model (CS20-Sig31)
High Resolution UKCS Model (CS20-Sig16)

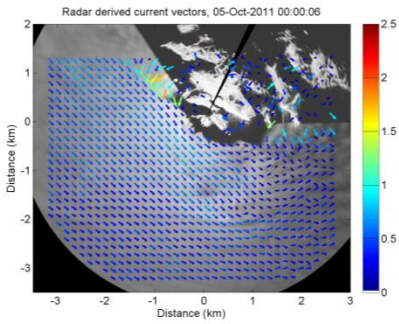
Radar derived current vectors, 05-Oct-2011 00:00:06
Distance (km)
Distance (km)

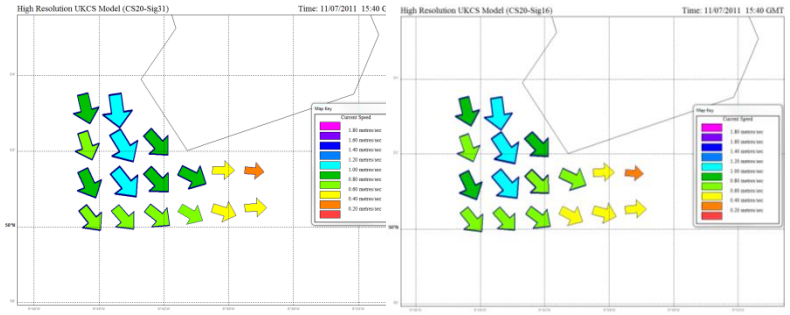
High Resolution UKCS Model (CS20-Sig31)
High Resolution UKCS Model (CS20-Sig16)

HW+3

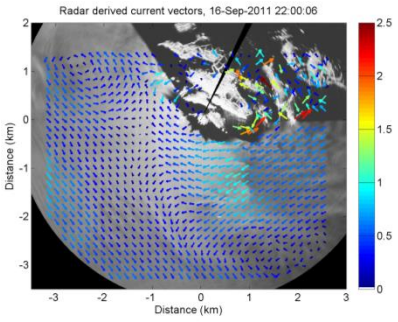
Radar derived current vectors, 16-Sep-2011 22:00:06
Distance (km)
Distance (km)

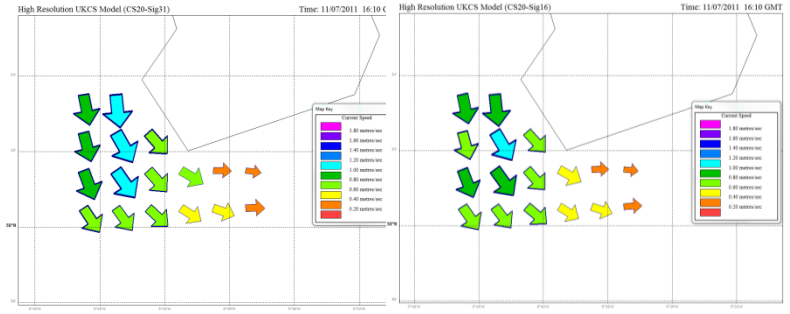
High Resolution UKCS Model (CS20-Sig31)
High Resolution UKCS Model (CS20-Sig16)

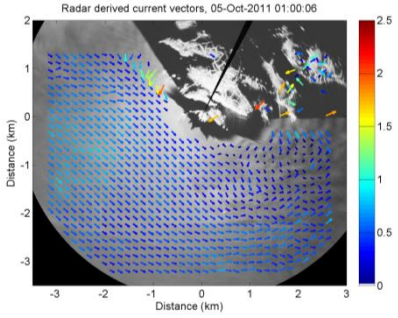
Radar derived current vectors, 05-Oct-2011 01:00:06
Distance (km)
Distance (km)

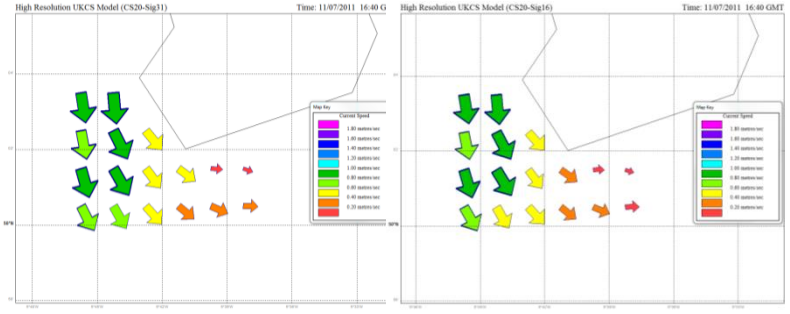
High Resolution UKCS Model (CS20-Sig31)
High Resolution UKCS Model (CS20-Sig16)

HW+4

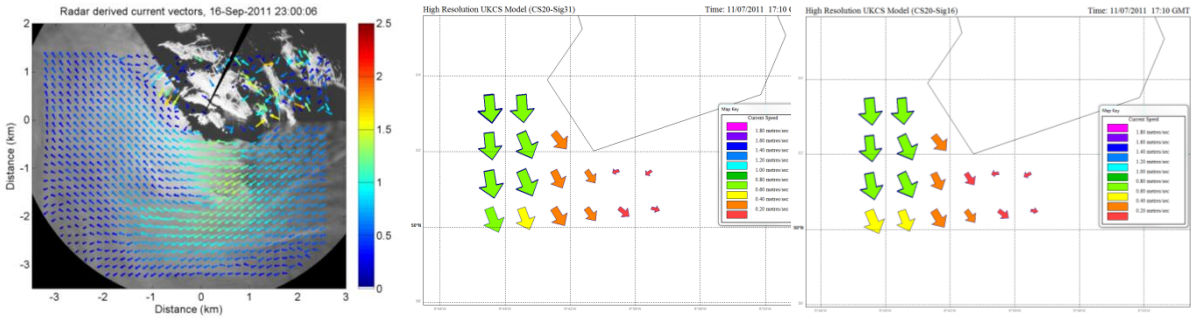
Radar derived current vectors, 16-Sep-2011 23:00:06
High Resolution UKCS Model (CS20-Sig31)
Time: 11/07/2011 17:10 GMT
High Resolution UKCS Model (CS20-Sig16)
Time: 11/07/2011 17:10 GMT
Distance (km)

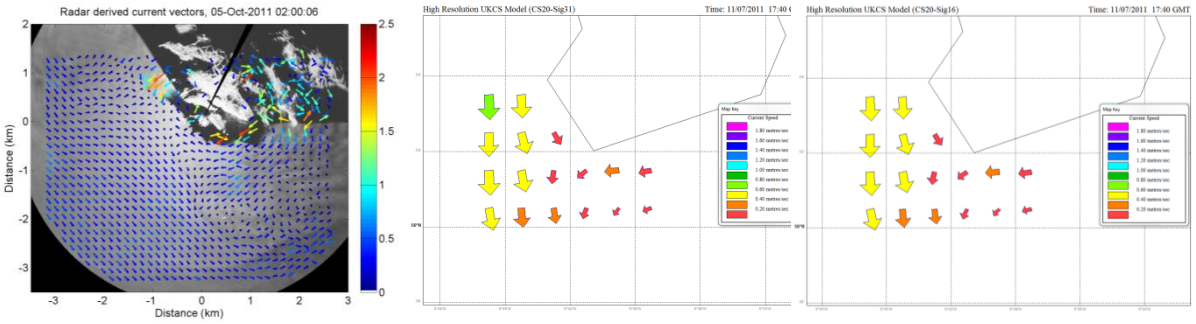
Radar derived current vectors, 05-Oct-2011 02:00:06
High Resolution UKCS Model (CS20-Sig31)
Time: 11/07/2011 17:40 GMT
High Resolution UKCS Model (CS20-Sig16)
Time: 11/07/2011 17:40 GMT
Distance (km)

HW+5

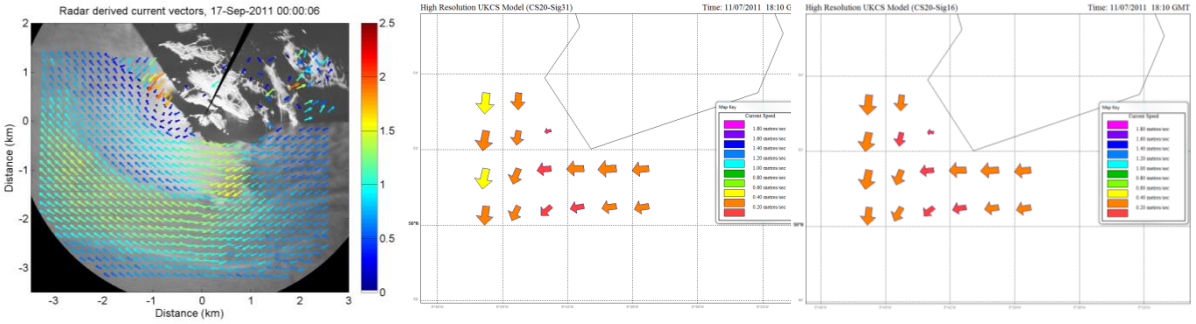
Radar derived current vectors, 17-Sep-2011 00:00:06
High Resolution UKCS Model (CS20-Sig31)
Time: 11/07/2011 18:10 GMT
High Resolution UKCS Model (CS20-Sig16)
Time: 11/07/2011 18:10 GMT
Distance (km)

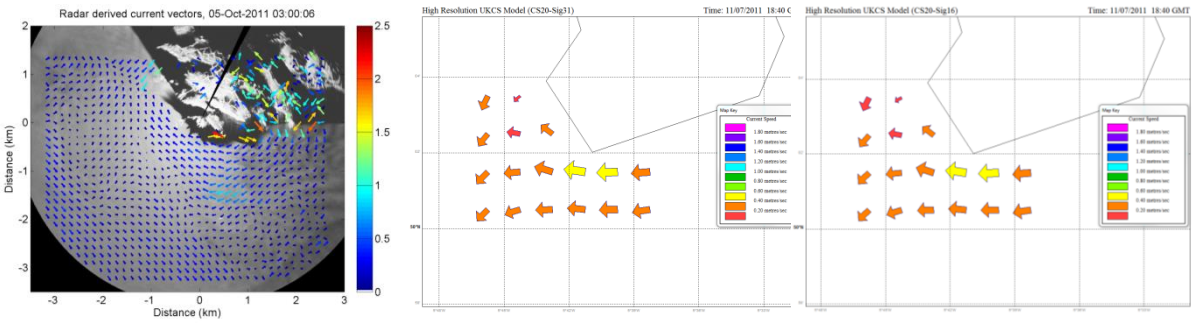
Radar derived current vectors, 05-Oct-2011 03:00:06
High Resolution UKCS Model (CS20-Sig31)
Time: 11/07/2011 18:40 GMT
High Resolution UKCS Model (CS20-Sig16)
Time: 11/07/2011 18:40 GMT
Distance (km)

HW+6

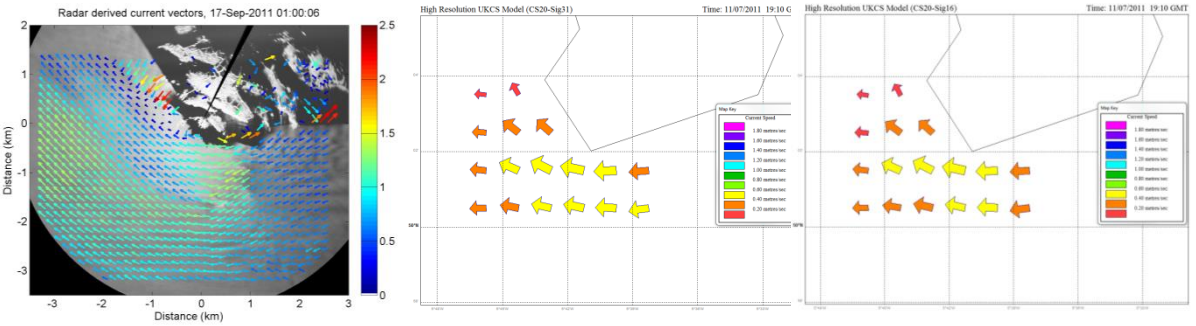
Radar derived current vectors, 17-Sep-2011 01:00:06
High Resolution UKCS Model (CS20-Sig31)
Time: 11/07/2011 19:10 GMT
High Resolution UKCS Model (CS20-Sig16)
Time: 11/07/2011 19:10 GMT
Distance (km)

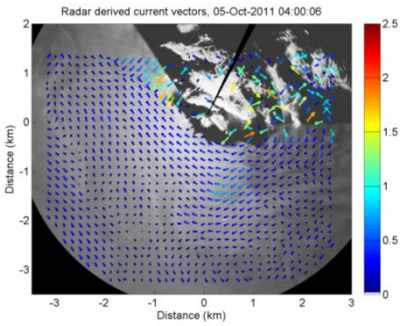
Radar derived current vectors, 05-Oct-2011 04:00:06
Distance (km)
Distance (km)

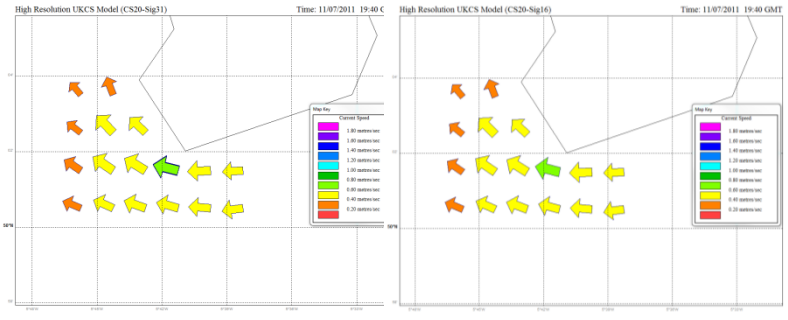
High Resolution UKCS Model (CS20-Sig31)
High Resolution UKCS Model (CS20-Sig16)

LW

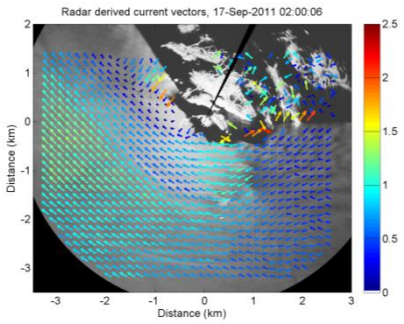
Radar derived current vectors, 17-Sep-2011 02:00:06
Distance (km)
Distance (km)

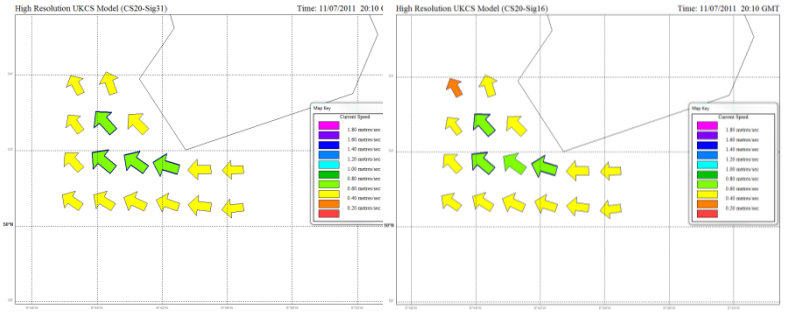
High Resolution UKCS Model (CS20-Sig31)
High Resolution UKCS Model (CS20-Sig16)

Appendix F Local-scale tidal flow schematics of the Runnel Stone Reef.

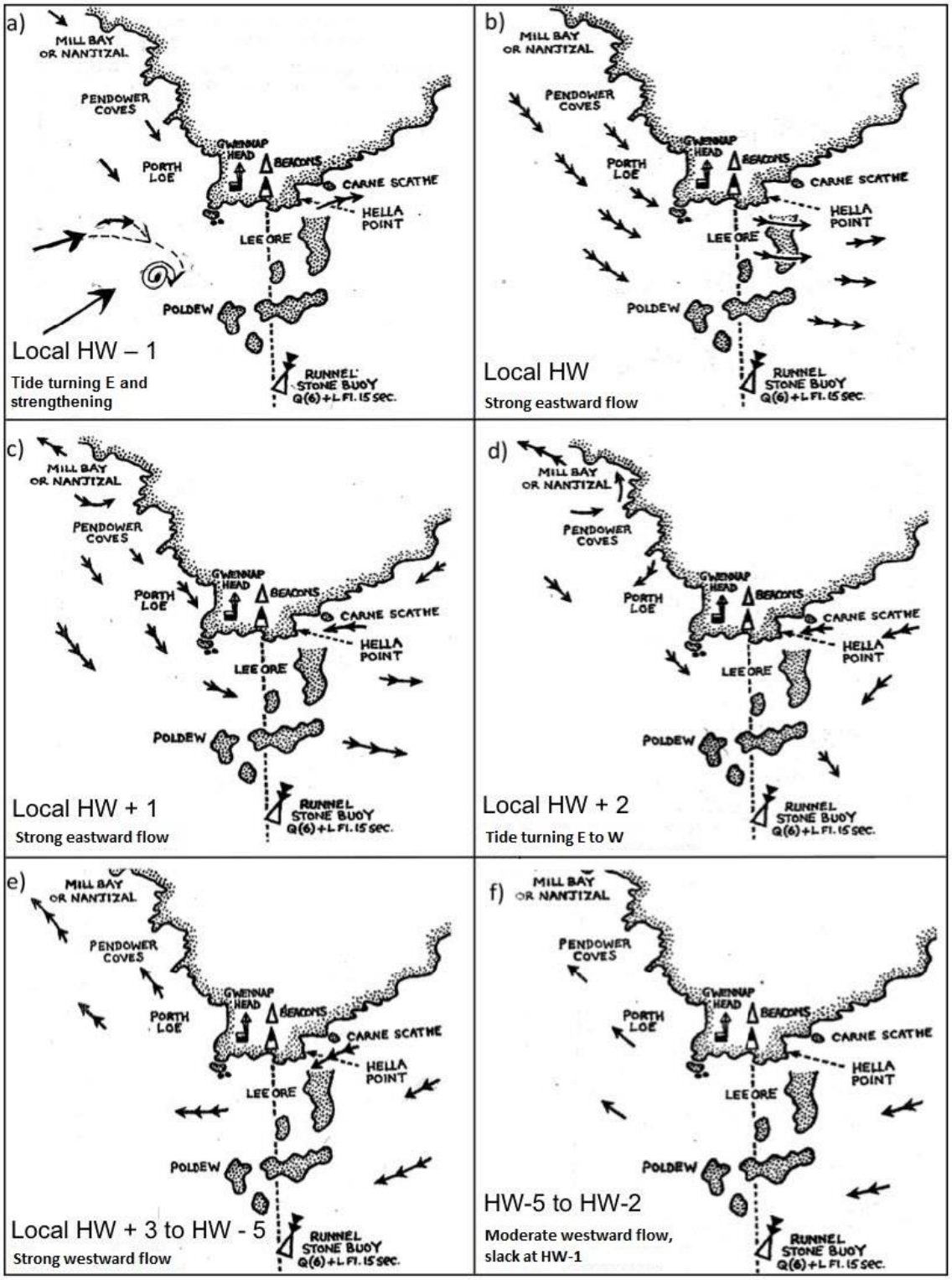

Schematics originally drawn by local fishermen and provided by the Gwennap Head NCI. Arrows indicate tidal flow direction, number of arrow heads signify relative tidal speed (knots).

Appendix G Categorisation table of criteria for birds of 'amber' conservation importance.

	Amber list criteria
1	Species with unfavourable conservation status in Europe (SPEC = Species of European Conservation Concern)
2	Historical population decline during 1800–1995, but recovering; population size has more than doubled over last 25 years
3	Moderate (25-49%) decline in UK breeding population over last 25 years, or the longer-term period
4	Moderate (25-49%) contraction of UK breeding range over last 25 years, or the longer-term period
5	Moderate (25-49%) decline in UK non-breeding population over last 25 years, or the longer-term period
6	Rare breeder; 1–300 breeding pairs in UK
7	Rare non-breeders; less than 900 individuals
8	Localised; at least 50% of UK breeding or non-breeding population in 10 or fewer sites, but not applied to rare breeders or non-breeders
9	Internationally important; at least 20% of European breeding or non-breeding population in UK (NW European and East Atlantic Flyway populations used for non-breeding wildfowl and waders respectively)

Appendix H Additional spatial analyses for harbour porpoises at the Runnel Stone Reef.

Appendix H.1 Evidence of spatial clustering.

The average point intensity within the 2 217 600-m^2 sampling window is $9.78x10^{-6}$ per m^2 ($9.78x10^{-12}$ points per km^2). The Pearson χ^2 goodness-of-fit test of the null hypothesis of complete spatial randomness (CSR) using quadrat counts is 317.22 (p = <0.0002), indicating the process is not a homogenous Poisson process (either because there is non-uniform intensity or because it exhibits dependence between points).

Appendix H.2 Ripley's K function test of observed distribution of porpoise sightings (n = 217).

Observations filtered by the 600-m grid compared to complete spatial randomness (CSR) within the survey area. The red dashed line shows the expected number of sightings within a radius of a sighting under the assumption of CSR. The black line represents the observed distribution, *K*, with "best" edge correction. The Ripley's *K* analysis (Appendix H.2) of spatial point patterns (with edge correction) on the filtered porpoise sightings data indicates strong spatial clustering, as the observed distributions lie above the dashed red line at all spatial scales, particularly where r > 100 m.

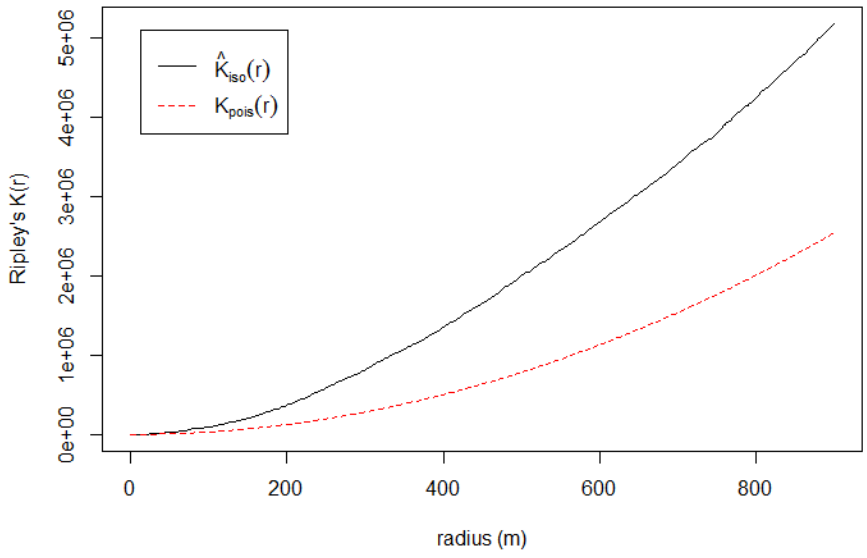

Appendix H.3 Pair correlation function for porpoise sightings (n = 217) filtered by the 600-m grid.

The dotted green line represents no spatial correlation at any spatial scale. The red and black lines are the observed spatial correlations. Since the value *g(r)* = 1 corresponds to CSR, results of the pair correlation function, shown in Appendix H.3, suggest strong correlation between pairs of sightings at small scales, but much less clustering at distances greater than *r* = 100 m.

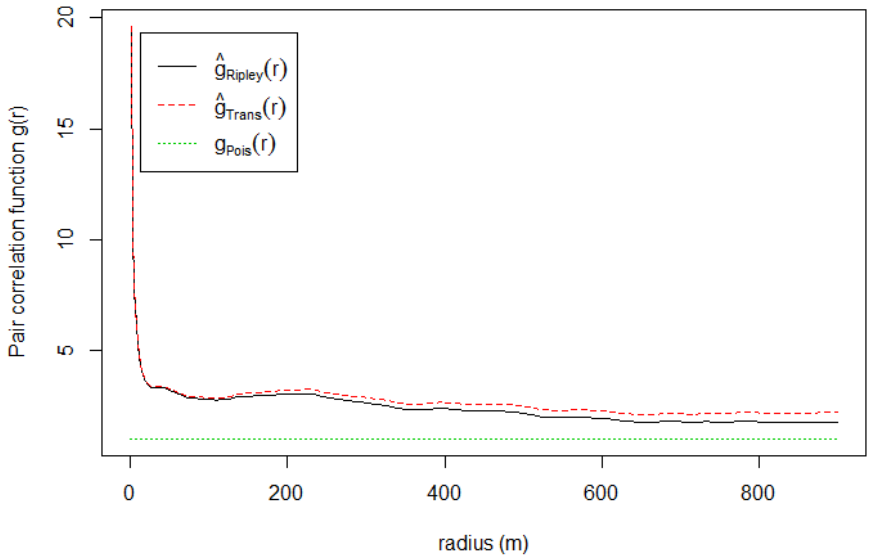

Appendix H.4 **Percentage volume isopleths of porpoise surfacing locations, filtered by 300-m grid.**

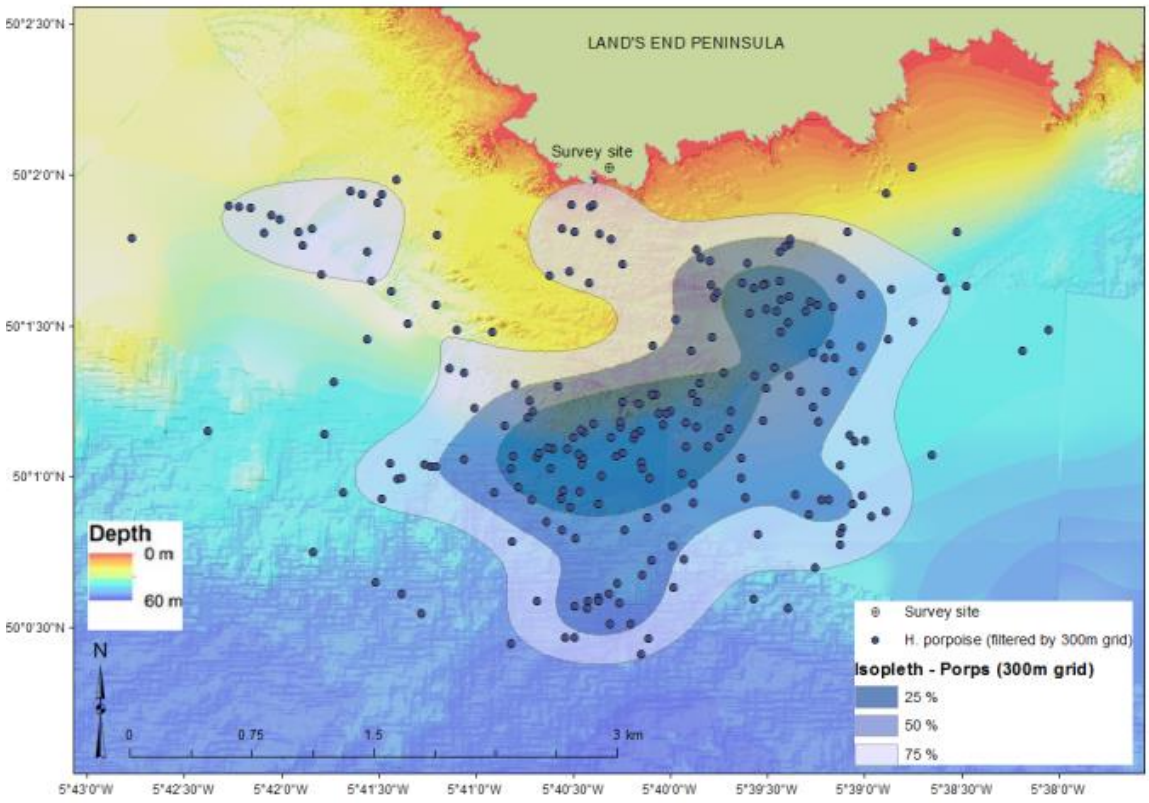

Kernel density estimations (25%, 50%, 75%) calculated from surfacing locations (blue dots) filtered by the 300-m radial grid (n = 232) within Beyer's (2012) Geospatial Modelling Environment (bandwidth = 400 m; plug-in), mapped onto high resolution (1 m) bathymetry data (courtesy of CCO/MCA © Crown copyright). Observation team located at survey site 'crosshairs'. Theodolite data collected across years 2011-2013.

Appendix H.5 Sightings and covariate data summarised by 300-m radial grid.

Parameter	Value
Number of (300-m) grid cells	190
Number of 'absence' cells (%)	77 (41%)
Number of (filtered) sightings: Harbour porpoise	232
Range of sightings per grid cell	0 – 8
Mean sightings per cell (s.d.)	1.3 (1.72)
Static physical variables	
Depth (m)	
Range	3.5 – 61.1
Mean (s.d.)	32.5 (15.3)
Aspect (degrees)	
Range	27.7 – 248.0
Mean (s.d.)	154.4 (54.7)
Slope (degrees)	
Range	0.15 – 21.9
Mean (s.d.)	5.1 (4.4)
Distance from shore to centre of grid cell (m)	
Range	2.4 – 2729.5
Mean (s.d.)	1107.6 (792.4)
Grid cell area (m^2)	
Range	344.5 – 152631
Mean (s.d.)	77701.5 (45980)

Porpoise relative densities per km^2 comparing effect of filtering by different grid cell sizes. When uncorrected by detection probability, both density grids highlight increased observations at the southern and south-eastern reef margin, with notable absences over the reef plateau and in deeper waters (> 50 m). Whether sightings are filtered by the 300-m (Fig. A) or 600-m radial grid (Fig. B), the same patterns are evident. The main effect of correcting for detection probability on the 600-m gridded sightings data is an increased number of higher density cells in deeper waters to the south (Fig. A), rather than solely along the south, south-eastern reef margins (Fig. B).

A) Filtering by 300 m grid

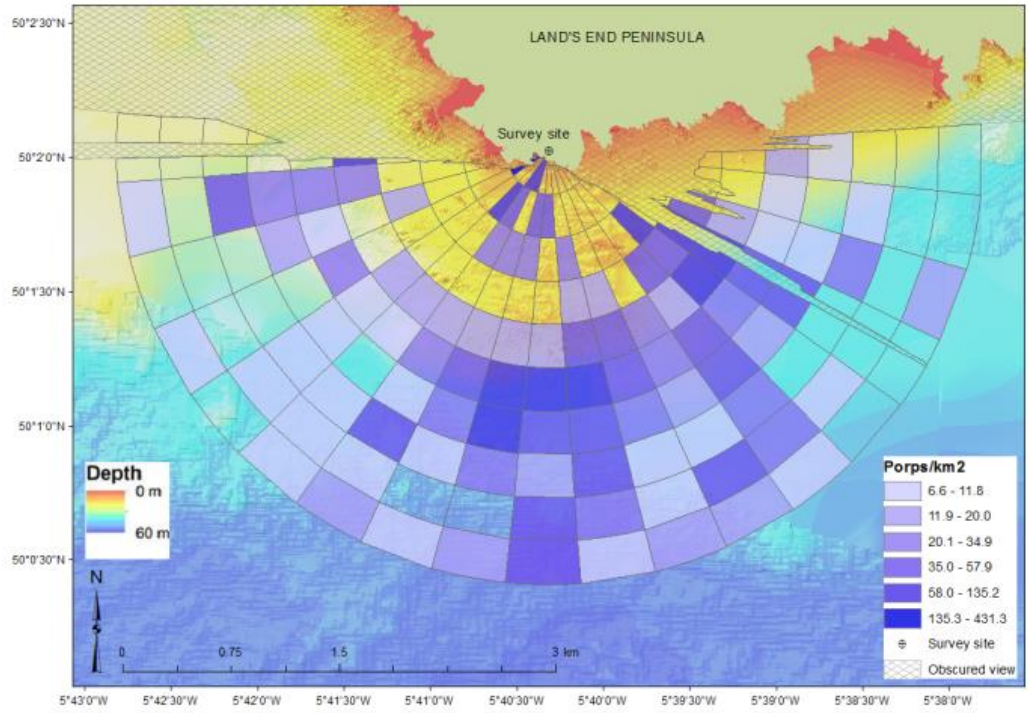

B) Filtering by 600-m grid

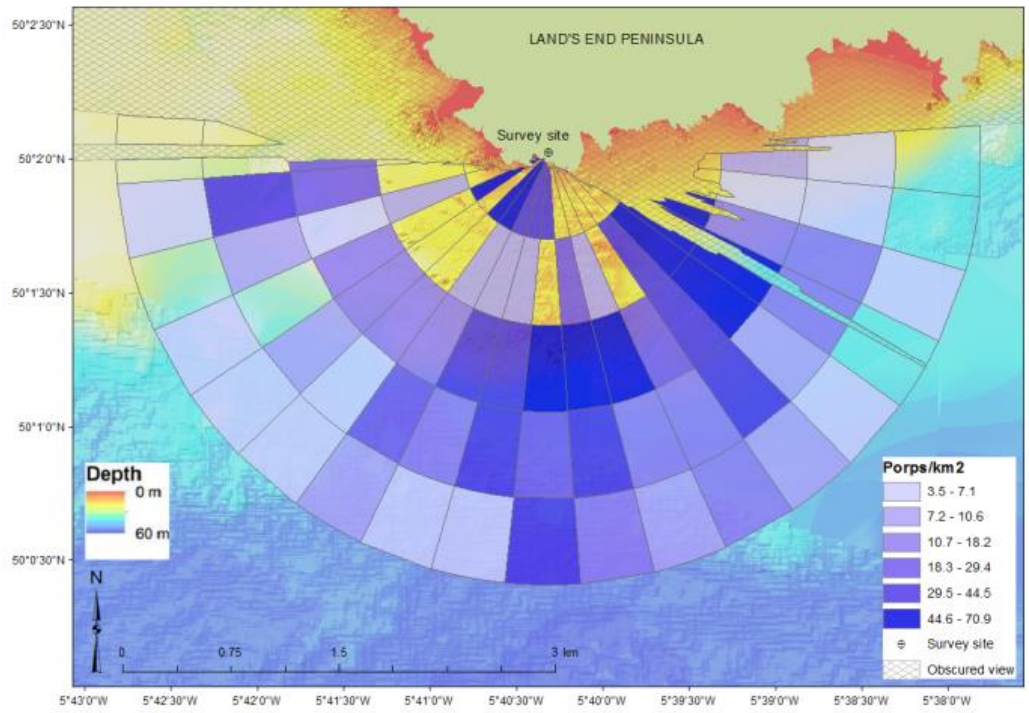

Appendix H.6 Spatial data exploration of porpoise sightings at Gwennap Head.

Boxplots of static variables conditional on the absence/presence of porpoise within 600-m grid cells (n = 90).

Boxplots of A): Mean depth, B): Mean slope, C): Mean aspect, and D): Distance from shore to grid cell centre. Solid black lines show median values; boxes show interquartile range (i.e. location of middle 50% of data); whiskers indicate range of the data. (When outliers are present, they show the largest data point that is <1.5 times either side of the IQR). Notches indicate potential significant difference between two medians, i.e. if notches do not overlap, medians may be significantly different at the 5 % level (Chambers et al., 1983).

Grid cells with porpoise presence were in deeper water (median = 36.07 m) than those cells with no recorded sightings (median = 19.79 m) (Appendix H.6-A). Additionally, the notches do not overlap suggesting the medians may be significantly different (Chambers et al., 1983; Crawley, 2012). This is also shown in the boxplot of distance from shore (Appendix H.6-D), showing that cells further from shore were more likely positive for sightings than those closer.

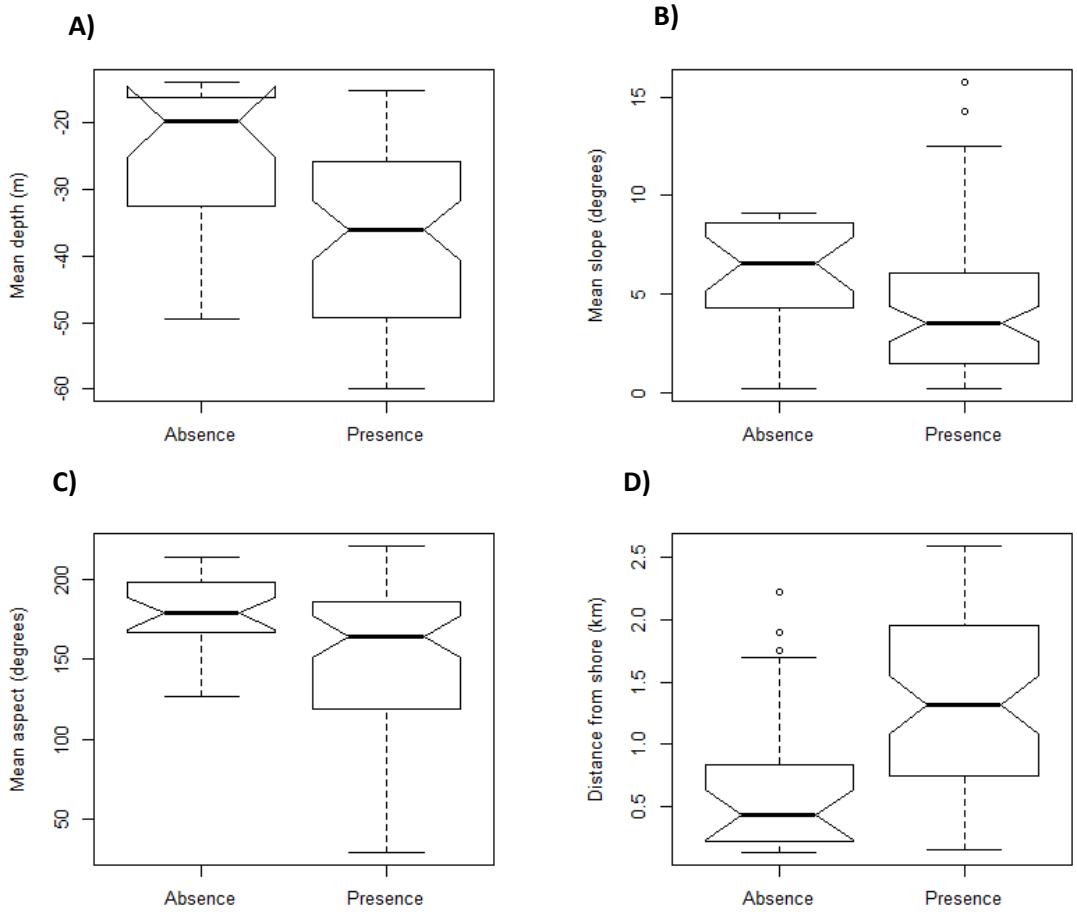

There is a lower median slope value (Appendix H.6-B) within the presence cells than within the absence cells (3.49° and 6.53°, respectively), and the notches suggest them to be significantly different. Median average aspect values are south, south-easterly for both presence and

absence (164° and 179°, respectively), with overlapping notches suggesting these medians are not significantly different. There is a notably larger spread of values within the presence cells relative to aspect (Appendix H.6-C) compared to the other static variables. However, there will be a larger spread of values within presence cells across all the independent variables, as 77 % of grid cells were positive for sightings, so will naturally cover a larger range of values.

Scatterplot of static variables.

Plots show A): Mean depth, B): Mean slope, and C): Mean aspect, against detection-corrected sightings of Harbour porpoise in each 600-m grid cell (n = 90). Loess scatterplot smooths (locally-weighted polynomial regressions) are fitted with the default smoothing span (α = 0.75).

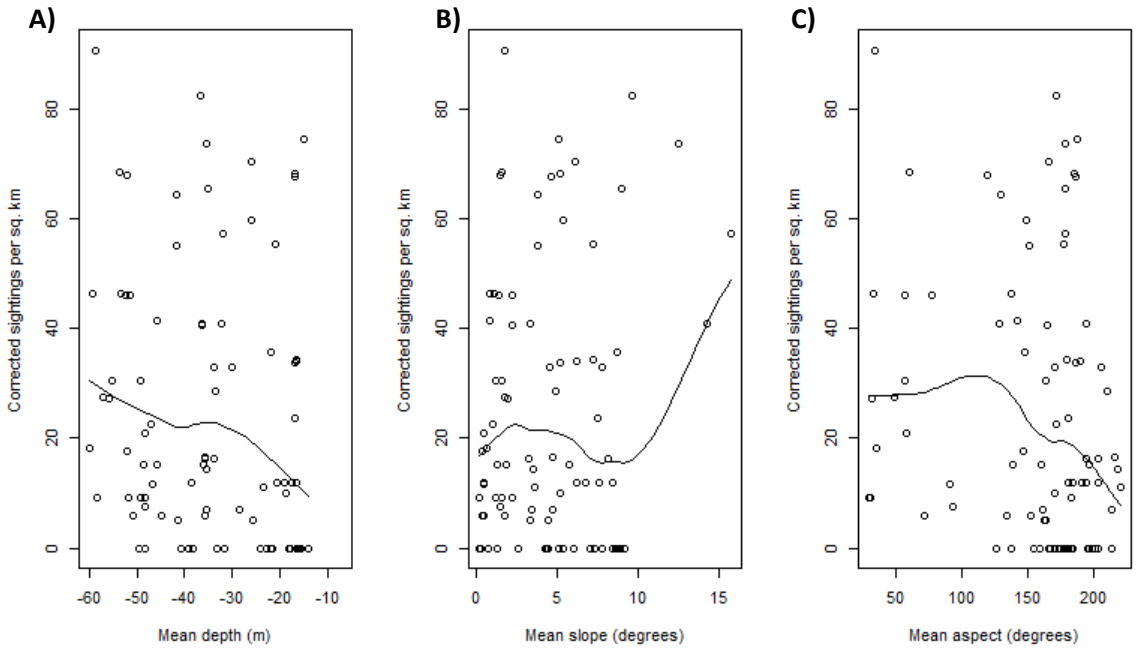

Exploratory scatterplots of corrected porpoise sightings per km^2 indicate that increased sightings are recorded with increasing depth, with the highest numbers between 35 and 60 m water depth, and the lowest recorded sightings in shallower depths of <15 m (0-A). The loess smooth suggests there are increased sightings per unit area with steeper slopes (>10°) and with slopes between 2° and 6° (0-B). The scatterplot of mean aspect against sightings per km^2 (0-C) suggest there is a higher number of recorded sightings for easterly facing slopes, peaking around 100-120° (ESE – SE). There appears decreased sightings in grid cells with more southerly and south-westerly aspects (>130°).

Appendix H.7 Pairplot of candidate static variables used in the porpoise spatial model at Gwennap Head.

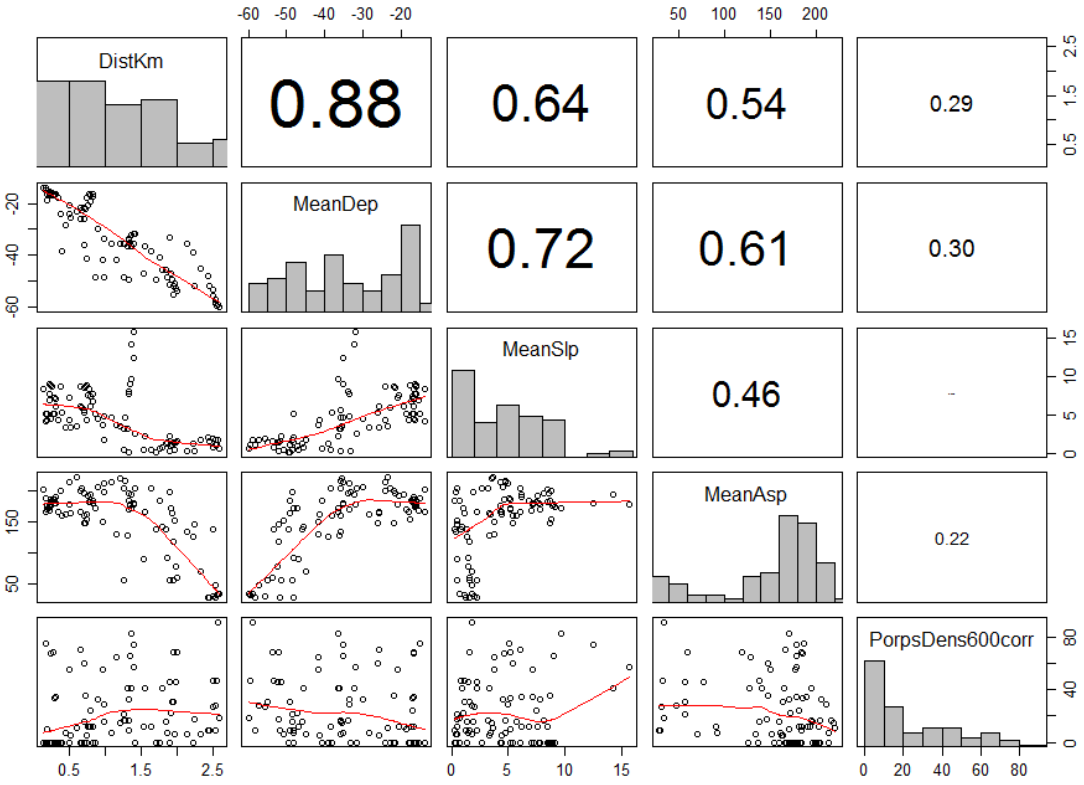

Pairplot of the four candidate static variables with the response, detection-corrected density of porpoise sightings per grid cell, "PorpsDens600corr" (n = 90). Smoothing curves are added to aid visual interpretation, and histograms on the diagonal show distribution of the data. Values on the edges represent units of the variables. Font size of Spearman's absolute correlation coefficients (Rho) in the upper panel is proportional to their value. Response variable: bottom row of panels' y-axes.

Appendix H.8 Spatial model validation plots from Gwennap porpoise model.

Underlying assumptions of homogeneity and normality, and potential influential observations, are verified Appendix H.8 (Figs. A-E). The deviance residuals in the QQ-plot (Fig. A) should ideally lie on the straight line (representing the theoretical quantiles of a negative binomial distribution) but, as the model only explains 50.8% of the variation in the data, some discrepancies are expected.

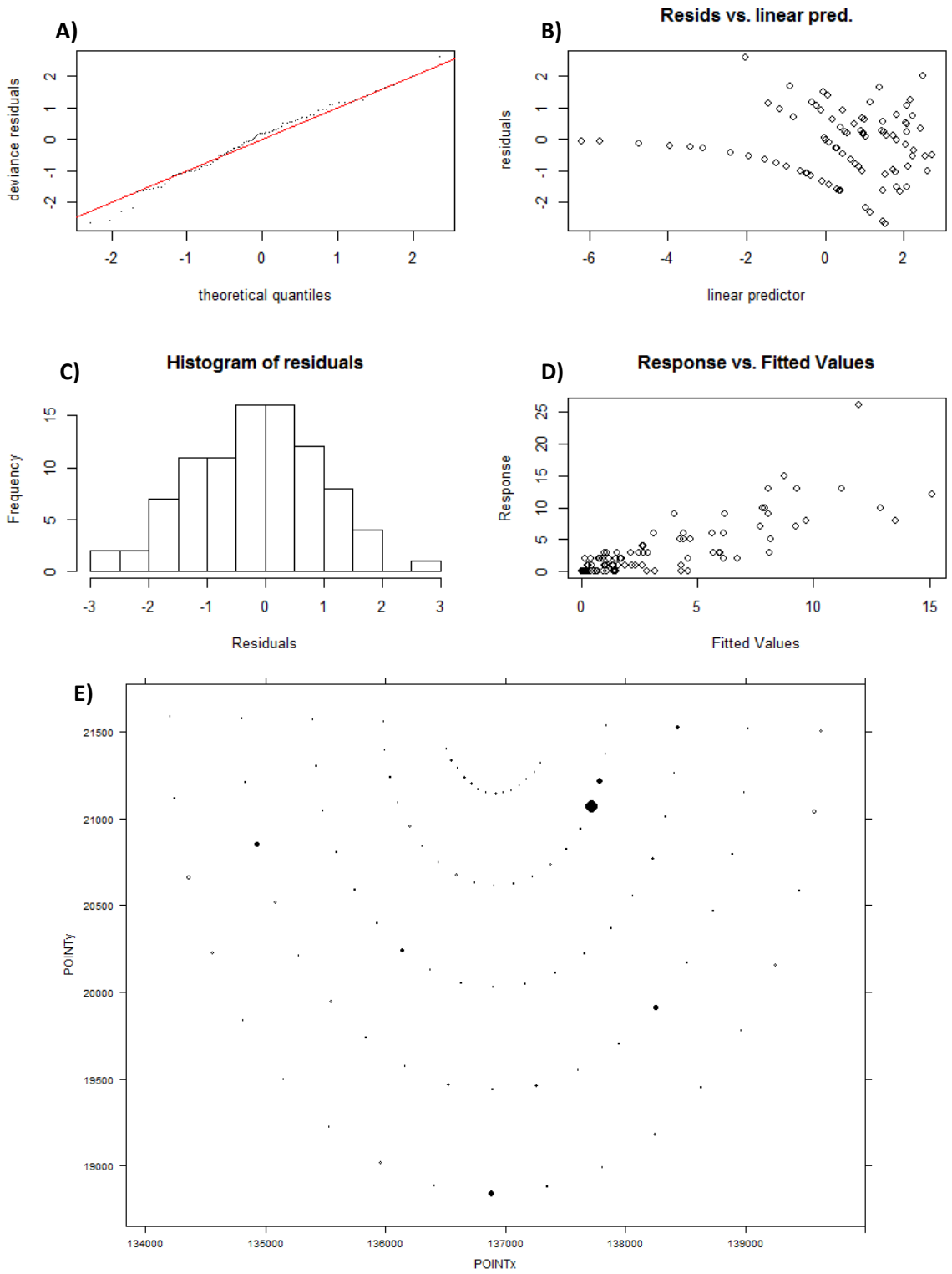

Model validation plots obtained by applying a negative binomial GAM on the detection-corrected porpoise sightings data.

Recorded surfacings were filtered by the 600-m radial grid (n = 90). A): QQ-plot; B): residuals vs. linear predictor; C): histogram of residuals; D): response values vs. fitted values; E): normalised residuals vs. spatial coordinates (black dots are negative residuals; empty dots are positive; size proportional to value of residual). QQ-plot and histogram are used to assess normality; and residuals versus fitted values to assess homogeneity. Response versus fitted values should ideally show a straight line.

Based on the residuals histogram (Fig. C) normality can reasonably be assumed. The residuals plot (Fig. B) suggests much of the heterogeneity in the data has been accounted for, since influential observations were removed prior to the final model selection process. The response versus fitted values of the response variable (Fig. D) should ideally show a straight line, though the level of spread is acceptable. The panel representing spatial dependence (Fig. E) shows little pattern (e.g. clustering of either negative or positive residuals, or their values), except perhaps with those nearest to shore, where there is a string of negative residuals to the west and positives to the east (though their values are comparatively small in context of the whole survey area). Overall, the validation plots do not indicate any obvious problems.

Appendix I Additional temporal analyses for harbour porpoises at the Runnel Stone Reef.

Appendix I.1 Temporal data exploration of porpoise sightings at Gwennap Head.

Sea surface conditions, such as sea state, appear to negatively impact on the number of porpoise sightings recorded during surveys (Appendix I.2-A). The highest rate was 0.41 porpoises per 30-minute survey unit during a sea state 1, reducing to 0.13 during a sea state 3, a three-fold decrease. Although sightings rate appears lowest during sea state 0, this is likely a consequence of very few sampling units during these periods (<1 % of survey effort), so not representative of actual sightings rate.

There are two peaks in the frequency density of sightings rate with SST (Appendix I.2-B) but since the majority of sampling occurred during the summer months with warmer waters, and only over a few days during the winter, the uneven effort over seasons means it is included here for reference but will not be included in the statistical modelling. Additionally, SST was measured at Penzance, several km from the watch point at a coarse resolution both in space and time, so may not be a representative dataset for Gwennap Head.

Appendix I.2 Histograms of effort-corrected sightings (n = 157).

Sightings as a function of A): significant wave height (m), and B): and SST (degrees).

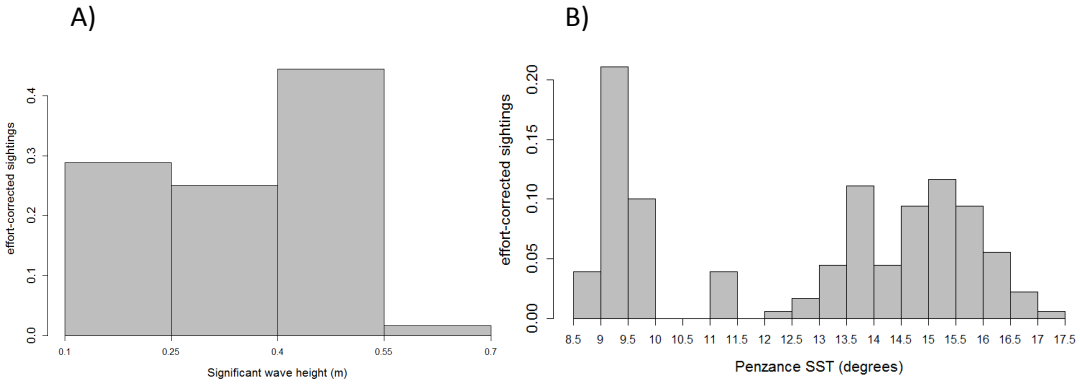

Appendix I.3 Boxplots to explore effect of continuous covariates on the occurrence of harbour porpoises over 737 30-minute units of survey effort across years 2011 – 2013.

A): Wind speed (kmh^{-1}), B): Wind direction (degrees), C): Tidal flow speed (ms^{-1}), D): Tide height (m), E): Tidal range (m), F): Tidal flow direction (degrees), G): Daylight hour (ratio, sunrise:sunset), H): Significant wave height (m), I): Tidal hour (relative to HW, where HW = 0), J): SST (degrees C), and K): Cloud cover (oktas).

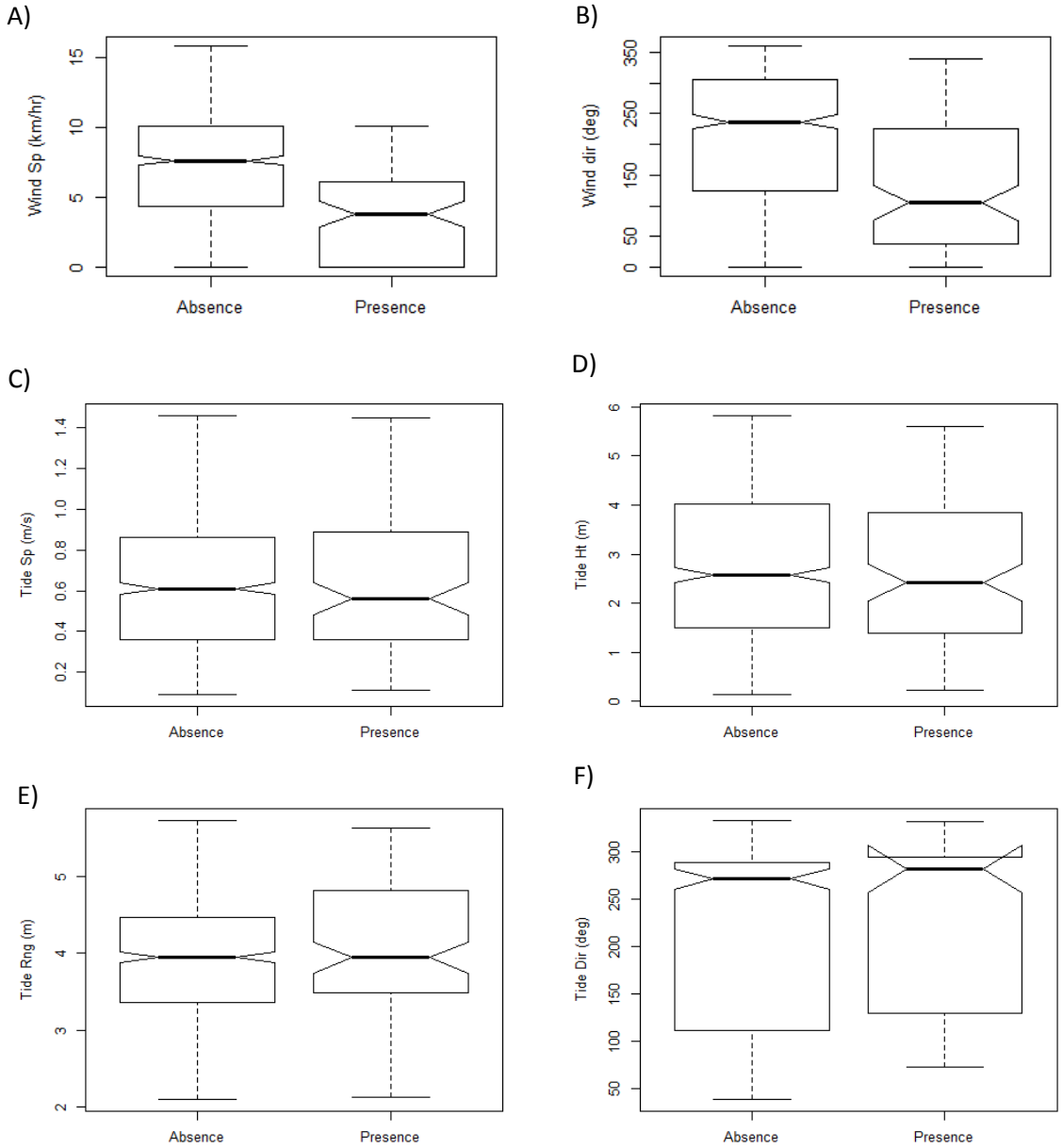

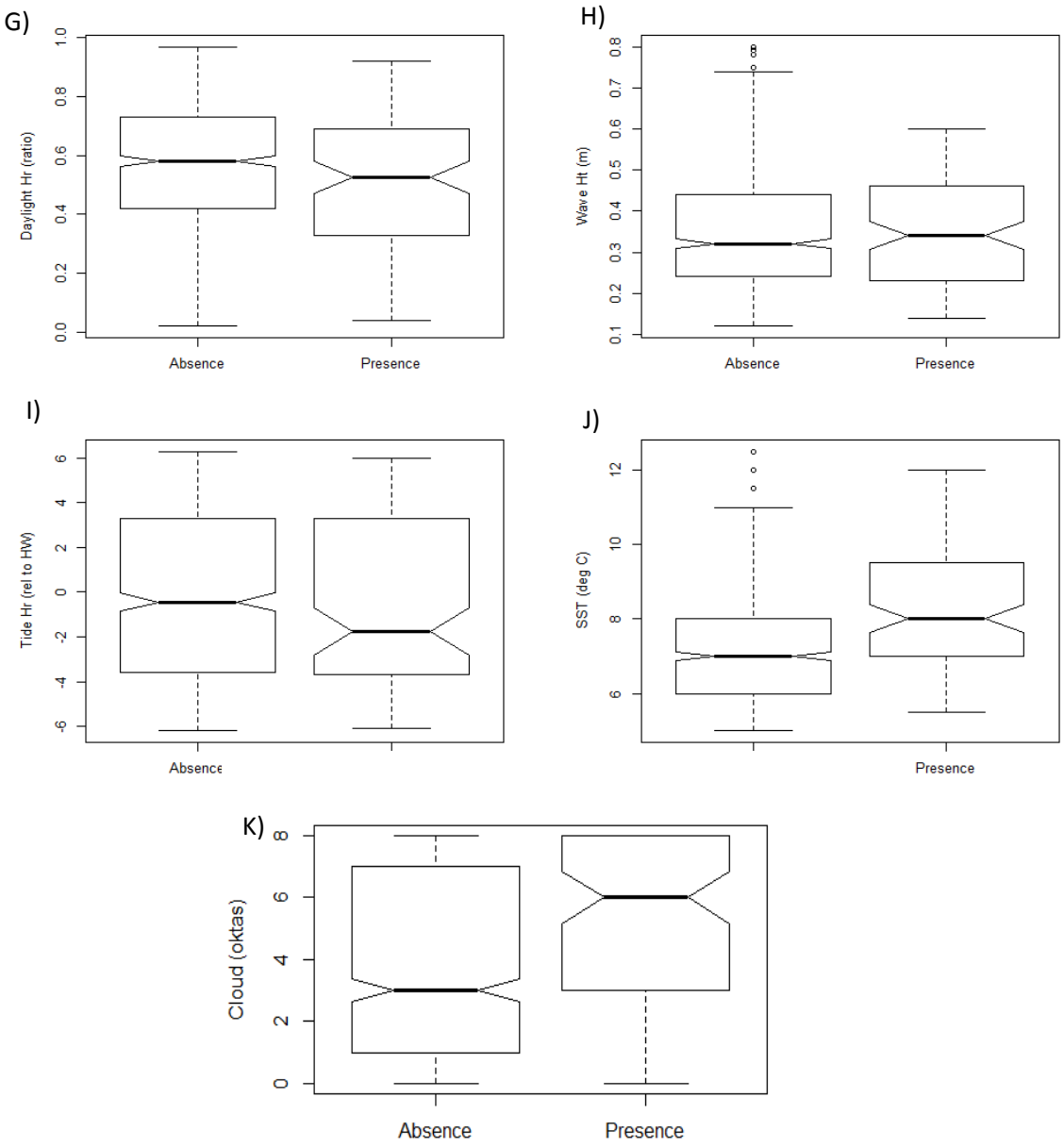

Boxplots to explore the effect of the continuous environmental variables on the presence-absence of porpoise per 30-minute survey unit are shown in Appendix I.3. For both presence and absence, the spread of values covers nearly the entire range of the covariate, except for wind speed, where there is no porpoise occurrence in high speeds above 10 kmh^{-1} (Appendix I.3-A). The medians appear significantly different at the 5 % level (notches do not overlap), with absence occurring at a median value of 7.6 kmh^{-1}, and presence at a considerably slower speed of 3.8 kmh^{-1}. There may be an important influence of wind direction on the occurrence of porpoise (Appendix I.3-B). Absence occurs during south-westerly winds (IQR: 120° – 260°, median: 237°), while more sampling units were positive for sightings during easterlies (median:

105°). The boxplots of the tidal variables (speed, height, range and direction) show that not only are the IQR's very similar between presence and absence but, also, since the notches overlap, this may indicate the medians are not significantly different either (Appendix I.3-C – F). This may suggest that that simple occurrence data (opposed to numbers of sightings) does not have a relationship with these covariates.

Though daylight hour appears to influence sightings rate (Appendix I.3-B), the boxplot suggests that it does not affect the simple presence-absence of the animals to the same extent (Appendix I.3-G). It does appear, however, that porpoise presence occurs slightly earlier in the day than absence time (IQR's: 0.32 – 0.68 and 0.41 – 0.73, respectively), although the medians are very similar (0.58 and 0.53). There appears little correspondence between significant wave height and porpoise presence-absence each 30-minute survey unit (Appendix I.3-H), though it is worth noting that no sampling units were positive for sightings where Hs >0.59 m. There is high variability in the tidal hour data associated with porpoise occurrence (Appendix I.3-I), indicated by the wide and overlapping IQR's, though the median for presence occurs at 1.75 hours before HW while the median for absence occurs at 0.45 before HW. The average SST during absence time (7°C) is cooler by 1°C than during presence time (8°C), though there is greater variability associated with the absence data (Appendix I.3-J). Appendix I.3-K indicates that more presence survey samples are associated with increased cloud cover (median = 6), whereas there is more absence during periods of clearer skies (median = 3).

Appendix I.4 **Pairplot of candidate temporal variables per 30-minute sampling unit of visual survey effort at Gwennap Head.**

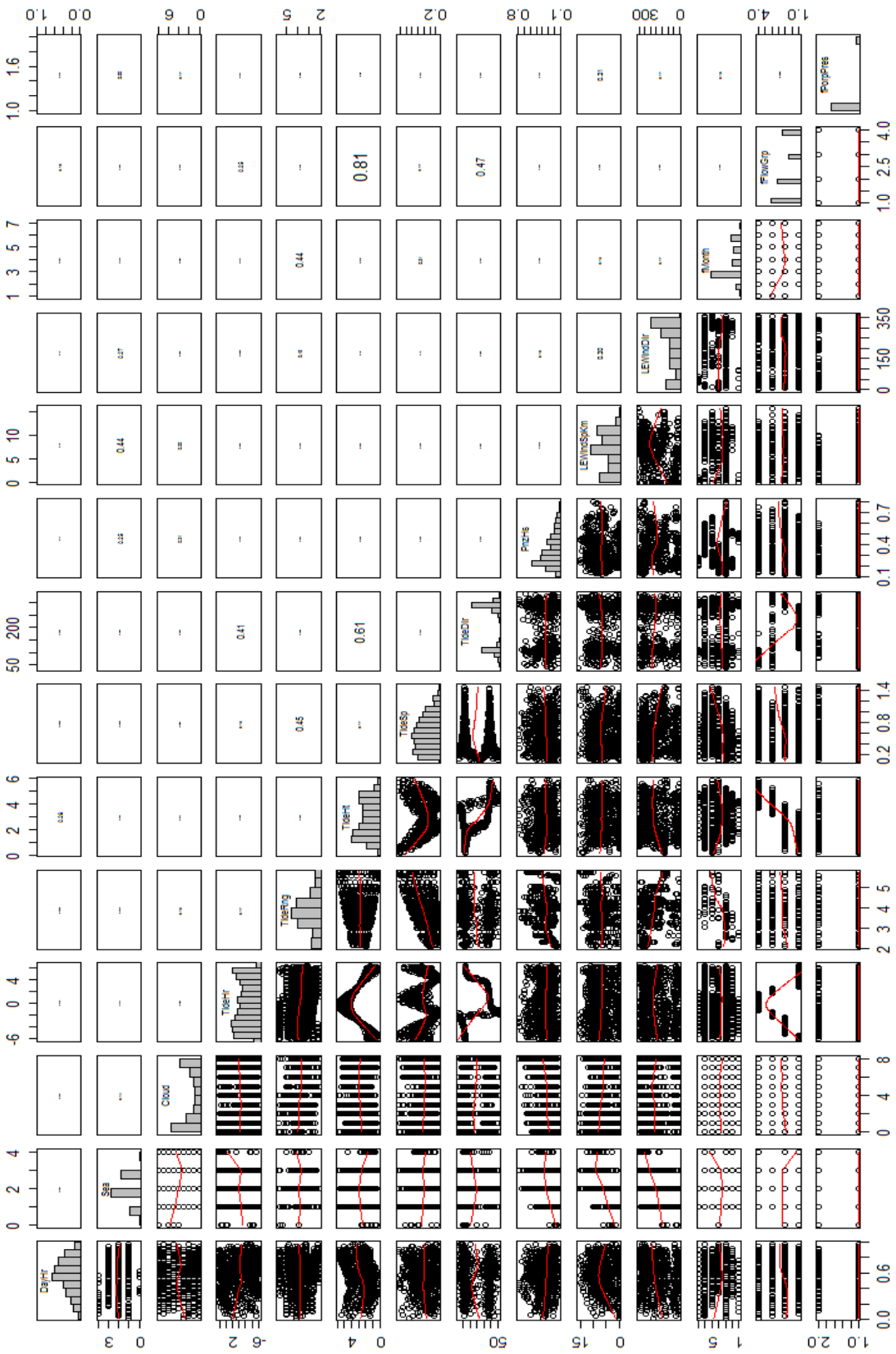

Appendix I.5 **ACF of temporal model residuals for porpoise at the Runnel Stone Reef (blue dotted lines = significance thresholds).**

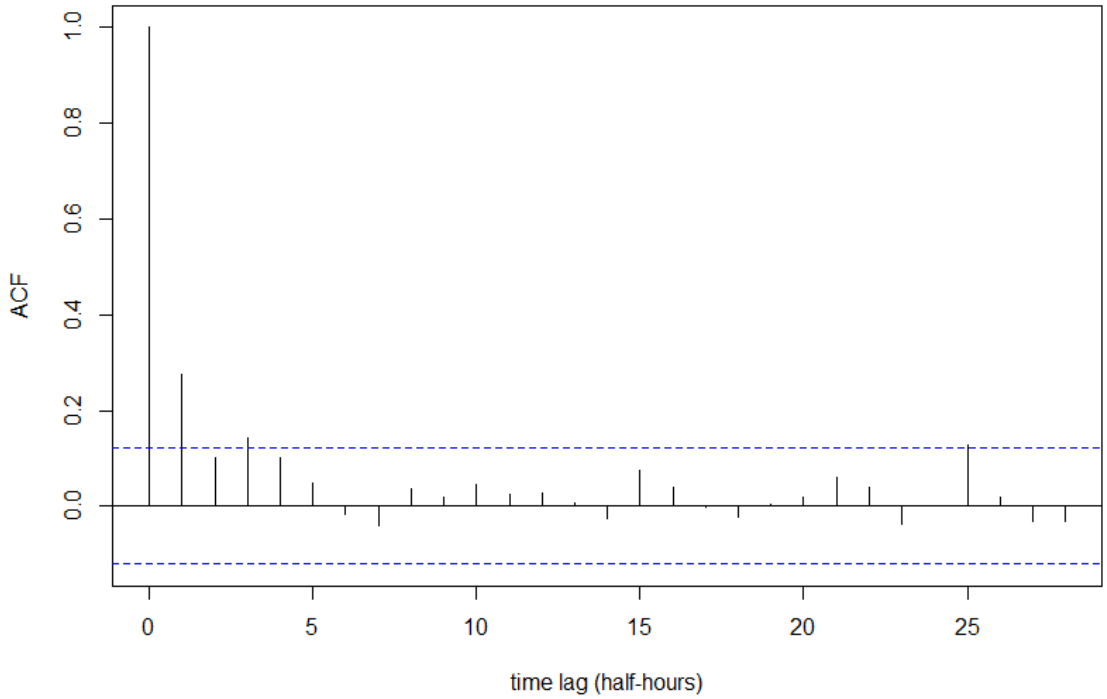

Appendix J Additional acoustic data analyses for cetacean species at the Runnel Stone Reef.

Appendix J.1 Frequency density histograms of DPM by hour of the day, dependent on the threshold value of "%TimeLost" selected to exclude data.

First panel of each species shows unfiltered DPM data; second panel shows 'cDPM' (DPM data *corrected* by the value of "%TimeLost").

Harbour porpoises:

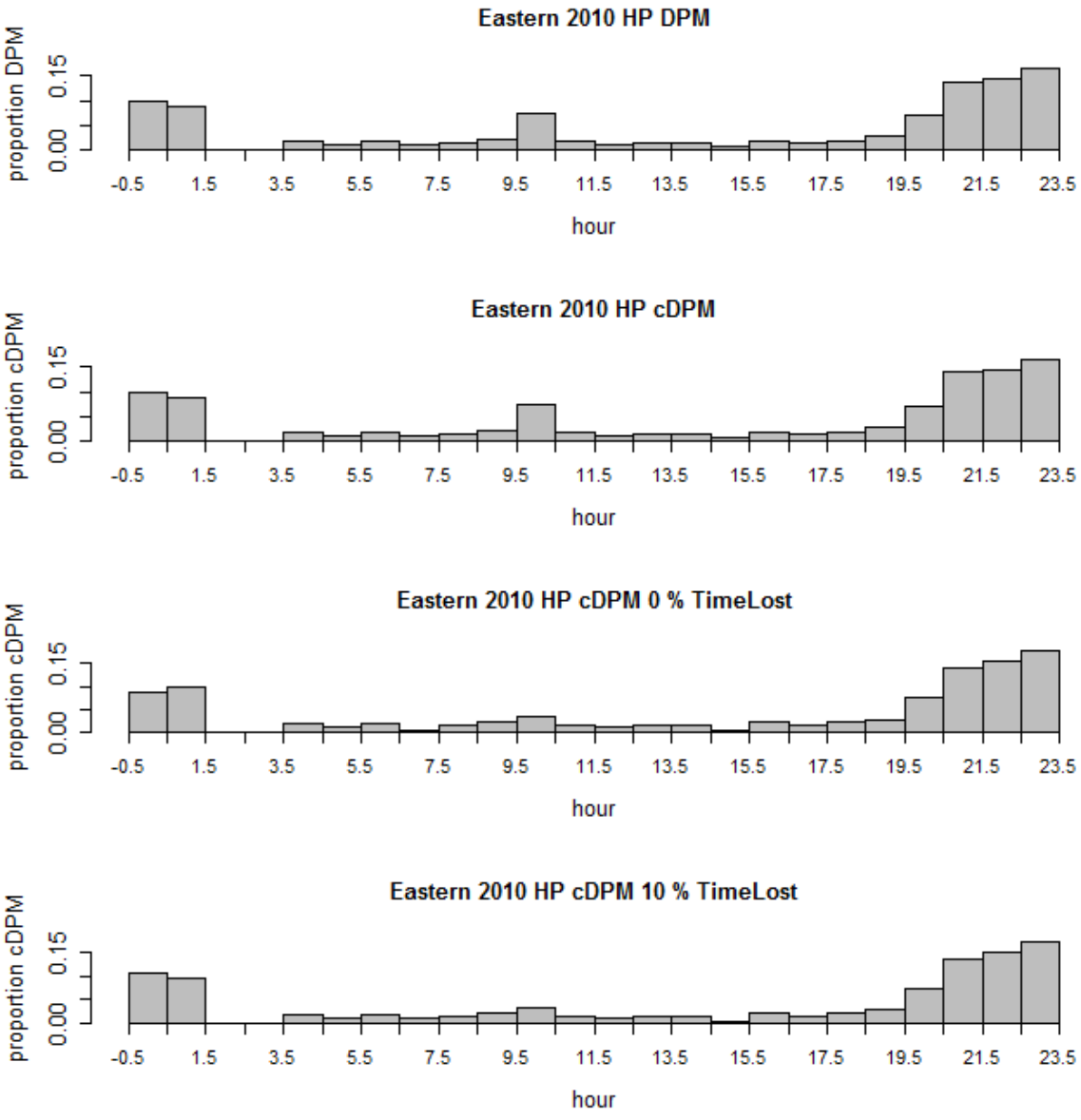

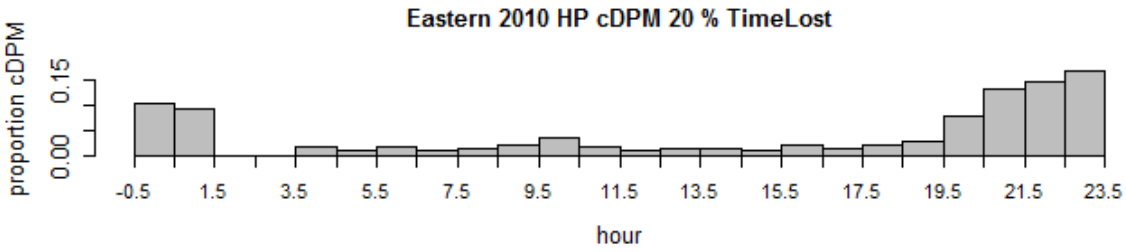
Eastern 2010 HP cDPM 20 % TimeLost
proportion cDPM
0.00
0.15
-0.5
1.5
3.5
5.5
7.5
9.5
11.5
13.5
15.5
17.5
19.5
21.5
23.5
hour

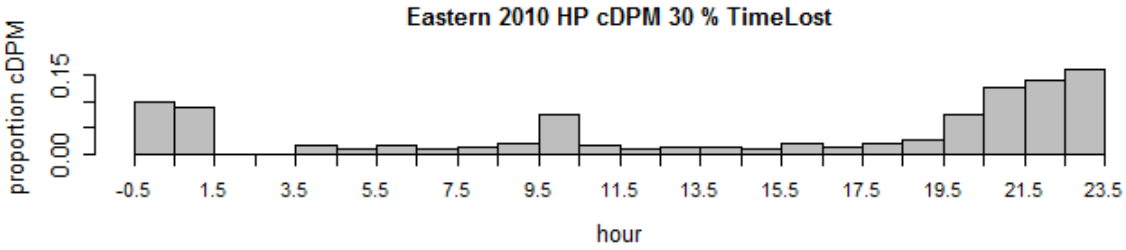
Eastern 2010 HP cDPM 30 % TimeLost
proportion cDPM
0.00
0.15
-0.5
1.5
3.5
5.5
7.5
9.5
11.5
13.5
15.5
17.5
19.5
21.5
23.5
hour

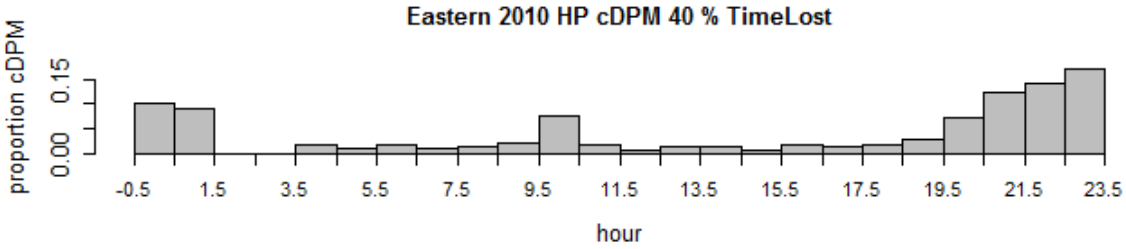
Eastern 2010 HP cDPM 40 % TimeLost
proportion cDPM
0.00
0.15
-0.5
1.5
3.5
5.5
7.5
9.5
11.5
13.5
15.5
17.5
19.5
21.5
23.5
hour

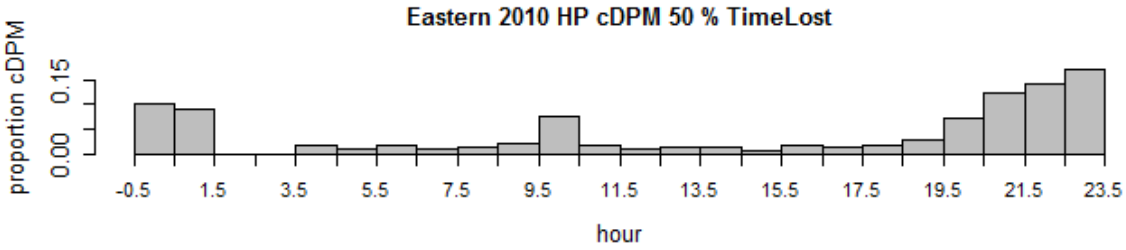
Eastern 2010 HP cDPM 50 % TimeLost
proportion cDPM
0.00
0.15
-0.5
1.5
3.5
5.5
7.5
9.5
11.5
13.5
15.5
17.5
19.5
21.5
23.5
hour

Dolphins:

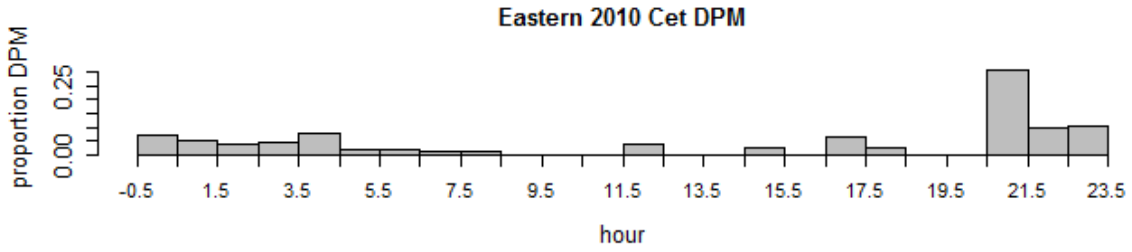
Eastern 2010 Cet DPM
proportion DPM
0.00
0.25
-0.5
1.5
3.5
5.5
7.5
9.5
11.5
13.5
15.5
17.5
19.5
21.5
23.5
hour

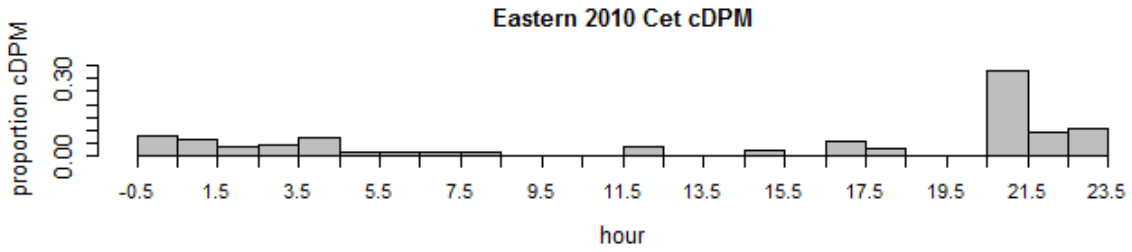
Eastern 2010 Cet cDPM
proportion cDPM
0.00
0.30
-0.5
1.5
3.5
5.5
7.5
9.5
11.5
13.5
15.5
17.5
19.5
21.5
23.5
hour

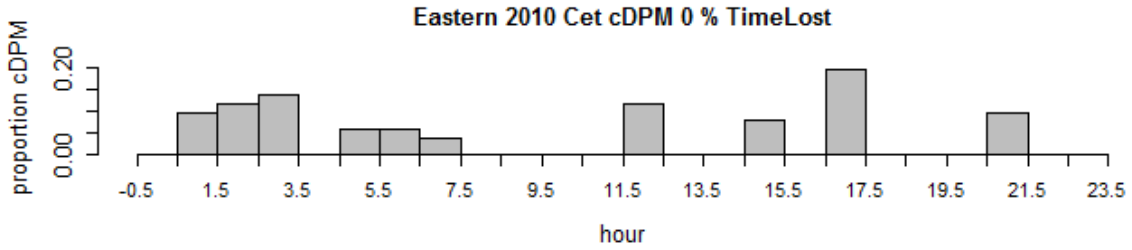
Eastern 2010 Cet cDPM 0 % TimeLost
proportion cDPM
0.00
0.20
-0.5
1.5
3.5
5.5
7.5
9.5
11.5
13.5
15.5
17.5
19.5
21.5
23.5
hour

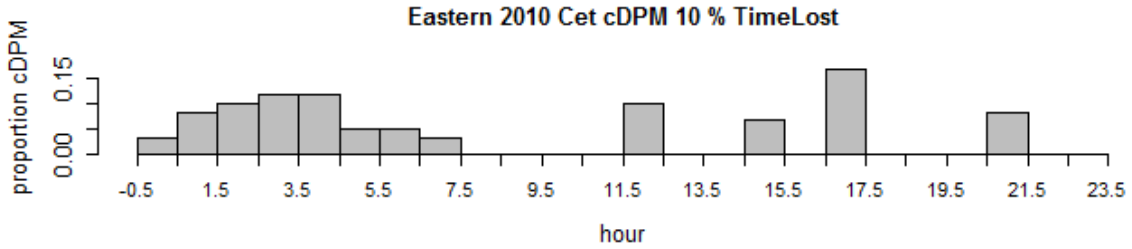
Eastern 2010 Cet cDPM 10 % TimeLost
proportion cDPM
0.00
0.15
-0.5
1.5
3.5
5.5
7.5
9.5
11.5
13.5
15.5
17.5
19.5
21.5
23.5
hour

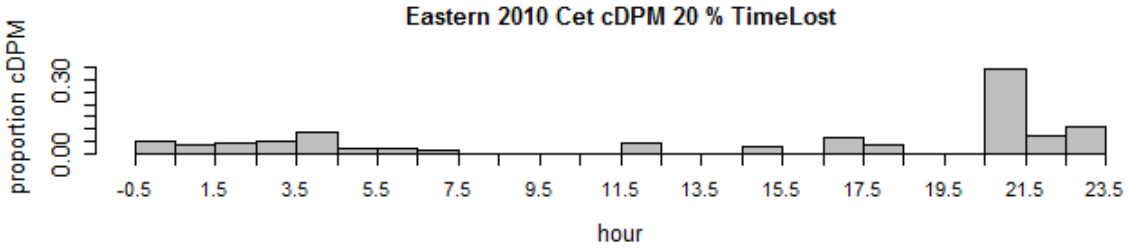
Eastern 2010 Cet cDPM 20 % TimeLost
proportion cDPM
0.00
0.30
-0.5
1.5
3.5
5.5
7.5
9.5
11.5
13.5
15.5
17.5
19.5
21.5
23.5
hour

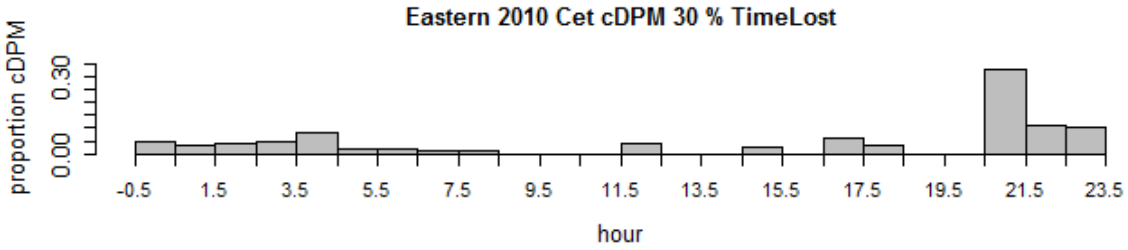
Eastern 2010 Cet cDPM 30 % TimeLost
proportion cDPM
0.00
0.30
-0.5
1.5
3.5
5.5
7.5
9.5
11.5
13.5
15.5
17.5
19.5
21.5
23.5
hour

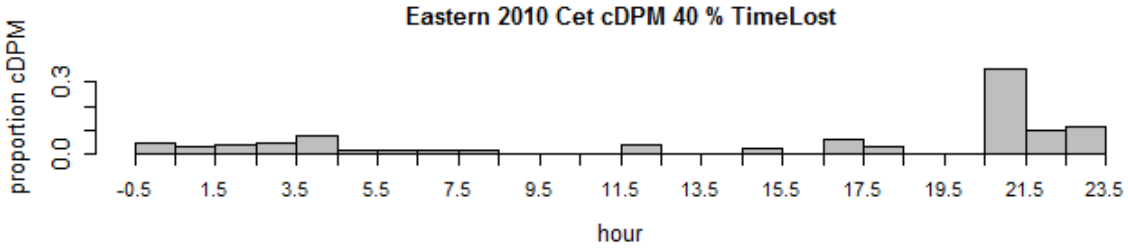
Eastern 2010 Cet cDPM 40 % TimeLost
proportion cDPM
0.0
0.3
-0.5
1.5
3.5
5.5
7.5
9.5
11.5
13.5
15.5
17.5
19.5
21.5
23.5
hour

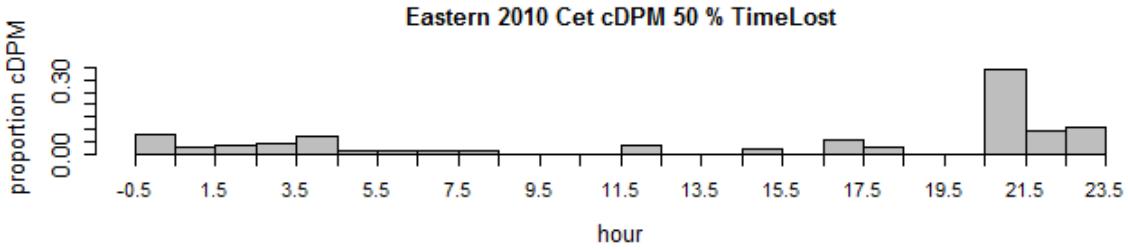
Eastern 2010 Cet cDPM 50 % TimeLost
proportion cDPM
0.00
0.30
-0.5
1.5
3.5
5.5
7.5
9.5
11.5
13.5
15.5
17.5
19.5
21.5
23.5
hour

Appendix J.2 **Pairplot of candidate temporal variables per hour unit of acoustic survey effort at the Runnel Stone Reef study site.**

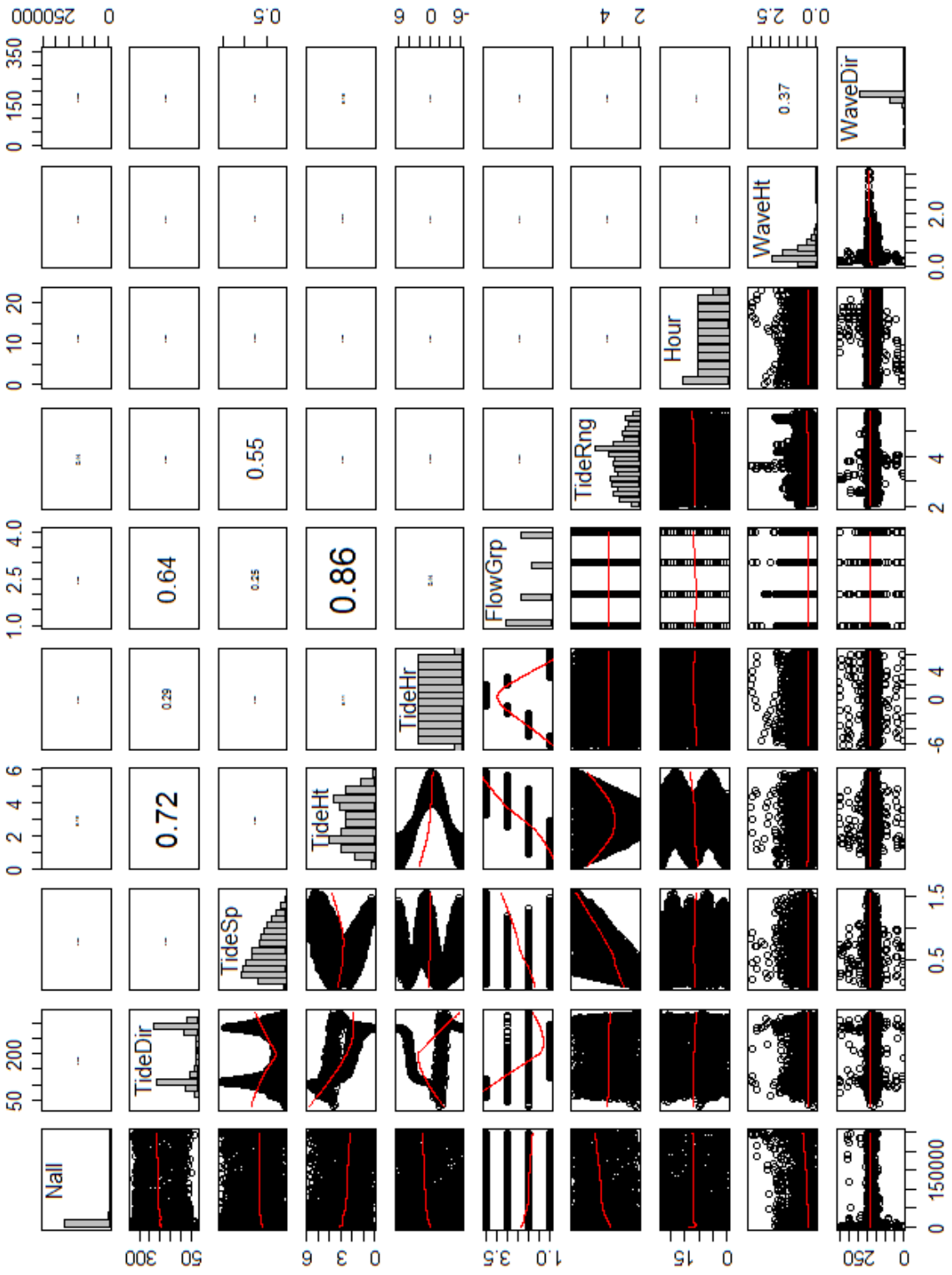

Appendix J.3 Auto-correlation functions of residuals from the acoustic models (blue dotted lines = significance thresholds).

Eastern reef edge (porpoises):

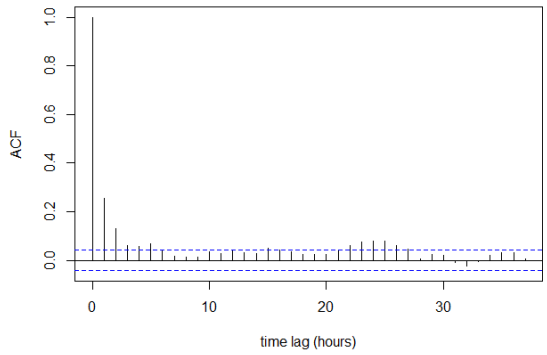

Reef margin (porpoises):

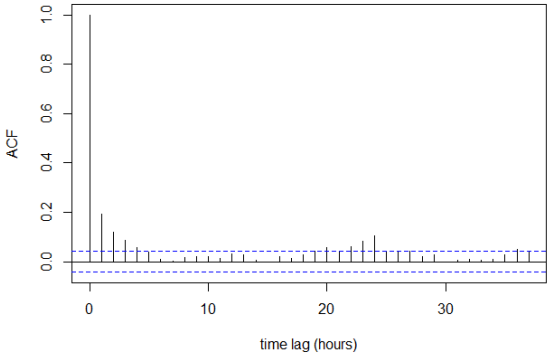

Penberth (porpoises):

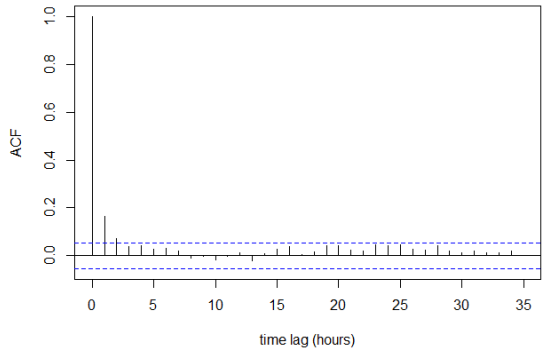

Sites pooled for dolphins:

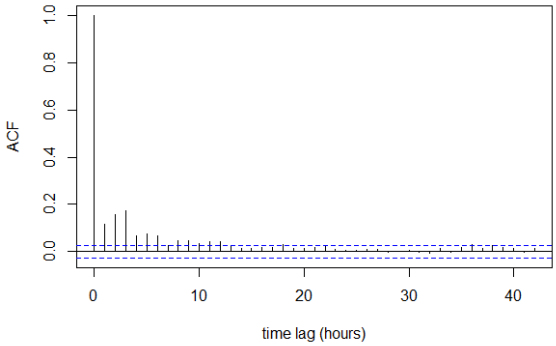

Appendix J.4 Results from acoustic model for porpoise when data was pooled across sites.

To determine the influence of tidal and temporal variables on porpoise acoustic activity at each site, the hourly presence-absence of detections was modelled with a range of candidate survey, tidal and temporal covariates (given in Table 4.5) using a binomial GAM with a logit-link function. Collinearity between the candidate variables was explored using a pairplot (Appendix J.2). Tide height and flow group were highly collinear (r = 0.81), which was dealt with during model selection, according to the procedure to deal with collinearity, detailed in Section 4.2.5. Through forward step-wise selection, the modelling process first compensated for survey effects (site, wave height, wave direction), then tidal variables, and finally temporal variables (as explained in the statistical methods).

The model selected site, tidal range, tidal hour, year, month, hour of the day, and other dolphin acoustic activity ('Cet cDPM') as significant predictors on the presence or absence of porpoise acoustic activity within the Runnel Stone Reef survey area. It took the form:

Porpoise DPM occurrence ~ Site + s(TideRng) + s(TideHr) + fYear + fMonth + s(Hour) + Cet cDPM

The model explained 7.56% of deviance in the occurrence of DPM over 15,974 hours of survey effort across years 2010-2012. All selected variables were highly significant ($p < 0.001$). Model smooths and rate of detection histograms for the significant factor variables are shown below in Figs. A – G. The auto-correlation function of model residuals (Fig. H) shows significant residual correlation of ~12 hours that the model has not accounted for, despite tidal hour and hour of the day having been included as significant variables.

The fitted smooth in Fig. A shows a clear decrease in detections where tidal range >3.5 m, almost half-way through the lunar cycle, i.e. steadily decreasing recorded activity between neaps and springs. Fig. B shows higher number of detections between tidal hours HW0 and HW+3 (when the current switches flow direction from a strong eastward to a strong westward) with a clear peak in the occurrence of acoustic activity at HW+1.5 (strong eastward flow). Acoustic porpoise detections decrease towards a low at 1000 hrs (Fig. C) and increase during the hours of darkness, particularly between 2000 hrs and 0100 hrs. There is a strong (linear) negative correlation between porpoise detection and increasing acoustic activity of other cetacean species (Fig. D).

Fig. E demonstrates the influence of location on the number of detections, even within a relatively small survey area, such as in this study, as well as an effect of year when the data is pooled (Fig. F). The highest and very similar rates of porpoise echolocation activity are found at the two reef sites within the survey area itself. The eastern reef edge has a marginally higher probability of detection of 0.2 hr^{-1}, while the reef margin site has a probability of 0.185 hr^{-1}. There is a lower detection rate at the Penberth control site, with a value of 0.14 hr^{-1}.

There appears an increase in the rate of detections each year of the survey and, even though 2012 has the highest rate of detection, which may be falsely inflated by the fact that the CPOD at the site with the lowest probability (Penberth) was not recording, the increase is still apparent between the first two years of survey when all three loggers did record successfully. There is a consistent detection rate of approximately 0.17 hr^{-1} between the months of July and September (Fig. G), though this increases to 0.25 hr^{-1} in October.

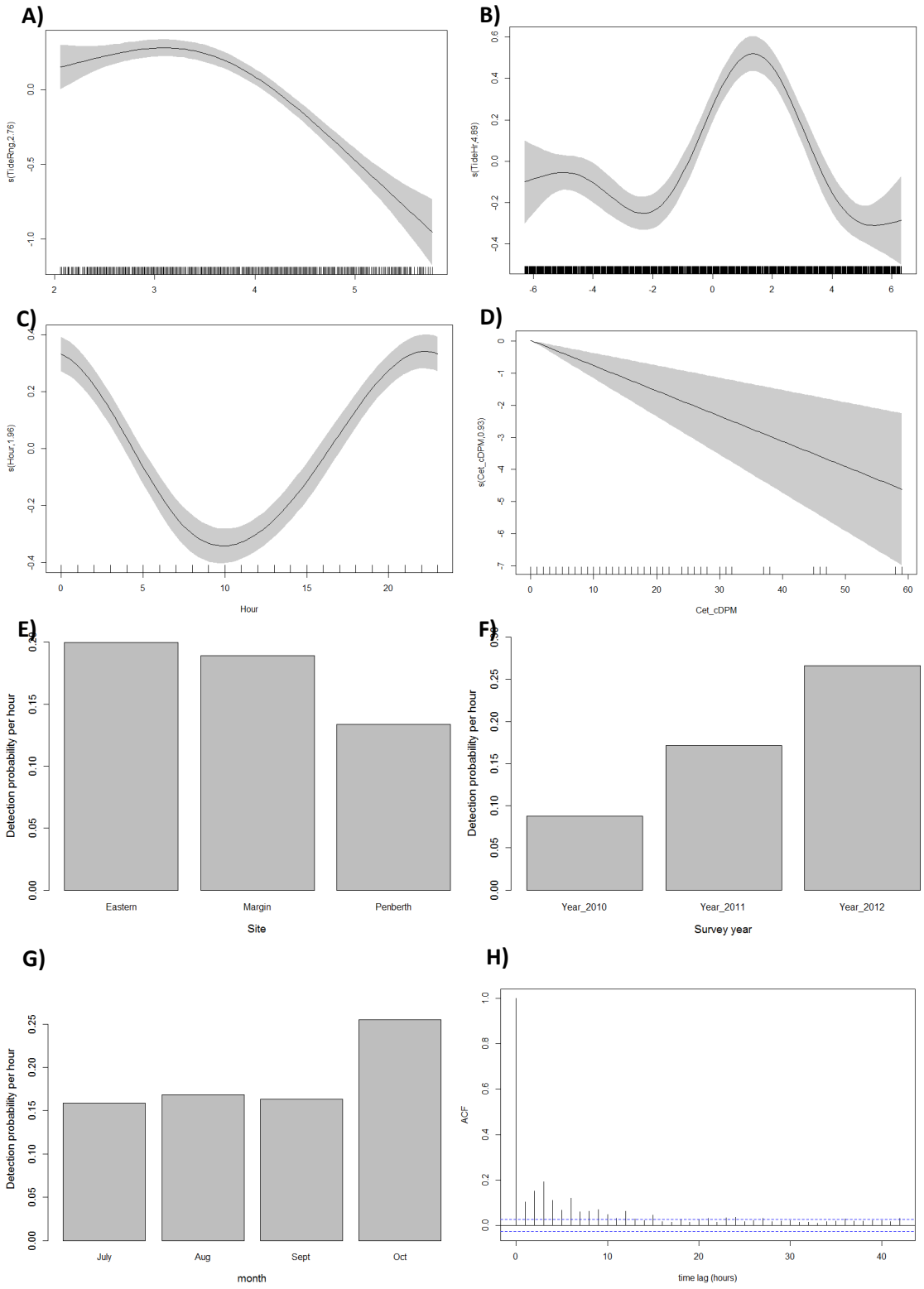
A)
s(TideRng,2.76)
B)
s(TideHt,4.89)
C)
s(Hour,1.96)
Hour
D)
s(Cet_cDPM,0.93)
Cet_cDPM
E)
Detection probability per hour
Eastern
Margin
Penberth
Site
F)
Detection probability per hour
Year_2010
Year_2011
Year_2012
Survey year
G)
Detection probability per hour
July
Aug
Sept
Oct
month
H)
ACF
time lag (hours)

Appendix J.5 **Negative binomial GAM showing significant (p < 0.001) negative relationship between total noise "Nall" and tide height at the reef margin CPOD site.**

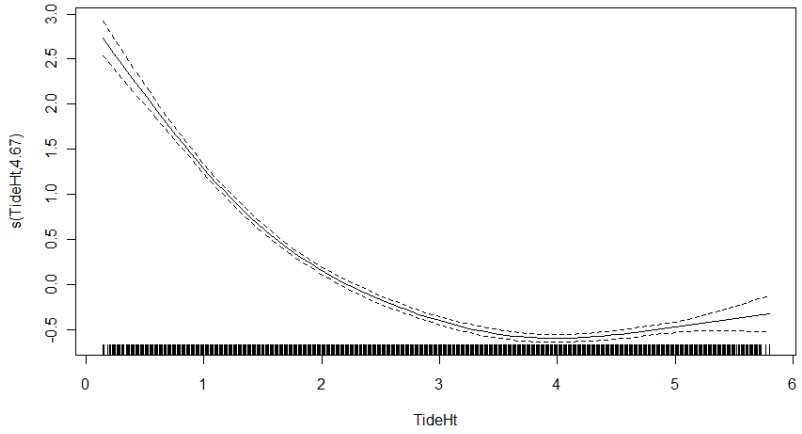

Appendix J.6 **Negative binomial GAM showing significant (p < 0.001) correlation between total noise "Nall" and tidal range on the pooled CPOD data.**

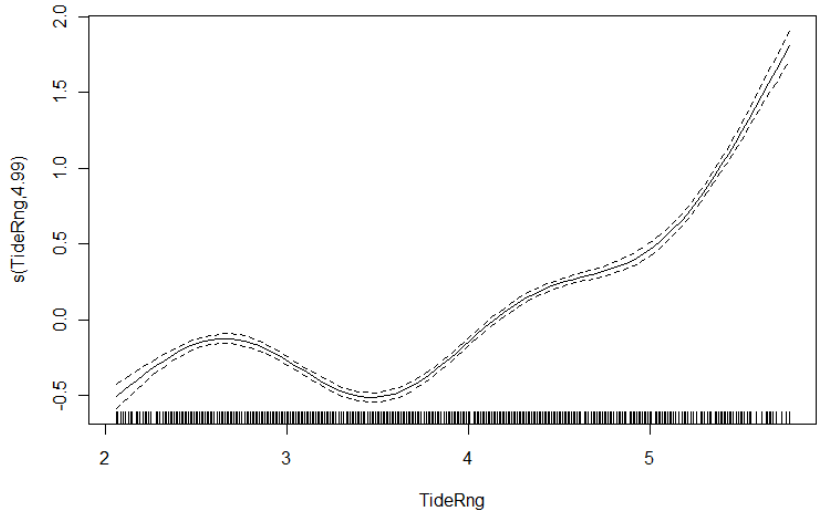

Appendix K Additional spatial analyses for seabird foraging events at the Runnel Stone Reef.

Appendix K.1 Kernels of foraging events filtered by the 300-m grid.

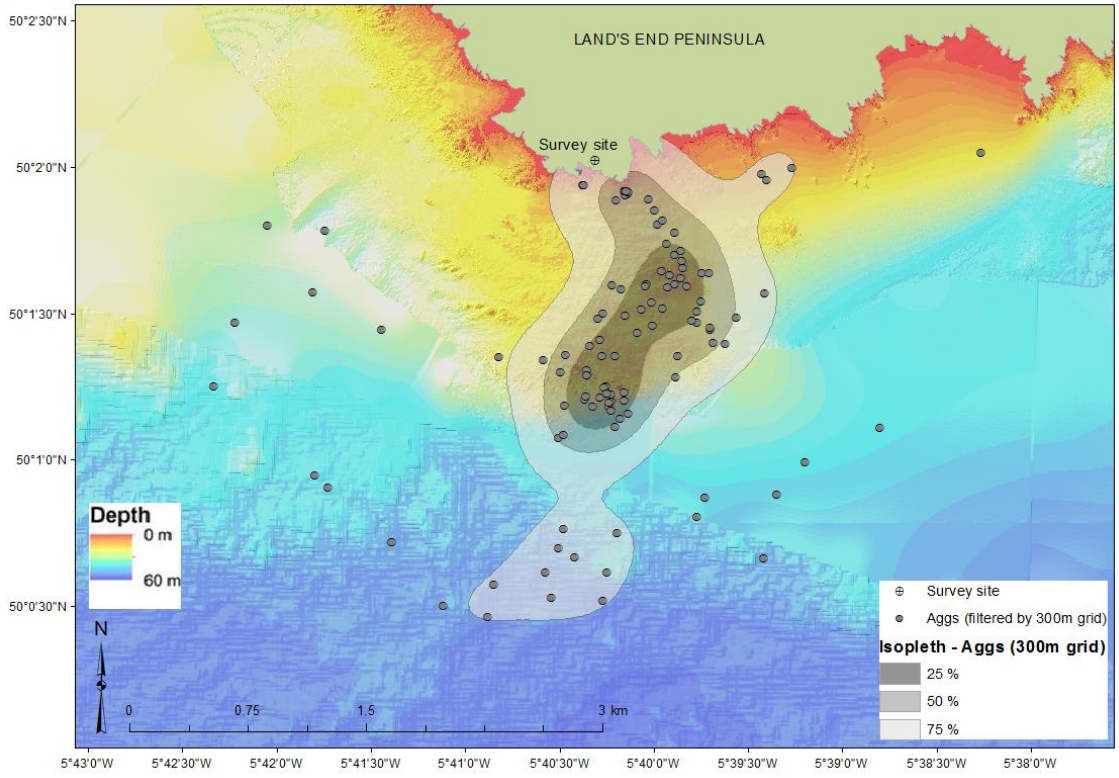

Appendix K.2 Sightings and covariate data summarised by the 300-m radial grid.

Parameter	Value
Number of (300-m) grid cells	190
Number of 'absence' cells (%)	125 (66%)
Number of (filtered) sightings: foraging seabird aggregations	113
Range of sightings per grid cell	0 – 9
Mean sightings per cell (s.d.)	0.63 (1.43)
Static physical variables	
Depth (m)	
Range	3.5 – 61.1
Mean (s.d.)	32.5 (15.3)
Aspect (degrees)	
Range	27.7 – 248.0
Mean (s.d.)	154.4 (54.7)
Slope (degrees)	
Range	0.15 – 21.9
Mean (s.d.)	5.1 (4.4)
Distance from shore to centre of grid cell (m)	
Range	2.4 – 2729.5
Mean (s.d.)	1107.6 (792.4)
Grid cell area (m^2)	
Range	344.5 – 152631.4
Mean (s.d.)	77701.5 (45980)

To visually compare whether there is a difference in high density areas dependent on grid cell size used, calculations were carried out for both. Whether filtered by the finer (Appendix K.2; Fig. A) or coarser (Appendix K.2; Fig. B) grids, results show increased observations clearly associated with the eastern reef margin, particularly where the reef inflects near the lee ore, an area ~0.16 km^2 around the southern pinnacles, and the shallow, nearshore zones to the east of the watch point.

Aggregation relative densities per km^2 comparing effect of filtering by different grid cell sizes:

A) Filtering by 300 m grid

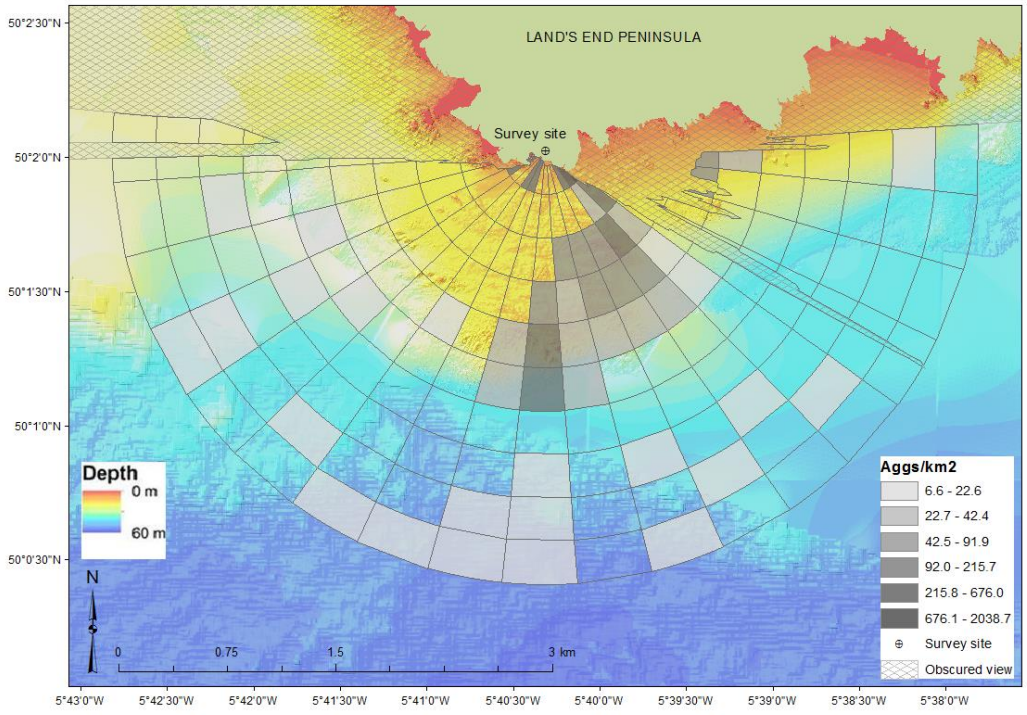

B) Filtering by 600-m grid

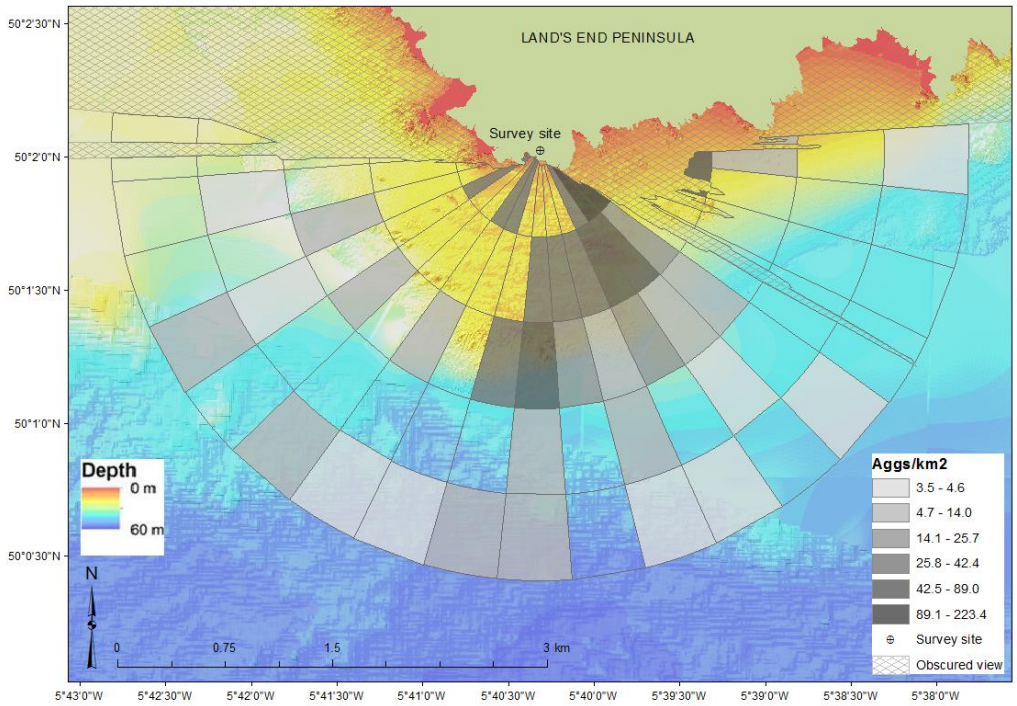

Appendix K.3 **Boxplots of the presence-absence of foraging seabird aggregations at Gwennap Head, as a function of static covariates.**

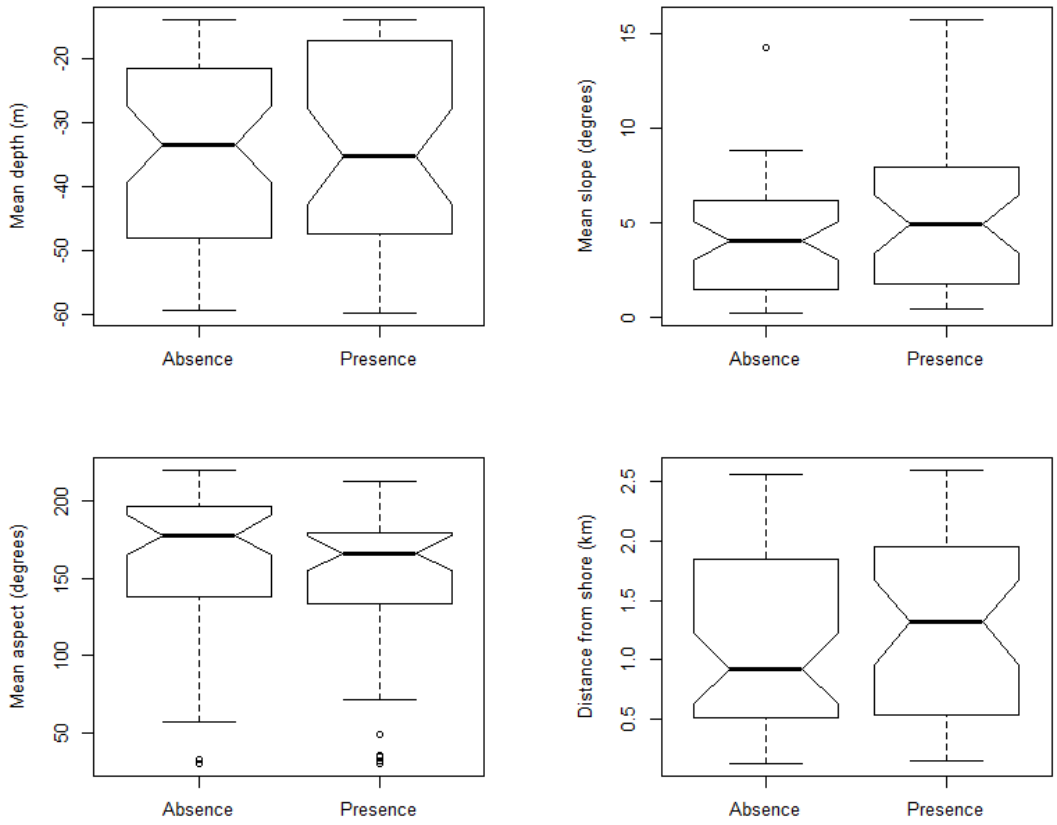

Appendix K.4 **Pairplot of candidate static variables used in the spatial model for foraging seabird aggregations at Gwennap Head.**

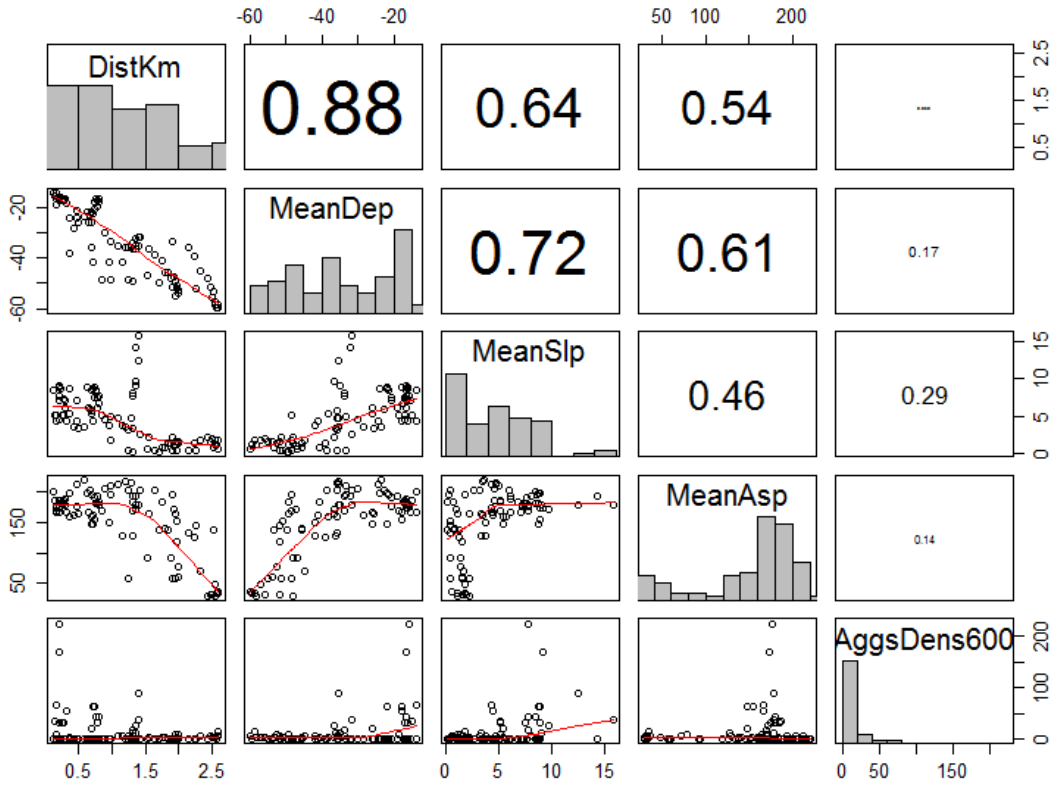

Pairplot of the four candidate static variables with the response, area-corrected density of foraging seabird aggregation sightings per grid cell, "AggsDens600" (n = 90). Smoothing curves are added to aid visual interpretation, and histograms on the diagonal show distribution of the data. Values on the edges represent units of the variables. Font size of Spearman's absolute correlation coefficients (Rho) in the upper panel is proportional to their value. Response variable: bottom row of panels' y-axes.

Appendix K.5 **Model validation plots for the spatial model of seabird foraging events at the Runnel Stone Reef.**

Underlying assumptions of homogeneity and normality, and potential influential observations, are verified in the model validation plots. The deviance residuals in the QQ-plot (Fig. A) should ideally lie on the straight line (representing the theoretical quantiles of a negative binomial distribution) but, as the model explains 63.4% of variation in the data, these discrepancies are minimal.

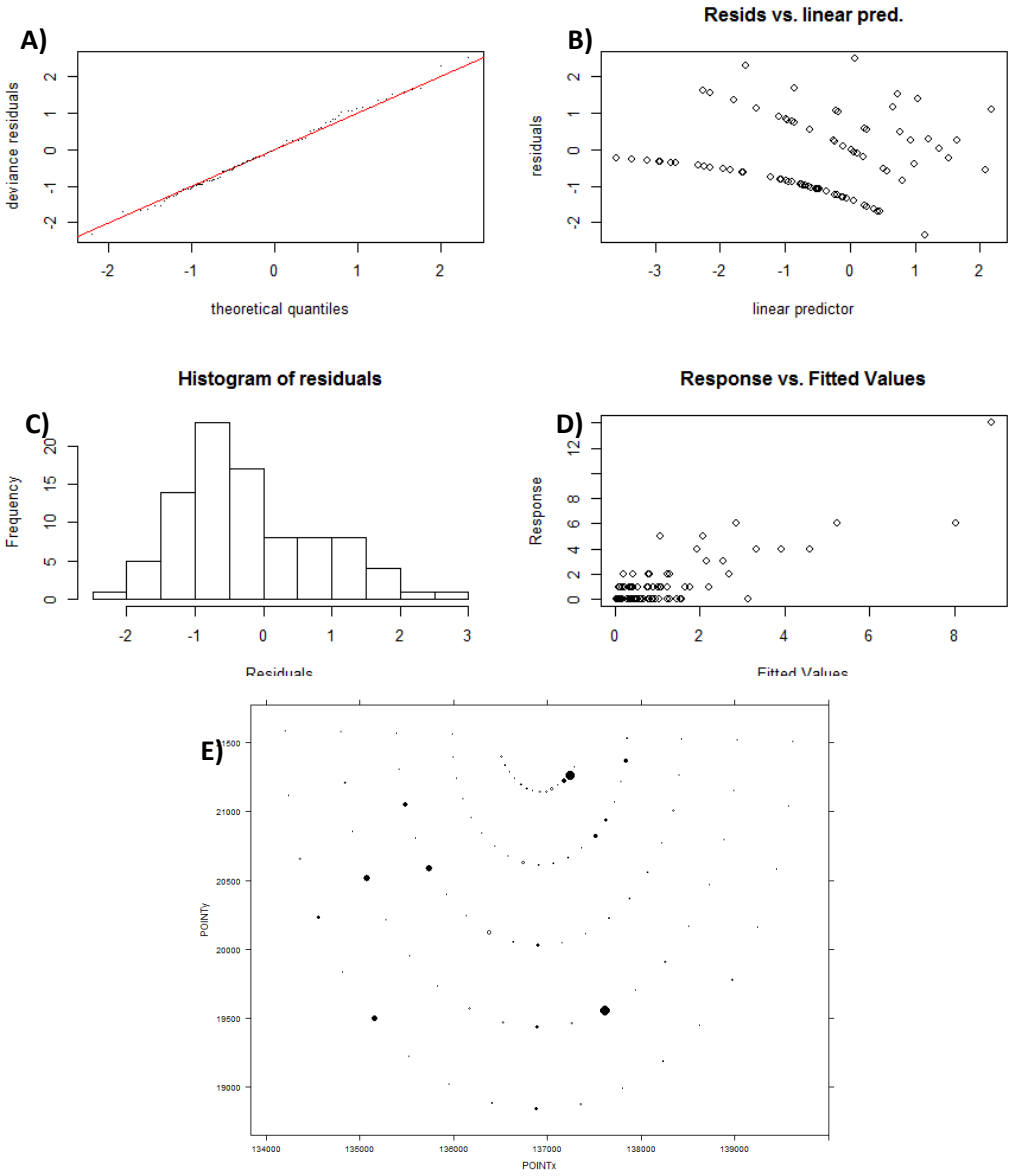

The residuals' plot (Fig. B) suggests much of the heterogeneity in the data has been accounted for, since influential observations were removed prior to the final model selection process. Based on the residuals histogram (Fig. C) normality can reasonably be assumed. The response versus fitted values of the response variable (Fig. D) should ideally show a straight line, though the level of spread is acceptable. The panel representing spatial dependence (Fig. E) shows little pattern (e.g. either clustering of negative or positive residuals, or their values). Overall, the validation plots do not indicate any obvious problems, so the spatial model can be accepted.

Appendix L Additional temporal analyses for seabird foraging events at the Runnel Stone Reef.

A thorough data exploration was carried out on the temporal aggregation sightings data prior to modelling and provided below.

Appendix L.1 Effort-corrected seabird foraging events (n = 100) as a function of temporal covariates.

Preliminary analysis indicates more sightings are observed with increasing sea states (Fig. A) reaching 0.5 events-hr^{-1} in a sea state 2, but after sea state 3, the rate falls, though this is likely a false, given the low number of sea states below 2 that were observed. Increasing cloud cover (Fig. B) is associated with decreased foraging events in the survey area. There are >0.2 events hr^{-1} during periods of clear skies (0 oktas), falling to 0.7 when fully overcast (8 oktas).

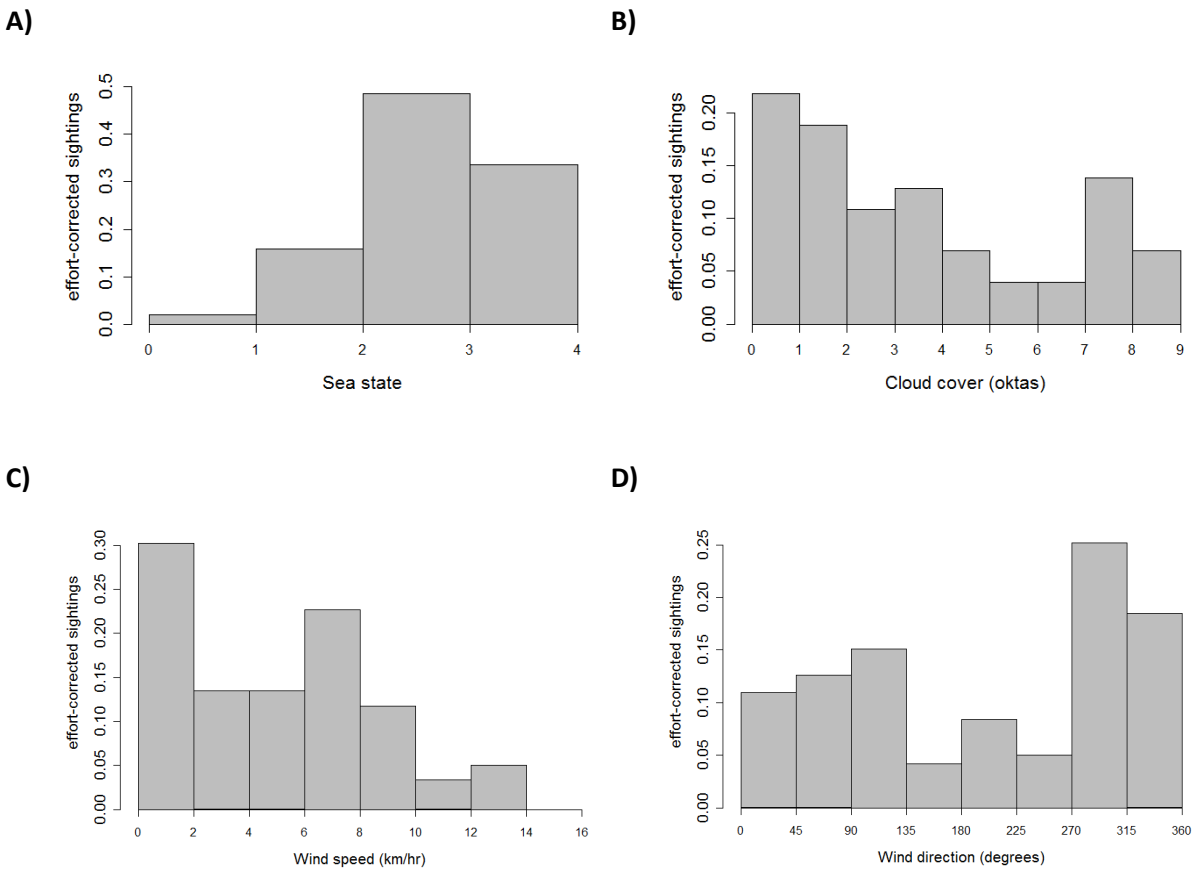

Sightings rates as a function of wind speed indicates decreased sightings are associated with increasing wind speeds (Fig. C), which fall from 0.3 aggregations hr^{-1} in calm conditions, to 0.04 hr^{-1}

during speeds >10 km hr^{-1}. The highest probabilities of observing foraging events are during north-westerly winds (~300°) and to a lesser extent during easterlies (Fig. D). The lowest sightings rates occur during southerly winds (~180°), which blow straight across the survey area directly north at the watch point.

Fig. E shows marginally increased sightings rates with increasing tide height, though no observable differences in the relationship with tidal flow direction (Fig. H), as the rate is ~0.38 aggregations hr^{-1} during both eastward (~120°) and westward flows (~275°).The number of sightings appears to increase around neap tides, as indicated in Fig. F, that evidences the association between foraging aggregations and tidal range, which is a proxy for time in the spring-neap cycle. The probability of seabird foraging events changes throughout the tidal cycle (Fig. G), with decreased sightings rates around the site-specific hours of slack water (HW-2 to HW, and HW+2 to HW+3), which carries over into the first hour of the subsequent flow directions, both eastward and westward. Peak sightings rates appear to coincide when eastward and westward flows are in full force (~HW-3, HW+1 and HW+5). Fig. I shows a clear peak in foraging seabird sightings (0.12 aggregations hr^{-1}) shortly after first light (~daylight hour 0.15), which drops dramatically towards midday (daylight hour 0.5), before increasing to a second, higher peak (0.16 aggregations hr^{-1}) in the hours just before sunset, ~daylight hour 0.8.

E)

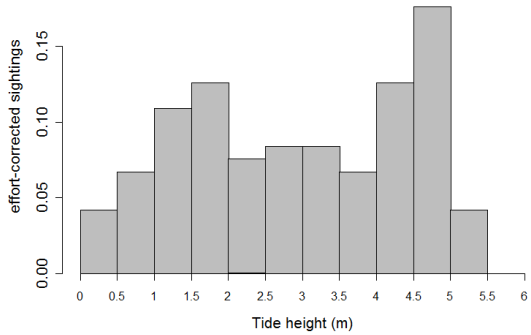
effort-corrected sightings
0.00
0.05
0.10
0.15
0 0.5 1 1.5 2 2.5 3 3.5 4 4.5 5 5.5 6
Tide height (m)

F)

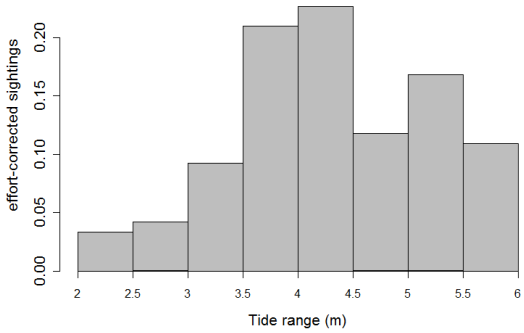
effort-corrected sightings
0.00
0.05
0.10
0.15
0.20
2 2.5 3 3.5 4 4.5 5 5.5 6
Tide range (m)

G)

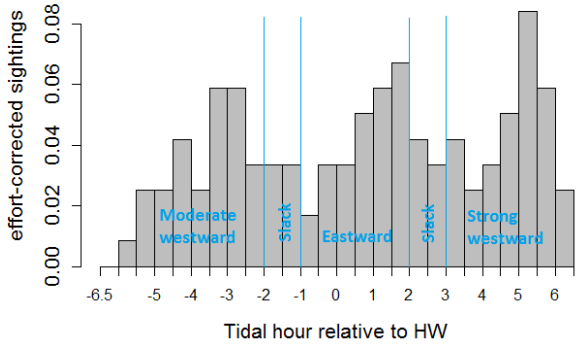
effort-corrected sightings
0.00
0.02
0.04
0.06
0.08
Moderate westward
Slack
Eastward
Slack
Strong westward
-6.5 -5 -4 -3 -2 -1 0 1 2 3 4 5 6
Tidal hour relative to HW

H)

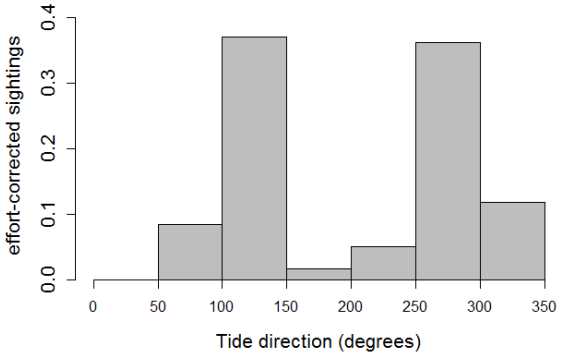
effort-corrected sightings
0.0
0.1
0.2
0.3
0.4
0 50 100 150 200 250 300 350
Tide direction (degrees)

I)

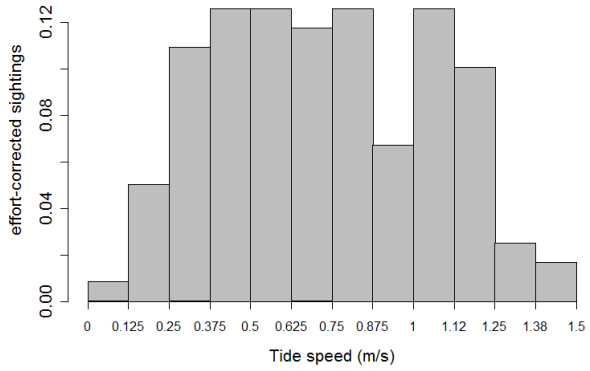
effort-corrected sightings
0.00
0.04
0.08
0.12
0 0.125 0.25 0.375 0.5 0.625 0.75 0.875 1 1.12 1.25 1.38 1.5
Tide speed (m/s)

J)

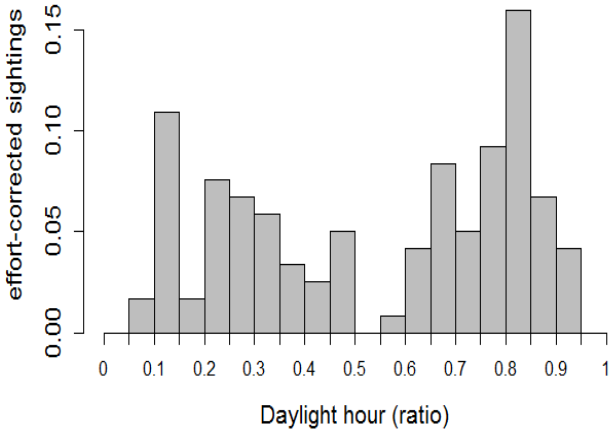
effort-corrected sightings
0.00
0.05
0.10
0.15
0 0.1 0.2 0.3 0.4 0.5 0.6 0.7 0.8 0.9 1
Daylight hour (ratio)

Appendix L.2 Boxplots to explore effect of continuous covariates on the occurrence of seabird aggregations over 737 30-minute units of survey effort across years 2011 – 2013.

A): Wind speed (kmh^{-1}), B): Wind direction (degrees), C): Tidal flow speed (ms^{-1}), D): Tide height (m), E): Tidal range (m), F): Tidal flow direction (degrees), G): Daylight hour (ratio, sunrise:sunset), H): Significant wave height (m), I): Tidal hour (relative to HW, where HW = 0), and J): Cloud cover (oktas).

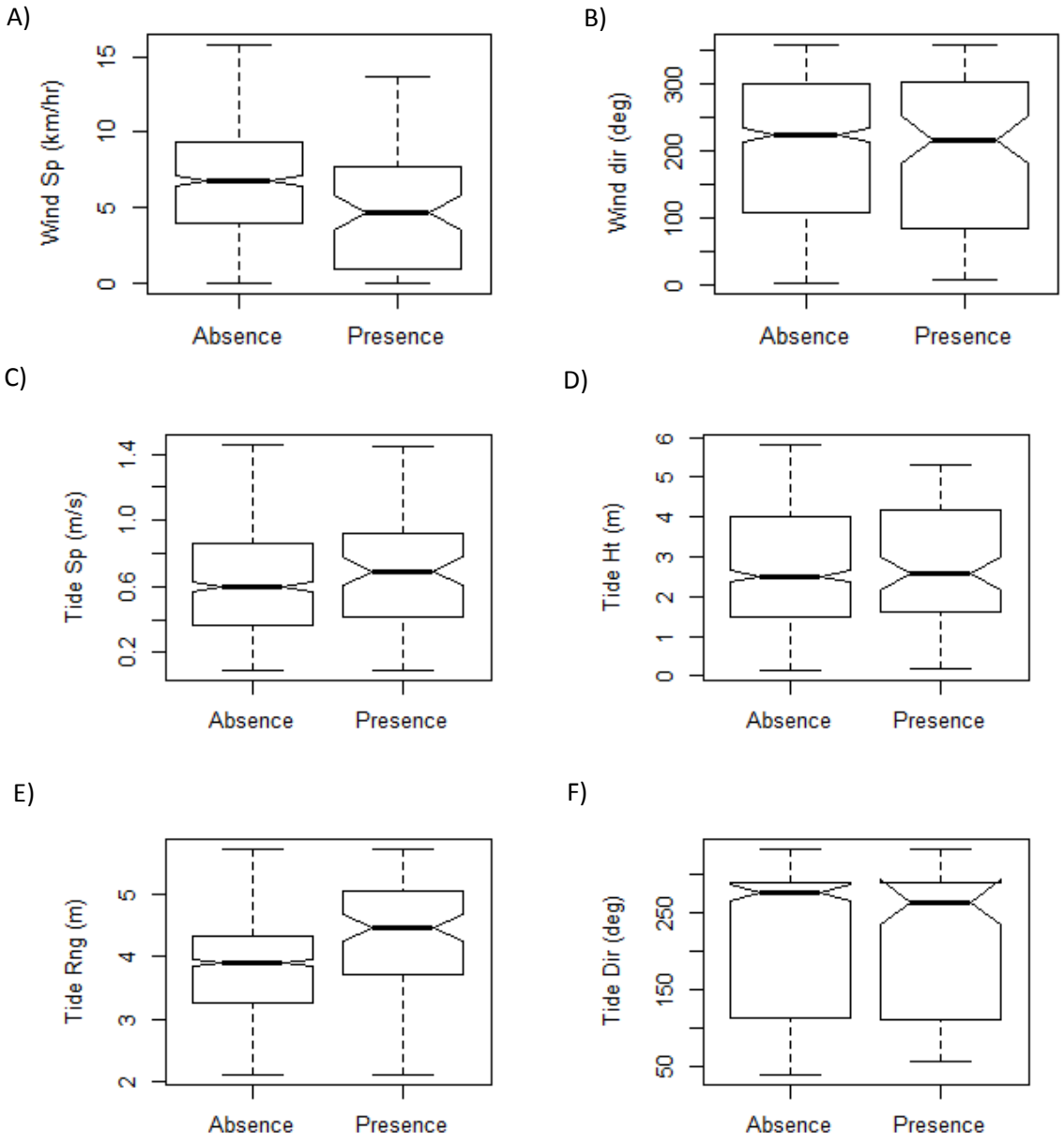

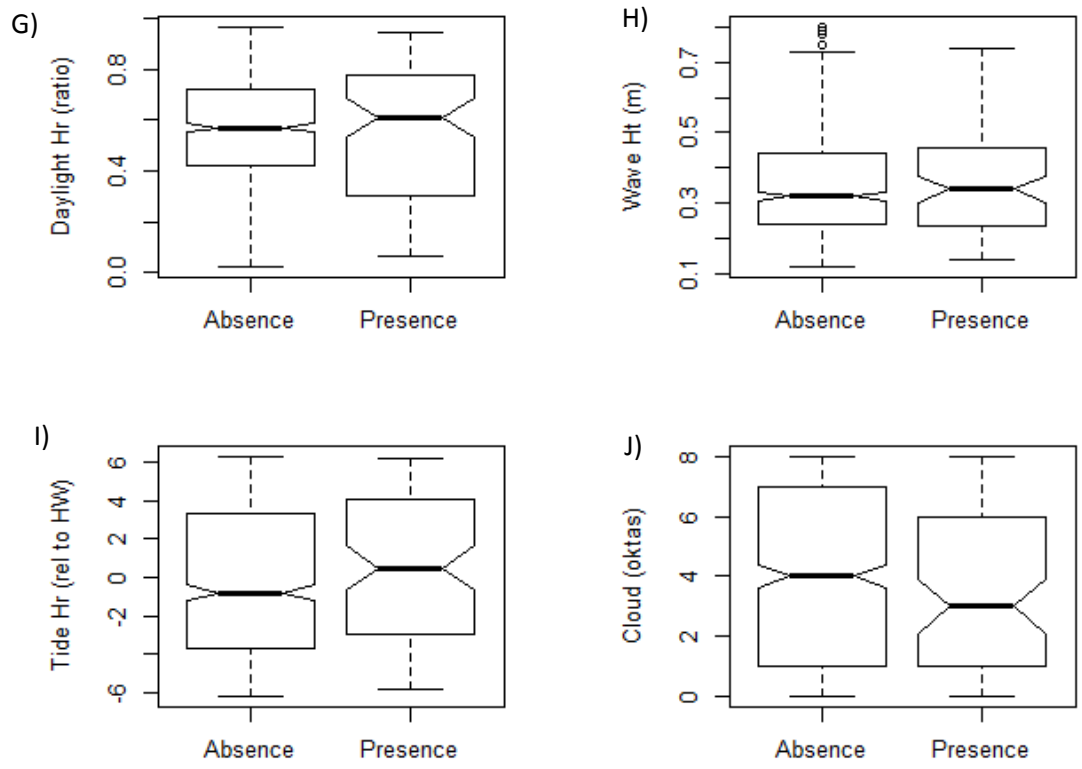

Appendix L.3 **Auto-correlation of temporal model residuals for foraging seabirds at the Runnel Stone Reef study site (blue dotted lines = significance thresholds).**

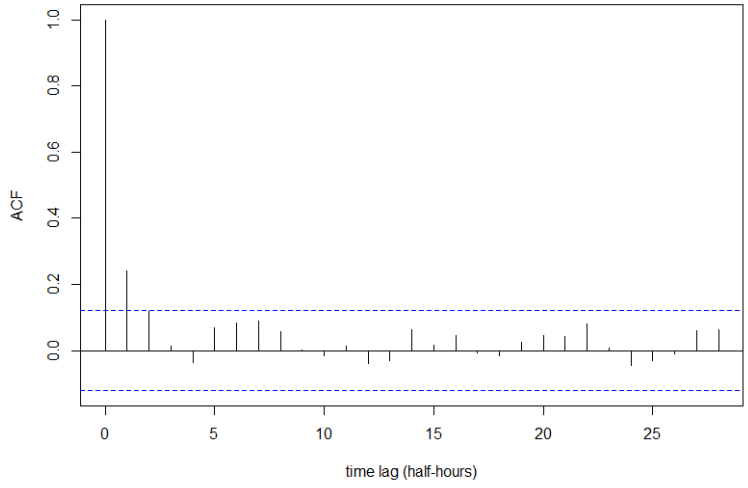

Appendix M St Ives Bay – supplementary material.

Appendix M.1 St Ives Bay Gillnet Fishery, 1999.

CORNWALL SEA FISHERIES COMMITTEE

SEA FISHERIES REGULATION ACT 1966

The Committee for the Cornwall Sea Fisheries District in exercise of their powers under Section 5 of the Sea Fisheries Regulation Act 1966 hereby make the following byelaw.

ST IVES BAY GILLNET FISHERY
(Enacted 11th November 1999)

1. No person shall use in fishing for seafish, any gillnet, within that part of the District which lies to the landward side of a line drawn 119°True from St Ives Head to the northern extremity of the Black Cliffs which is to the east of the Hayle Estuary, during any temporary closure of the fishery.

2. A temporary closure will be implemented by the Chief Fishery Officer, or a Senior Fishery Officer, when the deaths of birds through entanglement with gillnets, as witnessed by fishery officers and other relevant officials, exceeds a predetermined level over any consecutive five day period.

3. Notice of such a closure will be posted in prominent locations and notice boards around St Ives and Hayle harbours, within one working day of the predetermined level of bird deaths being exceeded. A closure shall have effect from midday, the day following a notice being posted, until midday, 21 days thereafter.

4. This byelaw shall not apply to any person using herring nets between 1 October and 31 December each year.

5. The byelaw shall not apply to any person fishing for scientific purposes with the written authority in that behalf of the Local Fisheries Committee signed by their Clerk and in accordance with any conditions contained therein.

6. For the purposes of this byelaw:-

   (a) "temporary closure" shall mean a total prohibition on the use of gillnets for fishing within the area defined in Paragraph 1, for a period of 21 days from the introduction of the closure.

   (b) "gillnet" shall mean any fixed or freefloating gillnet, tangle net, driftnet, ray net, trammel net, or similar enmeshing net.

   (c) "predetermined level" shall mean a sum agreed annually between the Committee, English Nature, nature conservation interests and local fishing representatives. Information concerning the agreed sum will be posted in prominent locations and notice boards around St Ives and Hayle harbour, subsequent to each annual meeting.

   (d) "relevant officials" shall mean established officers from either the Environment Agency or English Nature.

   (e) "herring nets"shall mean traditional, non-monofilament nets with a mesh size of 29 to 32 rows to the yard (28.5 millimetres to 31.5 millimetres), set on the sea bed.

6. This byelaw shall come into operation on the confirmation hereof by the Minister of Agriculture, Fisheries and Food and may be cited as the Cornwall Sea Fisheries District St Ives Bay Gillnet Fishery Byelaw 1999

Appendix M.2 CIFCA closure notice, 2012.

IMPORTANT NOTICE

ST. IVES BAY GILLNET FISHERY BYELAW 2011

The 2012 pre-determined number of sea-bird deaths through entanglement with nets has been exceeded.

Under Paragraph 2 of the above byelaw
a TEMPORARY CLOSURE of the fishery will commence
from midday 05 JANUARY 2012 until midday 26 JANUARY 2012.

During the closure period it will be an offence to use any net for sea fish in the specified area. Any person found guilty of such an offence is liable to a fine of up to £50 000 on summary conviction.

Further information on this byelaw can be found on the Cornwall Inshore Fisheries and Conservation Authority (CIFCA) website
www.cornwall-ifca.gov.uk

Contact the office on (01736) 336842 or email: enquiries@cornwall-ifca.gov.uk

Appendix M.3 CIFCA Code of Practice for fishing nets used in and adjacent to St Ives Bay.

Cornwall IFCA
Inshore Fisheries and Conservation Authority

FISHING NETS USED IN & ADJACENT TO ST. IVES BAY

CODE OF PRACTICE

To avoid significant numbers of sea bird deaths through their accidental capture in fishing nets, the points listed below should be followed by any fisherman using nets in and adjacent to St. Ives Bay:

- If seabirds are seen gathering to prey on fish in any area where you want to use nets, only shoot and haul them in the dark when birds are not diving below the surface of the sea;
- If there is a significant chance that weather conditions may prevent retrieval of nets before daylight in an area where birds are feeding, do not shoot nets there;
- If you shoot a net in the dark to avoid sea birds and find that you cannot haul it before daylight, ask for assistance from other fishermen who may be in a position to help. If nets cannot be hauled before daylight, contact the Cornwall IFCA (01736 336842) to report the situation. Cornwall IFCA may be able to assist with net recovery.
- If you do accidentally catch birds in your nets, ensure that other net fishermen in the area, officers of the Cornwall IFCA and harbour masters at St Ives and Hayle are informed as soon as possible;
- If you are informed of an area where accidental capture of sea birds in nets has just occurred, any nets you may have there during daylight must be hauled as soon as possible. No nets are to be used in the affected area during daylight until sea birds have moved away;
- If sea birds are feeding in an area where net fishing is required during daylight hours, net fishermen are to discuss with each other and consider a voluntary ban on netting during the day in the affected area. Any decision to act together on a voluntary basis will be assessed daily to ensure that it is or remains effective.

EXPLANATORY NOTE

This Code of Practice (CoP) was developed with St Ives and Hayle fishermen. It supplements the aim of the Cornwall Sea Fisheries District St Ives Bay Gill Net Fishery Byelaw which is to reduce the accidental capture of sea birds in nets set at the eastern end of St Ives Bay.

Interactions between sea birds and nets in the relevant area have historically been low. However, incidents in January 2012 whereby a pre-determined number of sea bird deaths was exceeded, did lead to a temporary closure of the fishery using nets, as prescribed by the byelaw. In pursuit of earning a living, fishermen then used their nets legally in other parts of St Ives Bay and along the adjacent coast where some of these nets also caused a problem for a significant number of sea birds.

The CoP is to be applied by fishermen wishing to use nets both in the area covered by the byelaw and in adjacent areas which are not. Barring exceptional circumstances, the chances of sea birds being accidentally caught in nets should be greatly reduced if the CoP is followed. Fishermen understand and appreciate the need to avoid sea birds in their nets and that the Cornwall IFCA will take further action, which may mean greater netting restrictions, if such problems persist.

Appendix N Additional spatial analyses at St Ives Bay.

Appendix N.1 Area-corrected relative densities of cetacean surfacings per km^2 per grid cell (n = 110 sightings) in St Ives Bay.

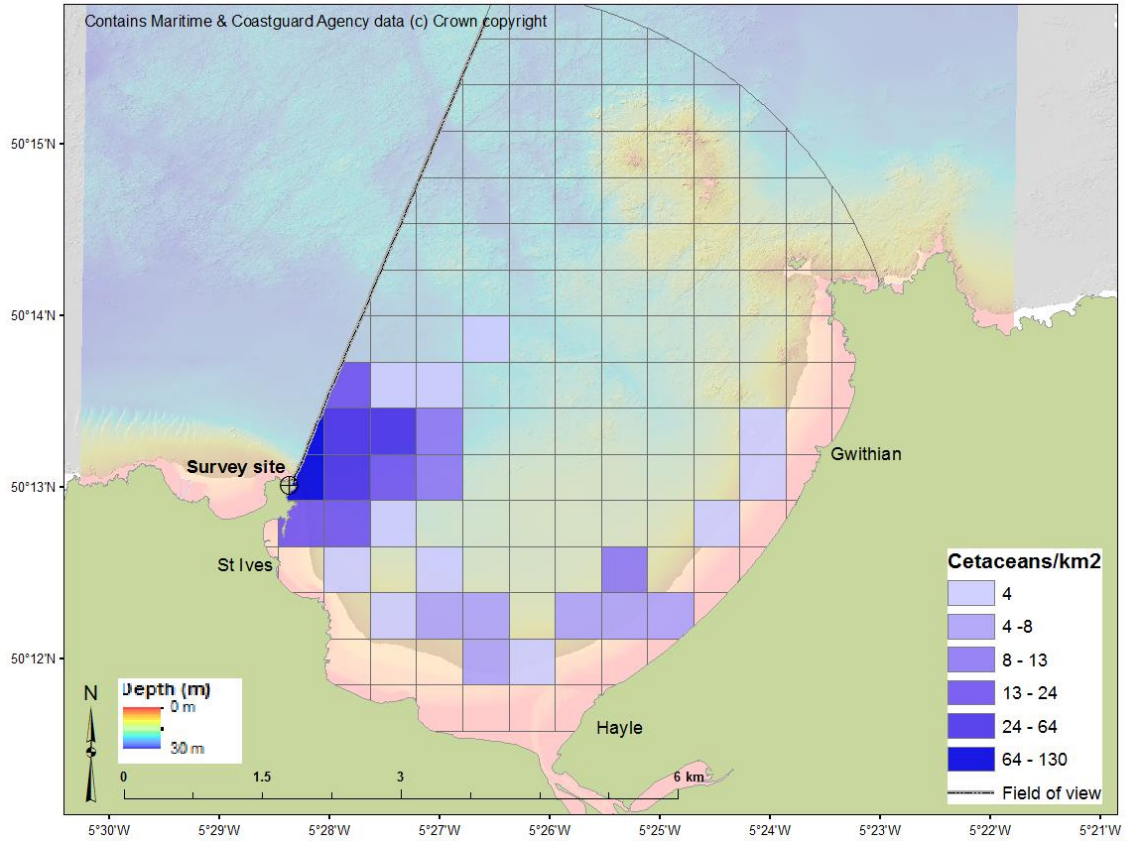

Appendix N.2 Boxplots of foraging seabird aggregation occurrence with environmental covariates.

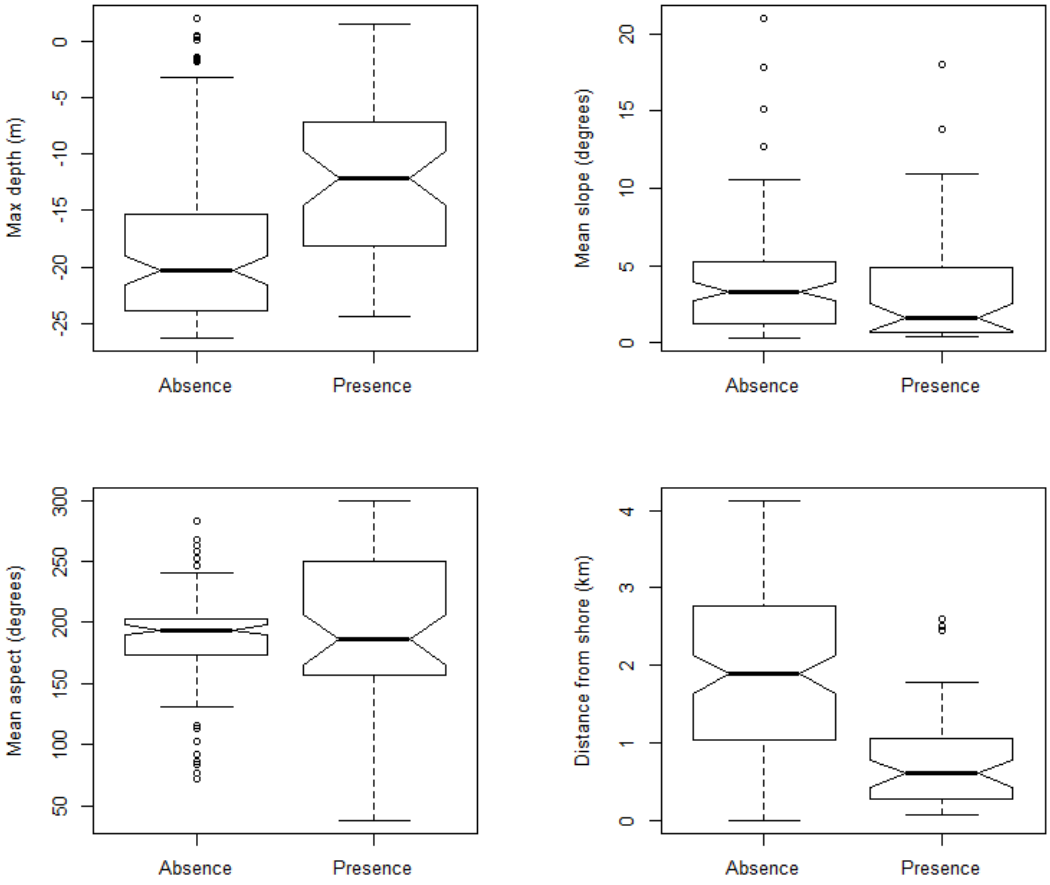

Appendix N.3 **Pairplot of candidate static variables used in the spatial model for foraging seabird aggregations at St Ives Bay.**

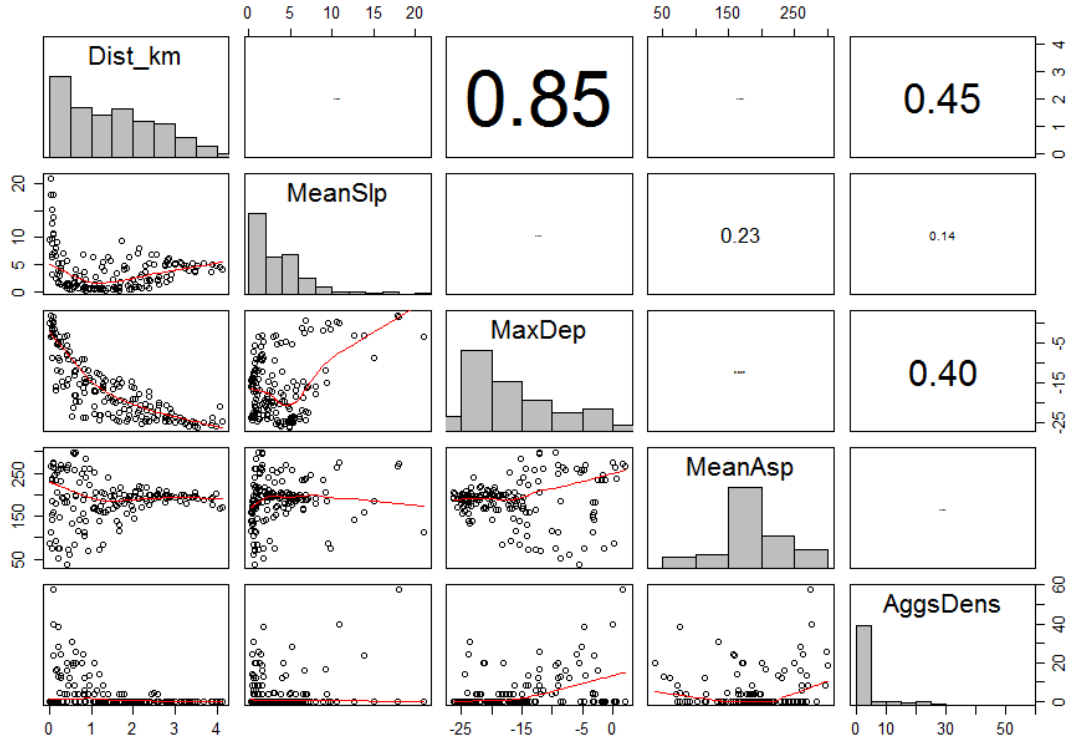

Pairplot of the four candidate static variables with the response, area-corrected density of foraging seabird aggregation sightings per grid cell, "AggsDens" (n = 164). Smoothing curves are added to aid visual interpretation, and histograms on the diagonal show distribution of the data. Values on the edges represent units of the variables. Font size of Spearman's absolute correlation coefficients (Rho) in the upper panel is proportional to their value. Response variable: bottom row of panels' y-axes.

Appendix N.4 **Model validation plots obtained by applying a negative binomial GAM on the area-corrected St Ives Bay seabird aggregation data.**

Underlying assumptions of homogeneity and normality, and potential influential observations, are verified. The deviance residuals in the QQ-plot (Fig. A) should ideally lie on the straight line (representing the theoretical quantiles of a negative binomial distribution) and, since the model explains 46.1% of variation in the data, these discrepancies are minimal.

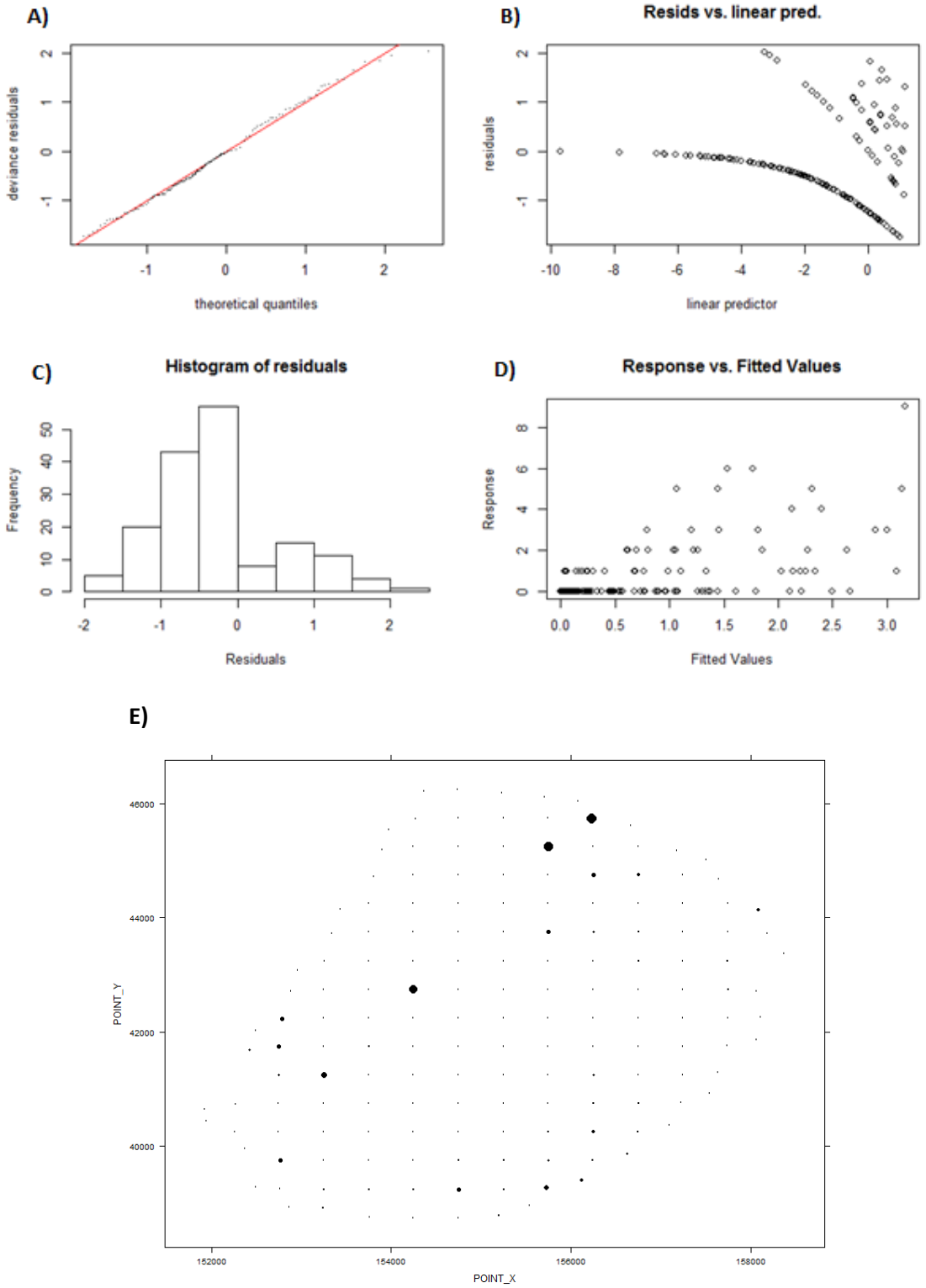

Recorded sightings were filtered by the 500 m radial grid (n = 164). A): QQ-plot; B): residuals vs. linear predictor; C): histogram of residuals; D): response values vs. fitted values; E): normalised residuals vs. spatial coordinates (black dots are negative residuals; empty dots are positive; size proportional to value of residual). QQ-plot and histogram are used to assess normality; and residuals versus fitted values to assess homogeneity. Response versus fitted values should ideally show a straight line.

Based on the residuals histogram (Fig. C) normality can reasonably be assumed. The residuals plot (Fig. B) suggests much of the heterogeneity in the data has been accounted for, since influential observations were removed prior to the final model selection process. The response versus fitted values of the response variable (Fig. D) should ideally show a straight line, though some level of spread is acceptable, this may be problematic. The panel representing spatial dependence (Fig. E) shows little pattern between clustering of negative and positive residuals, but some pattern in their values. Overall, the validation plots do not indicate any serious problems.

Appendix O Additional temporal analyses at St Ives Bay.

Appendix O.1 Effort-corrected number of foraging events as a function of significant wave height.

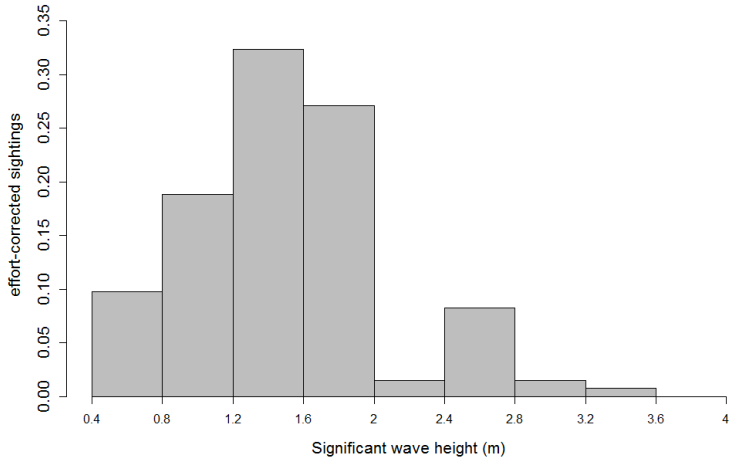

Boxplots of seabird aggregation presence-absence data with environmental covariates.

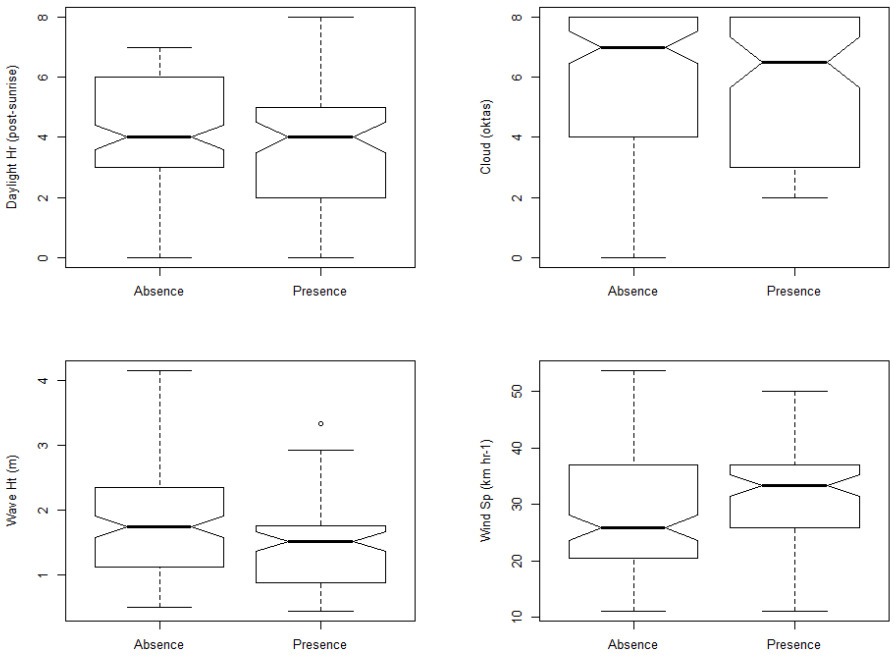

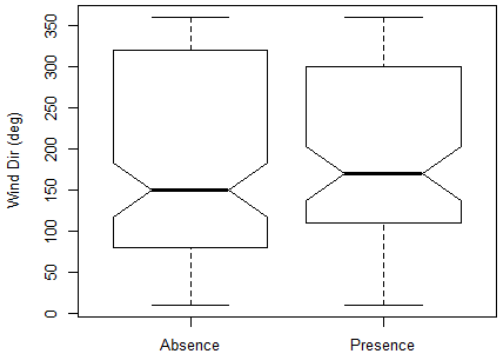
Wind Dir (deg)
0
50
100
150
200
250
300
350
Absence
Presence

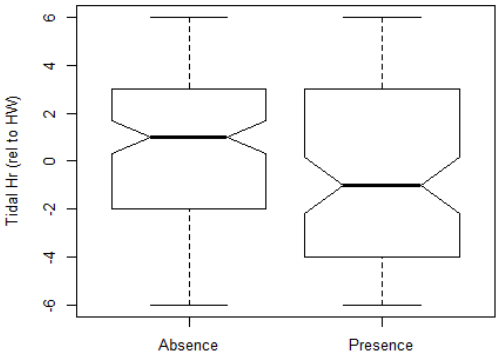
Tidal Hr (rel to HW)
-6
-4
-2
0
2
4
6
Absence
Presence

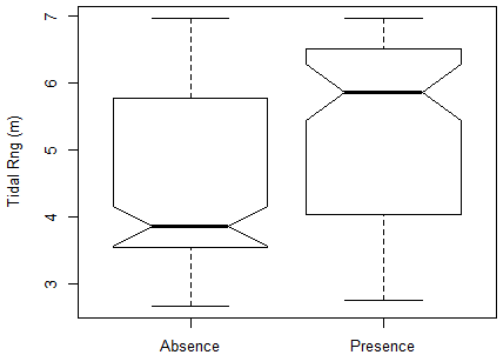
Tidal Rng (m)
3
4
5
6
7
Absence
Presence

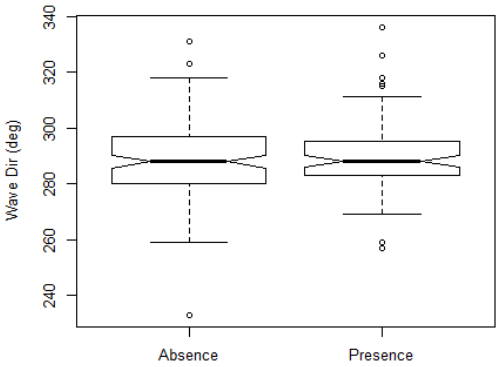
Wave Dir (deg)
240
260
280
300
320
340
Absence
Presence

Appendix O.2 Plots showing the probability of sighting cetaceans in St Ives Bay, given a range of temporal variables (n = 45 individual sightings).

Cetacean sightings rate as a function of A): sea state, B): tidal range (a proxy for time in the spring-neap cycle), C): tidal hour, and D): daylight hour.

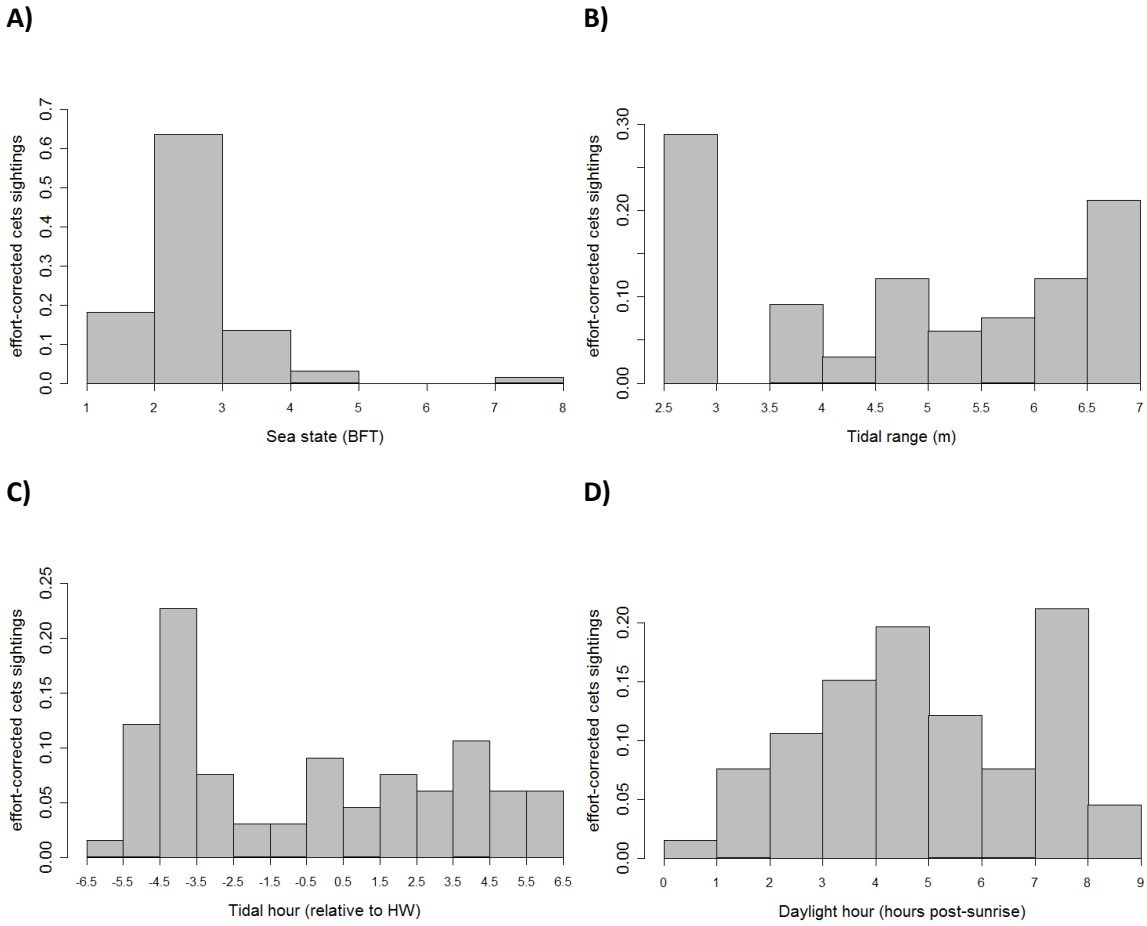

Appendix O.3 **Pairplot of candidate temporal variables per 30-minute sampling unit of visual survey effort at St Ives Bay.**

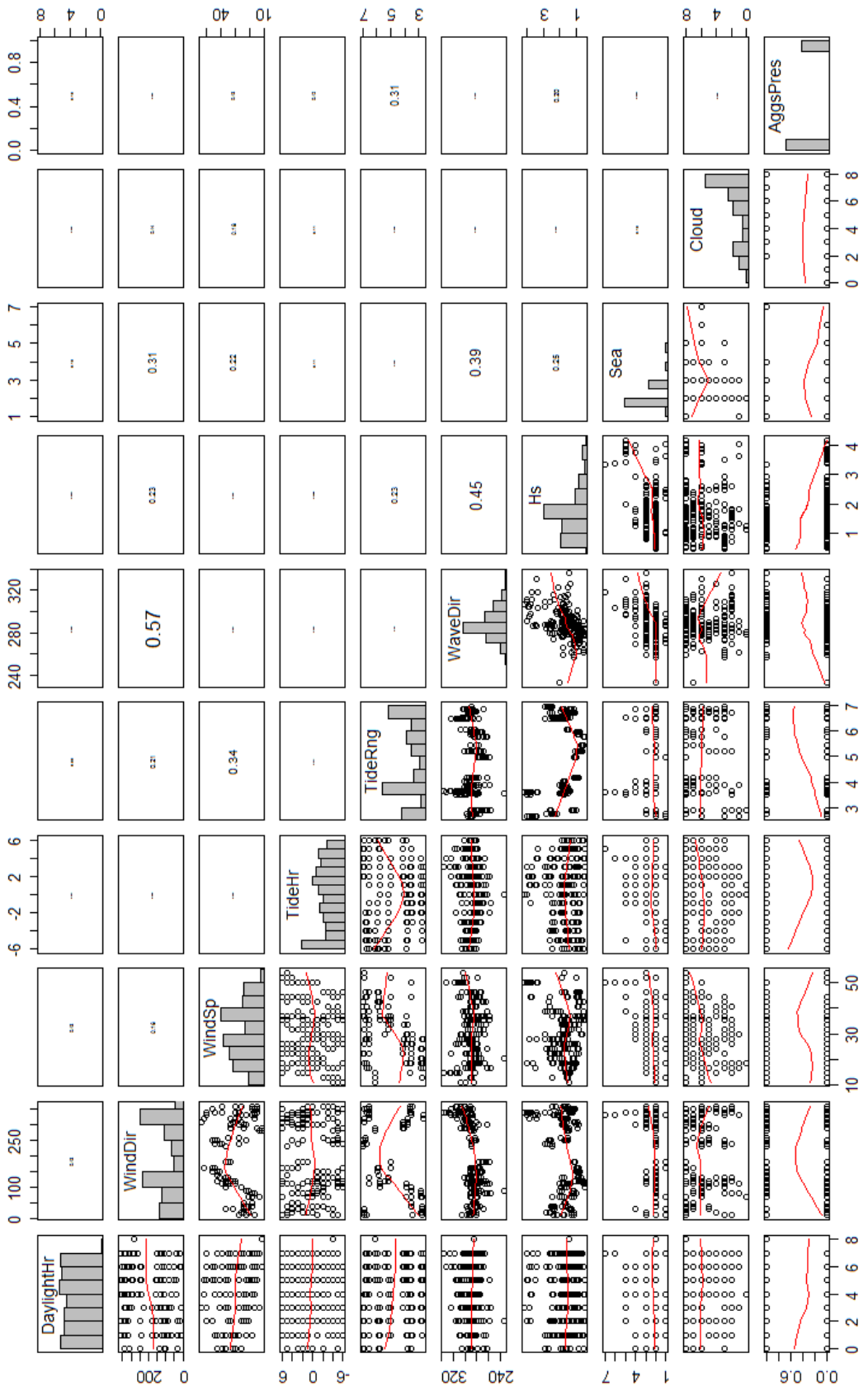

Appendix O.4 Results of forward GAM model selection for the presence-absence of foraging events.

The final model selected wind direction, significant wave height (Hs) and wave direction, as variables that best explain the fine-scale temporal distribution of foraging seabird occurrence in St Ives Bay. It took the form:

Seabird foraging occurrence ~ s(WindDir) + s(Hs) + s(WaveDir)

The model explained 10.2% of deviance (see Table) over 221 30-minute units of survey over 19 days between December 2012 and January 2013. Wind direction was the most significant predictor influencing sightings occurrence ($p < 0.002$), followed by significant wave height ($p < 0.004$). Wave direction was significant at the $p < 0.005$ level.

Variables are shown in order of importance, first compensating for survey effects (wind and sea conditions, cloud cover). Smooths are shown with the number of estimated degrees of freedom (e.d.f.) in parentheses; AIC_{Δ} is the reduction in AIC score caused by the addition of the significant variable to the model, with the first score in bold showing the starting AIC; % Dev is the additional deviation (%) in the data explained by adding the selected variable to the model. Surveys conducted over 19 days between December 2012 and January 2013 at St Ives (n = 110.5 hours).

	Aggregation presence-absence per 30-minutes		
Order	Smooth (e.d.f.)	% Dev	AIC_{Δ}
1	s(WindDir, 1.8)	4.61	**287.29**
2	s(Hs, 1.2)	+2.47	-5.36
3	s(WaveDir, 1.1)	+3.09	-6.47
Total		10.2	

The fitted model for wind direction (Fig. A) shows a marked increase in the occurrence of foraging seabird aggregations during south-westerly winds (~230°), i.e. those blowing from behind St Ives town out across the bay. There is near-linear negative correlation between sightings and significant wave height (Fig. B), indicating more foraging events occur during calmer sea conditions. The smooth for wave direction (Fig. C) shows sightings increase as tidal flows orientate from westward (~270°) to north-westward (~330°), though the wide confidence intervals either side of the smooth, where there are minimal observations (dashed lines of the rug plot), suggests any temporal preferences are marginal.

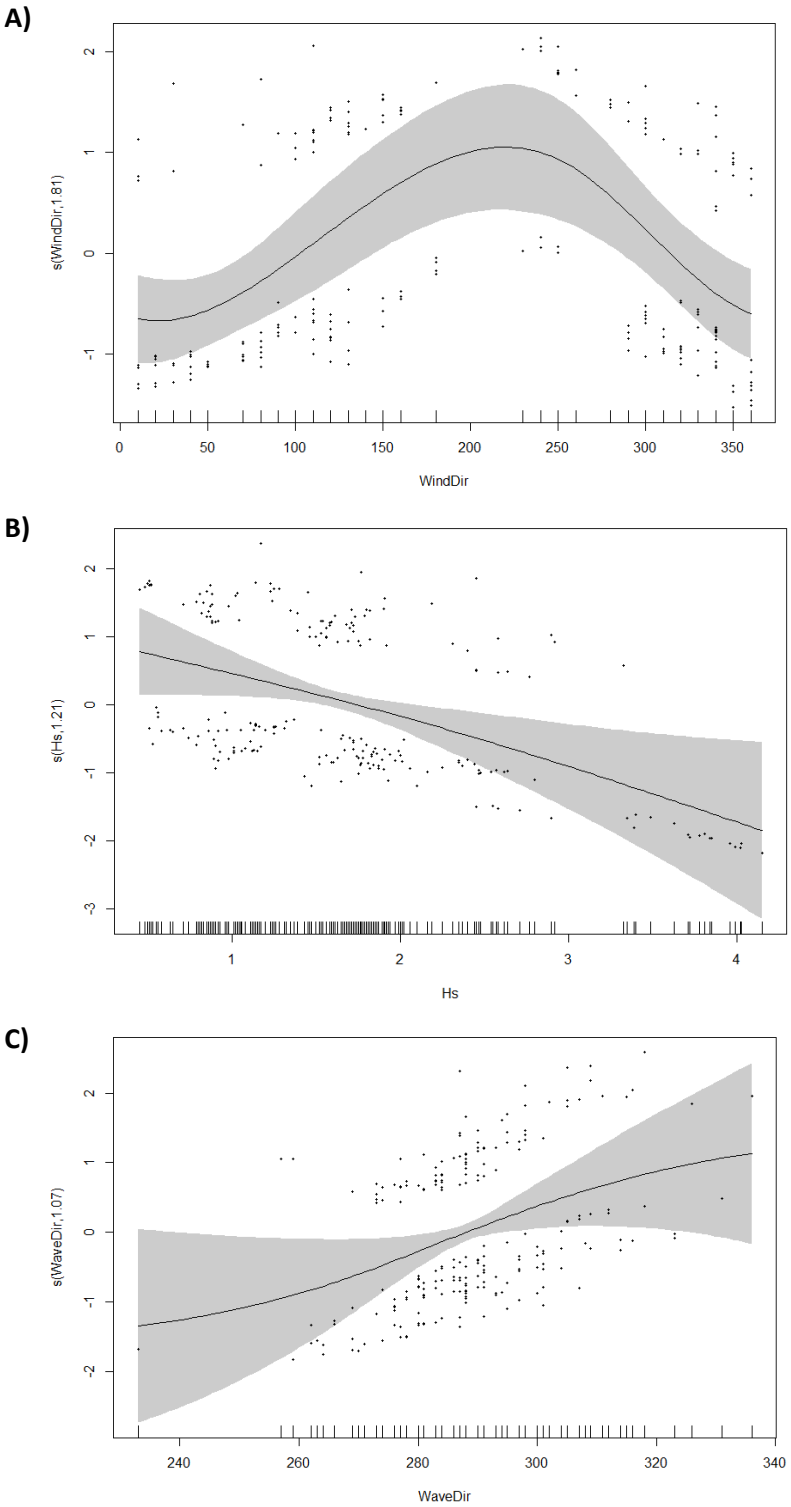

Relationships between foraging seabird occurrence and temporal predictor variables (n = 221 samples), as selected by the final binomial GAM.

A): Wind direction (e.d.f. = 1.81), B): Significant wave height (e.d.f. = 1.21), and C): Wave direction (e.d.f. = 1.07). Results reported on the scale of the linear predictor. Numbers in brackets in y-axis captions are estimated degrees of freedom (e.d.f.) of the smooths. Rug plots at bottom of figures are covariate values. Shaded regions around smooths represent 95% confidence intervals.

Appendix O.5 **Auto-correlation function of residuals from the temporal model for foraging seabirds at St Ives.**

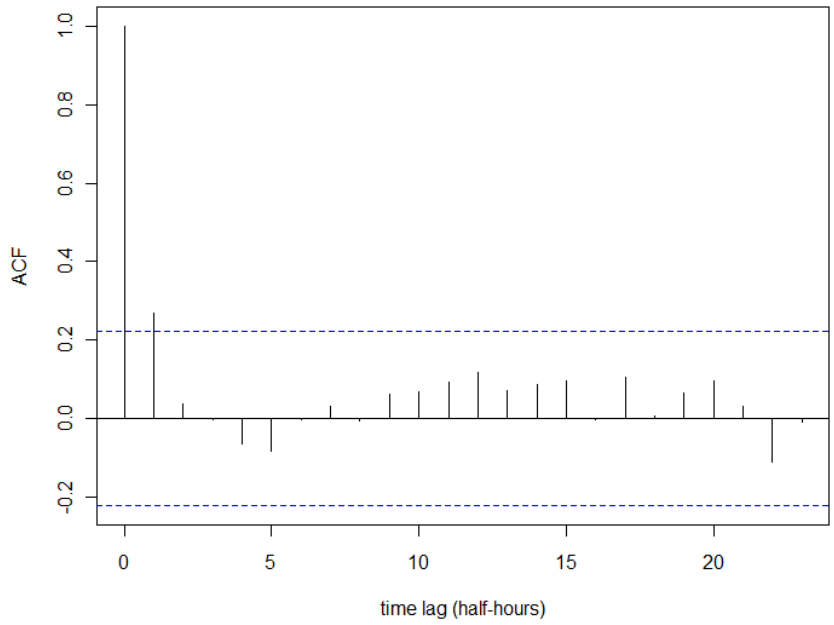

Appendix P Further work.

Appendix P.1 Fine-scale spatio-temporal distribution of basking shark *Cetorhinus maximus* in a recommended Marine Conservation Zone off southwest UK.

Context

Proposals for the 360 km^2 Argyll Array offshore wind farm, 5 km west of Tiree, Scotland, were dropped following both technical and environmental impact assessment studies (BBC News - Scotland Business 13/12/2013: http://www.bbc.co.uk/news/uk-scotland-scotland-business-25364699). One of the contributing factors for Scottish Power Renewables and the Crown Estate dropping the project was not only the 'significant presence' of basking sharks in the area (Speedie et al., 2009), whose fine-scale movement patterns remain poorly understood (Witt et al., 2012a), but also the presence of seabirds and other cetacean species, highlighting the site's 'international importance' for a range of marine wildlife (RSPB Scotland, 2013). On-going research by environmental groups, Scottish Natural Heritage and the University of Exeter, has involved attaching satellite tags to 21 individual sharks in July 2012 to better understand how these animals use the waters between Skye and Mull, including residency time, behaviour and seasonal distribution. The tagging work will not only help assess this area's potential as a possible MPA (pMPA), as part of the Scottish MPA Project (The Scottish MPA Project: http://jncc.defra.gov.uk/page-5469), but also inform on the potential interactions between basking sharks and at-sea engineering projects, such as offshore tidal and wind farms.

Other studies show large scale basking shark movements in relation to tidal flows (e.g. Sims & Quayle, 1998; Sims et al., 2005; Rowat & Gore, 2007), whilst satellite tracking methods have revealed their tortuosity relationship with bathymetric features. This study, however, will reveal extremely fine-scale movement patterns of these animals that can therefore be analysed with both fine-scale bathymetric (1-m resolution) and high resolution tidal flow metrics (160-m resolution each hour) to better understand the impact of their environment on their behavioural ecology.

Methods

In ArcGIS®, all point features of theodolite basking shark sightings at the surface were plotted (n = 1372). Using the Points to Line tool in Arc Toolbox to plot the tracks of the animals, connecting the points by Sighting ID. Cell values at locations specified in the point feature class

were extracted from multiple rasters (e.g. depth, slope and aspect), so static bathymetric values at each shark sighting location could be attributed to the attribute table of the point feature class, using the Extract Multi Values to Points tool. Using the 'movement.pathmetrics' tool in Beyer's (2012) GME environment, angles, step lengths, bearings and time intervals were calculated for the point time series dataset, whilst specifying the individual Sighting ID as the 'groupfield', which represents the collection of points of the same observation, i.e. a tracked shark(s).

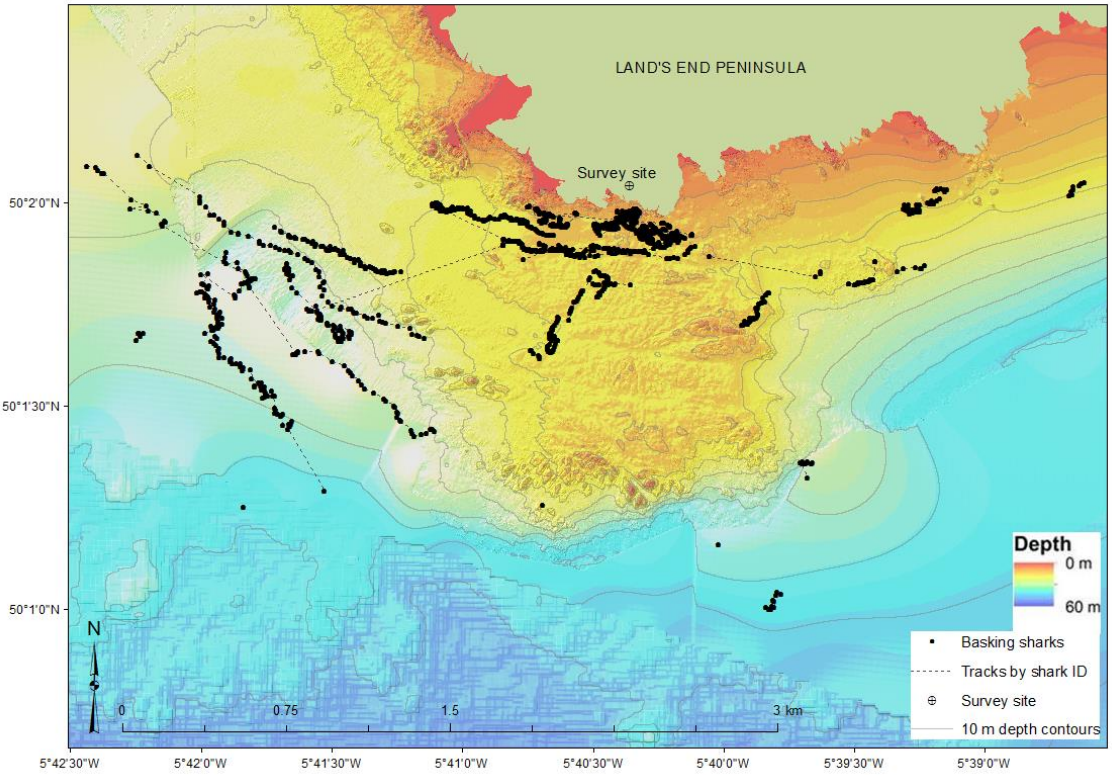

Individual sharks (black dots) joined by dotted lines representing surface movements between observations with the same Sighting ID (n = 35).

Data Filtering

Of 1372 individual theodolite fixes of surfacing basking shark locations, 35 had been allocated the same Sighting ID. Of these, 11 were selected for further fine-scale analysis, as these animals had each been observed for a minimum duration of 10 minutes.

Proposed Analysis

Basking shark IDs used in the tracks' analyses, with minimum duration 10 minutes (n = 11).

Basking shark track ID	Date	Start time	End time	Duration	Track length (m)	Number of fixes	'Fix rate'
s001	27/05/2011	14:37	14:49	00:12	481	42	17 s
s008	18/08/2011	12:09	12:34	00:25	1461	45	33 s
s012	10/06/2012	12:22	12:32	00:10	660	39	15 s
s017	10/06/2012	18:36	18:47	00:11	969	97	07 s
s019	11/06/2012	08:47	09:18	00:31	1418	81	23 s
s025	11/06/2012	12:26	12:40	00:14	878	89	09 s
s026	11/06/2012	14:22	14:39	00:17	627	38	27 s
s029	17/06/2012	12:42	14:06	01:24	3182	290	17 s
s030	17/06/2012	17:42	18:20	00:38	3648	122	19 s
s034	20/06/2012	10:14	10:35	00:21	1741	58	22 s
s036	14/10/2012	09:21	09:38	00:17	1064	13	78 s

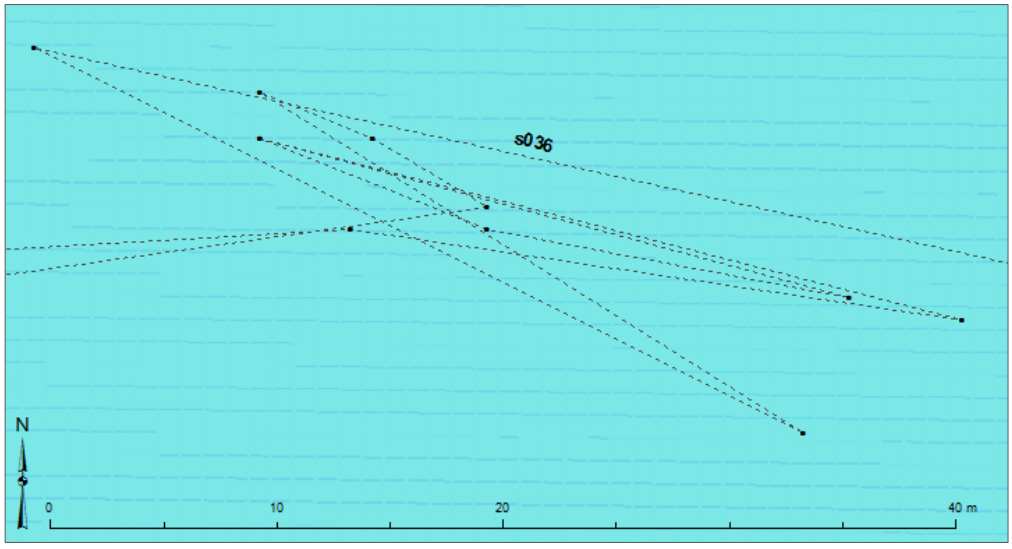

Sample high resolution (<20 m) track of shark 's036' swimming back and forth over a 40-m distance for ~18 minutes.

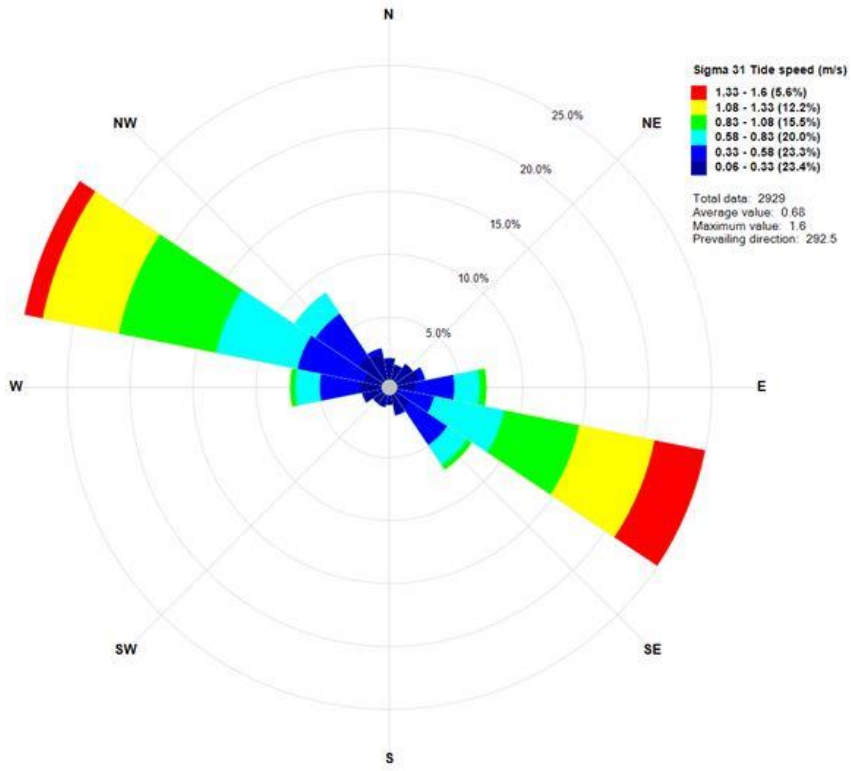

Tidal rose calculated in WindRosePRO3 using Polpred-predicted data with prevailing currents.

Given coarser resolution predicted tidal flow data, there appears a correlation between prevailing flow direction and the orientation of the sharks in the survey area.

Initially, it seems as though the majority of shark tracks, particularly in the western quadrant of the survey area, are running parallel to the complex topographic contours of the Runnelstone Reef. On further investigation, however, there is actually a slight offset between these contours and the tracks. When the tracks are visually compared alongside the plot of prevailing current flows (292°), there is closer alignment in orientation between the animals and the flow direction. Despite the contours of the complex heterogeneous environment, tidal flow direction may be more influential on tortuosity of the basking sharks, particularly when they interact together, perhaps explaining the preference for the western reef edge.

Highly resolved (~160-m resolution) radar-derived flow vector (speed and direction) will therefore be attributed to each fine-scale shark track by interpolating the values given the length of each ‘segment’. Each track will have a speed and bearing of travel, which will be adjusted depending on the flow information for any particular segment Once normalised,

tracks can be analysed in relation to extremely high-resolution flow information, along with static bathymetric covariates of depth, slope and aspect.

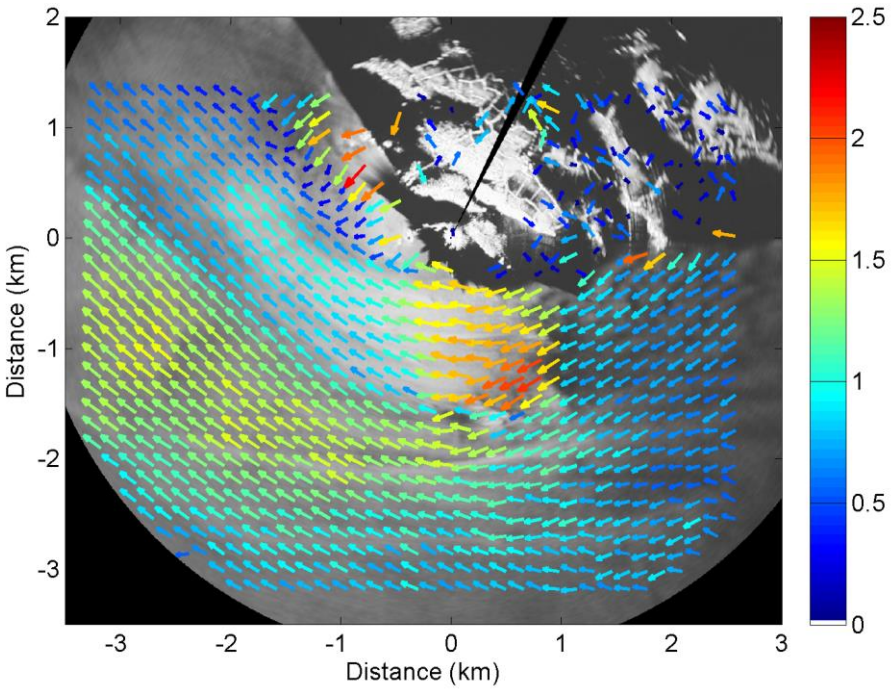

Radar-derived high resolution (~160-m) tidal flow image for one example hour for the Runnel Stone Reef survey area. Vectors scaled logarithmically according the speed in m s^{-1}.

Point_ID	ID	Time_BST	Date_BST	Eastings	Northings	TideHr	TideRng	TideHt	TideSp	TideDir	DayHr	AvAsp	Slp	AvSlp	Dep	TURNANG	STEPLENG	BEARING	TIMEINTVL
7	s001	15:37:46	27/05/2011	136788	21049	2.1	2.44	3.56	0.63	112	0.64	189.7669	13.7773	6.114377	17.13	-999	16.97056	225	50
8	s001	15:38:36	27/05/2011	136776	21037	2.1	2.44	3.56	0.63	112	0.65	182.978	5.311864	5.121116	18.105	45	4	270	19
9	s001	15:38:55	27/05/2011	136772	21037	2.1	2.44	3.56	0.63	112	0.65	182.978	0.308032	5.121116	18.355	90	1	0	2
10	s001	15:38:57	27/05/2011	136772	21038	2.1	2.44	3.56	0.63	112	0.65	182.978	0.835159	5.121116	18.35	0	0	180	13
11	s001	15:39:10	27/05/2011	136772	21038	2.1	2.44	3.55	0.63	112	0.65	182.978	0.835159	5.121116	18.35	0	21.09502	31.42957	16
12	s001	15:39:26	27/05/2011	136783	21056	2.1	2.44	3.55	0.63	112	0.65	189.7669	5.667193	6.114377	17.955	72.60668	4.123106	104.0362	7
13	s001	15:39:33	27/05/2011	136787	21055	2.1	2.44	3.55	0.63	112	0.65	189.7669	5.896497	6.114377	17.845	-66.1613	11.40175	37.87498	13
14	s001	15:39:46	27/05/2011	136794	21064	2.1	2.44	3.55	0.63	112	0.65	189.7669	3.219121	6.114377	17.74	52.12502	4	90	8
15	s001	15:39:54	27/05/2011	136798	21064	2.1	2.44	3.55	0.63	112	0.65	189.7669	2.933863	6.114377	17.72	-58.3925	15.26434	31.6075	11
16	s001	15:40:05	27/05/2011	136806	21077	2.1	2.44	3.54	0.63	112	0.65	189.7669	0.432691	6.114377	17.195	-20.2976	10.19804	11.30993	12
17	s001	15:40:17	27/05/2011	136808	21087	2.1	2.44	3.54	0.63	112	0.65	189.7669	8.490096	6.114377	18.035	-146.31	2.828427	225	7
18	s001	15:40:24	27/05/2011	136806	21085	2.1	2.44	3.54	0.63	112	0.65	189.7669	15.85873	6.114377	17.545	158.1986	15.23155	23.19859	15
19	s001	15:40:39	27/05/2011	136812	21099	2.1	2.44	3.54	0.63	112	0.65	189.7669	5.62891	6.114377	18.255	6.159163	18.35756	29.35775	18
20	s001	15:40:57	27/05/2011	136821	21115	2.1	2.44	3.54	0.63	112	0.65	189.7669	0.81652	6.114377	18.195	34.0772	2.236068	63.43495	7
21	s001	15:41:04	27/05/2011	136823	21116	2.2	2.44	3.53	0.62	112	0.65	189.7669	3.101069	6.114377	18.23	-57.0948	9.055385	6.340192	7
22	s001	15:41:11	27/05/2011	136824	21125	2.2	2.44	3.53	0.62	112	0.65	189.7669	3.226631	6.114377	18.21	-37.3039	5.830952	329.0362	14
23	s001	15:41:25	27/05/2011	136821	21130	2.2	2.44	3.53	0.62	112	0.65	189.7669	2.234622	6.114377	18.035	-119.291	8.062258	209.7449	5
24	s001	15:41:30	27/05/2011	136817	21123	2.2	2.44	3.53	0.62	112	0.65	189.7669	0.963466	6.114377	18.14	116.5651	7.211103	326.3099	13
25	s001	15:41:43	27/05/2011	136813	21129	2.2	2.44	3.53	0.62	112	0.65	189.7669	3.834126	6.114377	18.035	<Null>	7.211103	326.3099	9
26	s001	15:41:52	27/05/2011	136809	21135	2.2	2.44	3.53	0.62	112	0.65	189.7669	13.02765	6.114377	17.685	-56.3099	10	270	20
27	s001	15:42:12	27/05/2011	136799	21135	2.2	2.44	3.53	0.62	113	0.65	182.978	3.687641	5.121116	17.97	14.03624	8.246211	284.0362	18
28	s001	15:42:30	27/05/2011	136791	21137	2.2	2.44	3.53	0.62	113	0.65	182.978	3.046234	5.121116	17.75	22.83365	5	306.8699	11
29	s001	15:42:41	27/05/2011	136787	21140	2.2	2.44	3.53	0.62	113	0.65	182.978	5.349921	5.121116	17.815	29.16761	9.848858	336.0375	16
30	s001	15:42:57	27/05/2011	136783	21149	2.2	2.44	3.53	0.62	113	0.65	182.978	3.495877	5.121116	17.955	-47.6026	3.162278	288.4349	9
31	s001	15:43:06	27/05/2011	136780	21150	2.2	2.44	3.52	0.62	113	0.65	182.978	8.661761	5.121116	17.885	17.10273	17.20465	305.5377	35
32	s001	15:43:41	27/05/2011	136766	21160	2.2	2.44	3.52	0.62	113	0.65	182.978	9.146826	5.121116	17.57	-84.9364	9.219544	220.6013	12
33	s001	15:43:53	27/05/2011	136760	21153	2.2	2.44	3.52	0.62	113	0.65	182.978	11.68377	5.121116	17.555	-3.7314	35	216.8699	46
34	s001	15:44:39	27/05/2011	136739	21125	2.2	2.44	3.51	0.62	113	0.65	182.978	5.222311	5.121116	17.535	-3.17983	7.211103	213.6901	11
35	s001	15:44:50	27/05/2011	136735	21119	2.2	2.44	3.51	0.62	113	0.65	182.978	0.761292	5.121116	17.64	-5.38931	59.05929	208.3008	72
36	s001	15:46:02	27/05/2011	136707	21067	2.2	2.44	3.5	0.61	113	0.65	182.978	2.521372	5.121116	18.68	5.389312	3.605551	213.6901	12
37	s001	15:46:14	27/05/2011	136705	21064	2.2	2.44	3.5	0.61	113	0.65	182.978	2.174234	5.121116	18.625	1.84761	8.602325	215.5377	14
38	s001	15:46:28	27/05/2011	136700	21057	2.2	2.44	3.5	0.61	113	0.65	182.978	0.791004	5.121116	18.7	-8.97263	4.472136	206.5651	8
39	s001	15:46:36	27/05/2011	136698	21053	2.2	2.44	3.5	0.61	113	0.65	182.978	6.045295	5.121116	18.57	1.735705	14.76482	208.3008	18
40	s001	15:46:54	27/05/2011	136691	21040	2.2	2.44	3.5	0.61	113	0.65	182.978	4.388889	5.121116	17.99	5.389312	14.42221	213.6901	27
41	s001	15:47:21	27/05/2011	136683	21028	2.3	2.44	3.49	0.61	113	0.65	182.978	14.65778	5.121116	18.17	-4.63546	10.29563	209.0546	9
42	s001	15:47:30	27/05/2011	136678	21019	2.3	2.44	3.49	0.61	113	0.65	182.978	3.143237	5.121116	17.89	28.94001	9.433981	237.9946	28
43	s001	15:47:58	27/05/2011	136670	21014	2.3	2.44	3.49	0.61	113	0.65	182.978	5.501919	5.121116	17.67	17.96914	4.123106	255.9638	14
44	s001	15:48:12	27/05/2011	136666	21013	2.3	2.44	3.48	0.61	113	0.66	182.978	2.602276	5.121116	17.55	-56.8703	27.51363	199.0935	38

Screenshot of spreadsheet containing data on shark ID (with distance and time interval between points, turn angle, and bearing), matched with a suite of environmental static and temporal variables.

Appendix Q Recommendations for future theodolite use.

Following more than 500 hours spent in the field using a theodolite, some of the following considerations should be taken into account to benefit fully from the method, prior to carrying out any investigation:

- Initial cost of the instrument
- The method is fairly labour-intensive for the theodolite operator, and requires specialised knowledge for its use
- At least two other members of the survey team, apart from the theodolite operator, should be experienced observers of the target species, particularly during multi-species surveys, as operating the instrument, as well as filling out recording forms, is an arduous task during 'busy' days with many sightings
- More than one theodolite operator should be included in the observation team to prevent fatigue, due to the small eye-piece designed for surveying buildings. This is particularly relevant when tracking inconspicuous species, such as cetaceans, or where focal species are likely to be sighted frequently, i.e. when the theodolite will be used intensively during surveys
- The observation station needs to be located at a sufficient height above sea level, which will vary depending on the maximum extent (distance from the watch point) of the survey area required for the research, i.e. as the distance from the watch point increases, the height above sea level of the observation station needs to increase to counteract increasing error with distance (a consequence of trigonometric calculations)
- The survey team must be able to acquire precise GPS coordinates of the observation station, and of the reference point (used for zeroing the horizontal angle)
- It is recommended that the instrument is set up in a GPS coordinate system daily (if using a Total Station). This will streamline and reduce the risk of errors during data processing, as height-above-sea-level measurements, and coordinates of recorded targets, will be derived instantaneously in the field and automatically stored on-board
- Upload the data daily!
- Access to environmental data of similar resolutions as theodolite accuracy (given height above sea level and maximum distance of sightings from the watch point) should be confirmed, otherwise observation data collected using conventional visual monitoring techniques would be adequate

List of References

Abrams, R.W. and Griffiths, A.M. (1981). "Ecological Structure of the Pelagic Seabird Community in the Benguela Current Region." *Marine Ecology Progress Series* 6: 269-277.

Acevedo, A. (1991). "Interactions between boats and bottlenose dolphins, *Tursiops truncatus*, in the entrance to Ensenada De La Paz, Mexico." *Aquatic Mammals* 17: 120-124.

Adams, J. and Flora, S. (2009). "Correlating seabird movements with ocean winds: linking satellite telemetry with ocean scatterometry." *Marine Biology* 157(4): 915-929.

Ainley, D.G. and Boekelheide, R.J. (1983). "An ecological comparison of oceanic seabird communities of the South Pacific Ocean." *Studies in Avian Biology* 8: 2-23.

Allen, M.C., Read, A.J., Gaudet, J. and Sayigh, L.S. (2001). "Fine-scale habitat selection of foraging bottlenose dolphins *Tursiops truncatus* near Clearwater, Florida." *Marine Ecology Progress Series* 222: 253-264.

Atwood, T.C., Weeks, H.P. and Gehring, T.M. (2004). "Spatial Ecology of Coyotes Along a Suburban-to-Rural Gradient." *Journal of Wildlife Management* 68(4): 1000-1009.

Au, W.W. (1993). *The sonar of dolphins*: Springer Science & Business Media.

Au, W.W., Benoit-Bird, K.J. and Kastelein, R.A. (2007). "Modeling the detection range of fish by echolocating bottlenose dolphins and harbor porpoises." *The Journal of the Acoustical Society of America* 121(6): 3954-3962.

Baddeley, A. (2010). Analysing spatial point patterns in R. U.o.W. Australia. Perth, WA: CSIRO: 1-232.

Baddeley, A. and Turner, R. (2005). "Spatstat: an R package for analysing spatial point patterns." *Journal of Statistical Software* 12: 1-42.

Bailey, H., Clay, G., Coates, E.A., Lusseau, D., Senior, B. and Thompson, P.M. (2010). "Using T-PODs to assess variations in the occurrence of coastal bottlenose dolphins and harbour porpoises." *Aquatic Conservation-Marine and Freshwater Ecosystems* 20(2): 150-158.

Bailey, H. and Lusseau, D. (2004). "Increasing the precision of theodolite tracking: modified technique to calculate the altitude of land-based observation sites." *Marine Mammal Science* 20(4): 880-885.

Bailey, H. and Thompson, P. (2006). "Quantitative analysis of bottlenose dolphin movement patterns and their relationship with foraging." *Journal of Animal Ecology* 75(2): 456-465.

Bailey, H. and Thompson, P. (2010). "Effect of oceanographic features on fine-scale foraging movements of bottlenose dolphins." *Marine Ecology Progress Series* 418: 223-233.

Bailey, H. and Thompson, P.M. (2009). "Using marine mammal habitat modelling to identify priority conservation zones within a marine protected area." *Marine Ecology Progress Series* 378: 279-287.

Barrett, R.T. (2002). "Atlantic puffin *Fratercula arctica* and common guillemot *Uria aalge* chick diet and growth as indicators of fish stocks in the Barents Sea." *Marine Ecology Progress Series* 230: 275-287.

Baumgartner, M.F., Cole, T.V.N., Clapham, P.J. and Mate, B.R. (2003). "North Atlantic right whale habitat in the lower Bay of Fundy and on the SW Scotian Shelf during 1999-2001." *Marine Ecology Progress Series* 264: 137-154.

Bell, P. (2008). *Mapping shallow water coastal areas using a standard marine x-band radar*. International Federation of Hydrographic Societies, 4-6 November, Liverpool.

Bell, P.S. (2011). *Submerged dunes and breakwater eembayments mapped using wave inversions of shore-mounted marine X-band radar data*. IEEE International Geoscience & Remote Sensing Symposium, 9-14 August, Honolulu, Hawaii, U.S.A.

Bell, P.S. and Osler, J.C. (2011). "Mapping bathymetry using X-band marine radar data recorded from a moving vessel." *Ocean Dynamics* 61(12): 2141-2156.

Bertrand, A., Gerlotto, F., Bertrand, S., Gutiérrez, M., Alza, L., Chipollini, A., Díaz, E., Espinoza, P., Ledesma, J., Quesquén, R., Peraltilla, S. and Chavez, F. (2008). "Schooling behaviour and environmental forcing in relation to anchoveta distribution: An analysis across multiple spatial scales." *Progress In Oceanography* 79(2-4): 264-277.

Beyer, H.L. (2012) *Geospatial Modelling Environment (GME). Version 0.7.2.0*. http://www.spatialecology.com/gme.

BirdLife International (2004). *Birds in Europe: population estimates, trends and conservation status*. Cambridge, UK: BirdLife International.

Bogdanova, M.I., Wanless, S., Harris, M.P., Lindström, J., Butler, A., Newell, M.A., Sato, K., Watanuki, Y., Parsons, M. and Daunt, F. (2014). "Among-year and within-population variation in foraging distribution of European shags Phalacrocorax aristotelis over two decades: Implications for marine spatial planning." *Biological Conservation* 170: 292-299.

Booth, C.G., Embling, C., Gordon, J., Calderan, S.V. and Hammond, P.S. (2013). "Habitat preferences and distribution of the harbour porpoise Phocoena phocoena west of Scotland." *Marine Ecology Progress Series* 478: 273-285.

Borchers, D.L., Buckland, S.T., Goedhart, P.W., Clarke, E.D. and Hedley, S.L. (1998a). "Horvitz-Thompson estimators for double-platform line transect surveys." *Biometrics* 54: 1221-1237.

Borchers, D.L., Zucchini, W. and Fewster, R.M. (1998b). "Mark-recapture models for line transect surveys." *Biometrics* 54: 1207-1220.

Brierley, A.S. and Fernandes, P.G. (2001). "Diving depths of northern gannets: acoustic observations of Sula bassana from an autonomous underwater vehicle." *The Auk* 118(2): 529-534.

Buckland, S.T., Anderson, D.R., Burnham, K.P., Laake, J.L., Borchers, D.L. and Thomas, L. (2001). *Introduction to Distance Sampling*. Oxford: Oxford University Press.

Buckland, S.T., Anderson, D.R., Burnham, K.P., Laake, J.L., Borchers, D.L. and Thomas, L., Eds. (2010). *Advanced Distance Sampling: Estimating abundance of biological populations*. Oxford: Oxford University Press.

Bull, L.S. (2007). "Reducing seabird bycatch in longline, trawl and gillnet fisheries." *Fish and Fisheries* 8: 31-56.

Burger, A.E. and Shaffer, S.A. (2008). "Application of Tracking and Data-Logging Technology in Research and Conservation of Seabirds." *The Auk* 125(2): 253-264.

Burnham, K.P. and Anderson, D.R. (2002). *Model Selection and Multimodal Inference. A Practical Information-Theoretic Approach*. New York: Springer-Verlag.

Calderan, S.V. (2003). Fine-scale Temporal Distribution by Harbour Porpoise (*Phocoena phocoena*) in North Wales: Acoustic and Visual Survey Techniques. Bangor: University of Wales. MSc.

Camphuysen, C.J. (2011). "Northern Gannets in the North Sea: foraging distribution and feeding techniques around the Bass Rock." *British Birds* 104: 60-76.

Camphuysen, C.J., Scott, B.E. and Wanless, S. (2006). Distribution and foraging interactions of seabirds and marine mammals in the North Sea: a metapopulation analysis. *Top Predators in Marine Ecosystems: Their role in Monitoring and Management*. I. Boyd, S. Wanless and C.J. Camphuysen. New York: Cambridge University Press: 82-97.

Camphuysen, K., Shamoun-Baranes, J., Bouten, W. and Garthe, S. (2012). "Identifying ecologically important marine areas for seabirds using behavioural information in combination with distribution patterns." *Biological Conservation* 156: 22-29.

Cañadas, A., Desportes, G. and Borchers, D.L. (2004). "The estimation of the detection function and g(0) for short-beaked common dolphins (Delphinus delphis), using double-platform data collected during the NASS-95 Faroese survey." *Journal of Cetacean Research and Management* 6(2): 191-198.

Cañadas, A. and Hammond, P.S. (2006). "Model-based abundance estimates for bottlenose dolphin (Tursiops truncatus) off southern Spain: implications for conservation and management." *Journal of Cetacean Research and Management* 8(1): 13-27.

Cañadas, A., Sagarminaga, R., De Stephanis, R., Urquiola, E. and Hammond, P.S. (2005). "Habitat preference modelling as a conservation tool: proposals for marine protected areas for cetaceans in southern Spanish waters." *Aquatic Conservation: Marine and Freshwater Ecosystems* 15(5): 495-521.

Cañadas, A., Sagarminaga, R. and Garcia-Tisar, S. (2002). "Cetacean distribution related with depth and slope in the Mediterranean waters off southern Spain." *Deep Sea Research Part I* 49: 2053-2073.

Carlström, J. (2005). "Diel variation in echolocation behaviour of wild harbour porpoises." *Marine Mammal Science* 21(1): 1-12.

CCO (2011). *Channel Coastal Observatory*. http://www.channelcoast.org/data_management/online_data_catalogue/. [Accessed 02/02/2011].

Chambers, J.M., Cleveland, W.S., Kleiner, B. and Tukey, P.A. (1983). *Graphical Methods for Data Analysis*. Pacific Grove, CA: Wadsworth & Brooks/Cole.

Chambers, L.E., Devney, C.A., Congdon, B.C., Dunlop, N., Woehler, E.J. and Dann, P. (2011). "Observed and predicted effects of climate on Australian seabirds." *Emu* 111(3): 235-251.

Chelonia (2013) *Chelonia Ltd Cetacan Monitoring Systems*. http://www.chelonia.co.uk/. Mousehole, Cornwall: Chelonia Ltd.

CIFCA (2012). Cornwall Inshore Fisheries & Conservation Authority Enforcement Plan 2012 to 2013. Penzance, Cornwall: CIFCA: 1-32.

ClientEarth (2013). *Harbour porpoise Special Areas of Conservation*. ClientEarth: http://www.clientearth.org/biodiversity/biodiversity-publications/harbour-porpoise-special-areas-of-conservation-2400. [Accessed 10/01/2015].

Collins, P. (2011). The spatio-temporal distribution of seabird foraging flocks, focusing on the Northern Gannet, *Morus bassanus*, over a tidally dominated reef system in Southwest UK. Southampton: University of Southampton. MSc: 1-108.

Cooper, J., Croxall, J.P. and Rivera, K.S. (2001). *Off the hook? Initiatives to reduce seabird bycatch in longline fisheries*. Proceedings of the Symposium Seabird Bycatch: Trends, Roadblocks and Solutions.

Cox, T.M. and Read, A.J. (2004). "Echolocation behavior of harbor porpoises Phocoena phocoena around chemically enhanced gill nets." *Marine Ecology Progress Series* 279: 275-282.

Crawley, M.J. (2012). *The R book*. Chichester, UK: John Wiley & Sons Ltd.

Croxall, J.P., Butchart, S.H.M., Lascelles, B., Stattersfield, A.J., Sullivan, B., Symes, A. and Taylor, P. (2012). "Seabird conservation status, threats and priority actions: a global assessment." *Bird Conservation International* 22: 1-34.

Dapling, T.M., Clark, R.W., Vause, B.J., Medley, P. and Carleton, C.R.C. (2010). Navigating the Future. Developing Sustainable Inshore Fisheries. *The UK Inshore Fisheries Sustainability Project Summary Report.* Shoreham by Sea, Sussex: Sussex Sea Fisheries Committe.

Darlaston, M. and Wynn, R.B. (2012). "A record influx of Balearic shearwaters off Devon and Cornwall." *British Birds* 105: 37-38.

Daunt, F., Afanasyev, V., Silk, J. and Wanless, S. (2006). "Extrinsic and intrinsic determinants of winter foraging and breeding phenology in a temperate seabird." *Behavioral Ecology and Sociobiology* 59(3): 381-388.

De Boer, M.N., Simmonds, M.P., Reijnders, P.J. and Aarts, G. (2014). "The influence of topographic and dynamic cyclic variables on the distribution of small cetaceans in a shallow coastal system." *PLoS ONE* 9(1): 1-15.

Decker, M.B. and Hunt, G.L. (1996). "Foraging by murres (*Uria* spp.) at tidal fronts surrounding the Pribilof Islands, Alaska, USA." *Marine Ecology Progress Series* 139: 1-10.

Dehnhard, N., Ludynia, K., Poisbleau, M., Demongin, L. and Quillfeldt, P. (2013). "Good days, bad days: wind as a driver of foraging success in a flightless seabird, the southern Rockhopper Penguin." *PLoS ONE* 8(11): e79487.

Denardo, C., Dougherty, M., Hastie, G., Leaper, R., Wilson, B. and Thompson, P.M. (2001). "A new technique to measure spatial relationships within groups of free-ranging coastal cetaceans." *Journal of Applied Ecology* 38: 888-895.

Deruiter, S.L., Bahr, A., Blanchet, M.A., Hansen, S.F., Kristensen, J.H., Madsen, P.T., Tyack, P.L. and Wahlberg, M. (2009). "Acoustic behaviour of echolocating porpoises during prey capture." *The Journal of experimental biology* 212(19): 3100-3107.

Diamond, A.W. and Devlin, C.M. (2003). "Seabirds as Indicators of Changes in Marine Ecosystems: Ecological Monitoring on Machias Seal Island." *Environmental Monitoring and Assessment* 88: 153-175.

DiGiacomo, P.M., Hammer, W.M., Hamner, P.P. and Caldeira, R.M.A. (2002). "Phalaropes feeding at a coastal front in Santa Monica Bay, California " *Journal of Marine Systems* 37: 199-212.

Dolman, S.J., Hodgins, N.K., MacLeod, C.D., Pierce, G.J. and Weir, C.R. (2013). "Harbour porpoises (Phocoena phocoena) and minke whales (Balaenoptera acutorostrata) observed during land-based surveys in The Minch, north-west Scotland." *Journal of the Marine Biological Association of the United Kingdom*: 1-10.

Dos Santos, M.E. and Almada, V.C. (2004). A case for passive sonar: analysis of click train production patterns by bottlenose dolphins. *Echolocation in bats and dolphins*. J. Thomas. Chicago, Illinois: University of Chicago Press: 400-403.

Dunn, E.K. (1973). "Changes in fishing ability of terns associated with windspeed and sea surface conditions." *Nature* 244: 520-521.

Durant, J.M., Stenseth, N.C., Anker-Nilssen, T., Harris, M.P., Thompson, P.M. and Wanless, S. (2004). Marine birds and climate fluctuation in the North Atlantic. *Marine Ecosystems and Climate Variation*. N.C. Stenseth, G. Ottersen, J.M. Hurrell and A. Belgrano. Oxford: Oxford University Press: 95-105.

Eaton, M.A., Brown, A.F., Noble, D.G., Musgrove, A.J., Hearn, R., Aebischer, N.J., Gibbons, D.W., Evans, A. and Gregory, A.D. (2009). "Birds of Conservation Concern 3: the population status of birds in the United Kingdom, Channel Islands and the Isle of Man." *British Birds* 102: 296-341.

Elkins, N. (1995). *Weather and bird behaviour*. London: T. & A. D. Poyser.

Embling, C.B., Gillibrand, P.A., Gordon, J., Shrimpton, J., Stevick, P.T. and Hammond, P.S. (2010). "Using habitat models to identify suitable sites for marine protected areas for harbour porpoises (Phocoena phocoena)." *Biological Conservation* 143(2): 267-279.

Embling, C.B., Illian, J., Armstrong, E., van der Kooij, J., Sharples, J., Camphuysen, K.C.J. and Scott, B.E. (2012). "Investigating fine-scale spatio-temporal predator-prey patterns in dynamic marine ecosystems: a functional data analysis approach." *Journal of Applied Ecology* 49(2): 481-492.

Embling, C.B., Sharples, J., Armstrong, E., Palmer, M.R. and Scott, B.E. (2013). "Fish behaviour in response to tidal variability and internal waves over a shelf sea bank." *Progress In Oceanography* 117: 106-117.

Enviroware (2013) *WindRose PRO3. Version 3.1.54.0*. http://www.enviroware.com. Concorezzo, Italy: Enviroware srl.

ESRI (2012) *ArcGIS Desktop. Version 10.0*. http://www.esri.com. Redlands, CA: Environmental Systems Research Institute.

Farmer, D.M., D'Asaro, E.A., Trevorrow, M.V. and Dairiki, G.T. (1995). "Three-dimensional structure in a tidal convergence front." *Continental Shelf Research* 15(13): 1649-1673.

Fauchald, P. (2009). "Spatial interaction between seabirds and prey: review and synthesis." *Marine Ecology Progress Series* 391: 139-151.

Forney, K.A. (2000). "Environmental Models of Cetacean Abundance: Reducing Uncertainty in Population Trends." *Conservation Biology* 14(5): 1271-1286.

Forward, R.B. (1988). "Diel vertical migration: zooplankton photobiology and behaviour." *Oceaongr. Mar. Biol. Annu. Rev.* 26(36): 361-393.

Frank, K.T., Perry, R.I. and Drinkwater, K.F. (1990). "Predicted response of northwest Atlantic invertebrate and fish stocks to CO2-induced climate change." *Transactions of the American Fisheries Society*(119): 353-365.

Franks, P.J.S. (1992a). "Phytoplankton Blooms at Fronts: Patterns, Scales, and Physical Forcing Mechanisms." *Reviews in Aquatic Sciences* 6(2): 121-137.

Franks, P.J.S. (1992b). "Sink or swim: accumulation of biomass at fronts." *Marine Ecology Progress Series* 82: 1-12.

Fretwell, S.D. and Lucas, H.L. (1969). "On territorial behavior and other factors influencing habitat distribution in birds." *Acta Biotheor* 19: 16-36.

Fritz, H., Said, S. and Weimerskirch, H. (2003). "Scale–dependent hierarchical adjustments of movement patterns in a long–range foraging seabird." *Proceedings of the Royal Society of London B: Biological Sciences* 270(1520): 1143-1148.

Furness, R.W. and Bryant, D.M. (1996). "Effect of wind on field metabolic rates of breeding northern fulmars." *Ecology*: 1181-1188.

Furness, R.W. and Camphuysen, C.J. (1997). "Seabirds as monitors of the marine environment." *ICES Journal of Marine Science* 54: 726-737.

Gabrielsen, G.W., Mehlum, F. and Nagy, K.A. (1987). "Daily energy expenditure and energy utilization of free-ranging black-legged kittiwakes." *Condor*: 126-132.

Gannon, D.P., Barros, N.B., Nowacek, D.P., Read, A.J., Waples, D.M. and Wells, R.S. (2005). "Prey detection by bottlenose dolphins, Tursiops truncatus: an experimental test of the passive listening hypothesis." *Animal Behaviour* 69(3): 709-720.

Gargett, A. (1988). "A large-eddy approach to acoustic remote sensing of turbulent kinetic energy dissipation rate E." *Atmosphere-Ocean* 26: 483-508.

Garthe, S., Benvenuti, S. and Montevecchi, W.A. (2000). "Pursuit plunging by Northern Gannets (*Sula bassana*) feeding on capelin (*Mallotus villosus*)." *Proceedings of the Royal Society of London B* 267: 1717-1722.

Garthe, S., Benvenuti, S. and Montevecchi, W.A. (2003). "Temporal patterns of foraging activities of northern gannets, Morus bassanus, in the northwest Atlantic Ocean." *Canadian Journal of Zoology* 81(3): 453-461.

Garthe, S. and Hüppop, O. (2004). "Scaling possible adverse effects of marine wind farms on seabirds: developing and applying a vulnerability index." *Journal of Applied Ecology* 41: 724-734.

Gaston, A.J. and Nettleship, D.N. (1982). "The Thick-billed Murres of Prince Leopold Island - a study of the breeding biology of a colonial high arctic seabird." *Canadian Wildlife Service Monograph Series* 6: 350 pp.

Genin, A. (2004). "Bio-physical coupling in the formation of zooplankton and fish aggregations over abrupt topographies." *Journal of Marine Systems* 50(1-2): 3-20.

Georges, J.Y., Bonadonna, F. and Guinet, C. (2000). "Foraging habitat and diving activity of lactating subantarctic fur seals in relation to sea surface temperature at Amsterdam Island." *Marine Ecology Progress Series* 196: 291-304.

Georges, J.Y., Guinet, C., Jouventin, P. and Weimerskirch, H. (1997). "Satellite tracking of seabirds: interpretation of activity pattern from the frequency of satellite locations." *Ibis* 139(2): 403-405.

Goodson, D.A. and Mayo, R.H. (1995). Interactions between free-ranging dolphins (*Tursiops truncatus*) and passive acoustic gill-net deterrent devices. *Sensory Systems of Aquatic Mammals*. R.A. Kastelein, J.A. Thomas and P.E. Nachtigall. Woerden, NL: De Spil: 365-379.

Goodwin, L. and Speedie, C. (2008). "Relative abundance, density and distribution of the harbour porpoise (*Phocoena phocoena*) along the west coast of the UK." *Journal of the Marine Biological Association of the United Kingdom* 88(06).

GOV.UK (2014). *Marine conservation zone 2013 designations*. Crown copyright: https://www.gov.uk/government/collections/marine-conservation-zone-2013-designations. [Accessed 20/01/2015].

Grecian, W.J., Witt, M.J., Attrill, M.J., Bearhop, S., Godley, B.J., Grémillet, D., Hamer, K.C. and Votier, S.C. (2012). "A novel projection technique to identify important at-sea areas for seabird conservation: An example using Northern gannets breeding in the North East Atlantic." *Biological Conservation*.

Guilford, T., Wynn, R., McMinn, M., Rodriguez, A., Fayet, A., Maurice, L., Jones, A. and Meier, R. (2012). "Geolocators reveal migration and pre-breeding behaviour of the critically endangered Balearic Shearwater *Puffinus mauretanicus*." *PLoS ONE* 7(3): 1-8.

Guinet, C., Dubroca, L., Lea, M.A., Goldsworthy, S., Cherel, Y., Duhamel, G., Bonadonna, F. and Donnay, J.P. (2001). "Spatial distribution of foraging in female Antarctic fur seals *Arctocephalus gazella* in relation to oceanographic variables: a scale-dependent approach using geographic information systems." *Marine Ecology Progress Series* 219: 251-264.

Halpern, B.S., Walbridge, S., Selkoe, K.A., Kappel, C.V., Micheli, F., D'Agrosa, C., Bruno, J.F., Casey, K.S., Ebert, C. and Fox, H.E. (2008). "A global map of human impact on marine ecosystems." *Science* 319(5865): 948-952.

Hamazaki, T. (2002). "Spatiotemporal prediction models of cetacean habitats in the mid-western North Atlantic Ocean (from Cape Hatteras, North Carolina, USA to Nova Scotia, Canada)." *Marine Mammal Science* 18(4): 920-939.

Haney, J.C. (1986). "Seabird patchiness in tropical oceanic waters: the influence of *Sargassum* "reefs"." *Auk* 103: 141-151.

Hao, W., Jian, S., Ruijing, W., Lei, W. and Yi'an, L. (2003). "Tidal front and the convergence of anchovy (*Engraulis japonicus*) eggs in the Yellow Sea." *Fisheries Oceanography* 12(4-5): 434-442.

Hardy, T., Williams, R., Caslake, R. and Tregenza, N.C. (2012). "An investigation of acoustic deterrent devices to reduce cetacean bycatch in an inshore set net fishery." *Journal of Cetacean Research and Management* 12(1): 85-90.

Harzen, S.E. (2002). "Use of an electronic theodolite in the study of movements of the bottlenose dolphin (*Tursiops truncatus*) in the Sado Estuary, Portugal." *Aquatic Mammals* 28(3): 251-260.

Hastie, G., Swift, R., Slesser, G., Thompson, P. and Turrell, W. (2005). "Environmental models for predicting oceanic dolphin habitat in the Northeast Atlantic." *ICES Journal of Marine Science* 62(4): 760-770.

Hastie, G.D., Wilson, B., Wilson, L.J., Parsons, K.M. and Thompson, P.M. (2004). "Functional mechanisms underlying cetacean distribution patterns: hotspots for bottlenose dolphins are linked to foraging." *Marine Biology* 144(2): 397-403.

Hastie, T.J. and Tibshirani, R.J. (1999). *Generalized Additive Models*. Boca Raton: Chapman & Hall/CRC.

Hayhow, D.B., Conway, G., Eaton, M.A., Grice, P.V., Hall, C., Holt, C.A., Kuepfer, A., Noble, D.G., Oppel, S., Risely, K., Stringer, C., Stroud, D.A., Wilkinson, N. and Wotton, S. (2014). The state of the UK's birds 2014. RSPB, BTO, WWTet al. Sandy, Bedfordshire.

Hedd, A., Gales, R. and Brothers, N. (2001). "Foraging strategies of shy albatross Thalassarche cauta breeding at Albatross Island, Tasmania, Australia." *Marine Ecology Progress Series* 224: 267-282.

Herr, H., Fock, H.O. and Siebert, U. (2009). "Spatio-temporal associations between harbour porpoise Phocoena phocoena and specific fisheries in the German Bight." *Biological Conservation* 142(12): 2962-2972.

Hessner, K. and Bell, P.S. (2009). *High resolution current & Bathymetry Determined by Nautical X-Band Radar in Shallow Waters*. Oceans 2009 - Europe, 11-14 May.

Hooker, S.K. and Gerber, L.R. (2004). "Marine reserves as a tool for ecosystem based management: the potential importance of megafauna." *Bioscience* 54: 27-39.

Hooker, S.K., Whitehead, H. and Gowans, S. (2001). "Marine Protected Area Design and the Spatial and Temporal Distribution of Cetaceans in a Submarine Canyon." *Conservation Biology* 13(3): 592-602.

Horne, J. and Garton, E. (2006). "Likelihood Cross-Validation Versus Least Squares Cross-Validation for Choosing the Smoothing Parameter in Kernel Home-Range Analysis." *Journal of Wildlife Management* 70(3): 641-648.

Houghton, J.D.R., Doyle, T.K., Davenport, J. and Hays, G.C. (2006). "The ocean sunfish Mola mola: insights into distribution, abundance and behaviour in the Irish and Celtic Seas." *Journal of the Marine Biological Association of the United Kingdom* 86(05): 1237-1243.

Hunt, G.L. (1991a). "Marine ecology of seabirds in polar oceans." *American Zoologist* 31: 131-142.

Hunt, G.L. (1991b). "Occurrence of polar seabirds in relation to prey concentrations and oceanographic factors." *Polar Research* 10: 553-559.

Hunt, G.L., Mehlum, F., Russell, R.W., Irons, D., Decker, M.B. and Becker, P.H. (1999). *Physical processes, prey abundance, and the foraging ecology of seabirds*. Proceedings of the International Ornithological Congress, Durban: BirdLife South Africa.

Hunt, G.L., Russell, R.W., Coyle, K.O. and Weingartner, T. (1998). "Comparative foraging ecology of planktivorous auklets in relation to ocean physics and prey availability." *Marine Ecology Progress Series* 167: 241-259.

Hunt, G.L. and Schneider, D.C. (1987). Scale-dependent processes in the physical and biological environment of marine birds. *Seabirds: feeding ecology and role in marine ecosystems*. J. Croxall: Cambridge University Press: 7-41.

Ingram, S.N., Englund, A., O'Donovan, M., Walshe, L. and Rogan, E. (2005). An assessment of the potential for dolphin-listening ecotourism at sites on the Kerry shore of the outer Shannon Estuary. *Report to Tuatha Chiarrai Teo*: University College Cork: 1-15.

Ingram, S.N. and Rogan, E. (2002). "Identifying critical areas and habitat preferences of bottlenose dolphins *Tursiops truncatus*." *Marine Ecology Progress Series* 244: 247-255.

Ingram, S.N., Walshe, L., Johnston, D. and Rogan, E. (2007). "Habitat partitioning and the influence of benthic topography and oceanography on the distribution of fin and minke whales in the Bay of Fundy, Canada." *Journal of the Marine Biological Association of the UK* 87(01): 149.

Irons, D.B. (1998). "Foraging area fidelity of individual seabirds in relation to tidal cycles and flock feeding." *Ecology* 79(2): 647-655.

IUCN (2014). *IUCN Red List of Threatened Species. Version 2014.3*. International Union for Conservation of Nature: http://www.iucnredlist.org. [Accessed 12/12/2014].

JNCC (2009). Part 1: Background to site selection. The Habitats Directive: selection of Special Areas of Conservation in the UK. Version 4, September 2009, Tranche 37. Peterborough: 1-34.

Johnston, D.W., Thorne, L.H. and Read, A.J. (2005a). "Fin whales *Balaenoptera physalus* and minke whales *Balaenoptera acutorostrata* exploit a tidally driven island wake ecosystem in the Bay of Fundy." *Marine Ecology Progress Series* 305: 287-295.

Johnston, D.W., Westgate, A.J. and Read, A.J. (2005b). "Effects of fine-scale oceanographic features on the distribution and movements of harbour porpoises *Phocoena phocoena* in the Bay of Fundy." *Marine Ecology Progress Series* 295: 279-292.

Jones, A.R. (2012). *The spatio-temporal distribution and habitat associations of marine megavertebrates off southwest UK*. *School of Ocean and Earth Science*. Southampton: University of Southampton. PhD thesis: 329.

Jones, A.R., Hosegood, P., Wynn, R.B., De Boer, M.N., Butler-Cowdry, S. and Embling, C.B. (2014a). "Fine-scale hydrodynamics influence the spatio-temporal distribution of harbour porpoises at a coastal hotspot." *Progress In Oceanography* 128: 30-48.

Jones, A.R., Wynn, R.B., Yésou, P., Thébault, L., Collins, P., Suberg, L., Lewis, K.M. and Brereton, T.M. (2014b). "Using integrated land- and boat-based surveys to inform conservation of the Critically Endangered Balearic shearwater." *Endangered Species Research* 25(1): 1-18.

Jones, G.J. and Sayigh, L.S. (2002). "Geographic variation in rates of vocal production of free-ranging bottlenose dolphins." *Marine Mammal Science* 18(2): 374-393.

Kaschner, K., Watson, R., Trites, A.W. and Pauly, D. (2006). "Mapping world-wide distributions of marine mammal species using a relative environmental suitability (RES) model." *Marine Ecology Progress Series* 316: 285-310.

Kastelein, R.A., Janssen, M., Verboom, W.C. and de Haan, D. (2005). "Receiving beam patterns in the horizontal plane of a harbor porpoise (Phocoena phocoena)." *The Journal of the Acoustical Society of America* 118(2): 1172.

Kastelein, R.A., Verlaan, M. and Jennings, N. (2008). "Number and duration of echolocation click trains produced by a harbor porpoise (Phocoena phocoena) in relation to target and performance." *The Journal of the Acoustical Society of America* 124(1): 40-43.

Katzir, G. (1993). Visual mechanisms of prey capture in water birds. *Vision, Brain, and Behavior in Birds*. H.P. Zeigler and H.J. Bischof. Cambridge, Massachusetts: MIT Press, Cambridge: 301-315.

Kernohan, B.J., Gitzen, R. and Millspaugh, J. (2001). Analysis of animal space use and movements. *Radio tracking and animal populations*. J. Millspaugh and J. Marzluff. New York: Academic: 125-166.

Kim, H.-J., Miller, A.J., McGowan, J. and Carter, M.L. (2009). "Coastal phytoplankton blooms in the Southern Californian Bight." *Progress In Oceanography* 82: 137-147.

Koopman, H.N., Pabst, D.A., McLellan, W.A., Dillaman, R.M. and Read, A.J. (2002). "Changes in blubber distribution and morphology associated with starvation in the harbor porpoise (*Phocoena phocoena*): evidence fo regional differences in blubber structure and function." *Physiological and Biochemical Zoology* 75: 498-512.

Koschinski, S., Diederichs, A. and Amundin, M. (2008). "Click train patterns of free-ranging harbour porpoises acquired using T-PODs may be useful as indicators of their behaviour." *Journal of Cetacean Research and Management* 10(2): 147-155.

Kruse, S. (1991). The interaction between killer whales and boats in Johnstone Strait, B.C. *Dolphin Societies*. K.W. Pryor and K.S. Norris. Berkeley, C.A.: University of California Press: 149-159.

Kyhn, L.A., Tougaard, J., Thomas, L., Rosager Duve, L., Stenback, J., Amundin, M., Desportes, G. and Teilmann, J. (2012). "From echolation clicks to animal density - Acoustic sampling of harbour porpoise with static dataloggers." *Journal of Acoustic Society of America* 131(1): 550-560.

Largier, J.L. (1992). "Tidal Intrusion Fronts." *Estuaries* 15(1): 26-39.

Lascelles, B.G., Langham, G.M., Ronconi, R.A. and Reid, J.B. (2012). "From hotspots to site protection: Identifying Marine Protected Areas for seabirds around the globe." *Biological Conservation* 156: 5-14.

Le Fevre, J. (1986). "Aspects of the biology of frontal systems." *Advances in Marine Biology* 23: 163-299.

Leeney, R.H., Witt, M.J., Broderick, A.C., Buchanan, J., Jarvis, D.S., Richardson, P.B. and Godley, B.J. (2012). "Marine megavertebrates of Cornwall and the Isles of Scilly: relative abundance and distribution." *Journal of the Marine Biological Association of the United Kingdom* 92(08): 1823-1833.

Lehodey, P., Alheit, J., Barange, M., Baumgartner, T., Beaugrand, G., Drinkwater, K., Fromentin, J.-M., Hare, S., Ottersen, G. and Perry, R. (2006). "Climate variability, fish, and fisheries." *Journal of Climate* 19(20): 5009-5030.

Lewis, S., Benvenuti, S., Daunt, F., Wanless, S., Dall'Antonia, L., Luschi, P., Elston, D.A., Hamer, K.C. and Sherratt, T.N. (2004). "Partitioning of diving effort in foraging trips of northern gannets." *Canadian Journal of Zoology* 82(12): 1910-1916.

Lopez, A., Pierce, G.J., Valeiras, X., Santos, M.B. and Guerra, A. (2004). "Distribution patterns of small cetaceans in Galician waters." *Journal of the Marine Biological Association of the United Kingdom* 84(1): 283-294.

Lwiza, K.M.M., Bowers, D.G. and Simpson, J.H. (1991). "Residual and tidal flow at a tidal mixing front in the North Sea." *Continental Shelf Research* 11(11): 1379-1395.

Lynch, D.R., Werner, F.E., Greenberg, D.A. and Loder, J.W. (1992). "Diagnostic model for baroclinic, wind-driven and tidal circulation in shallow seas." *Continental Shelf Research* 12(1): 37-64.

Lythgoe, J.N. (1979). *The ecology of vision*. Oxford: Oxford University Press.

MacLeod, C.D., Santos, M.B., Reid, R.J., Scott, B.E. and Pierce, G.J. (2007a). "Linking sandeel consumption and the likelihood of starvation in harbour porpoises in the Scottish North Sea: could climate change mean more starving porpoises?" *Biology letters* 3(2): 185-188.

MacLeod, C.D., Weir, C.R., Pierpoint, C. and Harland, E.J. (2007b). "The habitat preferences of marine mammals west of Scotland (UK)." *Journal of the Marine Biological Association of the UK* 87(1): 157.

MacLeod, C.D. and Zuur, A.F. (2005). "Habitat utilization by Blainville's beaked whales off Great Abaco, northern Bahamas, in relation to seabed topography." *Marine Biology* 147(1): 1-11.

Macleod, K., Fairbairns, R., Gill, A., Fairbairns, B., Gordon, J., Blair-Myers, C. and Parsons, E.C.M. (2004). "Seasonal distribution of minke whales Balaenoptera acutorostrata in relation to physiography and prey off the Isle of Mull, Scotland." *Marine Ecology Progress Series* 277: 262-274.

Maravelias, C.D. (1999). "Habitat selection and clustering of a pelagic fish: effects of topography and bathymetry on species dynamics." *Canadian Journal of Fisheries and Aquatic Sciences* 56: 437-450.

Marques, T.A., Munger, L., Thomas, L., Wiggins, S. and Hildebrand, J.A. (2011). "Estimating North Pacific right whale Eubalaena japonica density using passive acoustic cue counting." *Endangered Species Research* 13(3): 163-172.

Marques, T.A., Thomas, L., Ward, J., DiMarzio, N. and Tyack, P.L. (2009). "Estimating cetacean population density using fixed passive acoustic sensors: An example with Blainville's beaked whales." *The Journal of the Acoustical Society of America* 125(4): 1982-1994.

Martin, S.W., Marques, T.A., Thomas, L., Morrissey, R.P., Jarvis, S., DiMarzio, N., Moretti, D. and Mellinger, D.K. (2013). "Estimating minke whale (Balaenoptera acutorostrata) boing sound density using passive acoustic sensors." *Marine Mammal Science* 29(1): 142-158.

Marubini, F., Gimona, A., Evans, P.G.H., Wright, P.J. and Pierce, G.J. (2009). "Habitat preferences and interannual variability in occurrence of the harbour porpoise Phocoena phocoena off northwest Scotland." *Marine Ecology Progress Series* 381: 297-310.

Mayo, R.H. and Goodson, D.A. (1993). *Land-based tracking of cetaceans - the practical use of surveying instruments*. Proceedings of the 7th Annual Conference ECS, Inverness, Scotland: European Research on Cetaceans-7.

McClellan, C.M., Brereton, T., Dell'amico, F., Johns, D.G., Cucknell, A.C., Patrick, S.C., Penrose, R., Ridoux, V., Solandt, J.L., Stephan, E., Votier, S.C., Williams, R. and Godley, B.J. (2014). "Understanding the Distribution of Marine Megafauna in the English Channel Region: Identifying Key Habitats for Conservation within the Busiest Seaway on Earth." *PLoS ONE* 9(2): e89720.

McFarlane Tranquilla, L.A., Montevecchi, W.A., Hedd, A., Fifield, D.A., Burke, C.M., Smith, P.A., Regular, P.M., Robertson, G.J., Gaston, A.J. and Phillips, R.A. (2013). "Multiple-colony winter habitat use by murres Uria spp. in the Northwest Atlantic Ocean: implications for marine risk assessment." *Marine Ecology Progress Series* 472: 287-303.

McPhee-Shaw, E.E., Nielsen, K.J., Largier, J.L. and Menge, B.A. (2011). "Nearshore chlorophyll-a events and wave-driven transport." *Geophysical Research Letters* 38(2).

Melvin, E.F., Parrish, J. and Conquest, L. (1999). "Novel Tools to Reduce Seabird Bycatch in Coastal Gillnet Fisheries." *Conservation Biology* 13(6): 1386-1397.

Mendes, S., Turrell, W., Lutkebohle, T. and Thompson, P. (2002). "Influence of the tidal cycle and a tidal intrusion front on the spatio-temporal distribution of coastal bottlenose dolphins." *Marine Ecology Progress Series* 239: 221-229.

Merchant, N.D., Fristrup, K.M., Johnson, M.P., Tyack, P.L., Witt, M.J., Blondel, P. and Parks, S.E. (2014). "Measuring acoustic habitats (Appendix S1)." *Methods in Ecology and Evolution*: 1-42.

Mikkelsen, L., Mouritsen, K.N., Dahl, K., Teilmann, J. and Tougaard, J. (2013). "Re-established stony reef attracts harbour porpoises Phocoena phocoena." *Marine Ecology Progress Series* 481: 239-248.

Miller, L.A. and Wahlberg, M. (2013). "Echolocation by the harbour porpoise: life in coastal waters." *Frontiers in physiology* 4: 52.

Montevecchi, W.A. (1993). Birds as indicators of change in marine prey stocks. *Birds as Monitors of Environmental Change*. R.W. Furness and J.J.D. Greenwood. London: Chapman & Hall.

Munilla, I., Díez, C. and Velando, A. (2007). "Are edge bird populations doomed to extinction? A retrospective analysis of the common guillemot collapse in Iberia." *Biological Conservation* 137(3): 359-371.

Nash, J.D. and Moum, J.N. (2001). "Internal hydraulic flows on the continental shelf: High drag states over a small bank." *Journal of Geophysical Research: Oceans* 106: 4593-4611.

Nelson, J.B. (1978). *The Sulidae: Gannets and Boobies*. Oxford: Oxford University Press.

NIEA (2011). Inshore Special Area of Conservation: Skerries and Causeway. Conservation Objectives and Advice on Operations. Northern Ireland Environment Agency. NIEA: 1-18.

Nowacek, D.P. (2005). "Acoustic ecology of foraging Bottlenose dolphins (*Tursiops truncatus*), habitat-specific use of three sound types." *Marine Mammal Science* 21(4): 587-602.

Nuuttila, H.K., Thomas, L., Hiddink, J.G., Meier, R., Turner, J.R., Bennell, J.D., Tregenza, N.J. and Evans, P.G. (2013). "Acoustic detection probability of bottlenose dolphins, Tursiops truncatus, with static acoustic dataloggers in Cardigan Bay, Wales." *The Journal of the Acoustical Society of America* 134(3): 2596-2609.

Ohizumi, H., Kuramochi, T., Amano, N. and Miyazaki, N. (2000). "Prey switching of Dall's porpoise, *Phocoenoides dalli*, with population decline of Japanese pilchard, *Sardinops melanostictus*, around Hokkaido, Japan." *Marine Ecology Progress Series* 200: 265-275.

Otani, S., Naito, Y., Kawamura, A., Kawasaki, M., Nishiwaki, S. and Kato, A. (1998). "Diving behaviour and performance of Harbor porpoises, Phocoena phocoena, in Funka Bay, Kokkaido, Japan." *Marine Mammal Science* 14(2): 209-220.

Ottersen, G., Alheit, J., Drinkwater, K., Friedland, K., Hagen, E. and Stenseth, N.C. (2004). The responses of fish populations to ocean climate fluctuations. *Marine Ecosystems and Climate Variation*. N.C. Stenseth, G. Ottersen, J.M. Hurrell and A. Belgrano. Oxford: Oxford University Press. `: 73-94.

Paiva, V.H., Guilford, T., Meade, J., Geraldes, P., Ramos, J.A. and Garthe, S. (2010). "Flight dynamics of Cory's shearwater foraging in a coastal environment." *Zoology* 113(1): 47-56.

Palka, D. (1996). Effects of Beaufort sea state of the sightability of harbor porpoises in the Gulf of Maine: International Whaling Commission. 46: 575-582.

Pennycuick, C.J. (2002). "Gust soaring as a basis for the flight of petrels and albatrosses (Procellariiformes)." *Avian Science* 2(1): 1-12.

Philpott, E., Englund, A., Ingram, S. and Rogan, E. (2007). "Using T-PODs to investigate the echolocation of coastal bottlenose dolphins." *Journal of the Marine Biological Association of the UK* 87(01): 11.

Pierpoint, C. (2008). "Harbour porpoise (Phocoena phocoena) foraging strategy at a high energy, near-shore site in south-west Wales, UK." *Journal of the Marine Biological Association of the United Kingdom* 88(06).

Pikesley, S.K., Witt, M.J., Hardy, T., Loveridge, J., Loveridge, J., Williams, R. and Godley, B.J. (2011). "Cetacean sightings and strandings: evidence for spatial and temporal trends." *J Mar Biol Ass DOI* 10: S0025315411000464.

Pirotta, E., Thompson, P.M., Miller, P.I., Brookes, K.L., Cheney, B., Barton, T.R., Graham, I.M., Lusseau, D. and Costa, D. (2013). "Scale-dependent foraging ecology of a marine top predator modelled using passive acoustic data." *Functional Ecology* 28(1): 206-217.

Pocklington, R. (1979). "An oceanographic interpretation of seabird distributions in the Indian Ocean." *Marine Biology*(51): 9-21.

Pollet, I.L., Ronconi, R.A., Jonsen, I.D., Leonard, M.L., Taylor, P.D. and Shutler, D. (2014). "Foraging movements of Leach's storm-petrels Oceanodroma leucorhoaduring incubation." *Journal of Avian Biology* 45(4): 305-314.

POLPRED (2013) *Offshore tidal prediction software. Version 2.4.1.0*. Liverpool: National Oceanography Centre.

Prado, J.H.F., Secchi, E.R. and Kinas, P.G. (2013). "Mark-recapture of the endangered franciscana dolphin (Pontoporia blainvillei) killed in gillnet fisheries to estimate past bycatch from time series of stranded carcasses in southern Brazil." *Ecological Indicators* 32: 35-41.

R Development Core Team (2012) *R: a language and environment for statistical computing*. http://www.R-project.org. Vienna: R Foundation for Statistical Computing.

Raum-Suryan, K.L. and Harvey, J.T. (1998). "Distribution and abundance of and habitat use by harbour porpoise, *Phocoena phocoena*, off the northern San Juan Islands, Washington." *Fishery Bulletin US*(96): 802-822.

Read, A.J. and Westgate, A.J. (1997). "Monitoring the movements of harbour porpoises (*Phocoena phocoena*) with satellite telemetry." *Marine Biology* 130: 315-322.

Redfern, J.V., Ferguson, M.C., Becker, E.A., Hyrenbach, K.D., Good, C., Barlow, J., Kaschner, K., Baumgartner, M.F., Forney, K.A., Ballance, L.T., Fauchald, P., Halpin, P., Hamazaki, T., Pershing, A.J., Qian, S.S., Read, A., Reilly, S.B., Torres, L. and Werner, F. (2006). "Techniques for cetacean-habitat modelling." *Marine Ecology Progress Series* 310: 271-295.

Roberts, T. and Jones, P.J.S. (2013). "North East Kent European marine site: Overcoming barriers to conservation through community engagement." *Marine Policy* 41: 33-40.

Rodrigues, J.M.G. (2014). Echolocation activity of Harbour Porpoise *Phocoena phocoena* in the Eastern Scheldt estuary (The Netherlands) and the North Sea. F. Zanderink: The Rugvin Foundation: 1-38.

Roff, J.C. (2014). "Networks of marine protected areas - the demonstrability dilemma." *Aquatic Conservation: Marine and Freshwater Ecosystems* 24(1): 1-4.

Ronconi, R.A., Lascelles, B.G., Langham, G.M., Reid, J.B. and Oro, D. (2012). "The role of seabirds in Marine Protected Area identification, delineation, and monitoring: Introduction and synthesis." *Biological Conservation*.

Ross, H.M. and Wilson, B. (1996). "Violent interactions between bottlenose dolphins and harbour porpoises." *Proceedings of the Royal Society of London. Series B: Biological Sciences* 263(1368): 283-286.

Rowat, D. and Gore, M. (2007). "Regional scale horizontal and local scale vertical movements of whale sharks in the Indian Ocean off Seychelles." *Fisheries Research* 84(1): 32-40.

RSPB (2012). *Seabird death toll rises off Cornish Coast*. Royal Society for the Protection of Birds: http://www.rspb.org.uk/news/details.aspx?id=302190. [Accessed 02/07/2013].

Sagnol, O., Reitsma, F., Richter, C. and Field, L.H. (2014). "Correcting Positional Errors in Shore-Based Theodolite Measurements of Animals at Sea." *Journal of Marine Biology* 2014: 1-8.

Sanchez, P., Demestre, M., Recasens, L., Maynou, F. and Martin, P. (2008). "Combining GIS and GAMs to identify potential habitats of squid Loligo vulgaris in the Northwestern Mediterranean." *Hydrobiologia* 612(1): 91-98.

Scales, K.L., Miller, P.I., Hawkes, L.A., Ingram, S.N., Sims, D.W., Votier, S.C. and Punt, A. (2014). "On the Front Line: frontal zones as priority at-sea conservation areas for mobile marine vertebrates." *Journal of Applied Ecology* 51(6): 1575-1583.

Schneider, D.L. (1997). "Habitat selection by marine birds in relation to water depth." *Ibis*(139): 175-177.

Schneider, D.L. and Piatt, J.F. (1986). "Scale-dependent correlation of seabirds with schooling fish in a coastal ecosystem." *Marine Ecology Progress Series* 32: 237-246.

Schreiber, E.A. and Burger, J., Eds. (2002). *Biology of Marine Birds*. CRC Marine Biology Series. Boca Raton: CRC Press LLC.

Scott, B.E., Sharples, J., Ross, O.N., Wang, J., Pierce, G.J. and Camphuysen, C.J. (2010). "Sub-surface hotspots in shallow seas: fine-scale limited locations of top predator foraging habitat indicated by tidal mixing and sub-surface chlorophyll." *Marine Ecology Progress Series* 408: 207-226.

Scott, B.E., Webb, A., Palmer, M.R., Embling, C.B. and Sharples, J. (2013). "Fine scale bio-physical oceanographic characteristics predict the foraging occurrence of contrasting seabird species; Gannet (Morus bassanus) and storm petrel (Hydrobates pelagicus)." *Progress In Oceanography* 117: 118-129.

SeaWatch SW (2014). *SeaWatch South West*. http://www.seawatch-sw.org. [Accessed 06/12/2014].

Secchi, E. (2010). "Review on the threats and conservation status of franciscana, Pontoporia blainvillei (Cetacea, Pontoporiidae)." *Biology, evolution and conservation of river dolphins within South America and Asia. 1st ed. Hauppange (NY): Nova Science Publishers Inc*: 323-339.

Senko, J., White, E.R., Heppell, S.S. and Gerber, L.R. (2013). "Comparing bycatch mitigation strategies for vulnerable marine megafauna." *Animal Conservation*: 1-20.

Sharples, J. (2007). "Potential impacts of the spring-neap tidal cycle on shelf sea primary production." *Journal of Plankton Research* 30(2): 183-197.

Sharples, J., Ellis, J.R., Nolan, G. and Scott, B.E. (2013a). "Fishing and the oceanography of a stratified shelf sea." *Progress In Oceanography* 117: 130-139.

Sharples, J., Scott, B.E. and Inall, M.E. (2013b). "From physics to fishing over a shelf sea bank." *Progress In Oceanography* 117: 1-8.

Shealer, D.A. (1996). "Foraging habitat use and profitability in tropical Roseate Terns and Sandwich Terns." *Auk* 113: 209-217.

Simon, M., Nuuttila, H., Reyes-Zamudio, M.M., Ugarte, F., Verfub, U. and Evans, P.G. (2010). "Passive acoustic monitoring of bottlenose dolphin and harbour porpoise, in Cardigan Bay, Wales, with implications for habitat use and partitioning." *Journal of the Marine Biological Association of the United Kingdom* 90(08): 1539-1545.

Sims, D.W. and Merrett, D.A. (1997). "Determination of zooplankton characteristics in the presence of surface feeding basking sharks *Cetorhinus maximus*." *Marine Ecology Progress Series* 158: 297-302.

Sims, D.W. and Quayle, V.A. (1998). "Selective foraging behaviour of basking sharks on zooplankton in a small-scale front." *Nature*(393): 460-464.

Sims, D.W. and Southall, E.J. (2002). "Occurrence of ocean sunfish, Mola mola near fronts in the western English Channel." *Journal of the Marine Biological Association of the United Kingdom* 82(5): 927-928.

Sims, D.W., Southall, E.J., Humphries, N.E., Hays, G.C., Bradshaw, C.J., Pitchford, J.W., James, A., Ahmed, M.Z., Brierley, A.S., Hindell, M.A., Morritt, D., Musyl, M.K., Righton, D., Shepard, E.L., Wearmouth, V.J., Wilson, R.P., Witt, M.J. and Metcalfe, J.D. (2008). "Scaling laws of marine predator search behaviour." *Nature* 451(7182): 1098-1102.

Sims, D.W., Southall, E.J., Richardson, A.J., Reid, P.C. and Metcalfe, J.D. (2003). "Seasonal movements and behaviour of basking sharks from archival tagging: no evidence of winter hibernation." *Marine Ecology Progress Series* 248: 187-196.

Sims, D.W., Southall, E.J., Tarling, G.A. and Metcalfe, J.D. (2005). "Habitat-specific normal and reverse diel vertical migration in the plankton-feeding basking shark." *Journal of Animal Ecology* 74(4): 755-761.

Sims, D.W., Witt, M.J., Richardson, A.J., Southall, E.J. and Metcalfe, J.D. (2006). "Encounter success of free-ranging marine predator movements across a dynamic prey landscape." *Proceedings. Biological sciences / The Royal Society* 273(1591): 1195-1201.

Skov, H., Gunnlaugsson, T., Budgell, W., Horne, J., Nøttestad, L., Olsen, E., Søiland, H., Víkingsson, G. and Waring, G. (2008). "Small-scale spatial variability of sperm and sei whales in relation to oceanographic and topographic features along the Mid-Atlantic Ridge." *Deep Sea Research Part II: Topical Studies in Oceanography* 55(1): 254-268.

Skov, H. and Thomsen, F. (2008). "Resolving fine-scale spatio-temporal dynamics in the harbour porpoise Phocoena phocoena." *Marine Ecology Progress Series* 373: 173-186.

Soanes, L.M., Arnould, J.P., Dodd, S.G., Milligan, G. and Green, J.A. (2014). "Factors affecting the foraging behaviour of the European shag." *Marine Biology* 161(6): 1335-1348.

Sonntag, N., Schwemmer, H., Fock, H.O., Bellebaum, J. and Garthe, S. (2012). "Seabirds, set-nets, and conservation management: assessment of conflict potential and vulnerability of birds to bycatch in gillnets." *ICES Journal of Marine Science* 69(4): 578-589.

Sostres Alonso, M. and Nuuttila, H.K. (2014). "Detection rates of wild harbour porpoises and bottlenose dolphins using static acoustic click loggers vary with depth." *Bioacoustics*: 1-10.

Speedie, C.D., Johnson, L.A. and Witt, M.J. (2009). *Basking Shark Hotspots on the West Coast of Scotland: Key sites, threats and implications for conservation of the species*.

Stevick, P.T., Incze, L.S., Kraus, S.D., Rosen, S., Wolff, N. and Baukus, A. (2008). "Trophic relationships and oceanography on and around a small offshore bank." *Marine Ecology Progress Series* 363: 15-28.

Sveegaard, S., Andreasen, H., Mouritsen, K.N., Jeppesen, J.P., Teilmann, J. and Kinze, C.C. (2012a). "Correlation between the seasonal distribution of harbour porpoises and their prey in the Sound, Baltic Sea." *Marine Biology* 159(5): 1029-1037.

Sveegaard, S., Nabe-Nielsen, J., Stæhr, K.J., Jensen, T.F., Mouritsen, K.N. and Teilmann, J. (2012b). "Spatial interactions between marine predators and their prey: herring abundance as a driver for the distributions of mackerel and harbour porpoise." *Marine Ecology Progress Series* 468: 245-253.

Sveegaard, S., Teilmann, J., Berggren, P., Mouritsen, K.N., Gillespie, D. and Tougaard, J. (2011a). "Acoustic surveys confirm the high-density areas of harbour porpoises found by satellite tracking." *ICES Journal of Marine Science* 68(5): 929-936.

Sveegaard, S., Teilmann, J., Tougaard, J., Dietz, R., Mouritsen, K.N., Desportes, G. and Siebert, U. (2011b). "High-density areas for harbor porpoises (Phocoena phocoena) identified by satellite tracking." *Marine Mammal Science* 27(1): 230-246.

Thaxter, C.B., Lascelles, B., Sugar, K., Cook, A.S.C.P., Roos, S., Bolton, M., Langston, R.H.W. and Burton, N.H.K. (2012). "Seabird foraging ranges as a preliminary tool for identifying candidate Marine Protected Areas." *Biological Conservation* 156: 53-61.

Thetmeyer, H. and Kils, U. (1995). "To see and not be seen: the visibility of predator and prey with respect to feeding behaviour." *Marine Ecology Progress Series* 126(1): 1-8.

Thomas, L., Buckland, S.T., Burnham, K.P., Anderson, D.R., Laake, J.L., Borchers, D.L. and Strindberg, S. (2012). Distance sampling. *Encyclopedia of Environmetrics Second Edition*. A.H. El-Shaarawi and W.W. Piegorsch. Chichester: John Wiley & Sons Ltd: 1-10.

Thompson, P., White, S. and Dickson, E. (2004). "Co-variation in the probabilities of sighting Harbour porpoises and Bottlenose dolphins." *Marine Mammal Science* 20(2): 322-328.

Thompson, P.M., Wilson, B., Grellier, K. and Hammond, P.S. (2000). "Combining power analysis and population viability analysis to compare traditional and precautionary approaches to conservation of coastal cetaceans." *Conservation Biology* 14: 1253-1263.

Todd, V.L.G., Pearse, W.D., Tregenza, N.C., Lepper, P.A. and Todd, I.B. (2009). "Diel echolocation activity of harbour porpoises (*Phocoena phocoena*) around North Sea offshore gas installations." *ICES Journal of Marine Science* 66(4): 734-745.

Tougaard, J., Carstensen, J., Teilmann, J., Skov, H. and Rasmussen, P. (2009). "Pile driving zone of responsiveness extends beyond 20 km for harbor porpoises (Phocoena phocoena (L.))." *The Journal of the Acoustical Society of America* 126(1): 11-14.

Tregenza, N.C., Berrow, S.D., Hammond, P.S. and Leaper, R. (1997). "Harbour porpoise (*Phocoena phocoena* L.) by-catch in set gillnets in the Celtic Sea." *ICES Journal of Marine Science* 54: 896-904.

Trujillo, A.P. and Thurman, H.V. (2008). *Essentials of Oceanography*. New Jersey, US: Pearson Prentice Hall.

Van Eerden, M.R. and Voslamber, B. (1995). "Mass fishing by cormorants Phalacrocorax carbo sinensis at Lake Ijsselmeer, the Netherlands-A recent and successful adaptation to a turbid environment." *Ardea* 83(1): 199-212.

Verfuß, U.K., Honnef, C.G., Meding, A., Dähne, M., Mundry, R. and Benke, H. (2007). "Geographical and seasonal variation of harbour porpoise (Phocoena phocoena) presence in the German Baltic Sea revealed by passive acoustic monitoring." *Journal of the Marine Biological Association of the UK* 87(01): 165.

Verfuß, U.K., Miller, L.A., Pilz, P.K. and Schnitzler, H.U. (2009). "Echolocation by two foraging harbour porpoises (Phocoena phocoena)." *The Journal of experimental biology* 212(Pt 6): 823-834.

Votier, S.C., Bearhop, S., Witt, M.J., Inger, R., Thompson, D. and Newton, J. (2010). "Individual responses of seabirds to commercial fisheries revealed using GPS tracking, stable isotopes and vessel monitoring systems." *Journal of Applied Ecology* 47: 487-497.

Waggitt, J. and Scott, B. (2014). "Using a spatial overlap approach to estimate the risk of collisions between deep diving seabirds and tidal stream turbines: A review of potential methods and approaches." *Marine Policy* 44: 90-97.

Wakefield, E.D., Phillips, R.A. and Matthiopoulos, J. (2009a). "Quantifying habitat use and preferences of pelagic seabirds using individual movement data: a review." *Marine Ecology Progress Series* 391: 165-182.

Wakefield, E.D., Phillips, R.A., Matthiopoulos, J., Fukuda, A., Higuchi, H., Marshall, G.J. and Trathan, P.N. (2009b). "Wind field and sex constrain the flight speeds of central-place foraging albatrosses." *Ecological Monographs* 79(4): 663-679.

Wanless, S., Frederiksen, M., Daunt, F., Scott, B.E. and Harris, M.P. (2007). "Black-legged kittiwakes as indicators of environmental change in the North Sea: Evidence from long-term studies." *Progress In Oceanography* 72(1): 30-38.

Watts, P. and Gaskin, D. (1985). "Habitat Index Analysis of the Harbor Porpoise (Phocoena phocoena) in the Southern Coastal Bay of Fundy, Canada." *Journal of Mammalogy* 66(4): 733-744.

Webster, M.S., Marra, P.P., Haig, S.M., Bensch, S. and Holmes, R.T. (2002). "Links between worlds: unraveling migratory connectivity." *Trends in Ecology & Evolution* 17(2): 76-83.

Weimerskirch, H., Guionnet, T., Martin, J., Shaffer, S.A. and Costa, D.P. (2000). *Fast and fuel efficient? Optimal use of wind by flying albatrosses*.

Wenz, G.M. (1962). "Acoustic ambient noise in the ocean: spectra and sources." *The Journal of the Acoustical Society of America* 34(12): 1936-1956.

Westgate, A.J., Head, A.J., Berggren, P., Koopman, H.N. and Gaskin, D.E. (1995). "Diving behaviour of harbour porpoises, Phocoena phocoena." *Canadian Journal of Fisheries and Aquatic Sciences* 52(5): 1064-1073.

Wilson, B., Reid, R.J., Grellier, K., Thompson, P.M. and Hammond, P.S. (2004). "Considering the temporal when managing the spatial: a population range expansion impacts protected areas-based management for bottlenose dolphins." *Animal Conservation* 7(4): 331-338.

Wilson, B., Thompson, P.M. and Hammond, P.S. (1997). "Habitat use by bottlenose dolphins: seasonal distribution and stratified movement patterns in the Moray Firth, Scotland." *Journal of Applied Ecology* 34: 1365-1374.

Wilson, L.J., McSorley, C.A., Gray, C.M., Dean, B.J., Dunn, T.E., Webb, A. and Reid, J.B. (2009). "Radio-telemetry as a tool to define protected areas for seabirds in the marine environment." *Biological Conservation* 142(8): 1808-1817.

Wilson, R.P., Grémillet, D., Syder, J., Kierspel, M.A., Garthe, S., Weimerskirch, H., Schäfer-Neth, C., Scolaro, J.A., Bost, C. and Plötz, J. (2002). "Remote-sensing systems and seabirds: their use, abuse and potential for measuring marine environmental variables." *Marine Ecology Progress Series* 228: 241-261.

Witt, M.J., Doherty, P.D., Hawkes, L.A., Godley, B.J., Graham, B.J. and Henderson, S.M. (2013). Basking shark satellite tagging project: post-fieldwork report.

Witt, M.J., Hardy, T., Johnson, L., McClellan, C.M., Pikesley, S.K., Ranger, S., Richardson, P.B., Solandt, J.L., Speedie, C., Williams, R. and Godley, B.J. (2012a). "Basking sharks in the northeast Atlantic: spatio-temporal trends from sightings in UK waters." *Marine Ecology Progress Series* 459: 121-134.

Witt, M.J., Sheehan, E.V., Bearhop, S., Broderick, A.C., Conley, D.C., Cotterell, S.P., Crow, E., Grecian, W.J., Halsband, C., Hodgson, D.J., Hosegood, P., Inger, R., Miller, P.I., Sims, D.W., Thompson, R.C., Vanstaen, K., Votier, S.C., Attrill, M.J. and Godley, B.J. (2012b). "Assessing wave energy effects on biodiversity: the wave hub experience." *Philosophical transactions. Series A, Mathematical, physical, and engineering sciences* 370(1959): 502-529.

Wolanski, E. and Hamner, W.M. (1988). "Topographically Controlled Fronts in the Ocean and Their Biological Influence." *Science* 241(4862): 177-181.

Wood, S. (2006a) *The mgcv Package: GAMs with GCV smoothness estimation and GAMMs by REML/PQL. Version 1.3.17*. www.r-project.org: R project.

Wood, S.N. (2006b). *Generalized Additive Models: An Introduction with R*. Boca Raton: Chapman & Hall/CRC.

Worton, B.J. (1995). "Using Monte Carlo simulation to evaluate kernel-based home range estimators." *Journal of Wildlife Management* 59: 794-800.

Wursig, B. and Wursig, M. (1979). "Behaviour and ecology of bottlenose dolphin, *Tursiops truncatus*, in the South Atlantic." *Fisheries Bulletin* 77: 399-412.

Wursig, B.W., Cipriano, F. and Wursig, M. (1991). Dolphin movement patterns. Information on radio and theodolite tracking studies. *Dolphin Societies*. K.W. Pryor and K.S. Norris. Berkeley, C.A.: University of California Press: 79-111.

Wynn, R.B. (2009). "Balearic shearwaters in UK and Irish waters from 2004 to 2006." *British Birds* 102: 320-354.

Wynn, R.B., Josey, S.A., Martin, A.P., Johns, D.G. and Yesou, P. (2007). "Climate-driven range expansion of a critically endangered top predator in northeast Atlantic waters." *Biol Lett* 3(5): 529-532.

Wynn, R.B., Josey, S.A., Martin, A.P., Johns, D.G. and Yesou, P. (2008). "Reply to comment: is climate change the most likely driver of range expansion of a critically endangered top predator in northeast Atlantic waters?" *Biology Letters* 4(2): 206-207.

Yen, P. (2004). "Marine bird and cetacean associations with bathymetric habitats and shallow-water topographies: implications for trophic transfer and conservation." *Journal of Marine Systems* 50(1-2): 79-99.

Zheng, X. (2002). "Does the North Atlantic current affect spatial distribution of whiting? Testing environmental hypotheses using statistical and GIS techniques." *ICES Journal of Marine Science* 59(2): 239-253.

Zuur, A.F., Ieno, E.N. and Smith, G.M. (2007). *Analysing Ecological Data*. New York: Springer Science+Business Media.

Zuur, A.F., Ieno, E.N., Walker, N.J., Saveliev, A.A. and Smith, G.M. (2009). *Mixed Effects Models and Extensions in Ecology with R*. New York: Springer Science+Business Media.

Žydelis, R., Small, C. and French, G. (2013). "The incidental catch of seabirds in gillnet fisheries: A global review." *Biological Conservation* 162: 76-88.